April 2019

High-Resolution Investigation of Event Driven Sedimentation: Response and Evolution of the Deepwater Horizon Blowout in the Sedimentary System

Rebekka A. Larson
University of South Florida, larsonra@eckerd.edu

High-Resolution Investigation of Event Driven Sedimentation:

Response and Evolution of the Deepwater Horizon Blowout in the Sedimentary System

by

Rebekka A. Larson

A dissertation submitted in partial fulfillment
of the requirements for the degree of
Doctor of Philosophy
College of Marine Science
University of South Florida

Major Professor: David J. Hollander, Ph.D.
Brad Rosenheim, Ph.D.
Steven Murawski, Ph.D.
Gregg R. Brooks, Ph.D.
Gert-Jan Reichart, Ph.D.

Date of Approval:
March, 19, 2019

Keywords: Geochronology, Sedimentology, High-Resolution, Short-lived Radioisotopes, Gulf of Mexico, Event Stratigraphy

DEDICATION

This dissertation is dedicated to mentors, clleagues, and friends Charles “Chuck” Holmes, Benjanmin “Ben” Flower, and Terry Edgar, as well as my father Ross Larson who always was supportive of pursuing what made you happy. Charles “Chuck” Holmes advanced geologic studies in the Gulf of Mexico and beyond, tand without his guidance and knowledge, the advancement and use of short-lived radioisotopes for investigating sediment records at high-resolution, in this study and others, would not have been as far-reaching. Benjamin “Ben” Flower was a great advisor and paleoceanography, and integral to this study as a promopter of the 2mm high-resolution sampling and innovative concepts such as the “dirty blizzard” and “bathtub ring”. Terry Edgar was my first scientific internship, at the USGS in St. Petersburg, FL as well as a great mentor, colleague and advisor in the early years of my scientific education and carreer.

ACKNOWLEDGMENTS

This research was made possible by a grants from The Gulf of Mexico Research Initiative C-IMAGE I, C-IMAGE II, and DEEP-C, as well as NSF RAPID grant 1049586. Data are publicly available through the Gulf of Mexico Research Initiative Information & Data Cooperative (GRIIDC) at https://data.gulfresearchinitiative.org (doi: 10.7266/N7FJ2F94, 10.7266/N79S1PJZ, 10.7266/N7610XTJ, 10.7266/N7FJ2F94, 10.7266/N74B2Z7K, 10.7266/n7-k9s6-4b11, 10.7266/n7-pb9j-t538, 10.7266/n7-c88d-pn57, 10.7266/n7-qzyx-sz24, 10.7266/N7BR8QHJ, 10.7266/n7-kzww-0995, 10.7266/n7-c8va-fr98, 10.7266/n7-bkvk-wr98, 10.7266/n7-ebqz-4476, 10.7266/n7-b0y2-f117, 10.7266/n7-g60e-wd38, 10.7266/n7-380p-k210, 10.7266/n7-81nq-dq02, 10.7266/n7-p0xt-6209, 10.7266/n7-qzw5-kc72, 10.7266/n7-xsrd-fq25, 10.7266/n7-1vvs-ef02, 10.7266/n7-4j4h-7w93, 10.7266/n7-cdrm-g239, 10.7266/n7-0n8j-b448, 10.7266/n7-4vxx-7a70, 10.7266/n7-srx5-bm38, 10.7266/n7-pny9-4794, 10.7266/n7-bddk-cj34, 10.7266/n7-tf6e-ct11, 10.7266/n7-5gnm-zd54).

I would like to acknowledge the assistance in field collection by the Florida Institute of Oceanography including the crew of the R/V Weatherbird II, the assistance in laboratory analyses by multiple Eckerd College students over the duration of this project.

TABLE OF CONTENTS

LIST OF TABLES

LIST OF FIGURES

ABSTRACT

This Dissertation combines the investigation of the sedimentological impacts of the Deepwater Horizon (DwH) blowout event in the deep-sea benthos, with the refinement and advancement of methods and approaches for high-resolution investigations of events preserved in sedimentary records. An approach that combined, rapid collection of cores, a continued annual time series collection of cores, and high-resolution sampling and analyses, in particular short-lived Radioisotopes (SLRad), enabled the temporal resolution required to detect the sedimentary response to the short-duration DwH event, and evaluate post-event sedimentation patterns at a comparable time scale (months).

The collection of 179 sediment cores from 80 sites between the fall of 2010 and 2016 included four sites that were utilized as an annual time-series collection to define the sedimentary response to the DwH blowout event and how the sedimentary system evolved/recovered post-event. High-resolution (2mm) sub-sampling was utilized to maximize the temporal resolution of analyses and age control using SLRad. The rapid collection of cores to define the immediate benthic impact(s), as well as the use of time-sensitive indicators of the event that may degrade over time, as well as indicators for very short time scale (months) sedimentation, such as $^{234}Th_{xs}$. $^{234}Th_{xs}$ inventories and mass accumulation rates (MAR's) were one of the most diagnostic characteristics of the sedimentary response. The DwH blowout event led to a Marine Oil Snow Sedimentation and Flocculent Accumulation (MOSSFA) event that caused a depositional pulse to the seafloor.

This was defined by increased sedimentation rates and the shutdown of bioturbation as indicated by $^{234}Th_{xs}$ inventories and MAR's. The annual collection of sediment cores as a time-series allowed for continued high-resolution analyses and use of $^{234}Th_{xs}$ to determine post-event sedimentation rates and baselines on monthly time scales for direct comparison to the depositional pulse. Within ~one year sedimentation rates decreased and within three years site specific return of bioturbation occurred and sedimentation rates on monthly scale ($^{234}Th_{xs}$) stabilized. Also, within ~three years the sedimentary signature of the depositional pulse became undetectable with respect to sediment texture and composition possibly due to dilution of this indicator by mixing/bioturbation and/or compaction of the event layer.

Without the use of high-resolution sampling and geochronological tools such as $^{234}Th_{xs}$ the depositional pulse would not have been detected in the sedimentary system. The continued use of these high-resolution methods allowed for further defining the magnitude of the sedimentary response to the DwH event as well as provide baseline sedimentation patterns at a monthly time scale. The annual time series defines the post-event evolution of the sedimentary system as well as the assessment of the post-depositional alterations that influence the integration and preservation of such sedimentation events in the sedimentary record. This includes the potential for re-mobilization of event sediments, potential re-exposure of ecosystems to contaminated sediments and redistribution of event sediments. Alternatively, burial and alteration of the sedimentary signature over time influences the preservation potential of sedimentation events such as DwH, with decreasing ability to detect events due to bioturbation, degradation of signature and compaction.

The refinement of methodology and approaches, in particular short-lived radioisotope (SLRad) geochronology, allowed for the high-resolution determination of the sedimentary impacts

of the DwH blowout event. In turn, the opportunity to investigate the DwH event in real time provided the opportunity to advance high-resolution methodologies in an applied fashion. Continued refinement of high-resolution approaches and methods, in particular geochronologies, will allow for the detection of short-duration and subtle sedimentary events in real time as well as in the sedimentary record. Through the application of such approaches and methods to real events, these methods can be further refined and assessed for their utility and limitations.

CHAPTER ONE:

INTRODUCTION

1.1 Introduction

Natural events, such as tropical cyclones, and anthropogenic events, such as oil spills/contamination, land use changes, etc. are common occurrences and can have significant influences on sedimentary processes and the benthic ecosystem. These include changes in sedimentation, chemical conditions and benthic habitat, as well as harmful exposure to contaminants and injury to benthic biology and the ecosystem. Such injury is often associated with anthropogenic events such as the Deepwater Horizon blowout (DwH) (White et al., 2012; Fisher et al., 2016; Murawski et al., 2016). Detection of these types of events and their potential impacts to the sedimentary system can be challenging depending on the magnitude of the sedimentary response(s) to an event, and its integration into the sedimentary record. Understanding the sedimentary response to an event, how it is manifested in the sedimentary system and the ability to detect them in the sedimentary record are fundamental to assessing impacts of event driven sedimentation. Sedimentary records of events combined with high-resolution age control can be investigated to determine the variability in timing and frequency of events in the past. For natural events, this can provide insight into the variety of factors controlling these events such as tropical cyclones. For anthropogenic events, it can link a specific anthropogenic activity (land use change, spill/contamination) to the sedimentary response and impacts. Accurate age control of sedimentary records to provide timing of events has been of critical importance particularly for

high-resolution climate records (Sadler, 1981; Jones et al., 2009) and in studies of anthropogenic events and their impact(s) on the environment. For events of short-duration (months), there is increased importance for high-resolution approaches and investigations to define impacts of events on sub-annual to decadal time scales pertinent to human populations and relevant to natural ecosystems.

The focus of this study is to refine and advance high-resolution geochronological approaches using short-lived radioisotopes (SLRad) and analytical methods for investigating the sedimentary response(s), integration and detection in the sedimentary record of the 2010 DwH blowout event in the northeastern Gulf of Mexico (NEGoM) deep sea. Applying these methods to a real-time study of the sedimentary response to the DwH event, and its evolution in the sedimentary system over the subsequent 6 years will 1) define the impacts of the DwH blowout on the benthic sedimentary system, and 2) refine the methods and approaches for detecting short-duration sedimentation events, including the strengths and limitations of such an approach. Investigating how the DwH event is manifested in the sedimentary record will improve the ability to detect and interpret event-scale features in the geologic record, as well as create a basis to characterize sedimentological, biological and chemical impacts from the DwH event that may not be detected in longer-term sedimentary records due to lack of analytical resolution and or preservation.

1.1.1 Event Stratigraphy

In the sedimentary system, events are defined by deviations from baseline or natural sedimentation patterns, but the detection of these deviations is often challenging. This is particularly true for events that produce subtle deviations in sedimentary response, are of short-duration, and/or occur in sedimentologic settings that are not conducive to strong manifestation

and/or preservation in the sedimentary record. Detection of events in the sedimentary record include defining a measurable sedimentary signature(s) of the event, and developing accurate age control to link events to the sedimentary signature(s) in the record. This is influenced by: 1) the sedimentary response, 2) preservation potential, and 3) influence of time on the detectability in the sedimentary record. The magnitude of the sedimentary response is often reflected by how it is different sedimentologically (i.e., signature), as well as timing and rates of sedimentation. Preservation potential can influence the detection of events by compromising the stratigraphic integrity due to mixing/bioturbation, erosion/re-mobilization of sediments, chemical/diagenetic degradation of the sedimentary signature, and/or compaction of the event layers. With increase in time (post-event) these factors that reduce the preservation potential, often lead to reduced ability to detect events and underestimation of the original magnitude of an event in the sedimentary system (Figure 1.1).

The development of high-resolution sampling and analytical techniques have considerably improved the ability to resolve small-scale (mm to cm) sedimentary records in aquatic settings. Advances in core sampling methods (Schwing et al., 2016) and core scanning methods (scanning X-ray Fluorescence (XRF), Laser ablation inductively coupled plasma mass spectroscopy (LA-ICPMS) smaller scale and more subtle deviations in sedimentology can be measured to identify the signature of short-term sedimentation events. The use of short-lived radioisotopes (SLRad) such as $^{210}Pb_{xs}$, $^{234}Th_{xs}$, ^{137}Cs, and ^{7}Be at high-sampling resolution, can provide high temporal resolution age control for multiple time-scales over the past ~100 years (Appleby, 2001; Holmes, 1998; Swarzenski, 2014). This is particularly useful for correlating sedimentary events with historical records as well as real-time investigations of sedimentary events (Alonso-Hernandez et al., 2006; Diaz-Asencio et al., 2011; Jones et al. 2009).

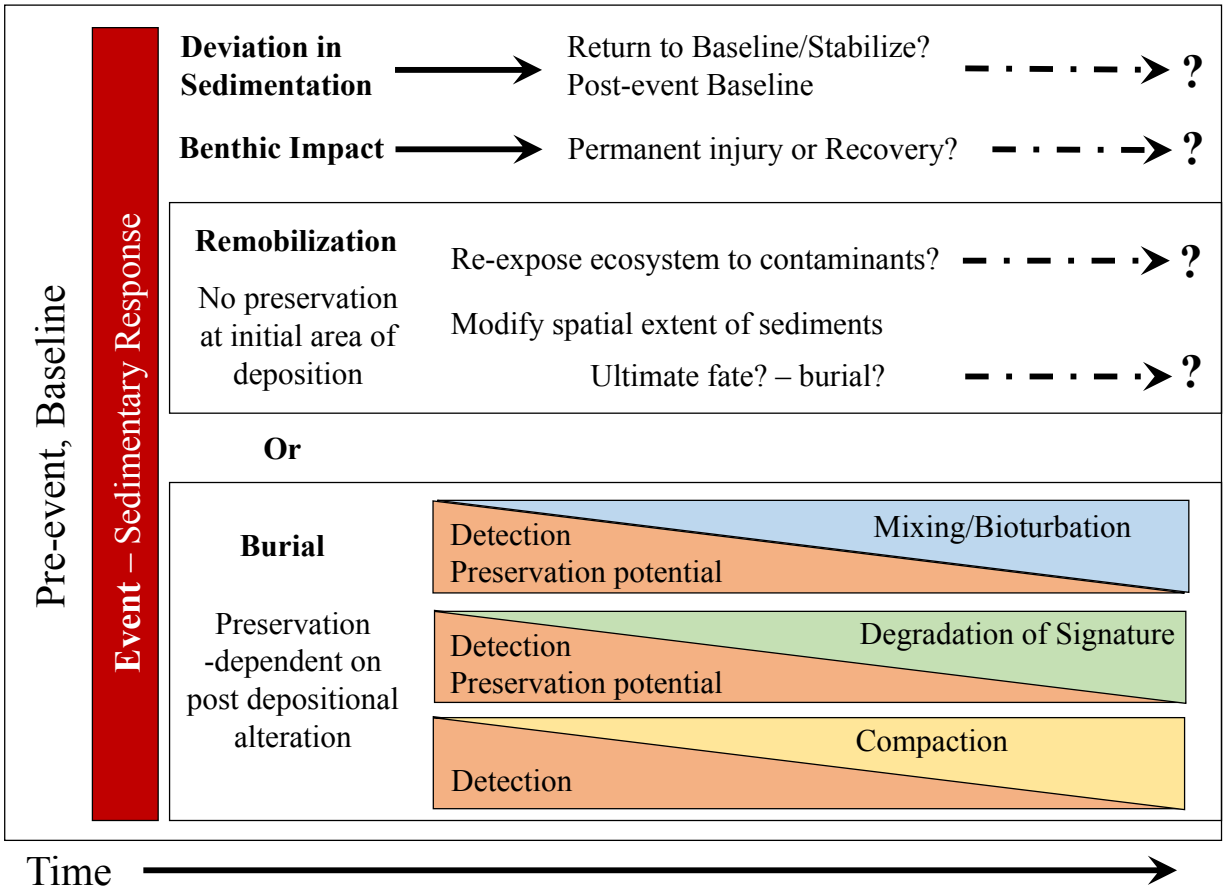

Figure 1.1. Conceptual diagram of the sedimentary response to events and how time influences different components with regards to detection and preservation in the sedimentary record. This includes pre-event (downcore) baselines, the sedimentary response, subsequent deviations in sedimentation and benthic impacts, as well as the duration of impacts. Detection and preservation in the sedimentary record as determined by remobilization vs burial and influence of time on post depositional alteration with respect to detection and preservation potential.

1.1.2 Deepwater Horizon Oil Spill

The April 2010, the 2010 DwH blowout in the northeastern Gulf of Mexico (NEGoM) led to the release of oil and gas at a water depth of ~1500 m for 87 days (McNutt et al., 2012; Passow and Hetland, 2016). From the seafloor, a rising plume formed with a subsurface plume (comprised of oil microdroplets and dissolved hydrocarbons) centered at ~1,000 m water depth (Camilli et al., 2010; Diercks et al., 2010; Joye et al., 2011), and an oil slick at the sea surface (Thibodeaux et al.,

2011) (Figure 1.2). Response strategies to stop the release of oil and mitigate impacts included addition of dispersants (Corexit) at the wellhead as well as at sea surface slicks (Yan et al., 2016), skimming and burning at the sea surface,, and the addition of drilling mud at the wellhead (Liu et al., 2018). The object of these response and mitigation strategies was to attempt to contain, remove, and influence the distribution, and degradation (biotic and abiotic) of released oil (US Coast Guard, 2010; BOEM, 2010).

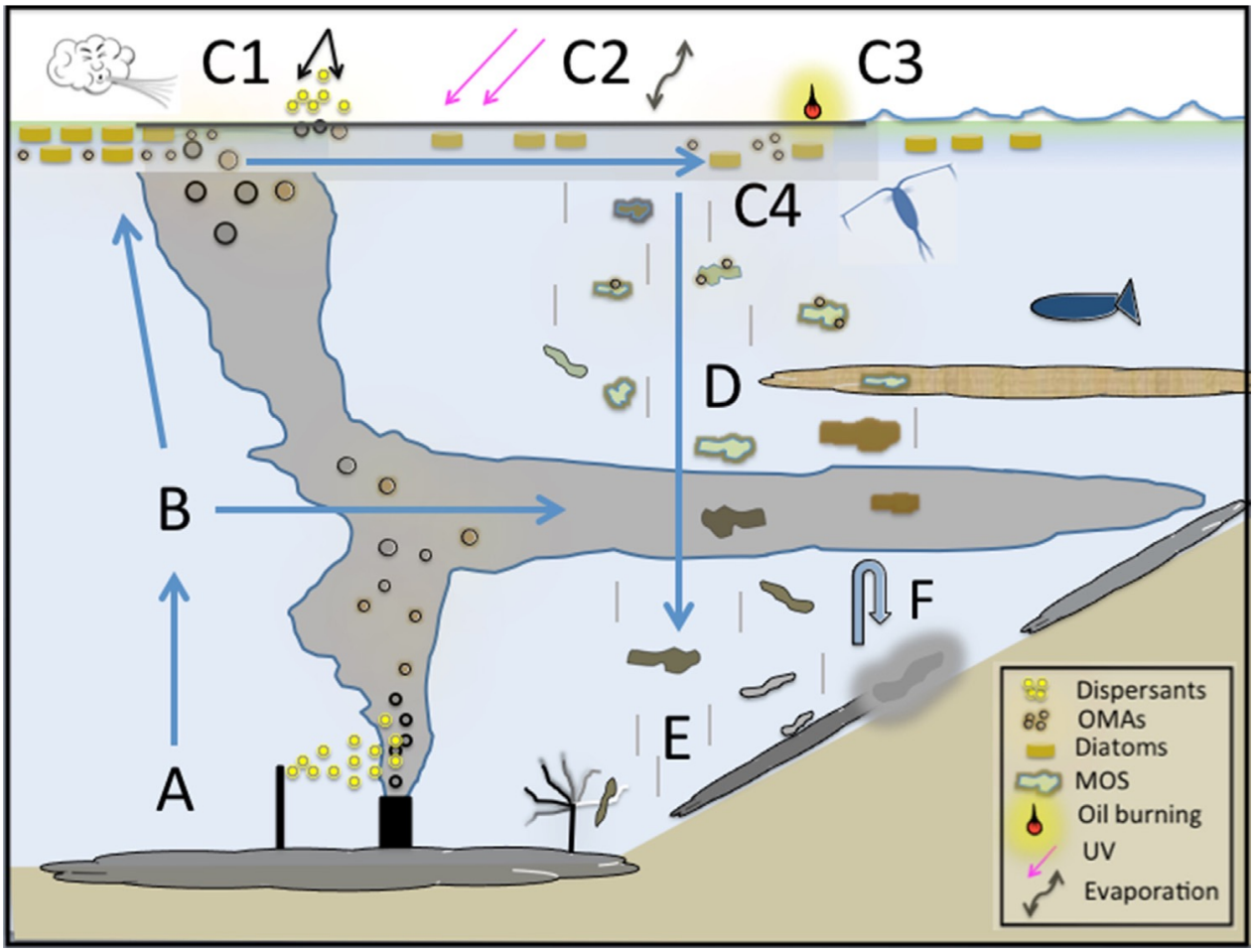

Figure 1.2. Conceptual diagram of components of the DwH oil spill, MOSSFA formation, and sedimentation to the deep-sea benthos including A) Wellhead, release of oil, B) Formation of rising plume of oil droplets and gas bubbles, C1-C4) Processes influences formation of marine oil snow at the sea surface with C4) representing processes influencing the sinking marine oil snow, D) sinking of marine oil snow, E) sedimentation of marine oil snow, F) resuspension and remobilization of sediment from seafloor (from Daly et al., 2016).

An observed Marine Oil Snow Sedimentation and Flocculent Accumulation (MOSSFA) event was the primary depositional mechanism of oil-contaminated sedimentation to the seafloor and consisted of surface oil interacting with biogenic, lithogenic particles, and exopolymeric substances that were released as a stress response from surface-dwelling organisms, resulting in a massive marine snow event (MOS) (Quigg et al, 2018; Daly et al., 2016; Passow, 2016; Ziervogel et al., 2012; Passow et al., 2012; Passow and Ziervogel, 2016). Aggregation of this marine oil snow, lea to a loss of buoyancy causing the rapid settling of MOS through the water column, stripping particles, and transporting them to the sea floor as MOSSFA (Passow et al., 2012; Brooks et al., 2015) (Figure 1.2).

The DwH blowout provided a unique opportunity to investigate, at very high-resolution, the sedimentary impacts of a singular event in real time including if/how sediment and oil-contaminated sediment reached the deep-sea benthos and how it was integrated into the sedimentary system. The MOSSFA event was detected in sediment cores collected in the fall of 2010 and early 2011, as a depositional pulse characterized by deviations in sediment texture and composition as well as increased sedimentation rates (Brooks et al., 2015). This included increased sediments indicative of sea surface origin including pyrogenic hydrocarbons from surface burning (Romero et al., 2015), increased planktic foraminifera accumulation rates (Fridrik et al., 2016), and chloroplast 16SRNA gene sequences (Brooks et al., 2015). A diagnostic feature was short-term (months) increases in sedimentation rate leading to a 10-20 mm thick blanket of oil contaminated sediment on the NEGoM seafloor (Brooks et al., 2015; Romero et al, 2015; Chanton et al., 2015). This depositional pulse impacted bottom-dwelling organisms such as benthic foraminifera, which were nearly absent (Schwing et al., 2015), shutdown/cessation of bioturbation in surface sediments (Brooks et al., 2015), and rapid upward shift in the redox boundary within

surficial sediments (Brooks et al., 2015; Hastings et al., 2016). The MOSSFA event was estimated to have affected broad areas of the continental slope and shelf, ranging from 1,030 to 35,425km^2 (Valentine et al., 2014; Chanton et al., 2015; Romero et al., 2015; Passow & Ziervogel, 2016; Romero et al., 2017; Schwing et al., 2017; Stout & German, 2017). It occurred in a region comprised of two sedimentary regimes. West of the DeSoto Canyon sediments are dominantly siliciclastic, associated with Mississippi River discharge and east of the DeSoto Canyon seafloor sediments are dominantly carbonate, associated with the west Florida Platform (Balsam and Beeson, 2003; Holmes, 1976; Harbison et al., 1968) (Figure 1.3).

The DwH event was of short duration (geologically), on the scale of months. Investigating the impacts of DwH on the benthos required a rapid response to determine the initial distribution patterns of oil-contaminated sediments and benthic impacts. Sediment studies continued over subsequent years to determine the potential redistribution of oil-contaminated sediments, the duration of benthic impacts and if/when the sedimentary system stabilized/recovered, and ultimate fate of oil-contaminated sediments. This also includes assessment of preservation potential in the sedimentary records as a funcionto of potential remobilization, as well burial rate with respect to bioturbation depth. Of equal importance were adaptive approaches and high-resolution methods to detect such a short-duration event, the continued evaluation of sedimentary processes at high-temporal resolution, and the determination of baseline (pre- and post-event) sedimentation patterns at the similar time scale (month).

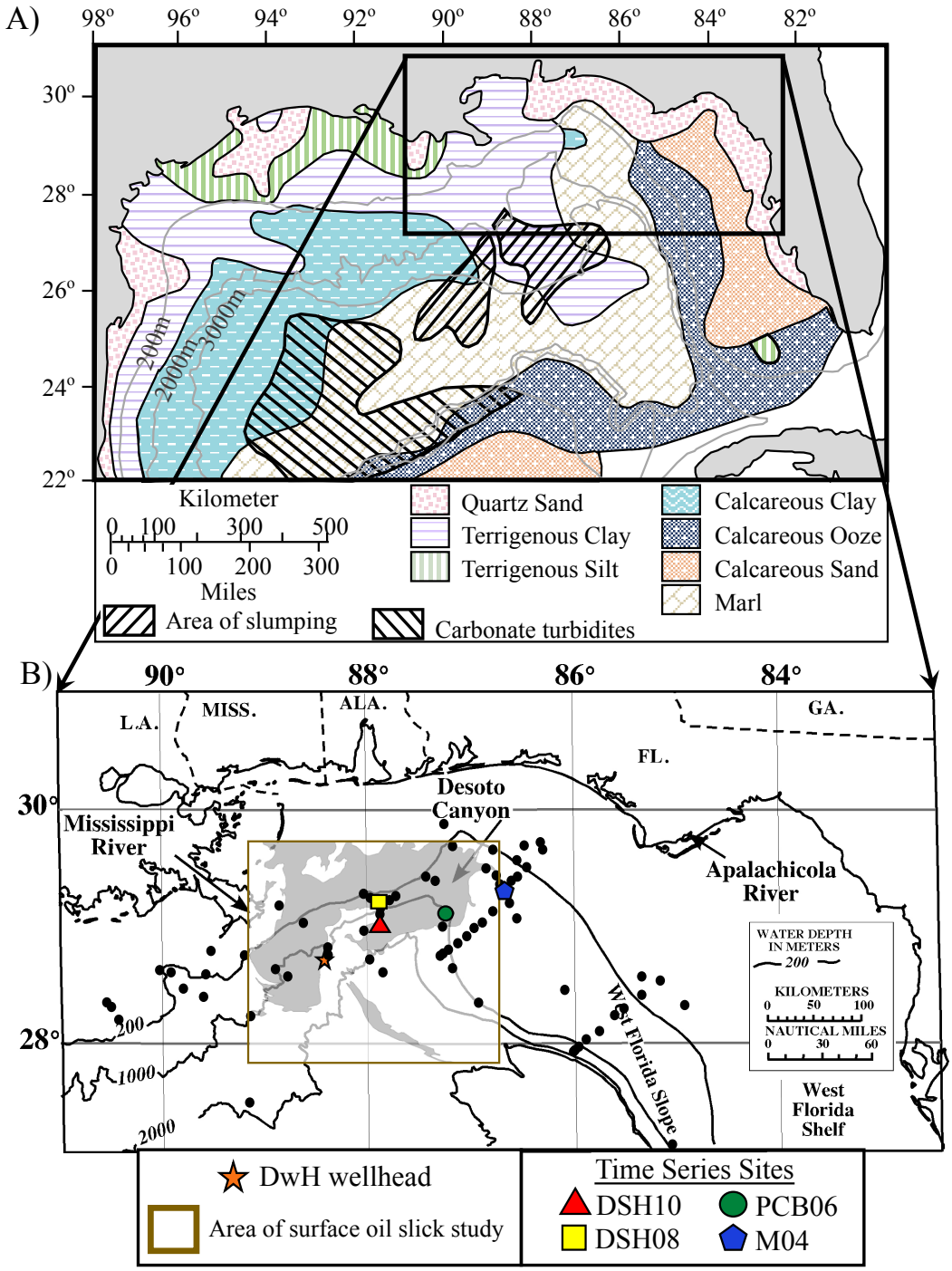

Figure 1.3. Maps of the Gulf of Mexico (GoM) showing the physiographic features: A) Map indicating the study area in the NEGoM with sedimentologic regions (modified from Brooks et al., 2018; Balsam and Beeson, 2003; Holmes, 1976), B) Map of NEGoM showing location of the DWH wellhead (orange star), surface sediment slick (gray shading in brown box, from Garcia-Pineda et al., 2013 and C-IMAGE sediment core locations (black circles) and time-series sites (DSH10 = red triangle, DSH08 = yellow square, PCB06 = green circle, and M04 = blue pentagon) (from Larson et al., 2018, Chapter 4).

1.2 Approach/Methods

1.2.1 Sediment Records – Cores

A total of 179 sediment cores were collected between 2010 and 2016 at 80 sites following the blowout event, ranging from ~100 m to >1500 m water depths to investigate the sedimentary impacts (Figure 1.3). Cores were collected using an Ocean Instruments MC-800 multicorer, whichsimultaneously collects eight sediment cores, up to ~60 cm in length, while maintaining the sediment-water interface. This ensures the preservation of the most recent sedimentation and sufficient core length to capture sediment accumulation over the past ~100 years to use for pre-DwH baseline sedimentation patterns. All cores were investigated for stratigraphic integrity to maximize the selection of cores with higher potential for continuous sedimentation and detection of the depositional pulse. This included visible stratigraphy (core photography and inspection), lack of mixing/bioturbation and lack of indications of re-mobilization/erosion.

1.2.1 Rapid Collection and Time Series

Cores were first collected immediately following the DwH blowout event, in 2010 and 2011, to determine if there were sedimentological impacts and to characterize the sedimentary signature of the event. This allowed for the use of time-sensitive indicators of the event that may degrade over time, as well as indicators for very short time scale (months) sedimentation. It also provided the opportunity to define the full magnitude of the benthic impacts that may not later be detectable in the sedimentary record. The continued collection of cores, in 2011 through 2016, as a time-series provided a temporal record to define the duration of benthic impacts, and how the sedimentary system evolved and stabilized over subsequent years. It also allowed for continued high-resolution analysis to determine baseline sedimentation patterns on the same time scale (months) as the DwH blowout for direct comparison. A time-series collection of cores in this field

of study is rare, and is unique in its ability to detect an event in the sedimentary record, determine the evolution of the event deposit over the subsequent years, and the potential burial and preservation of the DwH signature in the sedimentary system.

1.2.2 High-Resolution Sampling

The sub-sampling resolution of cores defines the temporal resolution of data, with coarser (cm-scale) sampling integrating larger periods of time as compared to finer sub-sampling (mm-scale). High temporal resolution is often desired for detection of short-duration events in the sedimentary system as it increases the potential detection of a single short-term event as well as increases the magnitude of the event signature. For this project, cores collected in the NEGoM high-resolution sub-sampling, at 2 mm and 5mm intervals, provided the highest temporal resolution possible for subsequent chronological and sedimentological analyses (Schwing et al., 2016). The 2 mm resolution sub-sampling in surficial sections was maintained downcore to obtain comparable baseline sedimentation prior to the DwH event.

1.2.3 Sedimentary Signature, Sedimentology

The sedimentary signature of events is diagnostic of the sedimentary response to an event and how it deviates from non-event sedimentation patterns. For the DwH blowout event, the sedimentological signature was investigated with respect to bulk sediment texture and composition (carbonate, organic matter, terrigenous) as well as organic and inorganic geochemical indicators and biological responses. Approaches to identify oil-contaminated sediments and to specifically isolate DwH oil-contamination, included petrocarbon signatures (Chanton et al., 2015), and molecular organic geochemical fingerprinting were utilized (Romero et al. 2018). These are also combined with shifts in redox geochemistry (Brooks et al., 2015; Hastings et al., 2018), and

biological indicators of oil-contaminated sedimentation as well as benthic impacts (benthic foraminifera and macrofauna) (Schwing et al., 2018; Montagna et al., 2018).

1.2.4 Age Control, Short-lived Radioisotopes

Defining the timing of sedimentation is critical to correlate the deviations in the sedimentary record with events. Therefore, the selection of the most appropriate geochronological tools for the time scale being investigated (months, years, decades, etc.) is of vital importance. The most commonly used chronometers for recent sediment records are short-lived radioisotopes including excess ^{234}Th ($^{234}Th_{xs}$), excess ^{210}Pb ($^{210}Pb_{xs}$), ^{137}Cs, and ^{7}Be (Swarzenski, 2014; Holmes, 1998; Appleby, 2001). The months to year time scale was the focus for investigating the sedimentological response to the DwH blowout event, with the primary tools being $^{234}Th_{xs}$ (months) and $^{210}Pb_{xs}$ (years, and baseline sedimentation to ~1900). Due to the differences in time scales between $^{234}Th_{xs}$ and $^{210}Pb_{xs}$ they are often not able to be directly compared and therefore when possible, the use of the same chronometer is advisable (Sadler, 1981). The rapid collection of cores, the continued time-series collection of cores, and high-resolution sampling allowed for the use of $^{234}Th_{xs}$ to determine sedimentation on monthly time-scales for the event, and in subsequent years. This chronometer is more appropriate for monthly timescales than $^{210}Pb_{xs}$, which was initially unable to detect the depositional pulse associated with the DwH blowout, but provides age control for pre-event downcore baselines, and detection of the sedimentation pulse in subsequent years (2012-2016). A consequence of high-resolution sampling is that often there are small amounts of sediment for analyses, which requires assessment and refinement of methods to produce quality data. This includes assessment of analytical methods as well as interpretations for age control for sediment records.

1.3 Detecting Short Time-scale Events in the Sedimentary System: Advances of this Dissertation

The objectives of this dissertation are twofold: 1) the investigation of the sedimentological impacts of the DwH blowout event in the deep-sea benthos, and 2) refining and advancing the methods and approaches for high-resolution investigations of events in the sedimentary system and sedimentary records. Each component was critical for the success of the other. Without the refinement of methodology and approaches in particular geochronological tools, much of the characterization of the DwH event in the deep-sea benthos would not have been possible. Refining methods and approaches is often an iterative process, and were advanced here through the application to the real-time investigation of the sedimentary impacts of the DwH blowout. The advancement of short-lived radioisotope geochronology for determining age control and sedimentation rates is a major focus of this study, with the development of analytical methods, interpretations, and application to event stratigraphy, and was critical for age correlation of the sedimentary signature of the DwH depositional pulse.

1.4 Chapter Summaries

Chapters 3 is presented in Appendix A and Chapter 4 is presented in Appendix B and have been published. Supplemental tables and figures for Chapter 2 are preseted in Appendix C and for Chapter 3 in Appendx D. Appedicies E-K include the supportive figures and tables of the data utiliesd in this dissertation.

1.4.1 Chapter 2: Refining Short-lived Radioisotope Geochronology Analysis and Application to High-resolution Sediment Records

In Chapter 2, short-lived radioisotope (SLRad) analysis and interpretation methods using two calibration standards are evaluated, and applied, to two sediment cores from the Gulf of

Mexico to determine the robustness of results and age determinations. Analyses focused on small sample masses (<10g), which are often a product of high-resolution sampling of sedimentary records to obtain high temporal resolution age control. The objective of this chapter is to evaluate and refine geochronological analyses, interpretations, and application to sedimentary records to improve the temporal resolution and confidence in geochronologies produced from these SLRad.

1.4.2 Chapter 3: High-Resolution Investigation of Event Driven Sedimentation: Northeastern Gulf of Mexico

In Chapter 3, (presented in Appendix A) the high-resolution methods and approach used to identify the sedimentary response to the DwH event are continued to assess the of the post-DwH sedimentary system. This chapter builds on the Brooks et al. 2015 publication by further assessing the high-resolution approaches used to define the depositional pulse, and the continued high-resolution sampling and analyses to determine the post-DwH evolution and stabilization of the sedimentary system.

1.4.3 Chapter 4: Characterization of the Sedimentation Associated with the *Deepwater Horizon* Blowout: Depositional Pulse, Initial Response, and Stabilization

In Chapter 4, (presented in Appendix B) a synthesis of the DwH sedimentary response and evolution from a sedimentary perspective are described as well as assessment of the utility of the high-resolution approach used in this study. This includes evaluating the utility and comparisons of SLRad at different time scales to identify event driven sedimentation. Factors that may influence the modification of the sedimentary signature of event, its detection and preservation potential are discussed including burial, bioturbation, degradation of the pulse signature, and re-mobilization of pulse sediments.

1.5 Literature Cited

Alonso-Hernandez, C.M., Diaz-Asencio, M., Munoz-Caravaca, A., Delfanti, R., Papucci, C., Ferretti, O., Crovato, C., 2006, Recent Changes in Sedimentation Regime in Cienfuegos Bay, Cuba, as Inferred from ^{210}Pb and ^{137}Cs Vertical Profiles, Continental Shelf Research, vol. 26, pg. 153-167, doi:10.1016/j.csr.2005.08.026

Appleby, P.G., 2001, Chronostratigraphic Techniques in Recent Sediments, Ch 9 In: Tracking Environmental Change Using Lake Sediments Volume 1, Ed. Last, W.M., Smol, J.P., Kluwer Academic Publishers, The Netherlands, Holmes, C.W., 1998, Short-lived Isotopic Chronometers – A Means of Measuring Decadal Sedimentary Dynamics, U.S. Geological Survey, Dept. of the Interior, Fact Sheet FS-073-98.

Balsam W.L., Beeson J.P., 2003, Sea-floor Sediment Distribution in the Gulf of Mexico, Deep Sea Res Part I: Oceanographic Research Papers, vol. 50, pg. 1421-1444.

BOEM, 2011, Report Regarding the Causes of the April 20, 2010 Macondo Well Blowout, https://www.bsee.gov/sites/bsee.gov/files/reports/blowout-prevention/DWHfinaldoi-volumeii.pdf

Brooks, G. R., Larson, R. A., Schwing, P. T., Romero, I., Moore, C., Reichart, G.-J., Jilbert, T., Chanton, J. P., Hastings, D. W., Overholt, W. A., Marks, K.P., Kostka, J.E., Holmes, C.W., Hollander, D., 2015, Sedimentation Pulse in the NE Gulf of Mexico Following the 2010 DWH Blowout, PLOSone, vol. 10 (7), e0132341.

Brooks GR, Larson RA, Schwing PT, Diercks AR, Armenteros-Almanza M, Diaz-Asencio M, Martinez-Suarez A, Sánchez-Cabeza JA, Ruiz-Fernandez AC, Herguera Garcia JC, Perez-Bernal LH, Hollander DJ (2020) Gulf of Mexico (GoM) bottom sediments and depositional processes: A baseline for future oil spills (Chap. 5). In: Murawski SA, Ainsworth C, Gilbert S, Hollander D, Paris CB, Schlüter M, Wetzel D (eds) Scenarios and Responses to Future Deep Oil Spills – Fighting the Next War. Springer, Cham

Camilli, R., Reddy, C.M., Yoerger, D.R., Van Mooy, B.A.S., Jakuba, M.V., Kinsey, J.C., McIntyre, C.P., Sylva, S.P., Maloney, J.V., 2010, Tracking Hydrocarbon Plume Transport and Biodegradation at Deepwater Horizon, Scienc, vol. 330(8), pg. 201-204.

Chanton J., Zhao T., Rosenheim B.E., Joye S., Bosman S., Bruner C., Yeager K.M., Diercks A.R., Hollander D., 2015, Using Natural Abundance Radiocarbon to Trace the Flux of Petrocarbon to the Seafloor Following the Deepwater Horizon Oil Spill. Environmental Science and Technology, vol. 49(2), pg. 847–854 http://doi.org/10.1021/es5046524

Daly K.L., Passow U., Chanton J., Hollander D.J., 2016, Assessing the impacts of oil-associated marine snow formation and sedimentation during and after the Deepwater Horizon oil spill, Anthropocene, vol. 13, pg. 18–33 https://doi.org/10.1016/j.ancene.2016.01.006

Diaz-Asencio, M., Corcho Alvarado, J.A., Alonso-Hernandez, C., Quijedo-Cabezas, A., Ruiz-Fernanadez, A.C., Sanchez-Sanchez, M., Gomez-Mancebo, M.B., Froidevaux, P., Sanchez-Cabeza, J.A., 2011, Reconstruction of Metal Pollution and Recent Sedimentation Processes in Havana Bay (Cuba): A Tool for Coastal Ecosystem Management, Journal of Hazardous Materials, vol. 196, pg. 402-411.

Diercks A.R., Highsmith R.C., Asper V.L., Joung D., Zhou Z., Guo L., Shiller A.M., Joye S.B., Teske A.P., Guinasso Jr N.L., Wade T.L., Lohrenz S.E., 2010, Characterization of Subsurface Polycyclic Aromatic Hydrocarbons at the Deepwater Horizon Site, Geophysical Research Letters, vol. 37, L20602, DOI: 10.1029/2010GL045046

Fisher, C.R., Montagna, P.A., Sutton, T.T., 2016, How Did the Deepwater Horizon Oil Spill Impact Deep-Sea Ecosystems?, Oceanography, vol. 29(3), pg. 192-195.

Fridrik, E.E., Schwing, P.T., Ramirez, H., Larson, R.A., Brooks, G.R., O'Malley, B.J., Hollander, D.J., 2016, Comparative Records of Planktic Foraminiferal Mass Accumulation Rates Following the DwH and IXTOC Events, In Proceedings of the Gulf of Mexico Oil Spill and Ecosystem Science Conference; Tampa, FL.

Garcia-Pineda O., MacDonald I., Hu C., Svejkovsky J., Hess M., Dukhovskoy D., Morey S.L., 2013, Detection of Floating Oil Anomalies from the Deepwater Horizon Oil Spill with Synthetic Aperture Radar, Oceanography, vol. 26, pg. 124–137.

Harbison R.N., 1968, Geology of DeSoto Canyon. Journal of Geophysical Research, vol. 73, pg. 5175-5185.

Hastings, D.W., Schwing, P.T., Brooks, G.R., Larson, R.A., Morford, J.L., Roeder, T., Quinn, K.A., Bartlett, T., Romero, I.C., Hollander, D.J., 2016, Changes in Sediment Redox Conditions Following the BP DwH Blowout Event, Deep Sea Res. Part II Topical Studies in Oceanography, vol. 129, pg. 167–178.

Hastings DW, Bartlett R, Brooks R, Larson RA, Quinn KA, Razionale D, Schwing PT, Pérez Bernal LH, Ruiz-Fernández AC, Sánchez-Cabeza JA, Hollander DJ (2020) Changes in redox conditions of surface sediments following the BP Deepwater horizon and Ixtoc 1 events (Chap. 16). In: Murawski SA, Ainsworth C, Gilbert S, Hollander D, Paris CB, Schlüter M, Wetzel D (eds) Deep oil spills – facts, fate and effects. Springer, Cham

Holmes C.W., 1998, Short-lived Isotopic Chronometers – A Means of Measuring Decadal Sedimentary Dynamics, U.S. Geological Survey, Dept. of the Interior, Fact Sheet FS-073-98.

Holmes C.W., 1976, Distribution, Regional Variation, and Geochemical Coherence of Selected Elements in the Sediments of the Central Gulf of Mexico, Geological Survey Professional Paper 928, Washington, D.C., US Government Printing Office.

Jones, P.D.; Briffa, K.R., Osborn, T.J., Lough, J.M., Van Ommen, T.D., Vinther, B.M., Luterbacher, J., Wahl, E.R., Zwiers, F.W., Mann, M.E., Schmidt, G.A., Ammann, C.M., Buckley, B.M., Cobb, K.M., Esper, J., Goosse, H., Graham, N., Jansen, E., Kiefer, T., Kull, C., Küttel, M., Mosley-Thompson, E., Overpeck, J.T., Riedwyl, N., Schulz, M., Tudhope, A.W., Villablba, R., Wanner, H., Wolff, E., Xoplaki, E., 2009, High-Resolution Palaeoclimatology of the Last Millennium: A Review of Current Status and Future Prospects, The Holocene, vol. 19 (1), pg. 3–49.

Joye S.B., MacDonald L.R., Leifer I., Asper V., 2011, Magnitude and Oxidation Potential of Hydrocarbon Gases Released from the BP Oil Well Blowout, Nature Geosciences, vol. 4, pg.160-164.

Larson, R.A., Brooks, G.R., Schwing, P.T., Diercks, A.R., Holmes, C.W., Chanton, J., Diaz-Asencio, M., Hollander, D.J., 2019, Characterization of the Sedimentation Associated with the Deepwater Horizon Blowout: Depositional Pulse, Initial Response, and Stabilization (Chap. 14). In: Murawski SA, Ainsworth C, Gilbert S, Hollander D, Paris CB, Schlüter M, Wetzel D (eds) Deep oil spills – facts, fate and effects. Springer, Cham

Liu G., Bracco A., Passow U., 2018, The Influence of Mesoscale and Submesoscale Circulation on Sinking Particles in the Northern Gulf of Mexico, Elementa: Science of the Anthropocene, vol. 6(1), pg. 1-16. DOI: http://doi.org/10.1525/elementa.292

McNutt, M.K., Camilli,R., Crone, T.J., Cuthrie, G.D., Hsieh, P.A., Ryerson, T.B., Savas, O., Shaffer, F., 2012, Review of Flow Rate Estimates of the Deepwater Horizon Oil Spill, PNAS, vol. 109(50) 20260-20267, https://doi.org/ 10.1073/pnas.1112139108

Montagna P.A., Girard F., 2018, Deep-sea Benthic Faunal Impacts and Community Evolution Before, During and After the Deepwater Horizon Event, In: Murawski S.A., Ainsworth C., Gilbert S., Hollander D., Paris C.B., Schlüter M., Wetzel D. (Eds.), Deep Oil Spills – Facts, Fate and Effects. Springer xxx, pp: xx-xx,

Murawski, S.A., Fleeger, J.W., Patterson, W.F., Chuanmin, H., Daly, K., Romero, I., Toro-Farmer, A., 2016, How Did the Oil Spill Affect Coastal and Continental Deepwater Horizon Shelf Ecosystems of the Gulf of Mexico?, Oceanography, vol. 29(3), pg. 160-172, doi: 10.2307/24862718

Passow U., 2016, Formation of Rapidly-Sinking, Oil-Associated Marine Snow, Deep Sea Research Part II: Topical Studies in Oceanography, The Gulf of Mexico Ecosystem - before, during and after the Macondo Blowout, vol. 129, pg. 232–240 https://doi.org/10.1016/j.dsr2.2014.10.001

Passow U., Ziervogel K., Asper V.L., Diercks A.R., 2012, Marine Snow Formation in the Aftermath of the Deepwater Horizon Oil Spill in the Gulf of Mexico, Environmental Research Letters, vol. 7, 035301. DOI: 10.1088/1748-9326/7/3/035301

Passow U., Hetland R., 2016, What Happened to All of the Oil?, Oceanography, vol. 29, pg. 88–95, https://doi.org/10.5670/oceanog.2016.73

Passow, U., Ziervogel, K., 2016, Marine Snow Sedimented Oil Released during the Deepwater Horizon Spill, Oceanography, vol. 29 (3), pg. 118–125.

Quigg A, Passow U, Hollander DJ, Daly KL, Burd A, Lee K (2020) Formation and sinking of MOSSFA (Marine Oil Snow Sedimentation and Flocculent Accumulation) Events: Past and present (Chap. 12). In: Murawski SA, Ainsworth C, Gilbert S, Hollander D, Paris CB, Schlüter M, Wetzel D (eds) Deep oil spills – facts, fate and effects. Springer, Cham

Romero I.C., Schwing P.T., Brooks G.R., Larson R.A., Hastings D.W., Ellis G.E., Goddard E.A., Hollander D.J., 2015, Hydrocarbons in Deep-Sea Sediments Following the 2010 Deepwater Horizon Blowout in the Northeast Gulf of Mexico, PLOSone, vol. 10(5), e0128371.

Romero I.C., Toro-Farmer G., Diercks A.R., Schwing P.T., Muller-Karger F., Murawski S., Hollander D.J., 2017, Large Scale Deposition of Weathered Oil in the Gulf of Mexico Following a Deepwater Oil Spill, Environmental Pollution, vol. 228, pg. 179-189 http://dx.doi.org/10.1016/j.envpol.2017.05.019.

Romero IC, Chanton JP, Rosenheim BE, Radović J, Schwing PT, Hollander DJ, Larter SR, Oldenburg TBP (202020) Long-term preservation of oil spill events in sediments: the case for the Deepwater Horizon Spill in the Northern Gulf of Mexico (Chap. 17). In: Murawski SA, Ainsworth C, Gilbert S, Hollander D, Paris CB, Schlüter M, Wetzel D (eds) Deep oil spills – facts, fate and effects. Springer, Cham.

Sadler P., 1981, Sedimentation Rates and the Completeness of Stratigraphic Sections, Journal of Geology, vo. 89, pg. 569–584

Schwing, P.T., Romero, I.C., Brooks, G.R., Hastings, D.W., Larson, R.A., Hollander, D.J., 2015, A Decline in Deep-Sea Benthic Foraminifera Following the Deepwater Horizon Event in the Northeastern Gulf of Mexico, PLOSone, vol. 10 (3), pg. 1–14.

Schwing, P.T., Romero, I.C., Larson, R.A., O'Malley, B.J., Fridrik, E.E., Goddard, E.A., Brooks, G.R.; Hastings, D.W.; Rosenheim, B.E., Hollander, D.J., Grant, G., Mulhollan, J., 2016 Sediment Core Extrusion Method at Millimeter Resolution Using a Calibrated Threaded-Rod, Journal of Visualized Experiments: JoVE, vol. 114, doi: 10.3791/54363.

Schwing P.T., Brooks G.R., Larson R.A., Holmes C.W., O'Malley B.J., Hollander D.J., 2017, Constraining the Spatial Extent of the Marine Oil Snow Sedimentation and Accumulation (MOSSFA) Following the DWH Event Using a $^{210}Pb_{xs}$ Inventory Approach, Environmental Science & Technology, vol. 51, pg. 5962−5968. DOI: 10.1021/acs.est.7b00450

Schwing PT, Machain Castillo ML (2020) Impact and resilience of benthic foraminifera in the aftermath of the Deepwater Horizon and Ixtoc 1 oil spills (Chap. 23). In: Murawski SA, Ainsworth C, Gilbert S, Hollander D, Paris CB, Schlüter M, Wetzel D (eds) Deep oil spills – facts, fate and effects. Springer, Cham.

Stout, S.A., German, C.R., 2017, Characterization and Flux of Marine Oil Snow Settling Toward the Sea Floor in the Northern Gulf of Mexico During the Deepwater Horizon Incident : Evidence for Input from Surface Oil and Impact on Shallow Shelf Sediments, Marine Pollution Bulletin, vol. 129, pg. 695-713.

Swarzenski, P.W., 2014, ^{210}Pb Dating, In: Encyclopedia of Scientific Dating Methods, Springer Science and Business Media, Dordrecht, doi: 10.1007/978-94-007-6326-5_236-1.

Thibodeaux, L.J., Valsaraj, K.T., John V.J., Papadopoulos K.D., Pratt L.R., Pesika N.S., 2011, Marine Oil Fate: Knowledge Gaps, Basic Research, and Development Needs: A Perspective Based on the Deepwater Horizon Spill, Environmental Engineering Science, vol. 28(2) pg. 87-93, doi: 10.1089/eex.2010.0276

US Coast Guard, 2010, Report of Investigation into the Circumstances Surrounding the Explosion, Fire, Sinking and Loss of Eleven Crew Members Aboard the Mobile Offshore Drilling Unit Deepwater Horizon in the Gulf of Mexico April 20-22, 2010. Volume I MISLE Activity Number: 3721503. https://www.bsee.gov/newsroom/library/deepwater-horizon-reading-room/joint-investigation-team-report

White, J., Hsing, P.Y., Cho, W., Shank, T.M., Cordes, E.E., Quattrini, A.M., Nelson, R.K., Camilli, R., Demopoulos, A.W.J., German, C.R., Brooks, J.M., Roberts, H.H., Shedd, W., Reddy, C.M., Risher, C.R., 2012, Impact of the Deepwater Horison Oil Spill on a Deep-water Coral Community in the Gulf of Mexico, PNAS, vol. 109(50), 20303-20308, https://doi.org/ 10.1073/pnas.1118029109

Yan B., Passow U., Chanton J.P., Nöthig E.M., Asper V., Sweet J., Pitiranggon M., Diercks A.R., Pak D., 2016, Sustained Deposition of Contaminants from the Deepwater Horizon Spill. PNAS, vol. 113, 24E3332-E3340. DOI: 10.1073/pnas.1513156113

Valentine, D.L., Fisher, G.B., Bagby, S.C., Nelson, R.K., Reddy, C.M., Sylva, S.P., 2014, Fallout Plume of Submerged Oil from Deepwater Horizon, PNAS, vol. 111(45), pg. 15906-15911, doi.org/10.1073/pnas.1414873111.

Ziervogel K., McKay L., Rhodes B., Osburn C.L., Dickson-Brown J., Arnosti C., Teske A., 2012, Microbial Activities and Dissolved Organic Matter Dynamics in Oil-Contaminated Surface Seawater from the Deepwater Horizon Oil Spill Site, PLOSOne, vol. 7(4), e34816.

CHAPTER TWO:

REFINING SHORT-LIVED RADIOISOTOPE GEOCHRONOLOGY ANALYSIS AND APPLICATION TO HIGH-RESOLUTION SEDIMENT RECORDS.

Abstract

In this study, short-lived radioisotope (SLRad) analysis and interpretation methods using two calibration standards are evaluated, and applied to two sediment cores from the Gulf of Mexico to determine the robustness of results and age determinations. Analyses focused on small sample masses (<10g), which are often a product of high-resolution sampling of sedimentary records to obtain high temporal resolution age control. Calibrations to convert analyzed data (counts/minute/gram) to activity (disintegrations/minute/gram) were developed using standards IAEA RGU-1 and IAEA-447 for commonly used SLRad, total ^{210}Pb, and supported ^{210}Pb (determined using ^{214}Pb and ^{214}Bi activities) to calculate excess ^{210}Pb for age dating over the past ~100 years, as well as ^{234}Th, and ^{137}Cs. Over a range of analyzed masses (1g-50g), the IAEA RGU-1 and IAEA-447 calibration lines were substantially different, particularly at the small and large analyzed masses. When applied to sediment cores collected from the Gulf of Mexico, the IAEA RGU-1 calibration overestimated all SLRad activities for samples less than 10 g. The IAEA-447 standard has a similar composition to sediment core samples and thus calibrations produced using this standard yielded more accurate activities for all SLRad. This difference (IAEA RGU-1 calibrations vs IAEA-447 calibrations) in activities led to variability in age model results and potential misinterpretation of sedimentary processes. The IAEA-447 calibration also

yielded accurate calibration for ^{137}Cs when compared to a ^{137}Cs standard, IAEA-375. The selection of the most appropriate SLRad calibration standard is critical for application to sedimentary records. The advantage of this approach is the ease of application as these calibrations also account for self-absorption and changes in sample geometry (height/mass).

2.1 Introduction

Natural and anthropogenic events play significant roles in sedimentary processes on various spatial and temporal scales. These events lead to sedimentary deposits that record the event itself and/or the potential impacts of the event. It has become increasingly important to investigate these types of records at higher temporal resolution to understand variability on annual to decadal time scales pertinent to human populations and natural ecosystems. When event-scale deposits are preserved in the sedimentary record they can be investigated with respect to timing, variability, and connections/linkages to larger scale processes (natural and/or anthropogenic). The challenge with these types of records is the ability to resolve small (mm to cm) scale changes in the sedimentary record, as well as developing high-resolution age control. In a review of the results of the 2006 PAGES/CLIVAR Intersection Panel meeting, a working group of the Intergovernmental Panel on Climate Change, Jones et al. (2009) stated that accuracy of absolute dating is of critical importance for utilizing high-resolution proxies for climate records.

The ability to resolve small-scale (mm to cm) sedimentary records has been improved with advances in core sampling (Schwing et al., 2016) and core scanning methods (scanning X-ray Fluorescence (XRF), Laser ablation inductively coupled plasma mass spectroscopy). The use of short-lived radioisotopes (^{210}Pb, ^{137}Cs, etc.), to provide age control over the past ~120 years, makes it possible to directly correlate sediment records of events to instrumental/historical data (Alonso-Hernandez et al., 2006; Diaz-Asencio, et al., 2011; Jones, et al. 2009). Further refinement of age

dating methods is required in order to resolve sub-annual, annual and decadal-scale depositional processes by increasing accuracy and confidence in age models developed from high-resolution sediment records.

This study focuses on refining techniques to increase the temporal resolution and accuracy of results and chronologies produced from short-lived radioisotope (SLRad) analysis of sediment cores by gamma spectroscopy. A consequence of increased temporal resolution is often finer sampling resolution, which result in small (often < 10g) sediment sample masses. Two cores collected in the Gulf of Mexico (GoM), and sub-sampled at 2mm resolution, are discussed here with respect to the influence of small sediment sample mass on SLRad sample analysis, data processing, and interpretation (Appendix C, Figure C.1).

2.1.1 SLRad in the Sedimentary System.

The integration of SLRad into the sedimentary record is controlled by the sources, distribution patterns, and depositional mechanisms of SLRad (Figure 2.1). SLRad readily attach to particles (i.e. sediments) and are transported, deposited, and eventually accumulate with the sediments (Appleby, 2001). The most commonly used SLRad for age dating over the past ~120 years include ^{210}Pb, ^{137}Cs, ^{234}Th, and ^{7}Be (not discussed in this study), which can all be measured by gamma spectroscopy. Age dating for sedimentary records using SLRad is made possible by understanding their properties (chemistry, half-life, sources, change in activity only due to radioactive decay, and ease of measurement), and how they are incorporated into the sedimentary record (Holmes, 1998; Appleby, 2001; Swarzenski, 2014).

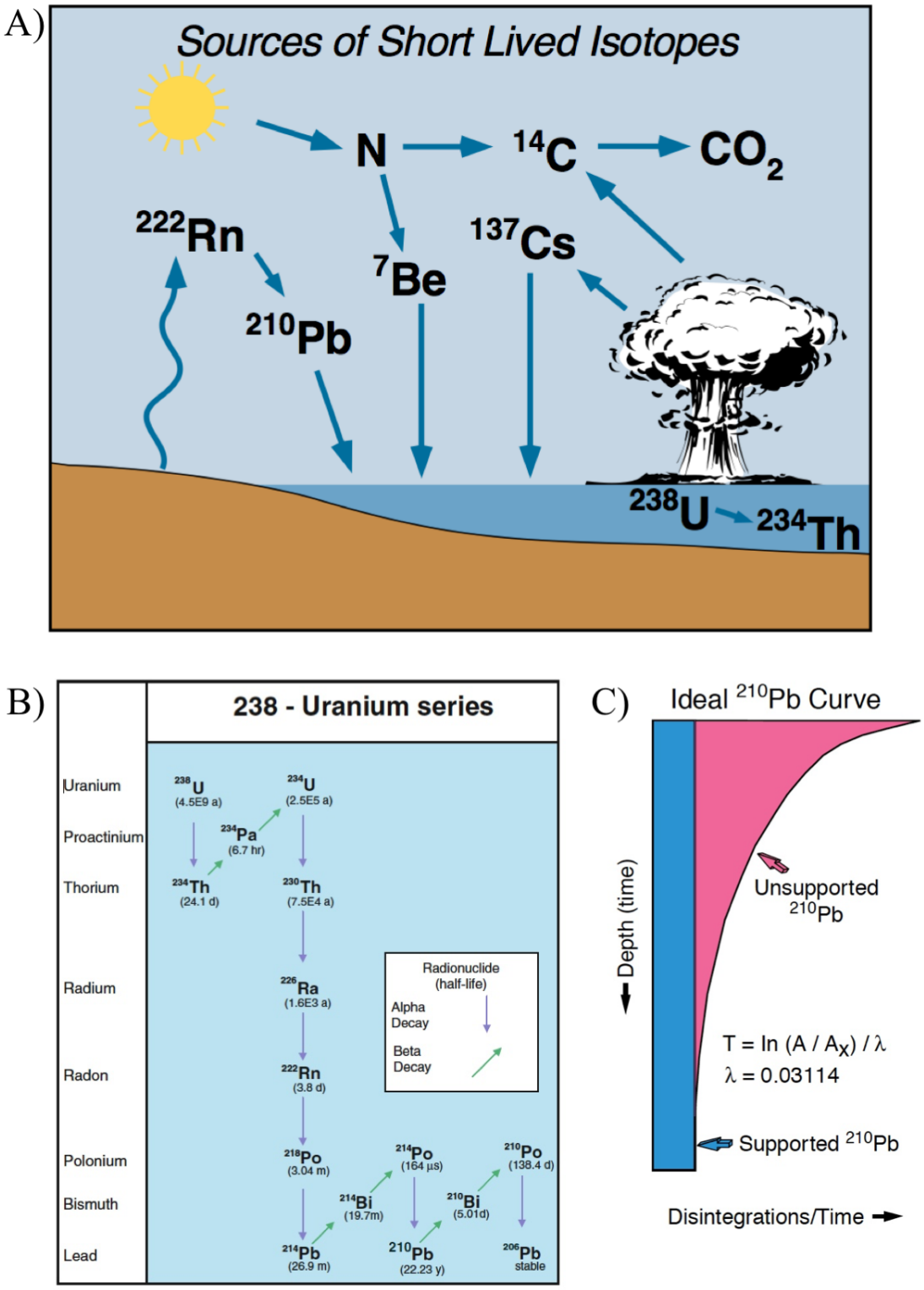

Figure 2.1. A) Diagram of sources of SLRad in the environment and pathways to the sedimentary system (from Holmes, 1998). B) Diagram of ^{238}U decay series showing daughter products of ^{234}Th, ^{226}Ra, ^{222}Rn (gaseous), ^{214}Pb, ^{214}Bi, and ^{210}Pb (from Swarzenski, 2014). C) Diagram of idealized ^{210}Pb curve indicating supported ^{210}Pb ($^{210}Pb_{Sup}$) and unsupported ^{210}Pb ($^{210}Pb_{xs}$) used for age dating sediment cores (from Holmes, 1998).

Sources of these SLRad include anthropogenic thermonuclear byproducts (^{137}Cs), spallation in the upper atmosphere (^{7}Be), and the natural ^{238}U decay series (^{234}Th, ^{210}Pb) within continental rocks and ocean waters (Figure 2.1) (Holmes, 1998; Swarzenski, 2014; Winkler and Rosner, 2000). The ^{238}U decay series (Figure 2.1) produces a sequence of SLRad and when in a closed system (i.e. no loss in the decay series) all SLRad in the series are of equal concentration/activity, referred to as secular equilibrium (Appleby and Oldfield, 1983). Disequilibrium can occur in the series with respect to ^{234}Th and ^{210}Pb, which leads to higher activities of ^{234}Th and ^{210}Pb in sediments than the ^{238}U supported daughter products. This excess ^{234}Th ($^{234}Th_{xs}$) and excess ^{210}Pb ($^{210}Pb_{xs}$) decays according to properties of each radioisotope, and provides the opportunity to use $^{234}Th_{xs}$ and $^{210}Pb_{xs}$ as chronometers (Appleby, 2001). $^{210}Pb_{xs}$ is produced by the gaseous release of ^{222}Rn to the atmosphere and oceanic waters (i.e. loss in the ^{238}U decay series) and subsequent decay to ^{210}Pb, which attaches to particles in the atmosphere and/or water column and is eventually deposited on the seafloor. $^{210}Pb_{xs}$, with a 22.3 yr. half-life, is useful for dating the past ~120 years (Chisté and Bé, 2007a; Appleby, 2001) (Table 2.1).

To determine $^{210}Pb_{xs}$, the supported ^{210}Pb ($^{210}Pb_{Sup}$) is subtracted from the measured total ^{210}Pb ($^{210}Pb_{Tot}$). ^{226}Ra represents the supported in situ radioisotope production from sediment (i.e. $^{210}Pb_{Sup}$) as it is prior to the decay to ^{222}Rn (gaseous). Even though ^{226}Ra can be measured directly by gamma emission spectroscopy at the 186keV energy, but there is potential interference at this energy as ^{235}U also produces gamma emissions with 186 keV energy. Due to secular equilibrium, ^{214}Pb and ^{214}Bi radioisotopes have the same activity as ^{226}Ra (i.e. $^{210}Pb_{Sup}$) and can be measured by gamma emission spectroscopy. Therefore, ^{214}Pb at 295keV, ^{214}Pb at 351keV and ^{214}Bi are commonly used to estimate $^{210}Pb_{Sup}$ (Baskaran, et al. 2014, MacKenzie, et al., 2011, Smith et al., 2002).

Table 2.1. Short-lived Radioisotope (SLRad) characteristics used for gamma spectroscopy analysis and activities (dpm/g) of standards IAEA RGU-1 (no reference date, in secular equilibrium), IAEA-447 (decay correction reference date 11/15/09) and IAEA-375 (decay correction reference date 12/31/91) (Chisté, et al., 2007a, Chisté, et al., 2007b, Chisté, et al., 2010, Steger, 1987; IAEA, 2012; Strachnov et al., 1996).

Radioisotope (SLRad)	^{210}Pb	^{234}Th	^{214}Pb	^{214}Pb	^{214}Bi	^{137}Cs
Energy (keV)	46.5	63	295	352	609	661.6
Emission probability (% decay measured)	4.25	3.7	18.28	35.34	45.16	84.99
Emission probability uncertainty (% decay measured)	0.04	0.06	0.14	0.27	0.33	0.002
Half-life (m=minutes, d=days, y=years)	22.3 (y)	24.1 (d)	26.8 (m)	26.8 (m)	19.9 (m)	30.1 (y)
IAEA RGU-1 Activity (dpm/g)	296.4	296.4	296.4	296.4	296.4	*NA
IAEA RGU-1 Activity error (dpm/g)	1.8	1.8	1.8	1.8	1.8	*NA
IAEA-447 Activity (dpm/g)	25.4	1.5	1.6	1.6	1.5	25.5
IAEA-447 Activity error (dpm/g)	1.2	0.2	0.1	0.1	0.1	0.6
IAEA-375 Activity (dpm/g)	*NA	*NA	*NA	*NA	*NA	316.8
IAEA-375 Activity error (dpm/g)	*NA	*NA	*NA	*NA	*NA	4.8

*NA = Not Analyzed

$^{234}Th_{xs}$ is produced in oceanic waters from the decay of soluble ^{238}U to ^{234}Th, which adsorbs to particulate matter in the water column and is deposited on the seafloor (Figure 2.1). $^{234}Th_{xs}$, with a half-life of ~24 days, is usually only detectable at the sediment surface, and is typically used as an indicator of surface mixing (i.e. bioturbation) (Table 2.1) (Luca, 2008; Pope et al., 1996; Yeager et al, 2004; McClintic et al., 2008). Where sediments are unmixed and sedimentation rates are high enough to detect a $^{234}Th_{xs}$ profile (decay curve) it can be used as a geochronological tool (Brooks et al., 2015).

^{137}Cs is a thermonuclear byproduct and is utilized as a chronostratigraphic marker in sediment records representing the height of nuclear bomb testing in the early-mid 1960s (Figure 2.1), and/or other thermonuclear incidents such as the Chernobyl event in 1986 (Appleby, 2001). ^{137}Cs is often used to validate $^{210}Pb_{xs}$ age dating as an independent chronostratigraphic marker.

All of these SLRad can be integrated into sedimentary records and utilized to provide age control to investigate natural and anthropogenic environmental change. The analytical approach and measurement of these SLRad is of importance, but of equal or greater importance is understanding the sedimentological parameters that may influence SLRad in sediment records. Factors that will not be discussed in this paper, but should always be considered when analyzing and interpreting SLRad in sedimentary records include stratigraphic integrity, and sedimentology (i.e. grain size and composition).

2.1.2 International Atomic Energy Association (IAEA) Calibration Standards

Calibration standards of known activity are used in this study to convert analytical measurements of SLRad (counts per minute per gram, cpm/g) to activities (disintegrations per minute per gram, dpm/g), which are used to interpret sedimentary records and provide age dating. The standards used in this study (IAEA RGU-1, IAEA-447, and IAEA-375) are characterized by

the International Atomic Energy Association (IAEA) and are readily available. They vary in sedimentological properties and composition, and were assessed to determine the most appropriate standard for determining activities of SLRad in high-resolution sedimentary records.

The IAEA RGU-1 standard is a uranium ore diluted with silica sand developed to use as a U standard reference material for calibrating laboratory gamma-ray spectrometers (Steger, 1987). It has relatively high activities of daughter products of the ^{238}U decay series, which are in secular equilibrium (i.e. all ^{238}U series SLRad have the same activity and do not change over time (Figure 2.1, Table 2.1). Advantages of the RGU-1 standard are shorter analysis time (hours) and no requirements for decay correction of SLRad. Decay correction accounts for the decrease in activity due to decay between the known activity at the reference date and date of analysis of the standard (Table 2.1). Therefore, a calibration curve of many different sample masses can be produced for a specific detector in a relatively short period of time. A potential disadvantage is that the uranium ore/silica composition is not similar to most natural sediments. Also, this standard does not contain ^{137}Cs and, therefore, an alternate standard is required for calibration of this radioisotope.

The IAEA-447 sediment standard is a moss-soil collected in Hungary in 2007 with an intended use for determination of natural and artificial SLRad of similar composition and density (IAEA, 2012). This standard has a similar composition to many natural sediments generally analyzed and, therefore, may be more appropriate in many sedimentologic studies. The IAEA-447 standard contains the ^{238}U series as well as ^{137}Cs and, therefore, can be used for calibration of the most commonly used radioisotopes in sediment studies (Table 2.1). SLRad activities for IAEA-447 are similar to natural sediment samples and counting times range from 24-48 hours, depending on sample mass. This requires significantly more analysis time to produce a calibration curve over a range of sample masses as compared to the IAEA RGU-1 standard. Also, decay corrections are

required for $^{210}Pb_{xs}$ and ^{137}Cs to determine activities at time of analysis, and the utility of the IAEA-447 will diminish over time due to the decay of these SLRad.

The IAEA-375 standard consists of top soil collected from a farm in Brjansk, Russia in July 1990 and was irradiated to a known activity, with the intended use as a reference material for measurement of SLRad in soil samples (Strachnov et al., 1996). This standard specifically contains high activity of ^{137}Cs and is generally similar in composition to natural sediments (Table 2.1). It should be noted that there is the potential for additional ^{137}Cs activity in this standard resulting from the Chernobyl accident of 1986, leading to higher measured activities as compared to the known irradiated activity reported for this standard. With a half-life of 30 years, decay corrections are required for ^{137}Cs to determine activities at time of analysis, and the utility of IAEA-375 will diminish over time due to the decay of this radioisotope (Helmer and Chechev, 2006).

2.1.3 Application: Case Study, GoM

Analytical calibrations using the IAEA RGU-1 and IAEA-447 are applied to two sediment cores collected in the northeastern Gulf of Mexico (NEGoM) and southwestern Gulf of Mexico (SWGoM) to compare results and interpretations of SLRad activities, age models, and sedimentation/accumulation rates. These cores were collected to assess variability in sedimentation over the past ~100 years at high temporal resolution, and to detect potential impacts associated with anthropogenic oil platform blowout events: specifically, the 2010 Deepwater Horizon (DwH) blowout event (NEGoM) and the 1979 IXTOC-1 blowout event (SWGoM) (Appendix B, Figure B.1; Table B.1, Table B.2, Table S1, Table S2). The DwH Blowout event occurred over the course of 87 days and the IXTOC-1 event, 290 days (Passow and Hetland, 2016; Jernelöv and Lindén, 1981). Detection of these events in the sedimentary record required high-

resolution sampling and analysis (2mm sub-sampling), to detect intervals that potentially contain sedimentation associated with these events.

2.2 Approach and Methods

The IAEA RGU-1 and IAEA-447 calibration standards are applied to SLRad results from two sediment core records, described above, to determine differences between the standards and how calculated activities may be influenced by small sample mass. This includes assessing results for SLRad commonly used in sediment studies including, ^{210}Pb, ^{214}Pb (295 Kev), ^{214}Pb (351 Kev), ^{214}Bi, total ^{234}Th, and ^{137}Cs. Assessment of the IAEA-447 standard for determining ^{137}Cs activities is performed by analysis of an additional known standard (IAEA-375) as ^{137}Cs was below detection limits in the two sediment cores.

Assessment of different sediment standards includes:

1) Calibration, converting counts (measured) to activity: Comparison of IAEA RGU-1 and IAEA-447 standards (i.e. data processing).
2) Application of calibration: NEGoM and SWGoM sediment cores.
    a) $^{234}Th_{xs}$ results, interpretation and comparisons: IAEA RGU-1 vs. IAEA-447.
    b) $^{210}Pb_{xs}$ results, interpretation and comparisons: IAEA RGU-1 vs. IAEA-447.
3) Calibration for ^{137}Cs using the IAEA-447 standard: IAEA-375 standard of known activity.

2.2.1 SLRad Gamma Spectroscopy Analysis

Standards and samples were analyzed by gamma spectroscopy on Series HPGe (High-Purity Germanium) Coaxial Planar Photon Detectors simultaneously measuring activities for ^{210}Pb (46.5Kev), ^{214}Pb (295 keV and 351 keV), ^{214}Bi (609 keV), ^{137}Cs (661 keV), and ^{234}Th (63 keV). A range of sample masses, as a proxy for sample geometry (greater mass = greater sample height),

were analyzed for standards of known activity, IAEA RGU-1 (1g, 3g, 5g, 7g, 9g, 12g, 15g, 17g, 20g, 30g, 40g and 50g), and IAEA-447, (1g, 3g, 5g, 7g, 10g, 20g, 30g, 40g and 50g). The IAEA RGU-1 standard was analyzed for a minimum of 1 hour for samples >10g dry mass and a minimum of 2 hours for samples <10g dry mass. The IAEA-447 standard was analyzed for a minimum of 24 hours for samples >10g dry mass and a minimum of 48 hours for samples <10g dry mass. The IAEA-375 standard was analyzed for a minimum of 12 hours for samples >10g dry mass and a minimum of 24 hours for samples <10g dry mass. GoM samples were analyzed for ~48hrs regardless of sample mass. Analyses yielded counts of gamma emissions for each SLRad measured. Data were corrected for the emission probability (% of total decay at energy measured, i.e. 4.25% of total decay of ^{210}Pb produces gamma emissions of 46.5keV) of each SLRad at the measured energy in the spectrum (Table 1), analysis time (minutes), and sample mass (g) yielding counts/minute/gram (cpm/g) for each SLRad. Results of the IAEA-447 standard were decay corrected for $^{210}Pb_{xs}$ and ^{137}Cs, and results of the IAEA-375 standard were also decay corrected for ^{137}Cs. The IAEA RGU-1 standard does not require decay correction as it is in secular equilibrium and activities do not change with time.

2.2.2 Calibration: Counts to Activity

The IAEA RGU-1 and IAEA-447 standards were utilized to convert measured cpm/g to activity (disintegrations/minute/gram, dpm/g) in a method similar to Kitto (1991). This was performed for each standard in a series of steps.

1) A numerical conversion factor (CF) was calculated for each SLRad (i.e. ^{210}Pb, ^{214}Pb (295 keV and 351 keV), ^{214}Bi, ^{137}Cs, and ^{234}Th) for each analysis of the standard. This was used to convert the measured cpm/g to the known activity (dpm/g) of the standard using the equation below (Table 2.1, Table 2.2).

CF (conversion factor) = known dpm/g of standard ÷ cpm/g measured

2) For each SLRad, the CF for each analysis of the standard was plotted versus the sample mass (1g-50g) (Figure 2.2).

3) For each SLRad, a calibration curve (second-order polynomial fit of data) was developed to define how the CF changes with sample mass (1g-50g) (Figure 2.2).

4) The second-order polynomial fit of the plotted CF vs sample mass (g) mathematically describes how the CF changes with respect to sample mass (g). This mathematical equation is used to convert the measured cpm/g (measured) to activity (dpm/g) of sediment samples. For example:

$$^{210}\text{Pb activity (dpm/g)} = \text{measured } ^{210}\text{Pb cpm/g} * ((0.0006(x^2) + 0.1953(x) + 5.2987))$$

Where: x = the sample mass analyzed (grams), and constant values are defined by the second-order polynomial equation of the calibration curve for ^{210}Pb.

This method of calibration takes into consideration detector efficiency as well as changes in gamma emission detection associated with varying sample mass/sample geometry including effects of self-absorption for each SLRad. Comparison of the calibration curves produced from the two standards are used to determine the potential differences of the two standards in calculating SLRad activities and subsequent age models of sediment records.

Table 2.2. Conversion factor (Conv. Factor, CF) maximum and minimum values for each radioisotope for standards IAEA RGU-1 and IAEA-447 over range of sample masses (i.e. geometry/height).

IAEA	RGU-1	Mass (g)	1.1	3.0	5.1	7.0	9.2	12.0	15.0	17.0	20.1	30.5	41.5	50.4
	447	Mass (g)	1.0	3.0	5.0	7.0	10.0	*NA	*NA	*NA	20.0	30.0	40.0	50.0
^{210}Pb	RGU-1 Conv. Factor	Max.	7.0	7.0	6.9	7.3	7.3	8.5	8.4	8.6	9.9	11.1	12.4	14.9
		Min.	6.3	5.8	6.5	6.4	6.7	7.3	7.8	7.8	8.8	9.9	11.7	12.8
	447 Conv. Factor	Max.	5.4	6.2	6.6	7.0	7.5	*NA	*NA	*NA	10.0	12.4	14.0	17.6
		Min.	5.0	5.8	6.3	6.7	7.3	*NA	*NA	*NA	8.8	11.3	13.3	16.3
^{234}Th	RGU-1 Conv. Factor	Max.	7.4	6.8	6.6	6.9	6.7	7.4	7.8	7.7	8.9	9.7	10.9	12.4
		Min.	5.6	5.8	6.1	6.2	6.2	6.7	7.0	7.1	7.9	9.0	9.9	10.9
	447 Conv. Factor	Max.	0.6	1.5	2.2	2.7	3.1	*NA	*NA	*NA	5.3	7.2	8.7	10.2
		Min.	0.5	1.2	1.8	2.3	2.8	*NA	*NA	*NA	4.8	6.7	8.3	10.0
^{214}Pb (295 keV)	RGU-1 Conv. Factor	Max.	23.6	21.3	22.9	23.5	22.5	25.1	25.5	25.2	28.5	30.6	33.8	38.9
		Min.	19.8	20.1	20.6	21.1	20.4	22.5	24.0	24.2	26.5	27.2	31.3	34.4
	447 Conv. Factor	Max.	6.9	11.3	16.1	17.3	20.1	*NA	*NA	*NA	31.0	36.4	41.7	52.2
		Min.	6.0	9.5	14.0	16.5	17.5	*NA	*NA	*NA	26.4	34.3	*NA	49.2
^{214}Pb (351 keV)	RGU-1 Conv. Factor	Max.	28.4	27.0	28.6	29.5	28.1	31.3	32.1	32.7	35.7	38.0	41.9	49.7
		Min.	24.0	25.6	26.0	26.8	26.6	29.0	30.2	29.7	33.1	35.8	39.3	43.3
	447 Conv. Factor	Max.	8.5	14.6	19.7	21.7	24.7	*NA	*NA	*NA	36.5	45.5	*NA	61.2
		Min.	6.1	13.7	17.0	20.7	22.3	*NA	*NA	*NA	32.6	41.4	*NA	56.2
^{214}Bi	RGU-1 Conv. Factor	Max.	76.3	63.5	68.6	66.2	63.3	73.7	73.2	72.8	80.9	86.2	94.6	108.3
		Min.	58.8	57.1	59.7	63.6	61.9	66.4	68.2	68.2	73.9	79.5	87.7	96.1
	447 Conv. Factor	Max.	11.2	24.1	36.6	40.7	52.4	*NA	*NA	*NA	72.0	90.4	*NA	114.9
		Min.	10.4	20.2	32.6	37.6	44.2	*NA	*NA	*NA	66.5	83.4	*NA	107.7
^{137}Cs	447 Conv. Factor	Max.	64.1	65.9	67.7	69.2	71.8	*NA	*NA	*NA	79.6	96.5	102.9	120.3
		Min.	60.6	62.0	65.9	67.8	67.8	*NA	*NA	*NA	77.5	89.8	96.1	119.1

*NA = Not Analyzed

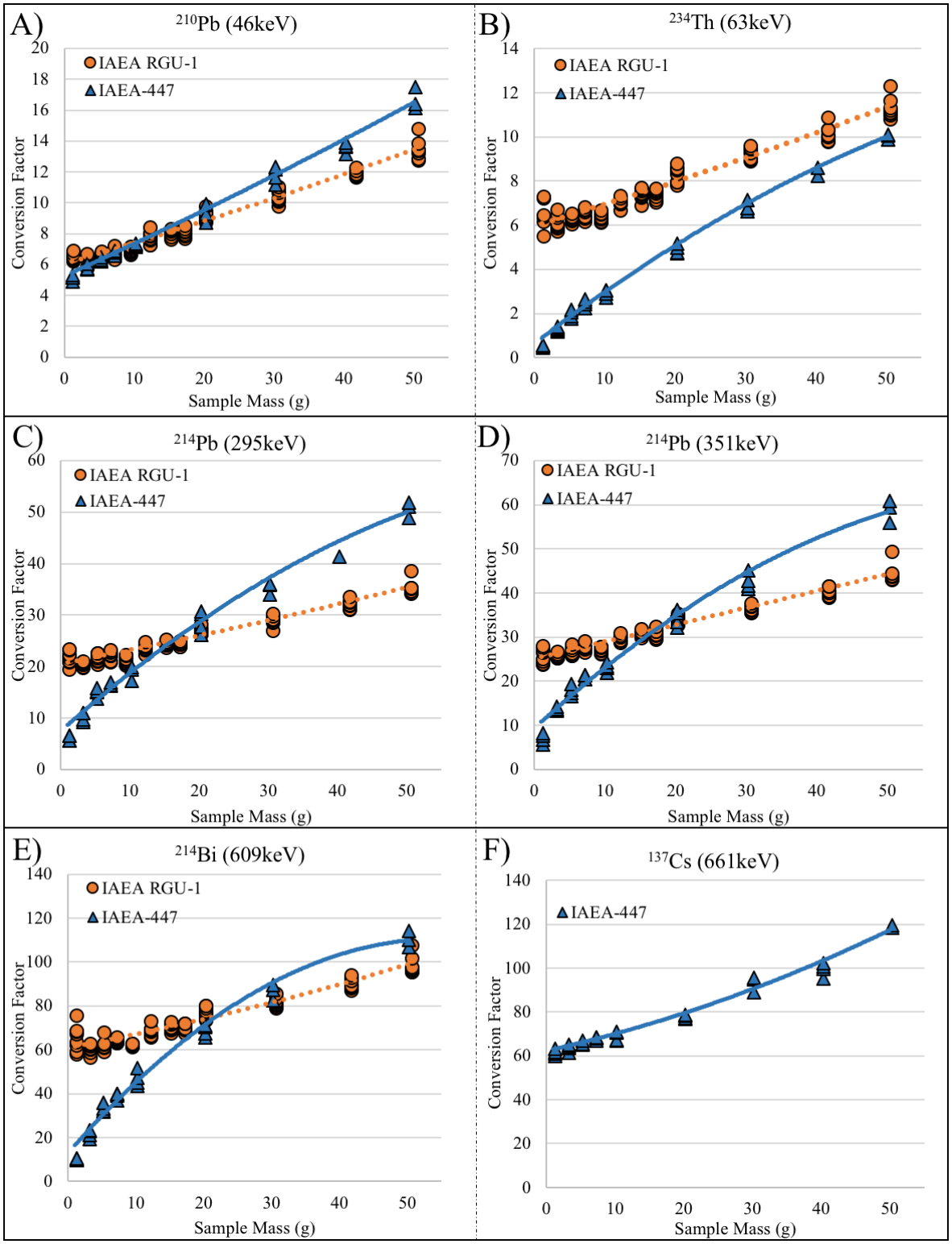

Figure 2.2. Plots of conversion factor vs sample mass (g) of A) ^{210}Pb, B) ^{234}Th, C) ^{214}Pb (295keV), D) ^{214}Pb (351keV), E) ^{214}Bi, and F) ^{137}Cs for range of sample masses of IAEA RGU-1 (orange circles) and IAEA-447 (blue triangles) analyzed to determine calibration lines (i.e. counts to activity). Note the higher conversion factors of IAEA RGU-1 for small sample masses, <10g as compared to IAEA-447.

2.2.3 Application: NEGoM and SWGoM sediment cores

Cores were collected with an Ocean Instruments MC-800 multicore to preserve the sediment water interface. Core DSH08 was collected in the NEGoM from 1,143m water depth and was extruded at 2mm resolution from 0-50mm and 50 mm resolution from 50mm to the core base at 280mm (Appendix B, Figure B.1; Table B.1) (Schwing, et al., 2016). Core IXW250 was collected in the SWGoM from 583m water depth and extruded at 2mm resolution from 0-100mm and 5 mm resolution from 100mm to the core base at 345mm (Appendix B, Figure B.1; Table B.2) (Scwhing, et al., 2016). All core sub-samples were weighed for sample wet mass (during extrusion) and dry mass to calculate dry bulk density (g/cm^3) (Appleby, 2001, Binford, 1900, Sanchez-Cabeza, et al., 2012). Sub-samples from both cores were analyzed on the same detector and activities for SLRad were determined using the IAEA RGU-1 and IAEA-447 calibration equations.

2.2.4 Excess ^{234}Th ($^{234}Th_{xs}$)

$^{234}Th_{Tot}$ activities for cores DSH08 and IXW250 were calculated using the IAEA RGU-1 and IAEA-447 calibration lines for ^{234}Th. For core DSH08, $^{234}Th_{Sup}$ was determined by re-analysis of the same sample >120 days (~5 half-lives) after core collection (i.e., all $^{234}Th_{xs}$ decayed) as well as comparison to downcore $^{234}Th_{Tot}$ activities (i.e. older and no $^{234}Th_{xs}$). $^{234}Th_{Sup}$ was subtracted from the $^{234}Th_{Tot}$ to calculate $^{234}Th_{xs}$ activities in the surficial sub-sample(s).

2.2.5 Supported ^{210}Pb ($^{210}Pb_{Sup}$)

^{214}Pb (295 keV), ^{214}Pb (351 keV) and ^{214}Bi activities for cores DSH08 and IXW250 were calculated using the IAEA RGU-1 and IAEA-447 calibration lines for ^{214}Pb (295 keV), ^{214}Pb (351 keV) and ^{214}Bi . ^{214}Pb (295 Kev), ^{214}Pb (351 Kev), and ^{214}Bi (609 Kev) activities were averaged

as an estimate of the $^{210}Pb_{Sup}$ in sediment sample (Baskaran, et al. 2014, MacKenzie, et al., 2011, Smith et al., 2002).

2.2.6 Excess ^{210}Pb ($^{210}Pb_{xs}$)

$^{210}Pb_{Tot}$ activities for cores DSH08 and IXW250 were calculated using the IAEA RGU-1 and IAEA-447 calibration lines for ^{210}Pb. $^{210}Pb_{Sup}$ activities were subtracted from $^{210}Pb_{Tot}$ activities to calculate $^{210}Pb_{xs}$ activities. The Constant Rate of Supply (CRS) algorithm was employed to assign specific ages to sedimentary intervals within the $^{210}Pb_{xs}$ profile. The CRS algorithm is appropriate under conditions of varying accumulation rates (Appleby and Oldfield, 1983; Binford, 1990). Mass accumulation rates (MAR) were calculated for each data point (i.e., "date"), based upon the CRS model results. The use of MAR corrects for differential sediment compaction down core, thereby enabling a direct comparison of $^{210}Pb_{xs}$ accumulation rates throughout a core (i.e., over the last ~120 years). Mass accumulation rates were calculated as follows:

$$MAR\ (g/cm^2/yr) = \text{dry bulk density X LAR}$$

Where: dry bulk density (g/cm^3) = sample dry mass (g) ÷ sample volume (cm^3)

LAR = linear accumulation rate (cm/yr)

2.2.7 ^{137}Cs

A range of sample masses (g) of the IAEA-375 standard was analyzed and converted from counts to activity using the IAEA-447 calibration line for ^{137}Cs. Activities were decay corrected to account for decay (loss in activity) between the known activity reference date and the analysis date. Activity results determined using the IAEA-447 calibration line were compared to the known activity of the IAEA-375 standard.

2.3 Results

There was variability between the IAEA RGU-1 and IAEA-447 calibration lines and subsequent SLRad activities measured in the subsamples of the cores collected in the NEGoM and SWGoM, especially for analysis of small sample masses. IAEA RGU-1 calibration lines consistently overestimated activities in sediment samples of small mass for all SLRad (Figure 2.3-2.7, Appendix B, Table B.3 – Table B.17) with the IAEA-447 calibration lines yielding more consistent SLRad activities/results.

2.3.1 Conversion Factor (CF): Counts to Activity

For both standards (IAEA RGU-1 and IAEA-447), CF (conversion factor) values increased with increasing sample mass (g) for all SLRad (Figure 2.2, Table 2.2). At smaller sample masses (<10g) the IAEA-447 standard CF values was smaller than the IAEA RGU-1 standard CF values for all SLRad. For 5g masses, IAEA RGU-1 CF values for ^{210}Pb ranged from 6.5-6.9 and for IAEA-447 from 6.3-6.6. For 5g masses, IAEA RGU-1 CF values for ^{234}Th ranged from 6.1-6.6 and for IAEA-447 from 1.8-2.2. For 5g masses, IAEA RGU-1 CF values for ^{214}Pb (295keV) ranged from 20.6-22.9 and for IAEA-447 from 14.0-16.1. For 5g masses, IAEA RGU-1 CF values for ^{214}Pb (351keV) ranged from 26.0-28.6 and for IAEA-447 from 17.0-19.7. For 5g masses, IAEA RGU-1 CF values for ^{214}Bi ranged from 59.7-68.6 and for IAEA-447 from 32.6-36.6 and the (Table 2.2). The difference between the IAEA RGU-1 and IAEA-447 CF values became greater with decreasing sample mass. This difference was greatest at the smallest sample mass with a difference in CF value for ^{210}Pb up to 0.6, ^{234}Th up to 4.8, ^{214}Pb (295keV) up to 8.9, ^{214}Pb (352keV) up to 11.6, and ^{214}Bi up to 36 (Figure 2.2, Table 2.2). For ^{137}Cs, the IAEA-447 CF values ranged from 65.9-67.7 for 5g sample mass, 77.5-79.6 for 20g sample mass, and 119.1-120.3 for 50g sample mass (Table 2.2).

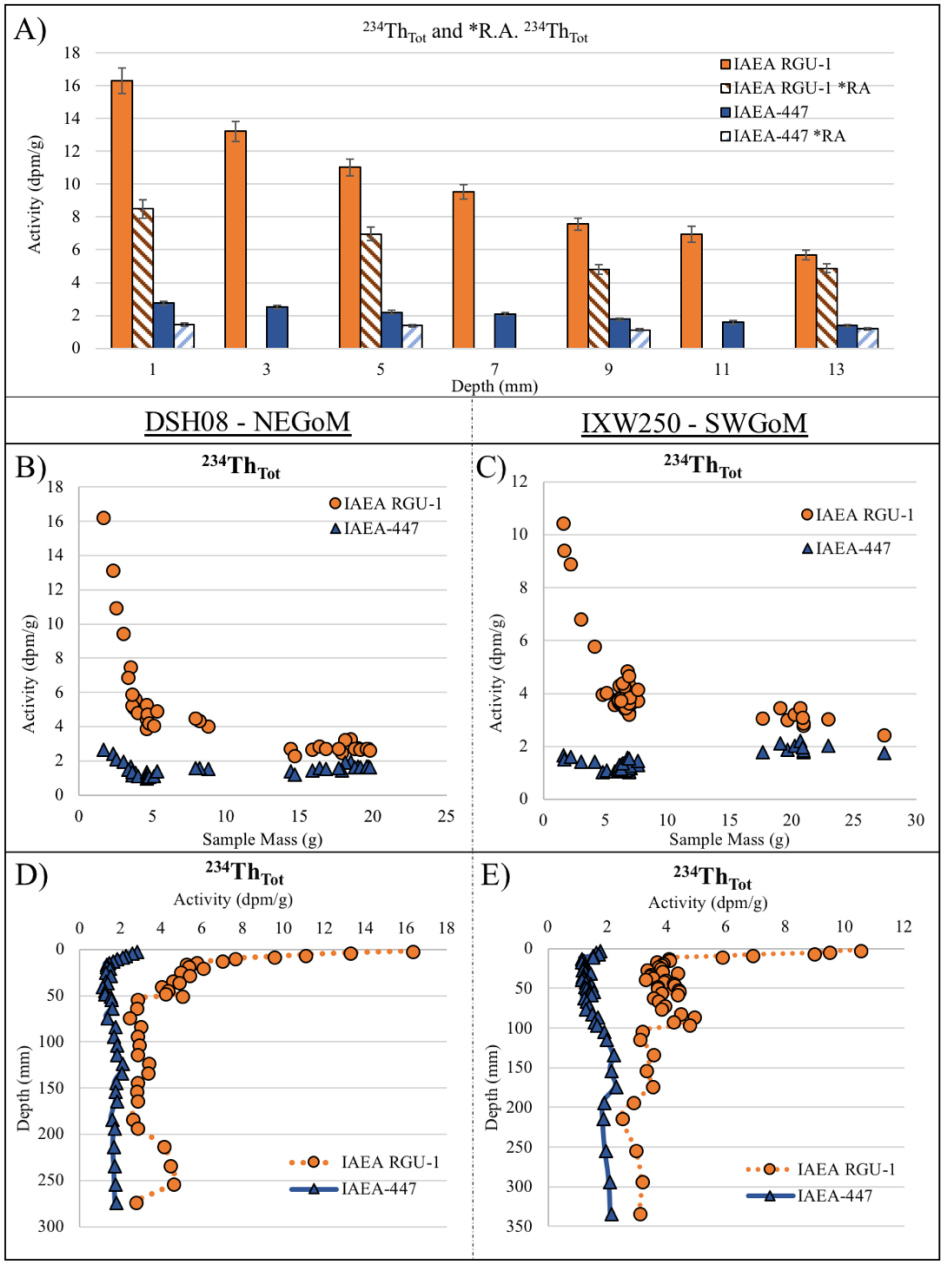

Figure 2.3. $^{234}Th_{Tot}$ activities for cores collected in the GoM. A) Plot of $^{234}Th_{Tot}$ activities analyzed promptly after core collection using IAEA RGU-1 (orange bar) and IAEA-447 (blue bar) calibration lines, as well as re-analysis (RA) activities ($^{234}Th_{Sup}$) using IAEA RGU-1 (orange stripe bar), and IAEA-447 (blue stripe bar) calibration lines (Appendix B, Table B.3 – B.6). Note the change in ^{234}Th RA activities with sample depth (i.e. sample mass) indicating a decrease in $^{234}Th_{Sup}$ activity. B) DSH08 (Appendix B, Table B.3) and C) IXW250 (Appendix B, Table B.5) $^{234}Th_{Tot}$ activities determined using IAEA RGU-1 (orange circles) and IAEA-447 (blue triangle) calibration lines versus analyzed mass. Note the overestimation of $^{234}Th_{Tot}$ of IAEA RGU-1 for small sample masses (>10g). D) DSH08 (Appendix B, Table B.3) and E) IXW250 (Appendix B, Table B.5) $^{234}Th_{Tot}$ activities determined using IAEA RGU-1 (orange circles) and IAEA-447 (blue triangle) calibration lines vs depth downcore, with samples 12mm and deeper reflecting $^{234}Th_{Sup}$ activities. Note the overestimation of $^{234}Th_{Tot}$ by IAEA RGU-1 for small sample mass, specifically 2mm sampling intervals (DSH08 0-50mm and IXW250 0-100mm) and intervals 200-260mm in DSH08 (<10g mass).

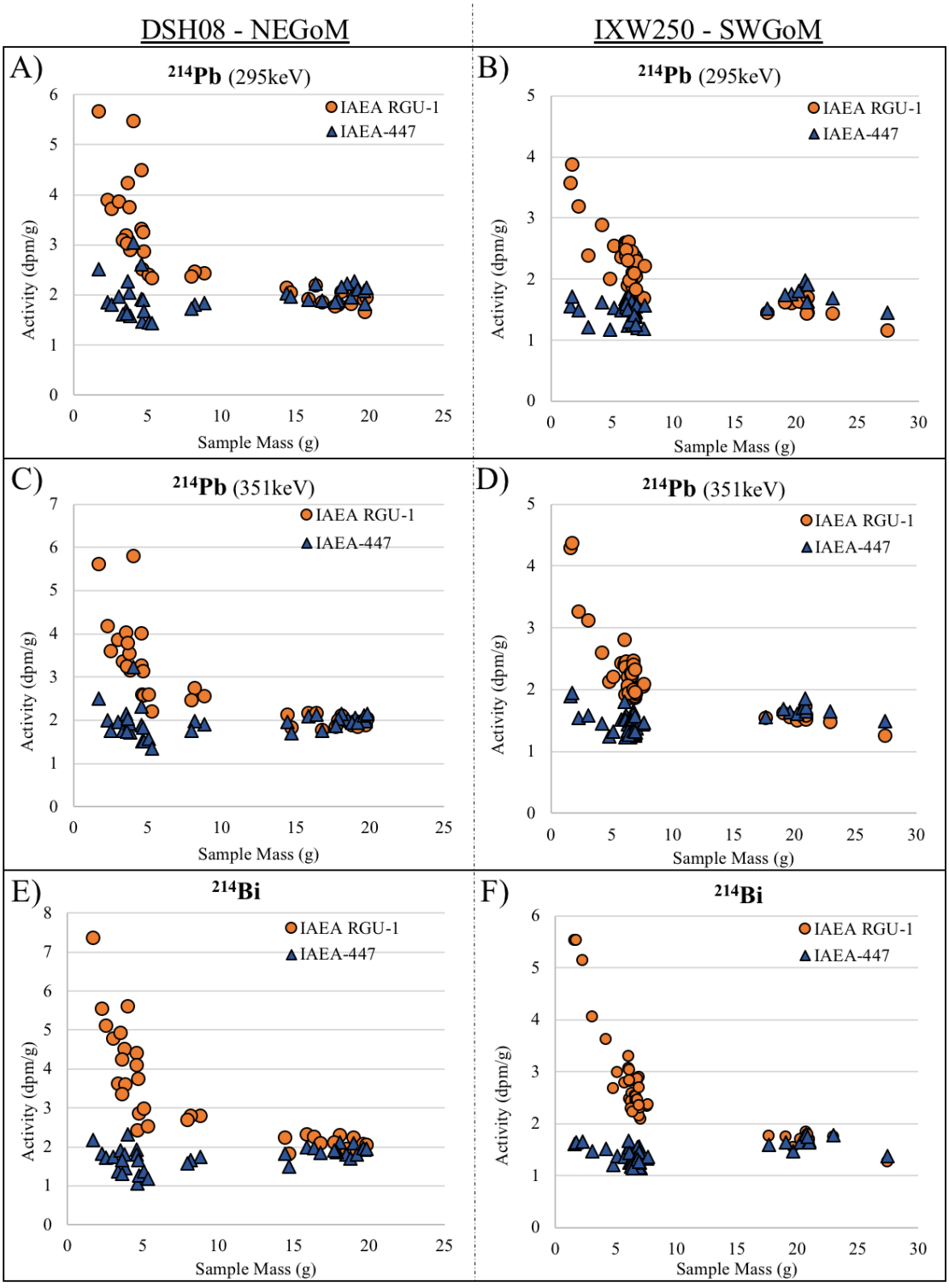

Figure 2.4. Activities of SLRad used for determining $^{210}Pb_{Sup}$ calculated using IAEA RGU-1 (orange circles) and IAEA-447 (blue triangles) calibration lines compared to sample analysis mass (g) for A) DSH08 ^{214}Pb (295keV), B) IXW250 ^{214}Pb (295keV), C) DSH08 ^{214}Pb (351keV), D) IXW250 ^{214}Pb (351keV), E) DSH08 ^{214}Bi, F) IXW250 ^{214}Bi. Note the overestimation of activity, of small sample mass (>10g), by IAEA RGU-1 for all SLRad proxies for $^{210}Pb_{Sup}$ and agreement over the range of sample masses with activities calculated using the IAEA-447 calibration lines.

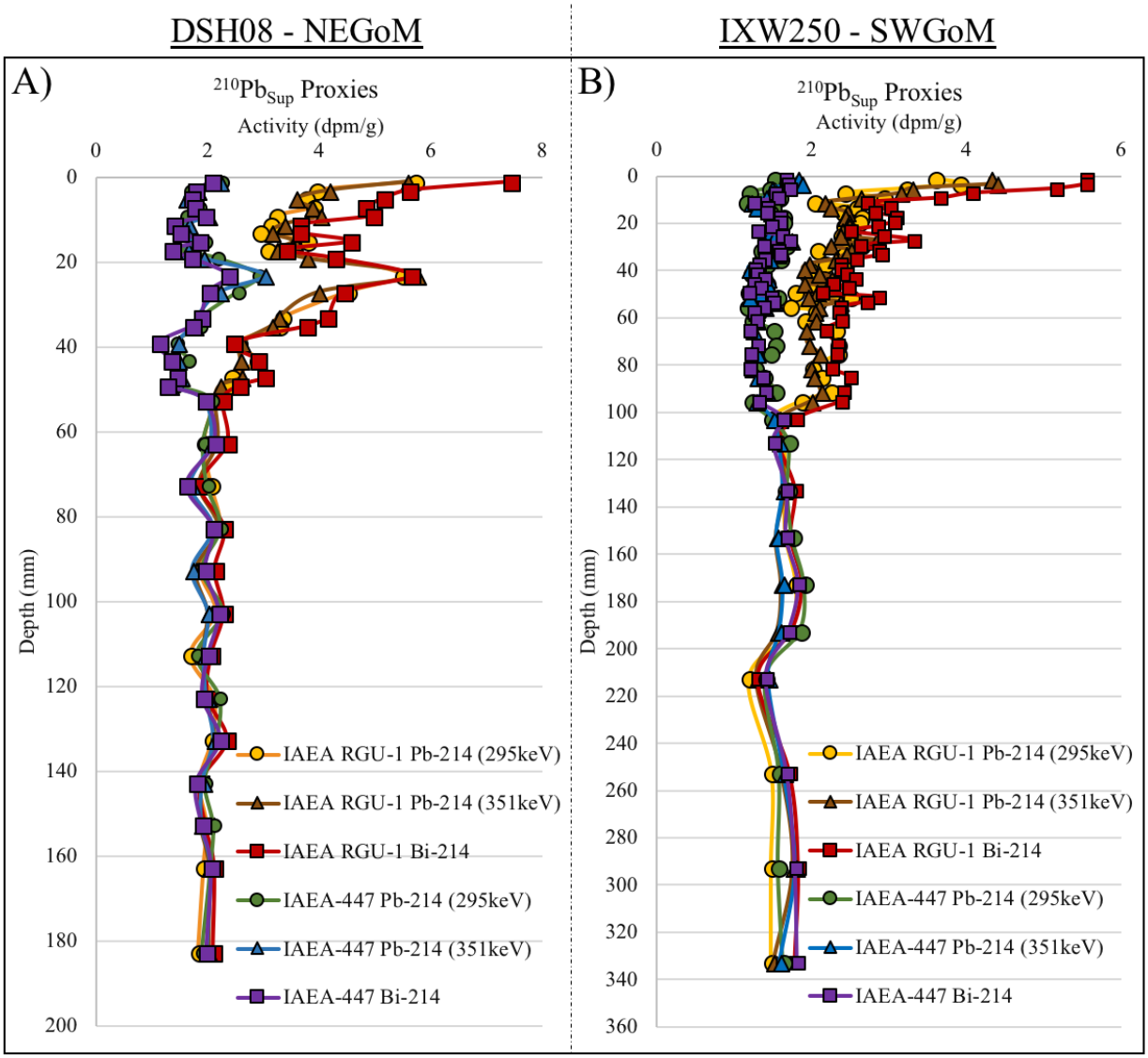

Figure 2.5. Depth profiles of SLRad proxies (^{214}Pb (295keV), ^{214}Pb (351keV), and ^{214}Bi) used for determining $^{210}Pb_{Sup}$ calculated using IAEA RGU-1 (yellow, brown, red) and IAEA-447 (green, blue, purple) calibration lines for A) core DSH08, B) core IXW250. Note the agreement in activity of all six proxies downcore (DSH08 below 50mm and IXW250 below 100mm) associated with 5mm sampling resolution and larger sample masses. Both cores have deviations between IAEA RGU-1 and IAEA-447 activities associated with smaller (<10g) in surficial 50mm (DSH08) and 100mm (IXW250) due to overestimation of activity by IAEA RGU-1 and activities calculated using the IAEA-447 calibration lines are more consistent with downcore activities.

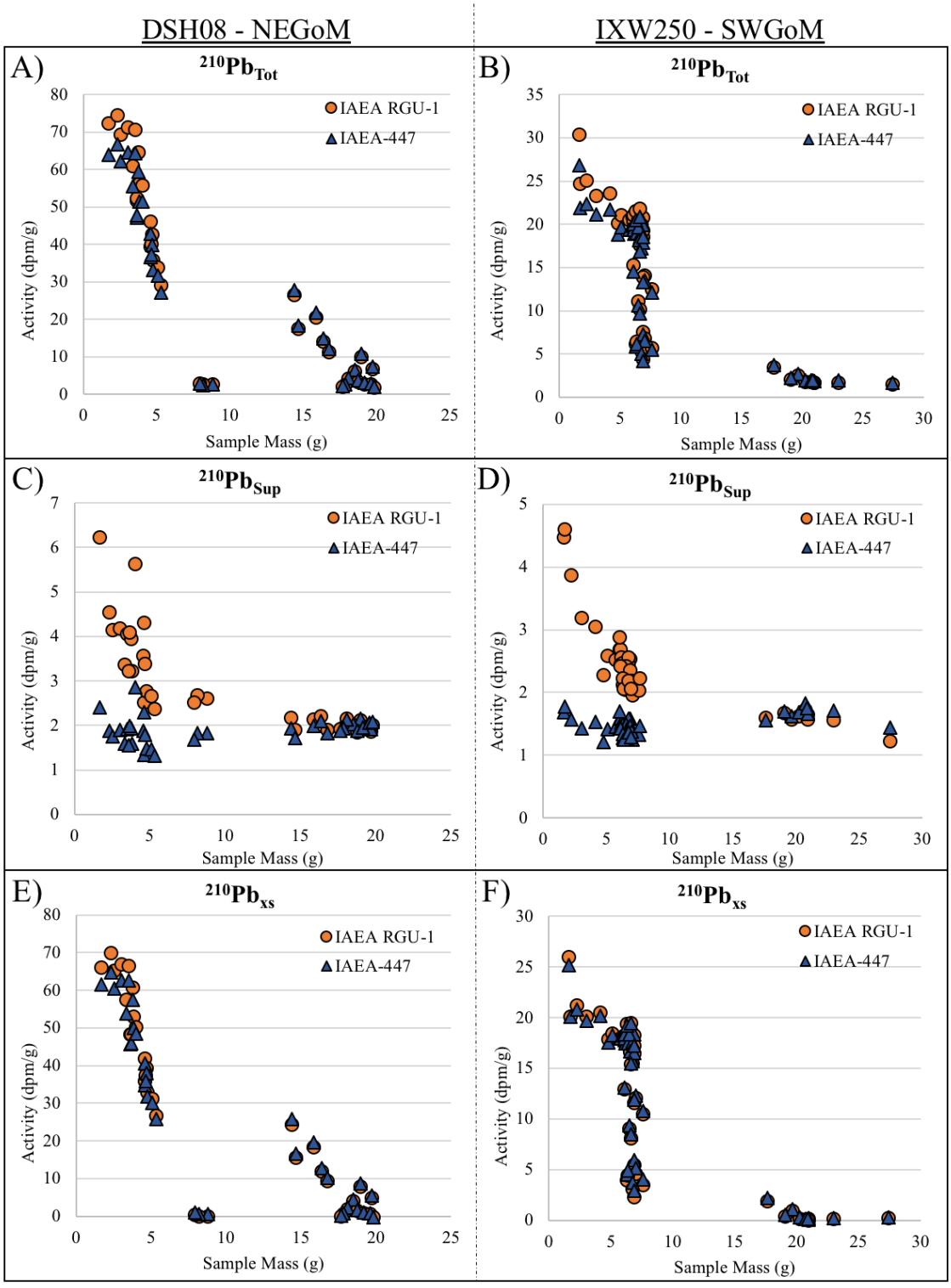

Figure 2.6. Activities of A) core DSH08 $^{210}Pb_{Tot}$, B) core IXW250 $^{210}Pb_{Tot}$, C) core DSH08 $^{210}Pb_{Sup}$, D) core IXW250 $^{210}Pb_{Sup}$, E) core DSH08 calculated $^{210}Pb_{xs}$, F) core IXW250 calculated $^{210}Pb_{xs}$ using IAEA RGU-1 (orange circles) and IAEA-447 (blue triangles) calibration lines compared to sample analysis mass (g). Note the overestimation of activity, of small samples (>10g), by IAEA RGU-1 for $^{210}Pb_{Tot}$, $^{210}Pb_{Sup}$ and calculated $^{210}Pb_{xs}$. Due to the overestimation of $^{210}Pb_{Tot}$ and $^{210}Pb_{Sup}$ the overestimation of $^{210}Pb_{xs}$ is reduced.

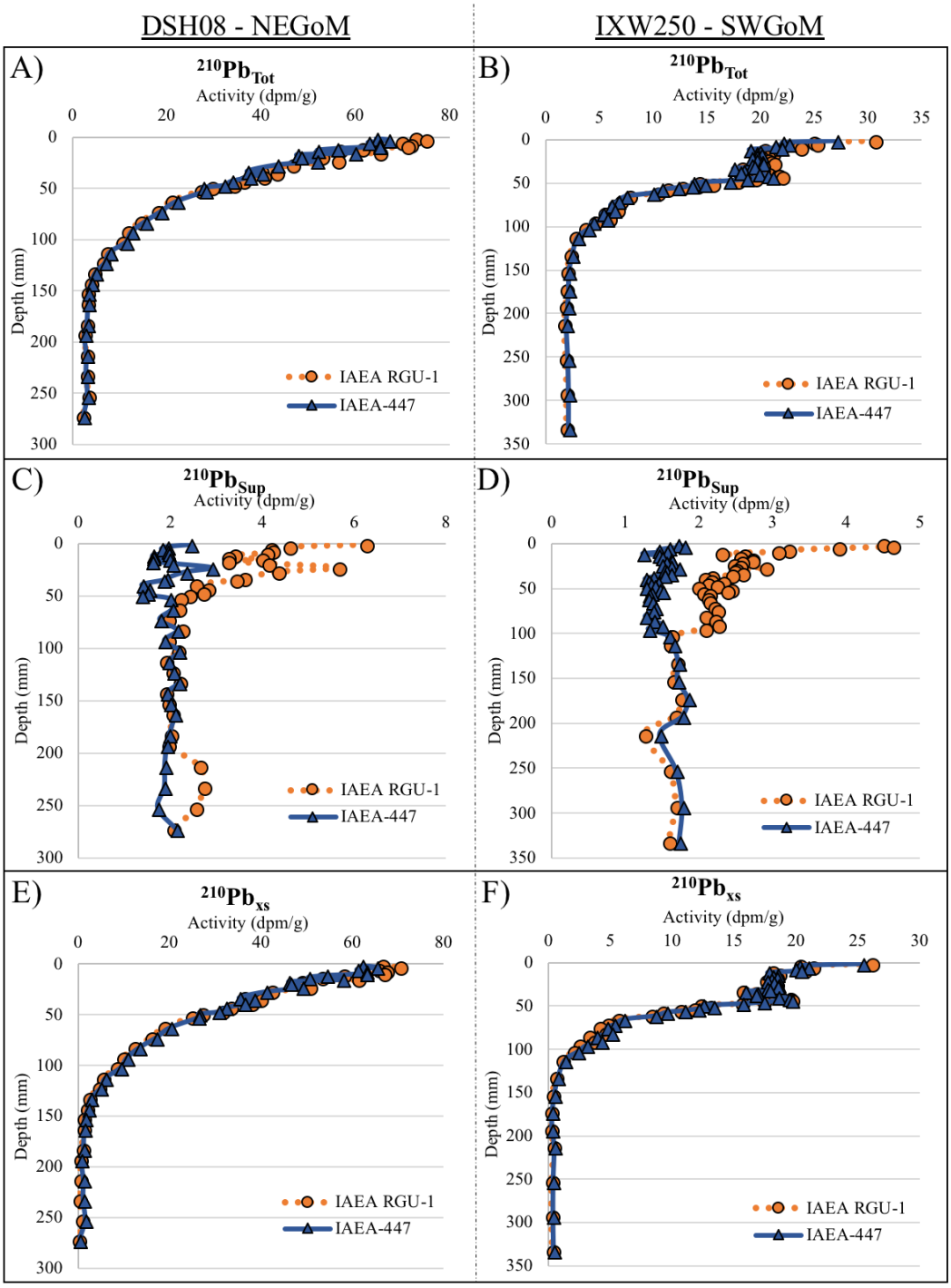

Figure 2.7. Activity profiles vs depth of A) core DSH08 $^{210}Pb_{Tot}$, B) core IXW250 $^{210}Pb_{Tot}$, C) core DSH08 $^{210}Pb_{Sup}$, D) core IXW250 $^{210}Pb_{Sup}$, E) core DSH08 calculated $^{210}Pb_{xs}$, F) core IXW250 calculated $^{210}Pb_{xs}$ using IAEA RGU-1 (orange circles) and IAEA-447 (blue triangles) calibration lines compared to sample analysis mass (g). Note the agreement in activity proxies (DSH08 below 50mm and IXW250 below 100mm) associated with 5mm sampling resolution and larger sample masses. The higher activities of $^{210}Pb_{Sup}$ in DSH08 between 200mm and 250mm is due to analysis of smaller sample mass for these intervals (7.8-8.7g). Both cores have deviations between IAEA RGU-1 and IAEA-447 associated with the overestimation of activity, of small samples (>10g) by IAEA RGU-1 for $^{210}Pb_{Tot}$, $^{210}Pb_{Sup}$ and calculated $^{210}Pb_{xs}$. Due to the overestimation of $^{210}Pb_{Tot}$ and $^{210}Pb_{Sup}$ the overestimation of $^{210}Pb_{xs}$ is reduced.

2.3.2 Calibration Curves

The IAEA RGU-1 and IAEA-447 calibration lines reflect the changes in the CF values over the range of sample masses (1-50g) (Figure 2.2, Table 2.2). Both the IAEA RGU-1 and IAEA-447 calibration lines show an increase in the CF value with increasing sample mass. For all radioisotopes, the IAEA RGU-1 calibration lines are more linear with a smaller range of CF values as compared to the IAEA-447 calibration lines, with the exception of ^{137}Cs (IAEA RGU-1 contains no ^{137}Cs for comparison). For 1g (smallest CF) to 50g (largest CF) sample mass the IAEA RGU-1 standard CF values ranged for ^{210}Pb from 6.3-14.9, for ^{234}Th from 5.6-12.4, for ^{214}Pb (295keV) from 19.8-38.9, for ^{214}Pb (351keV) from 24.0-49.7, and for ^{214}Bi from 58.8-108.3 (Table 2.2). For 1g (smallest CF) to 50g (largest CF) sample mass the IAEA-447 standard CF values ranged for ^{210}Pb from 5.0-17.6, for ^{234}Th from 0.5-10.2, for ^{214}Pb (295keV) from 6.0-52.2, for ^{214}Pb (351keV) from 6.1-61.2, and for ^{214}Bi from 10.4-114.9 (Table 2.2). The difference between the IAEA RGU-1 and IAEA-447 CF values is greater with decreasing sample mass, below 10g sample mass. This difference was greatest at the smallest sample mass with a difference in CF value for ^{210}Pb up to 0.6, CF value for ^{234}Th up to 4.8, CF value for ^{214}Pb (295keV) up to 8.9, CF value for ^{214}Pb (352keV) up to 11.6, and CF value for ^{214}Bi up to 36 (Figure 2.2, Table 2.2).

2.3.3 NEGoM and SWGoM Sediment Cores

Sediment cores DSH08 (NEGoM) and IXW250 (SWGoM) consist of grayish tan muds with brown to dark brown surficial layers associated with redox geochemistry (Brooks et al. 2015). Both are comprised of 99% mud throughout (Appendix B, Table B.1 and B.2). Core DSH08 yielded 1.59g-5.21g of dry sediment from 2mm sampling intervals and 14.30g-19.59g of dry sediment from 5mm sampling intervals for gamma spectroscopy analysis, with some 5mm intervals sub-sampled and analyzed at smaller sample masses (7.84g-8.70g) (Appendix B, Table

B.3). Core IXW250 yielded 1.48g-7.49g of dry sediment from 2mm sampling intervals and 17.50g-27.30g of dry sediment from 5mm sampling intervals for gamma spectroscopy analysis (Appendix B, Table B.5).

2.3.4 Application of Calibration: ^{234}Th

For both cores, DSH08 and IXW250, the IAEA RGU-1 calibration line overestimated activities of ^{234}Th for all samples (particularly for small sample masses) by up to 13.56 dpm/g for DSH08 and 8.77 dpm/g for IXW250 (Figure 2.3, Appendix B, Table B.3, Table B.5). Activities determined using the IAEA-447 calibration line are more consistent over the range of analyzed sample masses, and downcore activities are comparable to the re-analyzed activities used for determining $^{234}Th_{Sup}$ (Figure 2.3, Appendix B, Table B.3, Table B.5).

In core DSH08 $^{234}Th_{xs}$ was detected to a depth of 12mm (Figure 2.3, Appendix B, Table B.3). Re-analysis of samples for $^{234}Th_{Sup}$ yielded activities ranging between 1.12 and 1.37 dpm/g using the IAEA-447 calibration line and between 3.27 and 5.85 dpm/g using the IAEA RGU-1 calibration line (Appendix B, Table B.3). $^{234}Th_{Tot}$ activities below 12mm, using IAEA-447 calibration line, ranged between 1.07 and 2.04 dpm/g with no apparent relationship to analyzed sample mass. $^{234}Th_{Tot}$ activities below 12mm, using the IAEA RGU-1 calibration line, ranged between 2.39 and 5.68 dpm/g and activities increased with decreasing analyzed sample mass (Appendix B, Table B.3). For core IXW250 $^{234}Th_{Tot}$ activities below 12mm, using IAEA-447 calibration line, ranged between 1.10 and 2.26 dpm/g with no apparent relationship to sample mass. $^{234}Th_{Tot}$ activities below 12mm, using the IAEA RGU-1 calibration line, ranged between 2.85 and 4.73 dpm/g and activities increased with decreasing analyzed sample mass (Appendix B, Table B.3).

2.3.5 Application of Calibration: $^{210}Pb_{Sup}$

The calculation of $^{210}Pb_{Sup}$ consisted of averaging 3 SLRad, that are in secular equilibrium and should have similar measured activities, including ^{214}Pb for 2 energies (295keV and 351keV) and ^{214}Bi (Figure 2.1). ^{214}Pb (295keV and 351keV) and ^{214}Bi had higher calculated activities for smaller sample masses (<10g) using the IAEA RGU-1 calibration lines as compared to the IAEA-447 calibration lines, leading to higher $^{210}Pb_{Sup}$ activities (Figure 2.4, Figure 2.5, Appendix B, Table B.12, Table B.13). Generally, $^{210}Pb_{Sup}$ activities are relatively constant in sediment records with consistent sediment composition, and should be comparable to downcore activities.

For core DSH08, all ^{214}Pb (295keV), ^{214}Pb (351keV), and ^{214}Bi activities were higher in the upper 50mm of the core when calculated using the IAEA RGU-1 calibration lines compared to the IAEA-447 calibration lines (Figure 2.4, Appendix B, Table B.6 – Table B.8). Activities calculated using the IAEA RGU-1 calibration lines were higher near the surface and decreased with increasing sample mass. Calculated activities for ^{214}Pb (295keV) ranged from 5.71 to 1.70 dpm/g, ^{214}Pb (351keV) activities ranged from 5.83 to 1.80 dpm/g, and ^{214}Bi activities ranged from 7.41 to 1.87 dpm/g. All three SLRad yielded similar activities using the IAEA- 447 calibration lines with calculated activities for ^{214}Pb (295keV) ranging from 3.08 to 1.47 dpm/g, ^{214}Pb (351keV) ranging from 3.26 to 1.38 dpm/g, and ^{214}Bi ranging from 2.35 to 1.10 dpm/g. ^{214}Pb (295kev) and ^{214}Pb(351keV) yielded similar activities using the IAEA RGU-1 calibration lines, but varied with the ^{214}Bi calibration line by up to 1.7 dpm/g. Calculated $^{210}Pb_{Sup}$ activities using the IAEA RGU-1 calibration lines ranged from 6.25 to 1.88 dpm/g and were higher in the upper 50mm of the core by up to 3.82 dpm/g as compared to the IAEA-447 calculated activities (Figure 2.6, Figure 2.7, Appendix B, Table B.6 – Table B.8). Calculated $^{210}Pb_{Sup}$ activities using the IAEA-447 calibration

lines were more consistent throughout the core and ranged from 2.90 to 1.36 dpm/g (Figure 2.7, Figure 2.8, Appendix B, Table B.12).

All ^{214}Pb (295keV), ^{214}Pb (351keV), and ^{214}Bi activities in core IXW250 were also higher in the upper 50mm of the core when calculated using the IAEA RGU-1 calibration lines compared to the IAEA-447 calibration lines (Figure 2.4, Figure 2.5, Appendix B, Table B.9 – Table B.11). Activities calculated using the IAEA RGU-1 calibration lines were higher near the surface and decreased with increasing sample mass with calculated activities for ^{214}Pb (295keV) ranging from 3.90 to 1.47 dpm/g, ^{214}Pb (351keV) ranging from 4.40 to 1.28 dpm/g, and ^{214}Bi ranging from 5.57 to 1.30 dpm/g. All three SLRad yielded similar activities using the IAEA-447 calibration lines with calculated activities for ^{214}Pb (295keV) ranging from 2.00 to 1.22 dpm/g, ^{214}Pb (351keV) ranging from 1.98 to 1.25 dpm/g, and ^{214}Bi ranging from 1.82 to 1.17 dpm/g. ^{214}Pb (295kev) and ^{214}Pb(351keV) SLRad yielded similar activities using the RGU-1 calibration lines but the ^{214}Bi calibration line varied by up to 1.7 dpm/g. Calculated $^{210}Pb_{Sup}$ activities using the IAEA RGU-1 calibration lines ranged from 4.62 to 1.25 dpm/g and were higher in the upper 50mm of the core by up to 2.83 dpm/g compared to IAEA-447 calculated activities (Figure 2.6, Figure 2.7, Appendix B, Table B.13). Calculated $^{210}Pb_{Sup}$ activities using the IAEA-447 calibration lines were more consistent throughout the core and ranged from 1.85 to 1.24 dpm/g (Figure 2.6, Figure 2.7, Appendix B, Table B.13). This is an indication that, for small sample masses the IAEA RGU-1 calibration lines overestimate background ^{210}Pb, which is consistent with the other SLRad.

2.3.6 Application of Calibration: $^{210}Pb_{Tot}$

Samples with small mass (<10g) had higher activities of $^{210}Pb_{Tot}$ calculated using the IAEA RGU-1 compared to the IAEA-447 calibration lines in both DSH08 and IXW250. The difference in activities between the calibration lines decreases with increasing sample mass (Figure 2.6,

Appendix B, Table B.14, Table B.15). For core DSH08, the difference in activities of $^{210}Pb_{Tot}$ between the IAEA RGU-1 and IAEA-447 calibration lines ranged from 8.29 dpm/g to 1.76 dpm/g in the upper 50mm (2mm sampling resolution) with a decrease in difference as sample mass increased. Differences in activity (IAEA RGU-1 vs IAEA-447) below 50mm ranged from -1.17 to 0.08 dpm/g (Figure 2.6, Figure 2.7, Appendix B, Table B.14). For core IXW250, the differences in activities of $^{210}Pb_{Tot}$ between the IAEA RGU-1 and IAEA-447 calibration lines ranged from 3.54 dpm/g to 0.53 dpm/g in the upper 50mm (2mm sampling resolution) and variability between the two calibration lines decreased as sample mass increased. From 50mm to 100mm, continued 2mm sampling indicated differences between calibration lines ranging from 0.76 to 0.18 dpm/g. Differences below 100mm (5mm sampling resolution) ranged from -0.26 to -0.18 dpm/g (Figure 2.6, Figure 2.7, Appendix B, Table B.15).

2.3.7 Application of Calibration: $^{210}Pb_{xs}$, CRS age and MAR

Core DSH08 had an exponential $^{210}Pb_{xs}$ profile and core IXW250 had a deviation in the exponential $^{210}Pb_{xs}$ profile with a plateau between 15mm and 40mm (Figure 2.7). The difference in the $^{210}Pb_{xs}$ profiles of these two cores provides the opportunity to compare results and interpretations for $^{210}Pb_{xs}$ age dating on exponential and non-exponential $^{210}Pb_{xs}$ sediment records using IAEA RGU-1 and IAEA-447 calibration lines to determine activities. The determination of $^{210}Pb_{xs}$ activities includes the measurement of $^{210}Pb_{Tot}$ and $^{210}Pb_{Sup}$. The higher activities, using the IAEA RGU-1 calibration lines, of both $^{210}Pb_{Tot}$ and $^{210}Pb_{Sup}$, for small sample masses, reduces the differences of $^{210}Pb_{xs}$ between the IAEA RGU-1 and IAEA 447 calibration line, leading to better agreement between the $^{210}Pb_{xs}$ profiles.

For core DSH08, the $^{210}Pb_{xs}$ activities calculated using the IAEA RGU-1 calibration lines were higher compared to the IAEA 447 calibration lines by up to 5.13 dpm/g near the sediment

surface and decreased to 0.72 dpm/g in the upper 50mm. Once again, differences in activities decreased as sample mass increased (Figure 2.6, Figure 2.7, Appendix B, Table B.16). For core IXW250, the $^{210}Pb_{xs}$ activities calculated using the IAEA RGU-1 calibration lines were more similar to the IAEA-447 calibration lines with higher activities (IAEA RGU-1) by up to 0.77 dpm/g near the surface, and decreased to 0.72 dpm/g in the upper 50mm (Figure 2.6, Figure 2.7, Appendix B, Table B.17). Using the CRS model to calculate sample ages shows that the differences between the IAEA RGU-1 and IAEA-447 dates increase with depth (age) due to the influence of $^{210}Pb_{xs}$ on the $^{210}Pb_{xs}$ inventory (summation of activity in the sediment core), which is required for the CRS algorithm. The IAEA RGU-1 calibration lines consistently yields younger ages with depth compared to the IAEA-447, and also yields consistently lower MAR values (Figure 2.8, Appendix B, Table B.18 - Table B.21). The difference in age between the IAEA RGU-1 and IAEA-447 is within analytical error of the method, but the consistent offset to younger ages by the IAEA RGU-1 standard leads to decreased certainty in ages, particularly for older ages. Depending on the objective of a study this may be acceptable, but with increased desire for high-temporal resolution age dating, increased confidence in age dating is critical.

2.3.8 Application of Calibration, ^{137}Cs

Activities of the IAEA-375 standard were decay corrected and ranged between 310 dpm/g and 356 dpm/g with a targeted known activity of 316 dpm/g (Figure 2.9, Appendix B, Table B.22). The IAEA-447 calibration line may slightly overestimate ^{137}Cs activities, but the potential additional activity of ^{137}Cs in the IAEA-375 standard from the Chernobyl accident of 1986 likely accounts for some of the variability and higher than expected activities.

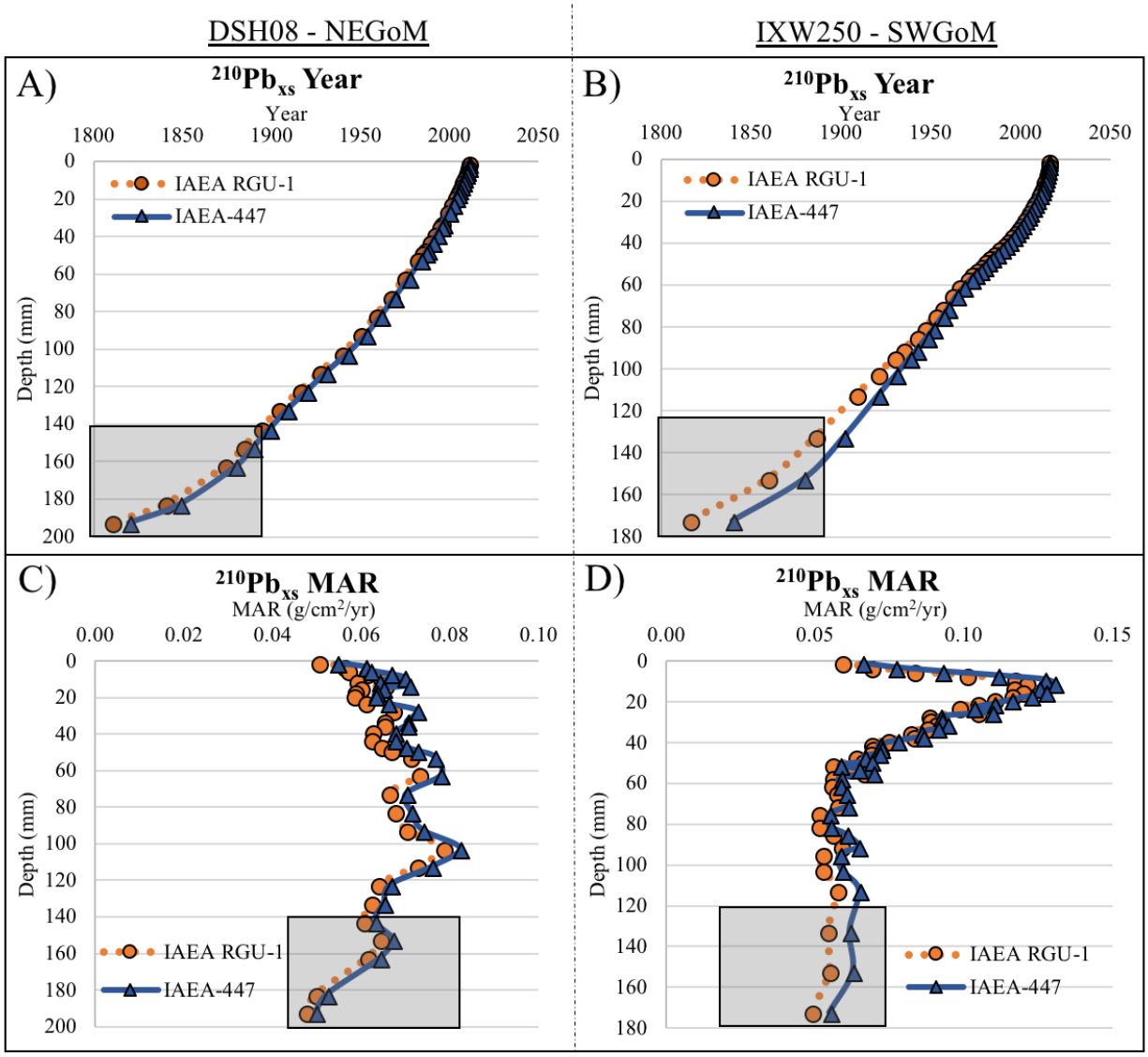

Figure 2.8. Profiles vs depth of A) core DSH08 $^{210}Pb_{xs}$ CRS chronology with depth, B) core IXW250 $^{210}Pb_{xs}$ CRS chronology with depth, C) core DSH08 $^{210}Pb_{xs}$ MAR with depth, and D) core IXW250 $^{210}Pb_{xs}$ MAR with depth using IAEA RGU-1 (orange circles) and IAEA-447 (blue triangles) calibration lines. Gray shaded box denotes dating beyond the capabilities of $^{210}Pb_{xs}$ (>120yrs). The results of CRS age models using the IAEA RGU-1 calibration lines yields lower MAR, as well as younger ages as compared to IAEA-447 CRS ages, particularly for older ages (i.e. early 1900's).

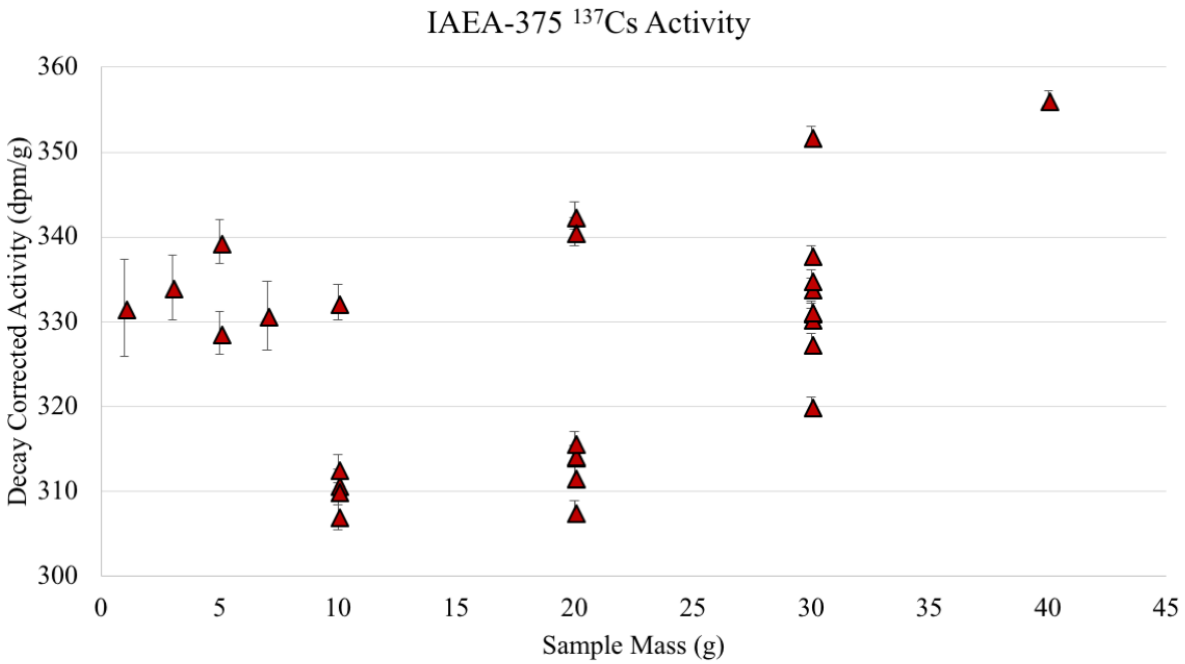

Figure 2.9. Plot of decay corrected IAEA-375 standard ^{137}Cs activities versus sample mass (g) calculated using the IAEA-447 calibration line. The known activity of the IAEA-375 is 316 dpm/g +/- 0.6 dpm/g. The IAEA-375 sediment was collected in Russia near Chernobyl and irradiated to the known activity. There is the potential for additional activity in this standard from the Chernobyl accident of 1986 leading to higher measured activities as compared to the known irradiated activity reported for this standard (Strachnov et al., 1996).

2.4 Discussion

The differences in DSH08 and IXW250 SLRad activities calculated using the IAEA RGU-1 and IAEA-447 standards are primarily a function of differences in CF values (Table 2.2, Figure 2.2). The CF value is the representation of the efficiency of measurement/detection of a specific SLRad for a specific detector. A higher CF value reflects a less efficient measurement/detection of the SLRad (e.g. fewer cpm/g detected for the same activity, dpm/g). For a specific SLRad (i.e. ^{210}Pb) the detector efficiency at the measured energy (i.e. 46keV) influences the measurement/detection of the SLRad, but this is relatively constant as compared to other variables. Variables that can influence SLRad with respect to measurement/detection that vary with analysis

of IAEA standards and sediment samples include, 1) self-absorption of standard/sample, 2) activity of standard/sample, and 3) geometry/height of standard/sample (estimated by sample mass) (Figure 2.10).

Sediment composition can influence the self-absorption of a standard/sample, with more dense sediment leading to increased self-absorption. Self-absorption occurs when gamma photons (i.e. radioisotope decay) collide with particles causing the initial gamma photon to be fragmented into multiple gamma photons of lesser energy (i.e. Compton scattering) (Nelson and Reilly, 1991). Higher self-absorption causes lower count detection and subsequently a higher CF value. Higher self-absorption causes increased occurrence of scattering of higher energy SLRad (i.e. ^{214}Bi at 609keV, and ^{137}Cs at 661kev), relative to lower energy SLRad (i.e. ^{210}Pb at 46keV and ^{234}Th at 63keV) (Nelson and Reilly, 1991; Smith and Lucas, 1991). This reduces the detection of SLRad measured at higher energies in the spectrum, as seen by the increase in CF values with increases in measured emission energy (Figure 2.2, Table 2.2). The scattering of higher energy SLRad produces lower energy gammas leading to increased noise in the lower energy range of the spectrum, which can influence detection of lower energy SLRad (Nelson and Reilly, 1991; Kitto, 1991; Plagnard et al., 2008).

Increased standard/sample activity (dpm/g) with increased gamma emissions causes increased occurrence of scattering as compared to a standard/sample of lower activity. This is particularly applicable to standards/samples that have higher activities of SLRad and emit gamma photons of higher energy. An increase in scattering due to higher activities has the same implications as increased self-absorption, with higher activities (IAEA RGU-1) leading to decreased detection of SLRad and higher CF values as compared to lower activities (IAEA-447 and sediment cores) (Table 2.2, Figure 2.2).

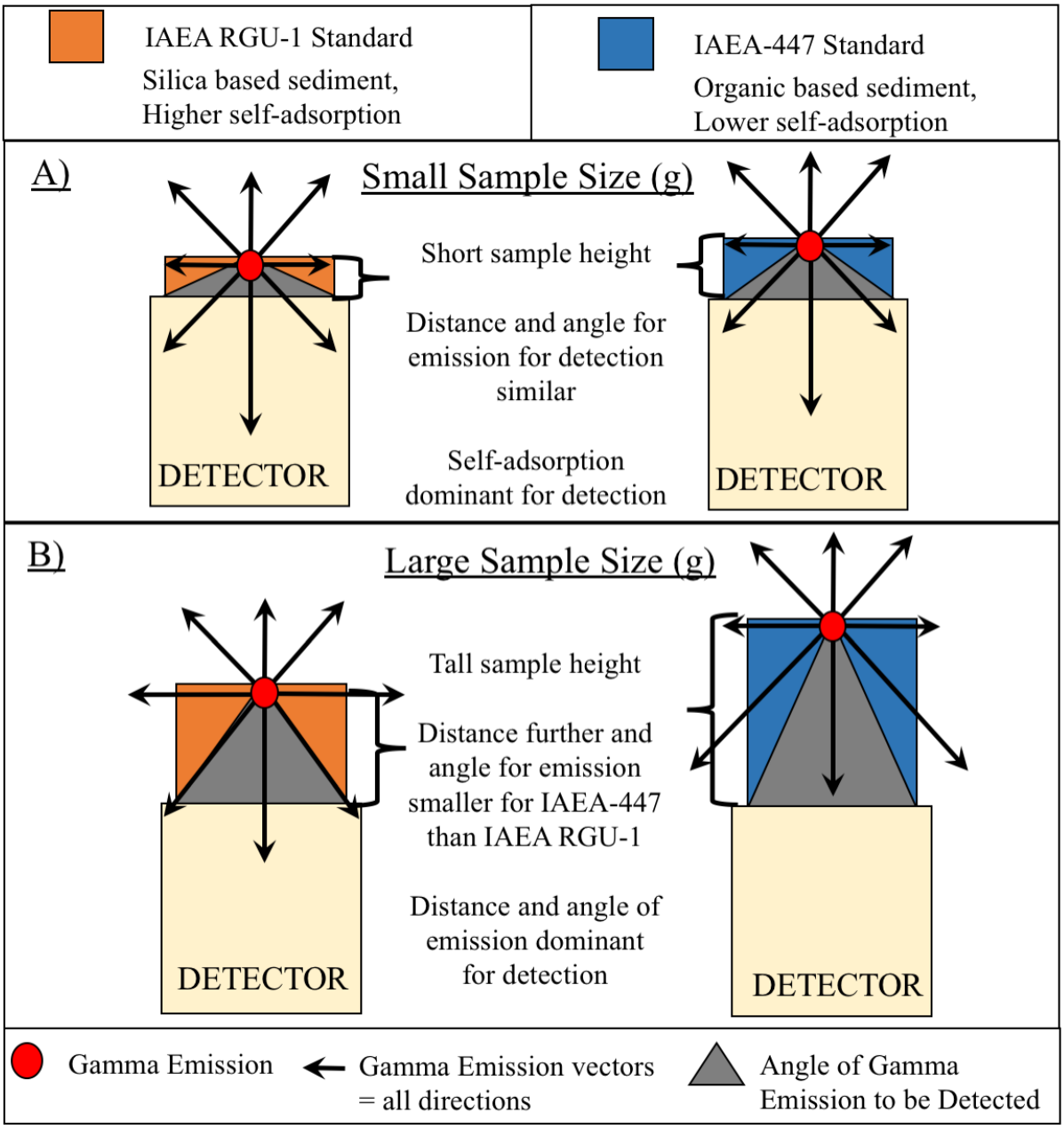

Figure 2.10. Two-dimensional diagram of variables influencing detection of gamma emissions (red circle) for the IAEA RGU-1 standard compared to the IAEA-447 standard. Gamma emission can have vectors in all directions (denoted by black arrows) and only gamma emissions that interact with the detector (angle of emissions that will be detected, denoted by gray shaded triangles) will be measured/detected. Changes in sample height (orange box for IAEA RGU-1 and blue box for IAEA-447) change the angle of emissions that are measured/detected as well as the distance emissions travel to reach the detector. Increased distance of travel increases interaction of gamma emission with particles (i.e. sediment) and increases self-absorption, lowering efficiency of measurement/detection. Differences in sediment composition lead to differences in self-absorption (i.e. Compton scattering) with the IAEA RGU-1 having higher self-absorption compared to the IAEA-447. Higher activities, particularly at higher energies, will increase self-absorption and interference at lower energies.

Sediment composition may also influence the geometry of standard/samples analyzed. A relatively low density standard/sample has a taller sample geometry for the same mass (g) as compared to a denser standard/sample. Standard/sample height can change detection of SLRad in two ways. Firstly, with increased sample height, the distance gamma emissions travel to reach the detector increases (assuming the use of a planar detector), which also increases the potential interaction with particles (sediment) and self-absorption (Figure 2.10). Secondly, sample geometry (height as estimated by sample mass) affects the percentage of gamma emissions that intercept the detector and are measured. Gamma emissions can be emitted in all directions, but with planar detectors there is a limited area of detection and only gammas emitted at acute, downward angles will intercept the detector and be measured. With increased sample height, the angles/directions for emissions to intercept the detector decreases leading to decreased detection and a higher CF value (Figure 2.10).

The expressed differences in CF values, and subsequent calculated activities of SLRad for cores DSH08 and IXW250, using the IAEA RGU-1 and IAEA-447 calibration lines are primarily a function of how these three parameters (self-absorption, activity, and geometry) change for each standard as a function of analyzed mass (Table 2.2, Figures 2.2-2.7). The IAEA RGU-1 (silica based standard) is denser and has higher self-absorption as compared to the IAEA-447 standard and the sediment core (DSH08, IXW250) sub-samples. The IAEA RGU-1 standard also has higher activities (dpm/g) than the IAEA-447 standard and sediment cores, particularly for SLRad with gamma emission at higher energy. For the IAEA RGU-1 standard, this leads to increased occurrence of scattering of the higher energy SLRad and increased noise in the lower energy SLRad range of the spectrum. Due to its higher density, the IAEA RGU-1 standard has less variability in sample height (geometry) with different sample mass. The IAEA-447 standard and

core sediment samples are of similar composition and density. They have greater variability in sample height with changes in sample mass as compared to the IAEA RGU-1 standard. For small sample masses (<10g) the sample height of the IAEA RGU-1 and IAEA-447 standards are similar and therefore sample height (geometry) is not a significant influence on the differences in CF values between the standards. The higher self-absorption, and increased scattering due to higher activities of the IAEA RGU-1 standard are the dominant influences on the lower detection of SLRad and higher CF values, as compared to the IAEA-447 (Figure 2.10) (Nelson and Reilley, 1991). For the IAEA-447, as sample mass increases sample height increases at a greater rate than RGU-1. The influence of sample height on CF values becomes more important for defining the differences between the IAEA RGU-1 and IAEA-447 as sample mass increases. For all but ^{234}Th, the CF values for IAEA-447 standard become higher than the IAEA RGU-1 CF values near 20 g sample mass (Tables 2.2, Figure 2.2). The increased height of the IAEA-447 standard decreases the detection of emissions due to longer travel distances of emissions and decreased angles/directions at which emissions will intercept the detector (Figure 2.10).

As stated, the IAEA-447 standard is an organic based sediment standard that is of similar composition to sediment cores, specifically those used in this study. Therefore, the self-absorption, activities, and change in geometry (height) with sample mass, of sediment core samples is similar to that of the IAEA-447 standard. This results in more accurate CF values, calibration lines, and calculated activities, particularly for small sample masses. The calibration of cpm/g, to determine activity (dpm/g) as a function of sample mass, is useful as it includes influences of self-absorption and sample height. This is reflected in the increased consistency and similarities in $^{210}Pb_{Sup}$ activities and ^{234}Th activities in cores DSH08 and IXW250 using the IAEA-447 standard for calibration. The IAEA-447 standard may also be utilized for determination of ^{137}Cs activities, but

further refinement may be warranted depending on the scientific objective and required accuracy of measured activity of sediment samples.

2.5 Conclusions

This approach to obtain SLRad activities for sediment records is advantageous and relatively easy to 1) execute the analysis of standards, 2) calculate conversion factors (CF), 3) create calibration lines (CF vs sample mass), and 4) determine the second order polynomial calibration equation to convert cpm/g to dpm/g for analyzed samples as a function of analyzed mass (g). It also includes the influences of self-absorption and changes in sample geometry (height/mass) in the calibration specific for each SLRad over a range of sample masses. This allows for SLRad data processing with only the calibration equation, sample mass (g), analysis time (minutes), counts of SLRad measured, and emission probability of each SLRad.

For this study, the IAEA-447 standard provided more accurate calculation of SLRad activities for the sediment cores (DSH08 and IXW250), in particular for small sample masses as compared to the IAEA RGU-1 standard. Differences in activities obtained from calibration lines using the IAEA RGU-1 and IAEA-447 standards likely influence age dating, but can also lead to significant variability when calculating SLRad inventories and investigating radioisotope distribution patterns. Therefore, it is important to determine the most appropriate calibration standard for the analyzed sediment type in order to attain high resolution SLRad age control, MAR, and inventories, specifically on short time scales such as ^{234}Th (~5 months).

Refinement and advancement in SLRad age dating is critical for accurate and high-resolution age control on sedimentary records. Improvements in the analytical methods and interpretation can produce higher temporal resolution records with increased confidence in chronologies. Further work to understand how SLRad standards can be used to improve age data

is warranted. In particular, the development of additional sediment standards that can be tailored to sediment type and composition would greatly improve the quality of SLRad data using this approach. This would aid in increasing the temporal resolution and production of high-resolution radiochronologies.

2.6 Literature Cited

Alonso-Hernandez, C.M., Diaz-Asencio, M., Munoz-Caravaca, A., Delfanti, R., Papucci, C., Ferretti, O., Crovato, C., 2006, Recent Changes in Sedimentation Regime in Cienfuegos Bay, Cuba, as Inferred from ^{210}Pb and ^{137}Cs Vertical Profiles, Continental Shelf Research, vol., 26, pg. 153-167.

Appleby, P. G., Oldfield, F., 1983, The Assessment of ^{210}Pb Data from Sites with Varying Sediment Accumulation Rates. Hydrobiologia, vol. 103, pg. 29–35.

Appleby, P.G., 2001, Chronostratigraphic Techniques in Recent Sediments, Ch 9 In: Tracking Environmental Change Using Lake Sediments Volume 1, Ed. Last, W.M., Smol, J.P., Kluwer Academic Publishers, The Netherlands.

Baskaran, M., Nix, J., Kuyper, C., Karunakara, N., 2014, Problems with the Dating of Sediment Cores Using Excess ^{210}Pb in a Freshwater System Impacted by Large Scale Watershed Changes, Journal of Environmental Radioactivity, vol., 138, pg. 355-363.

Brooks, G. R., Larson, R. A., Schwing, P. T., Romero, I., Moore, C., Reichart, G.-J., Jilbert, T., Chanton, J. P., Hastings, D. W., Overholt, W. A., Marks, K.P., Kostka, J.E., Holmes, C.W., Hollander, D., 2015, Sedimentation Pulse in the NE Gulf of Mexico Following the 2010 DWH Blowout. PLOSone, vol. 10 (7), e0132341.

Binford, M. W., 1990, Calculation and Uncertainty Analysis of ^{210}Pb Dates for PIRLA Project Lake Sediment Cores. J. Paleolimnol., vol. 3, 253–267.

Chisté, V., and Bé, M.M, 2007a, Table of Radionuclides ^{210}Pb – Comments on Evaluation of Decay Data, LNHB - Bureau International des Poids et Mesures, Vol. 8, Sevres Cedex, France, http://www.nucleide.org/DDEP_WG/DDEPdata.htm.

Chisté, V., and Bé, M.M, 2007b, Table of Radionuclides ^{214}Bi – Comments on Evaluation of Decay Data, LNHB - Bureau International des Poids et Mesures, Vol. 8, Sevres Cedex, France, http://www.nucleide.org/DDEP_WG/DDEPdata.htm.

Chisté, V., and Bé, M.M, 2010, Table of Radionuclides ^{214}Pb – Comments on Evaluation of Decay Data, LNHB - Bureau International des Poids et Mesures, Vol. 8, Sevres Cedex, France, http://www.nucleide.org/DDEP_WG/DDEPdata.htm.

Diaz-Asencio, M., Corcho Alvarado, J.A., Alonso-Hernandez, C., Quijedo-Cabezas, A., Ruiz-Fernanadez, A.C., Sanchez-Sanchez, M., Gomez-Mancebo, M.B., Froidevaux, P., Sanchez-Cabeza, J.A., 2011, Reconstruction of Metal Pollution and Recent Sedimentation Processes in Havana Bay (Cuba): A Tool for Coastal Ecosystem Management, Journal of Hazardous Materials, vol. 196, pg. 402-411.

Garrison, L.E., and Martin, R.G., Jr., 1973, Geologic Structures in the Gulf of Mexico basin, U.S. Geological Survey, Prof. Paper 773.

Helmer, R.G., Chechev, V.P., 2006, Table of Radionuclides ^{137}Cs – Comments on Evaluation of Decay Data, LNHB - Bureau International des Poids et Mesures, Vol. 8, Sevres Cedex, France, http://www.nucleide.org/DDEP_WG/DDEPdata.htm.

Holmes, C.W., 1998, Short-lived Isotopic Chronometers – A Means of Measuring Decadal Sedimentary Dynamics, U.S. Geological Survey, Dept. of the Interior, Fact Sheet FS-073-98.

IAEA, 2007, Update of X Ray and Gamma Ray Decay Data Standards for Detector Calibration and Other Applications, Volume 1: Recommended Decay Data, High Energy Gamma Ray Standards and Angular Correlation Coefficients, IAEA, Vienna, Austria, ISBN 92-0-113606-4.

IAEA, 2012, Worldwide Open Proficiency Test, Determination of Natural and Artificial Radionuclides in Moss-Soil and Water: IAEA-CU-2009-03, Vienna, Austria.

Jernelöv, A., Lindén, O., 1981, Ixtoc I: A Case Study of the World's Largest Oil Spill, Ambio, vol. 10, no. 6, pg. 299-306.

Jones, P. D.; Briffa, K. R., Osborn, T. J., Lough, J. M., van Ommen, T. D., Vinther, B. M., Luterbacher, J., Wahl, E. R., Zwiers, F. W., Mann, M. E., Schmidt, G.A., Ammann, C.M., Buckley, B.M., Cobb, K.M., Esper, J., Goosse, H., Graham, N., Jansen, E., Kiefer, T., Kull, C., Küttel, M., Mosley-Thompson, E., Overpeck, J.t., Riedwyl, N., Schulz, M., Tudhope, A.W., Villablba, R., Wanner, H., Wolff, E., Xoplaki, E., 2009, High-Resolution Palaeoclimatology of the Last Millennium: A Review of Current Status and Future Prospects. The Holocene, vol. 19 (1), pg. 3–49.

Kitto, M. E., 1991, Determination of Photon Self-Absorption Corrections for Soil Samples. Appl. Radiat. Isot., vol. 42, pg. 835–839.

Luca, A., 2008, Table of Radionuclides ^{234}Th – Comments on Evaluation of Decay Data, LNHB - Bureau International des Poids et Mesures, Vol. 8, Sevres Cedex, France, http://www.nucleide.org/DDEP_WG/DDEPdata.htm.

MacKenzie, A.B., Hardie, S.M.L., Farmer, J.G., Eades, L.J., Pulford, I.D., 2011, Analytical and Sampling Constraints in ^{210}Pb Dating, Science of the Total Environment, vol. 409, 1298-1304.

McClintic, M. A., DeMaster, D. J., Thomas, C. J., Smith, C. R., 2008, Testing the FOODBANCS Hypothesis: Seasonal Variations in near-Bottom Particle Flux, Bioturbation Intensity, and Deposit Feeding Based on 234Th Measurements. Deep Sea Res. Part II Top. Stud. Oceanogr., vol. 55 (22–23), pg. 2425–2437.

Nelson, G., Reilly. D., 1991, Gamma-Ray Interactions with Matter, Chapter 2, In Passive Nondestructive Assay of Nuclear Materials, Ed. Reilly, D., Ensslin, N., Smith, H. Jr., Kreiner, S., Office of Nuclear Regulatory Research, U.S. Nuclear Regulatory Commission, NUREG/CR-5550, ISBM 0-16-032724-5.

Passow, U., Hetland, R.D., 2016, What Happened to all the Oil?, Oceanography, Special Issue on GoMRI Deepwater Horizon Oil Spill and Ecosystem Science, vol. 29, no. 3, pg. 88-95.

Plagnard, J., Hamon, C., Lépy, M.C., 2008, Study of Scattering Effects in low-energy Gamma-ray Spectrometry, Applied Radiation and Isotopes, vol. 66, pg. 769-773, doi; 10.1016/j.apradiso.2008.02.016.

Pope, R. H., Demaster, J. D., Smith, C. R., Seltmann, H., 1996, Rapid Bioturbation in Equatorial Pacific Sediments: Evidence from Excess ^{234}Th Measurements. Deep. Res., vol. 43, pg.1339–1364.

Sanchez-Cabeza, J.A., Ruiz-Fernandez, A.C., 2012, ^{210}Pb Sediment Radiochronology: An Integrated Formulation and Classification of Dating Models, Geochimica et Cosmochimica Acta., vol. 82, pg. 183-200.

Schwing, P. T., Romero, I. C., Larson, R. A., O'Malley, B. J., Fridrik, E. E., Goddard, E. A., Brooks, G. R.; Hastings, D. W.; Rosenheim, B. E., Hollander, D. J., Grant, G., Mulhollan, J., 2016 Sediment Core Extrusion Method at Millimeter Resolution Using a Calbirated Threaded-Rod, Journal of Visualized Experiments: JoVE, vol. 114, doi: 10.3791/54363.

Smith, A.S. Jr., Lucas, M., 1991, Gamma-Ray Detectors, Chapter 3, In Passive Nondestructive Assay of Nuclear Materials, Ed. Reilly, D., Ensslin, N., Smith, H. Jr., Kreiner, S., Office of Nuclear Regulatory Research, U.S. Nuclear Regulatory Commission, NUREG/CR-5550, ISBM 0-16-032724-5.

Smith, M.L., Clark, A., Jennings, A.E., 2002, Accumultion in East Greenland Fjords and on the Continental Shelves Adjacent to the Denmark Strait Over the Last Century Based on ^{210}Pb Geochronology, Arctic, vol. 55, pg. 109-122.

Steger, H.F., 1987, The Prearation of RGU-1, A Uranium Radiometric Reference Material, In: The Preparation of Gamma-ray Spectrometry Reference Materials, RGU-1, RGTh-1, and RGK-1, Report IAEA/RL/148, Vienna, Austria.

Strachnov, V., LaRosa, J., Dekner, R., Zeisler, R., Fajgelj, A., 1996, Report of the Intercomparison run IAEA-375: Radionuclides in Soil, IAEA/AL/075, Vienna Austria.

Swarzenski, P.W., 2014, ^{210}Pb Dating, In: Encyclopedia of Scientific Dating Methods, Springer Science and Business Media, Dordrecht, doi: 10.1007/978-94-007-6326-5_236-1.

Winkler, R., Rosner, G., 2000, Seasonal and long-term variation in ^{210}Pb concentration in air, atmoshpere deposition rate and total deposition velocity in south Germany, The Science of the Total Environment, vol. 263, pg. 57-68.

Yeager, K. M., Stantschi, P. H., Owe, G. T., 2004 Sediment Accumulation and Radionuclide Inventories (^{239},^{240}Pu, ^{210}Pb and ^{234}Th) in the Northern Gulf of Mexico, as Influenced by Organic Matter and Macrofaunal Density. Mar. Chem., vol. 91, pg. 1–14.

CHAPTER THREE:

"HIGH-RESOLUTION INVESTIGATION OF EVENT DRIVEN SEDIMENTATION: NORTHEASTERN GULF OF MEXICO" Published in Anthropocene (2018)

3.1 Copyright Clearance

Appendix A: *High-resolution investigation of event driven sedimentation: northeastern Gulf of Mexico,* presents work previously published in the journal *Anthropocene*, published by Elsivier. DOI: 10.1016/j.ancene.2018.11.002, (https://doi.org/10.1016/j.ancene.2018.11.002). A complete reprint is provided with the authors' permission in Appendix C © 2018 RA Larson; Brooks, GR; Schwing, PT; Holmes, CW; Carter, SR; Hollander, DJ.

3.2 Research Overview

The original work in Appendix A and Appendix C addresses two primary objectives including 1) to describe a high-resolution approach to investigate sediment records at temporal resolutions pertinent to human time-scales (i.e. months, years, decades) for natural environmental variability as well as anthropogenic events, and 2) to present the sedimentological evolution of the depositional pulse in the northeastern Gulf of Mexico associated with the Deepwater Horizon oil spill event immediately following the event (2010) and over the subsequent 6 years at high temporal resolution. The combination of these two objectives advances the science of investigating sedimentary events with high-resolution sampling and at high temporal resolution. The application of this approach to the anthropogenic sedimentary event (Deepwater Horizon oil spill) in real time allows for the determination of the sedimentary impacts, as well as how the detection of these sedimentary impacts and the preservation of the signature of the event in the sedimentary record changes through time.

3.3 Author Contributions

The publication was primarily written by RAL with contributions and review by GRB, PTS, CWH, and SRC. Sedimentological analysis was performed, interpreted and synthesized by RAL, GRB, and SRC. Radioisotope analysis was performed, interpreted and synthesized by RAL, GRB, PTS, and CWH. The PI and co-PI on the project was DJH and GRB (respectively).

CHAPTER FOUR:

"CHARACTERIZATION OF THE SEDIMENTATION PULSE ASSOCIATED WITH THE *DEEPWATER HORIZON* BLOWOUT: DEPOSITIONAL PULSE, INITIAL RESPONSE, AND STABILIZATION" Published In: Deep Oil Spills – Facts Fate and Effects, Springer (2019)

3.1 Copyright Clearance

Appendix D: *Characterization of the sedimentation pulse associated with the Deepwater Horizon blowout: depositional pulse, initial response, and stabilization,* presents work previously published in book 1, entitled *Deep Oil Spills*, of a 2 book series, published by Springer…DOI: (web link). A complete reprint is provided with the authors' permission in Appendix D © 2019 RA Larson; Brooks, GR; Schwing, PT; Diercks, AR; Holmes, CW; Chanton, J; Diaz-Ascensio, M; Hollander, DJ.

3.2 Research Overview

The original work in Appendix D synthesizes the sedimentological response, impact, and stabilization in the northern Gulf of Mexico following the Deepwater Horizon blowout in 2010. This work is from a sedimentological perspective focusing on the application and use of radioisotopes to determine the sedimentary response to the event as well and the evolution in the sedimentary system including potential for preservation and influence of post depositional process such as re-mobilization and redistribution of oil-contaminated sediments.

3.3 Author Contributions

The publication was primarily written by RAL with contributions and review by GRB, PTS, ARD, CWH, JC, and MDA. Sedimentological analysis was performed, interpreted and synthesized by RAL and GRB. Radioisotope analysis was performed, interpreted and synthesized by RAL, GRB, PTS, and CWH. The PI and co-PI on the project was DJH and GRB (respectively).

CHAPTER FIVE:

CONCLUSIONS

5.1 Conclusions

The sedimentary impacts of the DwH blowout event on the deep-sea sedimentary environment included a depositional pulse that was able to be defined by using a high-resolution approach for investigating short-term sedimentation events. The combination of the rapid collection of cores, an annual time-series collection of cores with high-resolution sub-sampling and analysis, allowed for the use of time-sensitive indicators of sedimentation, and high temporal resolution (months) data to detect changes in sedimentation patterns associated with the DwH event. In turn, the application of these methods to an actual event in real time allowed for the adaptation and refinement of methodologies. Specifically, the analysis and interpretations of short-lived radioisotopes (SLRad) as geochronometers.

5.2 Deepwater Horizon Oil Spill

Sediment cores immediately following the 2010 DwH blowout event in the NEGoM detected recent surficial (~10-20mm) deviations in sedimentation patterns (Brooks et al., 2015). The detection of these deviations was possible due to the high-resolution methodologies developed and refined during the event and over subsequent years. As compared to downcore baselines, deviations were often subtle but were indicated by multiple independent lines of evidence showing an increase in sedimentation due to the observed MOSSFA event. Building on the identification of the depositional pulse (Brooks et al., 2015) and continued sediment studies over subsequent

years (2010-2016) the defined increases in sedimentation rates and post-event decreases (defined by $^{234}Th_{xs}$ Inventories and MARs) were a diagnostic characteristic of the depositional pulse, post-impact, and stabilization. The depositional pulse, as indicated by higher sedimentation rates and a lack of bioturbation, was only fully defined when compared to $^{234}Th_{xs}$ inventory and MARs in subsequent years, since pre-event baseline data was not available and $^{210}Pb_{xs}$ was unable to detect such short time-scales (months) events. The sedimentary signature of the depositional pulse was characterized by a decline in foraminifera and macrofaunal (Schwing et al., 2015; Montagna et al., 2018), and shifts in redox geochemistry (Hastings et al., 2016; Brooks et al,. 2015). The spatial extent of MOSSFA was indicated by increased oil-contaminated sediments at the sediment surface (Valentine et al., 2014; Chanton et al., 2015; Romero et al., 2015; Passow & Ziervogel, 2016; Romero et al., 2017; Schwing et al., 2017). Deviations in bulk sediment composition were not detectable indicating there were no major changes in sediment sources. Subtle shifts in sediment texture, % silt, were detected but were site-specific as they were relative changes as compares to baseline sedimentation patterns (Brooks et al., 2015).

The years following the depositional pulse (2011-2012) sedimentation rates as indicated by $^{234}Th_{xs}$ inventories and MARs decreased and continued absence of bioturbation as indicated by continued lower MARs persisted (Brooks et al., 2105). Deviations in sedimentation patterns became less pronounced possibly due to remobilization of the depositional pulse or the signature becoming below detection due to degradation, dilution due to mixing/bioturbation, and/or compaction of the event layer. Beginning in 2013, and continuing through 2016, site-specific return of bioturbation was seen as indicated by increases in $^{234}Th_{xs}$ apparent MARs (A-MARs), which was not supported by increases in $^{234}Th_{xs}$ inventories (Brooks et al., 2015). Sedimentation rates as indicated by $^{234}Th_{xs}$ inventories remained low and annual variability likely reflects

variability in baseline sedimentation patterns on this time-scale. A continuation of the time series and analysis of short-term sedimentation using $^{234}Th_{xs}$ would assist in defining baseline sedimentation rates on monthly time-scales. Also beginning in 2013, some sites indicated the ability of $^{210}Pb_{xs}$ to detect the depositional pulse as it was beginning to be buried in the sedimentary record. The use of $^{210}Pb_{xs}$ age control can assist in identifying if and where the sedimentation pulse is buried and preserved in the sedimentary record and possibly the influence of bioturbation, compaction, and degradation, as well as the role of remobilization and redistribution of MOSSFA derived sediments.

5.3 High-Resolution Event Stratigraphy

5.3.1 Rapid Collection and Time Series

The combination of rapid collection and time-series (annual) collection of sediment cores following the DwH blowout event was critical for identifying the immediate sedimentary response, benthic impacts, stabilization, and potential integration of the event in the sedimentary record. The rapid collection of cores allows for characterization of the sedimentary response at the most unaltered stage (2010-2011) and the use of time-sensitive indicators to define deviations in sedimentation associated with the event. This was particularly valuable for the use of $^{234}Th_{xs}$ as an indicator of higher sedimentation rates that defined the depositional pulse, which was possible due to the lack of bioturbation immediately following the depositional pulse (Brooks et al., 2015). When possible, the rapid collection of sediment cores following an event provides the opportunity to use short-lived radioisotopes such as $^{234}Th_{xs}$ (~4-5 months) and ^{7}Be (less than one year) to identify sedimentation associated with a natural or anthropogenic event. This greatly diminishes the uncertainty in age control that usually is associated with longer time-scale geochronometers such as $^{210}Pb_{xs}$. The rapid collection of cores also provides a more comprehensive assessment of

the event prior to post-depositional modification and degradation of the sedimentological, chemical and biological signatures.

A continued time-series collection of cores provides a temporal evolution of the sedimentary system following an event. The DwH time-series (2010-2016) allowed for the continuation of high temporal resolution sedimentation patterns post-event, using $^{234}Th_{xs}$ on a monthly time-scale to provide baselines as well as indications on stabilization and return of bioturbation. By using the same chronometer direct comparison of sedimentation rates and indications of bioturbated can be made. Also, this helps to define the duration of benthic impacts and how the sedimentary system evolves following such an event.

5.3.2 High-Resolution Sampling

High-resolution sub-sampling equates to high temporal resolution analyses and the ability to identify changes in sedimentation on short time-scales. Due to the short duration (months) of the DwH blowout event and subsequent strategy rapid collection of cores, the 2 mm sub-sampling of the surficial core sections provided the highest temporal resolution possible for detection of $^{234}Th_{xs}$ to identify sedimentation patterns and determine the influence of bioturbation. To maintain as comparable an approach as possible, 2 mm sub-sampling of cores collected in the years following 2010, also provided high temporal resolution dating using $^{210}Pb_{xs}$ (years to decades). As the depositional pulse was identified in the upper ~10 mm, coarser sampling resolution (>5mm), would not have been able to detect this change in sedimentation rates. The post-event decrease in sedimentation rates would not have been detected as coarser sampling would have integrated a longer time-interval of sedimentation, likely at annual scale. This would not have provided the monthly time-scale baseline provided by $^{234}Th_{xs}$ that was needed to define the depositional pulse. Coarser sampling would have also diluted the sedimentary signature of the depositional pulse, and

subtle deviations would not have been detected. As the depositional pulse layer is compacted (assuming preservation) it will require high-resolution sampling to resolve it in sedimentary records and may eventually become unresolvable.

Continued high-resolution sampling provides high temporal resolution sedimentation patterns baselines, which is critical providing pre-event information on the same time-scale as short-term events. The high-resolution approach provides short-term (seasonal to annual) variability to be defined prior to an event and to determine to what magnitude deviations in sedimentation patterns occur and if there is recovery post-event or if there is a permanent alteration of the sedimentary system. High-temporal resolution studies and baseline assessments are challenging as they often require significantly more analyses than lower resolution studies.

5.3.3 Short-lived Radioisotopes

Accurate and high-resolution age control on sedimentary records for identifying events in the sedimentation events are critical. However, with high-resolution studies, often the amount of sediment available for analysis often limited. The combination of improvements in analytical methods to accommodate small amounts of sediment and interpretations can provide high temporal resolution age control for sedimentary records of events. It is highly desirable to have multiple independent dating methods to corroborate age dating results, but this is not always possible, and due to differences in the temporal resolution of different chronometers, which may not be comparable. For example, $^{234}Th_{xs}$ can indicate sedimentation on monthly time-scales, but it is not directly comparable to $^{210}Pb_{xs}$, which integrates sedimentation on annual time-scales, and averages short-term (monthly) variability. Similarly, $^{210}Pb_{xs}$ is often not comparable to ^{14}C age dating as ^{14}C integrates longer periods of time as compared to $^{210}Pb_{xs}$ (Sadler, 1981). Therefore, multiple chronometers can be useful, but comparisons between chronometers with different temporal

resolution should be carefully considered. The combination of short-lived radioisotope chronometers can be useful to understand temporal differences in sedimentation patterns and sediment accumulation. For example, $^{234}Th_{xs}$ characterizes sedimentation but not necessarily sediment accumulation. Differences between $^{234}Th_{xs}$ and $^{210}Pb_{xs}$ may indicate that not all sedimentation is accumulating in an area and remobilization is occurring. It may also be advantageous to interpret a single short-lived radioisotope, such as $^{234}Th_{xs}$, in multiple ways including inventories for sedimentation rates, MARs for sedimentation and/or bioturbation, and profile depth.

5.4 Advancements in Event Stratigraphy

The application of a high-resolution approach for investigating the sedimentary response, impact, and stabilization of the DwH blowout on the deep-sea sedimentary environment highlights the importance of accurate time-scale with respect to such events. This includes use of SLRad of the appropriate time-scale, i.e. temporal resolution such as $^{234}Th_{xs}$. The depositional pulse (MOSSFA) was short-lived (months) and was only detectable due to the rapid collection of cores, within months, that allowed for the use of $^{234}Th_{xs}$ to identify increased sedimentation rates immediately following the event. This also applies to other time-sensitive indicators that are degraded, not preserved and/or undetectable in the sedimentary record. The approach defined in this dissertation provides a methodology to assess short-term sedimentary response and benthic impacts to evaluate how the sedimentary system stabilizes following an event and if it is permanently altered, or returns to previous conditions. The continuation of a time-series collection of sediment cores allowed for direct comparison of monthly sedimentation to characterize post-event evolution of the sedimentary system, and the integration of the longer time-scale methods such as $^{210}Pb_{xs}$. The eventual combination of multiple time-scales ($^{234}Th_{xs}$ and $^{210}Pb_{xs}$) can assess

the short event response/impact, with and longer term accumulation and modification in the sedimentary system over time including preservation potential, bioturbation/mixing, degradation, as well as resuspension and redistribution.

5.5 Chapter Summaries

5.5.1 Chapter 2: Refining Short-lived Radioisotope Geochronology Analysis and Application to High-resolution Sediment Records

In this study, short-lived radioisotope (SLRad) analysis and interpretation methods using two calibration standards are evaluated, and applied to two sediment cores from the Gulf of Mexico to determine the robustness of results and age determinations. Analyses focused on small sample masses (<10g), which are often a product of high-resolution sampling of sedimentary records to obtain high temporal resolution age control. Calibrations to convert analyzed data (counts/minute/gram) to activity (disintegrations/minute/gram) were developed using standards IAEA RGU-1 and IAEA-447 for commonly used SLRad, total ^{210}Pb, and supported ^{210}Pb (determined using ^{214}Pb and ^{214}Bi activities) to calculate excess ^{210}Pb for age dating over the past ~100 years, as well as ^{234}Th, and ^{137}Cs. Over a range of analyzed masses (1g-50g), the IAEA RGU-1 and IAEA-447 calibration lines were substantially different, particularly at the small and large analyzed masses. When applied to sediment cores collected from the Gulf of Mexico, the IAEA RGU-1 calibration overestimated all SLRad activities for samples less than 10 g. The IAEA-447 standard has a similar composition to sediment core samples and thus calibrations produced using this standard yielded more accurate activities for all SLRad. This difference (IAEA RGU-1 calibrations vs IAEA-447 calibrations) in activities led to variability in age model results and potential misinterpretation of sedimentary processes. The IAEA-447 calibration also yielded accurate calibration for ^{137}Cs when compared to a ^{137}Cs standard, IAEA-375. The

selection of the most appropriate SLRad calibration standard is critical for application to sedimentary records. The advantage of this approach is the ease of application as these calibrations also account for self-absorption and changes in sample geometry (height/mass).

5.5.2 Chapter 3: High-Resolution Investigation of Event Driven Sedimentation: Northeastern Gulf of Mexico

A rapid sedimentation pulse in the northeast Gulf of Mexico, associated with the Deepwater Horizon blowout in 2010, provided a unique opportunity to investigate a depositional event in real time and at very high resolution. Sediment cores were collected annually (2010-2016) from four sites and sub-sampled at 2 mm resolution to identify and characterize the sedimentary signature, as well as geochronology and accumulation rates using excess Lead-210 ($^{210}Pb_{xs}$) and excess Thorium-234 ($^{234}Th_{xs}$). The "time-series" collection of sediment cores on an annual basis allowed for the identification of changes in sedimentation on monthly to annual time-scales, which define the depositional pulse (2010-2011), initial post-event sedimentary impact and response (2011-2012), and post-event stabilization and preservation (2013-2016). The 2010 depositional pulse was short-lived (<1 year) with $^{234}Th_{xs}$ inventories and mass accumulation rates (MARs) indicating higher sedimentation rates and an absence of bioturbation as compared to subsequent years. The initial post-event impact/response (2011-2012) exhibited lower $^{234}Th_{xs}$ inventories and MARs indicating lower sedimentation rates. The stabilization in sedimentation (2013-2016) was indicated by site-specific apparent increases in MARs that are not supported by increased $^{234}Th_{xs}$ inventories, reflecting the re-establishment of bioturbation. Initially, $^{210}Pb_{xs}$ was unable to detect the sedimentation pulse, but with subsequent sedimentation and burial, it begins to resolve the event after 3-5 years. The ability to resolve the sedimentation pulse and the following short-term

response was possible due to the high-resolution sampling and analysis, unconventional methodologies, and utilization of high sedimentation rates.

5.5.3 Chapter 4: Characterization of the Sedimentation Associated with the *Deepwater Horizon* Blowout: Depositional Pulse, Initial Response, and Stabilization

The *Deepwater Horizon* (DWH) blowout led to a depositional pulse in the northeast Gulf of Mexico in the Fall of 2010 associated with an observed Marine Oil Snow Sedimentation and Flocculent Accumulation (MOSSFA) event. A time series (2010-2016) of annually collected sediment cores at four sites characterize the sedimentary response to the event, post event, and stabilization/recovery. The depositional pulse (2010-2011) was characterized by high sedimentation rates with little to no bioturbation and large excursions in % silt. The lack of changes in sediment composition indicate that the same sediment sources dominated during the event, but the rates of sedimentation increased. In the years following the event (2011-2012) sedimentation rates were lower, and bioturbation was absent, and the initial excursions in % silt began to become undetectable in the sedimentary record. Between 2013 and 2016, a spatially and temporally variable return of bioturbation was detected at most sites. Sedimentation rates at all sites remained low, but increases in $^{234}Th_{xs}$ apparent mass accumulation rates indicated a return of bioturbation and potential stabilization and/or recovery of the sedimentary system. The deepest site (~1500 m) did not have any indication of bioturbation as of the 2016 collections, which may reflect a lack of recovery or that bioturbation was never present. In 2012, $^{210}Pb_{xs}$ age dating began to resolve the depositional pulse suggesting it may be applied to determine changes in the pulse deposit over time, and/or its preservation in the sedimentary record. Factors that may influence preservation include burial, bioturbation, degradation of the pulse signature, and re-mobilization of pulse sediments.

5.6 Literature Cited

Brooks, G. R., Larson, R. A., Schwing, P. T., Romero, I., Moore, C., Reichart, G.-J., Jilbert, T., Chanton, J. P., Hastings, D. W., Overholt, W. A., Marks, K.P., Kostka, J.E., Holmes, C.W., Hollander, D., 2015, Sedimentation Pulse in the NE Gulf of Mexico Following the 2010 DWH Blowout, PLOSone, vol. 10 (7), e0132341.

Chanton J., Zhao T., Rosenheim B.E., Joye S., Bosman S., Bruner C., Yeager K.M., Diercks A.R., Hollander D., 2015, Using Natural Abundance Radiocarbon to Trace the Flux of Petrocarbon to the Seafloor Following the Deepwater Horizon Oil Spill. Environmental Science and Technology, vol. 49(2), pg. 847–854 http://doi.org/10.1021/es5046524

Hastings, D.W., Schwing, P.T., Brooks, G.R., Larson, R.A., Morford, J.L., Roeder, T., Quinn, K.A., Bartlett, T., Romero, I.C., Hollander, D.J., 2016, Changes in Sediment Redox Conditions Following the BP DwH Blowout Event, Deep Sea Res. Part II Topical Studies in Oceanography, vol. 129, pg. 167–178.

Valentine, D.L., Fisher, G.B., Bagby, S.C., Nelson, R.K., Reddy, C.M., Sylva, S.P., 2014, Fallout Plume of Submerged Oil from Deepwater Horizon, PNAS, vol. 111(45), pg. 15906-15911, doi.org/10.1073/pnas.1414873111.

Montagna PA, Girard F (2020) Deep-sea benthic faunal impacts and community evolution before, during and after the Deepwater Horizon event (Chap. 22). In: Murawski SA, Ainsworth C, Gilbert S, Hollander D, Paris CB, Schlüter M, Wetzel D (eds) Deep oil spills – facts, fate and effects. Springer, Cham.

Romero I.C., Schwing P.T., Brooks G.R., Larson R.A., Hastings D.W., Ellis G.E., Goddard E.A., Hollander D.J., 2015, Hydrocarbons in Deep-Sea Sediments Following the 2010 Deepwater Horizon Blowout in the Northeast Gulf of Mexico, PLOSone, vol. 10(5), e0128371.

Romero I.C., Toro-Farmer G., Diercks A.R., Schwing P.T., Muller-Karger F., Murawski S., Hollander D.J., 2017, Large Scale Deposition of Weathered Oil in the Gulf of Mexico Following a Deepwater Oil Spill, Environmental Pollution, vol. 228, pg. 179-189 http://dx.doi.org/10.1016/j.envpol.2017.05.019.

Sadler P., 1981, Sedimentation Rates and the Completeness of Stratigraphic Sections, Journal of Geology, vo. 89, pg. 569–584

Schwing, P.T., Romero, I.C., Brooks, G.R., Hastings, D.W., Larson, R.A., Hollander, D.J., 2015, A Decline in Deep-Sea Benthic Foraminifera Following the Deepwater Horizon Event in the Northeastern Gulf of Mexico, PLOSone, vol. 10 (3), pg. 1–14.

Schwing P.T., Brooks G.R., Larson R.A., Holmes C.W., O'Malley B.J., Hollander D.J., 2017, Constraining the Spatial Extent of the Marine Oil Snow Sedimentation and Accumulation (MOSSFA) Following the DWH Event Using a $^{210}Pb_{xs}$ Inventory Approach, Environmental Science & Technology, vol. 51, pg. 5962−5968. DOI: 10.1021/acs.est.7b00450

APPENDIX A:

CHAPTER THREE:

"HIGH-RESOLUTION INVESTIGATION OF EVENT DRIVEN SEDIMENTATION: NORTHEASTERN GULF OF MEXICO" Published In Anthropocene (2018)

Anthropocene 24 (2018) 40–50

Contents lists available at ScienceDirect

Anthropocene

journal homepage: www.elsevier.com/locate/ancene

Invited Research Article

High-resolution investigation of event driven sedimentation: Northeastern Gulf of Mexico

Rebekka A. Larson[a,b,*], Gregg R. Brooks[a], Patrick T. Schwing[b], Charles W. Holmes[c], Savannah R. Carter[a], David J. Hollander[b]

[a] Eckerd College, Marine Science Dept., 4200 54th Ave S., St. Petersburg, FL, 33711, United States
[b] University of South Florida, College of Marine Science, 140 7th Ave. S., St. Petersburg, FL, 33701, United States
[c] Environchron, 3988 Emerald Chase Dr., Tallahassee, FL, 32308, United States

ARTICLE INFO

Article history:
Received 25 July 2018
Received in revised form 9 November 2018
Accepted 10 November 2018
Available online 12 November 2018

Keywords:
High-resolution stratigraphy
Short-lived radioisotopes
Geochronology
Event stratigraphy
Sedimentology
Gulf of Mexico

ABSTRACT

A rapid sedimentation pulse in the northeast Gulf of Mexico, associated with the Deepwater Horizon blowout in 2010, provided a unique opportunity to investigate a depositional event in real time and at very high resolution. Sediment cores were collected annually (2010-2016) from four sites and sub-sampled at 2 mm resolution to identify and characterize the sedimentary signature, as well as geochronology and accumulation rates using excess Lead-210 ($^{210}Pb_{xs}$) and excess Thorium-234 ($^{234}Th_{xs}$). The "time-series" collection of sediment cores on an annual basis allowed for the identification of changes in sedimentation on monthly to annual time-scales, which define the depositional pulse (2010-2011), initial post-event sedimentary impact and response (2011-2012), and post-event stabilization and preservation (2013-2016). The 2010 depositional pulse was short-lived (<1 year) with $^{234}Th_{xs}$ inventories and mass accumulation rates (MARs) indicating higher sedimentation rates and an absence of bioturbation as compared to subsequent years. The initial post-event impact/response (2011-2012) exhibited lower $^{234}Th_{xs}$ inventories and MARs indicating lower sedimentation rates. The stabilization in sedimentation (2013-2016) was indicated by site-specific apparent increases in MARs that are not supported by increased $^{234}Th_{xs}$ inventories, reflecting the re-establishment of bioturbation. Initially, $^{210}Pb_{xs}$ was unable to detect the sedimentation pulse, but with subsequent sedimentation and burial, it begins to resolve the event after 3-5 years. The ability to resolve the sedimentation pulse and the following short-term response was possible due to the high-resolution sampling and analysis, unconventional methodologies, and utilization of high sedimentation rates.

1. Introduction

High-resolution studies of sedimentation in aquatic systems have become popular over the past few decades to investigate short-term (inter-annual to inter-decadal scale) events, which are essential elements of natural and anthropogenically-enhanced global environmental fluctuations. The development of very high-resolution techniques and their application to aquatic settings have considerably improved our capabilities to investigate these short-term events. The opportunity to study, in real time, how an event is manifested in the sedimentary record enables us to improve the ability to interpret event scale features in the geologic record, as well as characterize events that may not be detected in longer-term sedimentary records due to lack of analytical resolution and or preservation.

The 2010 Deepwater Horizon (DwH) blowout in the northeastern Gulf of Mexico occurred over the course of 87 days and provided a unique opportunity to investigate, at very high-resolution, the sedimentary impacts of a singular event in real time (Passow and Hetland, 2016). The surface oil slick (petrogenic) from the 2010 blowout (Fig. 1) combined with biogenic particles, lithogenic particles, and exopolymeric substances that were released as a stress response from surface dwelling organisms, resulting in a massive marine snow event (Passow et al., 2012; Daly et al., 2016; Passow and Ziervogel, 2016; Ziervogel et al., 2012). The marine snow lost buoyancy, stripped particulates out of the water column, and rapidly settled to the sea floor in what has since become known as "marine oil snow sedimentation and flocculent accumulation" (MOSSFA) (Daly et al., 2016). In sediment cores collected in the fall of 2010 and early 2011, this was manifested as a 10-20 mm thick blanket of sediment representing a short-term

* Corresponding author at: Eckerd College, Marine Science Dept., 4200 54th Ave S., St. Petersburg, FL, 33711, United States.
E-mail address: larsonra@eckerd.edu (R.A. Larson).

https://doi.org/10.1016/j.ancene.2018.11.002
2213-3054/

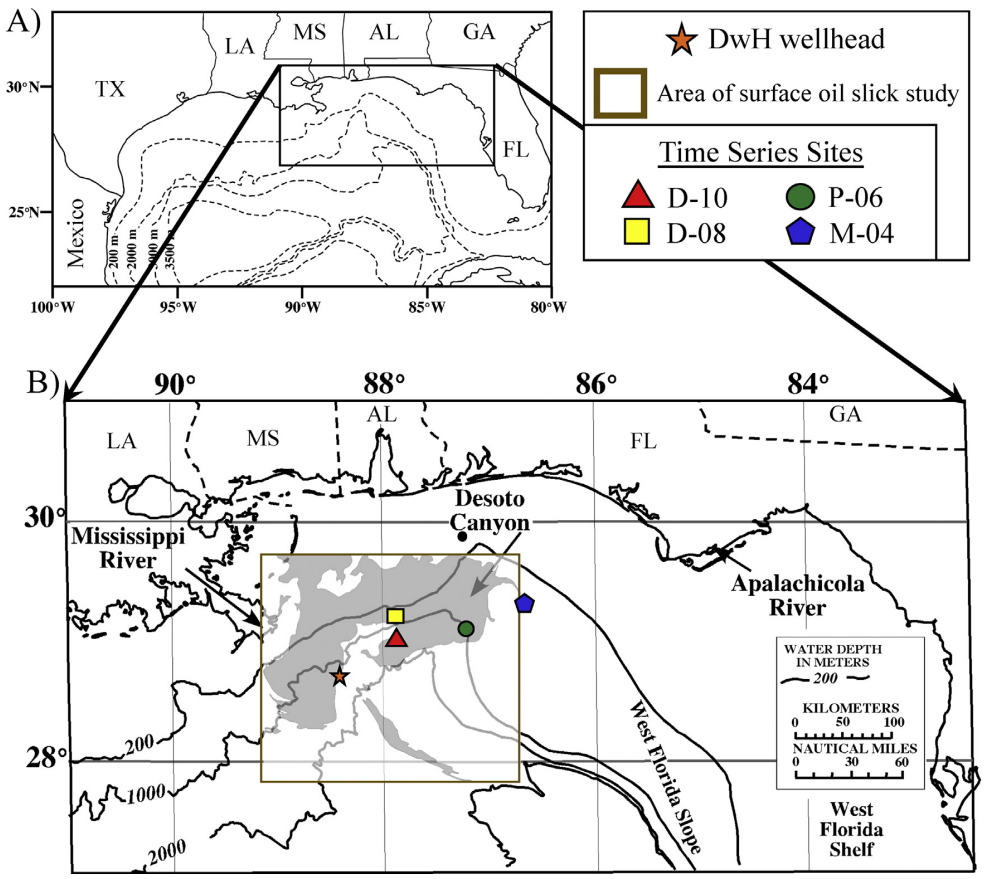

Fig. 1. Maps showing physiographic features of the Gulf of Mexico and core site locations. "DwH" is Deepwater Horizon, "TX" is Texas, "LA" is Louisiana, "MS" is Mississippi, "AL" is Alabama, "Ga" is Georgia, and "FL" is Florida: (A) Map of Gulf of Mexico indicating study area; (B) Map of study area in the northeastern Gulf of Mexico showing location of the Deepwater Horizon wellhead, time series sites (M-04, P-06, D-08, and D-10), and extent of the sea surface oil slick (gray shading within brown box, from Garcia-Pineda et al., 2013) modified from Brooks et al. (2015).

(months) depositional pulse defined by high sedimentation rates (Brooks et al., 2015). The depositional pulse contained sea surface characteristics, including pyrogenic hydrocarbons from surface burning (Romero et al., 2015), increased planktic foraminifera accumulation rates

(Fridrik et al., 2016) and chloroplast 16SRNA gene sequences (Brooks et al., 2015). Additionally, bottom-dwelling organisms such as benthic foraminifera were absent (Schwing et al., 2015), and bioturbation in surface sediments was shutdown (Brooks et al., 2015). It also resulted in a rapid upward shift in the redox boundary within surficial sediments (Brooks et al., 2015; Hastings et al., 2016). Studies showed that the MOSSFA event affected broad areas of the continental slope and shelf, with estimates ranging from 1,030 to 35,425 km^2 (Valentine et al., 2014; Chanton et al., 2015; Romero et al., 2015; Passow and Ziervogel, 2016; Romero et al., 2017; Schwing et al., 2017; Stout and German, 2017).

The detection of the depositional pulse in the sedimentary record required the rapid collection of cores, analysis of geochronological and sedimentological samples using new methodologies, the unconventional use of current methodologies, and standard methodologies at high-resolution. The annual collection of cores at the same sites created a geologic time-series, with analysis of cores collected between 2010 and 2012 identifying the depositional pulse associated with the DwH blowout (Brooks et al., 2015). Here we build on the short-lived radioisotope records from cores collected between 2010 and 2102 and sedimentology records collected between 2010 and 2011 presented by Brooks et al. (2015). The continuation of the annual time-series (2013-2016) and the continued high-resolution analysis of all cores collected between 2010 and 2016 provides a means to determine baseline sedimentation on monthly time-scales for direct comparison to further define the characteristics of the depositional pulse. It also describes the evolution of the sedimentary system over the subsequent years and the preservation potential of the depositional pulse in the geologic record.

2. Methods

A total of 73 core sites were occupied between 2010 and 2016 in the northeastern Gulf of Mexico following the 2010 DwH blowout event, ranging from ~100 m to >1500 m water depths along the Florida, Alabama, Mississippi, and Louisiana outer continental margins (Fig. 1, Table 1). This includes the annual collection of cores at four time-series sites (M-04, P-06, D-08, and D-10) using the same methods as presented by Brooks et al. (2015) to allow for direct comparison and interpretation of the entire 2010-2016 time-series (Fig. 1, Table 1). An Ocean Instruments MC – 800 multicorer was used to collect up to eight cores per deployment, with minimal

Table 1
Site location information including Collection Date, Latitude, Longitude, Water Depth (m is meters), the distance of re-collection at each site in subsequent years with respect to the collection in 2010, and distance of 2010 site from the DwH wellhead (2010-2012 cores from Brooks et al., 2015). Km is Kilometer, N is north, NE is northeast, NW is northwest, NNE is north northeast, E is east, W is west, WSW is west south west, WNW is west northwest, SE is southeast.

Site ID	Collection Date	Latitude	Longitude	Water Depth (m)	Direction/ Distance from 2010 collection	Distance from DwH wellhead
M-04	Nov. 2010	29.30465	−86.67677	400	0 km	178 km
M-04	Oct. 2012	29.30575	−86.67637	384	N 0.1 km	
M-04	Aug. 2013	29.30733	−86.67492	397	NE 0.3 km	
M-04	Aug. 2014	29.30733	−86.67492	399	NE 0.3 km	
M-04	Aug. 2015	29.30242	−86.66390	407	E 1.3 km	
M-04	Aug. 2016	29.30495	−86.67858	412	W 0.2 km	
P-06	Dec. 2010	29.09983	−87.26550	1043	0 km	117 km
P-06	Sept. 2011	29.13328	−87.26097	990	N 4.4 km	
P-06	Aug. 2012	29.12270	−87.26622	1011	N 3.0 km	
P-06	Aug. 2013	29.12455	−87.26375	940	N 3.2 km	
P-06	Aug. 2014	29.12285	−87.26547	1008	N 3.0 km	
P-06	Aug. 2015	29.12533	−87.26083	1023	N 3.4 km	
P-06	Aug. 2016	29.12407	−87.26568	1000	N 3.3 km	
D-08	Dec. 2010	29.12092	−87.86545	1143	0 km	65 km
D-08	Sept. 2011	29.12058	−87.86998	1130	WSW 0.8 km	
D-08	Aug. 2012	29.12278	−87.86773	1130	NW 0.6 km	
D-08	Aug. 2013	29.12630	−87.87147	1098	NW 1.6 km	
D-08	Aug. 2014	29.12297	−87.86818	1127	NW 0.7 km	
D-08	Aug. 2015	29.12283	−87.86813	1123	NW 0.6 km	
D-08	Aug. 2016	29.12077	−87.86803	1130	WSW 0.5 km	
D-10	Dec. 2010	28.97667	−87.87333	1520	0 km	57 km
D-10	Feb. 2011	29.09882	−87.86603	1500	NNE 1.5 km	
D-10	Sept. 2011	28.97617	−87.86833	1520	E 0.5 km	
D-10	Aug. 2012	28.97905	−87.89162	1504	W 1.8 km	
D-10	Aug. 2013	28.97363	−87.86810	1520	SE 0.6 km	
D-10	Aug. 2014	28.97812	−87.89063	1520	W 1.7 km	
D-10	Aug. 2015	28.97940	−87.89133	1490	W 1.8km	
D-10	Aug. 2016	28.98030	−87.89190	1495	WNW 1.8 km	

disturbance to surface sediments. For each site and collection, a core was extruded for short-lived radioisotope geochronology, which is non-destructive, and the same sediment was utilized for sedimentology analysis. For each site and collection, a core was split longitudinally for photography and visual description to assess stratigraphic integrity.

2.1. Extrusions, dry bulk density/porewater

The cores used for geochronology and sedimentology were extruded at 2 mm intervals from the sediment surface (0 mm) to depths downcore ranging from 20 to 100 mm to ensure the highest possible resolution of recently deposited sediments, and subsequently at 5 mm intervals to the base of the core. Cores were volumetrically extruded according to the method described in Schwing et al. (2016) using a calibrated threaded rod (1 turn = 2 mm) attached to a tight-fitting plunger to push the core vertically upward through a flat acrylic surface where samples were carefully extracted. Sample volume was calculated using the inner diameter of the core barrel and sampling interval (i.e., height). Once extruded, samples were weighed immediately to provide the wet mass required for determining pore water content. Each sample was then freeze-dried and weighed for dry mass to calculate dry bulk density (Appleby, 2001; Binford, 1990; Sanchez-Cabeza and Ruiz-Fernandez, 2012). Extruded samples were then analyzed for short-lived radioisotope geochronology and sedimentology as described in Sections 2.2 and 2.3.

2.2. Sedimentology

Sediment texture and composition analyses were conducted on extruded samples and included grain size, and calcium carbonate content (%$CaCO_3$). Grain size was determined by wet sieving the sample through a 63 μm screen. The fine-size (<63 μm) fraction was analyzed by pipette (Folk, 1965) to measure the relative percentage of silt (%silt) and clay (%clay). The sand-size (>63 μm) fraction was volumetrically too small to analyze further and is reported here as %sand. Carbonate content was determined by the acid leaching method according to Milliman (1974). Where there was not sufficient sediment from an interval for both sediment texture and composition, only sediment texture was performed.

2.3. Short-lived radioisotope geochronology

Samples were analyzed for short-lived radioisotopes by gamma spectrometry on Series HPGe (High-Purity Germanium) Coaxial Planar Photon Detectors for activities of total Lead-210 ($^{210}Pb_{Tot}$) at 46.5 kiloelectron volts (keV), Lead-214 (^{214}Pb) at 295 keV and 351 keV, Bismuth-214 (^{214}Bi) at 609 keV, and total Thorium-234 ($^{234}Th_{Tot}$) at 63 keV. Samples were also analyzed for Cesium-137 (^{137}Cs) at 661 keV, and Berilium-7 (^{7}Be) at 477 keV, but these radioisotopes were below detection in all samples and therefore will not be discussed. Data were corrected for emission probability at the measured energy, counting time, sample mass, and converted to activity (disintegrations per minute per gram, dpm/g), using the International Atomic Energy Association (IAEA) organic standard IAEA-447 for calibration by a method similar to Kitto (1991). The IAEA-447 organic standard, which has a similar density to the sediment analyzed in this study, was analyzed over a range of sample masses (1 g, 3 g, 5 g, 7 g, 9 g, 12 g, 15 g, 17 g, 20 g, 30 g, 40 g and 50 g) as a proxy for geometry (IAEA, 2012). A calibration equation was produced for each radionuclide, defining the relationship between the measured counts per minute per gram to the known activity of the standard over the range of sample masses. By using this approach of calibration over a range of sample masses, factors that can influence the detection of radionuclides and how they may change with sample geometry (mass), is included in the calibration (i.e., self-absorption, detector efficiency, cascade summing, etc.) (Hussain et al., 1996; Larson et al., 2017). The Cutshall method (Cutshall et al., 1983) was used on

select sediment samples, and results show that the self-absorption and variability are negligible and within detection error. Analytical error, determined from analysis of the known standard, IAEA-447, were all <3% of the measured activities.

With a half-life of ~24 days, excess Thorium-234 ($^{234}Th_{xs}$) is usually only detectable at the sediment surface. Supported Thorium-234 ($^{234}Th_{Sup}$) was determined by reanalysis of the same sample >120 days (~5 half-lives) after core collection as well as the comparison to downcore intervals (deeper than 20 mm, e.g., all $^{234}Th_{xs}$ decayed). The $^{234}Th_{Sup}$ activity was subtracted from the $^{234}Th_{Tot}$ activity to determine the $^{234}Th_{xs}$ activity. Activities of $^{234}Th_{xs}$ were decay corrected for activity lost due to natural decay between the time of core collection and sample analysis. Although $^{234}Th_{xs}$ is typically used as an indicator of surface mixing (e.g., bioturbation) (McClintic et al., 2008; Pope et al., 1996; Yeager et al., 2004), it can be used as a geochronological tool where sediments are deposited rapidly and are unmixed (Brooks et al., 2015).

The activities of the ^{214}Pb (295 keV), ^{214}Pb (351 keV), and ^{214}Bi (609 keV) were averaged as a proxy for the Radium-226 (^{226}Ra) activity of the sample or the "supported" Lead-210 ($^{210}Pb_{Sup}$) that is produced in situ (Baskaran et al., 2014; MacKenzie et al., 2011; Smith et al., 2002; Swarzenski, 2014). The $^{210}Pb_{Sup}$ activity was subtracted from the $^{210}Pb_{Tot}$ activity to calculate the "unsupported" or "excess" Lead-210 ($^{210}Pb_{xs}$), which is used for dating within the last ~100 years.

Investigating the ability of $^{210}Pb_{xs}$ age dating to detect the sedimentation pulse in subsequent years (2012-2016) was performed using the Constant Rate of Supply (CRS) model as it is appropriate under conditions of varying accumulation rates, which is common in sedimentary systems, and it is one of the most widely used age models (Appleby, 2001; Binford, 1990; Appleby and Oldfield, 1983). For each core, activity values vs. depth down core were plotted, and CRS model results applied to assign a date to each sample. Mass accumulation rates (MARs) were calculated for each data point (i.e., "date"), thereby giving MARs over the past ~ 100 years. The use of MARs corrects for differential sediment compaction down core, thereby enabling a direct comparison of $^{210}Pb_{xs}$ accumulation rates throughout the core. Linear accumulation rates from the CRS age model (cm/yr) were multiplied by the dry bulk density (g/cm^3) to calculate MARs (g/cm^2/yr). Dry bulk density (g/cm^3) was calculated by dividing the sediment dry weight (g) by the sampling volume (cm^3). The sampling volume was calculated as the volume of a cylinder using the inner diameter of the core barrel and the sample interval as the height of the cylinder.

Recognizing that $^{234}Th_{xs}$ profiles may represent deposition and not bioturbation, $^{234}Th_{xs}$ MARs were calculated according to the same equation as above using linear accumlation rates determined using the CRS model results in the same fashion as $^{210}Pb_{xs}$.

Sediment inventories of $^{234}Th_{xs}$ were calculated according to the method described in Baskaran and Santschi (2002) by multiplying the dry bulk density (g/cm^3) of the interval by the activity (dpm/g) and the thickness of the interval (cm). All $^{234}Th_{xs}$ inventories were determined using decay corrected $^{234}Th_{xs}$. Sediment inventories are independent of $^{234}Th_{xs}$ profile depth(s) and, therefore, not influenced by bioturbation.

3. Results

Sediment cores (100-550 mm in length) collected between 2010 and 2016 using the MC-800 multicorer showed little disturbance of the sediment water interface, with clear water overlying sediments when retrieved. The most recent sedimentation (surface) was intact allowing for high-resolution sampling (2 mm) over the surficial intervals and analyses for geochronology and sedimentology. Therefore, impacts to stratigraphy are dominantly attributed to in situ mixing by primarily bioturbation and not due to the coring process. Cores generally consisted of homogenous tan to tannish-gray sandy muds, to muds with a surficial dark brown to black unit, occasionally with multiple dark brown to black layers within this surficial unit. X-radiography of a subset of selected cores showed no visible stratigraphy or layering.

3.1. Extrusions, dry bulk density/porewater

From volumetrically extruded sediment sub-samples (2 mm and 5 mm sampling resolution) porewater content ranged between 50% and 88%, with increasing porewater content upcore. The surficial (0-20 mm) section of cores ranged between 65% and 88% porewater content. Sample sizes (g) for 2 mm sub-samples ranged between 0.8 g and 10 g, with most between 4 g and 7 g. Porewater content and sub-sample sizes (g) were comparable to those reported by Brooks et al. (2015) for the 2010-2012 collections.

3.2. Sedimentology - texture and composition

Sediments at all sites consisted dominantly of mud, with an increase in sand, in the eastern, carbonate dominated, portion of the study area. All sites contained low to no gravel size sediment. These are consistent with sedimentology reported by Brooks et al. (2015) for cores collected in 2010 and 2011 (they did not present sedimentology results from 2012 cores).

Cores collected from site M-04, over the time series (2012-2016), exhibited %sand ranging from 1.5% to 29.8%, with a decrease in %sand upcore, especially in the surficial 0-20 mm to 0-30 mm. Silt content ranged from 40.4% to 67.3% and with an increase in % silt upcore, especially in the surficial 0-20 mm to 0-30 mm, concurrent with the decrease in %sand. Clay content ranged from 21.9% to 48.4% and showed little variation throughout all cores. Carbonate content ranged from 50.7% to 61.9% with little to no variability.

Cores collected from site P-06, over the time series (2012-2016), exhibited %sand ranging from 0.1% to 4.7%, with little variation throughout. Silt and clay content exhibited an inverse relationship, with %silt ranging from 3.8% to 83.6% and %clay ranging from 8.0% to 95.8%. Carbonate content ranged from 30% to 42.8% and showed a slight decrease upcore with a slight decrease in the very surficial sediments.

Cores collected from site D-08, over the time series (2012-2016), exhibited %sand ranging from 0.0% to 2.0%, with little variation throughout. Silt and clay content exhibited an inverse relationship, with %silt ranging from 15.6% to 83.7% and %clay ranging from 31.7% to 95.8%. Carbonate content ranged from 18.6% to 62.9% with an increase upcore.

Cores collected from site D-10, over the time series (2012-2016), exhibited %sand ranging from 0.0% to 8.9%, with little variation throughout. Silt and clay content exhibited an inverse relationship, with %silt ranging from 5.0% to 51.5% with an increase in %silt in the surficial 0-30 mm, and %clay ranging from 47.5% to 92.0%. Carbonate content ranged from 20.3% to 39.1% with a decrease upcore from 250 mm to 150 mm, variability from 150 mm to 60 mm, and a slight increase from 60 mm to the surface.

3.3. Short-lived radioisotopes

Short-lived radioisotope analyses yielded activity profiles for decay corrected $^{234}Th_{xs}$ and $^{210}Pb_{xs}$ for all collection years for all sites with good consistency between collection years at each site, specifically with respect to $^{210}Pb_{xs}$ (Fig. 2, Fig. 3). Inventories and MARs determined using $^{234}Th_{xs}$ for each site over the time series allowed for comparison of short-term (months) sedimentation

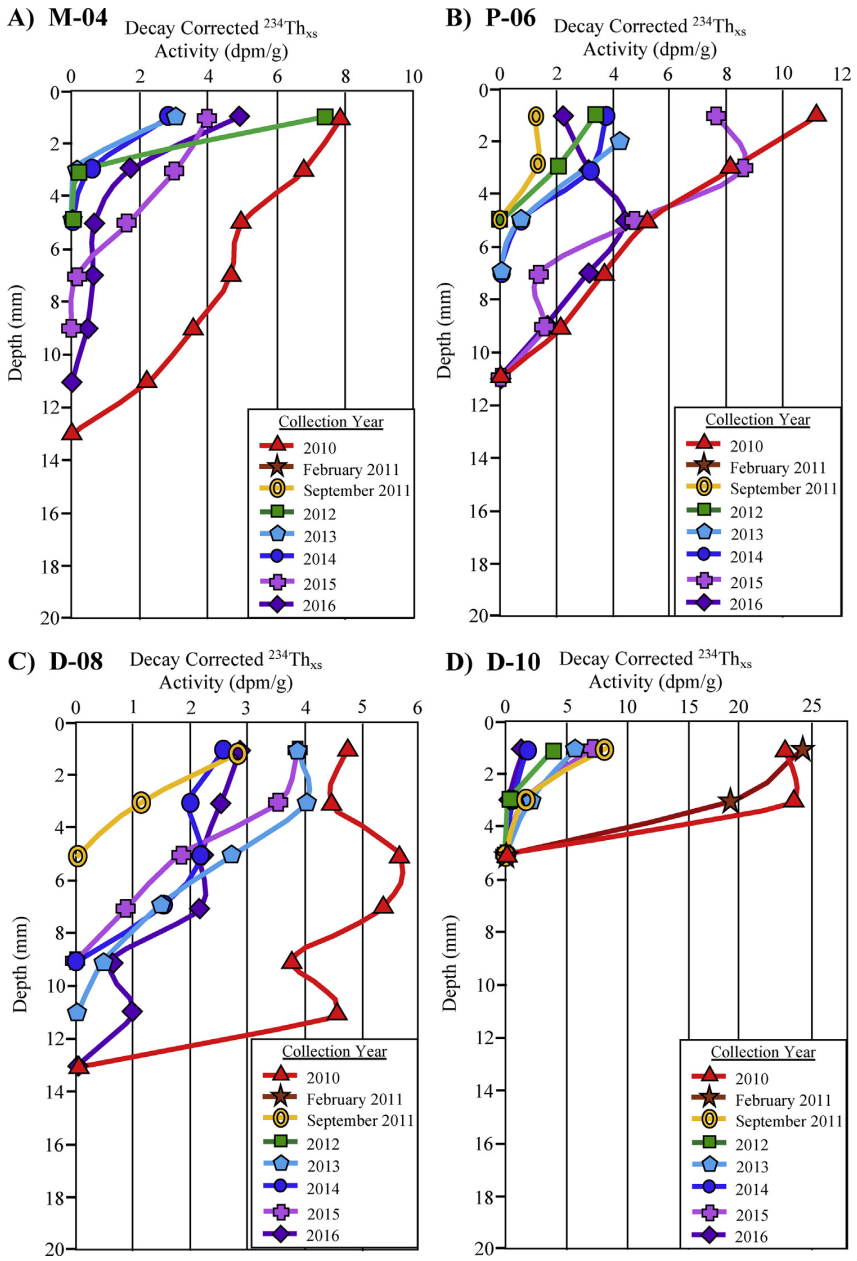

Fig. 2. Decay Corrected $^{234}Th_{xs}$ profiles vs. depth (mm) for time-series sites A) M-04, B) P-06, C) D-08, and D) D-10 collected in 2010, February 2011, September 2011, 2012 (2010-2012 cores from Brooks et al., 2015), 2013, 2014, 2015 and 2016 (note error bars not visible). Note the higher activities and deeper profiles in 2010 and February 2011, the decrease in activity and profile depth between September 2011 and 2012 and the increase in profile depths between 2013 and 2016 at sites M-04, P-06 and D-08.

processes for direct comparison of the event detected by Brooks et al. (2015) in the fall of 2010 and early 2011 to subsequent years (2012-2016) (Fig. 2, Fig. 4, Table 2).

Activities of $^{234}Th_{Tot}$ for site M-04 ranged between 0.7 dpm/g and 5.8 dpm/g with an average below 20 mm of 1.3 dpm/g (a proxy for $^{234}Th_{Sup}$). Activities of $^{234}Th_{Tot}$ for site P-06 ranged between 0.8 dpm/g and 6.4 dpm/g with an average below 20 mm of 1.4 dpm/g (a proxy for $^{234}Th_{Sup}$). Activities of $^{234}Th_{Tot}$ for site D-08 ranged between 0.8 dpm/g and 3.4 dpm/g with an average below 20 mm of 1.6 dpm/g (a proxy for $^{234}Th_{Sup}$). Activities of $^{234}Th_{Tot}$ for site D-10 ranged between 0.7 dpm/g and 4.8 dpm/g with an average below 20 mm of 1.2 dpm/g (a proxy for $^{234}Th_{Sup}$). For all sites collected over the time series (2010-2012 presented by Brooks et al., 2015, and 2013-2016 from this study), $^{234}Th_{xs}$ profile depths ranged from 0.2 to 1.2 cm downcore (Fig. 2, Table 2). Calculated $^{234}Th_{xs}$ inventories ranged from 0.04 dpm/cm^2 to 1.7 dpm/cm^2 with higher values in 2010 and early 2011, and decreased in subsequent collection years for all sites. Apparent MARs (A-MARs) $^{234}Th_{xs}$ values ranged from 0.2 g/cm^2/yr to 2.0 g/cm^2/yr. Higher A-MARs values in 2010 and early 2011 were concurrent with higher

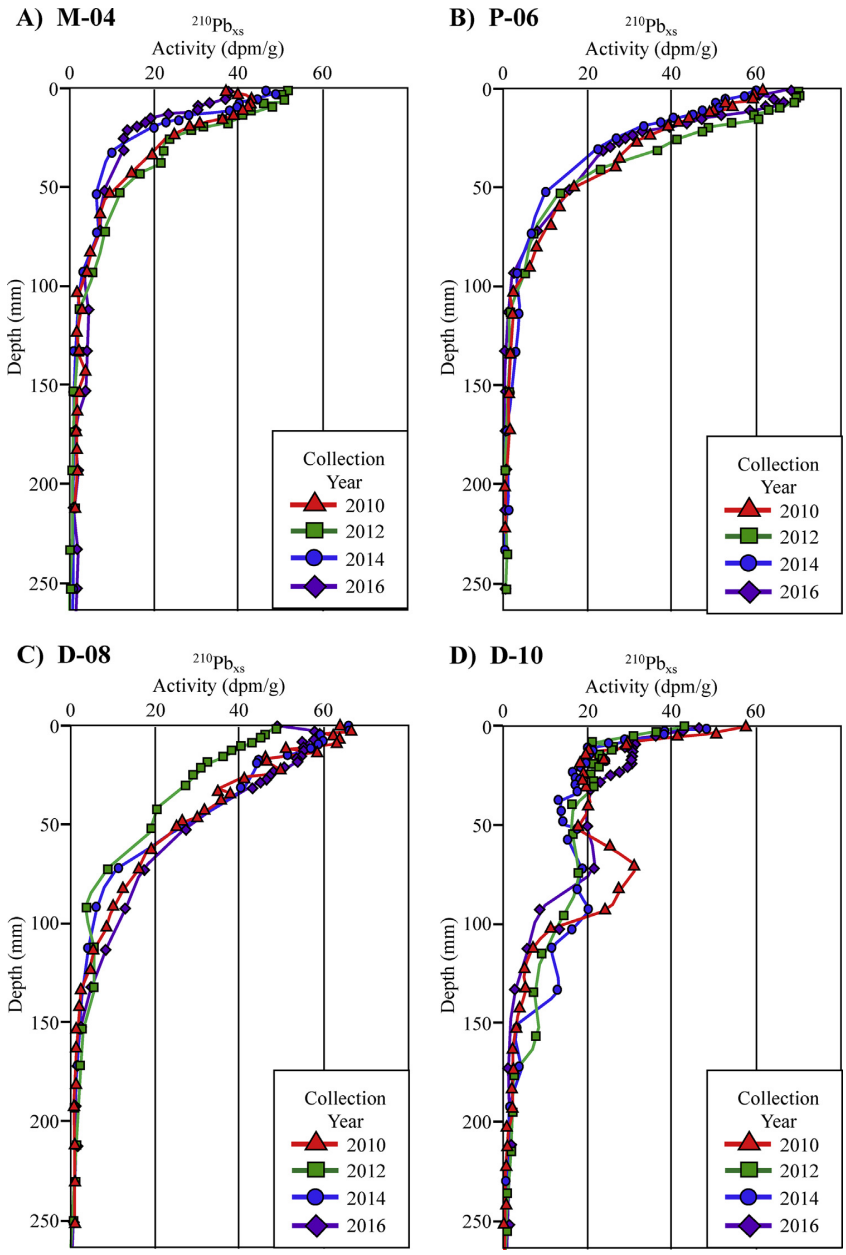

Fig. 3. Excess Lead-210 profiles vs. depth (mm) for time-series sites A) M-04, B) P-06, C) D-08, and D) D-10 collected in 2010 (2010 cores from Brooks et al., 2015), 2012, 2014 and 2016 (note error bars not visible. Note the reproducibility of profiles at all sites.

inventories. In subsequent collection years, A-MARs vary and increase without an increase in inventory, but the timing and occurrence are site specific, with the first observance at site D-08 followed by P-06 and M-04. Site D-10, to date, has shown no increase in A-MARs (Fig. 4, Table 2).

Activities of $^{210}Pb_{Sup}$ for site M-04 ranged between 0.8 dpm/g and 1.7 dpm/g with an average of 1.1 dpm/g and $^{210}Pb_{xs}$ surface activities ranged from 37.5 dpm/g to 51.5 dpm/g, with near to exponential profiles to depths between 150 mm and 200 mm downcore (Fig. 3). For site P-06, $^{210}Pb_{Sup}$ activities ranged between 1.2 dpm/g and 2.6 dpm/g with an average of 1.7 dpm/g and $^{210}Pb_{xs}$ surface activities ranged from 56.4 dpm/g to 70.4 dpm/g, with near to exponential profiles to depths between 150 mm and 200 mm downcore (Fig. 3). Activities of $^{210}Pb_{Sup}$ for site D-08 ranged between 1.2 dpm/g and 2.6 dpm/g with an average of 1.7 dpm/g and $^{210}Pb_{xs}$ surface activities for sites D-08 ranged from 37.5 dpm/g to 66.2 dpm/g, with near to exponential profiles to depths between 200 mm and 250 mm downcore (Fig. 3). For site D-10 $^{210}Pb_{Sup}$ activities ranged between 1.3 dpm/g and 3.3 dpm/g with an average of 2.0 dpm/g and $^{210}Pb_{xs}$ surface activities for sites D-10 ranged from 42.8 dpm/g to 70.9 dpm/g with, $^{210}Pb_{xs}$ profiles deviating from exponential to depths between 200 mm and 250 mm downcore (Fig. 3). Age dating of $^{210}Pb_{xs}$ profiles using the Constant Rate of Supply model provided

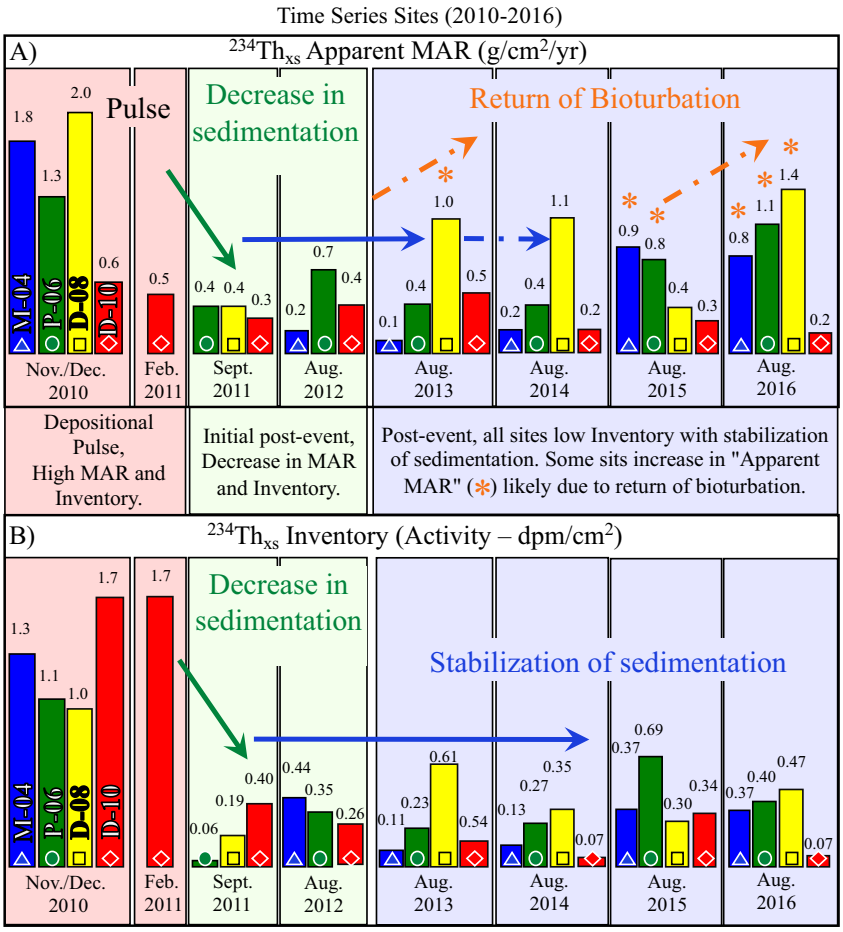

Fig. 4. Decay corrected $^{234}Th_{xs}$ apparent MARs (A-MARs) and inventories for the four time series sites collected between 2010 (2010-2012 cores from Brooks et al., 2015) and 2016 showing the evolution of sedimentation associated with the depositional pulse (pink shading), the initial post-event impact and response (green shading) and post-event stabilization and preservation (blue shading) (A) $^{234}Th_{xs}$ A- MARs of the four time series sites showing high A-MARs of the depositional pulse associated with the DwH blowout event (pink shading), decrease in A-MARs initial post-event (green shading), and site specific increases in A-MARs (orange *) that is not supported by the inventories, likely due to the return of bioturbation (blue shading); (B) $^{234}Th_{xs}$ inventories of the four time series sites showing high inventories (i.e. increased flux to the seafloor) of the depositional pulse associated with the DwH blowout event (pink shading), and decrease in inventories post-event (green and blue shading) as sedimentation patterns stabilized (data in Table 2).

sub-decadal to annual resolution ages and MARs. Mass Accumulation Rates for the time series sites were relatively consistent at each site between collections and deviations in the surficial units did not exceed downcore variability.

3.4. High-resolution analysis/sampling

Due to the small amount (1-10 g) of sediment available at high resolution sampling, some analyses were limited. Short-lived radioisotopes analysis required extended counting time (48 h) to increase peak counts and decrease analytical error, as well as data processing (measured counts to activity, dpm/g) using calibration lines established using a sediment standard (IAEA-447) of similar sedimentological characteristics as sediment analyzed from cores collected in this study. This approach proved to be of critical importance as activities of small samples size (<10 g) were more influenced to a greater degree by the calibration standard used as compared to larger sample sizes (Larson et al., 2017).

4. Discussion

The annual collection of sediment cores (2010-2016) at the four sites allowed for the investigation of the sedimentation event at the most unaltered stage (2010-2011) immediately following deposition, and the evolution of the sedimentary signature over subsequent years (2011-2016). It was critical to determine sedimentation patterns and rates on the same time-scale as the depositional event (months) for direct comparison. Due to the annual time-series core collections, $^{234}Th_{xs}$ could be utilized to identify variability in sedimentation on monthly scales over the 2010-2016 collection period due to the annual time-series core collections. The 2 mm sub-sampling of the surficial core sections provided the highest temporal resolution possible for detection of $^{234}Th_{xs}$ to identify sedimentation and determine influence of bioturbation. The 2 mm sub-sampling also provided high temporal resolution dating using $^{210}Pb_{xs}$ (years to decades) to determine the variability in sedimentation over the past ~100 years at annual

resolution, as well as assess the burial and preservation of the sedimentation event in the record (2012-2016) (Fig. 3).

4.1. Depositional pulse 2010–2011 - detecting the event

The depositional pulse detected in cores collected in late 2010 to early 2011 has been well documented (Brooks et al., 2015; Romero et al., 2015; Schwing et al., 2015; Hastings et al., 2016), and as such will be discussed here only in terms of the high-resolution methodologies utilized to detect the event. High-resolution sampling and analysis is critical for the detection of the depositional pulse in the sedimentary record. The 10–20 mm thick surficial layer was detectable as a result of the 2 mm sampling resolution yielding five samples per 10 mm for analyses versus the integration of 10 mm or more of sediment and thus, minimizing the dilution of the sedimentary signature. This was important for all analyses, but in particular for the time-series of $^{234}Th_{xs}$ as 10 mm sampling would not have detected $^{234}Th_{xs}$ profiles for the cores collected over the 6-year period (Fig. 2, Table 2). Using a coarser sampling resolution, the direct comparison of $^{234}Th_{xs}$ inventories, MARs, and A-MARs of the event, and post-event evolution would not have been detectable over the six-year period.

Detection of the depositional pulse that resulted in a 10-20 mm thick sediment layer required the unconventional use of $^{234}Th_{xs}$ as a geochronological tool. Due to the short (~24 day) half-life, $^{234}Th_{xs}$ has traditionally been used to determine the depth of bioturbation (McClintic et al., 2008; Pope et al., 1996; Yeager et al., 2004). The $^{234}Th_{xs}$ decay profiles allowed for the identification of the 10-20 mm thick sediment layer deposited within a 4-5 month period. The $^{234}Th_{xs}$ decay profiles were discernable due to the exceptionally high (2 mm) resolution sampling, the high sedimentation rate (Fig. 2) and the lack of bioturbation, such that the stratigraphy throughout the surficial 10-20 mm was intact (Brooks et al., 2015).

Excess ^{234}Th MARs and inventories (Fig. 4, Table 2) from the initial 2010-2011 collections appeared abnormally high over the surficial 10-20 mm (Brooks et al., 2015). Down-core $^{210}Pb_{xs}$ geochronologies recorded MARs an order of magnitude lower than surficial rates based on $^{234}Th_{xs}$ (Table 2). However, rates calculated by different methods representing different time frames cannot be directly compared due to the differences in time scales involved, which is commonly referred to as the Sadler Effect (Sadler, 1981). Unfortunately, the rapid increase in MARs of the depositional pulse that was detected using $^{234}Th_{xs}$ could not be confirmed initially (2010-2011), because pre-event $^{234}Th_{xs}$ data were unavailable for direct comparison. Additionally, analyses of cores collected before the depositional pulse, as well as down-core samples in this study, could not be utilized to detect pre-event $^{234}Th_{xs}$, as all pre-event $^{234}Th_{xs}$ had decayed to undetectable levels due to the short half-life (24 days, i.e., analysis within 4-5 months of core collection). Consequently, confirmation of the pulse required post-event assessment to document the decrease in $^{234}Th_{xs}$ MARs and inventories over the years following the event (Brooks et al., 2015).

With few exceptions, sedimentological parameters over the 10-20 mm-thick pulse layer showed little change compared to underlying sediments. Exceptions include the silt content, which exhibited major excursions in the surfaces of cores collected in late 2010 and early 2011 (Fig. 5). In the 2010 collections silt content (% silt) increased by ~10% at site M-04, and ~20% at site D-08, while site P-06 decreased by ~40% and site D-10 decreased by ~15%, which at this stage cannot be fully explained. However, all cores revealed a major change in silt content from underlying sediments, suggesting a significant deviation in sedimentation processes during 2010 and 2011. Compositionally, there were no detectable changes in carbonate content (%carbonate). The consistency in composition was initially problematic in that there are two distinct sedimentological regimes (carbonate-dominated east of DeSoto Canyon and siliceous-dominated west of DeSoto Canyon) (Harbison, 1968), and the increase in MARs would suggest an increase in one sediment source over the other, rather than the unlikely scenario of equivalent increases in both sediment types. However, MOSSFA stripped the overlying water column of particulates that would have eventually settled to the sea floor in each of the two sediment regimes, so composition may not be expected to change measurably (Brooks et al., 2015).

4.2. Post-event 2011–2012 - initial response

Cores collected annually at the four time series sites (Fig. 1, Table 1) in September 2011 and August 2012 exhibit a substantial decrease and apparent stabilization in $^{234}Th_{xs}$ MARs and inventories (Fig. 4, Table 2), which suggests a decrease in the rate of deposition by up to 90% (site M-04 between 2010 and 2012). The use of inventories and MARs, based on the same radioisotope ($^{234}Th_{xs}$), corroborates the initial observation that the sedimentation rates for the depositional pulse were exceptionally high, and eliminated any potential Sadler Effect. The corresponding decrease in $^{234}Th_{xs}$ inventories adds further support as inventories are a function of the $^{234}Th_{xs}$ flux associated with sediment delivery to the seafloor and are independent of bioturbation.

Short-lived radioisotope data for cores collected in August 2012 show that the 2010 depositional pulse began to be resolved by $^{210}Pb_{xs}$ (half-life ~22.3 years) methods (Fig. 6) in little more than two years following the event. The existence of several adjacent

Table 2
Decay Corrected $^{234}Th_{xs}$ profile depth, Apparent Mass Accumulation Rates (A-MARs), and Inventories for the four time series sites collected between November 2010 (2010-2012 cores from Brooks et al., 2015) and August 2016.

Site ID	Decay Corrected $^{234}Th_{xs}$	Nov. 2010	Dec. 2010	Feb. 2011	Sept. 2011	Aug. 2012	Oct. 2012	Aug. 2013	Aug. 2014	Aug. 2015	Aug. 2016
M-04	Profile depth (mm)	12	NC[1]	NC[1]	NC[1]	NC[1]	4	4	4	8	10
M-04	A-MARs (g/cm^2/yr)	1.76	NC[1]	NC[1]	NC[1]	NC[1]	0.20	0.10	0.24	0.90	0.83
M-04	Inventory (dpm/cm^2)	1.34	NC[1]	NC[1]	NC[1]	NC[1]	0.44	0.11	0.13	0.37	0.37
P-06	Profile depth (mm)	NC[1]	12	NA[2]	4	4	NC[1]	4	6	10	10
P-06	A-MARs (g/cm^2/yr)	NC[1]	1.31	NA[2]	0.40	0.70	NC[1]	0.40	0.40	0.80	1.1
P-06	Inventory (dpm/cm^2)	NC[1]	1.06	NA[2]	0.06	0.35	NC[1]	0.23	0.27	0.69	0.40
D-08	Profile depth (mm)	NC[1]	12	NA[2]	4	NA[2]	NC[1]	10	8	6	12
D-08	A-MARs (g/cm^2/yr)	NC[1]	2.00	NA[2]	0.40	NA[2]	NC[1]	1.00	1.10	0.40	1.40
D-08	Inventory (dpm/cm^2)	NC[1]	1.04	NA[2]	0.19	NA[2]	NC[1]	0.61	0.35	0.30	0.47
D-10	Profile depth (mm)	NC[1]	4	4	4	0.4	NC[1]	4	2	4	4
D-10	A-MARs (g/cm^2/yr)	NC[1]	0.61	0.50	0.25	0.44	NC[1]	0.50	0.23	0.30	0.19
D-10	Inventory (dpm/cm^2)	NC[1]	1.68	1.69	0.40	0.26	NC[1]	0.54	0.07	0.34	0.07

[1] NC = No core collected.
[2] NA = Not analyzed within the timeframe to detect $^{234}Th_{xs}$.

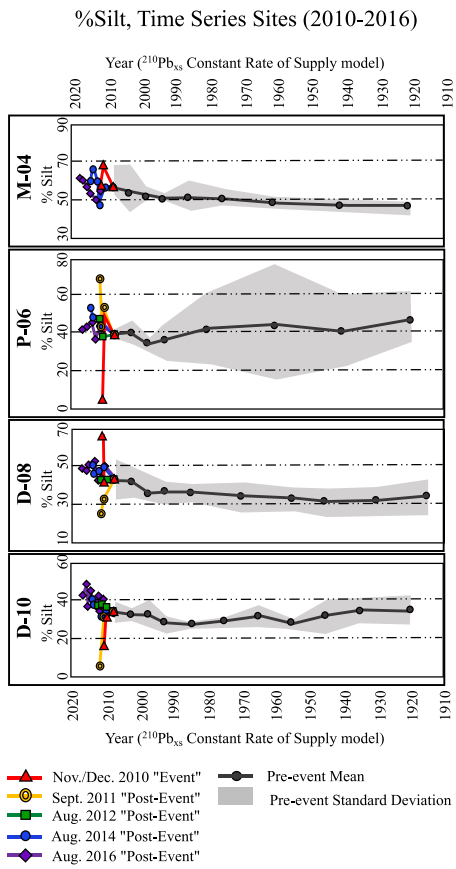

Fig. 5. Sediment texture represented as %silt content of four time series sites collected between 2010 (2010-2011 cores from Brooks et al., 2015) and 2016 showing the increased variability associated with the depositional event (red) and initial post-event (yellow, and green), and post-event stabilization (blue and purple) to similar pre-event downcore values and ranges (black and gray shading).

core-depth intervals exhibiting similar $^{210}Pb_{xs}$ activities (dpm/g) is consistent with the interpretation that they are all approximately the same age and therefore deposited at the same time (Fig. 6). The lack of similar adjacent core-depth activities (dpm/g) in the surfaces of cores collected in 2010 illustrates the ineffectiveness of using $^{210}Pb_{xs}$ within ~5 months after the event as the ~22.3 year half-life is too long to resolve the event in this time frame.

Texturally, the silt content in surficial sediments is less variable in cores collected in 2011 and 2012 as compared to those collected in 2010, with most cores exhibiting a stabilization in %silt closer to pre-event values (Fig. 5). Below the surficial 10-20 mm (i.e., the depositional pulse layer), sediments show little variability in silt content suggesting a relatively stable sedimentological regime for >100 years preceding the depositional pulse. It also confirms the high reproducibility of sampling and analysis and suggests little spatial heterogeneity in the sedimentology. Compositionally, sediments continued to show little temporal variability in carbonate content.

4.3. Post-event 2013–2016 - stabilization and preservation

Cores collected annually at the four time series sites from 2013 to 2016 showed that some aspects of the sedimentary system maintained continuity with the 2011 and 2012 collections, while other aspects of the system deviated. As shown in Fig. 4 and Table 2, site D-08 exhibited an apparent increase in $^{234}Th_{xs}$ MARs (A-MARs) beginning in August 2013, while sites M-04 and P-06 recorded increases beginning in August 2015. These A-MARs are not supported by increases in $^{234}Th_{xs}$ inventories, which remained relatively stable from late 2011 through August 2016 (Fig. 4, Table 2). Therefore, the increases in $^{234}Th_{xs}$ A-MARs are likely due to the re-establishment of bioturbation and not increases in the rates of deposition. Bioturbation likely mixed $^{234}Th_{xs}$ downward in the sediment column giving the false impression of an increase in accumulation rate, but the stability in $^{234}Th_{xs}$ inventories, which is independent of bioturbation, recorded no increase in the flux of $^{234}Th_{xs}$ to the sediments (Fig. 2, Table 2). The reason(s) that bioturbation re-established at different times at different sites remains unknown, as does the reason why there is still no evidence of bioturbation at site D-10, which may mean the system remains in transition. $^{210}Pb_{xs}$ dating continues to progressively resolve the depositional pulse from the 2012-2016 collections (Fig. 6). Activities (dpm/g) of the depositional pulse layer remained relatively stable between ~2012 and 2016.

The silt content is even less variable, remaining near pre-event values (Fig. 5). Down core (pre-event) values continue to support a relatively stable sedimentological regime over the >100 years prior to the depositional pulse, as well as the high reproducibility of sampling and analysis, and lack of spatial heterogeneity. There continues to be little temporal variability in carbonate content.

4.4. Synthesis 2010–2016 - evolution of event in the sedimentary system

The 2010 depositional pulse associated with the DwH oil spill and MOSSFA was short-lived as $^{234}Th_{xs}$ MARs and inventories relaxed and stabilized within ~1 year. It is only speculation at this point that they returned to pre-event rates because pre-event data are either nonexistent in the case of $^{234}Th_{xs}$, or not comparable (i.e., pre-event MARs were calculated using $^{210}Pb_{xs}$, which is not comparable to $^{234}Th_{xs}$ MARs). The decrease and stabilization of $^{234}Th_{xs}$ MARs and inventories over the six years following the depositional pulse were documented, using high-resolution sampling and analyses allowing for the measurement of inventories and MARs based upon the same radioisotope ($^{234}Th_{xs}$). Throughout the 2013-2016 collections, the 2010 depositional pulse remains preserved in the sedimentary record in some aspects, manifested as a rapid, but short-lived increase in MARs that is beginning to be resolved by $^{210}Pb_{xs}$ dating. The apparent increase in $^{234}Th_{xs}$ MARs in some cores beginning in 2013 is not a function of increased sedimentation, but is likely due to the return of bioturbation as the A-MARs increases in $^{234}Th_{xs}$ are not supported by increases in inventories. Bioturbation appears to have returned at the majority of the time-series sites through 2016, but still others (e.g., D-10) have yet to record a return of bioturbation suggesting the system is still in transition.

Sedimentologically, the initial deviation in %silt content has not been preserved past ~2011-2012, which may be due to the return of bioturbation (at some sites), or alternatively, sediments may have become compacted to the extent that the pulse layer is no longer detectable with respect to %silt. It is unknown at this stage whether the complete return of bioturbation will mix the surface sediments to the extent that the remaining characteristics of the pulse signature will become unresolvable, or whether the signature will eventually become buried below the bioturbation depth, thereby resulting in long-term preservation. Continued time series sampling and high-resolution analysis would help to answer this question.

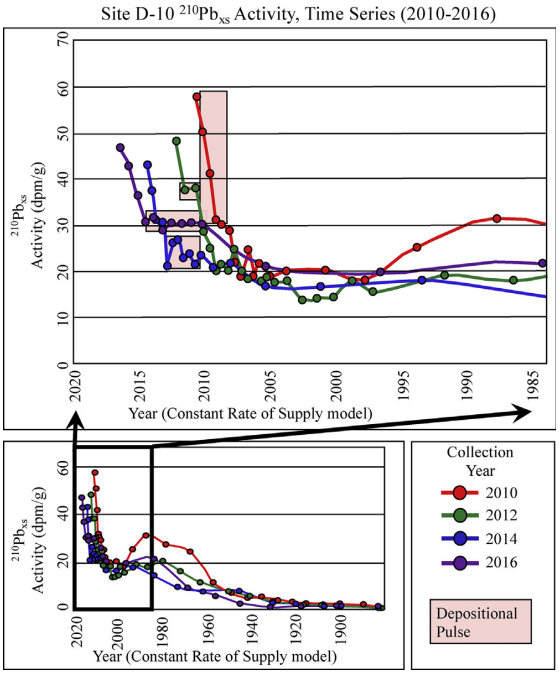

Fig. 6. Constant Rate of Supply age dating versus $^{210}Pb_{xs}$ activities for time series site D-10 showing consistency in profiles of cores collected between 2010 and 2016 and the ability of $^{210}Pb_{xs}$ to resolve the depositional pulse, primarily beginning in 2012. Pink shading denotes sections of the profile that have adjacent intervals with similar $^{210}Pb_{xs}$ activities, indicating similar age/single deposit associated with the depositional pulse with the exception of 2010, which is recording the depositional pulse in real time.

5. Conclusions

The ability to detect individual depositional events in the geologic record requires a number of factors. First, and most importantly, it is critical to have a well-preserved and undisturbed sedimentary record of the event. This begins with the careful collection and handling of cores that are most likely to contain sedimentation from the event and yield the best-preserved sedimentary record. The sub-sampling resolution (i.e., 2 mm vs. 5 mm vs. cm-scale) of sediment cores determines the temporal resolution that can be investigated depending on the event and objectives. However, it should be considered that records sampled at high temporal resolution may reflect short-term environmental variability that is undetectable in lower resolution studies. For example, finer sampling resolution may detect sedimentation associated with seasonal changes in surface productivity (e.g., months scale), whereas coarser resolution sampling averages sedimentation on longer time-scales (e.g., annual-decadal-centennial) and may not detect such short-term variations. This potential difference in temporal scale can also influence radiometric dating when using multiple radioisotopes with very different half-lives such as $^{234}Th_{xs}$ (monthly short-term variability) and $^{210}Pb_{xs}$ (annual to decadal variability). Comparison of accumulation rates determined using two distinctly different time scales are generally not comparable (e.g., the Sadler Effect), but can provide information with respect to processes on different time-scales. With this said, it is highly desirable to have independent dating methods for corroboration, which might be difficult at the event scale. Finally, although valid for any investigation, it is especially important for high-resolution investigations to have multiple independent lines of evidence, as they may help alleviate many of the challenges mentioned above.

Here we sampled accurately at 2 mm intervals, as shown by the repeatability of down-core $^{210}Pb_{xs}$ profiles and %silt values, and adapted analyses to accommodate the small sample sizes. This allowed the use of $^{234}Th_{xs}$ and $^{210}Pb_{xs}$ geochronologies to provide monthly to annual-scale resolution respectively. The combination of $^{234}Th_{xs}$ inventories and MARs from the 6 year time-series of cores allowed for the identification of the depositional pulse associated with the DwH blowout, as well as post-event stabilization of the sedimentary system and site specific return of bioturbation.

High-resolution studies can aid in our understanding of event-scale processes that can be important indicators of longer-term environmental change. This also includes the generation of baseline information (i.e., pre-event) at high temporal resolution (i.e., event scale) for better determination of impacts of events on the sedimentary system and their preservation in the sedimentary record. Detection of event-scale processes in the geologic record is becoming more feasible with recent improvements in technological capabilities.

Acknowledgments

This research was made possible by a grants from The Gulf of Mexico Research Initiative C-IMAGE I, C-IMAGE II, and DEEP-C consortia, as well as NSF RAPID grant 1049586. Data are publicly available through the Gulf of Mexico Research Initiative Information & Data Cooperative (GRIIDC) at https://data.gulfresearchinitiative.org (doi: 10.7266/N7FJ2F94, doi: 10.7266/N79S1PJZ, doi: 10.7266/N7610XTJ). We would like to acknowledge the assistance in field collection by the Florida Institute of Oceanography including the crew of the R/V Weatherbird II, the assistance in laboratory analyses by multiple Eckerd College students over the duration of this project.

Appendix A. Supplementary data

Supplementary material related to this article can be found, in the online version, at doi:https://doi.org/10.1016/j.ancene.2018.11.002.

References

Appleby, P.G., 2001. Chronostratigraphic techniques in recent sediments, Ch 9. In: Last, W.M., Smol, J.P. (Eds.), Tracking Environmental Change Using Lake Sediments, 1. Kluwer Academic Publishers, The Netherlands.
Appleby, P.G., Oldfield, F., 1983. The assessment of ^{210}Pb data from sites with varying sediment accumulation rates. Hydrobiologia 103, 29–35.
Baskaran, M., Santschi, P.H., 2002. Particulate and dissolved ^{210}Pb activities in the shelf and slope regions of the Gulf of Mexico waters. Cont. Shelf Res. 22, 1493–1510.
Baskaran, M., Nix, J., Kuyper, C., Karunakara, N., 2014. Problems with the dating of sediment cores using excess ^{210}Pb in a freshwater system impacted by large scale watershed changes. J. Environ. Radioact. 138, 355–363.
Binford, M.W., 1990. Calculation and uncertainty analysis of ^{210}Pb dates for PIRLA project lake sediment cores. J. Paleolimnol. 3, 253–267.
Brooks, G.R., Larson, R.A., Schwing, P.T., Romero, I., Moore, C., Reichart, G.-J., Jilbert, T., Chanton, J.P., Hastings, D.W., Overholt, W.A., Marks, K.P., Kostka, J.E., Holmes, C.W., Hollander, D., 2015. Sedimentation pulse in the NE Gulf of Mexico following the 2010 DWH blowout. PLoS One 10 (7), 1–24.
Chanton, J., Zhao, T., Rosenheim, B.E., Joye, S., Bosman, S., Brunner, C., Yeager, K.M., Diercks, A.R., Hollander, D., 2015. Using natural abundance radiocarbon to trace the flux of petrocarbon to the seafloor following the deepwater horizon oil spill. Environ. Sci. Technol. 49, 847–854.
Cutshall, N.H., Larsen, I.L., Olsen, C.R., 1983. Direct analysis of ^{210}Pb in sediment samples: self-absorption corrections. Nucl. Inst. Method 206, 309–312.
Daly, K.L., Passow, U., Chanton, J., Hollander, D.J., 2016. Assessing the impacts of oil-associated marine snow formation and sedimentation during and after the deepwater horizon oil spill. Anthropocene 13, 18–33.
Folk, R.L., 1965. Petrology of Sedimentary Rocks. Hemphillis, Austin, Texas.

Fridrik, E.E., Schwing, P.T., Ramirez, H., Larson, R.A., Brooks, G.R., O'Malley, B.J., Hollander, D.J., 2016. Comparative records of planktic foraminiferal mass accumulation rates following the DwH and IXTOC events. Proceedings of the Gulf of Mexico Oil Spill and Ecosystem Science Conference .
Garcia-Pineda, O., MacDonald, I., Hu, C., Svejkovsky, J., Hess, M., Dukhovskoy, D., Morey, S.L., 2013. Detection of floating oil anomalies from the deepwater horizon oil spill with synthetic aperture radar. Oceanography 26, 124–137.
Harbison, R.N., 1968. Geology of DeSoto canyon. J. Geophys. Res. 73, 5175–5185.
Hastings, D.W., Schwing, P.T., Brooks, G.R., Larson, R.A., Morford, J.L., Roeder, T., Quinn, K.A., Bartlett, T., Romero, I.C., Hollander, D.J., 2016. Changes in sediment redox conditions following the BP DwH blowout event. Deep Sea Res. Part II Top. Stud. Oceanogr. 129, 167–178.
Hussain, N., Kim, G., Church, T.M., Carey, W.A., 1996. Simplified technique for gamma-spectrometric analysis of ^{210}Pb in sediment samples. Appl. Radiat. Isot 42, 835–839.
IAEA, 2012. Worldwide Open Proficiency Test, Determination of Natural and Artificial Radionuclides in Moss-Soil and Water: IAEA-CU-2009-03. IAEA, Vienna, Austria.
Kitto, M.E., 1991. Determination of photon self-absorption corrections for soil samples. Appl. Radiat. Isot. 42, 835–839.
Larson, R.A., Brooks, G.R., Schwing, P.T., Holmes, C., Carter, S.R., Hollander, D.J., 2017. Post DwH sedimentation in the northeastern Gulf of Mexico: a 6-year overview. Proceedings of the Gulf of Mexico Research Oil Spill and Ecosystem (GoMOSES) Conference .
MacKenzie, A.B., Hardie, S.M.L., Farmer, J.G., Eades, L.J., Pulford, I.D., 2011. Analytical and sampling constraints in ^{210}Pb dating. Sci. Total Environ. 409, 1298–1304.
McClintic, M.A., DeMaster, D.J., Thomas, C.J., Smith, C.R., 2008. Testing the FOODBANCS hypothesis: seasonal variations in near-bottom particle flux, bioturbation intensity, and deposit feeding based on ^{234}Th measurements. Deep Sea Res. Part II Top. Stud. Oceanogr. 55 (22–23), 2425–2437.
Milliman, J.D., 1974. Marine Carbonates. Springer-Verlag, New York.
Passow, U., Hetland, R.D., 2016. What happened to all the oil? Oceanogr., Special Issue GoMRI Deepwater Horizon Oil Spill Ecosyst. Sci. 29 (3), 88–95.
Passow, U., Ziervogel, K., Asper, V., Diercks, A., 2012. Marine snow formation in the aftermath of the deepwater horizon oil spill in the Gulf of Mexico. Environ. Res. Lett. 7, 035301.
Passow, U., Ziervogel, K., 2016. Marine snow sedimented oil released during the deepwater horizon spill. Oceanography 29 (3), 118–125.
Pope, R.H., Demaster, J.D., Smith, C.R., Seltmann, H., 1996. Rapid bioturbation in equatorial pacific sediments: evidence from excess ^{234}Th measurements. Deep. Res. 43, 1339–1364.
Romero, I.C., Schwing, P.T., Brooks, G.R., Larson, R.A., Hastings, D.W., Ellis, G.E., Goddard, E.A., Hollander, D.J., 2015. Hydrocarbons in deep-sea sediments following the 2010 deepwater horizon blowout in the northeast Gulf of Mexico. PLoS One 10 (5) e0128371.
Romero, I.C., Toro-Farmer, G., Diercks, A.R., Schwing, P.T., Muller-Karger, F., Murawski, M., Hollander, D.J., 2017. Large scale deposition of weathered oil in the Gulf of Mexico following a deepwater oil spill. Environ. Pollut. 228, 179–189. doi:http://dx.doi.org/10.1016/j.envpol.2017.05.019.
Sadler, P., 1981. Sedimentation rates and the completeness of stratigraphic sections. J. Geol. 89, 569–584.
Sanchez-Cabeza, J.A., Ruiz-Fernandez, A.C., 2012. ^{210}Pb sediment radiochronology: an integrated formulation and classification of dating models. Geochimica Et Cosmochimica Acta. 82, 183–200.
Schwing, P.T., Romero, I.C., Brooks, G.R., Hastings, D.W., Larson, R.A., Hollander, D.J., 2015. A decline in deep-sea benthic foraminifera following the deepwater horizon event in the northeastern Gulf of Mexico. PLoS One 10 (3), 1–14.
Schwing, P.T., Romero, I.C., Larson, R.A., O'Malley, B.J., Fridrik, E.E., Goddard, E.A., Brooks, G.R., Hastings, D.W., Rosenheim, B.E., Hollander, D.J., Grant, G., Mulhollan, J., 2016. Sediment core extrusion method at millimeter resolution using a calbirated threaded-rod. J. Visual. Exp.: JoVE 114.
Schwing, P.T., Brooks, G.R., Larson, R.A., O'Malley, B.J., Hollander, D.J., 2017. Constraining the spatial extent of the marine oil snow sedimentation and accumulation (MOSSFA) following the DWH event using a ^{210}Pb$_{xs}$ inventory approach. Environ. Sci. Technol. 51, 5962–5968. doi:http://dx.doi.org/10.1021/acs.est.7b00450.
Smith, M.L., Clark, A., Jennings, A.E., 2002. Accumulation in East Greenland Fjords and on the continental shelves adjacent to the Denmark strait over the last century based on ^{210}Pb geochronology. Arctic 55, 109–122.
Stout, S.A., German, C.R., 2017. Characterization and flux of marine oil snow settling toward the sea floor in the northern Gulf of Mexico during the deepwater horizon incident : evidence for input from surface oil and impact on shallow shelf sediments. Mar. Pollut. Bull. 129, 695–713.
Swarzenski, P.W., 2014. ^{210}Pb Dating, In: Encyclopedia of Scientific Dating Methods. Springer Science and Business Media, Dordrecht.
Valentine, D.L., Fisher, G.B., Bagby, S.C., Nelson, R.K., Reddy, C.M., Sylva, S.P., 2014. Fallout plume of submerged oil from deepwater horizon. PNAS .
Yeager, K.M., Stantschi, P.H., Owe, G.T., 2004. Sediment accumulation and radionuclide inventories (^{239},^{240}Pu, ^{210}Pb, and ^{234}Th) in the northern Gulf of Mexico, as influenced by organic matter and macrofaunal density. Mar. Chem. 91, 1–14.
Ziervogel, K., McKay, L., Rhodes, B., Osburn, C.L., Dickson-Brown, J., Arnosti, C., Teske, A., 2012. Microbial activities and dissolved organic matter dynamics in oil-contaminated surface seawater from the deepwater horizon oil spill site. PLoS One 7 (4) e34816.

APPENDIX B:

CHAPTER FOUR:

"CHARACTERIZATION OF THE SEDIMENTATION PULSE ASSOCIATED WITH THE *DEEPWATER HORIZON* BLOWOUT: DEPOSITIONAL PULSE, INITIAL RESPONSE, AND STABILIZATION" Published In: Deep Oil Spills – Facts Fate and Effects, Springer (2019)

Chapter 14
Characterization of the Sedimentation Associated with the *Deepwater Horizon* Blowout: Depositional Pulse, Initial Response, and Stabilization

Rebekka A. Larson[1,2], Gregg R. Brooks[1], Patrick T. Schwing[2], Arne R. Diercks[3], Charles W. Holmes[4], Jeffrey P. Chanton[5], Misael Diaz-Asencio[6], David J. Hollander[2]

1. Eckerd College, Department of Marine Science, St. Petersburg, Florida 33711, USA

2. University of South Florida, College of Marine Science, St. Petersburg, Florida 33701, USA

3. University of Southern Mississippi, School of Ocean Science and Engineering, Stennis Space Center, Mississippi 39529, USA

4. Environchron, Tallahassee FL, 32308, USA

5. Florida State University, Department of Earth, Ocean and Atmospheric Science, Tallahassee, Florida 32306-4320, USA

6. Ensenada Center for Scientific Research and Higher Education, Ensenada, B.C., Mexico

Keywords: Sediment, Chronology, MOSSFA, Short-lived radioisotopes, Sedimentation

S. Murawski et al. (eds.), *Deep Oil Spills*,

Abstract
The *Deepwater Horizon* (DWH) blowout led to a depositional pulse in the northeast Gulf of Mexico in the Fall of 2010 associated with an observed Marine Oil Snow Sedimentation and Flocculent Accumulation (MOSSFA) event. A time series (2010-2016) of annually collected sediment cores at four sites characterize the sedimentary response to the event, post event, and stabilization/recovery. The depositional pulse (2010-2011) was characterized by high sedimentation rates with little to no bioturbation and large excursions in % silt. The lack of changes in sediment composition indicate that the same sediment sources dominated during the event, but the rates of sedimentation increased. In the years following the event (2011-2012) sedimentation rates were lower, and bioturbation was absent, and the initial excursions in % silt began to become undetectable in the sedimentary record. Between 2013 and 2016, a spatially and temporally variable return of bioturbation was detected at most sites. Sedimentation rates at all sites remained low, but increases in $^{234}Th_{xs}$ apparent mass accumulation rates indicated a return of bioturbation and potential stabilization and/or recovery of the sedimentary system. The deepest site (~1500 m) did not have any indication of bioturbation as of the 2016 collections, which may reflect a lack of recovery or that bioturbation was never present. In 2012, $^{210}Pb_{xs}$ age dating began to resolve the depositional pulse suggesting it may be applied to determine changes in the pulse deposit over time, and/or its preservation in the sedimentary record. Factors that may influence preservation include burial, bioturbation, degradation of the pulse signature, and re-mobilization of pulse sediments.

14.1 Introduction

The *Deepwater Horizon* (DWH) blowout resulted in multiple sequences of events leading to the deposition of sediment and oil-contaminated sediment to the deep-sea benthos and subsequent integration into the sedimentary system. Beginning in April 2010, the DWH blowout led to the release of oil and gas at a water depth of ~1500 m in the northeastern Gulf of Mexico (NEGoM) for a duration of 87 days (Passow and Hetland 2016). The released oil formed a rising plume from the leak at the seafloor to the sea surface, a subsurface plume at ~1,000 m water depth (Diercks et al. 2010; Joye et al. 2011), and a sea surface oil slick (Thibodeaux et al. 2011). A variety of strategies to stop the release of oil and mitigate impacts were utilized to contain, remove, and influence the distribution and degradation (biotic and abiotic) of released oil (US Coast Guard 2010; BOEM 2010). This included the addition of dispersants (Corexit) at the wellhead as well as at sea surface slicks (Yan et al. 2016), skimming and burning at the sea surface, water release from the Mississippi River, and the addition of drilling mud at the wellhead (Liu et al. 2018).

The DWH blowout occurred in a region that is sedimentologically complex (Fig. 14.1a). West of the DeSoto Canyon seafloor sediments are dominantly siliciclastic, associated with Mississippi River discharge. East of the DeSoto Canyon seafloor sediments are dominantly carbonate, associated with the west Florida Platform and low river influence (Balsam and Beeson 2003; Holmes 1976; Harbison et al. 1968). This resulted in the potential impacts of oil released in both siliciclastic and carbonate sedimentary regimes.

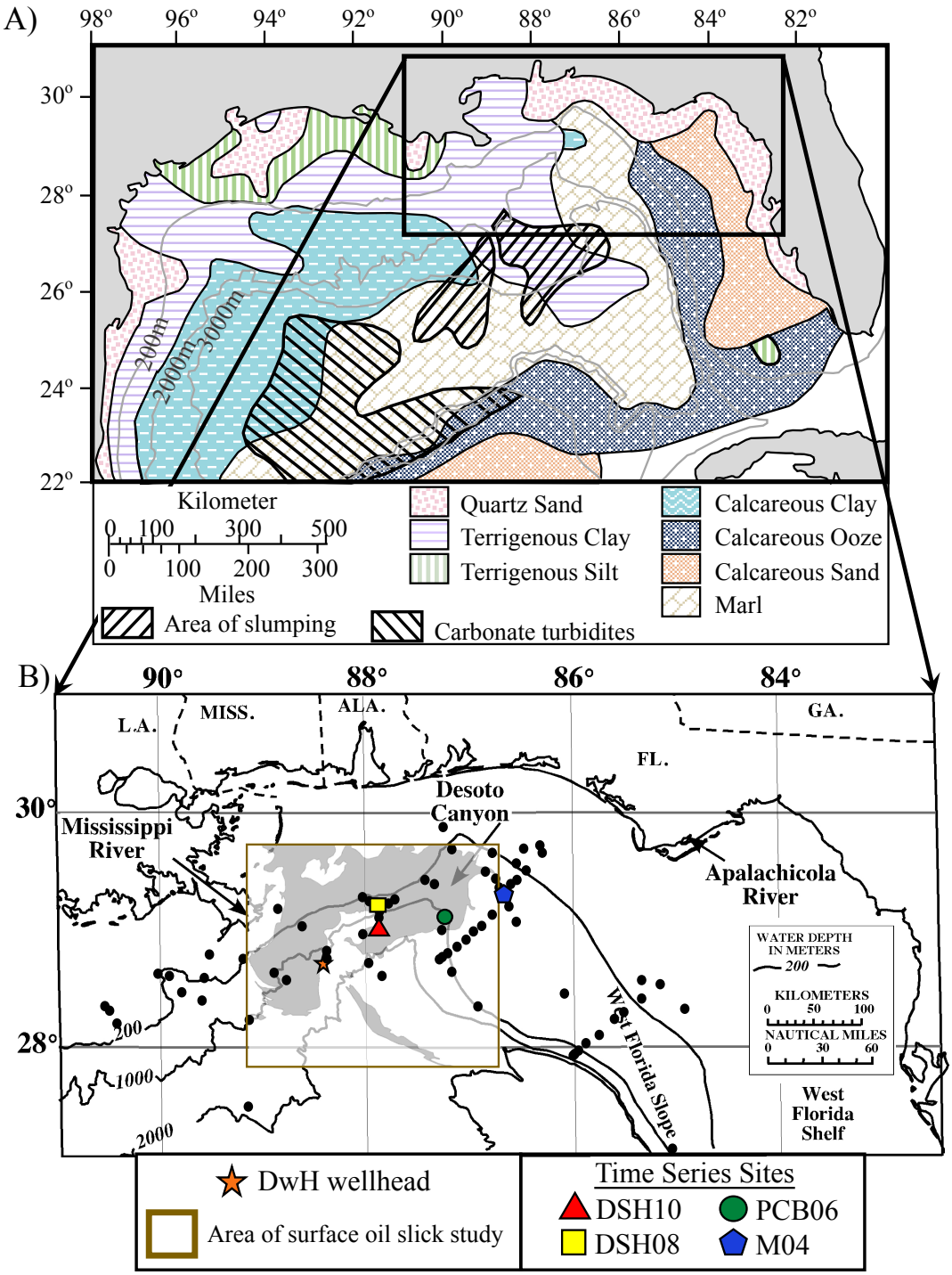

Fig. 14.1. Maps of the Gulf of Mexico (GoM) showing the physiographic features: (a) Map indicating the study area in the NEGoM with sedimentologic regions (modified from Brooks et al. 2020; Balsam and Beeson 2003; Holmes 1976), (b) map of NEGoM showing location of the DWH wellhead (orange star), surface sediment slick (gray shading in brown box, from Garcia-Pineda et al. 2013) and C-IMAGE sediment core locations (black circles) and time-series sites (DSH10 = red triangle, DSH08 = yellow square, PCB06 = green circle, and M04 = blue pentagon). (Modified from Brooks et al. 2015)

A primary depositional mechanism for oiled sedimentation was the observed Marine Oil Snow Sedimentation and Flocculent accumulation (MOSSFA), which consisted of surface oil interacting with biology, primarily phytoplankton (Quigg et al. 2020; Daly et al. 2016; Passow et al. 2016; Ziervogel et al. 2012; Passow et al. 2012). The interaction of this sticky substance combined with oil, dispersants, and clay particles in the water column leads to aggregation of marine oil snow, which lost buoyancy and rapidly settled through the water column, stripping particles and transporting them to the sea floor as MOSSFA (Passow et al. 2012; Brooks et al 2015).

The DWH blowout event was of short duration (geologically), on the scale of months. Understanding the manifestation of this event in the sedimentary system and impacts to the benthos required rapid response and adaptive approaches. Studying the sedimentary system before, during, and after an oil spill event, such as the DWH blowout, allows for the assessment of benthic sedimentological, biological and ecological implications ranging from acute/short-term to long-term/permanent impacts. The short- and long-term fate of oil-contaminated sediments can be described in terms of (1) the initial distribution patterns providing insight into the depositional mechanism(s) and source(s) of sedimented oil, such as MOSSFA, (2) the potential redistribution of oil-contaminated sediments and secondary deposition in benthic environments that may not have been initially impacted, and (3) the ultimate fate and potential for burial and sequestration of oil-contaminated sediments in deep-sea sediments and by the benthos.

14.2 Approach/Methods

A total of 179 sediment cores collected between 2010 and 2016 at 80 sites to investigate the sedimentary impacts of the DWH blowout (Fig. 14.1b). Due to the "real-time" nature of the sediment investigations immediately following the DWH event, it was expected that impacted sediments would be at the surface of the seafloor and core collection with an intact sediment water interface was of critical importance. Therefore, cores were collected using an Ocean Instruments MC-800 multicorer as it delicately collects sediment cores up to ~60 cm in length while preserving the sediment water interface, which is generally sufficient for capturing sedimentation over the past ~100 years to adequately assess baseline sedimentation patterns. Also, the MC-800 collects 8 cores simultaneously allowing for interdisciplinary studies (sedimentology, biology, chemistry, etc.) to fully characterize the benthic response and evolution during and following the event.

14.2.1 Time-Series Approach/High-Resolution Sampling

A time series of annually collected cores from the same sites allowed for the detection of the event in the sedimentary record, the annual-scale evolution of the sedimentary deposit over the subsequent years, and the potential burial and preservation in the sedimentary system. In the absence of any baseline information, such as for the DWH blowout, a time-series approach provides a post-event baseline. This approach also helps identify how indicators of oil-contaminated sediments may change over time in the sedimentary record. It also can assist in

determining the preservation potential of oil-contaminated sediments including influences of burial, bioturbation/mixing, post-depositional alteration, and resuspension/erosion.

Both the siliciclastic and carbonate sedimentary regimes are represented in the time series with sites DSH08 and DSH10 located on the siliciclastic side of the Desoto Canyon and sites PCB06 and M04 located on the carbonate side of the DeSoto Canyon (Fig. 14.1). High-resolution sub-sampling of cores provided high temporal resolution to define pre-event baselines (downcore), the event, and post-event sedimentation. Sub-sampling of cores at 2mm resolution by extrusion methods described by Schwing et al. (2016) provided the highest temporal resolution possible for analyses.

14.2.1 Time Series Approach/ High Resolution Sampling

A time-series of annually collected cores from the same sites allowed for the detection of the event in the sedimentary record, the annual-scale evolution of the sedimentary deposit over the subsequent years, and the potential burial and preservation in the sedimentary system. In the absence of any baseline information, such as for the DWH blowout, a time series approach provides a post-event baseline. This approach also helps identify how indicators of oil contaminated sediments may change over time in the sedimentary record. It also can assist in determining the preservation potential of oil contaminated sediments including influences of burial, bioturbation/mixing, post depositional alteration, and resuspension/erosion.

Both the siliciclastic and carbonate sedimentary regimes are represented in the time-series with sites DSH08 and DSH10 located on the siliciclastic side of the Desoto Canyon and sites PCB06 and M04 located on the carbonate side of the DeSoto Canyon (Fig. 14.1). High-resolution sub-sampling of cores provided high temporal resolution to define pre-event baselines (downcore), the event, and post-event sedimentation. Sub-sampling of cores at 2mm resolution by extrusion methods described by Schwing et al. (2016) provided the highest temporal resolution possible for analyses.

14.2.2 Chronometers – Timing of Deposition

Defining the timing of sedimentation is critical to correlate the deviations in the sedimentary record with the DWH event. The most commonly used chronometers for recent deposition are short-lived radioisotopes including excess ^{234}Th ($^{234}Th_{xs}$), excess ^{210}Pb ($^{210}Pb_{xs}$), ^{137}Cs, and ^{7}Be (Swarzenski 2014; Holmes 1998; Appleby 2001). Ideally, multiple chronometers would be utilized as they each have strengths and limitations. Sediment cores collected from the deep-sea oceanic setting (all analyzed to date) did not contain detectable ^{137}Cs or ^{7}Be, so they are not viable in this environment as chronometers or for corroborating other age dating techniques. Therefore, $^{234}Th_{xs}$ and $^{210}Pb_{xs}$ are the primary chronometers for defining sedimentation on monthly ($^{234}Th_{xs}$) and annual/decadal ($^{210}Pb_{xs}$) time scales. Sediment core samples were analyzed for short-lived radioisotopes by gamma spectrometry on Series HPGe (high-purity germanium) Coaxial Planar Photon Detectors for total ^{210}Pb (46.5keV), ^{214}Pb (295 keV and 351 keV), ^{214}Bi (609keV), and ^{234}Th (63 keV) in order to determine $^{234}Th_{xs}$ and $^{210}Pb_{xs}$ activities expressed as disintegrations per minute per gram (dpm/g) using methodology described by Brooks et al. (2015) and Larson et al. (2018).

The short duration of the sedimentation pulse required a high temporal resolution chronometer, such as $^{234}Th_{xs}$, to identify the most recent sedimentation that would be associated with the event. Uranium-238 is soluble in seawater and behaves conservatively with salinity (Chen et al. 1986), and the decay product, $^{234}Th_{xs}$, strongly adsorbs onto particles producing a flux of $^{234}Th_{xs}$ to the seafloor associated with sedimentation (Winkler and Rosner 2000). $^{234}Th_{xs}$ has a short half-life of ~24 days and is usually only detectable in surficial sediments representing sedimentation and/or bioturbation. Due to the short (~24 day) half-life, $^{234}Th_{xs}$ has traditionally been used to determine the depth of bioturbation (McClintic et al. 2008; Pope et al. 1996; Yeager et al. 2004), but under certain conditions (high sedimentation, high sampling resolution, stratigraphic integrity), it may be used as a chronological tool (Brooks et al. 2015). Activities of $^{234}Th_{xs}$ were decay corrected (DC $^{234}Th_{xs}$) for activity lost due to decay between the time of core collection and sample analysis, and data are expressed as Inventories and as mass accumulation rates (MAR) (Brooks et al. 2015; Larson et al. 2018). $^{234}Th_{xs}$ Inventory is the sum of activity in a core, which is an indicator of the flux of $^{234}Th_{xs}$ to the seafloor associated with sedimentation and is not influenced by bioturbation (Brooks et al. 2015). $^{234}Th_{xs}$ MAR is a function of the $^{234}Th_{xs}$ activity in a sediment core, as well as the depth downcore of the $^{234}Th_{xs}$ profile, and can be influenced by both sedimentation and bioturbation (downcore mixing deepening the $^{234}Th_{xs}$ profile). By utilizing the $^{234}Th_{xs}$ Inventory as a measure of sedimentation, the $^{234}Th_{xs}$ MAR can be used as an indicator of bioturbation/mixing in surficial sediments. Specifically, high Inventory with a high MAR indicates high sedimentation, and low Inventory with a low MAR indicates low sedimentation. The combination of a low Inventory with a high MAR indicates low sedimentation with the influence of bioturbation/mixing. Under these conditions, MAR is not an accurate indicator of sedimentation/accumulation due to the influence of bioturbation and is referred to as apparent MAR (A-MAR).

With a 22.3-year half-life, $^{210}Pb_{xs}$ provides age control and sedimentation rates over the past ~120 years but is less sensitive to monthly time scales (Chisté and Bé 2007; Appleby 2001). Therefore, $^{210}Pb_{xs}$ age dating is not as useful immediately following an event but becomes more useful as the primary dating tool in years to decades following a sedimentation event. The constant rate of supply (CRS) model, which is appropriate under conditions of varying accumulation rates, is used to provide $^{210}Pb_{xs}$ age dating for pre-event downcore baselines and to detect the sedimentation pulse in subsequent years (2012-2016) (Appleby 2001; Binford 1990; Appleby and Oldfield 1983).

14.2.3 Sediment Texture and Composition

Sediment texture and composition analyses were conducted on extruded samples and included grain size by methodology described by Folk (1965) and calcium carbonate content (%$CaCO_3$) by methodology by Milliman (1974) to determine variability in sediment sources and depositional mechanisms. Grain size is presented as % silt as this was the most indicative of changes in sediment texture (Larson et al. 2018). There are multiple indicators of oil-contaminated sediments and the benthic impacts including organic and inorganic geochemical indicators and biological responses. Organic geochemical fingerprinting is utilized to identify oil-contaminated sediments and specifically isolate DWH oil contamination and is described by Romero et al. (2020). Inorganic impacts and sedimentary signatures can include shifts in redox geochemistry as described by Hastings et al. (2020). Biological indicators of oil-contaminated

sedimentation and benthic impacts also include benthic foraminifera by Schwing et al. (2020) and macrofaunal by Montagna et al. (2020).

14.3 Sedimentary Response: Depositional Pulse (2010-2011)

The sedimentary response of the DWH event was manifested in sediment cores collected in the Fall of 2010 through early 2011 as increased rates of sedimentation and subtle changes in sedimentology at the time-series sites (DSH08, DSH10, PCB06, M04). This depositional pulse associated with MOSSFA was characterized by high $^{234}Th_{xs}$ Inventories and high $^{234}Th_{xs}$ MAR, indicating high sedimentation, over the surficial 10-20 mm (Fig. 14.2). Down-core $^{210}Pb_{xs}$ geochronologies recorded MAR an order of magnitude lower than surficial rates based on $^{234}Th_{xs}$ (Brooks et al. 2015). However, rates calculated by different methods representing different time frames cannot be directly compared due to the differences in time scales involved, which is commonly referred to as the Sadler effect (Sadler 1981). Where $^{234}Th_{xs}$ represents monthly time-scale sedimentation, $^{210}Pb_{xs}$ is more reflective of annual- to decadal-scale sediment accumulation. This leads to a consistently higher estimation of MAR by $^{234}Th_{xs}$ as compared to $^{210}Pb_{xs}$ (Sadler 1981) and provides evidence to support the importance of comparisons using the same chronometer. As there were no pre-event $^{234}Th_{xs}$ data available for direct comparison, the high $^{234}Th_{xs}$ Inventory and MAR measured in 2010 and early 2011, associated with the depositional pulse, initially could not be confirmed (Brooks et al. 2015). The continued measurement of $^{234}Th_{xs}$ Inventory and MAR over the 6-year time series allowed for the confirmation of the depositional pulse and evaluation of sedimentation (Inventory and MAR) and bioturbation (A-MAR) as the sedimentary system evolved following the DWH event.

There were no major systematic changes in sedimentological parameters over the 10-20 mm-thick pulse layer as compared to underlying sediments, the exception to this being silt content (% silt), which exhibited major excursions in the surfaces of the time-series cores collected in late 2010 and early 2011 (Fig. 14.3). The % silt increased dramatically in some cores and decreased dramatically in others as compared to consistent downcore (pre-event) values, suggesting a deviation in sedimentation processes during 2010 and 2011 concurrent with the depositional pulse (Brooks et al. 2015). Below the surficial 10-20 mm (i.e., the depositional pulse layer), silt content did not vary, indicating reproducibility of high-resolution analyses and little spatial heterogeneity and suggesting a relatively stable sedimentological regime for >100 years preceding the depositional pulse (Larson et al. 2018). Composition, as represented by carbonate content (%carbonate), showed no systematic or detectable changes within the surficial 10-20 mm of the time-series cores (Brooks et al. 2015). This indicates no detectable changes in sediment source(s) for the siliciclastic or carbonate regions of the study area during the event. This is due to MOSSFA stripping the overlying water column of particulates that would have eventually settled to the sea-floor in each of the two sediment regimes, so composition may not be expected to change measurably even though the rate of sedimentation increased (Brooks et al. 2015; Chanton et al. 2014; Romero et al. 2017; Schwing et al. 2017).

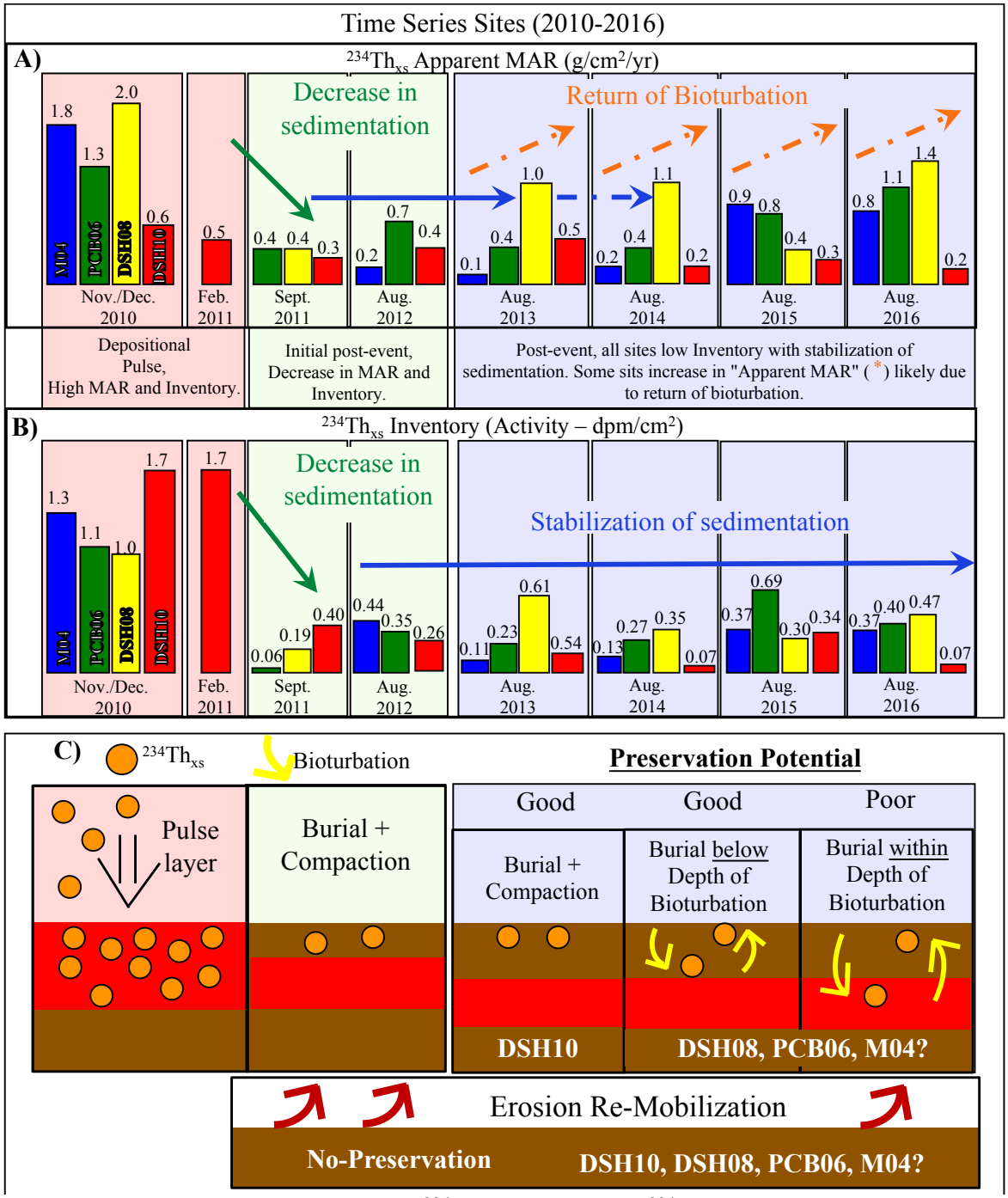

Fig. 14.2 2010-2016 time-series sites (a) $^{234}Th_{xs}$ A-MAR, (b) $^{234}Th_{xs}$ Inventory, showing the evolution of the sedimentation pulse (2010-Feb 2011) indicated by higher $^{234}Th_{xs}$ Inventory and MAR, initial post pulse impact and response (2011-2012) with decrease in $^{234}Th_{xs}$ Inventory and MAR, and stabilization with lower $^{234}Th_{xs}$ Inventory with variable return of bioturbation/mixing (higher $^{234}Th_{xs}$ A-MAR) at all sites except DSH10. (c) Diagram showing the influences on preservation potential of the pulse layer in the sedimentary record, with highest potential associated with burial and no bioturbation (DSH10) and poorest with bioturbation reaching the depth downcore of the pulse layer and remobilization of the pulse layer leading to no preservation at the sites of initial deposition (2010-2011). (Modified from Larson et al. 2018)

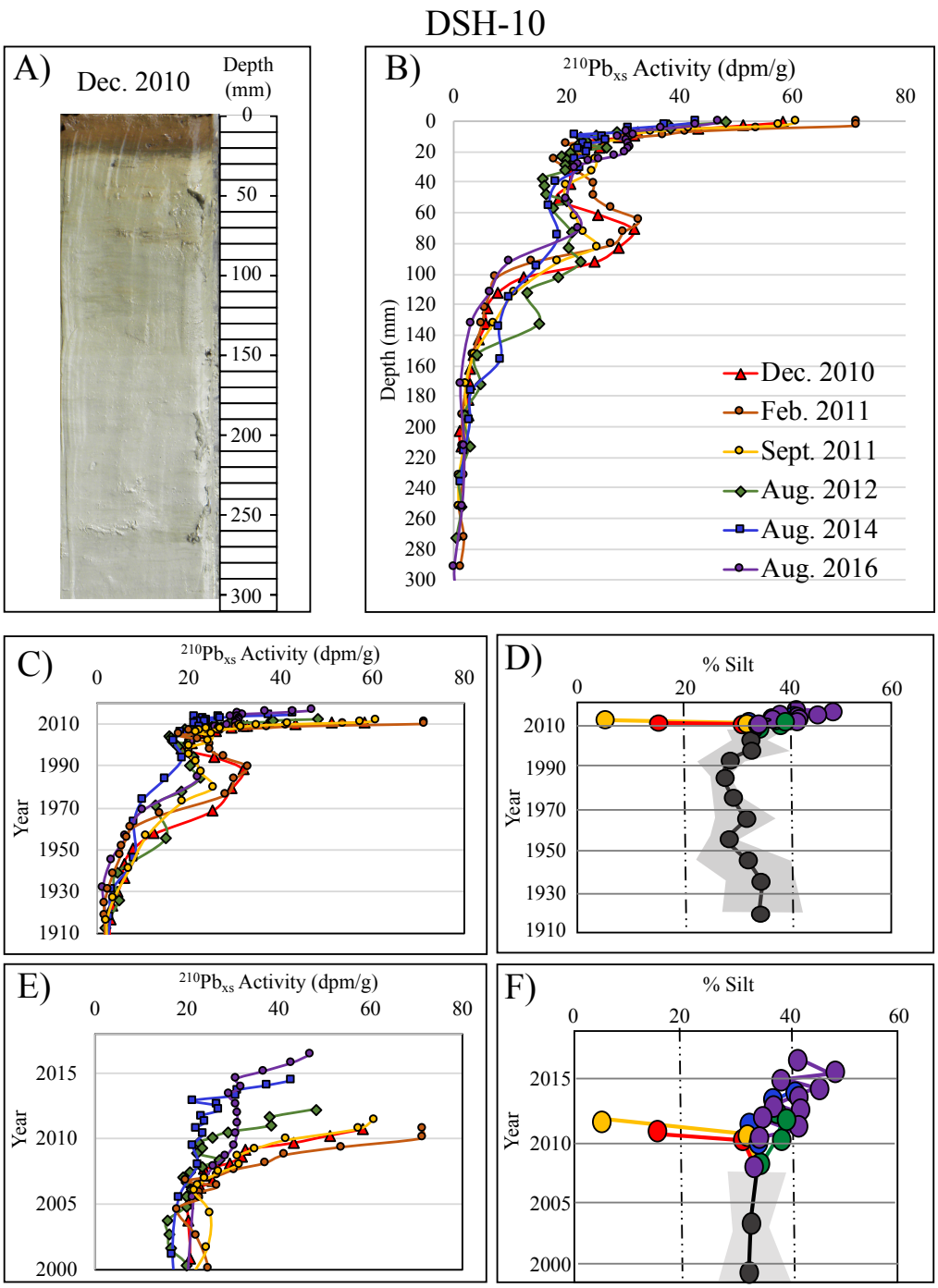

Fig. 14.3 Core data for site DSH-10. (a) Core photograph for December 2010 collection. (b) $^{210}Pb_{xs}$ profiles vs depth for all time series collections. Note the reproducibility of profiles. (c) $^{210}Pb_{xs}$ profiles vs year (CRS model). (d) % Silt profiles vs year for time series with averaged values and standard deviation shown as black line/circles and gray shading (modified from Larson et al. 2018). (e) $^{210}Pb_{xs}$ profiles vs year since 2000 for time series showing evolution of $^{210}Pb_{xs}$ signature of the depositional pulse. Note 2014 and 2016 cores have intervals of similar activity, which is possibly the detection of the depositional pulse. (f) % Silt profiles vs year since 2000 with decreases in % Silt in 2010 and 2011 cores associated with the depositional pulse, which is not detected in subsequent years. (Modified from Larson et al. 2018)

Detection of the depositional pulse within a 4-5-month period that resulted in a 10-20 mm thick sediment layer required the unconventional use of $^{234}Th_{xs}$ as a geochronological tool. This was due to the exceptionally high (2 mm)-resolution sampling, the high sedimentation rate for detection of $^{234}Th_{xs}$ profiles to determine Inventories and MAR, as well as the interruption of bioturbation by the event allowing for detection of the depositional pulse by $^{234}Th_{xs}$ and % silt (Brooks et al. 2015) (Figs. 14.2 and 14.3).

14.4 Initial Sedimentary Response: Post-event (2011-2012)

In the immediate years following the depositional pulse, a decrease in sedimentation was indicated by cores collected in September 2011 and 2012 at all of the time-series sites. This is expressed as lower $^{234}Th_{xs}$ Inventories and lower $^{234}Th_{xs}$ MARs as compared to the depositional pulse (Larson et al. 2018) (Fig. 14.2). As these Inventories and MARs are based upon the same chronometer ($^{234}Th_{xs}$), they are directly comparable to those associated with the depositional pulse. This also serves as initial baseline information indicating that the sedimentation rates of the depositional pulse were high. The low $^{234}Th_{xs}$ Inventory and low $^{234}Th_{xs}$ MAR also indicate a lack of bioturbation at all of the time-series sites for the first few years following the depositional pulse and possible lack of recovery of the benthic ecosystem over this period.

Sedimentologically, the subtle diagnostic indicator (% silt) of the depositional pulse was not as detectable in cores collected in 2011 and 2012 as compared to those collected in 2010 (Fig. 14.3). Most cores exhibited a stabilization in % silt toward pre-event (downcore) values. This may be an indication that % silt is not a strong diagnostic indicator of MOSSFA in sedimentary records, potentially due to challenges in detecting changes in % silt, and/or preservation (Fig.14.2).

Time-series cores collected in August 2012 showed that the 2010 depositional pulse began to be resolved by $^{210}Pb_{xs}$ (half-life ~22.3 years) in little more than 2 years following the event (Fig.14.3). $^{210}Pb_{xs}$ profiles began to reflect several adjacent depth intervals with similar $^{210}Pb_{xs}$ activities (dpm/g), indicating intervals were of approximately the same age and deposited at the same time (Larson et al. 2018). In the surface intervals of cores collected in 2010, the $^{210}Pb_{xs}$ profile is more exponential in shape, lacking intervals with similar activities (dpm/g) illustrating the ineffectiveness of $^{210}Pb_{xs}$ to resolve the depositional pulse.

14.5 Stabilization/Recovery: Post-event (2013-2016)

Beginning ~3 years after the DWH blowout and associated depositional pulse, there were indications of variability in the evolution of the sedimentary system as it stabilized/recovered. At the time-series sites collected between 2013 and 2016, lower $^{234}Th_{xs}$ Inventories did remain consistent with the post-depositional pulse Inventories for 2011 and 2012 indicating continued lower rates of sedimentation (Fig. 14.2). The $^{234}Th_{xs}$ MARs exhibited specific increases at different collection years. Site DSH08 exhibited an apparent increase in $^{234}Th_{xs}$ MAR (A-MAR) beginning in August 2013, while sites M04 and PCB06 recorded apparent increases in $^{234}Th_{xs}$ MAR (A-MAR) beginning in August 2015. These A-MAR are not supported by the relatively stable $^{234}Th_{xs}$ Inventories from late 2011 through August 2016 (Larson et al. 2018) (Fig. 14.2) and therefore are not a reflection of increased sedimentation rates, but are likely due to the re-

establishment of bioturbation. Bioturbation mixes $^{234}Th_{xs}$ downward, deepening the $^{234}Th_{xs}$ profile downcore and falsely increasing MARs (Larson et al. 2018). It is also unknown the reason(s) that bioturbation was re-established at specific sites at different times. Site DSH10 was the exception as $^{234}Th_{xs}$ MARs remained low through 2016 indicating low sedimentation rates and a lack of bioturbation (Larson et al. 2018) (Fig. 14.2). Whether bioturbation was never present at DSH10 (pre-event) or if this site remains in transition and/or has not recovered from the depositional pulse is unknown. The lack of bioturbation at site DSH10 increases the preservation potential of the depositional pulse at site DSH10 (Fig. 14.2). Alternatively, the return of bioturbation at sites DSH08, PCB06, and M04 decreases the preservation potential of the depositional pulse depending on if the depositional pulse layer is buried below the depth of bioturbation (Fig. 14.2).

The silt content continues to become more consistent/stable and similar to pre-event values in 2013-2016 cores as compared to the 2010-2011 event signature. This reinforces the time-sensitive nature of using % silt as an indicator of MOSSFA as it does not appear to be well preserved and/or detectable in the sedimentary record. In contrast, $^{210}Pb_{xs}$ dating continues to progressively resolve the depositional pulse beginning in the 2012 collections through the 2016 collections (Larson et al. 2018) (Fig. 14.3) with sequential intervals of similar activity capped by increases in activity from post-event deposition (Larson et al. 2018).

14.6 Preservation Potential in the Sedimentary Record

From a sedimentological perspective, the potential for preservation of deposited oil-contaminated sediments associated with the DWH event, and their detection in the sedimentary record, is dependent on a variety of factors including (1) bioturbation/mixing, (2) burial, (3) degradation of the signature, (4) sediment compaction, and (5) remobilization, transport, and secondary deposition (Fig. 14.2). The presence of bioturbation and mixing will decrease the potential for preservation/detection in the sedimentary record by smearing and diluting the signature to below detection. If there is a lack of bioturbation immediately following a deposition event, it is possible for burial by subsequent sedimentation to increase the preservation potential as long as the depositional layer is deeper (downcore) than the depth of bioturbation (Fig.14.2). Burial of the impacted layer by subsequent sedimentation will lead to the highest potential for preservation and detection in the sedimentary record (Fig. 14.2). Areas with higher sedimentation rates generally have a higher probability of burial. Some of the indicators of oiled sedimentation are susceptible to degradation and will become more difficult to detect over time (Romero et al. 2020). With subsequent burial, compaction will lead to thinning of the depositional layer, making it more difficult to detect and requiring high-resolution sampling. The remobilization of impacted sediments can lead to a lack of preservation at the location of the initial deposition, as well as modification of the geographic extent of oil-contaminated sediments on the seafloor. This often is a function of resuspension and downslope transport to deeper water with the potential for focusing contaminated sediments in areas of high deposition, and/or distribution over a broader area. Research shows that seafloor morphology affects resuspension (Diercks et al. 2018; Turnewitsch et al. 2017) and redistribution (Durrieu De Madron et al. 2017), as well as subsequent settling and deposition of material (Turnewitsch et al. 2013; 2004) focusing erosion and deposition on specific areas on the seafloor. This provides a mechanism for uneven sediment deposition and distribution within a given time frame.

14.7 Critical Approaches/Methods

The investigation of the DWH blowout in the sedimentary system was developed using a variety of approaches that maximized the detection of sedimentary impacts without pre-existing knowledge of the evolution and processes influencing sedimentation associated with a deep water oil blowout. This included the rapid collection of sediment cores, an annual time series to characterize the event and its evolution in the sedimentary system over subsequent years, high-resolution sampling to maximize temporal resolution, and a multi disciplinary approach to determine diagnostic as well as corroborative indicators of oil-contaminated sediment deposition.

14.7.1 Rapid Response and Collection of Cores

The rapid collection of sediment cores following the initiation of the blowout event allowed for investigation of the immediate sedimentary response and, benthic impacts and the use of time-sensitive indicators to define sedimentation associated with the event. Time sensitive indicators included short-lived chronometers ($^{234}Th_{xs}$) to identify recent sedimentation, as well as sedimentological, chemical, and biological indicators that are susceptible to degradation, rapid modification/change, and/or low preservation potential in the sedimentary record. Also, as mentioned, impacted sedimentation was expected to be at the very sediment surface, and this allowed for targeted analysis for rapid determination of oil-contaminated sedimentation.

14.7.2 Time Series

The continued collection of sediment cores over the subsequent years following DWH provided the ability to define how the sedimentary signature was distinctly different from non-event sedimentation and how the sedimentary signature evolved over the following months to years. This was particularly critical to be able to use the same chronometer ($^{234}Th_{xs}$) for direct comparison of sedimentation rates (event vs post-event) (Sadler 1981). The time series defined the duration of the event and timing of the post-event response and if/when the benthic system stabilizes and/or recovers following such an event. It also provided the opportunity to investigate how the sedimentary system, including the signature of oil-contaminated sediments, evolved over subsequent years and the preservation potential of oil-contaminated sediments in the sedimentary record.

14.7.3 Sampling Resolution

Due to the short duration (months) of the blowout event and subsequent rapid collection of cores, the appropriate sub-sampling resolution to detect sedimentation on a monthly time scale was also of critical importance. The utilization of high-resolution sampling (2 mm sub-sampling) of cores allowed for the highest temporal resolution to detect the sedimentary signature of the blowout event with multiple sample intervals that represented the depositional pulse. It also allowed for the utilization of $^{234}Th_{xs}$ as an indicator of short-term (months) sedimentation rates of the depositional pulse, as well as a direct comparison to post-event rates. This provided post-event

baselines to define the deviation in sedimentation rates associated with the depositional pulse. The continued use of 2 mm sampling resolution was critical for determining the post-event sedimentation rates using $^{234}Th_{xs}$ as this indicator was often only detectable in the upper 2-10 mm. Coarser sampling resolution would not have been able to define post-event sedimentation rates using $^{234}Th_{xs}$.

Factors to consider with respect to sub-sampling resolution for detection of an event in the sedimentary record are the thickness of the depositional event and the required sensitivity of the analytical measurements used to detect the sedimentary signature of the event. Coarser sampling resolution may be appropriate for depositional events of greater thickness, often associated with long duration and/or high magnitude/sedimentary responses. The thinner the depositional event the finer the sampling resolution as over sampling (i.e., more than just the depositional unit) will lead to dilution of event sedimentation with non-event sedimentation. Dilution of the sedimentary signature of an event can lead to changing interpretations of impact and/or making it more difficult to detect in the sedimentary record. This is particularly important for more subtle indicators of a sedimentation event, and increased sampling resolution would increase the potential for detection as well as the number of analyses performed providing a more robust record. Also, of consideration is the required sampling resolution to obtain comparable baseline sedimentological data on similar time scales (months/years) for direct comparison to determine deviations, from baseline, of sedimentation events. Often, baseline sedimentation is at lower rates as compared to events.

14.7.4 Multi-Disciplinary Approach

The simultaneous collection of up to eight cores allowed for a multi-disciplinary approach for investigating DWH blowout impacts in the sedimentary record. This provided a more robust definition of the sedimentary signature and detection of the event. As most diagnostic indicators were subtle, the combination of multiple lines of evidence for the presence of oil-contaminated sediments was extremely valuable for defining the impacts of spatial deposition. It also assisted in determining the sediment sources (i.e., surface waters, etc.), depositional mechanisms, and biological/ecological impacts.

14.8 Conclusions

The DWH blowout event led to the formation of MOSSFA and a depositional pulse to the deep-sea benthos in the NEGoM in the Fall of 2010. A time series of sediment cores from four sites collected annually between 2010 and 2016 characterizes the event, post-event response, and stabilization of the sedimentary system with respect to sedimentation rates, sedimentology, and preservation potential. All sites collected in 2010 and early 2011 had large excursions in % silt and high $^{234}Th_{xs}$ Inventories and MAR indicating a depositional pulse with high sedimentation rates associated with the observed MOSSFA event. There were no distinctive changes in sediment composition associated with the depositional pulse, as the MOSSFA event stripped existing particles from the water column and did not significantly change the source(s) of sediment in either the siliciclastic or carbonated dominated regions. In the following years, 2011 to 2012, $^{234}Th_{xs}$ Inventories and MAR were lower (at all sites) indicating lower sedimentation

rates and a lack of bioturbation following the event. Over this period the initial deviations in % silt began to become undetectable in the sedimentary record. Beginning in 2013 and continuing through 2016, there was a site-specific return of bioturbation and stabilization of the sedimentary system. Over the late 2011 to 2016 period, all sites had low $^{234}Th_{xs}$ Inventories indicating consistently low sedimentation rates and stabilization of sedimentation patterns. The return of bioturbation, as indicated by higher $^{234}Th_{xs}$ Apparent MAR with no supporting increase in $^{234}Th_{xs}$ Inventory, was spatially and temporally variable with site DSH08 beginning in 2013, sites PCB06 and M04 in 2015. The absence of bioturbation at site DSH10 over the 2010-2016 period may indicate a lack of recovery at this site or that bioturbation was never present (pre-event, event, and post-event). The return of bioturbation decreases the preservation potential of the depositional pulse with site DSH10 having the highest preservation potential. This is assuming remobilization of the depositional pulse did not occur at these sites. Beginning in 2012, $^{210}Pb_{xs}$ age dating for cores appeared to resolve the depositional pulse and may be used to assist in determining the burial and preservation of oil-contaminated sediments and their detection in the sedimentary record. The combination of the rapid collection of cores following the DWH event, high-resolution sampling, and time series of the annual collection of cores allowed for the detection of the event (2010-early 2011) and evolution of the sedimentary system over the post-event impact (2011-2012) and stabilization (2013-2016).

Dedication

This chapter is dedicated to Charles "Chuck" Holmes who was a mentor, colleague, and friend. In his career, he advanced geologic studies in the Gulf of Mexico and beyond, as well as the methods and applications of short-lived radioisotope geochronology. Without his guidance and knowledge, the use of short-lived radioisotopes for investigating sediment records at high resolution in this study and others would not have been as far-reaching.

Funding Information

This research was made possible by grants from The Gulf of Mexico Research Initiative through its consortia: The Center for the Integrated Modeling and Analysis of the Gulf Ecosystem (C-IMAGE) and Sea to Coast Connectivity in the Eastern Gulf of Mexico (Deep-C). Data are publicly available through the Gulf of Mexico Research Initiative Information & Data Cooperative (GRIIDC) at https://data.gulfresearchinitiative.org (doi: [10.7266/N7FJ2F94, 10.7266/N79S1PJZ, 10.7266/N7610XTJ]).

References

Appleby PG (2001) Chapter 9: Chronostratigraphic techniques in recent sediments, In: Last WM, Smol JP (eds) Tracking environmental change using lake sediments volume 1. Kluwer Academic Publishers, The Netherlands

Appleby PG, Oldfield F (1983) The assessment of ^{210}Pb data from sites with varying sediment accumulation rates. Hydrobiologia 103:29–35

Balsam WL and Beeson JP (2003) Sea-floor sediment distribution in the Gulf of Mexico. Deep Sea Res Part I Oceanogr Res Pap 50(12):1421-1444

Binford MW (1990) Calculation and uncertainty analysis of ^{210}Pb dates for PIRLA project lake sediment cores. J Paleolimnol 3:253–267

BOEM (2011) Report Regarding the Causes of the April 20, 2010 Macondo Well Blowout. https://www.bsee.gov/sites/bsee.gov/files/reports/blowout-prevention/DWHfinaldoi-volumeii.pdf

Brooks GR, Larson RA, Schwing PT, Romero I, Moore C, Reichart GJ, Jilbert T, Chanton J P, Hastings DW, Overholt WA, Marks KP, Kostka JE, Holmes CW, Hollander D (2015) Sedimentation pulse in the NE Gulf of Mexico following the 2010 DWH blowout. PLoS One 10(7): 1-24

Brooks GR, Larson RA, Schwing PT, Diercks AR, Armenteros-Almanza M, Diaz-Asencio M, Martinez-Suarez A, Sánchez-Cabeza JA, Ruiz-Fernandez AC, Herguera Garcia JC, Perez-Bernal LH, Hollander DJ (2020) Gulf of Mexico (GoM) bottom sediments and depositional processes: A baseline for future oil spills (Chap. 5). In: Murawski SA, Ainsworth C, Gilbert S, Hollander D, Paris CB, Schlüter M, Wetzel D (eds) Scenarios and Responses to Future Deep Oil Spills – Fighting the Next War. Springer, Cham

Chanton J, Zhao T, Rosenheim BE, Joye S, Bosman S, Bruner C, Yeager KM, Diercks AR, Hollander D (2014) Using natural abundance radiocarbon to trace the flux of Petrocarbon to the seafloor following the Deepwater horizon oil spill. Environ Sci and Technol 49(2): 847–854. http://doi.org/10.1021/es5046524

Chen JH, Lawrence ER, Wasserburg GJ (1986) ^{238}U,^{234}U and ^{232}Th in seawater. Earth Planet Sci Lett 80:241–251. http://doi:10.1016/0012-821X(86)90108-1

Chisté V and Bé M.M (2007) Table of radionuclides ^{210}Pb – comments on evaluation of decay data, LNHB - bureau international des Poids et Mesures. vol. 8, Sevres Cedex, France, http://www.nucleide.org/DDEP_WG/DDEPdata.htm

Daly KL, Passow U, Chanton J, Hollander DJ (2016) Assessing the impacts of oil-associated marine snow formation and sedimentation during and after the Deepwater Horizon oil spill. Anthropocene 13:18–33. https://doi.org/10.1016/j.ancene.2016.01.006

Diercks AR, Highsmith RC, Asper VL, Joung D, Zhou Z, Guo L, Shiller AM, Joye SB, Teske AP, Guinasso Jr NL, Wade TL, Lohrenz SE (2010) Characterization of subsurface polycyclic aromatic hydrocarbons at the Deepwater Horizon site. Geophys Res Lett 37:L20602. http://doi.org/ 10.10292010GL045046

Diercks AR, Dike C, Asper VL, DiMarco SF, Chanton JP, Passow U (2018) Scales of seafloor sediment resuspension in the northern Gulf of Mexico. Elementa: Science of the Anthropocene 6:32. https://doi.org/10.1525/elementa.285

Durrieu De Madron X, Ramondenc S, Berline L, Houpert L, Bosse A, Martini S, Guidi L, Conan P, Curtil C, Delsaut N, Kunesch S, Ghiglione JF, Marsaleix P, Pujo-Pay M, Séverin T, Testor P, Tamburini C (2017) Deep sediment resuspension and thick nepheloid layer generation by

open-ocean convection. J Geophys ResOceans 122: 2291–2318. https://doi.org/10.1002/2016JC012062
Folk RL (1965) Petrology of Sedimentary Rocks. Hemphillis, Austin, Texas.
Garcia-Pineda O, MacDonald I, Hu C, Svejkovsky J, Hess M, Dukhovskoy D, Morey SL (2013) Detection of floating oil anomalies from the Deepwater Horizon oil spill with synthetic aperture radar. Oceanography 26: 124–137
Harbison RN (1968) Geology of DeSoto Canyon. J Geophys Res 73:5175-5185.
Hastings DW, Bartlett R, Brooks R, Larson RA, Quinn KA, Razionale D, Schwing PT, Pérez Bernal LH, Ruiz-Fernández AC, Sánchez-Cabeza JA, Hollander DJ (2020) Changes in redox conditions of surface sediments following the BP Deepwater horizon and Ixtoc 1 events (Chap. 16). In: Murawski SA, Ainsworth C, Gilbert S, Hollander D, Paris CB, Schlüter M, Wetzel D (eds) Deep oil spills – facts, fate and effects. Springer, Cham
Holmes CW (1976) Distribution, regional variation, and geochemical coherence of selected elements in the sediments of the central Gulf of Mexico. Geological Survey Professional Paper 928. Washington, D.C.: US Government Printing Office.
Holmes CW (1998) Short-lived isotopic chronometers – a means of measuring decadal sedimentary dynamics. U.S. Geological Survey, Dept. of the Interior. Fact Sheet FS-073-98.
Joye SB, MacDonald LR, Leifer I, Asper V (2011) Magnitude and oxidation potential of hydrocarbon gases released from the BP oil well blowout. Nat Geosci 4:160-164
Larson RA, Brooks GR, Schwing PT, Carter S, Hollander DJ (2018) High resolution investigation of event-driven sedimentation: northeastern Gulf of Mexico. Anthropocene vol. 24, pg. 40-50. https://doi.org/10.1016/j.ancene.2018.11.002
Liu G, Bracco A, Passow U (2018) The influence of mesoscale and submesoscale circulation on sinking particles in the northern Gulf of Mexico. Elementa: Science of the Anthropocene 6(1):36. https://doiorg/10.1525/elementa.292
McClintic MA, DeMaster DJ, Thomas CJ, Smith CR (2008) Testing the FOODBANCS hypothesis: seasonal variations in near-bottom particle flux, bioturbation intensity, and deposit feeding based on ^{234}Th measurements. Deep Sea Research Part II: Topical Studies in Oceanography 55(22–23): 2425–2437.
Milliman JD (1974) Marine carbonates. Springer-Verlag, New York.
Montagna PA, Girard F (2020) Deep-sea benthic faunal impacts and community evolution before, during and after the Deepwater Horizon event (Chap. 22). In: Murawski SA, Ainsworth C, Gilbert S, Hollander D, Paris CB, Schlüter M, Wetzel D (eds) Deep oil spills – facts, fate and effects. Springer, Cham
Passow U (2016) Formation of rapidly-sinking, oil-associated marine snow. Deep Sea Research Part II: Topical Studies in Oceanography, The Gulf of Mexico Ecosystem - before, during and after the Macondo Blowout 129:232–240 https://doi.org/10.1016/j.dsr2.2014.10.001
Passow U, Hetland R (2016) What happened to all of the oil? Oceanography 29:88–95 https://doi.org/10.5670/oceanog.2016.73
Passow U, Ziervogel K, Asper VL, Diercks AR (2012) Marine snow formation in the aftermath of the Deepwater Horizon oil spill in the Gulf of Mexico. Environ Res Lett 7:035301. https://doi.org/10.1088/1748-9326/7/3/035301
Pope RH, Demaster JD, Smith CR, Seltmann H (1996) Rapid bioturbation in equatorial pacific sediments: evidence from excess ^{234}Th measurements. Deep Sea Research Part II: Topical Studies in Oceanography 43:1339–1364.

Quigg A, Passow U, Hollander DJ, Daly KL, Burd A, Lee K (2020) Formation and sinking of MOSSFA (Marine Oil Snow Sedimentation and Flocculent Accumulation) Events: Past and present (Chap. 12). In: Murawski SA, Ainsworth C, Gilbert S, Hollander D, Paris CB, Schlüter M, Wetzel D (eds) Deep oil spills – facts, fate and effects. Springer, Cham

Romero IC, Schwing PT, Brooks GR, Larson RA, Hastings DW, Ellis GE, Goddard E A, Hollander DJ (2015) Hydrocarbons in Deep-Sea Sediments following the 2010 Deepwater horizon blowout in the Northeast Gulf of Mexico. PLoS One, 10(5):e0128371

Romero IC, Toro-Farmer G, Diercks AR, Schwing PT, Muller-Karger F, Murawski S, Hollander DJ (2017) Large Scale deposition of weathered oil in the Gulf of Mexico following a deepwater oil spill. Environ Pollut 228:179-189. https://doi.org/10.1016/j.envpol.2017.05.019

Romero IC, Chanton JP, Rosenheim BE, Radović J, Schwing PT, Hollander DJ, Larter SR, Oldenburg TBP (202020) Long-term preservation of oil spill events in sediments: the case for the Deepwater Horizon Spill in the Northern Gulf of Mexico (Chap. 17). In: Murawski SA, Ainsworth C, Gilbert S, Hollander D, Paris CB, Schlüter M, Wetzel D (eds) Deep oil spills – facts, fate and effects. Springer, Cham

Sadler P (1981) Sedimentation rates and the completeness of stratigraphic sections. J Geol 89:569–584

Schwing PT, Machain Castillo ML (2020) Impact and resilience of benthic foraminifera in the aftermath of the Deepwater Horizon and Ixtoc 1 oil spills (Chap. 23). In: Murawski SA, Ainsworth C, Gilbert S, Hollander D, Paris CB, Schlüter M, Wetzel D (eds) Deep oil spills – facts, fate and effects. Springer, Cham

Schwing PT, Romero IC, Larson RA, O'Malley BJ, Fridrik EE, Goddard EA, Brooks GR, Hastings DW, Rosenheim BE, Hollander DJ, Grant G, Mulhollan J (2016) Sediment Core extrusion method at millimeter resolution using a calibrated, threaded-rod. J Vis Exp 114:e54363. https://doi.org/10.3791/54363

Schwing PT, Brooks GR, Larson RA, Holmes CW, O'Malley BJ, Hollander DJ (2017) Constraining the spatial extent of the Marine Oil Snow Sedimentation and Accumulation (MOSSFA) following the DWH event using a $^{210}Pb_{xs}$ inventory approach. Environ Sci Technol 51:5962−5968. https://doi.org/10.1021/acs.est.7b00450

Swarzenski PW (2014) ^{210}Pb Dating, In: Encyclopedia of scientific dating methods. Springer Science and Business Media, Dordrecht, https://doi.org/10.1007/978-94-007-6326-5_236-1.

Thibodeaux, LJ, Valsaraj, KT, John VJ Papadopoulos KD Pratt LR Pesika NS (2011) Marine oil fate: knowledge gaps, basic research, and development needs: a perspective based on the Deepwater horizon ppill. Environl Eng Sci 28(2):87-93. https://doi.org/10.1089/eex.2010.0276

Turnewitsch R, Dale A, Lahajnar N, Lampitt RS, Sakamoto K (2017) Can neap-spring tidal cycles modulate biogeochemical fluxes in the abyssal near-seafloor water column? Progress in Oceanography 154:1–24 https://doi.org/10.1016/j.pocean.2017.04.006

Turnewitsch R, Reyss JL, Chapman DC, Thomson J, Lampitt RS (2004) Evidence for a sedimentary fingerprint of an asymmetric flow field surrounding a short seamount. Earth Planet Sci Lett 222:1023–1036. https://doi.org/10.1016/j.epsl.2004.03.042

Turnewitsch R, Falahat S, Nycander J, Dale A, Scott RB, Furnival D (2013) Deep-sea fluid and sediment dynamics—Influence of hill- to seamount-scale seafloor topography. Earth Sci Rev 127:203–241. https://doi.org/10.1016/j.earscirev.2013.10.005

US Coast Guard (2010) Report of investigation into the circumstances surrounding the explosion, fire, sinking and loss of eleven crew members aboard the mobile offshore drilling

unit Deepwater horizon in the Gulf of Mexico April 20-22, 2010. Vol I MISLE Activity Number: 3721503. https://www.bsee.gov/newsroom/library/deepwater-horizon-reading-room/joint-investigation-team-report

Winkler R and Rosner G (2000) Seasonal and long-term variation in ^{210}Pb concentration in air, atmoshpere deposition rate and total deposition velocity in south Germany. Sci Total Environ 263: 57-68

Yan B, Passow U, Chanton JP, Nöthig EM, Asper V, Sweet J, Pitiranggon M, Diercks AR, Pak D (2016) Sustained deposition of contaminants from the Deepwater Horizon spill. PNAS 113:24E3332-E3340. https://doi.org/10.1073/pnas.1513156113

Yeager KM, Stantschi PH, Owe GT (2004) Sediment accumulation and radionuclide inventories (^{239},^{240}Pu, ^{210}Pb and ^{234}Th) in the northern Gulf of Mexico, as influenced by organic matter and macrofaunal density. Mar Chem 91: 1–14.

Ziervogel K, McKay L, Rhodes B, Osburn CL, Dickson-Brown J, Arnosti C, Teske A. (2012) Microbial activities and dissolved organic matter dynamics in oil-contaminated surface seawater from the Deepwater horizon oil spill site. PLoS One 7(4):e34816

APPENDIX C:

CHAPTER TWO SUPPLEMENTAL TABLES AND FIGURES

Appendix C. Supplemental Tables and Figures

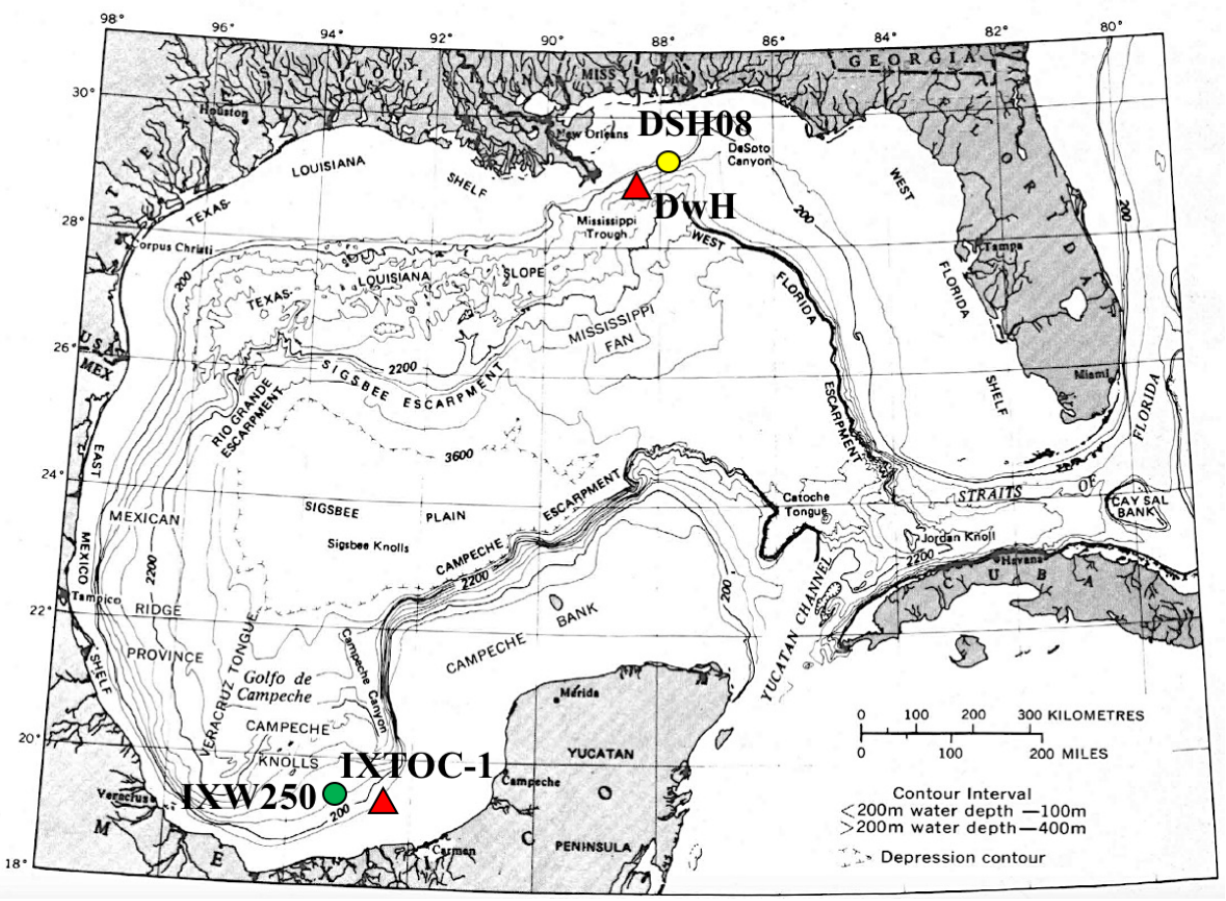

Figure C.1. Map of Gulf of Mexico Basin showing location of DwH blowout (red triangle) and site DSH08 (yellow circle) in NEGoM, as well as location of IXTOC-1 blowout (red triangle) and IXW250 (green circle) in the SWGoM (Garrison and Martin, 1973).

Figure C.1 Literature Cited

Garrison, L.E., and Martin, R.G., Jr., 1973, Geologic Structures in the Gulf of Mexico basin, U.S. Geological Survey, Prof. Paper 773.

Table C.1. Core DSH08, in the NEGoM, site information and sediment texture data.

Site ID	**Collection Date**	**Latitude**		**Longitude**		**Water Depth (m)**
DSH08	12/8/10	29.12092		-87.86545		1143
Top of interval (mm)	Bottom of interval (mm)	% Gravel	% Sand	% Silt	% Clay	% Mud (Silt + Clay)
0	2	0.0	0.9	67.4	31.7	99.1
2	4	0.0	0.8	42.1	57.1	99.2
4	6	0.0	0.5	48.4	51.2	99.5
6	8	0.0	0.4	50.3	49.3	99.6
8	10	0.0	0.7	46.3	53.0	99.3
10	12	0.0	0.5	44.8	54.7	99.5
12	14	0.0	0.5	55.5	44.0	99.5
14	16	0.0	0.9	47.6	51.5	99.1
16	18	0.0	0.6	46.4	53.0	99.4
18	20	0.0	0.9	49.9	49.2	99.1
22	24	0.0	0.5	41.9	57.6	99.5
26	28	0.0	0.8	35.4	63.8	99.2
32	34	0.0	0.7	31.7	67.6	99.3
34	36	0.0	0.3	39.0	60.7	99.7
38	40	0.0	0.9	30.1	69.0	99.1
42	44	0.0	0.5	30.6	68.9	99.5
46	48	0.0	0.5	33.4	66.1	99.5
48	50	0.0	0.5	26.4	73.1	99.5
50	55	0.0	0.3	32.8	66.9	99.7
70	75	0.0	0.4	26.5	73.1	99.6
80	85	0.0	0.3	26.8	72.9	99.7
90	95	0.0	0.4	31.0	68.7	99.6
100	105	0.0	0.5	25.5	74.0	99.5
110	115	0.0	0.6	28.2	71.3	99.4
120	125	0.0	0.7	25.3	74.0	99.3
130	135	0.0	0.3	31.6	68.1	99.7
140	145	0.0	1.3	27.9	70.8	98.7
150	155	0.0	1.2	30.2	68.7	98.8
160	165	0.0	0.8	25.8	73.4	99.2
180	185	0.0	0.8	24.4	74.8	99.2
210	215	0.0	0.6	36.1	63.3	99.4
220	225	0.0	0.6	29.4	70.0	99.4
230	235	0.0	0.6	30.3	69.1	99.4
240	245	0.0	0.5	29.8	69.7	99.5
250	255	0.0	1.8	40.1	58.1	98.2
260	265	0.0	1.0	31.7	67.3	99.0

Table C.2. Core IXW250, in the SWGoM, site information and sediment texture data.

Site ID	**Collection Date**	**Latitude**		**Longitude**		**Water Depth (m)**
IXW250	8/6/15	19.43068		-93.09497		583
Top of interval (mm)	Bottom of interval (mm)	% Gravel	% Sand	% Silt	% Clay	% Mud (Silt + Clay)
0	4	0.0	0.3	32.8	66.9	99.7
6	8	0.0	0.3	28.7	71.0	99.7
8	10	0.0	0.2	33.8	66.0	99.8
10	12	0.0	0.3	36.2	63.5	99.7
12	14	0.0	0.0	33.6	66.4	100.0
14	16	0.0	0.1	29.5	70.4	99.9
16	18	0.0	0.2	37.0	62.8	99.8
18	20	0.0	0.1	34.9	64.9	99.9
20	22	0.0	0.1	45.6	54.2	99.9
22	24	0.0	0.1	35.5	64.3	99.9
24	26	0.0	0.1	36.4	63.5	99.9
26	28	0.0	0.1	34.9	65.0	99.9
28	30	0.0	0.7	40.4	59.0	99.3
30	32	0.0	0.0	41.3	58.7	100.0
32	34	0.0	0.2	27.0	72.7	99.8
34	36	0.0	0.3	37.8	61.9	99.7
36	38	0.0	0.2	40.3	59.6	99.8
38	40	0.0	0.4	34.9	64.8	99.6
40	42	0.0	0.3	31.4	68.3	99.7
42	44	0.0	0.1	30.8	69.1	99.9
44	46	0.0	0.1	32.8	67.0	99.9
46	48	0.0	0.4	31.3	68.3	99.6
48	50	0.0	0.4	37.1	62.5	99.6
50	52	0.0	0.3	41.0	58.7	99.7
52	54	0.0	0.4	42.2	57.5	99.6
54	56	0.0	0.4	39.8	59.8	99.6
56	58	0.0	2.4	33.0	64.6	97.6
60	62	0.0	1.0	30.8	68.2	99.0
64	66	0.0	0.2	36.0	63.8	99.8
70	72	0.0	0.2	32.6	67.2	99.8
80	82	0.0	0.1	36.0	64.0	99.9
90	92	0.0	6.9	35.4	57.7	93.1
100	105	0.0	0.1	41.6	58.2	99.9
110	115	0.0	0.1	37.0	62.9	99.9
130	135	0.0	0.5	34.5	65.0	99.5
150	155	0.0	0.3	47.4	52.3	99.7
170	175	0.0	0.9	40.6	58.4	99.1
190	195	0.0	0.6	35.9	63.5	99.4
210	215	0.3	0.6	46.6	52.5	99.1

Table C.3. Core DSH08 $^{234}Th_{Tot}$ sample mass analyzed (g), and activity (dpm/g) calculated using the IAEA RGU-1 and IAEA-447 calibration lines.

			IAEA RGU-1	IAEA RGU-1	IAEA-447	IAEA-447	RGU-1 minus 447
Top of interval (mm)	Bottom of interval (mm)	Sample Mass (g)	$^{234}Th_{Tot}$ Activity (dpm/g)	$^{234}Th_{Tot}$ Activity Error (dpm/g)	$^{234}Th_{Tot}$ Activity (dpm/g)	$^{234}Th_{Tot}$ Activity Error (dpm/g)	$^{234}Th_{Tot}$ Activity Difference (dpm/g)
0	2	1.59	16.31	0.78	2.74	0.13	13.56
2	4	2.21	13.22	0.59	2.52	0.11	10.70
4	6	2.44	11.03	0.52	2.19	0.10	8.83
6	8	2.93	9.51	0.44	2.06	0.09	7.46
8	10	3.42	7.57	0.36	1.76	0.08	5.81
10	12	3.25	6.95	0.50	1.58	0.11	5.37
12	14	3.73	5.68	0.30	1.38	0.07	4.30
14	16	3.66	5.16	0.30	1.24	0.07	3.92
16	18	3.52	5.30	0.30	1.25	0.07	4.05
18	20	3.54	5.99	0.32	1.42	0.08	4.57
22	24	3.91	4.89	0.28	1.22	0.07	3.67
26	28	4.50	5.34	0.27	1.44	0.07	3.91
32	34	4.49	4.50	0.25	1.21	0.07	3.29
34	36	4.57	4.82	0.25	1.31	0.07	3.51
38	40	4.53	3.97	0.23	1.07	0.06	2.90
42	44	4.66	4.29	0.24	1.18	0.06	3.11
46	48	4.99	4.15	0.22	1.18	0.06	2.97
48	50	5.21	5.00	0.24	1.46	0.07	3.54
50	55	14.30	2.80	0.12	1.48	0.06	1.32
60	65	15.75	2.75	0.11	1.54	0.06	1.21
70	75	14.57	2.39	0.11	1.28	0.06	1.11
80	85	16.26	2.93	0.11	1.67	0.07	1.26
90	95	16.67	2.79	0.11	1.61	0.06	1.18
100	105	18.87	2.85	0.11	1.76	0.07	1.09
110	115	19.59	2.79	0.11	1.76	0.07	1.03
120	125	18.39	3.35	0.12	2.04	0.07	1.31
130	135	17.97	3.30	0.12	1.99	0.07	1.32
140	145	18.65	2.79	0.11	1.71	0.06	1.08
150	155	19.05	2.74	0.15	1.70	0.09	1.04
160	165	19.49	2.78	0.10	1.74	0.07	1.03
180	185	17.75	2.54	0.10	1.52	0.06	1.02
190	195	17.56	2.78	0.11	1.65	0.06	1.13
210	215	8.70	4.08	0.17	1.61	0.07	2.47
230	235	8.07	4.41	0.19	1.66	0.07	2.75
250	255	7.84	4.56	0.19	1.69	0.07	2.87
270	275	19.70	2.72	0.10	1.72	0.06	1.00

Table C.4. Core DSH08 $^{234}Th_{Tot}$ sample mass analyzed (g), and re-analysis activity (*RA) calculated using the IAEA RGU-1 and IAEA-447 calibration lines.

			IAEA RGU-1	IAEA RGU-1	IAEA-447	IAEA-447	RGU-1 minus 447
Top of interval (mm)	Bottom of interval (mm)	Sample Mass (g)	*R.A. $^{234}Th_{Tot}$ Activity (dpm/g)	*R.A. $^{234}Th_{Tot}$ Activity Error (dpm/g)	*R.A. $^{234}Th_{Tot}$ Activity (dpm/g)	*R.A. $^{234}Th_{Tot}$ Activity Error (dpm/g)	*R.A. $^{234}Th_{Tot}$ Activity Difference (dpm/g)
0	2	1.59	5.85	0.38	1.37	0.09	4.48
2	4	2.21	+N.A.	+N.A.	+N.A.	+N.A.	
4	6	2.44	4.78	0.28	1.36	0.08	3.41
6	8	2.93	+N.A.	+N.A.	+N.A.	+N.A.	
8	10	3.42	3.27	0.20	1.12	0.07	2.15
10	12	3.25	+N.A.	+N.A.	+N.A.	+N.A.	
12	14	3.73	3.32	0.19	1.20	0.07	2.13
14	16	3.66					
16	18	3.52					
18	20	3.54					
22	24	3.91					
26	28	4.50					
32	34	4.49					
34	36	4.57					
38	40	4.53					
42	44	4.66					
46	48	4.99					
48	50	5.21					
50	55	14.30					
60	65	15.75					
70	75	14.57					
80	85	16.26					
90	95	16.67					
100	105	18.87					
110	115	19.59					
120	125	18.39					
130	135	17.97					
140	145	18.65					
150	155	19.05					
160	165	19.49					
180	185	17.75					
190	195	17.56					
210	215	8.70					
230	235	8.07					
250	255	7.84					
270	275	19.70					

*RA = Re-analysis of sample >120 days (~5 half-lives) after core collection (i.e., all $^{234}Th_{xs}$ decayed) for determining $^{234}Th_{Sup}$.

+N.A. = Not Analyzed.

Table C.5. Core IXW250 $^{234}Th_{Tot}$ sample mass analyzed (g), activity (dpm/g) calculated using the IAEA RGU-1 and IAEA-447 calibration lines.

			IAEA RGU-1	IAEA RGU-1	IAEA-447	IAEA-447	RGU-1 minus 447
Top of interval (mm)	Bottom of interval (mm)	Sample Mass (g)	$^{234}Th_{Tot}$ Activity (dpm/g)	$^{234}Th_{Tot}$ Activity Error (dpm/g)	$^{234}Th_{Tot}$ Activity (dpm/g)	$^{234}Th_{Tot}$ Activity Error (dpm/g)	$^{234}Th_{Tot}$ Activity Difference (dpm/g)
0	2	1.48	10.49	0.53	1.72	0.09	8.77
2	4	1.58	9.45	0.60	1.59	0.10	7.86
4	6	2.1	8.94	0.50	1.67	0.09	7.27
6	8	2.91	6.87	0.37	1.48	0.08	5.39
8	10	4.03	5.83	0.29	1.48	0.07	4.35
10	12	4.67	4.02	0.23	1.10	0.06	2.92
12	14	4.99	4.07	0.22	1.16	0.06	2.91
14	16	5.61	3.63	0.20	1.11	0.06	2.53
16	18	5.91	3.85	0.20	1.21	0.06	2.64
18	20	5.99	3.79	0.20	1.20	0.06	2.59
20	22	6.02	3.68	0.19	1.16	0.06	2.51
22	24	5.96	3.76	0.20	1.18	0.06	2.58
24	26	6.76	3.32	0.18	1.12	0.06	2.19
26	28	5.94	3.82	0.20	1.20	0.06	2.62
28	30	6.2	4.32	0.21	1.39	0.07	2.93
30	32	6.65	3.40	0.18	1.14	0.06	2.26
32	34	6.64	3.37	0.18	1.13	0.06	2.24
34	36	6.45	3.48	0.18	1.15	0.06	2.33
36	38	6.77	3.25	0.17	1.10	0.06	2.15
38	40	6.37	3.94	0.20	1.29	0.06	2.65
40	42	6.15	3.86	0.20	1.24	0.06	2.62
42	44	6.52	4.18	0.20	1.39	0.07	2.79
44	46	6.75	4.22	0.19	1.43	0.07	2.79
46	48	6.51	3.66	0.19	1.21	0.06	2.45
48	50	6.91	3.65	0.18	1.25	0.06	2.40
50	52	5.98	4.35	0.21	1.37	0.07	2.98
52	54	6.77	4.37	0.20	1.48	0.07	2.89
54	56	7.46	3.79	0.18	1.36	0.06	2.43
56	58	6.38	4.32	0.21	1.42	0.07	2.90
60	62	6.50	3.51	0.18	1.16	0.06	2.35
64	66	6.76	3.68	0.19	1.25	0.06	2.44
70	72	6.86	3.88	0.19	1.33	0.06	2.56
74	76	6.15	3.79	0.19	1.21	0.06	2.57
80	82	6.24	4.43	0.20	1.43	0.07	3.00
84	86	6.65	4.89	0.21	1.64	0.07	3.25
90	92	7.49	4.20	0.19	1.51	0.07	2.69
94	96	6.78	4.73	0.21	1.60	0.07	3.12
100	105	17.50	3.13	0.12	1.85	0.07	1.27
110	115	19.51	3.06	0.11	1.92	0.07	1.14
130	135	18.93	3.51	0.12	2.17	0.07	1.34
150	155	20.10	3.27	0.11	2.09	0.07	1.18
170	175	20.58	3.49	0.12	2.26	0.07	1.24
190	195	20.83	2.85	0.14	1.85	0.09	1.00
210	215	27.30	2.47	0.09	1.82	0.06	0.65
250	255	20.82	2.93	0.10	1.90	0.07	1.03
290	295	20.74	3.14	0.11	2.04	0.07	1.11
330	335	22.82	3.07	0.10	2.09	0.07	0.98

Table C.6. Core DSH08 ^{214}Pb (295keV) activities (dpm/g) calculated using the IAEA RGU-1 and IAEA-447 calibration lines.

Top of interval (mm)	Bottom of interval (mm)	Sample Mass (g)	IAEA RGU-1 ^{214}Pb (295keV) Activity (dpm/g)	IAEA RGU-1 ^{214}Pb (295keV) Activity Error (dpm/g)	IAEA-447 ^{214}Pb (295keV) Activity (dpm/g)	IAEA-447 ^{214}Pb (295keV) Activity Error (dpm/g)	RGU-1 minus 447 ^{214}Pb (295keV) Activity Difference (dpm/g)
0	2	1.59	5.71	0.38	2.55	0.17	3.16
2	4	2.21	3.93	0.27	1.88	0.13	2.05
4	6	2.44	3.75	0.25	1.84	0.12	1.92
6	8	2.93	3.90	0.23	2.00	0.12	1.90
8	10	3.42	3.23	0.20	1.73	0.11	1.50
10	12	3.25	3.12	0.28	1.65	0.15	1.47
12	14	3.73	2.93	0.18	1.61	0.10	1.32
14	16	3.66	3.79	0.21	2.07	0.11	1.71
16	18	3.52	3.07	0.19	1.66	0.10	1.41
18	20	3.54	4.26	0.22	2.31	0.12	1.95
22	24	3.91	5.50	0.24	3.08	0.14	2.43
26	28	4.5	4.52	0.21	2.65	0.12	1.87
32	34	4.49	3.35	0.18	1.96	0.10	1.39
34	36	4.57	3.29	0.17	1.94	0.10	1.35
38	40	4.53	2.54	0.15	1.49	0.09	1.05
42	44	4.66	2.89	0.16	1.72	0.10	1.18
46	48	4.99	2.43	0.14	1.48	0.09	0.95
48	50	5.21	2.38	0.14	1.47	0.09	0.91
50	55	14.3	2.18	0.08	2.07	0.08	0.11
60	65	15.75	1.95	0.08	1.93	0.08	0.01
70	75	14.57	2.08	0.08	1.99	0.08	0.08
80	85	16.26	2.23	0.08	2.25	0.08	-0.02
90	95	16.67	1.89	0.07	1.92	0.07	-0.04
100	105	18.87	2.15	0.07	2.31	0.08	-0.16
110	115	19.59	1.70	0.07	1.85	0.07	-0.16
120	125	18.39	2.12	0.08	2.26	0.08	-0.14
130	135	17.97	2.09	0.08	2.20	0.08	-0.11
140	145	18.65	1.86	0.07	1.99	0.07	-0.13
150	155	19.05	1.99	0.10	2.15	0.11	-0.16
160	165	19.49	1.93	0.07	2.11	0.08	-0.17
180	185	17.75	1.84	0.07	1.92	0.08	-0.09
190	195	17.56	1.81	0.07	1.89	0.07	-0.08
210	215	8.7	2.46	0.11	1.87	0.08	0.59
230	235	8.07	2.50	0.12	1.84	0.09	0.66
250	255	7.84	2.41	0.11	1.75	0.08	0.66
270	275	19.7	1.98	0.07	2.17	0.08	-0.19

Table C.7. Core DSH08 ^{214}Pb (351keV) activities (dpm/g) calculated using the IAEA RGU-1 and IAEA-447 calibration lines.

			IAEA RGU-1	IAEA RGU-1	IAEA-447	IAEA-447	RGU-1 minus 447
Top of interval (mm)	Bottom of interval (mm)	Sample Mass (g)	^{214}Pb (351keV) Activity (dpm/g)	^{214}Pb (351keV) Activity Error (dpm/g)	^{214}Pb (351keV) Activity (dpm/g)	^{214}Pb (351keV) Activity Error (dpm/g)	^{214}Pb (351keV) Activity Difference (dpm/g)
0	2	1.59	5.64	0.30	2.54	0.14	3.10
2	4	2.21	4.22	0.22	2.03	0.11	2.19
4	6	2.44	3.63	0.20	1.78	0.10	1.85
6	8	2.93	3.90	0.19	2.01	0.10	1.90
8	10	3.42	4.07	0.18	2.18	0.09	1.88
10	12	3.25	3.40	0.23	1.80	0.12	1.60
12	14	3.73	3.18	0.15	1.75	0.08	1.43
14	16	3.66	3.59	0.16	1.96	0.09	1.62
16	18	3.52	3.28	0.16	1.77	0.08	1.50
18	20	3.54	3.82	0.17	2.07	0.09	1.75
22	24	3.91	5.83	0.20	3.26	0.11	2.57
26	28	4.5	4.04	0.16	2.36	0.09	1.68
32	34	4.49	3.31	0.14	1.93	0.08	1.38
34	36	4.57	3.18	0.14	1.87	0.08	1.31
38	40	4.53	2.64	0.12	1.55	0.07	1.09
42	44	4.66	2.62	0.12	1.55	0.07	1.07
46	48	4.99	2.64	0.12	1.60	0.07	1.04
48	50	5.21	2.25	0.11	1.38	0.07	0.87
50	55	14.3	2.16	0.07	2.00	0.06	0.16
60	65	15.75	2.20	0.07	2.12	0.06	0.08
70	75	14.57	1.87	0.06	1.75	0.06	0.12
80	85	16.26	2.21	0.07	2.16	0.06	0.05
90	95	16.67	1.80	0.06	1.78	0.06	0.02
100	105	18.87	2.02	0.06	2.09	0.06	-0.08
110	115	19.59	1.92	0.06	2.02	0.06	-0.11
120	125	18.39	2.00	0.06	2.06	0.06	-0.06
130	135	17.97	2.14	0.06	2.19	0.06	-0.04
140	145	18.65	1.92	0.06	1.99	0.06	-0.07
150	155	19.05	1.89	0.08	1.97	0.08	-0.08
160	165	19.49	2.04	0.06	2.15	0.06	-0.11
180	185	17.75	2.04	0.06	2.07	0.06	-0.03
190	195	17.56	1.88	0.06	1.90	0.06	-0.02
210	215	8.7	2.60	0.09	1.95	0.07	0.65
230	235	8.07	2.78	0.10	2.02	0.07	0.76
250	255	7.84	2.50	0.09	1.80	0.07	0.70
270	275	19.7	2.07	0.06	2.19	0.06	-0.12

Table C.8. Core DSH08 ^{214}Bi activities (dpm/g) calculated using the IAEA RGU-1 and IAEA-447 calibration lines.

			IAEA RGU-1	IAEA RGU-1	IAEA-447	IAEA-447	RGU-1 minus 447
Top of interval (mm)	Bottom of interval (mm)	Sample Mass (g)	^{214}Bi Activity (dpm/g)	^{214}Bi Activity Error (dpm/g)	^{214}Bi Activity (dpm/g)	^{214}Bi Activity Error (dpm/g)	^{214}Bi Activity Difference (dpm/g)
0	2	1.59	7.41	0.30	2.22	0.14	5.19
2	4	2.21	5.59	0.22	1.86	0.12	3.73
4	6	2.44	5.14	0.20	1.77	0.11	3.38
6	8	2.93	4.83	0.19	1.78	0.10	3.05
8	10	3.42	4.96	0.18	1.95	0.10	3.01
10	12	3.25	3.66	0.23	1.41	0.13	2.25
12	14	3.73	3.65	0.15	1.49	0.09	2.16
14	16	3.66	4.56	0.16	1.84	0.10	2.71
16	18	3.52	3.40	0.16	1.35	0.09	2.05
18	20	3.54	4.28	0.17	1.71	0.10	2.57
22	24	3.91	5.65	0.20	2.35	0.11	3.30
26	28	4.5	4.44	0.16	1.98	0.10	2.47
32	34	4.49	4.14	0.14	1.84	0.09	2.30
34	36	4.57	3.78	0.14	1.70	0.09	2.09
38	40	4.53	2.46	0.12	1.10	0.07	1.36
42	44	4.66	2.89	0.12	1.31	0.08	1.59
46	48	4.99	3.02	0.12	1.41	0.08	1.61
48	50	5.21	2.57	0.11	1.23	0.08	1.35
50	55	14.3	2.28	0.07	1.86	0.08	0.42
60	65	15.75	2.36	0.07	2.03	0.08	0.34
70	75	14.57	1.87	0.06	1.54	0.07	0.33
80	85	16.26	2.30	0.07	2.00	0.08	0.30
90	95	16.67	2.13	0.06	1.88	0.07	0.25
100	105	18.87	2.28	0.06	2.14	0.08	0.15
110	115	19.59	2.06	0.06	1.96	0.08	0.10
120	125	18.39	2.00	0.06	1.85	0.08	0.15
130	135	17.97	2.35	0.06	2.15	0.08	0.20
140	145	18.65	1.87	0.06	1.74	0.07	0.13
150	155	19.05	1.95	0.08	1.84	0.10	0.12
160	165	19.49	2.11	0.06	2.01	0.08	0.11
180	185	17.75	2.10	0.06	1.91	0.08	0.19
190	195	17.56	2.15	0.06	1.94	0.08	0.20
210	215	8.7	2.84	0.09	1.78	0.08	1.07
230	235	8.07	2.85	0.10	1.71	0.08	1.14
250	255	7.84	2.73	0.09	1.61	0.08	1.12
270	275	19.7	2.09	0.06	2.00	0.07	0.10

Table C.9. Core IXW250 ^{214}Pb (295keV) activities (dpm/g) calculated using the IAEA RGU-1 and IAEA-447 calibration lines.

Top of interval (mm)	Bottom of interval (mm)	Sample Mass (g)	IAEA RGU-1 ^{214}Pb (295keV) Activity (dpm/g)	IAEA RGU-1 ^{214}Pb (295keV) Activity Error (dpm/g)	IAEA-447 ^{214}Pb (295keV) Activity (dpm/g)	IAEA-447 ^{214}Pb (295keV) Activity Error (dpm/g)	RGU-1 minus 447 ^{214}Pb (295keV) Activity Difference (dpm/g)
0	2	1.48	3.59	0.26	1.58	0.11	2.01
2	4	1.58	3.90	0.32	1.74	0.14	2.16
4	6	2.1	3.22	0.25	1.52	0.12	1.70
6	8	2.91	2.41	0.18	1.23	0.09	1.18
8	10	4.03	2.92	0.17	1.65	0.10	1.27
10	12	4.67	2.03	0.13	1.20	0.08	0.82
12	14	4.99	2.57	0.15	1.56	0.09	1.01
14	16	5.61	2.39	0.13	1.52	0.09	0.87
16	18	5.91	2.63	0.13	1.70	0.09	0.92
18	20	5.99	2.61	0.14	1.70	0.09	0.91
20	22	6.02	2.41	0.13	1.57	0.08	0.84
22	24	5.96	2.51	0.13	1.63	0.09	0.88
24	26	6.76	2.37	0.12	1.62	0.08	0.75
26	28	5.94	2.54	0.13	1.65	0.09	0.89
28	30	6.2	2.64	0.13	1.74	0.09	0.90
30	32	6.65	2.07	0.12	1.41	0.08	0.66
32	34	6.64	2.41	0.12	1.63	0.08	0.77
34	36	6.45	2.47	0.13	1.66	0.09	0.81
36	38	6.77	2.17	0.12	1.49	0.08	0.69
38	40	6.37	1.95	0.11	1.30	0.08	0.65
40	42	6.15	1.92	0.12	1.27	0.08	0.66
42	44	6.52	2.14	0.12	1.44	0.08	0.70
44	46	6.75	2.16	0.12	1.48	0.08	0.68
46	48	6.51	1.94	0.11	1.31	0.08	0.63
48	50	6.91	1.78	0.11	1.23	0.07	0.55
50	52	5.98	2.50	0.13	1.63	0.09	0.87
52	54	6.77	2.07	0.11	1.41	0.08	0.65
54	56	7.46	1.71	0.10	1.22	0.07	0.49
56	58	6.38	2.04	0.12	1.36	0.08	0.68
60	62	6.50	1.90	0.11	1.28	0.08	0.62
64	66	6.76	2.31	0.12	1.58	0.08	0.73
70	72	6.86	2.32	0.12	1.60	0.08	0.73
74	76	6.15	2.33	0.13	1.54	0.08	0.80
80	82	6.24	2.01	0.11	1.33	0.08	0.68
84	86	6.65	2.12	0.12	1.44	0.08	0.68
90	92	7.49	2.24	0.11	1.60	0.08	0.64
94	96	6.78	1.87	0.11	1.28	0.07	0.59
100	105	17.50	1.48	0.07	1.54	0.07	-0.06
110	115	19.51	1.64	0.06	1.79	0.07	-0.15
130	135	18.93	1.64	0.06	1.77	0.07	-0.13
150	155	20.10	1.66	0.06	1.83	0.07	-0.17
170	175	20.58	1.79	0.07	2.00	0.08	-0.21
190	195	20.83	1.73	0.09	1.94	0.10	-0.21
210	215	27.30	1.19	0.05	1.47	0.06	-0.29
250	255	20.82	1.48	0.06	1.66	0.07	-0.18
290	295	20.74	1.47	0.06	1.65	0.07	-0.18
330	335	22.82	1.47	0.06	1.71	0.07	-0.24

Table C.10. Core IXW250 ^{214}Pb (351keV) activities (dpm/g) calculated using the IAEA RGU-1 and IAEA-447 calibration lines.

			IAEA RGU-1	IAEA RGU-1	IAEA-447	IAEA-447	RGU-1 minus 447
Top of interval (mm)	Bottom of interval (mm)	Sample Mass (g)	^{214}Pb (351keV) Activity (dpm/g)	^{214}Pb (351keV) Activity Error (dpm/g)	^{214}Pb (351keV) Activity (dpm/g)	^{214}Pb (351keV) Activity Error (dpm/g)	^{214}Pb (351keV) Activity Difference (dpm/g)
0	2	1.48	4.32	0.22	1.92	0.10	2.40
2	4	1.58	4.40	0.27	1.98	0.12	2.42
4	6	2.1	3.29	0.20	1.56	0.10	1.73
6	8	2.91	3.14	0.17	1.61	0.09	1.53
8	10	4.03	2.63	0.13	1.48	0.07	1.15
10	12	4.67	2.15	0.11	1.28	0.07	0.88
12	14	4.99	2.23	0.11	1.35	0.07	0.88
14	16	5.61	2.45	0.11	1.55	0.07	0.90
16	18	5.91	2.43	0.10	1.56	0.07	0.87
18	20	5.99	2.47	0.11	1.60	0.07	0.87
20	22	6.02	2.48	0.10	1.60	0.07	0.87
22	24	5.96	2.39	0.11	1.54	0.07	0.85
24	26	6.76	2.36	0.10	1.60	0.07	0.76
26	28	5.94	2.83	0.11	1.83	0.07	1.01
28	30	6.2	2.23	0.10	1.46	0.07	0.77
30	32	6.65	2.50	0.10	1.68	0.07	0.82
32	34	6.64	2.43	0.10	1.64	0.07	0.80
34	36	6.45	2.30	0.10	1.53	0.07	0.77
36	38	6.77	1.95	0.09	1.32	0.06	0.63
38	40	6.37	1.89	0.09	1.25	0.06	0.64
40	42	6.15	2.08	0.10	1.36	0.06	0.72
42	44	6.52	2.25	0.10	1.50	0.06	0.75
44	46	6.75	1.90	0.09	1.28	0.06	0.61
46	48	6.51	2.28	0.10	1.52	0.07	0.76
48	50	6.91	2.06	0.09	1.40	0.06	0.65
50	52	5.98	1.95	0.09	1.26	0.06	0.69
52	54	6.77	2.36	0.10	1.60	0.07	0.76
54	56	7.46	2.08	0.09	1.46	0.06	0.61
56	58	6.38	2.03	0.09	1.34	0.06	0.68
60	62	6.50	2.04	0.09	1.36	0.06	0.68
64	66	6.76	1.92	0.09	1.30	0.06	0.62
70	72	6.86	1.96	0.09	1.33	0.06	0.62
74	76	6.15	2.09	0.10	1.37	0.06	0.72
80	82	6.24	1.98	0.09	1.30	0.06	0.68
84	86	6.65	2.02	0.09	1.36	0.06	0.66
90	92	7.49	2.12	0.09	1.49	0.06	0.62
94	96	6.78	1.99	0.09	1.35	0.06	0.64
100	105	17.50	1.57	0.05	1.59	0.05	-0.01
110	115	19.51	1.58	0.05	1.67	0.05	-0.08
130	135	18.93	1.65	0.05	1.72	0.05	-0.07
150	155	20.10	1.53	0.05	1.63	0.05	-0.10
170	175	20.58	1.60	0.05	1.72	0.06	-0.12
190	195	20.83	1.55	0.07	1.67	0.07	-0.12
210	215	27.30	1.28	0.04	1.52	0.05	-0.24
250	255	20.82	1.60	0.05	1.73	0.05	-0.13
290	295	20.74	1.75	0.05	1.89	0.06	-0.14

Table C.11. Core IXW250 ^{214}Bi activities (dpm/g) calculated using the IAEA RGU-1 and IAEA-447 calibration lines.

			IAEA RGU-1	IAEA RGU-1	IAEA-447	IAEA-447	RGU-1 minus 447
Top of interval (mm)	Bottom of interval (mm)	Sample Mass (g)	^{214}Bi Activity (dpm/g)	^{214}Bi Activity Error (dpm/g)	^{214}Bi Activity (dpm/g)	^{214}Bi Activity Error (dpm/g)	^{214}Bi Activity Difference (dpm/g)
0	2	1.48	5.56	0.35	1.63	0.10	3.93
2	4	1.58	5.57	0.42	1.67	0.12	3.90
4	6	2.1	5.17	0.34	1.69	0.11	3.48
6	8	2.91	4.09	0.26	1.50	0.10	2.58
8	10	4.03	3.66	0.21	1.55	0.09	2.12
10	12	4.67	2.71	0.17	1.23	0.08	1.49
12	14	4.99	3.02	0.17	1.41	0.08	1.61
14	16	5.61	2.81	0.16	1.39	0.08	1.42
16	18	5.91	3.10	0.16	1.58	0.08	1.52
18	20	5.99	3.07	0.16	1.57	0.08	1.50
20	22	6.02	2.85	0.15	1.46	0.08	1.39
22	24	5.96	2.51	0.15	1.28	0.07	1.22
24	26	6.76	2.93	0.15	1.60	0.08	1.33
26	28	5.94	3.33	0.17	1.70	0.09	1.63
28	30	6.2	2.62	0.15	1.37	0.08	1.25
30	32	6.65	2.87	0.15	1.55	0.08	1.32
32	34	6.64	2.90	0.15	1.57	0.08	1.33
34	36	6.45	2.57	0.14	1.37	0.08	1.20
36	38	6.77	2.37	0.13	1.30	0.07	1.08
38	40	6.37	2.37	0.14	1.25	0.07	1.12
40	42	6.15	2.45	0.14	1.27	0.07	1.18
42	44	6.52	2.56	0.14	1.37	0.08	1.19
44	46	6.75	2.27	0.13	1.24	0.07	1.03
46	48	6.51	2.48	0.14	1.33	0.07	1.15
48	50	6.91	2.13	0.13	1.17	0.07	0.95
50	52	5.98	2.86	0.16	1.47	0.08	1.40
52	54	6.77	2.72	0.14	1.48	0.08	1.23
54	56	7.46	2.37	0.13	1.37	0.07	1.01
56	58	6.38	2.34	0.14	1.24	0.07	1.10
60	62	6.50	2.38	0.14	1.27	0.07	1.11
64	66	6.76	2.18	0.13	1.19	0.07	0.99
70	72	6.86	2.34	0.13	1.29	0.07	1.05
74	76	6.15	2.32	0.14	1.20	0.07	1.11
80	82	6.24	2.26	0.13	1.18	0.07	1.08
84	86	6.65	2.50	0.14	1.35	0.07	1.15
90	92	7.49	2.41	0.13	1.39	0.07	1.02
94	96	6.78	2.39	0.13	1.30	0.07	1.08
100	105	17.50	1.80	0.08	1.62	0.07	0.17
110	115	19.51	1.58	0.07	1.50	0.06	0.08
130	135	18.93	1.78	0.07	1.67	0.07	0.11
150	155	20.10	1.73	0.07	1.67	0.07	0.06
170	175	20.58	1.87	0.07	1.82	0.07	0.05
190	195	20.83	1.74	0.10	1.70	0.09	0.04
210	215	27.30	1.30	0.05	1.41	0.06	-0.10
250	255	20.82	1.71	0.07	1.67	0.07	0.04
290	295	20.74	1.82	0.07	1.78	0.07	0.04
330	335	22.82	1.78	0.07	1.81	0.07	-0.03

Table C.12. Core DSH08 $^{210}Pb_{Sup}$ activities (dpm/g) calculated by averaging ^{214}Pb (295keV), ^{214}Pb (351keV) and ^{214}Bi activities calculated using the IAEA RGU-1 and IAEA-447 calibration lines.

			IAEA RGU-1	IAEA RGU-1	IAEA-447	IAEA-447	RGU-1 minus 447
Top of interval (mm)	Bottom of interval (mm)	Sample Mass (g)	$^{210}Pb_{Sup}$ Activity (dpm/g)	$^{210}Pb_{Sup}$ Activity Error (dpm/g)	$^{210}Pb_{Sup}$ Activity (dpm/g)	$^{210}Pb_{Sup}$ Activity Error (dpm/g)	$^{210}Pb_{Sup}$ Activity Difference (dpm/g)
0	2	1.59	6.25	0.39	2.44	0.15	3.82
2	4	2.21	4.58	0.28	1.92	0.12	2.66
4	6	2.44	4.18	0.26	1.80	0.11	2.38
6	8	2.93	4.21	0.23	1.93	0.11	2.28
8	10	3.42	4.08	0.21	1.95	0.10	2.13
10	12	3.25	3.39	0.28	1.62	0.13	1.78
12	14	3.73	3.25	0.18	1.62	0.09	1.64
14	16	3.66	3.98	0.21	1.96	0.10	2.02
16	18	3.52	3.25	0.19	1.59	0.09	1.65
18	20	3.54	4.12	0.21	2.03	0.10	2.09
22	24	3.91	5.66	0.24	2.90	0.12	2.77
26	28	4.5	4.34	0.19	2.33	0.10	2.01
32	34	4.49	3.60	0.18	1.91	0.09	1.69
34	36	4.57	3.42	0.17	1.83	0.09	1.58
38	40	4.53	2.55	0.15	1.38	0.08	1.17
42	44	4.66	2.80	0.15	1.52	0.08	1.28
46	48	4.99	2.70	0.14	1.50	0.08	1.20
48	50	5.21	2.40	0.14	1.36	0.08	1.04
50	55	14.3	2.21	0.08	1.98	0.07	0.23
60	65	15.75	2.17	0.08	2.03	0.07	0.14
70	75	14.57	1.94	0.08	1.76	0.07	0.18
80	85	16.26	2.25	0.08	2.14	0.07	0.11
90	95	16.67	1.94	0.07	1.86	0.07	0.08
100	105	18.87	2.15	0.07	2.18	0.07	-0.03
110	115	19.59	1.89	0.07	1.95	0.07	-0.05
120	125	18.39	2.04	0.07	2.05	0.07	-0.01
130	135	17.97	2.19	0.07	2.18	0.07	0.02
140	145	18.65	1.88	0.07	1.91	0.07	-0.02
150	155	19.05	1.94	0.10	1.99	0.10	-0.04
160	165	19.49	2.03	0.07	2.09	0.07	-0.06
180	185	17.75	1.99	0.07	1.97	0.07	0.02
190	195	17.56	1.95	0.07	1.91	0.07	0.04
210	215	8.7	2.64	0.11	1.87	0.08	0.77
230	235	8.07	2.71	0.12	1.86	0.08	0.85
250	255	7.84	2.55	0.11	1.72	0.08	0.83
270	275	19.7	2.05	0.07	2.12	0.07	-0.07

Table C.13. Core IXW250 $^{210}Pb_{Sup}$ activities (dpm/g) calculated by averaging ^{214}Pb (295keV), ^{214}Pb (351keV) and ^{214}Bi activities calculated using the IAEA RGU-1 and IAEA-447 calibration lines.

			IAEA RGU-1	IAEA RGU-1	IAEA-447	IAEA-447	RGU-1 minus 447
Top of interval (mm)	Bottom of interval (mm)	Sample Mass (g)	$^{210}Pb_{Sup}$ Activity (dpm/g)	$^{210}Pb_{Sup}$ Activity Error (dpm/g)	$^{210}Pb_{Sup}$ Activity (dpm/g)	$^{210}Pb_{Sup}$ Activity Error (dpm/g)	$^{210}Pb_{Sup}$ Activity Difference (dpm/g)
0	2	1.48	4.49	0.28	1.71	0.10	2.78
2	4	1.58	4.62	0.33	1.79	0.13	2.83
4	6	2.1	3.89	0.26	1.59	0.11	2.30
6	8	2.91	3.21	0.20	1.45	0.09	1.76
8	10	4.03	3.07	0.17	1.56	0.09	1.51
10	12	4.67	2.30	0.14	1.24	0.07	1.06
12	14	4.99	2.61	0.14	1.44	0.08	1.17
14	16	5.61	2.55	0.13	1.49	0.08	1.06
16	18	5.91	2.72	0.13	1.61	0.08	1.10
18	20	5.99	2.72	0.14	1.62	0.08	1.09
20	22	6.02	2.58	0.13	1.55	0.08	1.03
22	24	5.96	2.47	0.13	1.49	0.08	0.98
24	26	6.76	2.55	0.12	1.61	0.08	0.95
26	28	5.94	2.90	0.14	1.72	0.08	1.18
28	30	6.2	2.50	0.13	1.52	0.08	0.97
30	32	6.65	2.48	0.12	1.55	0.08	0.93
32	34	6.64	2.58	0.12	1.61	0.08	0.97
34	36	6.45	2.45	0.12	1.52	0.08	0.93
36	38	6.77	2.17	0.11	1.37	0.07	0.80
38	40	6.37	2.07	0.11	1.27	0.07	0.80
40	42	6.15	2.15	0.12	1.30	0.07	0.85
42	44	6.52	2.32	0.12	1.44	0.07	0.88
44	46	6.75	2.11	0.11	1.33	0.07	0.78
46	48	6.51	2.23	0.12	1.39	0.07	0.85
48	50	6.91	1.99	0.11	1.27	0.07	0.72
50	52	5.98	2.44	0.13	1.45	0.08	0.99
52	54	6.77	2.38	0.12	1.50	0.07	0.88
54	56	7.46	2.05	0.10	1.35	0.07	0.70
56	58	6.38	2.14	0.12	1.31	0.07	0.82
60	62	6.5	2.11	0.11	1.31	0.07	0.80
64	66	6.76	2.14	0.11	1.36	0.07	0.78
70	72	6.86	2.21	0.11	1.41	0.07	0.80
74	76	6.15	2.25	0.12	1.37	0.07	0.88
80	82	6.24	2.08	0.11	1.27	0.07	0.81
84	86	6.65	2.21	0.11	1.38	0.07	0.83
90	92	7.49	2.25	0.11	1.49	0.07	0.76
94	96	6.78	2.08	0.11	1.31	0.07	0.77
100	105	17.5	1.62	0.07	1.58	0.06	0.03
110	115	19.51	1.60	0.06	1.65	0.06	-0.05
130	135	18.93	1.69	0.06	1.72	0.06	-0.03
150	155	20.1	1.64	0.06	1.71	0.06	-0.07
170	175	20.58	1.75	0.06	1.85	0.07	-0.09
190	195	20.83	1.67	0.09	1.77	0.09	-0.10
210	215	27.3	1.25	0.05	1.47	0.06	-0.21
250	255	20.82	1.60	0.06	1.69	0.06	-0.09
290	295	20.74	1.68	0.06	1.77	0.06	-0.09
330	335	22.82	1.58	0.06	1.73	0.06	-0.15

Table C.14. Core DSH08 $^{210}Pb_{Tot}$ activities (dpm/g) calculated using the IAEA RGU-1 and IAEA-447 calibration lines.

			IAEA RGU-1	IAEA RGU-1	IAEA-447	IAEA-447	RGU-1 minus 447
Top of interval (mm)	Bottom of interval (mm)	Sample Mass (g)	$^{210}Pb_{Tot}$ Activity (dpm/g)	$^{210}Pb_{Tot}$ Activity Error (dpm/g)	$^{210}Pb_{Tot}$ Activity (dpm/g)	$^{210}Pb_{Tot}$ Activity Error (dpm/g)	$^{210}Pb_{Tot}$ Activity Difference (dpm/g)
0	2	1.59	72.74	1.55	64.45	1.37	8.29
2	4	2.21	74.89	1.33	67.09	1.19	7.79
4	6	2.44	69.72	1.24	62.72	1.11	7.00
6	8	2.93	71.62	1.13	64.97	1.03	6.65
8	10	3.42	70.96	1.05	64.90	0.96	6.06
10	12	3.25	61.39	1.41	55.99	1.29	5.40
12	14	3.73	56.56	0.90	51.99	0.83	4.57
14	16	3.66	65.12	0.99	59.79	0.91	5.33
16	18	3.52	52.01	0.89	47.65	0.82	4.37
18	20	3.54	52.75	0.89	48.34	0.82	4.41
22	24	3.91	56.20	0.89	51.81	0.82	4.39
26	28	4.5	46.58	0.76	43.34	0.70	3.24
32	34	4.49	39.89	0.69	37.11	0.65	2.78
34	36	4.57	43.14	0.72	40.18	0.67	2.96
38	40	4.53	40.39	0.70	37.59	0.65	2.80
42	44	4.66	36.13	0.65	33.70	0.61	2.44
46	48	4.99	34.20	0.61	32.05	0.57	2.15
48	50	5.21	29.44	0.56	27.68	0.53	1.76
50	55	14.3	27.03	0.35	28.20	0.37	-1.17
60	65	15.75	20.94	0.30	22.12	0.32	-1.18
70	75	14.57	17.94	0.28	18.76	0.30	-0.82
80	85	16.26	14.50	0.25	15.38	0.26	-0.88
90	95	16.67	11.74	0.22	12.49	0.23	-0.75
100	105	18.87	10.46	0.20	11.31	0.21	-0.85
110	115	19.59	7.22	0.17	7.85	0.18	-0.63
120	125	18.39	6.40	0.16	6.90	0.18	-0.50
130	135	17.97	4.51	0.13	4.85	0.14	-0.34
140	145	18.65	3.74	0.12	4.04	0.13	-0.30
150	155	19.05	3.11	0.15	3.37	0.16	-0.26
160	165	19.49	3.07	0.11	3.33	0.12	-0.26
180	185	17.75	2.88	0.11	3.09	0.12	-0.21
190	195	17.56	2.38	0.10	2.55	0.10	-0.17
210	215	8.7	3.00	0.14	2.96	0.14	0.05
230	235	8.07	2.98	0.15	2.91	0.14	0.07
250	255	7.84	3.27	0.16	3.19	0.15	0.08
270	275	19.7	2.14	0.09	2.33	0.10	-0.19

Table C.15. Core IXW250 $^{210}Pb_{Tot}$ activities (dpm/g) calculated using the IAEA RGU-1 and IAEA-447 calibration lines.

			IAEA RGU-1	IAEA RGU-1	IAEA-447	IAEA-447	RGU-1 minus 447
Top of interval (mm)	Bottom of interval (mm)	Sample Mass (g)	$^{210}Pb_{Tot}$ Activity (dpm/g)	$^{210}Pb_{Tot}$ Activity Error (dpm/g)	$^{210}Pb_{Tot}$ Activity (dpm/g)	$^{210}Pb_{Tot}$ Activity Error (dpm/g)	$^{210}Pb_{Tot}$ Activity Difference (dpm/g)
0	2	1.48	30.61	0.85	27.06	0.75	3.54
2	4	1.58	24.88	0.91	22.04	0.81	2.84
4	6	2.1	25.23	0.79	22.56	0.71	2.67
6	8	2.91	23.50	0.66	21.31	0.60	2.19
8	10	4.03	23.72	0.56	21.91	0.52	1.81
10	12	4.67	20.34	0.49	18.98	0.46	1.37
12	14	4.99	21.22	0.48	19.89	0.45	1.33
14	16	5.61	20.68	0.45	19.56	0.43	1.12
16	18	5.91	21.08	0.44	20.02	0.41	1.06
18	20	5.99	20.59	0.44	19.58	0.42	1.01
20	22	6.02	20.13	0.43	19.15	0.41	0.98
22	24	5.96	20.61	0.44	19.59	0.42	1.02
24	26	6.76	20.94	0.42	20.13	0.41	0.82
26	28	5.94	21.26	0.45	20.20	0.43	1.06
28	30	6.2	20.09	0.43	19.15	0.41	0.93
30	32	6.65	20.15	0.42	19.34	0.40	0.82
32	34	6.64	18.21	0.39	17.47	0.38	0.74
34	36	6.45	19.19	0.41	18.36	0.39	0.83
36	38	6.77	18.76	0.40	18.03	0.38	0.73
38	40	6.37	20.72	0.43	19.81	0.41	0.91
40	42	6.15	21.67	0.45	20.65	0.42	1.02
42	44	6.52	21.97	0.44	21.04	0.42	0.93
44	46	6.75	19.46	0.40	18.70	0.38	0.76
46	48	6.51	17.81	0.39	17.05	0.38	0.75
48	50	6.91	14.25	0.35	13.72	0.34	0.53
50	52	5.98	15.51	0.38	14.74	0.36	0.76
52	54	6.77	14.09	0.34	13.54	0.33	0.55
54	56	7.46	12.66	0.31	12.27	0.30	0.38
56	58	6.38	11.31	0.32	10.81	0.31	0.50
60	62	6.5	10.36	0.30	9.92	0.29	0.44
64	66	6.76	7.73	0.26	7.43	0.25	0.30
70	72	6.86	6.98	0.24	6.71	0.23	0.26
74	76	6.15	6.33	0.24	6.04	0.23	0.30
80	82	6.24	6.65	0.24	6.34	0.23	0.30
84	86	6.65	5.47	0.22	5.25	0.21	0.22
90	92	7.49	5.87	0.21	5.70	0.21	0.18
94	96	6.78	4.56	0.20	4.38	0.19	0.18
100	105	17.5	3.66	0.12	3.92	0.13	-0.26
110	115	19.51	2.69	0.10	2.93	0.11	-0.23
130	135	18.93	2.26	0.09	2.45	0.10	-0.19
150	155	20.1	1.97	0.08	2.15	0.09	-0.18
170	175	20.58	1.93	0.08	2.11	0.09	-0.18
190	195	20.83	1.85	0.11	2.02	0.12	-0.18
210	215	27.3	1.67	0.07	1.89	0.08	-0.23
250	255	20.82	1.86	0.08	2.03	0.09	-0.18
290	295	20.74	1.92	0.08	2.10	0.09	-0.18
330	335	22.82	1.90	0.08	2.11	0.09	-0.21

Table C.16. Core DSH08 $^{210}Pb_{xs}$ activities (dpm/g) calculated using the IAEA RGU-1 and IAEA-447 calibration lines.

			IAEA RGU-1	IAEA RGU-1	IAEA-447	IAEA-447	RGU-1 minus 447
Top of interval (mm)	Bottom of interval (mm)	Sample Mass (g)	$^{210}Pb_{xs}$ Activity (dpm/g)	$^{210}Pb_{xs}$ Activity Error (dpm/g)	$^{210}Pb_{xs}$ Activity (dpm/g)	$^{210}Pb_{xs}$ Activity Error (dpm/g)	$^{210}Pb_{xs}$ Activity Difference (dpm/g)
0	2	1.59	66.49	1.60	62.01	1.38	4.48
2	4	2.21	70.30	1.36	65.17	1.20	5.13
4	6	2.44	65.55	1.26	60.93	1.12	4.62
6	8	2.93	67.41	1.16	63.04	1.03	4.37
8	10	3.42	66.87	1.07	62.94	0.97	3.93
10	12	3.25	57.99	1.44	54.37	1.30	3.62
12	14	3.73	53.30	0.92	50.37	0.83	2.94
14	16	3.66	61.14	1.02	57.83	0.92	3.31
16	18	3.52	48.77	0.91	46.05	0.82	2.71
18	20	3.54	48.63	0.92	46.31	0.82	2.32
22	24	3.91	50.54	0.93	48.91	0.83	1.63
26	28	4.5	42.25	0.78	41.01	0.71	1.24
32	34	4.49	36.29	0.72	35.19	0.65	1.10
34	36	4.57	39.73	0.74	38.35	0.68	1.38
38	40	4.53	37.84	0.72	36.21	0.66	1.63
42	44	4.66	33.33	0.67	32.17	0.61	1.16
46	48	4.99	31.51	0.63	30.56	0.58	0.95
48	50	5.21	27.04	0.58	26.32	0.54	0.72
50	55	14.3	24.82	0.36	26.22	0.37	-1.40
60	65	15.75	18.77	0.31	20.09	0.32	-1.32
70	75	14.57	16.00	0.29	17.00	0.31	-1.00
80	85	16.26	12.25	0.26	13.24	0.27	-0.99
90	95	16.67	9.79	0.23	10.62	0.24	-0.83
100	105	18.87	8.31	0.21	9.13	0.23	-0.82
110	115	19.59	5.33	0.18	5.90	0.20	-0.57
120	125	18.39	4.36	0.18	4.85	0.19	-0.48
130	135	17.97	2.32	0.15	2.67	0.16	-0.35
140	145	18.65	1.85	0.14	2.13	0.15	-0.28
150	155	19.05	1.17	0.18	1.38	0.19	-0.22
160	165	19.49	1.04	0.13	1.24	0.14	-0.21
180	185	17.75	0.89	0.13	1.12	0.14	-0.23
190	195	17.56	0.43	0.12	0.63	0.13	-0.21
210	215	8.7	0.37	0.18	1.09	0.16	-0.72
230	235	8.07	0.27	0.19	1.05	0.16	-0.78
250	255	7.84	0.72	0.19	1.47	0.17	-0.74
270	275	19.7	0.09	0.11	0.21	0.12	-0.12

Table C.17. Core IXW250 $^{210}Pb_{xs}$ activities (dpm/g) calculated using the IAEA RGU-1 and IAEA-447 calibration lines.

			IAEA RGU-1	IAEA RGU-1	IAEA-447	IAEA-447	RGU-1 minus 447
Top of interval (mm)	Bottom of interval (mm)	Sample Mass (g)	$^{210}Pb_{xs}$ Activity (dpm/g)	$^{210}Pb_{xs}$ Activity Error (dpm/g)	$^{210}Pb_{xs}$ Activity (dpm/g)	$^{210}Pb_{xs}$ Activity Error (dpm/g)	$^{210}Pb_{xs}$ Activity Difference (dpm/g)
0	2	1.48	26.12	0.89	25.35	0.76	0.77
2	4	1.58	20.26	0.97	20.25	0.82	0.01
4	6	2.1	21.33	0.83	20.97	0.71	0.37
6	8	2.91	20.29	0.69	19.86	0.60	0.43
8	10	4.03	20.66	0.59	20.35	0.53	0.30
10	12	4.67	18.05	0.51	17.74	0.46	0.31
12	14	4.99	18.61	0.50	18.45	0.46	0.17
14	16	5.61	18.13	0.47	18.07	0.44	0.06
16	18	5.91	18.36	0.46	18.41	0.42	-0.05
18	20	5.99	17.87	0.46	17.96	0.43	-0.08
20	22	6.02	17.55	0.45	17.60	0.41	-0.05
22	24	5.96	18.14	0.46	18.11	0.43	0.04
24	26	6.76	18.39	0.44	18.52	0.41	-0.13
26	28	5.94	18.36	0.47	18.47	0.43	-0.12
28	30	6.2	17.59	0.45	17.63	0.42	-0.04
30	32	6.65	17.67	0.43	17.79	0.41	-0.12
32	34	6.64	15.63	0.41	15.85	0.38	-0.23
34	36	6.45	16.74	0.43	16.84	0.40	-0.10
36	38	6.77	16.60	0.41	16.66	0.39	-0.07
38	40	6.37	18.65	0.45	18.54	0.42	0.11
40	42	6.15	19.52	0.46	19.35	0.43	0.17
42	44	6.52	19.65	0.45	19.60	0.43	0.05
44	46	6.75	17.35	0.41	17.37	0.39	-0.01
46	48	6.51	15.57	0.41	15.67	0.38	-0.09
48	50	6.91	12.26	0.37	12.45	0.34	-0.19
50	52	5.98	13.07	0.40	13.29	0.37	-0.22
52	54	6.77	11.71	0.36	12.04	0.34	-0.33
54	56	7.46	10.60	0.33	10.93	0.31	-0.32
56	58	6.38	9.17	0.34	9.49	0.31	-0.32
60	62	6.5	8.25	0.32	8.62	0.30	-0.36
64	66	6.76	5.60	0.28	6.07	0.26	-0.48
70	72	6.86	4.77	0.27	5.31	0.24	-0.54
74	76	6.15	4.09	0.27	4.67	0.24	-0.58
80	82	6.24	4.57	0.26	5.07	0.24	-0.51
84	86	6.65	3.26	0.24	3.87	0.22	-0.61
90	92	7.49	3.62	0.24	4.21	0.22	-0.59
94	96	6.78	2.48	0.22	3.07	0.20	-0.59
100	105	17.5	2.05	0.14	2.34	0.15	-0.29
110	115	19.51	1.09	0.12	1.28	0.13	-0.18
130	135	18.93	0.57	0.11	0.73	0.12	-0.16
150	155	20.1	0.33	0.10	0.43	0.11	-0.11
170	175	20.58	0.18	0.11	0.27	0.11	-0.09
190	195	20.83	0.17	0.14	0.25	0.15	-0.08
210	215	27.3	0.41	0.08	0.43	0.10	-0.02
250	255	20.82	0.26	0.10	0.35	0.11	-0.09
290	295	20.74	0.24	0.10	0.33	0.11	-0.09
330	335	22.82	0.31	0.10	0.37	0.11	-0.06

Table C.18. Core DSH08 $^{210}Pb_{xs}$ CRS age dating calculated using the IAEA RGU-1 and IAEA-447 calibration lines.

			IAEA RGU-1	IAEA RGU-1	IAEA-447	IAEA-447	RGU-1 minus 447
Top of interval (mm)	Bottom of interval (mm)	Sample Mass (g)	CRS Age (yrs)	CRS Age (yrs) Error	CRS Age (yrs)	CRS Age (yrs) Error	CRS Age (yrs) Difference
0	2	1.59	2010.7	1.1	2010.7	1.1	0.0
2	4	2.21	2010.2	1.1	2010.2	1.1	-0.1
4	6	2.44	2009.5	1.1	2009.6	1.1	-0.1
6	8	2.93	2008.7	1.1	2008.9	1.1	-0.2
8	10	3.42	2007.7	1.1	2008.0	1.1	-0.3
10	12	3.25	2006.7	1.2	2007.1	1.1	-0.3
12	14	3.73	2005.8	1.2	2006.2	1.1	-0.4
14	16	3.66	2004.8	1.2	2005.3	1.1	-0.5
16	18	3.52	2003.8	1.2	2004.3	1.1	-0.6
18	20	3.54	2002.9	1.2	2003.5	1.1	-0.6
22	24	3.91	2000.7	1.2	2001.5	1.2	-0.8
26	28	4.5	1998.3	1.2	1999.3	1.2	-0.9
32	34	4.49	1995.0	1.2	1996.2	1.2	-1.2
34	36	4.57	1993.8	1.2	1995.1	1.2	-1.3
38	40	4.53	1991.2	1.3	1992.7	1.2	-1.5
42	44	4.66	1988.5	1.3	1990.2	1.2	-1.7
46	48	4.99	1985.5	1.3	1987.6	1.3	-2.0
48	50	5.21	1984.1	1.3	1986.3	1.3	-2.2
50	55	14.3	1981.6	1.4	1983.9	1.3	-2.3
60	65	15.75	1974.4	1.5	1976.9	1.4	-2.4
70	75	14.57	1966.4	1.6	1969.1	1.6	-2.6
80	85	16.26	1958.4	1.9	1961.2	1.8	-2.9
90	95	16.67	1949.8	2.1	1952.9	2.0	-3.1
100	105	18.87	1939.1	2.6	1942.4	2.4	-3.4
110	115	19.59	1926.8	3.2	1930.5	3.0	-3.7
120	125	18.39	1915.5	4.0	1919.6	3.7	-4.1
130	135	17.97	1903.9	5.0	1908.5	4.5	-4.6
140	145	18.65	1894.0	6.0	1899.0	5.2	-5.0
150	155	19.05	1884.0	6.9	1889.5	5.9	-5.5
160	165	19.49	1873.7	7.8	1879.8	6.5	-6.1
180	185	17.75	1840.2	14.3	1848.6	10.6	-8.4
190	195	17.56	1810.2	26.9	1820.1	18.6	-9.9

Table C.19. Core DSH08 $^{210}Pb_{xs}$ CRS MAR (g/cm^2/yr) calculated using the IAEA RGU-1 and IAEA-447 calibration lines.

			IAEA RGU-1	IAEA-447	RGU-1 minus 447
Top of interval (mm)	Bottom of interval (mm)	Sample Mass (g)	MAR (g/cm^2/yr)	MAR (g/cm^2/yr)	MAR (g/cm^2/yr) Difference
0	2	1.59	0.050	0.054	-0.004
2	4	2.21	0.056	0.061	-0.005
4	6	2.44	0.057	0.062	-0.005
6	8	2.93	0.061	0.066	-0.005
8	10	3.42	0.064	0.070	-0.005
10	12	3.25	0.059	0.064	-0.005
12	14	3.73	0.065	0.071	-0.006
14	16	3.66	0.060	0.065	-0.005
16	18	3.52	0.058	0.063	-0.005
18	20	3.54	0.058	0.063	-0.005
22	24	3.91	0.061	0.066	-0.005
26	28	4.5	0.067	0.072	-0.005
32	34	4.49	0.065	0.070	-0.005
34	36	4.57	0.065	0.070	-0.005
38	40	4.53	0.062	0.067	-0.005
42	44	4.66	0.062	0.067	-0.005
46	48	4.99	0.064	0.070	-0.006
48	50	5.21	0.067	0.072	-0.006
50	55	14.3	0.071	0.077	-0.006
60	65	15.75	0.073	0.078	-0.005
70	75	14.57	0.066	0.070	-0.004
80	85	16.26	0.067	0.071	-0.004
90	95	16.67	0.070	0.074	-0.004
100	105	18.87	0.078	0.082	-0.004
110	115	19.59	0.073	0.076	-0.003
120	125	18.39	0.064	0.066	-0.003
130	135	17.97	0.062	0.065	-0.003
140	145	18.65	0.060	0.063	-0.003
150	155	19.05	0.064	0.067	-0.003
160	165	19.49	0.061	0.064	-0.003
180	185	17.75	0.050	0.052	-0.003
190	195	17.56	0.047	0.050	-0.002

Table C.20. Core IXW250 $^{210}Pb_{xs}$ CRS age dating calculated using the IAEA RGU-1 and IAEA-447 calibration lines.

			IAEA RGU-1	IAEA RGU-1	IAEA-447	IAEA-447	RGU-1 minus 447
Top of interval (mm)	Bottom of interval (mm)	Sample Mass (g)	CRS Age Model (yrs)	CRS Age Model (yrs) Error	CRS Age Model (yrs)	CRS Age Model (yrs) Error	CRS Age Model (yrs) Difference
0	2	1.48	2015.4	2.0	2015.4	2.0	-0.02
2	4	1.58	2015.1	2.0	2015.2	2.0	-0.05
4	6	2.10	2014.7	2.0	2014.8	2.0	-0.09
6	8	2.91	2014.3	2.0	2014.4	2.0	-0.13
8	10	4.03	2013.6	2.0	2013.8	2.0	-0.18
10	12	4.67	2012.7	2.0	2013.0	2.0	-0.22
12	14	4.99	2011.9	2.0	2012.1	2.0	-0.26
14	16	5.61	2010.9	2.0	2011.2	2.1	-0.30
16	18	5.91	2009.7	2.0	2010.1	2.1	-0.34
18	20	5.99	2008.6	2.0	2008.9	2.1	-0.38
20	22	6.02	2007.3	2.1	2007.8	2.1	-0.42
22	24	5.96	2006.1	2.1	2006.5	2.1	-0.46
24	26	6.76	2004.6	2.1	2005.1	2.2	-0.50
26	28	5.94	2003.1	2.1	2003.6	2.2	-0.55
28	30	6.20	2001.6	2.2	2002.2	2.2	-0.60
30	32	6.65	2000.0	2.2	2000.6	2.2	-0.66
32	34	6.64	1998.3	2.2	1999.0	2.3	-0.71
34	36	6.45	1996.6	2.3	1997.4	2.3	-0.77
36	38	6.77	1994.8	2.3	1995.6	2.4	-0.84
38	40	6.37	1992.7	2.4	1993.6	2.4	-0.91
40	42	6.15	1990.4	2.5	1991.4	2.5	-1.02
42	44	6.52	1987.8	2.5	1989.0	2.6	-1.13
44	46	6.75	1985.1	2.6	1986.3	2.7	-1.26
46	48	6.51	1982.4	2.7	1983.8	2.8	-1.39
48	50	6.91	1980.0	2.8	1981.5	2.9	-1.53
50	52	5.98	1977.7	2.9	1979.3	3.0	-1.67
52	54	6.77	1975.2	3.1	1977.1	3.1	-1.84
54	56	7.46	1972.6	3.2	1974.6	3.2	-2.01
56	58	6.38	1970.2	3.3	1972.3	3.3	-2.18
60	62	6.50	1965.6	3.6	1968.2	3.5	-2.58
64	66	6.76	1961.5	3.8	1964.5	3.7	-2.99
70	72	6.86	1956.0	4.1	1959.6	4.0	-3.62
74	76	6.15	1952.4	4.3	1956.5	4.1	-4.13
80	82	6.24	1946.3	4.8	1951.4	4.4	-5.12
84	86	6.65	1941.9	5.1	1947.8	4.7	-5.94
90	92	7.49	1934.7	5.8	1942.0	5.1	-7.44
94	96	6.78	1929.5	6.3	1938.1	5.3	-8.65
100	105	17.50	1920.4	7.5	1930.9	6.0	-10.46
110	115	19.51	1908.5	9.6	1920.8	7.2	-12.30
130	135	18.93	1885.8	14.7	1901.7	9.9	-15.86
150	155	20.10	1859.3	23.7	1879.3	13.9	-20.0

Table C.21. Core IXW250 $^{210}Pb_{xs}$ CRS MAR (g/cm^2/yr) calculated using the IAEA RGU-1 and IAEA-447 calibration lines.

Top of interval (mm)	Bottom of interval (mm)	Sample Mass (g)	IAEA RGU-1 MAR (g/cm^2/yr)	IAEA-447 MAR (g/cm^2/yr)	RGU-1 minus 447 MAR (g/cm^2/yr) Difference
0	2	1.48	0.059	0.066	-0.007
2	4	1.58	0.069	0.077	-0.008
4	6	2.10	0.083	0.093	-0.009
6	8	2.91	0.101	0.111	-0.010
8	10	4.03	0.117	0.127	-0.010
10	12	4.67	0.121	0.130	-0.010
12	14	4.99	0.117	0.125	-0.008
14	16	5.61	0.120	0.127	-0.008
16	18	5.91	0.116	0.123	-0.007
18	20	5.99	0.110	0.116	-0.006
20	22	6.02	0.105	0.110	-0.005
22	24	5.96	0.098	0.103	-0.005
24	26	6.76	0.105	0.109	-0.005
26	28	5.94	0.088	0.092	-0.004
28	30	6.20	0.088	0.092	-0.004
30	32	6.65	0.090	0.094	-0.004
32	34	6.64	0.087	0.091	-0.004
34	36	6.45	0.082	0.085	-0.003
36	38	6.77	0.083	0.086	-0.003
38	40	6.37	0.074	0.078	-0.003
40	42	6.15	0.069	0.072	-0.003
42	44	6.52	0.069	0.072	-0.003
44	46	6.75	0.068	0.071	-0.003
46	48	6.51	0.064	0.066	-0.003
48	50	6.91	0.066	0.069	-0.003
50	52	5.98	0.056	0.058	-0.003
52	54	6.77	0.062	0.065	-0.003
54	56	7.46	0.066	0.069	-0.003
56	58	6.38	0.056	0.059	-0.003
60	62	6.50	0.055	0.058	-0.003
64	66	6.76	0.057	0.060	-0.003
70	72	6.86	0.057	0.061	-0.004
74	76	6.15	0.051	0.055	-0.004
80	82	6.24	0.051	0.055	-0.004
84	86	6.65	0.056	0.060	-0.005
90	92	7.49	0.059	0.065	-0.006
94	96	6.78	0.052	0.058	-0.006
100	105	17.50	0.052	0.059	-0.007
110	115	19.51	0.057	0.065	-0.007
130	135	18.93	0.054	0.062	-0.008
150	155	20.10	0.055	0.063	-0.008

Table C.22. Decay corrected ^{137}Cs activities for analysis of IAEA-375 standard using the IAEA-447 calibration line. Target ^{137}Cs activity of IAEA-375 standard is 316 dpm/g.

Sample Mass (g)	Decay Corrected ^{137}Cs Activity (dpm/g)	Decay Corrected ^{137}Cs Activity error (dpm/g)
1	332	5.8
3	334	3.8
5	339	2.6
5	329	2.5
7	331	4.1
10	311	1.7
10	332	2.1
10	313	1.7
10	307	1.7
10	310	1.7
20	312	1.3
20	308	1.3
20	343	1.6
20	314	1.2
20	341	1.7
20	314	1.2
20	316	1.3
30	331	1.1
30	352	1.2
30	334	1.1
30	320	1.1
30	330	1.2
30	338	1.1
30	327	1.1
30	335	1.1
30	331	1.2
40	356	1.1

APPENDIX D:

CHAPTER THREE SUPPLEMENTAL FIGURES:

HIGH-RESOLUTION INVESTIGATION OF EVENT DRIVEN SEDIMENTATION:

NORTHEASTERN GULF OF MEXICO

Appendix D. Chapter 3 Supplemental Figures

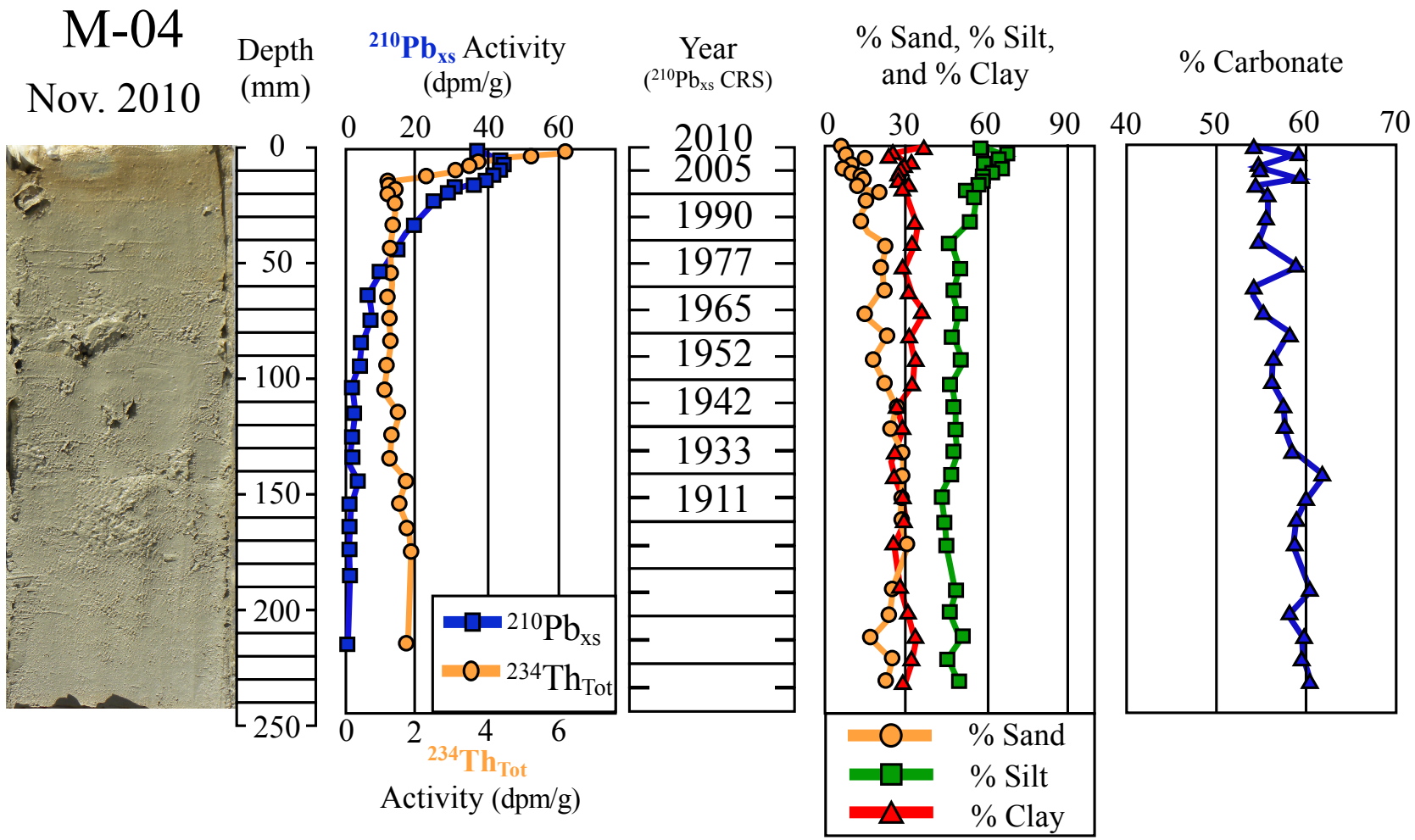

Figure D.1: Published as Figure S1, Site M-04 core collected in Nov. 2010 showing core photograph, $^{210}Pb_{xs}$ and $^{234}Th_{Tot}$ profiles, $^{210}Pb_{xs}$ CRS age dating (note error bars not visible), sediment texture (%sand, %silt, %clay) and %carbonate.

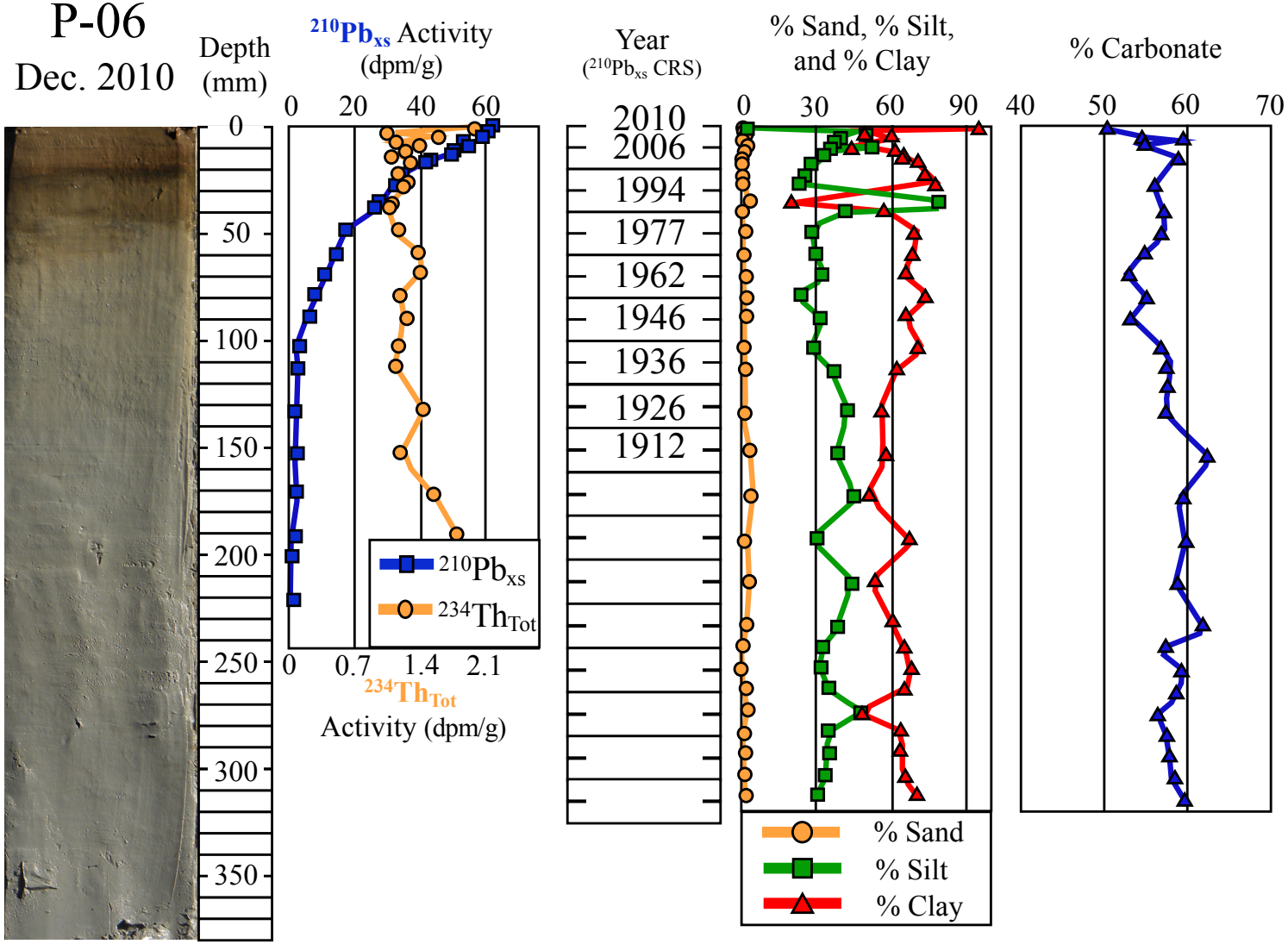

Figure D.2: Published as Figure S2, Site P-06 core collected in Nov. 2010 showing core photograph, $^{210}Pb_{xs}$ and $^{234}Th_{Tot}$ profiles, $^{210}Pb_{xs}$ CRS age dating (note error bars not visible), sediment texture (%sand, %silt, %clay) and %carbonate.

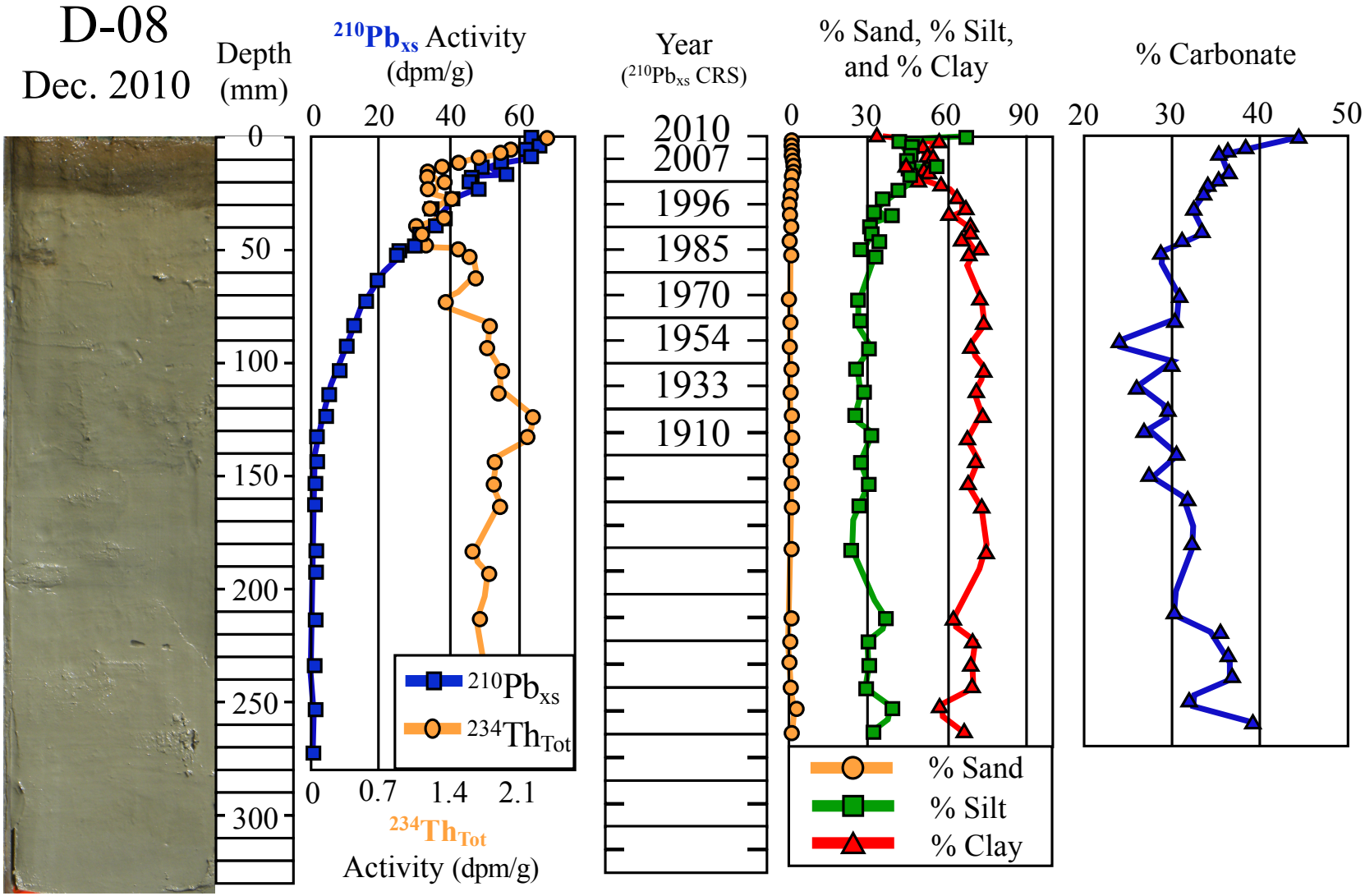

Figure D.3: Published as Figure S3, Site D-08 core collected in Nov. 2010 showing core photograph, $^{210}Pb_{xs}$ and $^{234}Th_{Tot}$ profiles, $^{210}Pb_{xs}$ CRS age dating (note error bars not visible), sediment texture (%sand, %silt, %clay) and %carbonate.

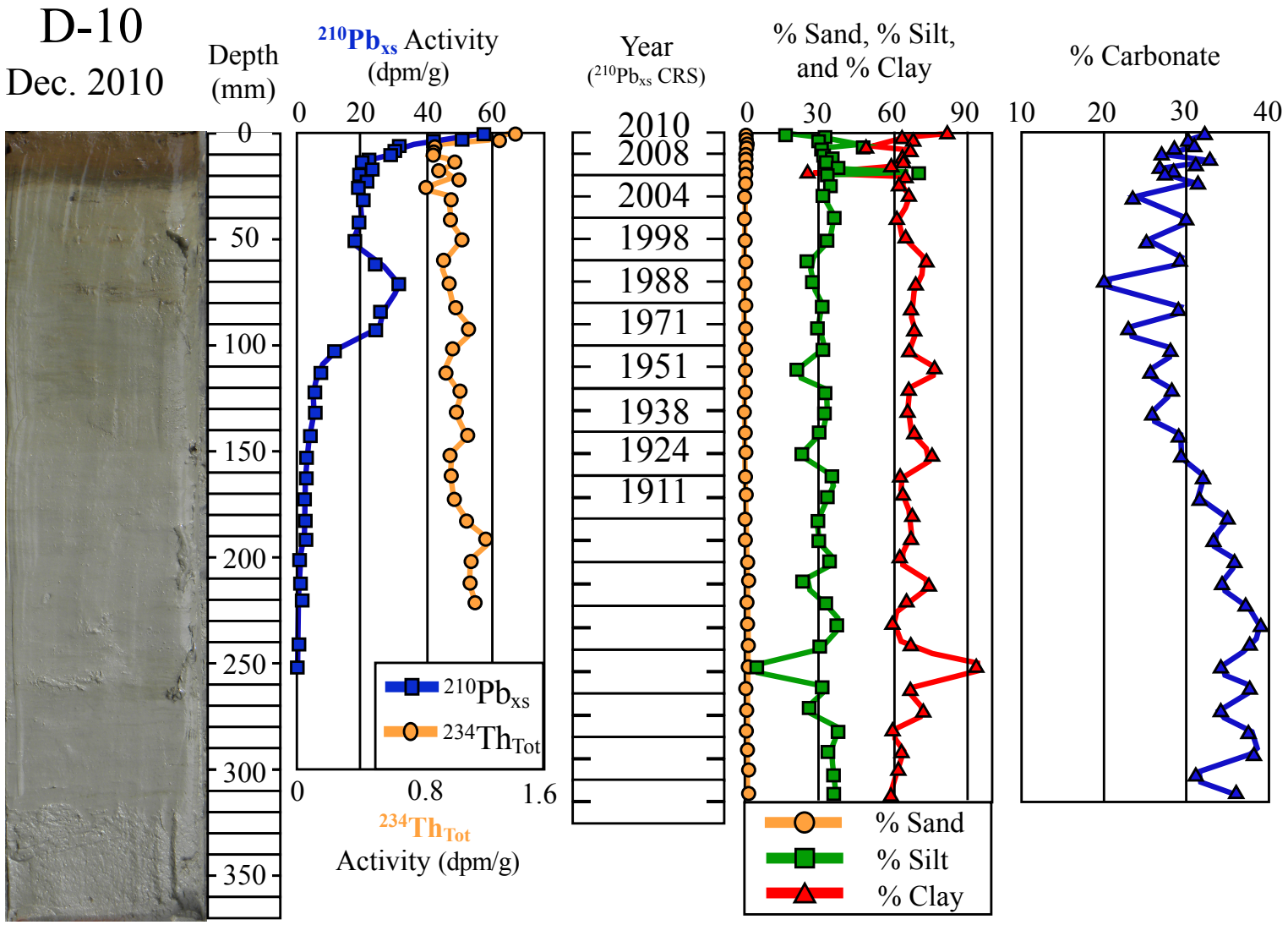

Figure D.4: Published as Figure S4, Site D-10 core collected in Nov. 2010 showing core photograph, $^{210}Pb_{xs}$ and $^{234}Th_{Tot}$ profiles, $^{210}Pb_{xs}$ CRS age dating (note error bars not visible), sediment texture (%sand, %silt, %clay) and %carbonate.

APPENDIX E:

CORE SITE LOCATION INFORMATION

Appendix E. Supplemental Table

Table E.1. Core site location information. List of core sites collected between 2010 and 2017 including the Collection Date, Latitude, Longitude, and Water Depth (m).

Site ID	Core ID	Collection Date	Latitude	Longitude	Water Depth (m)
DSH-10	2010-08 DSH-10 BC-A	8/11/10	28.97617	-87.86833	1520
M-01	WB-1109-MC-01	11/18/10	29.65990	-86.33143	108
M-02	WB-1109-MC-02	11/18/10	29.49940	-86.48068	202
M-03	WB-1109-MC-03	11/18/10	29.40747	-86.57533	302
M-04	WB-1109-MC-04	11/18/10	29.30465	-86.67677	400
M-05	WB-1109-MC-05-B	11/18/10	29.17473	-86.81493	504
M-06	WB-1109-MC-06	11/18/10	29.08355	-86.91452	600
M-07	WB-1109-MC-07	11/18/10	29.38533	-86.74525	400
M-08	WB-1109-MC-08	11/18/10	29.48540	-86.86525	404
M-09	WB-1109-MC-09	11/18/10	29.22008	-86.64042	406
M-10	WB-1109-MC-10	11/18/10	29.06738	-86.56320	399
DSH-07	WB-1110-MC-DSH-07	12/8/10	29.27012	-87.75615	399
DSH-08	WB-1110-MC-DSH-08	12/9/10	29.12092	-87.86545	1143
DSH-10	WB-1110-MC-DSH-10	12/9/10	28.97667	-87.87333	1520
PCB-03A	WB-1110-MC-PCB-03A	12/5/10	29.70880	-86.50445	130
PCB-04	WB-1110-MC-PCB-04	12/5/10	29.63352	-86.80787	221
PCB-06	WB-1110-MC-PCB-06	12/5/10	29.09983	-87.26550	1043
PPSED1	WB-1110-MC-PPSED-01	12/8/10	30.25923	-87.54627	9
DSH-08	WB-1114-MC-DSH-08	2/20/11	29.13215	-87.86668	1150
DSH-10	WB-1114-MC-DSH-10	2/20/11	28.98817	-87.86603	1500
DSH-11	WB-1114-MC-DSH-11	2/20/11	29.13637	-87.86447	1100
DSH-12	WB-1114-MC-DSH-12	2/20/11	29.10653	-87.86640	1200
DSH-13	WB-1114-MC-DSH-13	2/20/11	29.08337	-87.86542	1300
DSH-14	WB-1114-MC-DSH-14	2/20/11	29.18672	-87.80832	900
PCB-06	WB-1114-MC-PCB-06	2/21/11	29.11958	-87.26433	1002

Table E.1. (Continued)

Site ID	Core ID	Collection Date	Latitude	Longitude	Water Depth (m)
PCB-08	WB-1114-MC-PCB-08	2/21/11	28.89772	-87.16055	900
PCB-09	WB-1114-MC-PCB-09	2/21/11	28.85912	-87.21468	1000
PCB-10	WB-1114-MC-PCB-10	2/21/11	28.82227	-87.27302	1100
PCB-11	WB-1114-MC-PCB-11	2/21/11	28.80207	-87.30723	1200
PCB-12	WB-MAY-MC-PCB-12	5/20/11	28.97025	-87.00028	700
ST-1050	WB-1125-BC-ST-1050	6/26/11	27.04005	-85.09102	1047
NT-150	WB-1125-MC-NT-150	6/28/11	28.52638	-85.20272	150
NT-200	WB-1125-MC-NT-200	6/28/11	28.39547	-85.39603	233
NT-300	WB-1125-MC-NT-300	6/28/11	28.31227	-85.56702	306
NT-400	WB-1125-MC-NT-400	6/28/11	28.22650	-85.64850	400
NT-400	WB-1125-MC-NT-400	6/28/11	28.22650	-85.64850	400
NT-600	WB-1125-MC-NT-600	6/28/11	28.13462	-85.79408	600
NT-800	WB-1125-MC-NT-800	6/27/11	28.05412	-85.93167	825
NT-1000	WB-1125-BC-NT1000	6/27/11	28.00233	-85.99608	1000
NT-1200	WB-1125-BC-NT-1200	6/27/11	27.96637	-86.02313	1200
NT-1400	WB-1125-BC-NT-1400	6/27/11	27.92915	-86.02715	1400
DSH-07	WB-0911-MC-DSH-07	9/26/11	29.25482	-87.73210	449
DSH-08	WB-0911-BC-DSH-08	9/24/11	29.12058	-87.86998	1130
DSH-10	WB-0911-BC-DSH-10	9/25/11	28.97617	-87.86833	1520
DWH-01	WB-0911-BC-DWH-01	9/23/11	28.74987	-88.39287	1550
EL-01	WB-0911-MC-EL-01	9/23/11	28.71878	-88.00400	2100
NE-01	WB-0911-BC-NE-01	9/24/11	28.79057	-88.25998	1300
PCB-06	WB-0911-MC-PCB-06	9/26/11	29.13328	-87.26097	990
PCB-700	WB-0911-MC-PCB-700	9/27/11	29.02893	-86.99185	689
PCB-800	WB-0911-MC-PCB-800	9/27/11	28.96808	-87.07563	800
PCB-11	WB-0911-MC-PCB-11	9/25/11	28.80497	-87.30598	1167
SW-01	BP-0412-MC-SW-01	4/9/12	28.23898	-89.13146	1151
SW-02	BP-0412-MC-SW-02	4/10/12	27.53725	-90.36039	1120
DSH-07	WB-0812-MC-DSH-07	8/16/12	29.25578	-87.73238	451
DSH-08	WB-0812-MC-DSH-08	8/15/12	29.12278	-87.86773	1130
DSH-10	WB-0812-MC-DSH-10	8/15/12	28.97905	-87.89162	1504
DWH-01	WB-0812-MC-DWH-01	8/21/12	28.72437	-88.38728	1577
GP-01	WB-0812-MC-GP-01	8/23/12	28.61027	-88.88902	1018
GP-03	WB-0812-MC-GP-03	8/23/12	28.75337	-89.19600	199
MV-01	WB-0812-MC-MV-01	8/23/12	28.62990	-89.89053	323
MV-02	WB-0812-MC-MV-02	8/22/12	28.49417	-89.77937	550
MV-03	WB-0812-MC-MV-03	8/22/12	28.39825	-89.59933	759
PCB-03	WB-0812-MC-PCB-03	8/14/12	29.73833	-86.33833	100

Table E.1. (Continued)

Site ID	Core ID	Collection Date	Latitude	Longitude	Water Depth (m)
PCB-05	WB-0812-MC-PCB-05	8/14/12	29.44167	-86.78333	405
PCB-06	WB-0812-MC-PCB-06	8/15/12	29.12270	-87.26622	1011
PPSED1	WB-0812-MC-PPSED1	8/19/12	30.25833	-87.54500	20
SEEPA	WB-0812-MC-SEEPA	8/15/12	29.04328	-87.28222	1150
SEEPC	WB-0812-MC-SEEPC	8/15/12	28.99023	-88.04537	1086
SW-01	WB-0812-MC-SW-01	8/23/12	28.22087	-89.06950	1187
SW-03	WB-0812-MC-SW-03	8/22/12	28.57558	-88.80043	1200
SL-7-150	WB-0812-MC-SL-7-150	8/14/12	29.56833	-86.57833	196
SL-8-100	WB-0812-MC-SL-8-100	8/18/12	29.70167	-87.19167	230
SL-9-80	WB-0812-MC-SL-9-80	8/16/12	29.29153	-88.04135	156
SL-9-150	WB-0812-MC-SL9-150	8/16/12	29.24777	-87.99803	250
SL-10-40	WB-0812-MC-SL-10-40	8/16/12	29.19605	-88.86883	57
SL-14-60	WB-0812-MC-SL-14-60	8/17/12	29.45648	-87.45088	205
SL-14-100	WB-0812-MC-SL-14-100	8/17/12	29.40667	-87.38000	208
SL-16-150	WB-0812-MC-SL-16-150	8/23/12	28.63537	-90.00150	209
M-04	WB-1012-MC-04	10/18/12	29.30575	-86.67637	384
SE-01	WB-1012-MC-SE-01	10/18/12	28.64325	-87.20168	1000
SE-02	WB-1012-MC-SE-02	10/18/12	28.35917	-86.94427	977
SL-5-100	WB-1012-MC-SL-5-100	10/18/12	28.55352	-85.36810	186
M-04	WB-0813-MC-04	8/16/13	29.30733	-86.67492	397
DSH-07	WB-0813-MC-DSH-07	8/19/13	29.25223	-87.73725	458
DSH-08	WB-0813-MC-DSH-08	8/17/13	29.12630	-87.87147	1098
DSH-10	WB-0813-MC-DSH-10	8/20/13	28.97363	-87.86810	1520
DWH-01	WB-0813-MC-DWH-01	8/24/13	28.71630	-88.39190	1580
HC-01	WB-0813-MC-HC-01	8/25/13	28.37248	-90.51667	45
HC-02	WB-0813-MC-HC-02	8/25/13	28.31860	-90.47198	54
HC-03	WB-0813-MC-HC-03	8/25/13	28.21670	-90.41362	72
MV-02	WB-0813-MC-MV-02	8/26/13	28.50122	-89.78715	541
PCB-03	WB-0813-MC-PCB-03	8/15/13	29.89892	-86.29467	93
PCB-06	WB-0813-MC-PCB-06	8/16/13	29.12455	-87.26375	940
SE-02	WB-0813-MC-SE-02	8/28/13	28.35678	-86.94362	975
SW-01	WB-0813-MC-SW-01	8/27/13	28.22113	-89.06452	1192
SW-03	WB-0813-MC-SW-03	8/27/13	28.57555	-88.80865	1186
SL-5-100	WB-0813-MC-SL-5-100	8/28/13	28.55360	-85.36640	170
SL-5-200	WB-0813-MC-SL-5-200	8/28/13	28.47772	-86.12870	390
SL-7-150	WB-0813-MC-SL-7-150	8/15/13	29.58718	-86.38067	336
SL-8-100	WB-0813-MC-SL-8-100	8/17/13	29.74657	-87.19460	190
SL-9-80	WB-0813-MC-SL-9-80	8/20/13	29.29615	-88.01385	155

Table E.1. (Continued)

Site ID	Core ID	Collection Date	Latitude	Longitude	Water Depth (m)
SL-9-150	WB-0813-MC-SL-9-150	8/20/13	29.24997	-87.99412	249
SL-10-40	WB-0813-MC-SL-10-40	8/21/13	29.19627	-88.86673	56
SL-11-150	WB-0813-MC-SL-11-150	8/27/13	29.03808	-88.63330	286
SL-12-100	WB-0813-MC-SL-12-100	8/26/13	28.56963	-89.56572	212
SL-14-100	WB-0813-MC-SL-14-100	8/19/13	29.40420	-87.49347	222
SL-16-150	WB-0813-MC-SL-16-150	8/26/13	28.63557	-90.00605	207
DSH-09	WB-0913-MC-DSH-09	9/26/13	28.63785	-87.86791	2280
S36	WB-0913-MC-S36	9/27/13	28.91535	-87.66733	1834
S42	WB-0913-MC-S42	9/25/13	28.25152	-86.42195	768
M-04	WB-0814-MC-04	8/14/14	29.30733	-86.67483	399
M-06	WB-0814-MC-06	8/14/14	29.08355	-86.91452	595
DSH-08	WB-0814-MC-DSH-08 DEP 1	8/17/14	29.12297	-87.86818	1127
DSH-09	WB-0814-MC-DSH-09	8/27/14	28.63515	-87.87407	2293
DSH-10	WB-0814-MC-DSH-10 DEP 1	8/18/14	28.97812	-87.89063	1520
DSH-10	WB-0814-MC-DSH-10 DEP 2	8/22/14	28.97852	-87.97495	1515
DWH-01	WB-0814-MC-DWH-01	8/26/14	28.74017	-88.38492	1540
MV-02	WB-0814-MC-MV-02	8/23/14	28.49393	-89.77880	553
MV-03	WB-0814-MC-MV-03	8/23/14	28.39843	-89.59952	763
NT-400	WB-0814-MC-NT-400	8/28/14	28.22455	-85.65298	406
PCB-03	WB-0814-MC-PCB-03	8/14/14	29.89892	-86.29467	96
PCB-06	WB-0814-MC-PCB-06 DEP 2	8/19/14	29.12285	-87.26547	1008
PCB-09	WB-0814-MC-PCB-09	8/18/14	28.85973	-87.21480	981
SW-01	WB-0814-MC-SW-01 DEP 1	8/24/14	28.24048	-89.11903	1133
SW-03	WB-0814-MC-SW-03	8/25/14	28.57640	-88.79582	1208
SL-7-150	WB-0814-MC-SL-7-150	8/14/14	29.58718	-86.38067	196
SL-8-100	WB-0814-MC-SL-8-100	8/16/14	29.70713	-87.18897	226
SL-9-80	WB-0814-MC-SL-9-80	8/18/14	29.29188	-88.04187	150
SL-9-150	WB-0814-MC-SL-9-150	8/18/14	29.24928	-87.99583	251
SL-10-40	WB-0814-MC-SL-10-40	8/22/14	29.19707	-88.86843	58
SL-11-150	WB-0814-MC-SL-11-150	8/22/14	29.03880	-88.63950	296
SL-12-40	WB-0814-MC-SL-12-40	8/23/14	28.82653	-89.51327	62
SL-12-100	WB-0814-MC-SL-12-100	8/23/14	28.57272	-89.53805	171
SL-14-60	WB-0814-MC-SL-14-60	8/16/14	29.45580	-87.44990	212
SL-16-150	WB-0814-MC-SL-16-150	8/23/14	28.63575	-90.00212	209
M-04	WB-0815-MC-04	8/16/15	29.30242	-86.66390	407
M-06	WB-0815-MC-06	8/18/15	29.08542	-86.91340	616
DSH-07	WB-0815-MC-DSH-07	8/20/15	29.25582	-87.73238	447
DSH-08	WB-0815-MC-DSH-08-A	8/20/15	29.12283	-87.86813	1123

Table E.1. (Continued)

Site ID	Core ID	Collection Date	Latitude	Longitude	Water Depth (m)
DSH-09	WB-0815-MC-DSH-09	8/21/15	28.64107	-87.86087	2297
DSH-10	WB-0815-MC-DSH-10-A	8/19/15	28.97940	-87.89190	1490
DWH-01	WB-0815-MC-DWH-01-A	8/20/15	28.72428	-88.38675	1580
GP-03	WB-0815-MC-GP-03	8/25/15	28.74742	89.19432	208
HC-01	WB-0815-MC-HC-01	8/27/15	28.37118	-90.52048	46
HC-02	WB-0815-MC-HC-02	8/27/15	28.31670	-90.47363	55
HC-03	WB-0815-MC-HC-03	8/27/15	28.22267	-90.40702	81
MV-02	WB-0815-MC-MV-02	8/26/15	28.49320	-89.78060	550
NT-400	WB-0815-MC-NT-400	8/29/15	28.22205	-85.65080	396
PCB-03	WB-0815-MC-PCB-03	8/17/15	29.74530	-86.33932	94
PCB-06	WB-0815-MC-PCB-06-A	8/18/15	29.12533	-87.26083	1023
PCB-09	WB-0815-MC-PCB-09	8/18/15	28.85532	-87.21765	1012
SE-02	WB-0815-MC-SE-02	8/28/15	28.35985	-86.94742	973
SW-01	WB-0815-MC-SW-01-A	8/28/15	28.24125	-89.11855	1131
SW-03	WB-0815-MC-SW-03	8/28/15	28.57613	-88.79832	1190
SL-5-100	WB-0815-MC-SL-5-100	8/16/15	28.58850	85.21348	177
SL-7-150	WB-0815-MC-SL-7-150	8/17/15	29.49367	-85.67003	284
SL-8-100	WB-0815-MC-SL-8-100	8/22/15	29.73527	-87.18695	210
SL-9-80	WB-0815-MC-SL-9-80	8/19/15	29.29217	-87.99408	169
SL-9-150	WB-0815-MC-SL-9-150	8/19/15	29.24550	-87.96075	287
SL-10-40	WB-0815-MC-SL-10-40-A	8/20/15	29.20422	-88.87072	59
SL-11-150	WB-0815-MC-SL-11-150	8/25/15	29.04117	-88.61887	303
SL-12-40	WB-0815-MC-SL-12-40	8/26/15	28.82828	-89.18768	64
SL-12-100	WB-0815-MC-SL-12-100	8/26/15	28.55675	-87.55477	281
SL-14-60	WB-0815-MC-SL-14-60	8/22/15	29.46238	-87.43745	235
SL-16-150	WB-0815-MC-SL-16-150	8/26/15	28.63475	-89.98475	226
WFS-1	WB-0915-MC-WFS-1	10/1/15	26.52610	-84.97275	1587
M-04	WB-0816-MC-04	9/9/16	29.30495	-86.67858	412
DSH-08	WB-0816-MC-DSH-08-A	9/9/16	29.12077	-87.86803	1130
DSH-10	WB-0816-MC-DSH-10-A	9/8/16	28.98030	-87.89190	1495
DWH-01	WB-0816-MC-DWH-01-A	9/8/16	28.72515	-88.38727	1577
MV-02	WB-0816-MC-MV-02	9/7/16	28.49397	-89.78100	513
PCB-06	WB-0816-MC-PCB-06-A	9/9/16	29.12407	-87.26568	1000
SW-01	WB-0816-MC-SW-01-A	9/8/16	28.24030	-89.12170	1132
SW-02	WB-0816-MC-SW-02	9/7/16	27.53713	-90.36115	1110
M-04	WB-0717-MC-04	7/22/17	29.30728	-86.67412	394
DSH-08	WB-0717-MC-DSH-08-A	7/28/17	29.12310	-87.86918	1114
DSH-10	WB-0717-MC-DSH-10-A	7/28/17	28.98020	-87.89085	1489

Table E.1. (Continued)

Site ID	Core ID	Collection Date	Latitude	Longitude	Water Depth (m)
PCB-06	WB-0717-MC-PCB-06-A	7/23/17	29.12368	87.26587	991
SL-1-150	WB-0717-MC-SL-1-150	7/19/17	24.91595	-84.11690	255
SL-1-750	WB-0717-MC-SL-1-750	7/19/17	24.68002	-84.09957	1564
WFS-1-500	WB-0717-MC-WFS-1-500	7/20/17	26.52068	-84.87087	986
SW-01	WB-1217-MC-SW-01	12/5/17	28.23900	-89.12097	1125

APPENDIX F:

SEDIMENT CORE LOGS FOR TIME SERIES SITES

Appendix F. Supplemental Figures

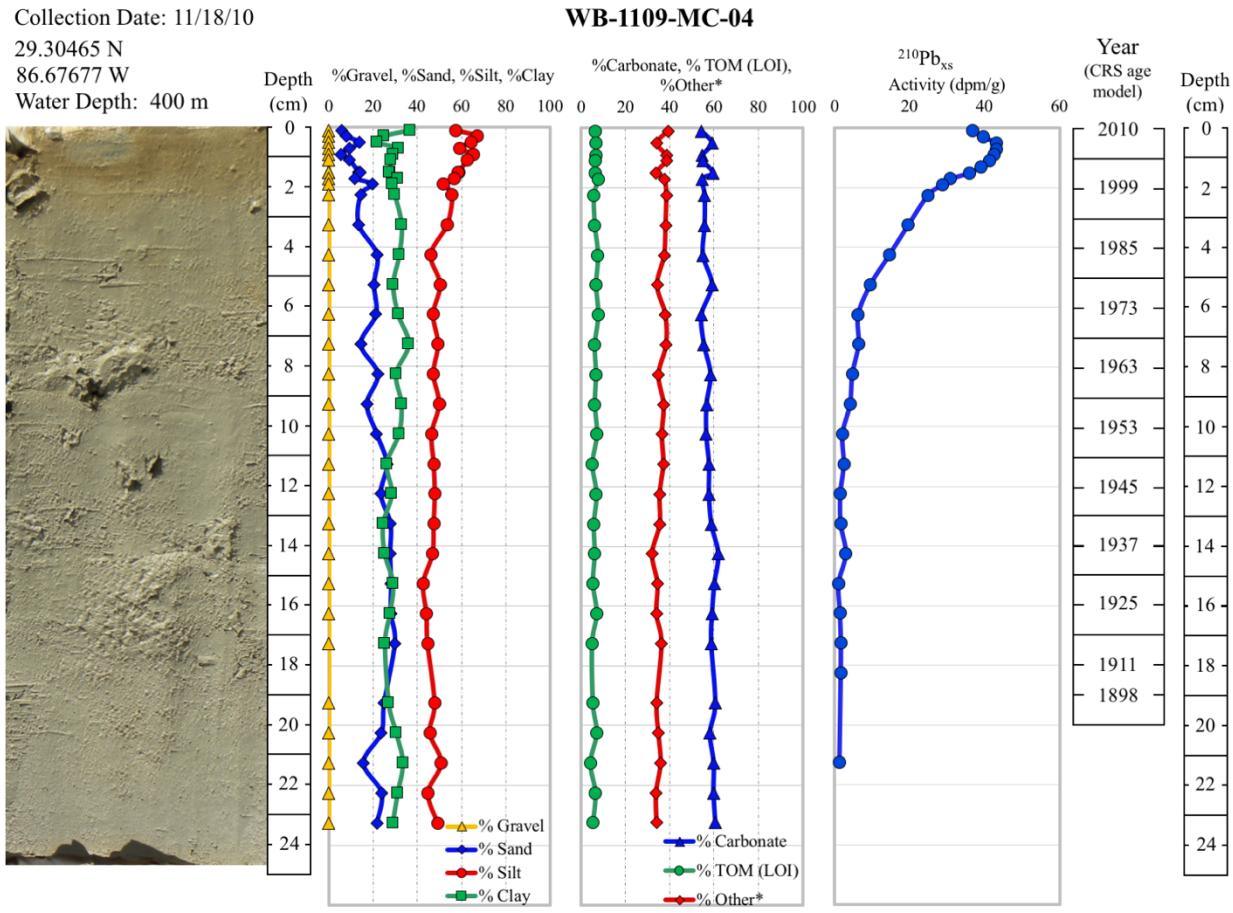

Figure F.1. Core Log for core WB-1109-MC-04. Core log including core collection date, latitude, longitude, water depth (m), core photograph, depth (cm), profiles of sediment texture, sediment composition, and $^{210}Pb_{xs}$ activity, as well as age control determined using CRS age model.

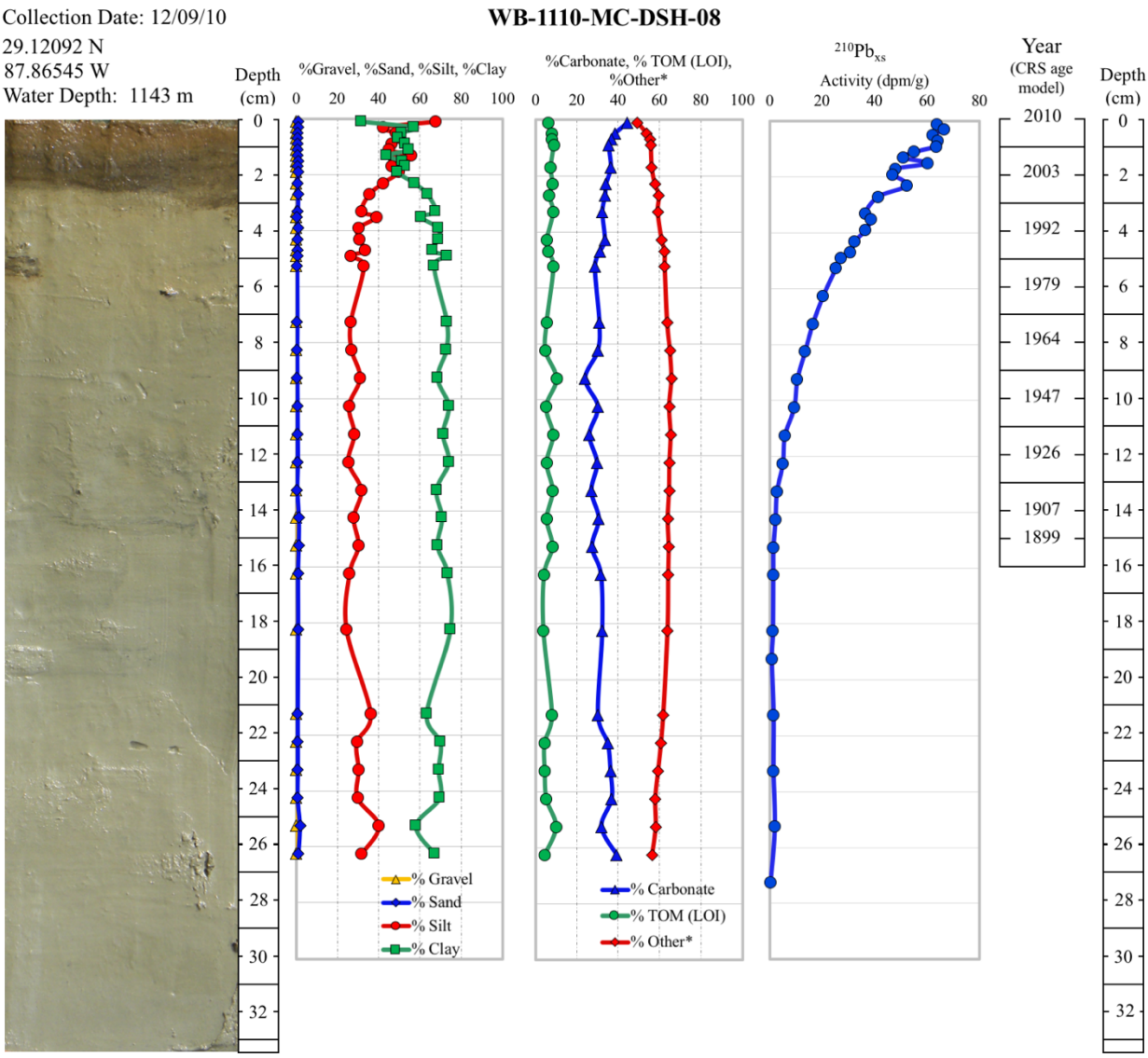

Figure F.2. Core Log for core WB-1110-MC-DSH-08. Core log including core collection date, latitude, longitude, water depth (m), core photograph, depth (cm), profiles of sediment texture, sediment composition, and $^{210}Pb_{xs}$ activity, as well as age control determined using CRS age model.

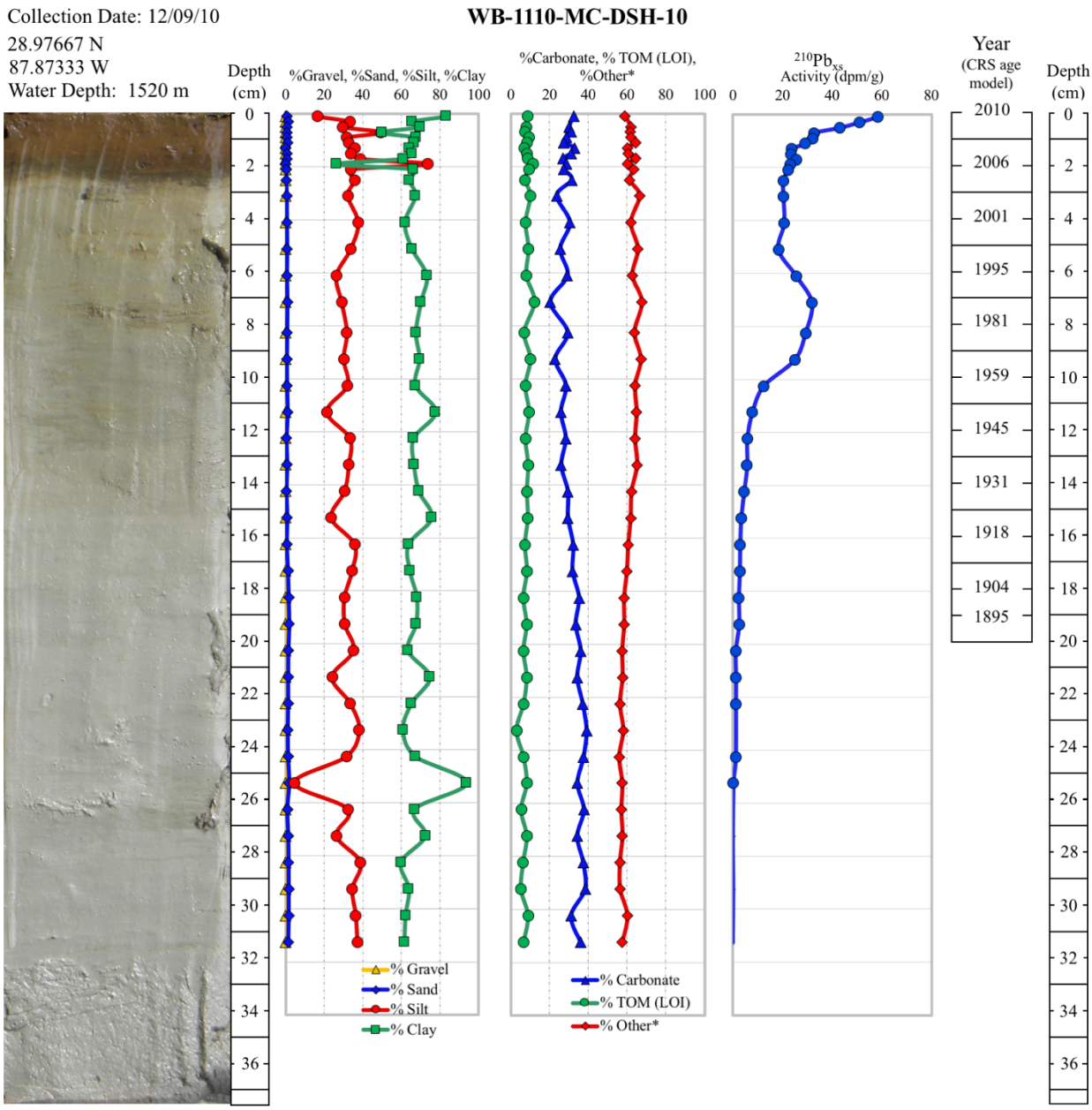

Figure F.3. Core Log for core WB-1110-MC-DSH-10. Core log including core collection date, latitude, longitude, water depth (m), core photograph, depth (cm), profiles of sediment texture, sediment composition, and $^{210}Pb_{xs}$ activity, as well as age control determined using CRS age model.

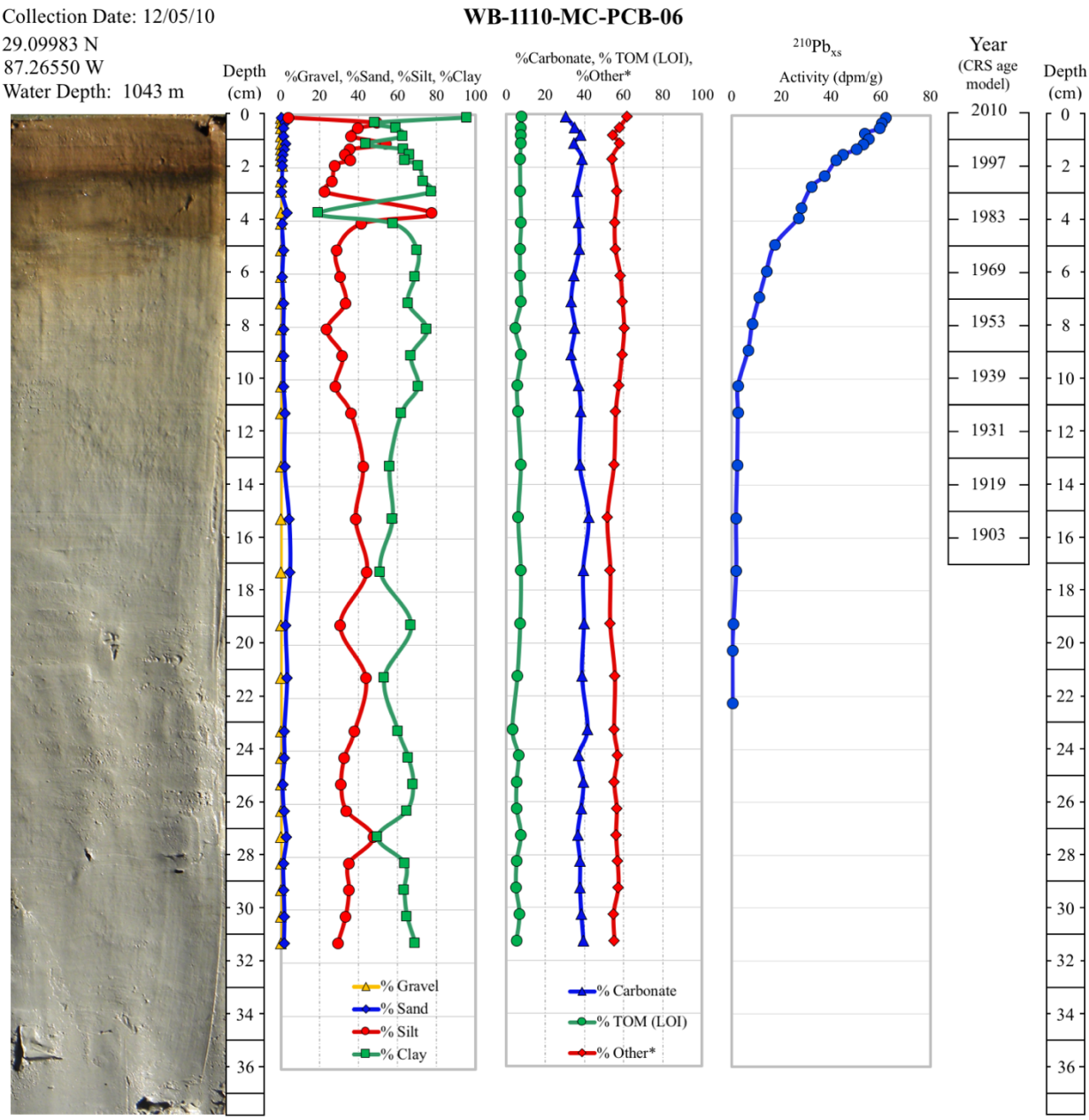

Figure F.4. Core Log for core WB-1110-MC-PCB-06. Core log including core collection date, latitude, longitude, water depth (m), core photograph, depth (cm), profiles of sediment texture, sediment composition, and $^{210}Pb_{xs}$ activity, as well as age control determined using CRS age model.

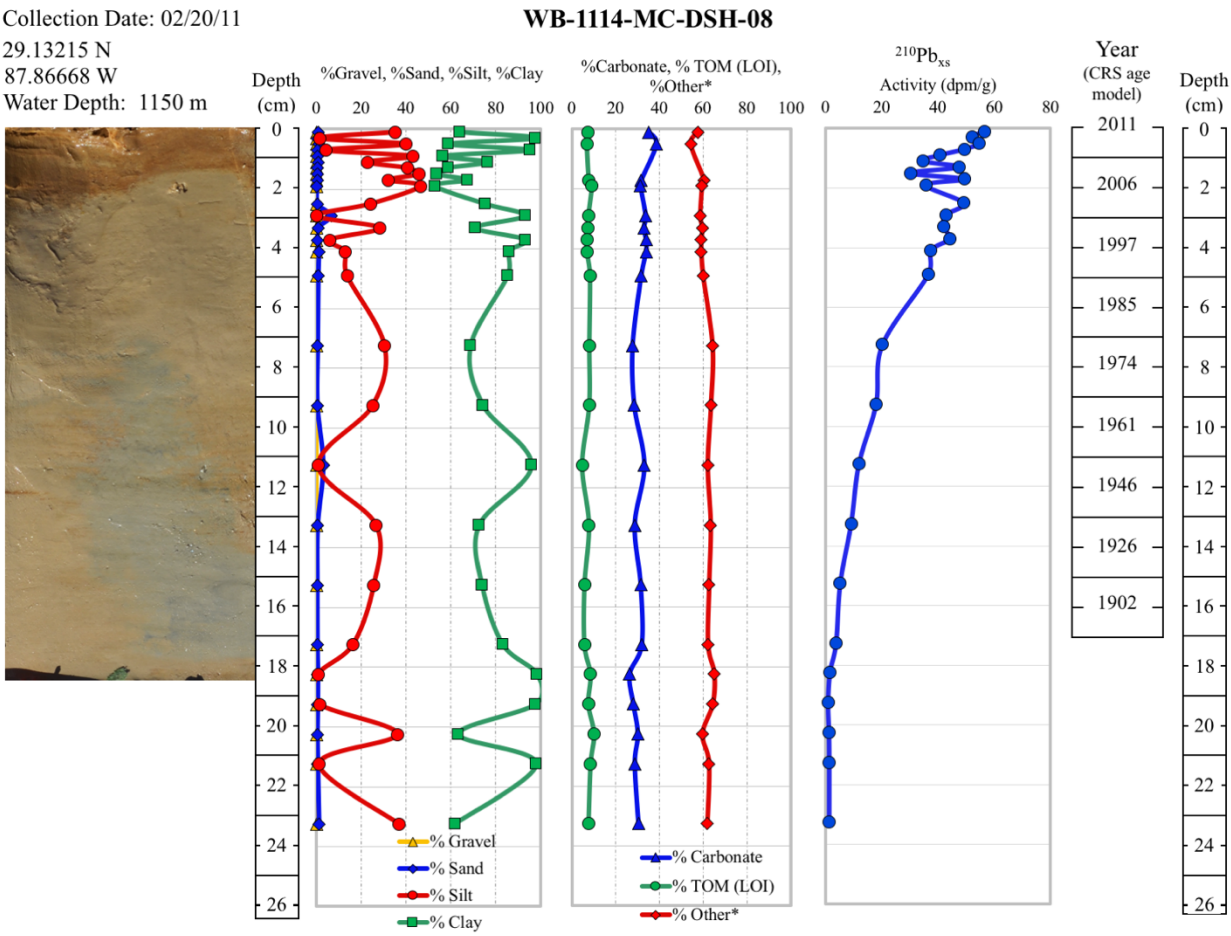

Figure F.5. Core Log for core WB-1114-MC-DSH-08. Core log including core collection date, latitude, longitude, water depth (m), core photograph, depth (cm), profiles of sediment texture, sediment composition, and $^{210}Pb_{xs}$ activity, as well as age control determined using CRS age model.

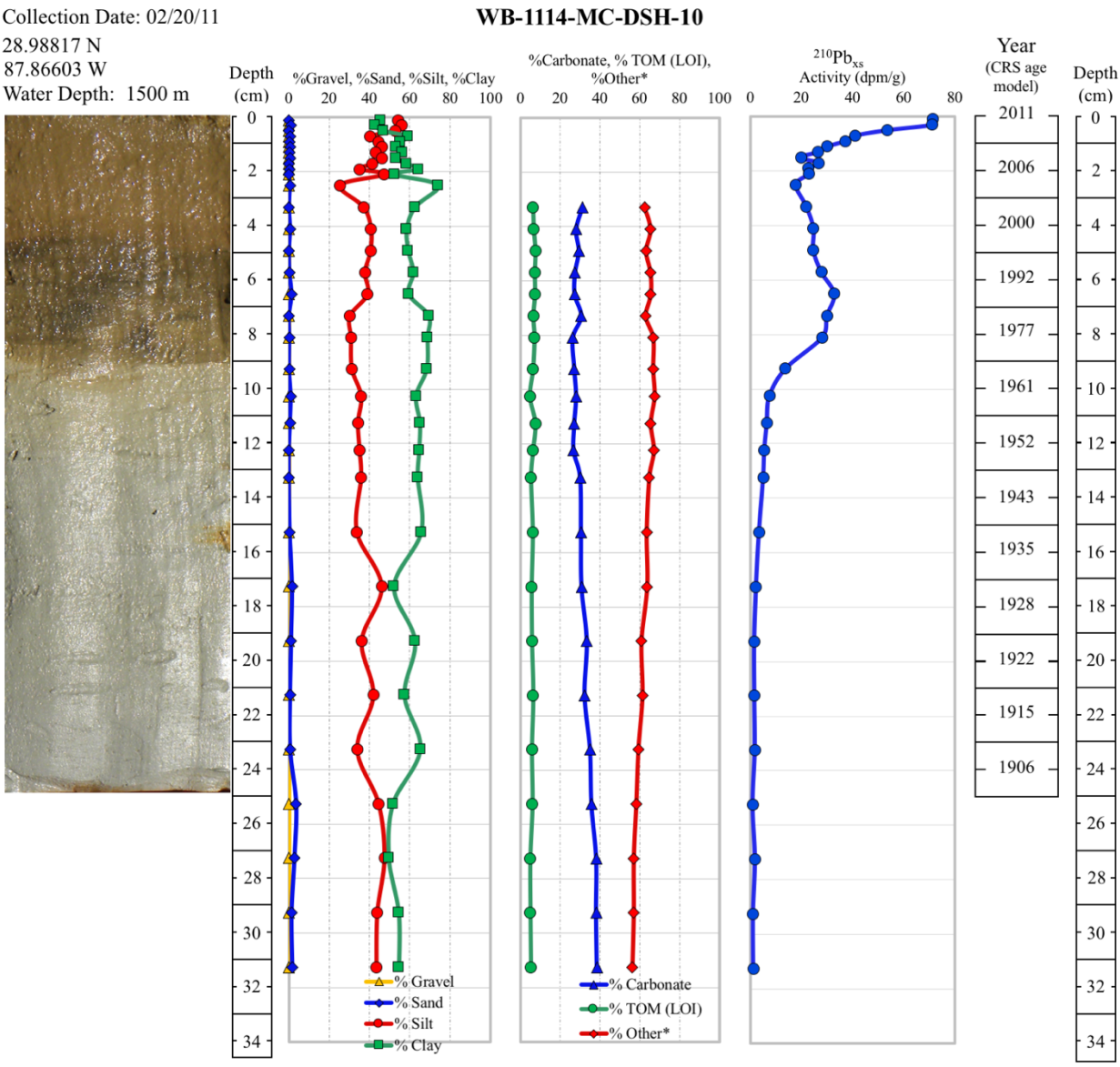

Figure F.6. Core Log for core WB-1114-MC-DSH-10. Core log including core collection date, latitude, longitude, water depth (m), core photograph, depth (cm), profiles of sediment texture, sediment composition, and $^{210}Pb_{xs}$ activity, as well as age control determined using CRS age model.

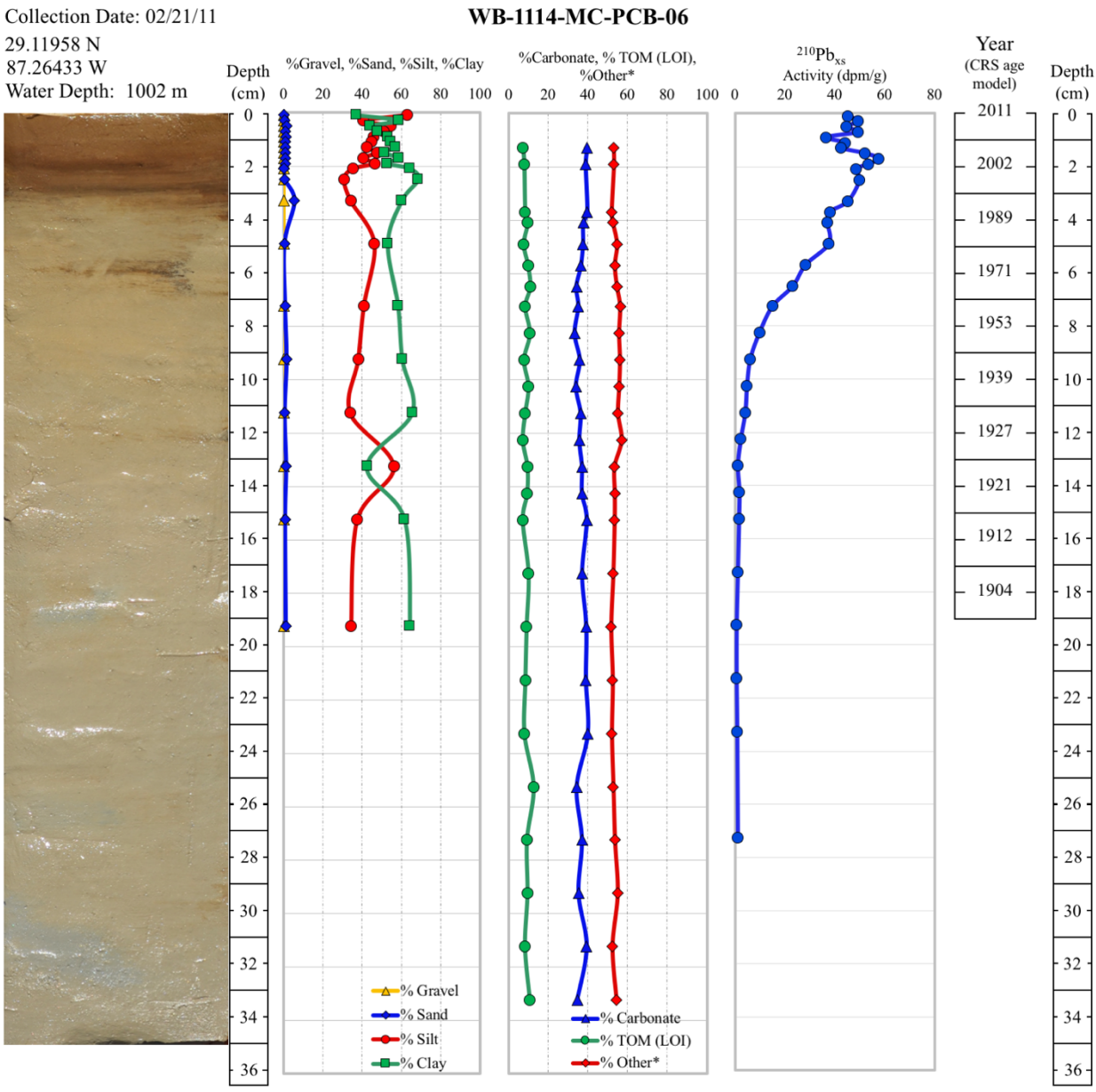

Figure F.7. Core Log for core WB-1114-MC-PCB-06. Core log including core collection date, latitude, longitude, water depth (m), core photograph, depth (cm), profiles of sediment texture, sediment composition, and $^{210}Pb_{xs}$ activity, as well as age control determined using CRS age model.

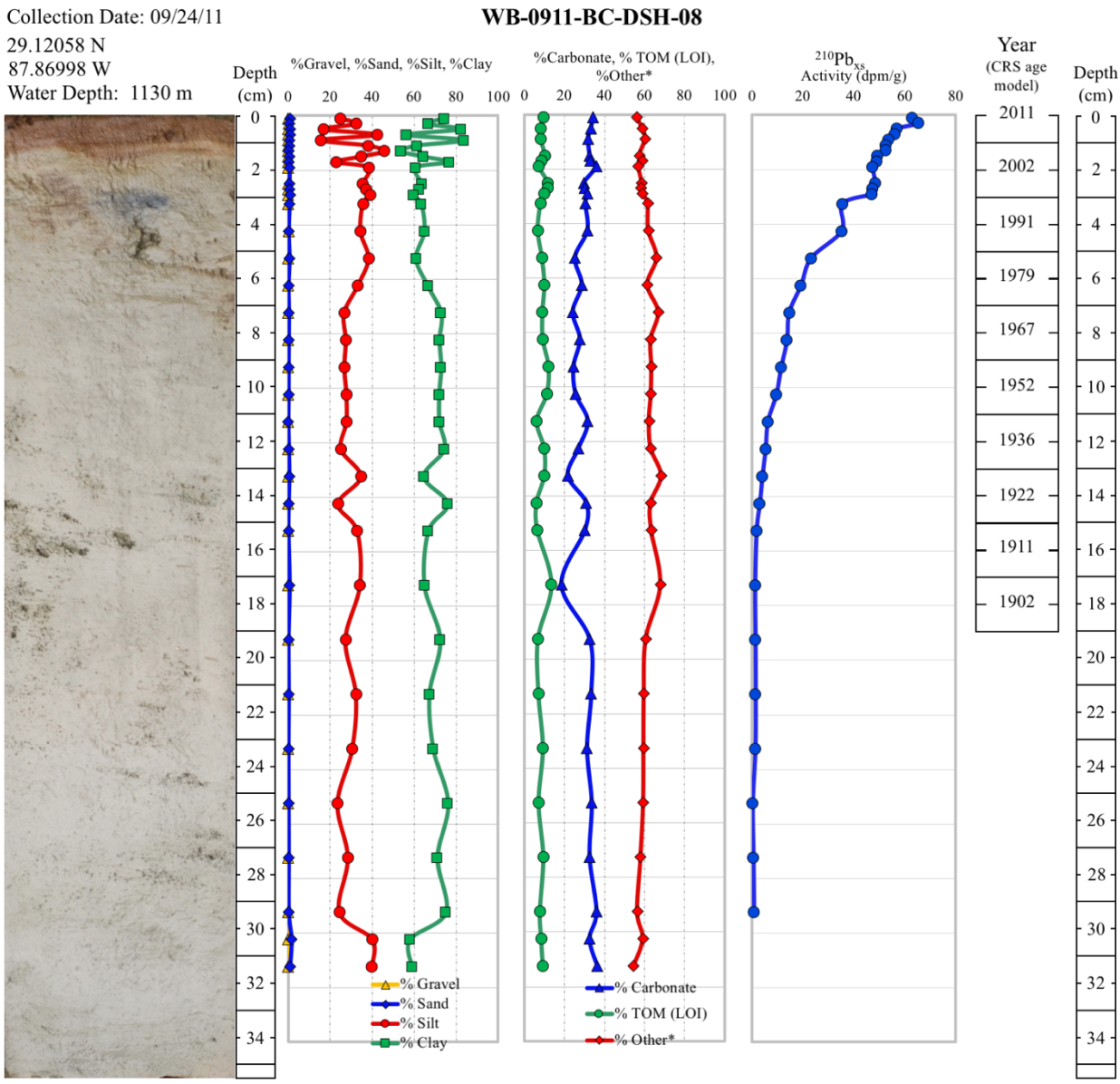

Figure F.8. Core Log for core WB-0911-BC-DSH-08. Core log including core collection date, latitude, longitude, water depth (m), core photograph, depth (cm), profiles of sediment texture, sediment composition, and $^{210}Pb_{xs}$ activity, as well as age control determined using CRS age model.

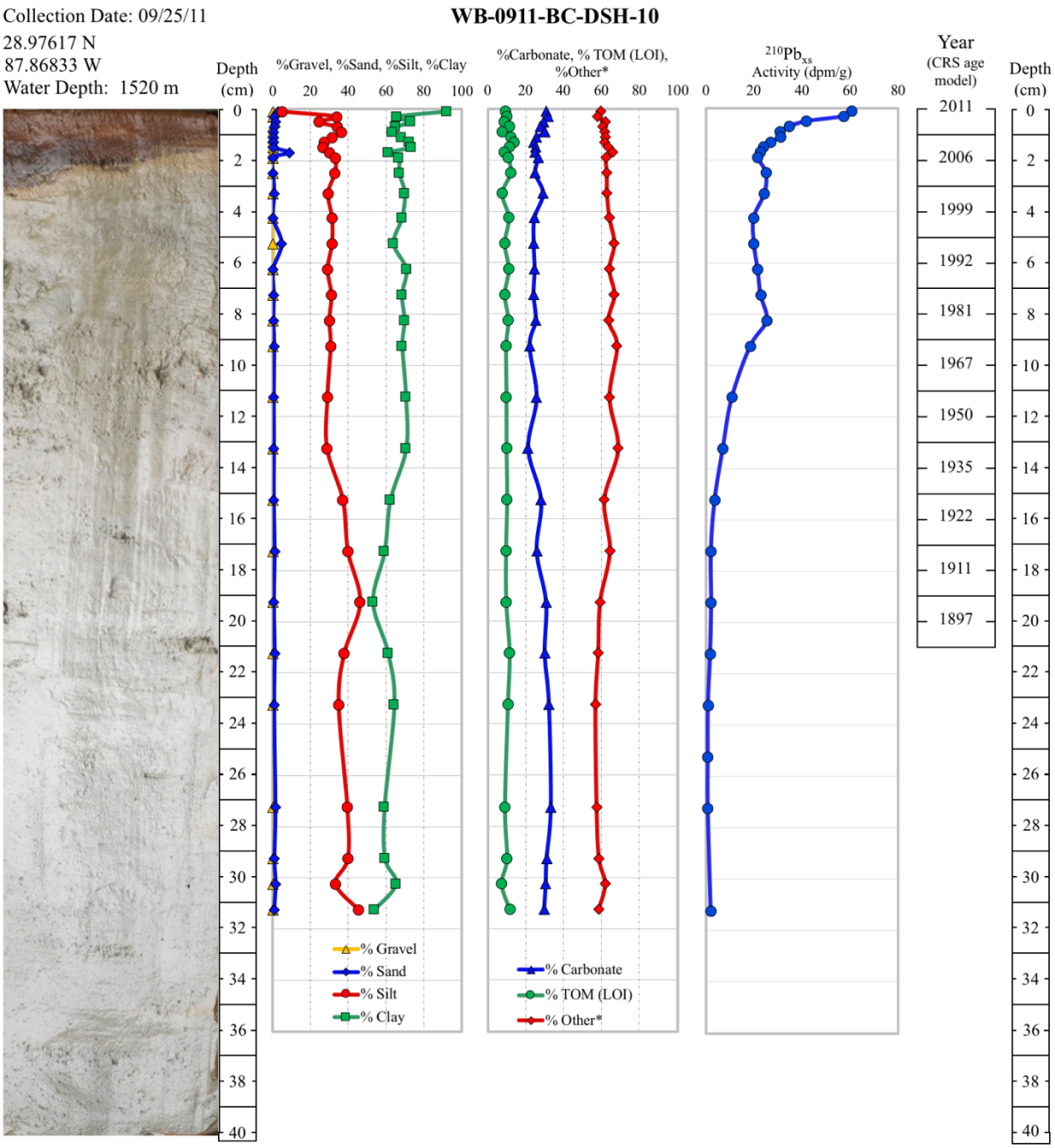

Figure F.9. Core Log for core WB-0911-BC-DSH-10. Core log including core collection date, latitude, longitude, water depth (m), core photograph, depth (cm), profiles of sediment texture, sediment composition, and $^{210}Pb_{xs}$ activity, as well as age control determined using CRS age model.

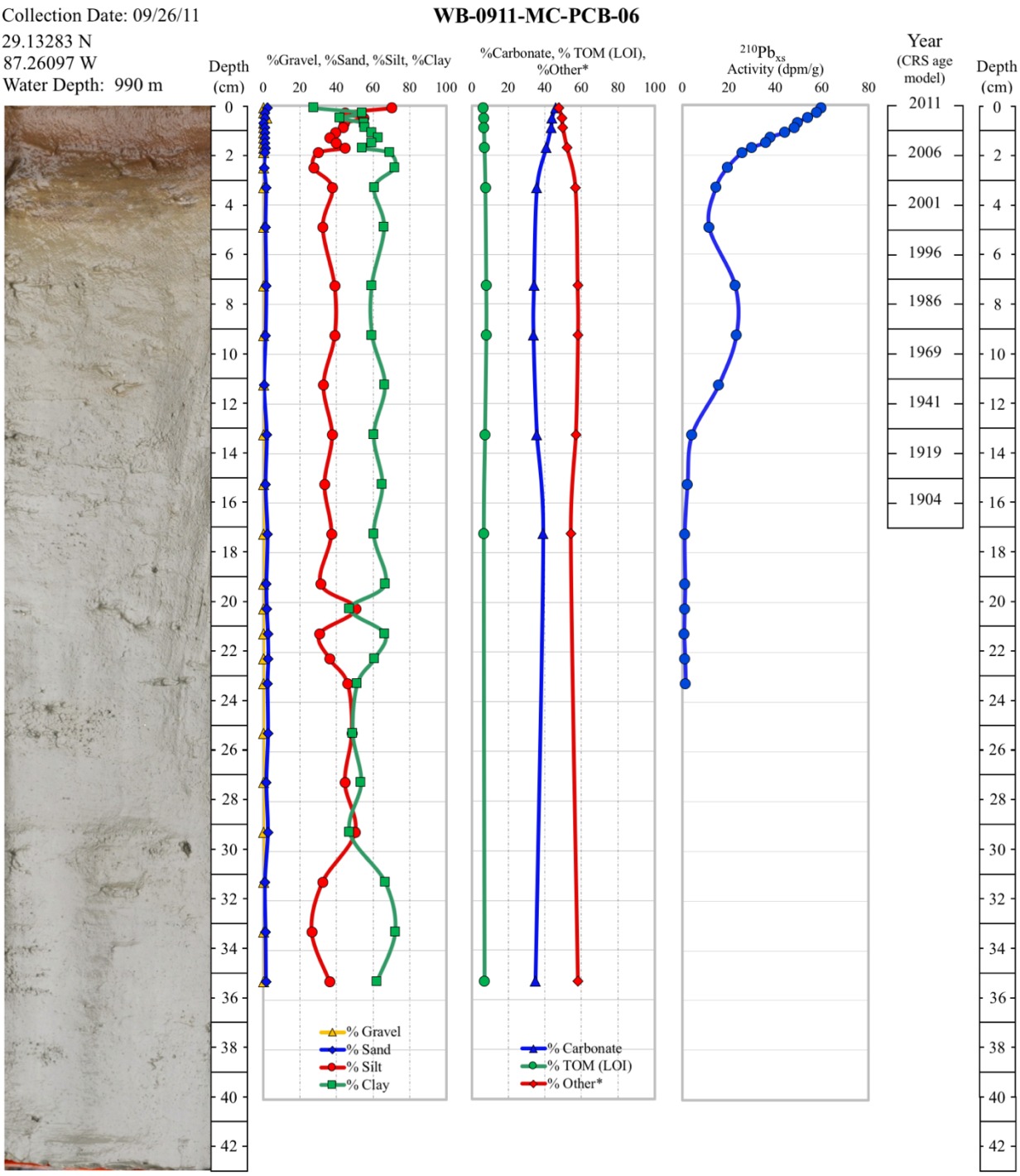

Figure F.10. Core Log for core WB-0911-MC-PCB-06. Core log including core collection date, latitude, longitude, water depth (m), core photograph, depth (cm), profiles of sediment texture, sediment composition, and $^{210}Pb_{xs}$ activity, as well as age control determined using CRS age model.

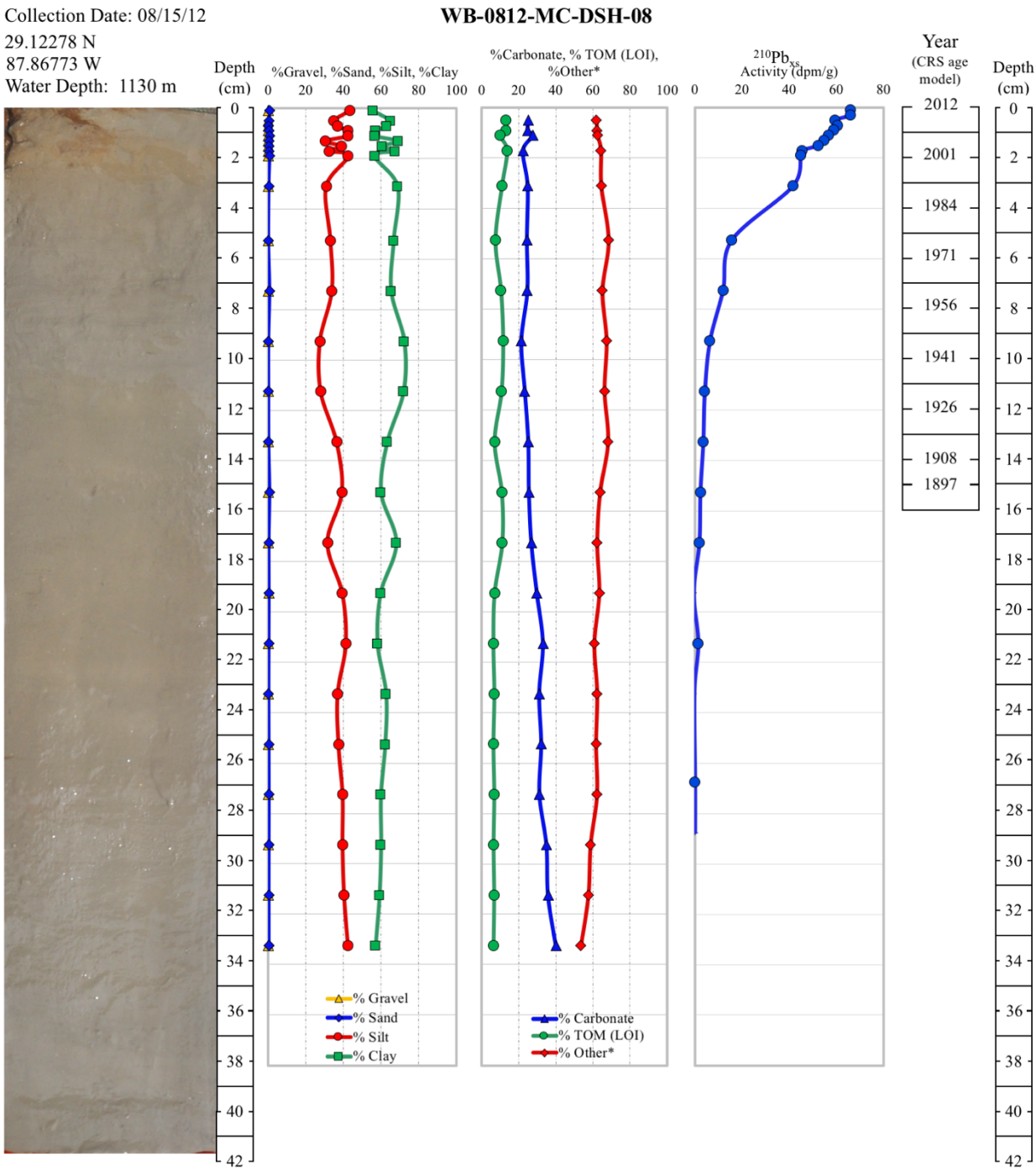

Figure F.11. Core Log for core WB-0812-MC-DSH-08. Core log including core collection date, latitude, longitude, water depth (m), core photograph, depth (cm), profiles of sediment texture, sediment composition, and $^{210}Pb_{xs}$ activity, as well as age control determined using CRS age model.

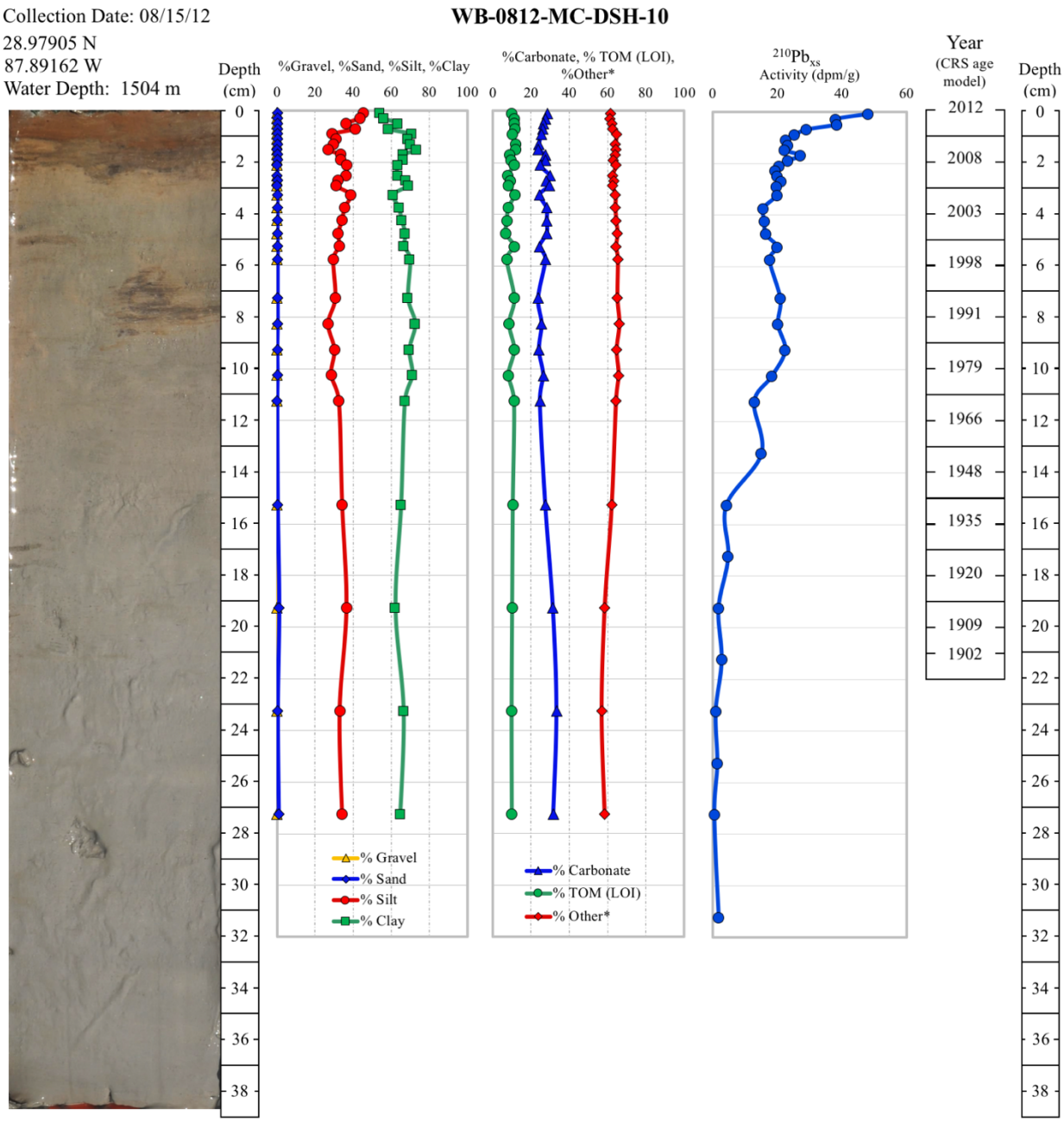

Figure F.12. Core Log for core WB-0812-MC-DSH-10. Core log including core collection date, latitude, longitude, water depth (m), core photograph, depth (cm), profiles of sediment texture, sediment composition, and $^{210}Pb_{xs}$ activity, as well as age control determined using CRS age model.

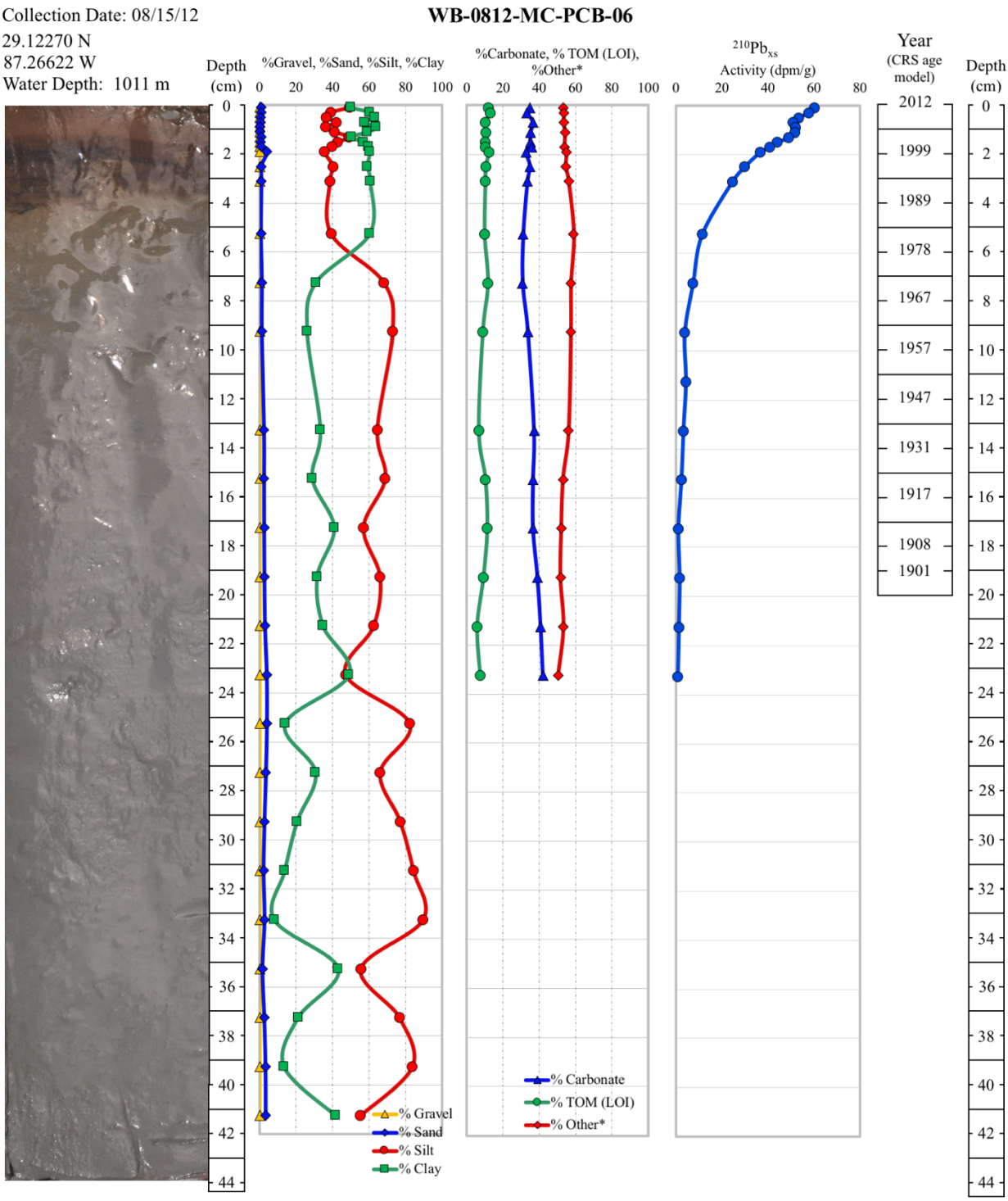

Figure F.13. Core Log for core WB-0812-MC-PCB-06. Core log including core collection date, latitude, longitude, water depth (m), core photograph, depth (cm), profiles of sediment texture, sediment composition, and $^{210}Pb_{xs}$ activity, as well as age control determined using CRS age model.

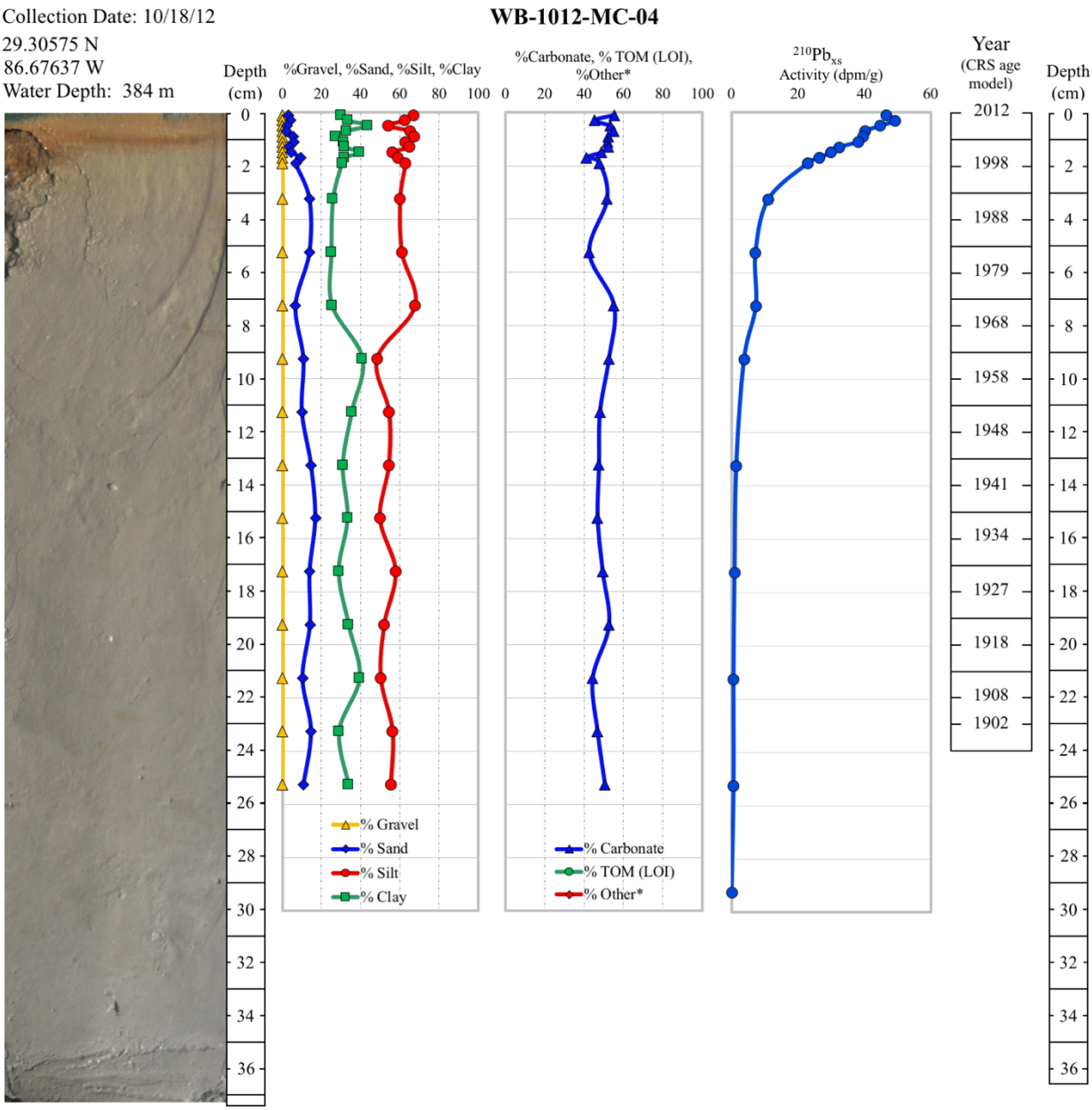

Figure F.14. Core Log for core WB-1012-MC-04. Core log including core collection date, latitude, longitude, water depth (m), core photograph, depth (cm), profiles of sediment texture, sediment composition, and $^{210}Pb_{xs}$ activity, as well as age control determined using CRS age model.

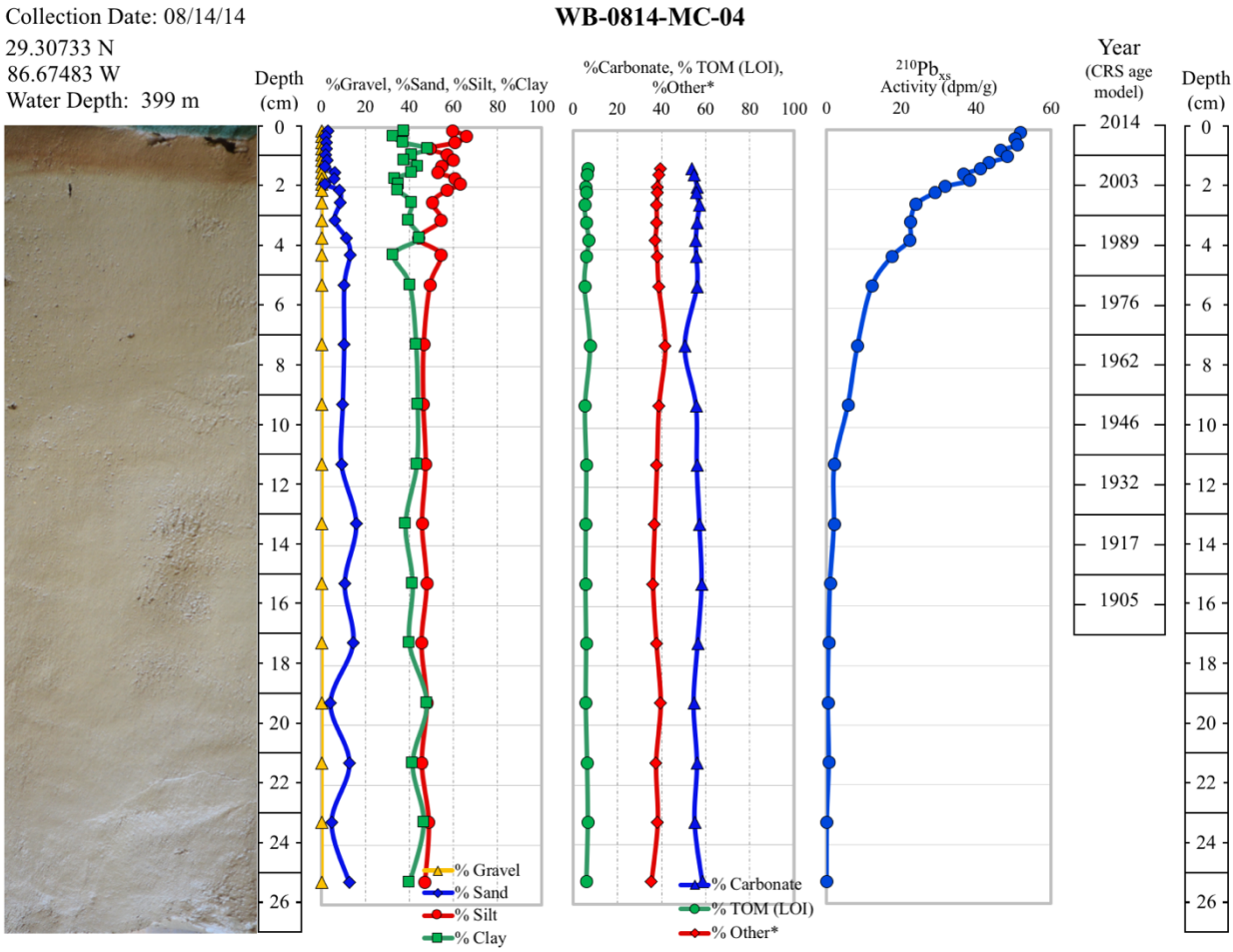

Figure F.15. Core Log for core WB-0814-MC-04. Core log including core collection date, latitude, longitude, water depth (m), core photograph, depth (cm), profiles of sediment texture, sediment composition, and $^{210}Pb_{xs}$ activity, as well as age control determined using CRS age model.

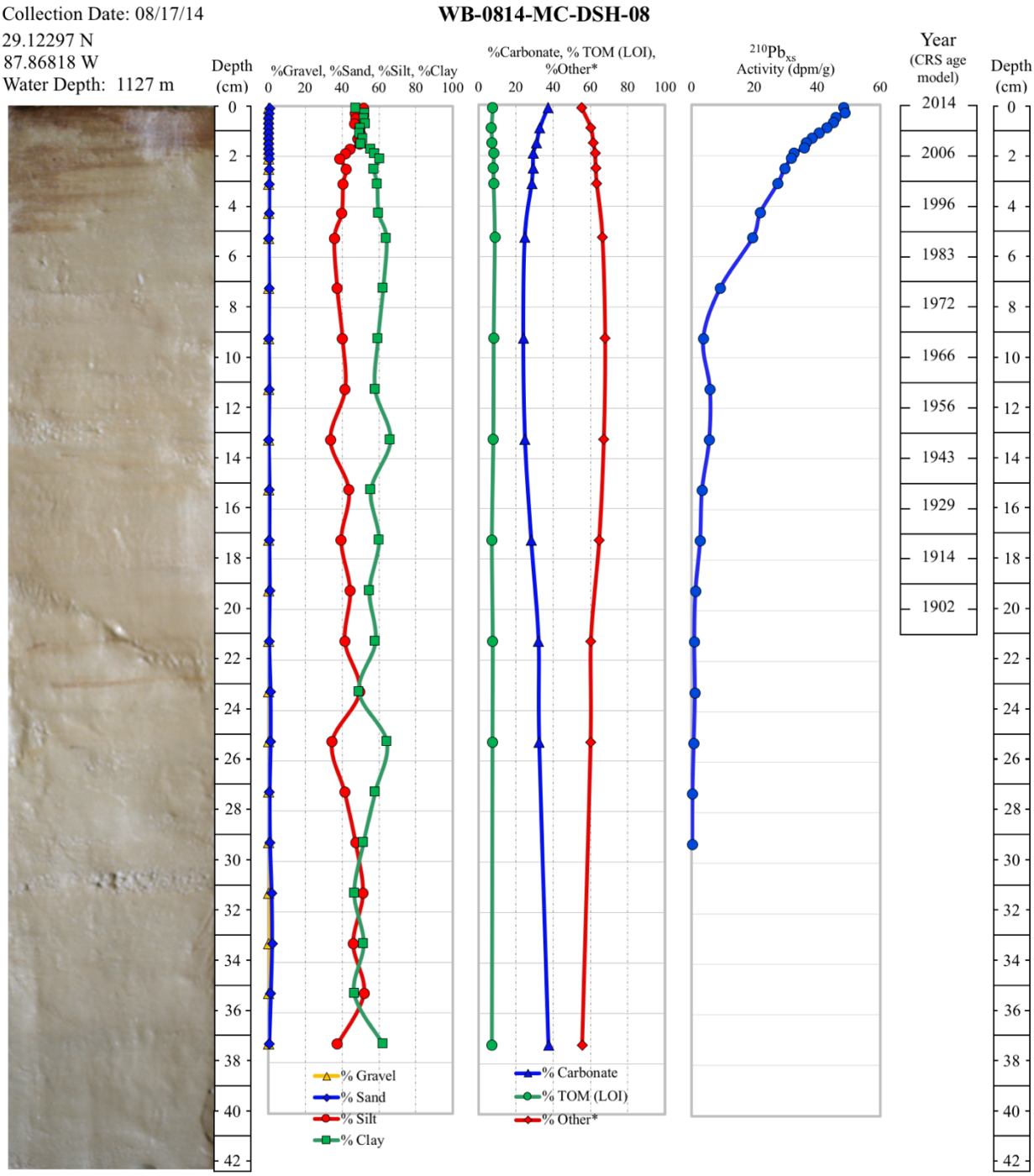

Figure F.16. Core Log for core WB-0814-MC-DSH-08. Core log including core collection date, latitude, longitude, water depth (m), core photograph, depth (cm), profiles of sediment texture, sediment composition, and $^{210}Pb_{xs}$ activity, as well as age control determined using CRS age model.

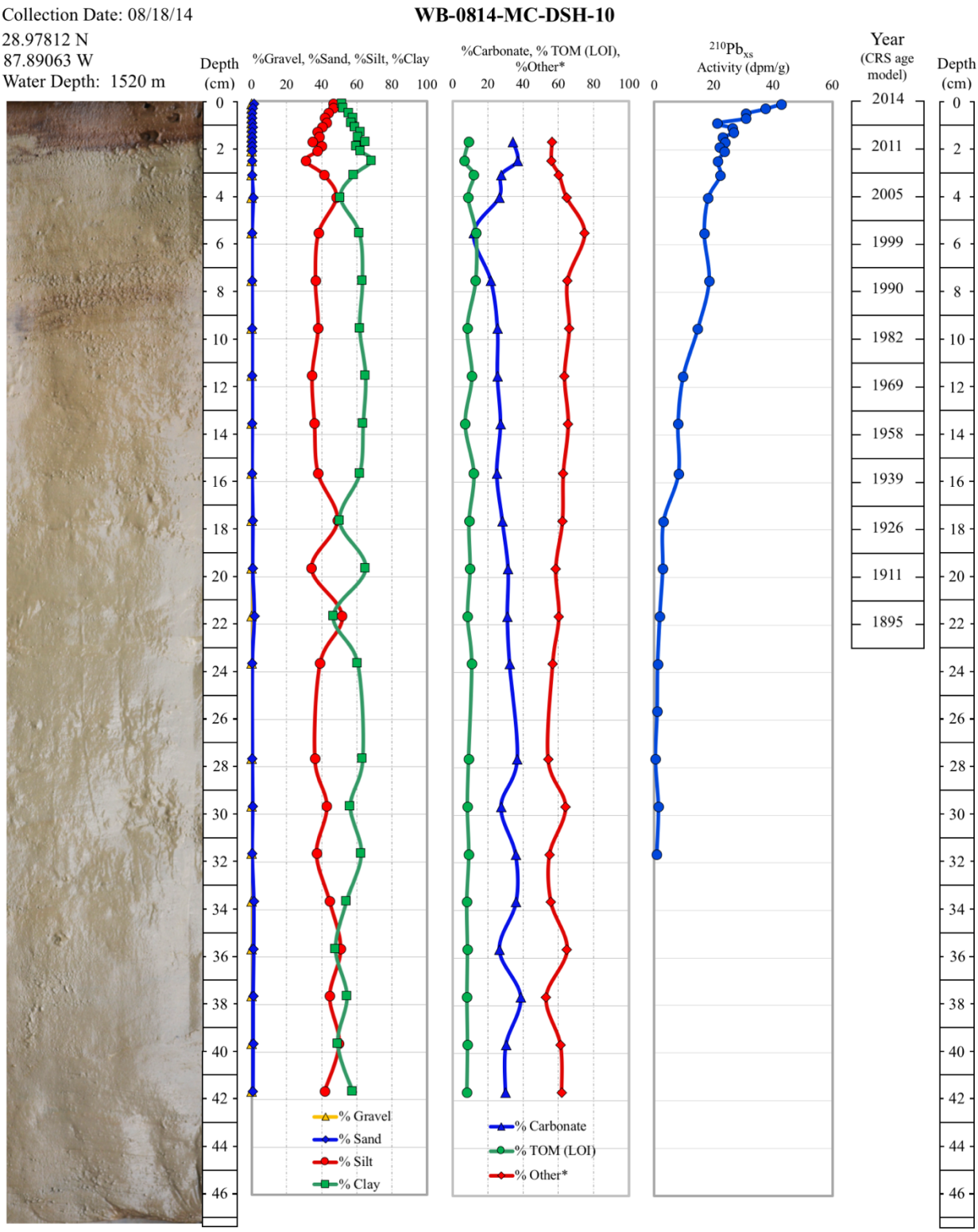

Figure F.17. Core Log for core WB-0814-MC-DSH-10. Core log including core collection date, latitude, longitude, water depth (m), core photograph, depth (cm), profiles of sediment texture, sediment composition, and $^{210}Pb_{xs}$ activity, as well as age control determined using CRS age model.

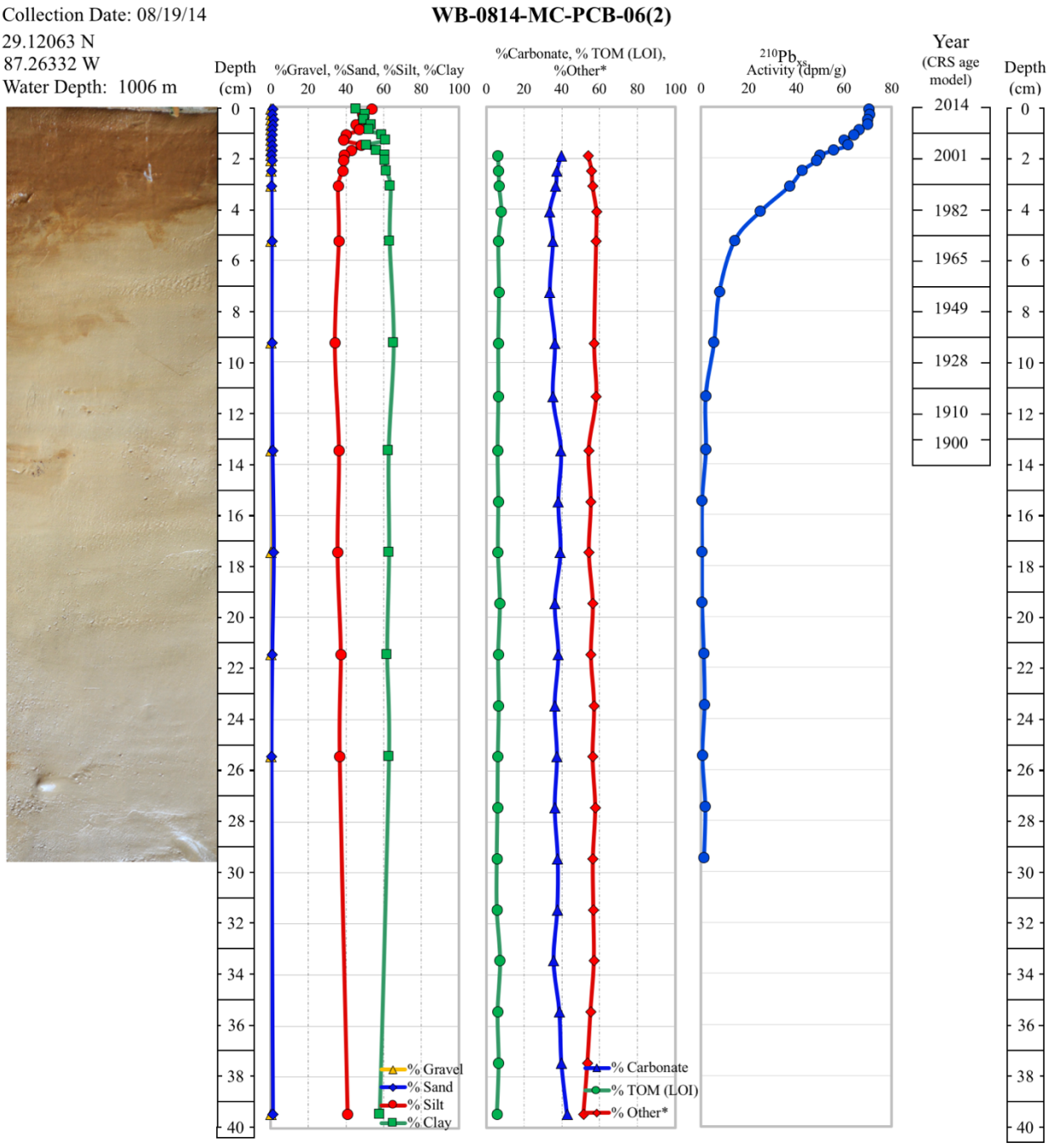

Figure F.18. Core Log for core WB-0814-MC-PCB-06(2). Core log including core collection date, latitude, longitude, water depth (m), core photograph, depth (cm), profiles of sediment texture, sediment composition, and $^{210}Pb_{xs}$ activity, as well as age control determined using CRS age model.

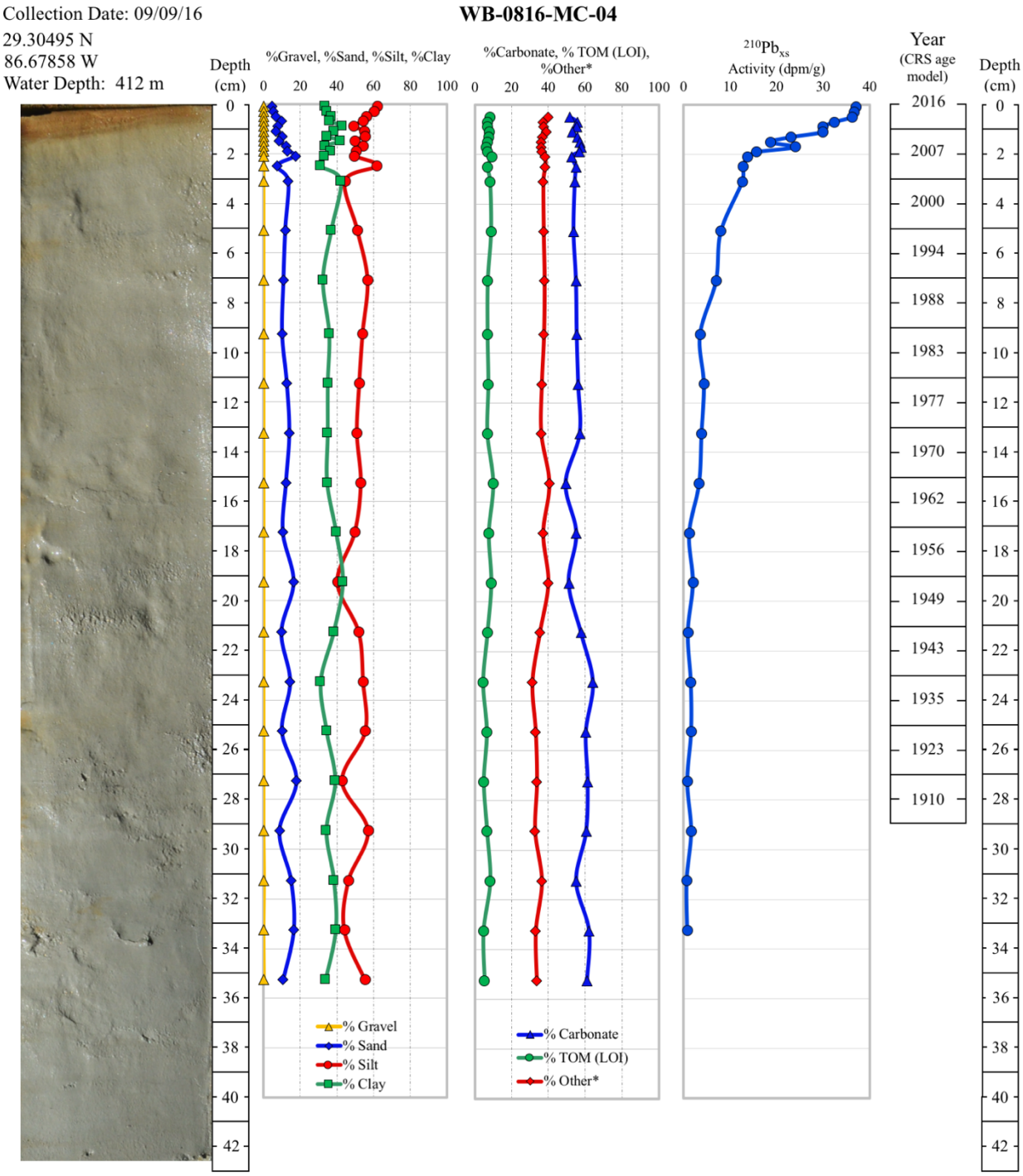

Figure F.19. Core Log for core WB-0816-MC-04. Core log including core collection date, latitude, longitude, water depth (m), core photograph, depth (cm), profiles of sediment texture, sediment composition, and $^{210}Pb_{xs}$ activity, as well as age control determined using CRS age model.

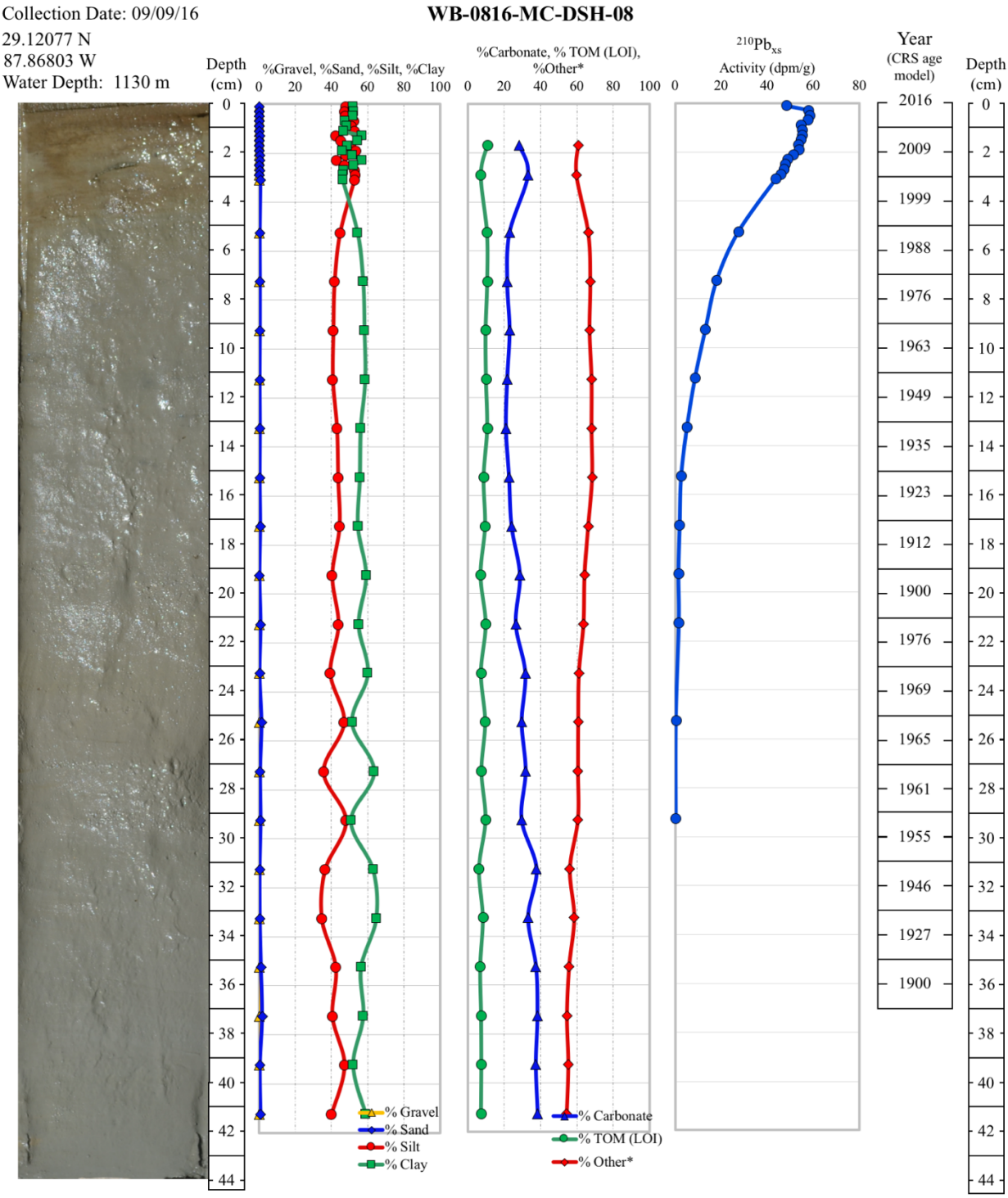

Figure F.20. Core Log for core WB-0816-MC-DSH-08. Core log including core collection date, latitude, longitude, water depth (m), core photograph, depth (cm), profiles of sediment texture, sediment composition, and $^{210}Pb_{xs}$ activity, as well as age control determined using CRS age model.

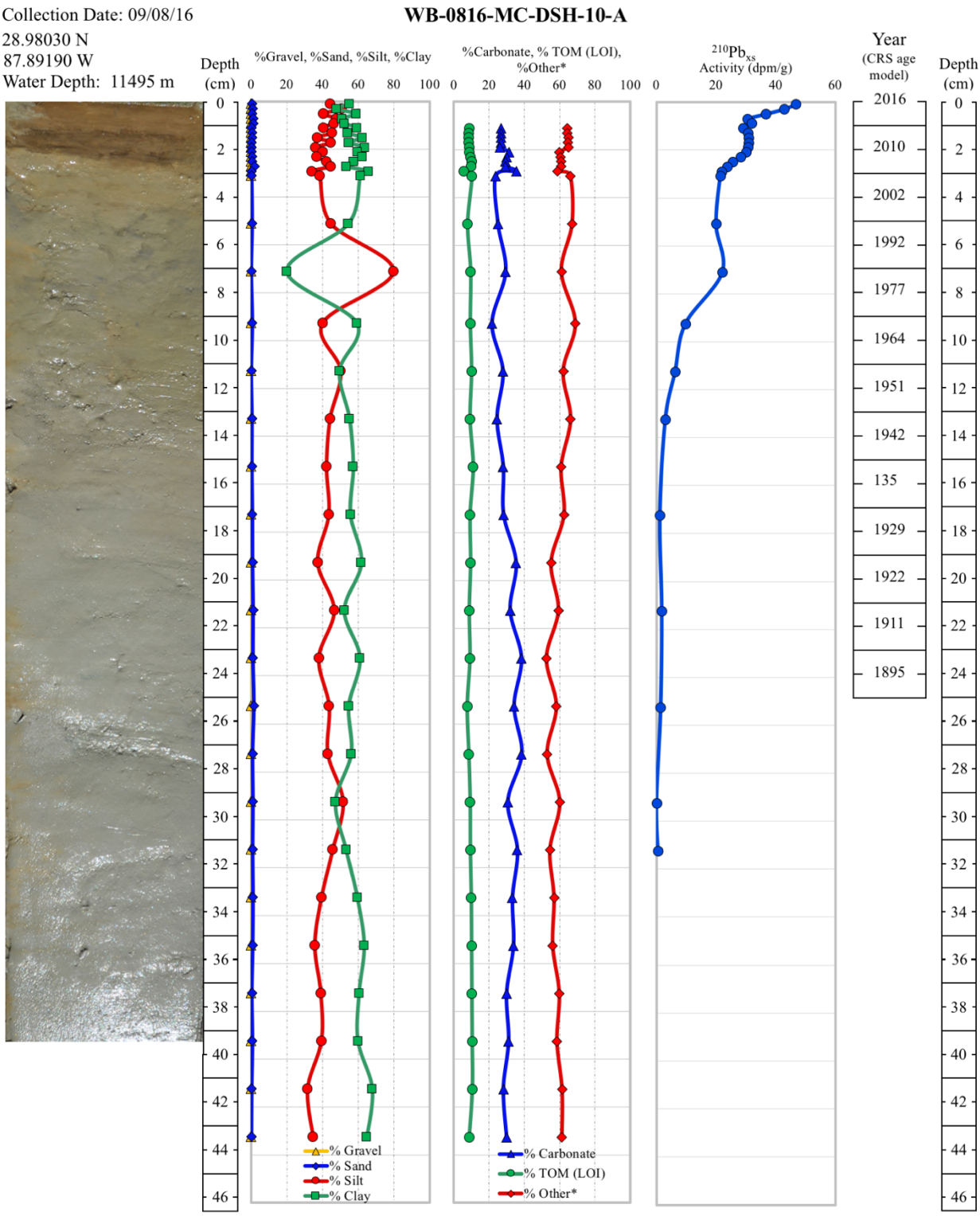

Figure F.21. Core Log for core WB-0816-MC-DSH-10-A. Core log including core collection date, latitude, longitude, water depth (m), core photograph, depth (cm), profiles of sediment texture, sediment composition, and $^{210}Pb_{xs}$ activity, as well as age control determined using CRS age model.

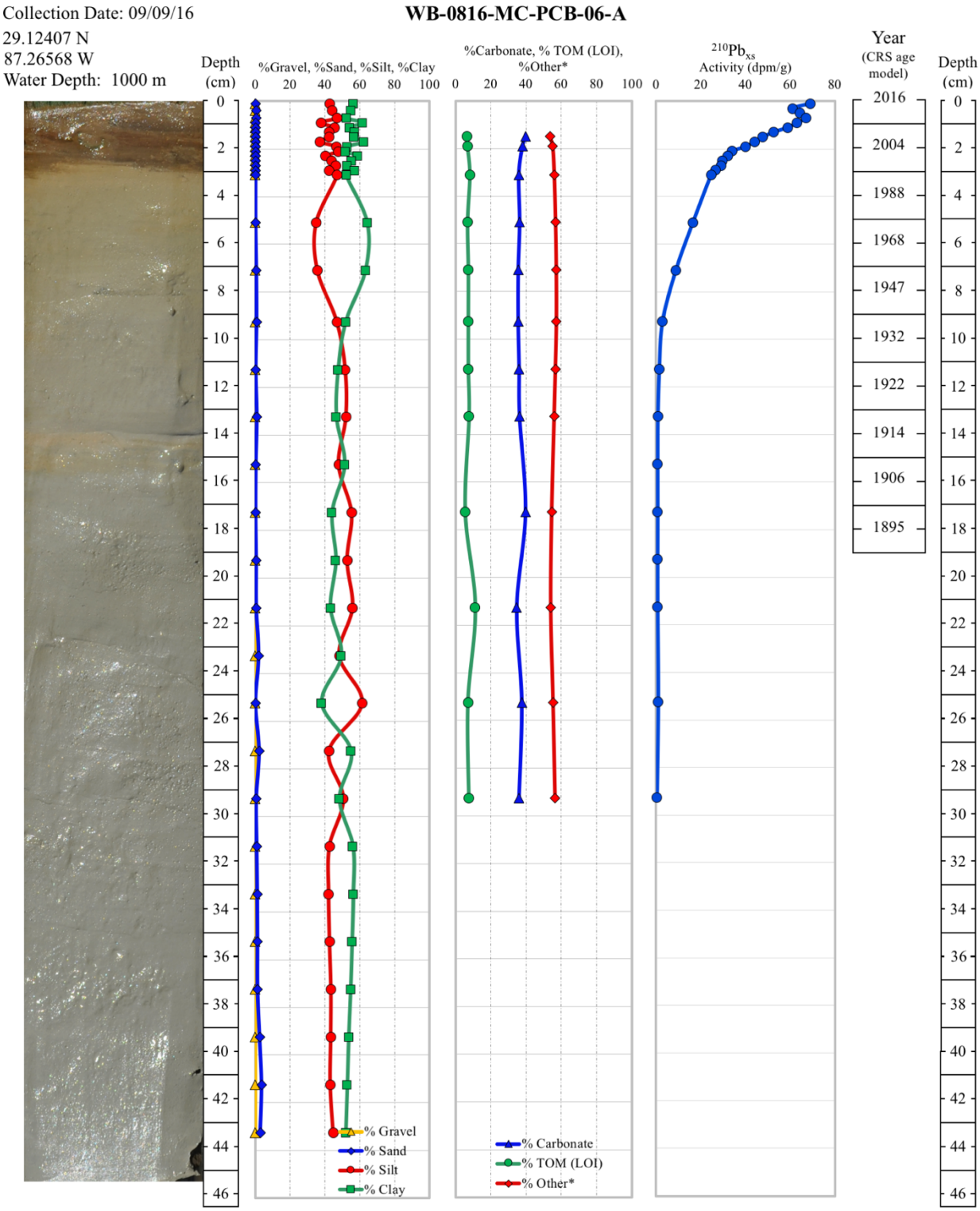

Figure F.22. Core Log for core WB-0816-MC-PCB-06-A. Core log including core collection date, latitude, longitude, water depth (m), core photograph, depth (cm), profiles of sediment texture, sediment composition, and $^{210}Pb_{xs}$ activity, as well as age control determined using CRS age model.

APPENDIX G:

SHORT-LIVED RADIOISOTOPE (SLRad) DATA: $^{234}Th_{Tot}$, $^{234}Th_{xs}$, and Decay Corrected (D.C.) $^{234}Th_{xs}$

Appendix G. Supplemental tables of short-lived radioisotope data for $^{234}Th_{Tot}$, $^{234}Th_{xs}$, and D.C. $^{234}Th_{xs}$.

Data are publicly available through the Gulf of Mexico Research Initiative Information & Data Cooperative (GRIIDC) at https://data.gulfresearchinitiative.org (doi: 10.7266/N7610XTJ, 10.7266/n7-81nq-dq02, 10.7266/n7-p0xt-6209, 10.7266/n7-qzw5-kc72, 10.7266/n7-xsrd-fq25, 10.7266/n7-1vvs-ef02, 10.7266/n7-4j4h-7w93, 10.7266/n7-cdrm-g239)

Table G.1. SLRad data of $^{234}Th_{Tot}$, $^{234}Th_{xs}$, and D.C. $^{234}Th_{xs}$ for core site WB-1109-MC-04. Sediment cores with sub-sample intervals (mm), and SLRad data for $^{234}Th_{Tot}$, Re-analysis of ^{234}Th as indicator of $^{234}Th_{Sup}$, $^{234}Th_{xs}$, and D.C. $^{234}Th_{xs}$ (Decay Corrected). Note: Blank cell denotes no analysis performed.

Core ID	Top Depth of Interval (mm)	Bottom Depth of Interval (mm)	Average Depth of Interval (mm)	$^{234}Th_{Tot}$ Activity (dpm/g)	$^{234}Th_{Tot}$ Activity error (dpm/g)	Re-Analysis; ^{234}Th Activity (dpmg/)	Re-Analysis; ^{234}Th error Activity (dpmg/)	$^{234}Th_{xs}$ Activity (dpm/g)	$^{234}Th_{xs}$ Activity error (dpm/g)	D.C. $^{234}Th_{xs}$ Activity (dpm/g)	D.C. $^{234}Th_{xs}$ Activity error (dpm/g)
WB-1109-MC-04	0	2	1	5.75	0.27			4.55	0.30	7.87	0.51
WB-1109-MC-04	2	4	3	4.92	0.22			3.72	0.26	6.80	0.47
WB-1109-MC-04	4	6	5	3.50	0.17			2.30	0.21	5.00	0.47
WB-1109-MC-04	6	8	7	3.29	0.17			2.09	0.21	4.67	0.48
WB-1109-MC-04	8	10	9	2.87	0.14			1.67	0.19	3.53	0.41
WB-1109-MC-04	10	12	11	2.17	0.14			0.97	0.19	2.24	0.44
WB-1109-MC-04	12	14	13	1.16	0.10			0.00	0.16	0.00	0.00
WB-1109-MC-04	14	16	15	1.17	0.09						
WB-1109-MC-04	16	18	17	1.35	0.09						
WB-1109-MC-04	18	20	19	1.16	0.09						
WB-1109-MC-04	20	25	22.5	1.32	0.09						
WB-1109-MC-04	30	35	32.5	1.24	0.08						
WB-1109-MC-04	40	45	42.5	1.08	0.08						
WB-1109-MC-04	50	55	52.5	0.99	0.07						
WB-1109-MC-04	60	65	62.5	0.94	0.07						
WB-1109-MC-04	70	75	72.5	1.16	0.07						
WB-1109-MC-04	80	85	82.5	1.20	0.07						
WB-1109-MC-04	90	95	92.5	1.03	0.07						
WB-1109-MC-04	100	105	102.5	1.05	0.07						
WB-1109-MC-04	110	115	112.5	1.41	0.08						
WB-1109-MC-04	120	125	122.5	1.24	0.08						
WB-1109-MC-04	130	135	132.5	1.18	0.07						
WB-1109-MC-04	140	145	142.5	1.46	0.08						

Table G.1 (Continued).

Core ID	Top Depth of Interval (mm)	Bottom Depth of Interval (mm)	Average Depth of Interval (mm)	$^{234}Th_{Tot}$ Activity (dpm/g)	$^{234}Th_{Tot}$ Activity error (dpm/g)	Re-Analysis; ^{234}Th Activity (dpmg/)	Re-Analysis; ^{234}Th error Activity (dpmg/)	$^{234}Th_{xs}$ Activity (dpm/g)	$^{234}Th_{xs}$ Activity error (dpm/g)	D.C. $^{234}Th_{xs}$ Activity (dpm/g)	D.C. $^{234}Th_{xs}$ Activity error (dpm/g)
WB-1109-MC-04	150	155	152.5	1.39	0.08						
WB-1109-MC-04	160	165	162.5	1.67	0.09						
WB-1109-MC-04	170	175	172.5	1.74	0.09						
WB-1109-MC-04	210	215	212.5	1.66	0.07						

Table G.2. SLRad data of $^{234}Th_{Tot}$, $^{234}Th_{xs}$, and D.C. $^{234}Th_{xs}$ for core site WB-1110-MC-DSH-08. Sediment cores with sub-sample intervals (mm), and SLRad data for $^{234}Th_{Tot}$, Re-analysis of ^{234}Th as indicator of $^{234}Th_{Sup}$, $^{234}Th_{xs}$, and D.C. $^{234}Th_{xs}$ (Decay Corrected). Note: Blank cell denotes no analysis performed.

Core ID	Top Depth of Interval (mm)	Bottom Depth of Interval (mm)	Average Depth of Interval (mm)	$^{234}Th_{Tot}$ Activity (dpm/g)	$^{234}Th_{Tot}$ Activity error (dpm/g)	Re-Analysis; ^{234}Th Activity (dpmg/)	Re-Analysis; ^{234}Th error Activity (dpmg/)	$^{234}Th_{xs}$ Activity (dpm/g)	$^{234}Th_{xs}$ Activity error (dpm/g)	D.C. $^{234}Th_{xs}$ Activity (dpm/g)	D.C. $^{234}Th_{xs}$ Activity error (dpm/g)
WB-1110-MC-DSH-08	0	2	1	2.23	0.11	1.16	0.08	1.33	0.13	4.59	0.46
WB-1110-MC-DSH-08	2	4	3	2.15	0.10			1.15	0.13	4.47	0.48
WB-1110-MC-DSH-08	4	6	5	1.90	0.09	1.20	0.07	0.85	0.12	5.70	0.80
WB-1110-MC-DSH-08	6	8	7	1.83	0.08			0.71	0.12	5.33	0.87
WB-1110-MC-DSH-08	8	10	9	1.60	0.08	1.01	0.06	0.43	0.11	3.76	0.96
WB-1110-MC-DSH-08	10	12	11	1.43	0.10			0.27	0.13	4.59	2.26
WB-1110-MC-DSH-08	12	14	13	1.27	0.07	1.09	0.06	0.00	0.10	0.00	0.00
WB-1110-MC-DSH-08	14	16	15	1.14	0.07						
WB-1110-MC-DSH-08	16	18	17	1.14	0.06						
WB-1110-MC-DSH-08	18	20	19	1.30	0.07						
WB-1110-MC-DSH-08	22	24	23	1.13	0.06						
WB-1110-MC-DSH-08	26	28	27	1.35	0.07						
WB-1110-MC-DSH-08	32	34	33	1.14	0.06						
WB-1110-MC-DSH-08	34	36	35	1.23	0.06						
WB-1110-MC-DSH-08	38	40	39	1.01	0.06						
WB-1110-MC-DSH-08	42	44	43	1.11	0.06						
WB-1110-MC-DSH-08	46	48	47	1.13	0.06						
WB-1110-MC-DSH-08	48	50	49	1.40	0.07						
WB-1110-MC-DSH-08	50	55	52.5	1.53	0.06						
WB-1110-MC-DSH-08	60	65	62.5	1.59	0.06						
WB-1110-MC-DSH-08	70	75	72.5	1.32	0.06						
WB-1110-MC-DSH-08	80	85	82.5	1.73	0.07						
WB-1110-MC-DSH-08	90	95	92.5	1.66	0.07						
WB-1110-MC-DSH-08	100	105	102.5	1.83	0.07						

Table G.2 (Continued).

Core ID	Top Depth of Interval (mm)	Bottom Depth of Interval (mm)	Average Depth of Interval (mm)	$^{234}Th_{Tot}$ Activity (dpm/g)	$^{234}Th_{Tot}$ Activity error (dpm/g)	Re-Analysis; ^{234}Th Activity (dpmg/)	Re-Analysis; ^{234}Th error Activity (dpmg/)	$^{234}Th_{xs}$ Activity (dpm/g)	$^{234}Th_{xs}$ Activity error (dpm/g)	D.C. $^{234}Th_{xs}$ Activity (dpm/g)	D.C. $^{234}Th_{xs}$ Activity error (dpm/g)
WB-1110-MC-DSH-08	110	115	112.5	1.82	0.07						
WB-1110-MC-DSH-08	120	125	122.5	2.11	0.08						
WB-1110-MC-DSH-08	130	135	132.5	2.06	0.07						
WB-1110-MC-DSH-08	140	145	142.5	1.77	0.07						
WB-1110-MC-DSH-08	150	155	152.5	1.76	0.09						
WB-1110-MC-DSH-08	160	165	162.5	1.81	0.07						
WB-1110-MC-DSH-08	180	185	182.5	1.57	0.06						
WB-1110-MC-DSH-08	190	195	192.5	1.71	0.07						
WB-1110-MC-DSH-08	210	215	212.5	1.61	0.07						
WB-1110-MC-DSH-08	230	235	232.5	1.66	0.07						
WB-1110-MC-DSH-08	250	255	252.5	1.68	0.07						
WB-1110-MC-DSH-08	270	275	272.5	1.78	0.07						

Table G.3. SLRad data of $^{234}Th_{Tot}$, $^{234}Th_{xs}$, and D.C. $^{234}Th_{xs}$ for core site WB-1110-MC-DSH-10. Sediment cores with sub-sample intervals (mm), and SLRad data for $^{234}Th_{Tot}$, Re-analysis of ^{234}Th as indicator of $^{234}Th_{Sup}$, $^{234}Th_{xs}$, and D.C. $^{234}Th_{xs}$ (Decay Corrected). Note: Blank cell denotes no analysis performed.

Core ID	Top Depth of Interval (mm)	Bottom Depth of Interval (mm)	Average Depth of Interval (mm)	$^{234}Th_{Tot}$ Activity (dpm/g)	$^{234}Th_{Tot}$ Activity error (dpm/g)	Re-Analysis; ^{234}Th Activity (dpmg/)	Re-Analysis; ^{234}Th error Activity (dpmg/)	$^{234}Th_{xs}$ Activity (dpm/g)	$^{234}Th_{xs}$ Activity error (dpm/g)	D.C. $^{234}Th_{xs}$ Activity (dpm/g)	D.C. $^{234}Th_{xs}$ Activity error (dpm/g)
WB-1110-MC-DSH-10	0	2	1	1.86	0.12			0.57	0.14	24.28	6.01
WB-1110-MC-DSH-10	2	4	3	1.72	0.10			0.45	0.13	24.89	7.13
WB-1110-MC-DSH-10	4	6	5	1.09	0.08			0.00	0.11	0.00	0.00
WB-1110-MC-DSH-10	6	8	7	1.18	0.08						
WB-1110-MC-DSH-10	8	10	9	1.18	0.08						
WB-1110-MC-DSH-10	10	12	11	1.19	0.08						
WB-1110-MC-DSH-10	12	14	13	1.37	0.08						
WB-1110-MC-DSH-10	16	18	17	1.21	0.08						
WB-1110-MC-DSH-10	20	22	21	1.41	0.08						
WB-1110-MC-DSH-10	24	26	25	1.11	0.07						
WB-1110-MC-DSH-10	30	32	31	1.32	0.08						
WB-1110-MC-DSH-10	40	42	41	1.34	0.08						
WB-1110-MC-DSH-10	50	52	51	1.43	0.08						
WB-1110-MC-DSH-10	60	62	61	1.25	0.07						
WB-1110-MC-DSH-10	70	72	71	1.30	0.08						
WB-1110-MC-DSH-10	80	85	82.5	1.38	0.07						
WB-1110-MC-DSH-10	90	95	92.5	1.47	0.07						
WB-1110-MC-DSH-10	100	105	102.5	1.34	0.07						
WB-1110-MC-DSH-10	110	115	112.5	1.28	0.06						
WB-1110-MC-DSH-10	120	125	122.5	1.40	0.07						
WB-1110-MC-DSH-10	130	135	132.5	1.38	0.07						
WB-1110-MC-DSH-10	140	145	142.5	1.46	0.07						
WB-1110-MC-DSH-10	150	155	152.5	1.32	0.07						
WB-1110-MC-DSH-10	160	165	162.5	1.34	0.07						

Table G.3 (Continued).

Core ID	Top Depth of Interval (mm)	Bottom Depth of Interval (mm)	Average Depth of Interval (mm)	$^{234}Th_{Tot}$ Activity (dpm/g)	$^{234}Th_{Tot}$ Activity error (dpm/g)	Re-Analysis; ^{234}Th Activity (dpmg/)	Re-Analysis; ^{234}Th error Activity (dpmg/)	$^{234}Th_{xs}$ Activity (dpm/g)	$^{234}Th_{xs}$ Activity error (dpm/g)	D.C. $^{234}Th_{xs}$ Activity (dpm/g)	D.C. $^{234}Th_{xs}$ Activity error (dpm/g)
WB-1110-MC-DSH-10	170	175	172.5	1.36	0.07						
WB-1110-MC-DSH-10	180	185	182.5	1.46	0.07						
WB-1110-MC-DSH-10	190	195	192.5	1.64	0.07						
WB-1110-MC-DSH-10	200	205	202.5	1.50	0.07						
WB-1110-MC-DSH-10	210	215	212.5	1.50	0.07						
WB-1110-MC-DSH-10	220	225	222.5	1.53	0.07						

Table G.4. SLRad data of $^{234}Th_{Tot}$, $^{234}Th_{xs}$, and D.C. $^{234}Th_{xs}$ for core site WB-1110-MC-PCB-06. Sediment cores with sub-sample intervals (mm), and SLRad data for $^{234}Th_{Tot}$, Re-analysis of ^{234}Th as indicator of $^{234}Th_{Sup}$, $^{234}Th_{xs}$, and D.C. $^{234}Th_{xs}$ (Decay Corrected). Note: Blank cell denotes no analysis performed.

Core ID	Top Depth of Interval (mm)	Bottom Depth of Interval (mm)	Average Depth of Interval (mm)	$^{234}Th_{Tot}$ Activity (dpm/g)	$^{234}Th_{Tot}$ Activity error (dpm/g)	Re-Analysis; ^{234}Th Activity (dpmg/)	Re-Analysis; ^{234}Th error Activity (dpmg/)	$^{234}Th_{xs}$ Activity (dpm/g)	$^{234}Th_{xs}$ Activity error (dpm/g)	D.C. $^{234}Th_{xs}$ Activity (dpm/g)	D.C. $^{234}Th_{xs}$ Activity error (dpm/g)
WB-1110-MC-PCB-06	0	2	1	1.89	0.10			1.09	0.13	10.57	1.26
WB-1110-MC-PCB-06	2	4	3	0.97	0.06						
WB-1110-MC-PCB-06	4	6	5	1.53	0.08			0.53	0.11	5.42	1.14
WB-1110-MC-PCB-06	6	10	8	0.98	0.05						
WB-1110-MC-PCB-06	10	12	11	1.30	0.07			0.20	0.10	2.14	1.14
WB-1110-MC-PCB-06	12	14	13	1.22	0.07			0.00	0.00	0.00	0.00
WB-1110-MC-PCB-06	14	16	15	1.02	0.06						
WB-1110-MC-PCB-06	16	18	17	1.17	0.06						
WB-1110-MC-PCB-06	18	20	19	1.23	0.06						
WB-1110-MC-PCB-06	24	26	25	1.12	0.06						
WB-1110-MC-PCB-06	28	30	29	1.20	0.06						
WB-1110-MC-PCB-06	36	38	37	1.02	0.06						
WB-1110-MC-PCB-06	40	42	41	1.00	0.06						
WB-1110-MC-PCB-06	50	52	51	1.11	0.06						
WB-1110-MC-PCB-06	60	62	61	1.33	0.06						
WB-1110-MC-PCB-06	70	72	71	1.33	0.06						
WB-1110-MC-PCB-06	80	82	81	1.10	0.06						
WB-1110-MC-PCB-06	90	92	91	1.18	0.06						
WB-1110-MC-PCB-06	100	105	102.5	1.10	0.05						
WB-1110-MC-PCB-06	110	115	112.5	1.08	0.05						
WB-1110-MC-PCB-06	130	135	132.5	1.38	0.06						
WB-1110-MC-PCB-06	150	155	152.5	1.15	0.05						
WB-1110-MC-PCB-06	170	175	172.5	1.47	0.06						
WB-1110-MC-PCB-06	190	195	192.5	1.71	0.07						

Table G.4 (Continued).

Core ID	Top Depth of Interval (mm)	Bottom Depth of Interval (mm)	Average Depth of Interval (mm)	$^{234}Th_{Tot}$ Activity (dpm/g)	$^{234}Th_{Tot}$ Activity error (dpm/g)	Re-Analysis; ^{234}Th Activity (dpmg/)	Re-Analysis; ^{234}Th error Activity (dpmg/)	$^{234}Th_{xs}$ Activity (dpm/g)	$^{234}Th_{xs}$ Activity error (dpm/g)	D.C. $^{234}Th_{xs}$ Activity (dpm/g)	D.C. $^{234}Th_{xs}$ Activity error (dpm/g)
WB-1110-MC-PCB-06	200	205	202.5	1.67	0.06						

Table G.5. SLRad data of $^{234}Th_{Tot}$, $^{234}Th_{xs}$, and D.C. $^{234}Th_{xs}$ for core site WB-1114-MC-DSH-08. Sediment cores with sub-sample intervals (mm), and SLRad data for $^{234}Th_{Tot}$, Re-analysis of ^{234}Th as indicator of $^{234}Th_{Sup}$, $^{234}Th_{xs}$, and D.C. $^{234}Th_{xs}$ (Decay Corrected). Note: Blank cell denotes no analysis performed.

Core ID	Top Depth of Interval (mm)	Bottom Depth of Interval (mm)	Average Depth of Interval (mm)	$^{234}Th_{Tot}$ Activity (dpm/g)	$^{234}Th_{Tot}$ Activity error (dpm/g)	Re-Analysis; ^{234}Th Activity (dpmg/)	Re-Analysis; ^{234}Th error Activity (dpmg/)	$^{234}Th_{xs}$ Activity (dpm/g)	$^{234}Th_{xs}$ Activity error (dpm/g)	D.C. $^{234}Th_{xs}$ Activity (dpm/g)	D.C. $^{234}Th_{xs}$ Activity error (dpm/g)
WB-1114-MC-DSH-08	0	2	1	1.73	0.04						
WB-1114-MC-DSH-08	2	4	3	1.50	0.04						
WB-1114-MC-DSH-08	4	6	5	1.57	0.04						
WB-1114-MC-DSH-08	6	8	7	1.58	0.04						
WB-1114-MC-DSH-08	8	10	9	1.13	0.03						
WB-1114-MC-DSH-08	10	12	11	1.41	0.04						
WB-1114-MC-DSH-08	12	14	13	1.60	0.04						
WB-1114-MC-DSH-08	14	16	15	1.00	0.03						
WB-1114-MC-DSH-08	16	18	17	1.63	0.04						
WB-1114-MC-DSH-08	18	20	19	1.14	0.03						
WB-1114-MC-DSH-08	24	26	25	1.63	0.04						
WB-1114-MC-DSH-08	28	30	29	1.52	0.04						
WB-1114-MC-DSH-08	32	34	33	1.43	0.04						
WB-1114-MC-DSH-08	36	38	37	1.58	0.04						
WB-1114-MC-DSH-08	40	42	41	1.54	0.04						
WB-1114-MC-DSH-08	48	50	49	1.55	0.04						
WB-1114-MC-DSH-08	70	75	72.5	1.62	0.04						
WB-1114-MC-DSH-08	90	95	92.5	1.58	0.04						
WB-1114-MC-DSH-08	110	115	112.5	1.60	0.04						
WB-1114-MC-DSH-08	130	135	132.5	1.62	0.04						
WB-1114-MC-DSH-08	150	155	152.5	1.74	0.04						
WB-1114-MC-DSH-08	170	175	172.5	1.68	0.04						
WB-1114-MC-DSH-08	180	185	182.5	1.71	0.04						
WB-1114-MC-DSH-08	190	195	192.5	1.68	0.04						

Table G.5 (Continued).

Core ID	Top Depth of Interval (mm)	Bottom Depth of Interval (mm)	Average Depth of Interval (mm)	$^{234}Th_{Tot}$ Activity (dpm/g)	$^{234}Th_{Tot}$ Activity error (dpm/g)	Re-Analysis; ^{234}Th Activity (dpmg/)	Re-Analysis; ^{234}Th error Activity (dpmg/)	$^{234}Th_{xs}$ Activity (dpm/g)	$^{234}Th_{xs}$ Activity error (dpm/g)	D.C. $^{234}Th_{xs}$ Activity (dpm/g)	D.C. $^{234}Th_{xs}$ Activity error (dpm/g)
WB-1114-MC-DSH-08	200	205	202.5	1.78	0.04						
WB-1114-MC-DSH-08	210	215	212.5	1.71	0.04						
WB-1114-MC-DSH-08	230	235	232.5	1.64	0.05						

Table G.6. SLRad data of $^{234}Th_{Tot}$, $^{234}Th_{xs}$, and D.C. $^{234}Th_{xs}$ for core site WB-1114-MC-DSH-10. Sediment cores with sub-sample intervals (mm), and SLRad data for $^{234}Th_{Tot}$, Re-analysis of ^{234}Th as indicator of $^{234}Th_{Sup}$, $^{234}Th_{xs}$, and D.C. $^{234}Th_{xs}$ (Decay Corrected). Note: Blank cell denotes no analysis performed.

Core ID	Top Depth of Interval (mm)	Bottom Depth of Interval (mm)	Average Depth of Interval (mm)	$^{234}Th_{Tot}$ Activity (dpm/g)	$^{234}Th_{Tot}$ Activity error (dpm/g)	Re-Analysis; ^{234}Th Activity (dpmg/)	Re-Analysis; ^{234}Th error Activity (dpmg/)	$^{234}Th_{xs}$ Activity (dpm/g)	$^{234}Th_{xs}$ Activity error (dpm/g)	D.C. $^{234}Th_{xs}$ Activity (dpm/g)	D.C. $^{234}Th_{xs}$ Activity error (dpm/g)
WB-1114-MC-DSH-10	0	2	1	4.09	0.14	1.31	0.09	2.79	0.16	24.92	1.45
WB-1114-MC-DSH-10	2	4	3	2.14	0.10	0.95	0.07	0.84	0.13	20.03	3.07
WB-1114-MC-DSH-10	4	6	5	0.89	0.07			0.00	0.10	0.00	0.00
WB-1114-MC-DSH-10	6	8	7	1.15	0.07						
WB-1114-MC-DSH-10	8	10	9	1.29	0.07						
WB-1114-MC-DSH-10	10	12	11	1.37	0.07						
WB-1114-MC-DSH-10	12	14	13	0.92	0.06						
WB-1114-MC-DSH-10	16	18	17	1.08	0.06						
WB-1114-MC-DSH-10	18	20	19	1.10	0.06						
WB-1114-MC-DSH-10	20	22	21	1.13	0.07						
WB-1114-MC-DSH-10	24	26	25	1.32	0.07						
WB-1114-MC-DSH-10	32	34	33	0.91	0.05						
WB-1114-MC-DSH-10	40	42	41	1.38	0.07						
WB-1114-MC-DSH-10	48	50	49	1.00	0.06						
WB-1114-MC-DSH-10	56	58	57	0.81	0.05						
WB-1114-MC-DSH-10	64	66	65	1.01	0.06						
WB-1114-MC-DSH-10	72	74	73	0.90	0.05						
WB-1114-MC-DSH-10	80	82	81	1.03	0.06						
WB-1114-MC-DSH-10	90	95	92.5	1.32	0.06						
WB-1114-MC-DSH-10	100	105	102.5	1.56	0.06						
WB-1114-MC-DSH-10	110	115	112.5	1.41	0.06						
WB-1114-MC-DSH-10	120	125	122.5	1.07	0.05						
WB-1114-MC-DSH-10	130	135	132.5	1.26	0.06						
WB-1114-MC-DSH-10	150	155	152.5	1.19	0.05						

Table G.6 (Continued).

Core ID	Top Depth of Interval (mm)	Bottom Depth of Interval (mm)	Average Depth of Interval (mm)	$^{234}Th_{Tot}$ Activity (dpm/g)	$^{234}Th_{Tot}$ Activity error (dpm/g)	Re-Analysis; ^{234}Th Activity (dpmg/)	Re-Analysis; ^{234}Th error Activity (dpmg/)	$^{234}Th_{xs}$ Activity (dpm/g)	$^{234}Th_{xs}$ Activity error (dpm/g)	D.C. $^{234}Th_{xs}$ Activity (dpm/g)	D.C. $^{234}Th_{xs}$ Activity error (dpm/g)
WB-1114-MC-DSH-10	170	175	172.5	1.37	0.06						
WB-1114-MC-DSH-10	190	195	192.5	1.31	0.06						
WB-1114-MC-DSH-10	210	215	212.5	1.61	0.06						
WB-1114-MC-DSH-10	230	235	232.5	1.69	0.06						
WB-1114-MC-DSH-10	250	255	252.5	1.42	0.06						
WB-1114-MC-DSH-10	270	275	272.5	1.15	0.05						
WB-1114-MC-DSH-10	310	315	312.5	1.54	0.07						

Table G.7. SLRad data of $^{234}Th_{Tot}$, $^{234}Th_{xs}$, and D.C. $^{234}Th_{xs}$ for core site WB-1114-MC-PCB-06. Sediment cores with sub-sample intervals (mm), and SLRad data for $^{234}Th_{Tot}$, Re-analysis of ^{234}Th as indicator of $^{234}Th_{Sup}$, $^{234}Th_{xs}$, and D.C. $^{234}Th_{xs}$ (Decay Corrected). Note: Blank cell denotes no analysis performed.

Core ID	Top Depth of Interval (mm)	Bottom Depth of Interval (mm)	Average Depth of Interval (mm)	$^{234}Th_{Tot}$ Activity (dpm/g)	$^{234}Th_{Tot}$ Activity error (dpm/g)	Re-Analysis; ^{234}Th Activity (dpmg/)	Re-Analysis; ^{234}Th error Activity (dpmg/)	$^{234}Th_{xs}$ Activity (dpm/g)	$^{234}Th_{xs}$ Activity error (dpm/g)	D.C. $^{234}Th_{xs}$ Activity (dpm/g)	D.C. $^{234}Th_{xs}$ Activity error (dpm/g)
WB-1114-MC-PCB-06	0	2	1	1.72	0.09	1.44	0.08				
WB-1114-MC-PCB-06	2	4	3	0.70	0.06						
WB-1114-MC-PCB-06	4	6	5	1.08	0.06						
WB-1114-MC-PCB-06	6	8	7	1.15	0.07						
WB-1114-MC-PCB-06	8	10	9	0.76	0.06						
WB-1114-MC-PCB-06	10	12	11	0.99	0.06						
WB-1114-MC-PCB-06	12	14	13	0.87	0.06						
WB-1114-MC-PCB-06	14	16	15	1.06	0.06						
WB-1114-MC-PCB-06	16	18	17	0.83	0.06						
WB-1114-MC-PCB-06	18	20	19	1.08	0.06						
WB-1114-MC-PCB-06	20	22	21	1.29	0.07						
WB-1114-MC-PCB-06	24	26	25	1.37	0.07						
WB-1114-MC-PCB-06	32	34	33	0.97	0.06						
WB-1114-MC-PCB-06	36	38	37	1.12	0.06						
WB-1114-MC-PCB-06	40	42	41	0.95	0.06						
WB-1114-MC-PCB-06	48	50	49	1.25	0.07						
WB-1114-MC-PCB-06	56	58	57	0.96	0.06						
WB-1114-MC-PCB-06	64	66	65	1.07	0.06						
WB-1114-MC-PCB-06	70	75	72.5	1.25	0.06						
WB-1114-MC-PCB-06	80	85	82.5	1.38	0.06						
WB-1114-MC-PCB-06	90	95	92.5	1.05	0.05						
WB-1114-MC-PCB-06	100	105	102.5	1.31	0.06						
WB-1114-MC-PCB-06	110	115	112.5	1.07	0.05						
WB-1114-MC-PCB-06	120	125	122.5	1.08	0.05						

Table G.7 (Continued).

Core ID	Top Depth of Interval (mm)	Bottom Depth of Interval (mm)	Average Depth of Interval (mm)	$^{234}Th_{Tot}$ Activity (dpm/g)	$^{234}Th_{Tot}$ Activity error (dpm/g)	Re-Analysis; ^{234}Th Activity (dpmg/)	Re-Analysis; ^{234}Th error Activity (dpmg/)	$^{234}Th_{xs}$ Activity (dpm/g)	$^{234}Th_{xs}$ Activity error (dpm/g)	D.C. $^{234}Th_{xs}$ Activity (dpm/g)	D.C. $^{234}Th_{xs}$ Activity error (dpm/g)
WB-1114-MC-PCB-06	140	145	142.5	1.45	0.06						
WB-1114-MC-PCB-06	150	155	152.5	1.75	0.07						
WB-1114-MC-PCB-06	170	175	172.5	1.48	0.06						
WB-1114-MC-PCB-06	190	195	192.5	1.31	0.06						
WB-1114-MC-PCB-06	210	215	212.5	1.36	0.06						
WB-1114-MC-PCB-06	230	235	232.5	1.77	0.07						
WB-1114-MC-PCB-06	270	275	272.5	1.49	0.07						

Table G.8. SLRad data of $^{234}Th_{Tot}$, $^{234}Th_{xs}$, and D.C. $^{234}Th_{xs}$ for core site WB-0911-BC-DSH-08. Sediment cores with sub-sample intervals (mm), and SLRad data for $^{234}Th_{Tot}$, Re-analysis of ^{234}Th as indicator of $^{234}Th_{Sup}$, $^{234}Th_{xs}$, and D.C. $^{234}Th_{xs}$ (Decay Corrected). Note: Blank cell denotes no analysis performed.

Core ID	Top Depth of Interval (mm)	Bottom Depth of Interval (mm)	Average Depth of Interval (mm)	$^{234}Th_{Tot}$ Activity (dpm/g)	$^{234}Th_{Tot}$ Activity error (dpm/g)	Re-Analysis; ^{234}Th Activity (dpmg/)	Re-Analysis; ^{234}Th error Activity (dpmg/)	$^{234}Th_{xs}$ Activity (dpm/g)	$^{234}Th_{xs}$ Activity error (dpm/g)	D.C. $^{234}Th_{xs}$ Activity (dpm/g)	D.C. $^{234}Th_{xs}$ Activity error (dpm/g)
WB-0911-BC-DSH-08	0	2	1	2.53	0.10			1.21	0.13	2.80	0.30
WB-0911-BC-DSH-08	2	4	3	1.78	0.08	1.39	0.07	0.46	0.11	1.27	0.31
WB-0911-BC-DSH-08	4	6	5	1.45	0.07			0.00	0.11	0.00	0.00
WB-0911-BC-DSH-08	6	8	7	1.32	0.07	1.11	0.06				
WB-0911-BC-DSH-08	8	10	9	1.38	0.07						
WB-0911-BC-DSH-08	10	12	11	1.33	0.07						
WB-0911-BC-DSH-08	12	14	13	1.44	0.07						
WB-0911-BC-DSH-08	14	16	15	1.25	0.07						
WB-0911-BC-DSH-08	16	18	17	1.26	0.06						
WB-0911-BC-DSH-08	18	20	19	1.24	0.06						
WB-0911-BC-DSH-08	24	26	25	1.18	0.06						
WB-0911-BC-DSH-08	26	28	27	1.26	0.06						
WB-0911-BC-DSH-08	28	30	29	1.22	0.06						
WB-0911-BC-DSH-08	30	35	32.5	1.39	0.06						
WB-0911-BC-DSH-08	40	45	42.5	1.48	0.06						
WB-0911-BC-DSH-08	50	55	52.5	1.39	0.06						
WB-0911-BC-DSH-08	60	65	62.5	1.41	0.06						
WB-0911-BC-DSH-08	70	75	72.5	1.70	0.07						
WB-0911-BC-DSH-08	80	85	82.5	1.66	0.07						
WB-0911-BC-DSH-08	90	95	92.5	2.06	0.07						
WB-0911-BC-DSH-08	100	105	102.5	1.96	0.07						
WB-0911-BC-DSH-08	110	115	112.5	1.83	0.07						
WB-0911-BC-DSH-08	120	125	122.5	1.95	0.07						
WB-0911-BC-DSH-08	130	135	132.5	1.86	0.07						

Table G.8 (Continued).

Core ID	Top Depth of Interval (mm)	Bottom Depth of Interval (mm)	Average Depth of Interval (mm)	$^{234}Th_{Tot}$ Activity (dpm/g)	$^{234}Th_{Tot}$ Activity error (dpm/g)	Re-Analysis; ^{234}Th Activity (dpmg/)	Re-Analysis; ^{234}Th error Activity (dpmg/)	$^{234}Th_{xs}$ Activity (dpm/g)	$^{234}Th_{xs}$ Activity error (dpm/g)	D.C. $^{234}Th_{xs}$ Activity (dpm/g)	D.C. $^{234}Th_{xs}$ Activity error (dpm/g)
WB-0911-BC-DSH-08	140	145	142.5	1.91	0.07						
WB-0911-BC-DSH-08	150	155	152.5	1.71	0.07						
WB-0911-BC-DSH-08	170	175	172.5	1.67	0.07						
WB-0911-BC-DSH-08	190	195	192.5	1.99	0.07						
WB-0911-BC-DSH-08	210	215	212.5	1.82	0.07						
WB-0911-BC-DSH-08	230	235	232.5	1.81	0.07						
WB-0911-BC-DSH-08	250	255	252.5	2.18	0.07						
WB-0911-BC-DSH-08	270	275	272.5	1.93	0.07						
WB-0911-BC-DSH-08	290	295	292.5	1.91	0.07						

Table G.9. SLRad data of $^{234}Th_{Tot}$, $^{234}Th_{xs}$, and D.C. $^{234}Th_{xs}$ for core site WB-0911-BC-DSH-10. Sediment cores with sub-sample intervals (mm), and SLRad data for $^{234}Th_{Tot}$, Re-analysis of ^{234}Th as indicator of $^{234}Th_{Sup}$, $^{234}Th_{xs}$, and D.C. $^{234}Th_{xs}$ (Decay Corrected). Note: Blank cell denotes no analysis performed.

Core ID	Top Depth of Interval (mm)	Bottom Depth of Interval (mm)	Average Depth of Interval (mm)	$^{234}Th_{Tot}$ Activity (dpm/g)	$^{234}Th_{Tot}$ Activity error (dpm/g)	Re-Analysis; ^{234}Th Activity (dpmg/)	Re-Analysis; ^{234}Th error Activity (dpmg/)	$^{234}Th_{xs}$ Activity (dpm/g)	$^{234}Th_{xs}$ Activity error (dpm/g)	D.C. $^{234}Th_{xs}$ Activity (dpm/g)	D.C. $^{234}Th_{xs}$ Activity error (dpm/g)
WB-0911-BC-DSH-10	0	2	1	4.77	0.16			3.64	0.18	8.15	0.40
WB-0911-BC-DSH-10	2	4	3	1.35	0.07	0.85	0.06	0.22	0.11	1.50	0.75
WB-0911-BC-DSH-10	4	6	5	1.14	0.06			0.00	0.10	0.00	0.00
WB-0911-BC-DSH-10	6	8	7	1.13	0.06						
WB-0911-BC-DSH-10	8	10	9	1.03	0.06						
WB-0911-BC-DSH-10	10	12	11	1.06	0.06						
WB-0911-BC-DSH-10	12	14	13	1.17	0.06						
WB-0911-BC-DSH-10	14	16	15	1.09	0.06						
WB-0911-BC-DSH-10	16	18	17	1.48	0.07						
WB-0911-BC-DSH-10	24	26	25	1.10	0.06						
WB-0911-BC-DSH-10	32	34	33	1.26	0.07						
WB-0911-BC-DSH-10	40	45	42.5	1.18	0.05						
WB-0911-BC-DSH-10	50	55	52.5	1.14	0.05						
WB-0911-BC-DSH-10	60	65	62.5	1.27	0.06						
WB-0911-BC-DSH-10	70	75	72.5	1.08	0.05						
WB-0911-BC-DSH-10	80	85	82.5	1.16	0.05						
WB-0911-BC-DSH-10	90	95	92.5	1.01	0.05						
WB-0911-BC-DSH-10	110	115	112.5	1.05	0.05						
WB-0911-BC-DSH-10	130	135	132.5	1.10	0.05						
WB-0911-BC-DSH-10	150	155	152.5	1.17	0.05						
WB-0911-BC-DSH-10	170	175	172.5	0.97	0.05						
WB-0911-BC-DSH-10	190	195	192.5	1.09	0.05						
WB-0911-BC-DSH-10	210	215	212.5	1.54	0.06						
WB-0911-BC-DSH-10	230	235	232.5	1.28	0.06						

Table G.9 (Continued).

Core ID	Top Depth of Interval (mm)	Bottom Depth of Interval (mm)	Average Depth of Interval (mm)	$^{234}Th_{Tot}$ Activity (dpm/g)	$^{234}Th_{Tot}$ Activity error (dpm/g)	Re-Analysis; ^{234}Th Activity (dpmg/)	Re-Analysis; ^{234}Th error Activity (dpmg/)	$^{234}Th_{xs}$ Activity (dpm/g)	$^{234}Th_{xs}$ Activity error (dpm/g)	D.C. $^{234}Th_{xs}$ Activity (dpm/g)	D.C. $^{234}Th_{xs}$ Activity error (dpm/g)
WB-0911-BC-DSH-10	250	255	252.5	1.37	0.06						
WB-0911-BC-DSH-10	270	275	272.5	0.85	0.05						
WB-0911-BC-DSH-10	310	315	312.5	1.28	0.06						

Table G.10. SLRad data of $^{234}Th_{Tot}$, $^{234}Th_{xs}$, and D.C. $^{234}Th_{xs}$ for core site WB-0911-MC-PCB-06. Sediment cores with sub-sample intervals (mm), and SLRad data for $^{234}Th_{Tot}$, Re-analysis of ^{234}Th as indicator of $^{234}Th_{Sup}$, $^{234}Th_{xs}$, and D.C. $^{234}Th_{xs}$ (Decay Corrected). Note: Blank cell denotes no analysis performed.

Core ID	Top Depth of Interval (mm)	Bottom Depth of Interval (mm)	Average Depth of Interval (mm)	$^{234}Th_{Tot}$ Activity (dpm/g)	$^{234}Th_{Tot}$ Activity error (dpm/g)	Re-Analysis; ^{234}Th Activity (dpmg/)	Re-Analysis; ^{234}Th error Activity (dpmg/)	$^{234}Th_{xs}$ Activity (dpm/g)	$^{234}Th_{xs}$ Activity error (dpm/g)	D.C. $^{234}Th_{xs}$ Activity (dpm/g)	D.C. $^{234}Th_{xs}$ Activity error (dpm/g)
WB-0911-MC-PCB-06	0	2	1	2.07	0.12			0.35	0.14	1.21	0.48
WB-0911-MC-PCB-06	2	4	3	1.90	0.12			0.18	0.14	1.25	1.00
WB-0911-MC-PCB-06	4	6	5	1.72	0.09			0.00	0.12	0.00	0.00
WB-0911-MC-PCB-06	6	8	7	1.76	0.09						
WB-0911-MC-PCB-06	8	10	9	1.80	0.09						
WB-0911-MC-PCB-06	10	12	11	1.50	0.08						
WB-0911-MC-PCB-06	12	14	13	1.56	0.08						
WB-0911-MC-PCB-06	14	16	15	1.13	0.07						
WB-0911-MC-PCB-06	16	18	17	1.16	0.07						
WB-0911-MC-PCB-06	18	20	19	1.01	0.06						
WB-0911-MC-PCB-06	24	26	25	0.80	0.06						
WB-0911-MC-PCB-06	32	34	33	1.01	0.06						
WB-0911-MC-PCB-06	48	50	49	1.01	0.06						
WB-0911-MC-PCB-06	70	75	72.5	0.82	0.05						
WB-0911-MC-PCB-06	90	95	92.5	1.17	0.05						
WB-0911-MC-PCB-06	110	115	112.5	0.98	0.05						
WB-0911-MC-PCB-06	130	135	132.5	1.46	0.06						
WB-0911-MC-PCB-06	150	155	152.5	1.47	0.06						
WB-0911-MC-PCB-06	170	175	172.5	1.54	0.06						
WB-0911-MC-PCB-06	200	205	202.5	1.47	0.06						
WB-0911-MC-PCB-06	210	215	212.5	1.47	0.06						
WB-0911-MC-PCB-06	220	225	222.5	1.51	0.06						

Table G.11. SLRad data of $^{234}Th_{Tot}$, $^{234}Th_{xs}$, and D.C. $^{234}Th_{xs}$ for core site WB-0812-MC-DSH-08. Sediment cores with sub-sample intervals (mm), and SLRad data for $^{234}Th_{Tot}$, Re-analysis of ^{234}Th as indicator of $^{234}Th_{Sup}$, $^{234}Th_{xs}$, and D.C. $^{234}Th_{xs}$ (Decay Corrected). Note: Blank cell denotes no analysis performed.

Core ID	Top Depth of Interval (mm)	Bottom Depth of Interval (mm)	Average Depth of Interval (mm)	$^{234}Th_{Tot}$ Activity (dpm/g)	$^{234}Th_{Tot}$ Activity error (dpm/g)	Re-Analysis; ^{234}Th Activity (dpmg/)	Re-Analysis; ^{234}Th error Activity (dpmg/)	$^{234}Th_{xs}$ Activity (dpm/g)	$^{234}Th_{xs}$ Activity error (dpm/g)	D.C. $^{234}Th_{xs}$ Activity (dpm/g)	D.C. $^{234}Th_{xs}$ Activity error (dpm/g)
WB-0812-MC-DSH-08	0	2	1	3.46	0.07			1.11	0.11	3.04	0.29
WB-0812-MC-DSH-08	2	4	3	3.22	0.07			0.87	0.10	2.69	0.32
WB-0812-MC-DSH-08	4	6	5	2.49	0.06			0.14	0.10	0.47	0.33
WB-0812-MC-DSH-08	6	8	7	2.35	0.06			0.00	0.10	0.00	0.00
WB-0812-MC-DSH-08	8	10	9	2.23	0.06						
WB-0812-MC-DSH-08	10	12	11	2.11	0.05						
WB-0812-MC-DSH-08	12	14	13	2.04	0.05						
WB-0812-MC-DSH-08	14	16	15	2.06	0.05						
WB-0812-MC-DSH-08	16	18	17	2.13	0.05						
WB-0812-MC-DSH-08	18	20	19	1.96	0.05						
WB-0812-MC-DSH-08	30	32	31	2.14	0.05						
WB-0812-MC-DSH-08	50	55	52.5	5.10	0.08						
WB-0812-MC-DSH-08	70	75	72.5	2.36	0.06						
WB-0812-MC-DSH-08	90	95	92.5	2.40	0.06						
WB-0812-MC-DSH-08	110	115	112.5	2.42	0.06						
WB-0812-MC-DSH-08	130	135	132.5	2.47	0.08						
WB-0812-MC-DSH-08	150	155	152.5	1.22	0.04						
WB-0812-MC-DSH-08	170	175	172.5	2.71	0.06						
WB-0812-MC-DSH-08	190	195	192.5	2.45	0.08						
WB-0812-MC-DSH-08	210	215	212.5	2.29	0.07						
WB-0812-MC-DSH-08	230	235	232.5	2.36	0.08						
WB-0812-MC-DSH-08	265	270	267.5	2.49	0.08						
WB-0812-MC-DSH-08	285	290	287.5	2.44	0.21						

Table G.12. SLRad data of $^{234}Th_{Tot}$, $^{234}Th_{xs}$, and D.C. $^{234}Th_{xs}$ for core site WB-0812-MC-DSH-10. Sediment cores with sub-sample intervals (mm), and SLRad data for $^{234}Th_{Tot}$, Re-analysis of ^{234}Th as indicator of $^{234}Th_{Sup}$, $^{234}Th_{xs}$, and D.C. $^{234}Th_{xs}$ (Decay Corrected). Note: Blank cell denotes no analysis performed.

Core ID	Top Depth of Interval (mm)	Bottom Depth of Interval (mm)	Average Depth of Interval (mm)	$^{234}Th_{Tot}$ Activity (dpm/g)	$^{234}Th_{Tot}$ Activity error (dpm/g)	Re-Analysis; ^{234}Th Activity (dpmg/)	Re-Analysis; ^{234}Th error Activity (dpmg/)	$^{234}Th_{xs}$ Activity (dpm/g)	$^{234}Th_{xs}$ Activity error (dpm/g)	D.C. $^{234}Th_{xs}$ Activity (dpm/g)	D.C. $^{234}Th_{xs}$ Activity error (dpm/g)
WB-0812-MC-DSH-10	0	2	1	3.24	0.11			2.24	0.14	4.61	0.28
WB-0812-MC-DSH-10	2	4	3	1.32	0.07			0.32	0.11	0.75	0.25
WB-0812-MC-DSH-10	4	6	5	0.54	0.04			0.00	0.09	0.00	0.00
WB-0812-MC-DSH-10	6	8	7	1.32	0.07						
WB-0812-MC-DSH-10	8	10	9	0.99	0.06						
WB-0812-MC-DSH-10	10	12	11	1.12	0.07						
WB-0812-MC-DSH-10	12	14	13	0.84	0.05						
WB-0812-MC-DSH-10	14	16	15	1.20	0.07						
WB-0812-MC-DSH-10	16	18	17	0.81	0.05						
WB-0812-MC-DSH-10	18	20	19	0.65	0.05						
WB-0812-MC-DSH-10	20	22	21	1.28	0.07						
WB-0812-MC-DSH-10	22	24	23	1.15	0.06						
WB-0812-MC-DSH-10	24	26	25	1.00	0.06						
WB-0812-MC-DSH-10	26	28	27	1.09	0.06						
WB-0812-MC-DSH-10	28	30	29	0.85	0.06						
WB-0812-MC-DSH-10	30	35	32.5	1.25	0.06						
WB-0812-MC-DSH-10	35	40	37.5	1.20	0.06						
WB-0812-MC-DSH-10	40	45	42.5	1.07	0.05						
WB-0812-MC-DSH-10	45	50	47.5	1.09	0.05						
WB-0812-MC-DSH-10	50	55	52.5	1.38	0.06						
WB-0812-MC-DSH-10	55	60	57.5	1.22	0.06						
WB-0812-MC-DSH-10	70	75	72.5	0.98	0.05						
WB-0812-MC-DSH-10	80	85	82.5	1.22	0.05						
WB-0812-MC-DSH-10	90	95	92.5	1.16	0.05						

Table G.12 (Continued).

Core ID	Top Depth of Interval (mm)	Bottom Depth of Interval (mm)	Average Depth of Interval (mm)	$^{234}Th_{Tot}$ Activity (dpm/g)	$^{234}Th_{Tot}$ Activity error (dpm/g)	Re-Analysis; ^{234}Th Activity (dpmg/)	Re-Analysis; ^{234}Th error Activity (dpmg/)	$^{234}Th_{xs}$ Activity (dpm/g)	$^{234}Th_{xs}$ Activity error (dpm/g)	D.C. $^{234}Th_{xs}$ Activity (dpm/g)	D.C. $^{234}Th_{xs}$ Activity error (dpm/g)
WB-0812-MC-DSH-10	100	105	102.5	1.20	0.05						
WB-0812-MC-DSH-10	110	115	112.5	1.51	0.06						
WB-0812-MC-DSH-10	130	135	132.5	1.15	0.06						
WB-0812-MC-DSH-10	150	155	152.5	1.46	0.06						
WB-0812-MC-DSH-10	170	175	172.5	1.07	0.06						
WB-0812-MC-DSH-10	190	195	192.5	1.40	0.06						
WB-0812-MC-DSH-10	210	215	212.5	1.43	0.10						
WB-0812-MC-DSH-10	230	235	232.5	1.57	0.06						
WB-0812-MC-DSH-10	250	255	252.5	0.90	0.08						
WB-0812-MC-DSH-10	270	275	272.5	1.03	0.05						
WB-0812-MC-DSH-10	310	315	312.5	1.29	0.06						

Table G.13. SLRad data of $^{234}Th_{Tot}$, $^{234}Th_{xs}$, and D.C. $^{234}Th_{xs}$ for core site WB-0812-MC-PCB-06. Sediment cores with sub-sample intervals (mm), and SLRad data for $^{234}Th_{Tot}$, Re-analysis of ^{234}Th as indicator of $^{234}Th_{Sup}$, $^{234}Th_{xs}$, and D.C. $^{234}Th_{xs}$ (Decay Corrected). Note: Blank cell denotes no analysis performed.

Core ID	Top Depth of Interval (mm)	Bottom Depth of Interval (mm)	Average Depth of Interval (mm)	$^{234}Th_{Tot}$ Activity (dpm/g)	$^{234}Th_{Tot}$ Activity error (dpm/g)	Re-Analysis; ^{234}Th Activity (dpmg/)	Re-Analysis; ^{234}Th error Activity (dpmg/)	$^{234}Th_{xs}$ Activity (dpm/g)	$^{234}Th_{xs}$ Activity error (dpm/g)	D.C. $^{234}Th_{xs}$ Activity (dpm/g)	D.C. $^{234}Th_{xs}$ Activity error (dpm/g)
WB-0812-MC-PCB-06	0	2	1	2.15	0.09			1.07	0.12	3.49	0.40
WB-0812-MC-PCB-06	2	4	3	1.68	0.08			0.60	0.11	2.07	0.39
WB-0812-MC-PCB-06	4	6	5	1.08	0.07			0.00	0.10	0.00	0.00
WB-0812-MC-PCB-06	6	8	7	1.20	0.06						
WB-0812-MC-PCB-06	8	10	9	1.03	0.06						
WB-0812-MC-PCB-06	10	12	11	1.09	0.06						
WB-0812-MC-PCB-06	12	14	13	1.01	0.06						
WB-0812-MC-PCB-06	14	16	15	0.85	0.05						
WB-0812-MC-PCB-06	16	18	17	0.94	0.06						
WB-0812-MC-PCB-06	18	20	19	1.01	0.06						
WB-0812-MC-PCB-06	24	26	25	1.19	0.07						
WB-0812-MC-PCB-06	30	32	31	1.25	0.07						
WB-0812-MC-PCB-06	50	55	52.5	0.94	0.05						
WB-0812-MC-PCB-06	70	75	72.5	1.01	0.05						
WB-0812-MC-PCB-06	90	95	92.5	0.95	0.05						
WB-0812-MC-PCB-06	110	115	112.5	1.12	0.05						
WB-0812-MC-PCB-06	130	135	132.5	1.40	0.06						
WB-0812-MC-PCB-06	150	155	152.5	1.48	0.06						
WB-0812-MC-PCB-06	170	175	172.5	1.43	0.06						
WB-0812-MC-PCB-06	190	195	192.5	1.39	0.06						
WB-0812-MC-PCB-06	210	215	212.5	1.47	0.06						
WB-0812-MC-PCB-06	230	235	232.5	1.71	0.06						

Table G.14. SLRad data of $^{234}Th_{Tot}$, $^{234}Th_{xs}$, and D.C. $^{234}Th_{xs}$ for core site WB-1012-MC-04. Sediment cores with sub-sample intervals (mm), and SLRad data for $^{234}Th_{Tot}$, Re-analysis of ^{234}Th as indicator of $^{234}Th_{Sup}$, $^{234}Th_{xs}$, and D.C. $^{234}Th_{xs}$ (Decay Corrected). Note: Blank cell denotes no analysis performed.

Core ID	Top Depth of Interval (mm)	Bottom Depth of Interval (mm)	Average Depth of Interval (mm)	$^{234}Th_{Tot}$ Activity (dpm/g)	$^{234}Th_{Tot}$ Activity error (dpm/g)	Re-Analysis; ^{234}Th Activity (dpmg/)	Re-Analysis; ^{234}Th error Activity (dpmg/)	$^{234}Th_{xs}$ Activity (dpm/g)	$^{234}Th_{xs}$ Activity error (dpm/g)	D.C. $^{234}Th_{xs}$ Activity (dpm/g)	D.C. $^{234}Th_{xs}$ Activity error (dpm/g)
WB-1012-MC-04	0	2	1	6.11	0.18			3.13	0.16	7.65	0.39
WB-1012-MC-04	2	4	3	2.13	0.11			0.10	0.11	0.38	0.45
WB-1012-MC-04	4	6	5	2.17	0.11			0.00	0.11	0.00	0.00
WB-1012-MC-04	6	8	7	2.01	0.10						
WB-1012-MC-04	8	10	9	1.61	0.09						
WB-1012-MC-04	10	12	11	0.91	0.07						
WB-1012-MC-04	12	14	13	1.51	0.09						
WB-1012-MC-04	14	16	15	1.59	0.09						
WB-1012-MC-04	16	18	17	1.63	0.09						
WB-1012-MC-04	18	20	19	1.40	0.08						
WB-1012-MC-04	30	35	32.5	1.54	0.08						
WB-1012-MC-04	50	55	52.5	1.60	0.07						
WB-1012-MC-04	70	75	72.5	1.80	0.08						
WB-1012-MC-04	90	95	92.5	1.69	0.08						
WB-1012-MC-04	130	135	132.5	1.64	0.08						
WB-1012-MC-04	170	175	172.5	1.83	0.08						
WB-1012-MC-04	210	215	212.5	2.17	0.09						
WB-1012-MC-04	250	255	252.5	2.57	0.09						
WB-1012-MC-04	290	295	292.5	3.14	0.10						

Table G.15. SLRad data of $^{234}Th_{Tot}$, $^{234}Th_{xs}$, and D.C. $^{234}Th_{xs}$ for core site WB-0813-MC-04. Sediment cores with sub-sample intervals (mm), and SLRad data for $^{234}Th_{Tot}$, Re-analysis of ^{234}Th as indicator of $^{234}Th_{Sup}$, $^{234}Th_{xs}$, and D.C. $^{234}Th_{xs}$ (Decay Corrected). Note: Blank cell denotes no analysis performed.

Core ID	Top Depth of Interval (mm)	Bottom Depth of Interval (mm)	Average Depth of Interval (mm)	$^{234}Th_{Tot}$ Activity (dpm/g)	$^{234}Th_{Tot}$ Activity error (dpm/g)	Re-Analysis; ^{234}Th Activity (dpmg/)	Re-Analysis; ^{234}Th error Activity (dpmg/)	$^{234}Th_{xs}$ Activity (dpm/g)	$^{234}Th_{xs}$ Activity error (dpm/g)	D.C. $^{234}Th_{xs}$ Activity (dpm/g)	D.C. $^{234}Th_{xs}$ Activity error (dpm/g)
WB-0813-MC-04	0	2	1	3.37	0.15			1.19	0.14	2.91	0.35
WB-0813-MC-04	2	4	3	1.74	0.10			0.06	0.11	0.22	0.43
WB-0813-MC-04	4	6	5	2.44	0.11			0.00	0.00	0.00	0.00
WB-0813-MC-04	6	8	7	1.98	0.10						
WB-0813-MC-04	8	10	9	2.54	0.11						
WB-0813-MC-04	10	14	12	1.81	0.08						
WB-0813-MC-04	14	16	15	1.80	0.09						
WB-0813-MC-04	16	18	17	1.74	0.09						

Table G.16. SLRad data of $^{234}Th_{Tot}$, $^{234}Th_{xs}$, and D.C. $^{234}Th_{xs}$ for core site WB-0813-MC-DSH-08. Sediment cores with sub-sample intervals (mm), and SLRad data for $^{234}Th_{Tot}$, Re-analysis of ^{234}Th as indicator of $^{234}Th_{Sup}$, $^{234}Th_{xs}$, and D.C. $^{234}Th_{xs}$ (Decay Corrected). Note: Blank cell denotes no analysis performed.

Core ID	Top Depth of Interval (mm)	Bottom Depth of Interval (mm)	Average Depth of Interval (mm)	$^{234}Th_{Tot}$ Activity (dpm/g)	$^{234}Th_{Tot}$ Activity error (dpm/g)	Re-Analysis; ^{234}Th Activity (dpmg/)	Re-Analysis; ^{234}Th error Activity (dpmg/)	$^{234}Th_{xs}$ Activity (dpm/g)	$^{234}Th_{xs}$ Activity error (dpm/g)	D.C. $^{234}Th_{xs}$ Activity (dpm/g)	D.C. $^{234}Th_{xs}$ Activity error (dpm/g)
WB-0813-MC-DSH-08	0	2	1	2.94	0.11			1.49	0.14	3.85	0.35
WB-0813-MC-DSH-08	2	4	3	2.75	0.10			1.30	0.13	4.00	0.39
WB-0813-MC-DSH-08	4	6	5	2.43	0.10			1.03	0.12	2.83	0.34
WB-0813-MC-DSH-08	6	8	7	1.89	0.08			0.49	0.11	1.60	0.37
WB-0813-MC-DSH-08	8	10	9	1.62	0.07			0.22	0.11	0.63	0.32
WB-0813-MC-DSH-08	10	12	11	1.29	0.07			0.00	0.00	0.00	0.00
WB-0813-MC-DSH-08	12	14	13	1.45	0.07						
WB-0813-MC-DSH-08	14	16	15	1.24	0.07						
WB-0813-MC-DSH-08	16	18	17	1.18	0.06						
WB-0813-MC-DSH-08	18	20	19	1.35	0.07						

Table G.17. SLRad data of $^{234}Th_{Tot}$, $^{234}Th_{xs}$, and D.C. $^{234}Th_{xs}$ for core site WB-0813-MC-DSH-10. Sediment cores with sub-sample intervals (mm), and SLRad data for $^{234}Th_{Tot}$, Re-analysis of ^{234}Th as indicator of $^{234}Th_{Sup}$, $^{234}Th_{xs}$, and D.C. $^{234}Th_{xs}$ (Decay Corrected). Note: Blank cell denotes no analysis performed.

Core ID	Top Depth of Interval (mm)	Bottom Depth of Interval (mm)	Average Depth of Interval (mm)	$^{234}Th_{Tot}$ Activity (dpm/g)	$^{234}Th_{Tot}$ Activity error (dpm/g)	Re-Analysis; ^{234}Th Activity (dpmg/)	Re-Analysis; ^{234}Th error Activity (dpmg/)	$^{234}Th_{xs}$ Activity (dpm/g)	$^{234}Th_{xs}$ Activity error (dpm/g)	D.C. $^{234}Th_{xs}$ Activity (dpm/g)	D.C. $^{234}Th_{xs}$ Activity error (dpm/g)
WB-0813-MC-DSH-10	0	2	1	3.29	0.11			2.29	0.13	5.60	0.33
WB-0813-MC-DSH-10	2	4	3	1.82	0.08			0.82	0.11	2.38	0.33
WB-0813-MC-DSH-10	4	6	5	1.29	0.07			0.00	0.00	0.00	0.00
WB-0813-MC-DSH-10	6	8	7	1.28	0.07						
WB-0813-MC-DSH-10	8	10	9	1.25	0.07						
WB-0813-MC-DSH-10	10	12	11	1.11	0.06						
WB-0813-MC-DSH-10	12	14	13	1.37	0.07						
WB-0813-MC-DSH-10	14	16	15	1.11	0.06						
WB-0813-MC-DSH-10	16	18	17	1.26	0.07						
WB-0813-MC-DSH-10	18	20	19	1.22	0.06						
WB-0813-MC-DSH-10	20	22	21	1.00	0.05						

Table G.18. SLRad data of $^{234}Th_{Tot}$, $^{234}Th_{xs}$, and D.C. $^{234}Th_{xs}$ for core site WB-0813-MC-PCB-06. Sediment cores with sub-sample intervals (mm), and SLRad data for $^{234}Th_{Tot}$, Re-analysis of ^{234}Th as indicator of $^{234}Th_{Sup}$, $^{234}Th_{xs}$, and D.C. $^{234}Th_{xs}$ (Decay Corrected). Note: Blank cell denotes no analysis performed.

Core ID	Top Depth of Interval (mm)	Bottom Depth of Interval (mm)	Average Depth of Interval (mm)	$^{234}Th_{Tot}$ Activity (dpm/g)	$^{234}Th_{Tot}$ Activity error (dpm/g)	Re-Analysis; ^{234}Th Activity (dpmg/)	Re-Analysis; ^{234}Th error Activity (dpmg/)	$^{234}Th_{xs}$ Activity (dpm/g)	$^{234}Th_{xs}$ Activity error (dpm/g)	D.C. $^{234}Th_{xs}$ Activity (dpm/g)	D.C. $^{234}Th_{xs}$ Activity error (dpm/g)
WB-0813-MC-PCB-06	0	4	2	2.49	0.09			1.26	0.12	4.48	0.42
WB-0813-MC-PCB-06	4	6	5	1.45	0.07			0.22	0.11	0.84	0.41
WB-0813-MC-PCB-06	6	8	7	1.23	0.07			0.00	0.10	0.00	0.00
WB-0813-MC-PCB-06	8	10	9	1.31	0.07						
WB-0813-MC-PCB-06	10	12	11	1.29	0.07						
WB-0813-MC-PCB-06	12	14	13	1.24	0.07						
WB-0813-MC-PCB-06	14	16	15	1.12	0.06						
WB-0813-MC-PCB-06	16	18	17	1.12	0.06						
WB-0813-MC-PCB-06	20	22	21	1.27	0.06						

Table G.19. SLRad data of $^{234}Th_{Tot}$, $^{234}Th_{xs}$, and D.C. $^{234}Th_{xs}$ for core site WB-0814-MC-04. Sediment cores with sub-sample intervals (mm), and SLRad data for $^{234}Th_{Tot}$, Re-analysis of ^{234}Th as indicator of $^{234}Th_{Sup}$, $^{234}Th_{xs}$, and D.C. $^{234}Th_{xs}$ (Decay Corrected). Note: Blank cell denotes no analysis performed.

Core ID	Top Depth of Interval (mm)	Bottom Depth of Interval (mm)	Average Depth of Interval (mm)	$^{234}Th_{Tot}$ Activity (dpm/g)	$^{234}Th_{Tot}$ Activity error (dpm/g)	Re-Analysis; ^{234}Th Activity (dpmg/)	Re-Analysis; ^{234}Th error Activity (dpmg/)	$^{234}Th_{xs}$ Activity (dpm/g)	$^{234}Th_{xs}$ Activity error (dpm/g)	D.C. $^{234}Th_{xs}$ Activity (dpm/g)	D.C. $^{234}Th_{xs}$ Activity error (dpm/g)
WB-0814-MC-04	0	2	1	2.30	0.10			0.89	0.13	3.17	0.55
WB-0814-MC-04	2	4	3	1.54	0.09			0.13	0.12	0.55	0.60
WB-0814-MC-04	4	6	5	1.58	0.08			0.00	0.00	0.00	0.00
WB-0814-MC-04	6	8	7	1.41	0.08						
WB-0814-MC-04	8	10	9	1.09	0.07						
WB-0814-MC-04	10	12	11	1.00	0.06						
WB-0814-MC-04	12	14	13	1.41	0.07						
WB-0814-MC-04	14	16	15	1.26	0.07						
WB-0814-MC-04	16	18	17	0.73	0.05						
WB-0814-MC-04	18	20	19	0.83	0.05						
WB-0814-MC-04	20	22	21	0.98	0.06						
WB-0814-MC-04	24	26	25	0.87	0.05						
WB-0814-MC-04	30	32	31	0.90	0.06						
WB-0814-MC-04	36	38	37	1.06	0.06						
WB-0814-MC-04	50	55	52.5	0.82	0.05						
WB-0814-MC-04	70	75	72.5	0.71	0.04						
WB-0814-MC-04	90	95	92.5	1.28	0.06						
WB-0814-MC-04	110	115	112.5	1.00	0.05						
WB-0814-MC-04	130	135	132.5	1.01	0.05						
WB-0814-MC-04	150	155	152.5	1.14	0.05						
WB-0814-MC-04	170	175	172.5	2.13	0.07						
WB-0814-MC-04	190	195	192.5	2.05	0.07						
WB-0814-MC-04	210	215	212.5	1.99	0.07						
WB-0814-MC-04	230	235	232.5	1.64	0.06						

Table G.19 (Continued).

Core ID	Top Depth of Interval (mm)	Bottom Depth of Interval (mm)	Average Depth of Interval (mm)	$^{234}Th_{Tot}$ Activity (dpm/g)	$^{234}Th_{Tot}$ Activity error (dpm/g)	Re-Analysis; ^{234}Th Activity (dpmg/)	Re-Analysis; ^{234}Th error Activity (dpmg/)	$^{234}Th_{xs}$ Activity (dpm/g)	$^{234}Th_{xs}$ Activity error (dpm/g)	D.C. $^{234}Th_{xs}$ Activity (dpm/g)	D.C. $^{234}Th_{xs}$ Activity error (dpm/g)
WB-0814-MC-04	250	255	252.5	2.29	0.07						

Table G.20. SLRad data of $^{234}Th_{Tot}$, $^{234}Th_{xs}$, and D.C. $^{234}Th_{xs}$ for core site WB-0814-MC-DSH-08 DEP 1. Sediment cores with sub-sample intervals (mm), and SLRad data for $^{234}Th_{Tot}$, Re-analysis of ^{234}Th as indicator of $^{234}Th_{Sup}$, $^{234}Th_{xs}$, and D.C. $^{234}Th_{xs}$ (Decay Corrected). Note: Blank cell denotes no analysis performed.

Core ID	Top Depth of Interval (mm)	Bottom Depth of Interval (mm)	Average Depth of Interval (mm)	$^{234}Th_{Tot}$ Activity (dpm/g)	$^{234}Th_{Tot}$ Activity error (dpm/g)	Re-Analysis; ^{234}Th Activity (dpmg/)	Re-Analysis; ^{234}Th error Activity (dpmg/)	$^{234}Th_{xs}$ Activity (dpm/g)	$^{234}Th_{xs}$ Activity error (dpm/g)	D.C. $^{234}Th_{xs}$ Activity (dpm/g)	D.C. $^{234}Th_{xs}$ Activity error (dpm/g)
WB-0814-MC-DSH-08 DEP 1	0	2	1	2.97	0.10			1.32	0.13	2.70	0.26
WB-0814-MC-DSH-08 DEP 1	2	4	3	2.39	0.09			0.74	0.12	1.92	0.32
WB-0814-MC-DSH-08 DEP 1	4	6	5	2.64	0.10			0.99	0.13	2.16	0.28
WB-0814-MC-DSH-08 DEP 1	6	8	7	2.22	0.09			0.57	0.12	1.55	0.32
WB-0814-MC-DSH-08 DEP 1	8	10	9	1.67	0.08			0.00	0.11	0.00	0.00
WB-0814-MC-DSH-08 DEP 1	10	12	11	1.69	0.08						
WB-0814-MC-DSH-08 DEP 1	12	14	13	1.52	0.07						
WB-0814-MC-DSH-08 DEP 1	14	16	15	1.33	0.07						
WB-0814-MC-DSH-08 DEP 1	16	18	17	1.52	0.07						
WB-0814-MC-DSH-08 DEP 1	18	20	19	1.15	0.06						
WB-0814-MC-DSH-08 DEP 1	20	22	21	1.28	0.07						
WB-0814-MC-DSH-08 DEP 1	24	26	25	1.12	0.06						
WB-0814-MC-DSH-08 DEP 1	30	32	31	1.20	0.06						
WB-0814-MC-DSH-08 DEP 1	40	45	42.5	1.69	0.07						
WB-0814-MC-DSH-08 DEP 1	50	55	52.5	1.92	0.07						
WB-0814-MC-DSH-08 DEP 1	70	75	72.5	2.29	0.08						
WB-0814-MC-DSH-08 DEP 1	90	95	92.5	2.19	0.07						
WB-0814-MC-DSH-08 DEP 1	110	115	112.5	1.99	0.07						
WB-0814-MC-DSH-08 DEP 1	130	135	132.5	1.97	0.07						
WB-0814-MC-DSH-08 DEP 1	150	155	152.5	1.78	0.07						
WB-0814-MC-DSH-08 DEP 1	170	175	172.5	1.79	0.07						
WB-0814-MC-DSH-08 DEP 1	190	195	192.5	1.75	0.07						
WB-0814-MC-DSH-08 DEP 1	210	215	212.5	1.87	0.07						
WB-0814-MC-DSH-08 DEP 1	230	235	232.5	2.14	0.08						

Table G.20 (Continued).

Core ID	Top Depth of Interval (mm)	Bottom Depth of Interval (mm)	Average Depth of Interval (mm)	$^{234}Th_{Tot}$ Activity (dpm/g)	$^{234}Th_{Tot}$ Activity error (dpm/g)	Re-Analysis; ^{234}Th Activity (dpmg/)	Re-Analysis; ^{234}Th error Activity (dpmg/)	$^{234}Th_{xs}$ Activity (dpm/g)	$^{234}Th_{xs}$ Activity error (dpm/g)	D.C. $^{234}Th_{xs}$ Activity (dpm/g)	D.C. $^{234}Th_{xs}$ Activity error (dpm/g)
WB-0814-MC-DSH-08 DEP 1	250	255	252.5	1.99	0.07						
WB-0814-MC-DSH-08 DEP 1	270	275	272.5	1.88	0.07						
WB-0814-MC-DSH-08 DEP 1	290	295	292.5	1.76	0.07						

Table G.21. SLRad data of $^{234}Th_{Tot}$, $^{234}Th_{xs}$, and D.C. $^{234}Th_{xs}$ for core site WB-0814-MC-DSH-10 DEP 1. Sediment cores with sub-sample intervals (mm), and SLRad data for $^{234}Th_{Tot}$, Re-analysis of ^{234}Th as indicator of $^{234}Th_{Sup}$, $^{234}Th_{xs}$, and D.C. $^{234}Th_{xs}$ (Decay Corrected). Note: Blank cell denotes no analysis performed.

Core ID	Top Depth of Interval (mm)	Bottom Depth of Interval (mm)	Average Depth of Interval (mm)	$^{234}Th_{Tot}$ Activity (dpm/g)	$^{234}Th_{Tot}$ Activity error (dpm/g)	Re-Analysis; ^{234}Th Activity (dpmg/)	Re-Analysis; ^{234}Th error Activity (dpmg/)	$^{234}Th_{xs}$ Activity (dpm/g)	$^{234}Th_{xs}$ Activity error (dpm/g)	D.C. $^{234}Th_{xs}$ Activity (dpm/g)	D.C. $^{234}Th_{xs}$ Activity error (dpm/g)
WB-0814-MC-DSH-10 DEP 1	0	2	1	2.24	0.11			1.24	0.14	2.35	0.26
WB-0814-MC-DSH-10 DEP 1	2	4	3	1.58	0.09			0.58	0.12	1.27	0.26
WB-0814-MC-DSH-10 DEP 1	4	6	5	1.09	0.07			0.00	0.11	0.00	0.00
WB-0814-MC-DSH-10 DEP 1	6	8	7	1.32	0.07						
WB-0814-MC-DSH-10 DEP 1	8	10	9	1.00	0.06						
WB-0814-MC-DSH-10 DEP 1	10	12	11	1.00	0.06						
WB-0814-MC-DSH-10 DEP 1	12	14	13	1.15	0.07						
WB-0814-MC-DSH-10 DEP 1	14	16	15	0.99	0.06						
WB-0814-MC-DSH-10 DEP 1	16	18	17	1.21	0.07						
WB-0814-MC-DSH-10 DEP 1	18	20	19	1.01	0.06						
WB-0814-MC-DSH-10 DEP 1	20	22	21	1.25	0.07						
WB-0814-MC-DSH-10 DEP 1	24	26	25	1.10	0.06						
WB-0814-MC-DSH-10 DEP 1	30	32	31	1.30	0.07						
WB-0814-MC-DSH-10 DEP 1	53	58	55.5	1.41	0.06						
WB-0814-MC-DSH-10 DEP 1	73	78	75.5	1.00	0.05						
WB-0814-MC-DSH-10 DEP 1	93	98	95.5	1.26	0.06						
WB-0814-MC-DSH-10 DEP 1	113	118	115.5	1.24	0.06						
WB-0814-MC-DSH-10 DEP 1	133	138	135.5	1.57	0.06						
WB-0814-MC-DSH-10 DEP 1	154	159	156.5	1.00	0.05						
WB-0814-MC-DSH-10 DEP 1	174	179	176.5	0.93	0.05						
WB-0814-MC-DSH-10 DEP 1	194	199	196.5	1.00	0.05						
WB-0814-MC-DSH-10 DEP 1	214	219	216.5	1.27	0.06						
WB-0814-MC-DSH-10 DEP 1	234	239	236.5	1.17	0.05						
WB-0814-MC-DSH-10 DEP 1	254	259	256.5	1.05	0.05						

Table G.21 (Continued).

Core ID	Top Depth of Interval (mm)	Bottom Depth of Interval (mm)	Average Depth of Interval (mm)	$^{234}Th_{Tot}$ Activity (dpm/g)	$^{234}Th_{Tot}$ Activity error (dpm/g)	Re-Analysis; ^{234}Th Activity (dpmg/)	Re-Analysis; ^{234}Th error Activity (dpmg/)	$^{234}Th_{xs}$ Activity (dpm/g)	$^{234}Th_{xs}$ Activity error (dpm/g)	D.C. $^{234}Th_{xs}$ Activity (dpm/g)	D.C. $^{234}Th_{xs}$ Activity error (dpm/g)
WB-0814-MC-DSH-10 DEP 1	274	279	276.5	1.11	0.05						
WB-0814-MC-DSH-10 DEP 1	294	299	296.5	1.48	0.06						
WB-0814-MC-DSH-10 DEP 1	314	319	316.5	1.17	0.05						

Table G.22. SLRad data of $^{234}Th_{Tot}$, $^{234}Th_{xs}$, and D.C. $^{234}Th_{xs}$ for core site WB-0814-MC-PCB-06 DEP 2. Sediment cores with sub-sample intervals (mm), and SLRad data for $^{234}Th_{Tot}$, Re-analysis of ^{234}Th as indicator of $^{234}Th_{Sup}$, $^{234}Th_{xs}$, and D.C. $^{234}Th_{xs}$ (Decay Corrected). Note: Blank cell denotes no analysis performed.

Core ID	Top Depth of Interval (mm)	Bottom Depth of Interval (mm)	Average Depth of Interval (mm)	$^{234}Th_{Tot}$ Activity (dpm/g)	$^{234}Th_{Tot}$ Activity error (dpm/g)	Re-Analysis; ^{234}Th Activity (dpmg/)	Re-Analysis; ^{234}Th error Activity (dpmg/)	$^{234}Th_{xs}$ Activity (dpm/g)	$^{234}Th_{xs}$ Activity error (dpm/g)	D.C. $^{234}Th_{xs}$ Activity (dpm/g)	D.C. $^{234}Th_{xs}$ Activity error (dpm/g)
WB-0814-MC-PCB-06 DEP 2	0	2	1	2.25	0.09			1.02	0.12	3.95	0.48
WB-0814-MC-PCB-06 DEP 2	2	4	3	2.02	0.09			0.79	0.12	3.44	0.53
WB-0814-MC-PCB-06 DEP 2	4	6	5	1.44	0.08			0.21	0.11	0.86	0.45
WB-0814-MC-PCB-06 DEP 2	6	8	7	1.53	0.08			0.00	0.11	0.00	0.00
WB-0814-MC-PCB-06 DEP 2	8	10	9	1.23	0.07						
WB-0814-MC-PCB-06 DEP 2	10	12	11	1.17	0.07						
WB-0814-MC-PCB-06 DEP 2	12	14	13	1.27	0.07						
WB-0814-MC-PCB-06 DEP 2	14	16	15	1.31	0.07						
WB-0814-MC-PCB-06 DEP 2	16	18	17	1.21	0.06						
WB-0814-MC-PCB-06 DEP 2	18	20	19	1.15	0.06						
WB-0814-MC-PCB-06 DEP 2	20	22	21	1.03	0.06						
WB-0814-MC-PCB-06 DEP 2	24	26	25	1.43	0.07						
WB-0814-MC-PCB-06 DEP 2	30	32	31	1.23	0.06						
WB-0814-MC-PCB-06 DEP 2	40	42	41	1.13	0.06						
WB-0814-MC-PCB-06 DEP 2	50	55	52.5	1.30	0.06						
WB-0814-MC-PCB-06 DEP 2	70	75	72.5	1.42	0.06						
WB-0814-MC-PCB-06 DEP 2	90	95	92.5	1.32	0.06						
WB-0814-MC-PCB-06 DEP 2	110	117	113.5	1.46	0.06						
WB-0814-MC-PCB-06 DEP 2	132	137	134.5	1.62	0.07						
WB-0814-MC-PCB-06 DEP 2	152	157	154.5	1.81	0.07						
WB-0814-MC-PCB-06 DEP 2	172	177	174.5	2.02	0.07						
WB-0814-MC-PCB-06 DEP 2	192	197	194.5	2.66	0.08						
WB-0814-MC-PCB-06 DEP 2	212	217	214.5	2.03	0.07						
WB-0814-MC-PCB-06 DEP 2	232	237	234.5	2.04	0.07						

Table G.22 (Continued).

Core ID	Top Depth of Interval (mm)	Bottom Depth of Interval (mm)	Average Depth of Interval (mm)	$^{234}Th_{Tot}$ Activity (dpm/g)	$^{234}Th_{Tot}$ Activity error (dpm/g)	Re-Analysis; ^{234}Th Activity (dpmg/)	Re-Analysis; ^{234}Th error Activity (dpmg/)	$^{234}Th_{xs}$ Activity (dpm/g)	$^{234}Th_{xs}$ Activity error (dpm/g)	D.C. $^{234}Th_{xs}$ Activity (dpm/g)	D.C. $^{234}Th_{xs}$ Activity error (dpm/g)
WB-0814-MC-PCB-06 DEP 2	252	257	254.5	2.55	0.08						
WB-0814-MC-PCB-06 DEP 2	272	277	274.5	1.93	0.08						
WB-0814-MC-PCB-06 DEP 2	292	297	294.5	1.48	0.07						
WB-0814-MC-PCB-06 DEP 2	292	297	294.5	1.48	0.07						

Table G.23. SLRad data of $^{234}Th_{Tot}$, $^{234}Th_{xs}$, and D.C. $^{234}Th_{xs}$ for core site WB-0815-MC-04. Sediment cores with sub-sample intervals (mm), and SLRad data for $^{234}Th_{Tot}$, Re-analysis of ^{234}Th as indicator of $^{234}Th_{Sup}$, $^{234}Th_{xs}$, and D.C. $^{234}Th_{xs}$ (Decay Corrected). Note: Blank cell denotes no analysis performed.

Core ID	Top Depth of Interval (mm)	Bottom Depth of Interval (mm)	Average Depth of Interval (mm)	$^{234}Th_{Tot}$ Activity (dpm/g)	$^{234}Th_{Tot}$ Activity error (dpm/g)	Re-Analysis; ^{234}Th Activity (dpmg/)	Re-Analysis; ^{234}Th error Activity (dpmg/)	$^{234}Th_{xs}$ Activity (dpm/g)	$^{234}Th_{xs}$ Activity error (dpm/g)	D.C. $^{234}Th_{xs}$ Activity (dpm/g)	D.C. $^{234}Th_{xs}$ Activity error (dpm/g)
WB-0815-MC-04	0	2	1	3.02	0.13			1.62	0.15	3.97	0.37
WB-0815-MC-04	2	4	3	2.53	0.10			1.13	0.13	3.01	0.35
WB-0815-MC-04	4	6	5	2.01	0.09			0.61	0.12	1.66	0.33
WB-0815-MC-04	6	8	7	1.43	0.07			0.03	0.11	0.14	0.53
WB-0815-MC-04	8	10	9	1.40	0.07			0.00	0.00	0.00	0.00
WB-0815-MC-04	10	12	11	0.91	0.06						
WB-0815-MC-04	12	14	13	1.34	0.07						
WB-0815-MC-04	14	16	15	0.97	0.06						
WB-0815-MC-04	16	18	17	1.15	0.06						

Table G.24. SLRad data of $^{234}Th_{Tot}$, $^{234}Th_{xs}$, and D.C. $^{234}Th_{xs}$ for core site WB-0815-MC-DSH-08-A. Sediment cores with sub-sample intervals (mm), and SLRad data for $^{234}Th_{Tot}$, Re-analysis of ^{234}Th as indicator of $^{234}Th_{Sup}$, $^{234}Th_{xs}$, and D.C. $^{234}Th_{xs}$ (Decay Corrected). Note: Blank cell denotes no analysis performed.

Core ID	Top Depth of Interval (mm)	Bottom Depth of Interval (mm)	Average Depth of Interval (mm)	$^{234}Th_{Tot}$ Activity (dpm/g)	$^{234}Th_{Tot}$ Activity error (dpm/g)	Re-Analysis; ^{234}Th Activity (dpmg/)	Re-Analysis; ^{234}Th error Activity (dpmg/)	$^{234}Th_{xs}$ Activity (dpm/g)	$^{234}Th_{xs}$ Activity error (dpm/g)	D.C. $^{234}Th_{xs}$ Activity (dpm/g)	D.C. $^{234}Th_{xs}$ Activity error (dpm/g)
WB-0815-MC-DSH-08-A	0	2	1	2.93	0.11			1.79	0.14	3.89	0.30
WB-0815-MC-DSH-08-A	2	4	3	2.60	0.11			1.46	0.14	3.37	0.31
WB-0815-MC-DSH-08-A	4	6	5	1.94	0.09			0.80	0.12	1.96	0.30
WB-0815-MC-DSH-08-A	6	8	7	1.58	0.08			0.30	0.11	0.91	0.35
WB-0815-MC-DSH-08-A	8	10	9	1.43	0.07			0.00	0.00	0.00	0.00
WB-0815-MC-DSH-08-A	10	12	11	1.65	0.08						
WB-0815-MC-DSH-08-A	12	14	13	1.65	0.08						
WB-0815-MC-DSH-08-A	14	16	15	1.39	0.07						
WB-0815-MC-DSH-08-A	16	18	17	1.53	0.07						
WB-0815-MC-DSH-08-A	18	20	19	1.14	0.07						

Table G.25. SLRad data of $^{234}Th_{Tot}$, $^{234}Th_{xs}$, and D.C. $^{234}Th_{xs}$ for core site WB-0815-MC-DSH-10-A. Sediment cores with sub-sample intervals (mm), and SLRad data for $^{234}Th_{Tot}$, Re-analysis of ^{234}Th as indicator of $^{234}Th_{Sup}$, $^{234}Th_{xs}$, and D.C. $^{234}Th_{xs}$ (Decay Corrected). Note: Blank cell denotes no analysis performed.

Core ID	Top Depth of Interval (mm)	Bottom Depth of Interval (mm)	Average Depth of Interval (mm)	$^{234}Th_{Tot}$ Activity (dpm/g)	$^{234}Th_{Tot}$ Activity error (dpm/g)	Re-Analysis; ^{234}Th Activity (dpmg/)	Re-Analysis; ^{234}Th error Activity (dpmg/)	$^{234}Th_{xs}$ Activity (dpm/g)	$^{234}Th_{xs}$ Activity error (dpm/g)	D.C. $^{234}Th_{xs}$ Activity (dpm/g)	D.C. $^{234}Th_{xs}$ Activity error (dpm/g)
WB-0815-MC-DSH-10-A	0	2	1	3.62	0.14			2.20	0.16	7.37	0.53
WB-0815-MC-DSH-10-A	2	4	3	1.85	0.09			0.43	0.12	1.52	0.42
WB-0815-MC-DSH-10-A	4	6	5	1.42	0.07			0.00	0.00	0.00	0.00
WB-0815-MC-DSH-10-A	6	8	7	1.51	0.11						
WB-0815-MC-DSH-10-A	8	10	9	1.42	0.07						
WB-0815-MC-DSH-10-A	12	14	13	1.19	0.07						
WB-0815-MC-DSH-10-A	16	18	17	0.95	0.06						

Table G.26. SLRad data of $^{234}Th_{Tot}$, $^{234}Th_{xs}$, and D.C. $^{234}Th_{xs}$ for core site WB-0815-MC-PCB-06-A. Sediment cores with sub-sample intervals (mm), and SLRad data for $^{234}Th_{Tot}$, Re-analysis of ^{234}Th as indicator of $^{234}Th_{Sup}$, $^{234}Th_{xs}$, and D.C. $^{234}Th_{xs}$ (Decay Corrected). Note: Blank cell denotes no analysis performed.

Core ID	Top Depth of Interval (mm)	Bottom Depth of Interval (mm)	Average Depth of Interval (mm)	$^{234}Th_{Tot}$ Activity (dpm/g)	$^{234}Th_{Tot}$ Activity error (dpm/g)	Re-Analysis; ^{234}Th Activity (dpmg/)	Re-Analysis; ^{234}Th error Activity (dpmg/)	$^{234}Th_{xs}$ Activity (dpm/g)	$^{234}Th_{xs}$ Activity error (dpm/g)	D.C. $^{234}Th_{xs}$ Activity (dpm/g)	D.C. $^{234}Th_{xs}$ Activity error (dpm/g)
WB-0815-MC-PCB-06-A	0	2	1	5.97	0.20			4.45	0.22	7.69	0.38
WB-0815-MC-PCB-06-A	2	4	3	6.25	0.16			4.73	0.18	8.66	0.33
WB-0815-MC-PCB-06-A	4	6	5	4.05	0.13			2.53	0.15	4.91	0.29
WB-0815-MC-PCB-06-A	6	8	7	1.92	0.08			0.40	0.12	1.43	0.41
WB-0815-MC-PCB-06-A	8	10	9	2.28	0.09			0.76	0.12	1.57	0.25
WB-0815-MC-PCB-06-A	10	12	11	1.47	0.07			0.00	0.11	0.00	0.00
WB-0815-MC-PCB-06-A	12	14	13	1.65	0.08						
WB-0815-MC-PCB-06-A	16	18	17	1.52	0.07						
WB-0815-MC-PCB-06-A	18	20	19	1.17	0.06						

Table G.27. SLRad data of $^{234}Th_{Tot}$, $^{234}Th_{xs}$, and D.C. $^{234}Th_{xs}$ for core site WB-0816-MC-04. Sediment cores with sub-sample intervals (mm), and SLRad data for $^{234}Th_{Tot}$, Re-analysis of ^{234}Th as indicator of $^{234}Th_{Sup}$, $^{234}Th_{xs}$, and D.C. $^{234}Th_{xs}$ (Decay Corrected). Note: Blank cell denotes no analysis performed.

Core ID	Top Depth of Interval (mm)	Bottom Depth of Interval (mm)	Average Depth of Interval (mm)	$^{234}Th_{Tot}$ Activity (dpm/g)	$^{234}Th_{Tot}$ Activity error (dpm/g)	Re-Analysis; ^{234}Th Activity (dpmg/)	Re-Analysis; ^{234}Th error Activity (dpmg/)	$^{234}Th_{xs}$ Activity (dpm/g)	$^{234}Th_{xs}$ Activity error (dpm/g)	D.C. $^{234}Th_{xs}$ Activity (dpm/g)	D.C. $^{234}Th_{xs}$ Activity error (dpm/g)
WB-0816-MC-04	0	2	1	2.33	0.11			1.46	0.14	4.24	0.40
WB-0816-MC-04	2	4	3	1.51	0.08			0.56	0.12	1.71	0.35
WB-0816-MC-04	4	6	5	1.25	0.07			0.20	0.11	0.67	0.35
WB-0816-MC-04	6	8	7	1.24	0.07			0.19	0.10	0.66	0.36
WB-0816-MC-04	8	10	9	1.18	0.07			0.13	0.10	0.52	0.40
WB-0816-MC-04	10	12	11	0.87	0.05			0.00	0.10	0.00	0.00
WB-0816-MC-04	12	14	13	1.11	0.06						
WB-0816-MC-04	14	16	15	0.99	0.06						
WB-0816-MC-04	16	18	17	1.07	0.06						
WB-0816-MC-04	18	20	19	0.88	0.05						
WB-0816-MC-04	20	22	21	0.91	0.06						
WB-0816-MC-04	24	26	25	0.77	0.05						
WB-0816-MC-04	30	32	31	0.81	0.05						
WB-0816-MC-04	50	52	51	0.80	0.05						
WB-0816-MC-04	70	72	71	0.82	0.05						
WB-0816-MC-04	90	95	92.5	1.04	0.05						
WB-0816-MC-04	110	115	112.5	1.29	0.05						
WB-0816-MC-04	130	135	132.5	0.99	0.05						
WB-0816-MC-04	150	155	152.5	1.31	0.05						
WB-0816-MC-04	170	175	172.5	1.50	0.06						
WB-0816-MC-04	190	195	192.5	1.61	0.06						
WB-0816-MC-04	210	215	212.5	1.59	0.06						
WB-0816-MC-04	230	235	232.5	1.45	0.08						
WB-0816-MC-04	250	255	252.5	1.46	0.06						

Table G.27 (Continued).

Core ID	Top Depth of Interval (mm)	Bottom Depth of Interval (mm)	Average Depth of Interval (mm)	$^{234}Th_{Tot}$ Activity (dpm/g)	$^{234}Th_{Tot}$ Activity error (dpm/g)	Re-Analysis; ^{234}Th Activity (dpmg/)	Re-Analysis; ^{234}Th error Activity (dpmg/)	$^{234}Th_{xs}$ Activity (dpm/g)	$^{234}Th_{xs}$ Activity error (dpm/g)	D.C. $^{234}Th_{xs}$ Activity (dpm/g)	D.C. $^{234}Th_{xs}$ Activity error (dpm/g)
WB-0816-MC-04	270	275	272.5	1.71	0.06						
WB-0816-MC-04	290	295	292.5	1.41	0.06						
WB-0816-MC-04	310	315	312.5	1.24	0.05						
WB-0816-MC-04	330	335	332.5	1.59	0.06						

Table G.28. SLRad data of $^{234}Th_{Tot}$, $^{234}Th_{xs}$, and D.C. $^{234}Th_{xs}$ for core site WB-0816-MC-DSH-08-A. Sediment cores with sub-sample intervals (mm), and SLRad data for $^{234}Th_{Tot}$, Re-analysis of ^{234}Th as indicator of $^{234}Th_{Sup}$, $^{234}Th_{xs}$, and D.C. $^{234}Th_{xs}$ (Decay Corrected). Note: Blank cell denotes no analysis performed.

Core ID	Top Depth of Interval (mm)	Bottom Depth of Interval (mm)	Average Depth of Interval (mm)	$^{234}Th_{Tot}$ Activity (dpm/g)	$^{234}Th_{Tot}$ Activity error (dpm/g)	Re-Analysis; ^{234}Th Activity (dpmg/)	Re-Analysis; ^{234}Th error Activity (dpmg/)	$^{234}Th_{xs}$ Activity (dpm/g)	$^{234}Th_{xs}$ Activity error (dpm/g)	D.C. $^{234}Th_{xs}$ Activity (dpm/g)	D.C. $^{234}Th_{xs}$ Activity error (dpm/g)
WB-0816-MC-DSH-08-A	0	2	1	3.42	0.12			1.76	0.14	2.87	0.23
WB-0816-MC-DSH-08-A	2	4	3	3.12	0.11			1.46	0.14	2.52	0.24
WB-0816-MC-DSH-08-A	4	6	5	2.85	0.10			1.19	0.13	2.18	0.24
WB-0816-MC-DSH-08-A	6	8	7	2.77	0.10			1.11	0.13	2.14	0.25
WB-0816-MC-DSH-08-A	8	10	9	1.88	0.08			0.22	0.11	0.61	0.31
WB-0816-MC-DSH-08-A	10	12	11	1.99	0.08			0.00	0.00	0.00	0.00
WB-0816-MC-DSH-08-A	12	14	13	1.66	0.08						
WB-0816-MC-DSH-08-A	14	16	15	1.56	0.07						
WB-0816-MC-DSH-08-A	16	18	17	1.75	0.08						
WB-0816-MC-DSH-08-A	18	20	19	1.47	0.07						
WB-0816-MC-DSH-08-A	20	22	21	1.23	0.07						
WB-0816-MC-DSH-08-A	22	24	23	0.98	0.06						
WB-0816-MC-DSH-08-A	24	26	25	1.15	0.06						
WB-0816-MC-DSH-08-A	26	28	27	1.02	0.06						
WB-0816-MC-DSH-08-A	28	30	29	0.84	0.05						
WB-0816-MC-DSH-08-A	30	32	31	1.16	0.06						
WB-0816-MC-DSH-08-A	50	55	52.5	1.44	0.06						
WB-0816-MC-DSH-08-A	70	75	72.5	1.70	0.07						
WB-0816-MC-DSH-08-A	90	95	92.5	2.08	0.07						
WB-0816-MC-DSH-08-A	110	115	112.5	1.76	0.07						
WB-0816-MC-DSH-08-A	130	135	132.5	1.87	0.07						
WB-0816-MC-DSH-08-A	150	155	152.5	1.83	0.07						
WB-0816-MC-DSH-08-A	170	175	172.5	1.92	0.07						
WB-0816-MC-DSH-08-A	190	195	192.5	1.61	0.06						

Table G.28 (Continued).

Core ID	Top Depth of Interval (mm)	Bottom Depth of Interval (mm)	Average Depth of Interval (mm)	$^{234}Th_{Tot}$ Activity (dpm/g)	$^{234}Th_{Tot}$ Activity error (dpm/g)	Re-Analysis; ^{234}Th Activity (dpmg/)	Re-Analysis; ^{234}Th error Activity (dpmg/)	$^{234}Th_{xs}$ Activity (dpm/g)	$^{234}Th_{xs}$ Activity error (dpm/g)	D.C. $^{234}Th_{xs}$ Activity (dpm/g)	D.C. $^{234}Th_{xs}$ Activity error (dpm/g)
WB-0816-MC-DSH-08-A	210	215	212.5	1.97	0.07						
WB-0816-MC-DSH-08-A	250	255	252.5	1.69	0.07						
WB-0816-MC-DSH-08-A	290	295	292.5	1.57	0.06						

Table G.29. SLRad data of $^{234}Th_{Tot}$, $^{234}Th_{xs}$, and D.C. $^{234}Th_{xs}$ for core site WB-0816-MC-DSH-10-A. Sediment cores with sub-sample intervals (mm), and SLRad data for $^{234}Th_{Tot}$, Re-analysis of ^{234}Th as indicator of $^{234}Th_{Sup}$, $^{234}Th_{xs}$, and D.C. $^{234}Th_{xs}$ (Decay Corrected). Note: Blank cell denotes no analysis performed.

Core ID	Top Depth of Interval (mm)	Bottom Depth of Interval (mm)	Average Depth of Interval (mm)	$^{234}Th_{Tot}$ Activity (dpm/g)	$^{234}Th_{Tot}$ Activity error (dpm/g)	Re-Analysis; ^{234}Th Activity (dpmg/)	Re-Analysis; ^{234}Th error Activity (dpmg/)	$^{234}Th_{xs}$ Activity (dpm/g)	$^{234}Th_{xs}$ Activity error (dpm/g)	D.C. $^{234}Th_{xs}$ Activity (dpm/g)	D.C. $^{234}Th_{xs}$ Activity error (dpm/g)
WB-0816-MC-DSH-10-A	0	2	1	2.05	0.10			0.94	0.13	1.66	0.23
WB-0816-MC-DSH-10-A	2	4	3	1.26	0.07			0.15	0.11	0.28	0.20
WB-0816-MC-DSH-10-A	4	6	5	1.16	0.07			0.00	0.00	0.00	0.00
WB-0816-MC-DSH-10-A	6	8	7	1.11	0.07						
WB-0816-MC-DSH-10-A	8	10	9	1.01	0.06						
WB-0816-MC-DSH-10-A	10	12	11	1.09	0.06						
WB-0816-MC-DSH-10-A	20	22	21	1.26	0.07						
WB-0816-MC-DSH-10-A	22	24	23	1.58	0.08						
WB-0816-MC-DSH-10-A	24	26	25	1.40	0.07						
WB-0816-MC-DSH-10-A	26	28	27	1.42	0.07						
WB-0816-MC-DSH-10-A	28	30	29	1.21	0.06						
WB-0816-MC-DSH-10-A	70	72	71	1.35	0.07						
WB-0816-MC-DSH-10-A	90	95	92.5	1.33	0.06						
WB-0816-MC-DSH-10-A	110	115	112.5	1.56	0.06						
WB-0816-MC-DSH-10-A	130	135	132.5	1.21	0.06						
WB-0816-MC-DSH-10-A	170	175	172.5	1.16	0.05						
WB-0816-MC-DSH-10-A	210	215	212.5	1.70	0.07						
WB-0816-MC-DSH-10-A	250	255	252.5	1.44	0.06						
WB-0816-MC-DSH-10-A	290	295	292.5	1.23	0.05						
WB-0816-MC-DSH-10-A	310	315	312.5	1.36	0.06						

Table G.30. SLRad data of $^{234}Th_{Tot}$, $^{234}Th_{xs}$, and D.C. $^{234}Th_{xs}$ for core site WB-0816-MC-PCB-06-A. Sediment cores with sub-sample intervals (mm), and SLRad data for $^{234}Th_{Tot}$, Re-analysis of ^{234}Th as indicator of $^{234}Th_{Sup}$, $^{234}Th_{xs}$, and D.C. $^{234}Th_{xs}$ (Decay Corrected). Note: Blank cell denotes no analysis performed.

Core ID	Top Depth of Interval (mm)	Bottom Depth of Interval (mm)	Average Depth of Interval (mm)	$^{234}Th_{Tot}$ Activity (dpm/g)	$^{234}Th_{Tot}$ Activity error (dpm/g)	Re-Analysis; ^{234}Th Activity (dpmg/)	Re-Analysis; ^{234}Th error Activity (dpmg/)	$^{234}Th_{xs}$ Activity (dpm/g)	$^{234}Th_{xs}$ Activity error (dpm/g)	D.C. $^{234}Th_{xs}$ Activity (dpm/g)	D.C. $^{234}Th_{xs}$ Activity error (dpm/g)
WB-0816-MC-PCB-06-A	0	2	1	2.50	0.11			1.06	0.13	2.17	0.27
WB-0816-MC-PCB-06-A	2	4	3	2.89	0.13			1.45	0.15	3.15	0.32
WB-0816-MC-PCB-06-A	4	6	5	3.38	0.12			1.94	0.15	4.47	0.34
WB-0816-MC-PCB-06-A	6	8	7	2.74	0.11			1.30	0.14	3.17	0.33
WB-0816-MC-PCB-06-A	8	10	9	2.09	0.09			0.65	0.12	1.68	0.31
WB-0816-MC-PCB-06-A	10	12	11	1.44	0.07			0.00	0.00	0.00	0.00
WB-0816-MC-PCB-06-A	12	14	13	1.56	0.07						
WB-0816-MC-PCB-06-A	14	16	15	1.30	0.07						
WB-0816-MC-PCB-06-A	16	18	17	1.24	0.06						
WB-0816-MC-PCB-06-A	18	20	19	1.17	0.06						
WB-0816-MC-PCB-06-A	20	22	21	0.75	0.05						
WB-0816-MC-PCB-06-A	22	24	23	1.07	0.06						
WB-0816-MC-PCB-06-A	24	26	25	1.12	0.06						
WB-0816-MC-PCB-06-A	26	28	27	1.19	0.06						
WB-0816-MC-PCB-06-A	28	30	29	1.35	0.07						
WB-0816-MC-PCB-06-A	30	32	31	1.14	0.05						
WB-0816-MC-PCB-06-A	50	52	51	1.00	0.06						
WB-0816-MC-PCB-06-A	70	72	71	1.28	0.06						
WB-0816-MC-PCB-06-A	90	95	92.5	1.57	0.06						
WB-0816-MC-PCB-06-A	110	115	112.5	1.44	0.06						
WB-0816-MC-PCB-06-A	130	135	132.5	1.53	0.06						
WB-0816-MC-PCB-06-A	150	155	152.5	1.84	0.07						
WB-0816-MC-PCB-06-A	170	175	172.5	2.01	0.07						
WB-0816-MC-PCB-06-A	190	195	192.5	1.71	0.07						

Table G.30 (Continued).

Core ID	Top Depth of Interval (mm)	Bottom Depth of Interval (mm)	Average Depth of Interval (mm)	$^{234}Th_{Tot}$ Activity (dpm/g)	$^{234}Th_{Tot}$ Activity error (dpm/g)	Re-Analysis; ^{234}Th Activity (dpmg/)	Re-Analysis; ^{234}Th error Activity (dpmg/)	$^{234}Th_{xs}$ Activity (dpm/g)	$^{234}Th_{xs}$ Activity error (dpm/g)	D.C. $^{234}Th_{xs}$ Activity (dpm/g)	D.C. $^{234}Th_{xs}$ Activity error (dpm/g)
WB-0816-MC-PCB-06-A	210	215	212.5	1.75	0.07						
WB-0816-MC-PCB-06-A	250	255	252.5	2.56	0.08						
WB-0816-MC-PCB-06-A	290	295	292.5	2.61	0.08						

APPENDIX H:

SHORT-LIVED RADIOISOTOPE (SLRad) DATA: $^{210}Pbs_{up}$ Data.

Appendix H. Supplemental tables of short-lived radioisotope data for $^{210}Pbs_{up}$ calculated from measured proxies (^{214}Pb at 295keV, ^{214}Pb at 351keV and ^{214}Bi at 609keV).

Data are publicly available through the Gulf of Mexico Research Initiative Information & Data Cooperative (GRIIDC) at https://data.gulfresearchinitiative.org (doi: 10.7266/N7610XTJ, 10.7266/n7-81nq-dq02, 10.7266/n7-p0xt-6209, 10.7266/n7-qzw5-kc72, 10.7266/n7-xsrd-fq25, 10.7266/n7-1vvs-ef02, 10.7266/n7-4j4h-7w93, 10.7266/n7-cdrm-g239)

Table H.1. SLRad data, $^{210}Pbs_{up}$ data for core site WB-1109-MC-04. Sediment cores with sub-sample intervals (mm), and SLRad's activities of ^{214}Pb (295keV), ^{214}Pb (351keV), and ^{214}Bi (351keV) used to calculate $^{210}Pb_{Sup}$. Note: Blank cell denotes no analysis performed.

Core ID	Top Depth of Interval (mm)	Bottom Depth of interval (mm)	Average Depth of Interval (mm)	^{214}Pb (295 keV) Activity (dpm/g)	^{214}Pb (295 keV) Activity error (dpm/g)	^{214}Pb (351 keV) Activity (dpm/g)	^{214}Pb (351 keV) Activity error (dpm/g)	^{214}Bi Activity (dpm/g)	^{214}Bi Activity error (dpm/g)	$^{210}Pb_{Sup}$ Activity (dpm/g)	$^{210}Pb_{Sup}$ Activity error (dpm/g)
WB-1109-MC-04	0	2	1	1.84	0.18	2.01	0.17	1.36	0.17	1.74	0.18
WB-1109-MC-04	2	4	3	1.46	0.14	1.85	0.14	1.55	0.16	1.62	0.15
WB-1109-MC-04	4	6	5	1.30	0.12	1.94	0.13	1.47	0.14	1.57	0.13
WB-1109-MC-04	6	8	7	1.49	0.13	1.58	0.12	1.84	0.16	1.63	0.14
WB-1109-MC-04	8	10	9	1.00	0.09	1.26	0.09	1.06	0.11	1.11	0.10
WB-1109-MC-04	10	12	11	1.89	0.15	1.36	0.11	1.58	0.15	1.61	0.14
WB-1109-MC-04	12	14	13	1.22	0.11	0.81	0.08	1.36	0.13	1.13	0.11
WB-1109-MC-04	14	16	15	1.16	0.11	1.61	0.11	1.28	0.12	1.35	0.11
WB-1109-MC-04	16	18	17	1.63	0.11	1.53	0.10	1.66	0.13	1.60	0.11
WB-1109-MC-04	18	20	19	0.91	0.09	1.32	0.10	1.31	0.12	1.18	0.10
WB-1109-MC-04	20	25	22.5	1.12	0.08	1.16	0.07	1.22	0.09	1.17	0.08
WB-1109-MC-04	30	35	32.5	0.94	0.07	0.85	0.05	1.18	0.08	0.99	0.07
WB-1109-MC-04	40	45	42.5	1.02	0.07	1.11	0.06	1.19	0.09	1.11	0.08
WB-1109-MC-04	50	55	52.5	0.94	0.07	1.20	0.06	0.92	0.07	1.02	0.07
WB-1109-MC-04	60	65	62.5	1.02	0.07	1.01	0.06	0.95	0.07	0.99	0.07
WB-1109-MC-04	70	75	72.5	0.93	0.06	0.98	0.05	1.06	0.07	0.99	0.06
WB-1109-MC-04	80	85	82.5	0.97	0.06	0.98	0.05	1.01	0.07	0.99	0.06
WB-1109-MC-04	90	95	92.5	1.01	0.07	1.11	0.06	1.03	0.08	1.05	0.07
WB-1109-MC-04	100	105	102.5	0.94	0.07	1.24	0.06	1.27	0.08	1.15	0.07
WB-1109-MC-04	110	115	112.5	1.07	0.07	1.16	0.06	1.07	0.08	1.10	0.07
WB-1109-MC-04	120	125	122.5	1.22	0.07	1.25	0.06	1.00	0.07	1.16	0.07
WB-1109-MC-04	130	135	132.5	0.85	0.06	1.02	0.05	1.03	0.07	0.97	0.06

Table H.1. (Continued).

Core ID	Top Depth of Interval (mm)	Bottom Depth of interval (mm)	Average Depth of Interval (mm)	^{214}Pb (295 keV) Activity (dpm/g)	^{214}Pb (295 keV) Activity error (dpm/g)	^{214}Pb (351 keV) Activity (dpm/g)	^{214}Pb (351 keV) Activity error (dpm/g)	^{214}Bi Activity (dpm/g)	^{214}Bi Activity error (dpm/g)	^{210}Pb$_{Sup}$ Activity (dpm/g)	^{210}Pb$_{Sup}$ Activity error (dpm/g)
WB-1109-MC-04	140	145	142.5	1.12	0.07	1.01	0.05	0.91	0.07	1.01	0.06
WB-1109-MC-04	150	155	152.5	1.04	0.07	0.98	0.06	0.93	0.07	0.98	0.07
WB-1109-MC-04	160	165	162.5	0.96	0.07	1.03	0.06	0.81	0.07	0.93	0.06
WB-1109-MC-04	170	175	172.5	0.95	0.07	1.02	0.06	0.83	0.07	0.93	0.06
WB-1109-MC-04	180	185	182.5	0.94	0.05	0.73	0.03	0.63	0.04	0.77	0.04
WB-1109-MC-04	210	215	212.5	1.12	0.06	0.99	0.05	0.92	0.06	1.01	0.06

Table H.2. SLRad data, $^{210}Pbs_{up}$ data for core site WB-1110-MC-DSH-08. Sediment cores with sub-sample intervals (mm), and SLRad's activities of ^{214}Pb (295keV), ^{214}Pb (351keV), and ^{214}Bi (351keV) used to calculate $^{210}Pb_{Sup}$. Note: Blank cell denotes no analysis performed.

Core ID	Top Depth of Interval (mm)	Bottom Depth of interval (mm)	Average Depth of Interval (mm)	^{214}Pb (295 keV) Activity (dpm/g)	^{214}Pb (295 keV) Activity error (dpm/g)	^{214}Pb (351 keV) Activity (dpm/g)	^{214}Pb (351 keV) Activity error (dpm/g)	^{214}Bi Activity (dpm/g)	^{214}Bi Activity error (dpm/g)	$^{210}Pb_{Sup}$ Activity (dpm/g)	$^{210}Pb_{Sup}$ Activity error (dpm/g)
WB-1110-MC-DSH-08	0	2	1	2.39	0.16	2.05	0.11	1.80	0.12	2.08	0.13
WB-1110-MC-DSH-08	2	4	3	1.74	0.12	1.68	0.09	1.55	0.10	1.66	0.10
WB-1110-MC-DSH-08	4	6	5	1.69	0.11	1.49	0.08	1.49	0.09	1.56	0.10
WB-1110-MC-DSH-08	6	8	7	1.83	0.11	1.71	0.08	1.52	0.09	1.68	0.09
WB-1110-MC-DSH-08	8	10	9	1.57	0.10	1.88	0.08	1.69	0.09	1.71	0.09
WB-1110-MC-DSH-08	10	12	11	1.50	0.13	1.55	0.11	1.21	0.11	1.42	0.12
WB-1110-MC-DSH-08	12	14	13	1.45	0.09	1.52	0.07	1.30	0.08	1.43	0.08
WB-1110-MC-DSH-08	14	16	15	1.87	0.10	1.70	0.08	1.61	0.09	1.73	0.09
WB-1110-MC-DSH-08	16	18	17	1.50	0.09	1.53	0.07	1.17	0.08	1.40	0.08
WB-1110-MC-DSH-08	18	20	19	2.09	0.11	1.79	0.08	1.48	0.08	1.79	0.09
WB-1110-MC-DSH-08	22	24	23	2.77	0.12	2.84	0.10	2.06	0.10	2.56	0.11
WB-1110-MC-DSH-08	26	28	27	2.37	0.11	2.09	0.08	1.75	0.09	2.07	0.09
WB-1110-MC-DSH-08	32	34	33	1.75	0.09	1.71	0.07	1.63	0.08	1.70	0.08
WB-1110-MC-DSH-08	34	36	35	1.73	0.09	1.65	0.07	1.51	0.08	1.63	0.08
WB-1110-MC-DSH-08	38	40	39	1.34	0.08	1.37	0.06	0.97	0.06	1.23	0.07
WB-1110-MC-DSH-08	42	44	43	1.53	0.08	1.37	0.06	1.16	0.07	1.36	0.07
WB-1110-MC-DSH-08	46	48	47	1.32	0.08	1.42	0.06	1.26	0.07	1.33	0.07
WB-1110-MC-DSH-08	48	50	49	1.31	0.08	1.24	0.06	1.10	0.07	1.22	0.07
WB-1110-MC-DSH-08	50	55	52.5	1.84	0.07	1.89	0.06	1.77	0.07	1.83	0.07
WB-1110-MC-DSH-08	60	65	62.5	1.73	0.07	2.01	0.06	1.92	0.07	1.89	0.07
WB-1110-MC-DSH-08	70	75	72.5	1.77	0.07	1.65	0.06	1.46	0.07	1.63	0.06
WB-1110-MC-DSH-08	80	85	82.5	2.02	0.07	2.05	0.06	1.90	0.07	1.99	0.07
WB-1110-MC-DSH-08	90	95	92.5	1.73	0.07	1.69	0.05	1.79	0.07	1.74	0.06

Table H.2 (Continued).

Core ID	Top Depth of Interval (mm)	Bottom Depth of interval (mm)	Average Depth of Interval (mm)	^{214}Pb (295 keV) Activity (dpm/g)	^{214}Pb (295 keV) Activity error (dpm/g)	^{214}Pb (351 keV) Activity (dpm/g)	^{214}Pb (351 keV) Activity error (dpm/g)	^{214}Bi Activity (dpm/g)	^{214}Bi Activity error (dpm/g)	^{210}Pb$_{Sup}$ Activity (dpm/g)	^{210}Pb$_{Sup}$ Activity error (dpm/g)
WB-1110-MC-DSH-08	100	105	102.5	2.10	0.07	1.98	0.06	2.03	0.07	2.04	0.07
WB-1110-MC-DSH-08	110	115	112.5	1.70	0.07	1.91	0.06	1.87	0.07	1.82	0.07
WB-1110-MC-DSH-08	120	125	122.5	2.05	0.08	1.94	0.06	1.76	0.07	1.92	0.07
WB-1110-MC-DSH-08	130	135	132.5	1.99	0.07	2.07	0.06	2.04	0.07	2.03	0.07
WB-1110-MC-DSH-08	140	145	142.5	1.81	0.07	1.88	0.06	1.66	0.07	1.78	0.06
WB-1110-MC-DSH-08	150	155	152.5	1.96	0.10	1.86	0.08	1.75	0.10	1.86	0.09
WB-1110-MC-DSH-08	160	165	162.5	1.93	0.07	2.03	0.06	1.91	0.07	1.95	0.07
WB-1110-MC-DSH-08	180	185	182.5	1.74	0.07	1.95	0.06	1.81	0.07	1.84	0.07
WB-1110-MC-DSH-08	190	195	192.5	1.71	0.07	1.80	0.06	1.85	0.07	1.78	0.06
WB-1110-MC-DSH-08	210	215	212.5	1.65	0.07	1.81	0.06	1.65	0.08	1.70	0.07
WB-1110-MC-DSH-08	230	235	232.5	1.62	0.07	1.87	0.07	1.58	0.07	1.69	0.07
WB-1110-MC-DSH-08	250	255	252.5	1.54	0.07	1.66	0.06	1.49	0.07	1.56	0.07
WB-1110-MC-DSH-08	270	275	272.5	1.99	0.07	2.07	0.06	1.90	0.07	1.98	0.07

Table H.3. SLRad data, $^{210}Pbs_{up}$ data for core site WB-1110-MC-DSH-10. Sediment cores with sub-sample intervals (mm), and SLRad's activities of ^{214}Pb (295keV), ^{214}Pb (351keV), and ^{214}Bi (351keV) used to calculate $^{210}Pb_{Sup}$. Note: Blank cell denotes no analysis performed.

Core ID	Top Depth of Interval (mm)	Bottom Depth of interval (mm)	Average Depth of Interval (mm)	^{214}Pb (295 keV) Activity (dpm/g)	^{214}Pb (295 keV) Activity error (dpm/g)	^{214}Pb (351 keV) Activity (dpm/g)	^{214}Pb (351 keV) Activity error (dpm/g)	^{214}Bi Activity (dpm/g)	^{214}Bi Activity error (dpm/g)	$^{210}Pb_{Sup}$ Activity (dpm/g)	$^{210}Pb_{Sup}$ Activity error (dpm/g)
WB-1110-MC-DSH-10	0	2	1	2.13	0.13	2.32	0.12	2.38	0.15	2.28	0.14
WB-1110-MC-DSH-10	2	4	3	1.79	0.11	2.11	0.10	1.99	0.12	1.96	0.11
WB-1110-MC-DSH-10	4	6	5	1.61	0.09	2.26	0.09	1.60	0.10	1.82	0.10
WB-1110-MC-DSH-10	6	8	7	2.10	0.11	2.13	0.10	1.77	0.11	2.00	0.11
WB-1110-MC-DSH-10	8	10	9	1.75	0.09	2.24	0.09	1.92	0.10	1.97	0.09
WB-1110-MC-DSH-10	10	12	11	1.56	0.09	2.03	0.08	1.48	0.09	1.69	0.09
WB-1110-MC-DSH-10	12	14	13	1.89	0.09	2.00	0.08	1.62	0.09	1.84	0.09
WB-1110-MC-DSH-10	14	16	15	1.99	0.09	2.31	0.09	1.74	0.10	2.01	0.09
WB-1110-MC-DSH-10	16	18	17	1.69	0.09	1.97	0.09	1.75	0.10	1.80	0.09
WB-1110-MC-DSH-10	18	20	19	1.96	0.10	2.25	0.09	2.02	0.11	2.08	0.10
WB-1110-MC-DSH-10	20	22	21	2.24	0.10	2.33	0.09	2.00	0.11	2.19	0.10
WB-1110-MC-DSH-10	24	26	25	1.68	0.09	2.12	0.08	1.69	0.09	1.83	0.09
WB-1110-MC-DSH-10	30	32	31	2.13	0.10	2.31	0.09	2.14	0.11	2.19	0.10
WB-1110-MC-DSH-10	40	42	41	1.79	0.09	2.12	0.08	1.74	0.09	1.88	0.09
WB-1110-MC-DSH-10	50	52	51	1.47	0.07	1.67	0.07	1.27	0.08	1.47	0.07
WB-1110-MC-DSH-10	60	62	61	1.86	0.08	2.19	0.08	1.90	0.09	1.98	0.09
WB-1110-MC-DSH-10	70	72	71	2.52	0.10	2.48	0.08	2.14	0.10	2.38	0.10
WB-1110-MC-DSH-10	80	85	82.5	2.45	0.08	2.67	0.07	2.40	0.08	2.51	0.07
WB-1110-MC-DSH-10	90	95	92.5	2.94	0.08	3.14	0.07	2.92	0.09	3.00	0.08
WB-1110-MC-DSH-10	100	105	102.5	2.09	0.07	2.25	0.06	2.14	0.08	2.16	0.07
WB-1110-MC-DSH-10	110	115	112.5	2.36	0.07	2.30	0.06	2.36	0.08	2.34	0.07
WB-1110-MC-DSH-10	120	125	122.5	2.74	0.08	2.69	0.06	2.34	0.08	2.59	0.07
WB-1110-MC-DSH-10	130	135	132.5	1.85	0.07	2.08	0.06	1.85	0.07	1.92	0.06

Table H.3 (Continued).

Core ID	Top Depth of Interval (mm)	Bottom Depth of interval (mm)	Average Depth of Interval (mm)	^{214}Pb (295 keV) Activity (dpm/g)	^{214}Pb (295 keV) Activity error (dpm/g)	^{214}Pb (351 keV) Activity (dpm/g)	^{214}Pb (351 keV) Activity error (dpm/g)	^{214}Bi Activity (dpm/g)	^{214}Bi Activity error (dpm/g)	^{210}Pb$_{Sup}$ Activity (dpm/g)	^{210}Pb$_{Sup}$ Activity error (dpm/g)
WB-1110-MC-DSH-10	140	145	142.5	2.07	0.07	2.18	0.06	1.85	0.07	2.03	0.07
WB-1110-MC-DSH-10	150	155	152.5	1.85	0.07	1.90	0.06	2.11	0.08	1.95	0.07
WB-1110-MC-DSH-10	160	165	162.5	1.84	0.07	1.95	0.06	2.07	0.08	1.95	0.07
WB-1110-MC-DSH-10	170	175	172.5	1.94	0.07	1.97	0.06	1.79	0.07	1.90	0.07
WB-1110-MC-DSH-10	180	185	182.5	1.89	0.07	2.10	0.06	2.01	0.08	2.00	0.07
WB-1110-MC-DSH-10	190	195	192.5	2.22	0.07	1.97	0.06	2.10	0.08	2.10	0.07
WB-1110-MC-DSH-10	200	205	202.5	1.84	0.07	1.95	0.06	1.95	0.08	1.91	0.07
WB-1110-MC-DSH-10	210	215	212.5	2.02	0.07	1.98	0.06	1.95	0.08	1.98	0.07
WB-1110-MC-DSH-10	220	225	222.5	1.98	0.07	1.93	0.05	2.08	0.08	1.99	0.07
WB-1110-MC-DSH-10	240	245	242.5	2.02	0.07	1.92	0.06	1.86	0.07	1.93	0.07
WB-1110-MC-DSH-10	250	255	252.5	1.54	0.07	1.72	0.06	1.76	0.08	1.68	0.07
WB-1110-MC-DSH-10	270	275	272.5	1.76	0.08	1.74	0.06	1.59	0.08	1.70	0.07
WB-1110-MC-DSH-10	290	295	292.5	1.87	0.08	1.78	0.06	1.66	0.08	1.77	0.07
WB-1110-MC-DSH-10	310	315	312.5	1.89	0.08	1.74	0.06	1.72	0.08	1.78	0.07

Table H.4. SLRad data, $^{210}Pbs_{up}$ data for core site WB-1110-MC-PCB-06. Sediment cores with sub-sample intervals (mm), and SLRad's activities of ^{214}Pb (295keV), ^{214}Pb (351keV), and ^{214}Bi (351keV) used to calculate $^{210}Pb_{Sup}$. Note: Blank cell denotes no analysis performed.

Core ID	Top Depth of Interval (mm)	Bottom Depth of interval (mm)	Average Depth of Interval (mm)	^{214}Pb (295 keV) Activity (dpm/g)	^{214}Pb (295 keV) Activity error (dpm/g)	^{214}Pb (351 keV) Activity (dpm/g)	^{214}Pb (351 keV) Activity error (dpm/g)	^{214}Bi Activity (dpm/g)	^{214}Bi Activity error (dpm/g)	$^{210}Pb_{Sup}$ Activity (dpm/g)	$^{210}Pb_{Sup}$ Activity error (dpm/g)
WB-1110-MC-PCB-06	0	2	1	2.28	0.17	1.80	0.11	1.24	0.10	1.77	0.13
WB-1110-MC-PCB-06	2	4	3	1.18	0.09	1.27	0.07	1.25	0.08	1.24	0.08
WB-1110-MC-PCB-06	4	6	5	1.25	0.09	1.29	0.07	1.08	0.07	1.21	0.08
WB-1110-MC-PCB-06	6	10	8	1.56	0.07	1.63	0.06	1.40	0.07	1.53	0.07
WB-1110-MC-PCB-06	10	12	11	1.41	0.08	1.29	0.06	1.05	0.07	1.25	0.07
WB-1110-MC-PCB-06	12	14	13	1.66	0.09	1.37	0.07	1.33	0.08	1.45	0.08
WB-1110-MC-PCB-06	14	16	15	1.58	0.09	1.32	0.07	1.22	0.08	1.37	0.08
WB-1110-MC-PCB-06	16	18	17	1.58	0.09	1.16	0.06	1.01	0.07	1.25	0.07
WB-1110-MC-PCB-06	18	20	19	1.46	0.08	1.27	0.06	1.23	0.07	1.32	0.07
WB-1110-MC-PCB-06	24	26	25	1.72	0.10	1.57	0.07	1.64	0.09	1.64	0.08
WB-1110-MC-PCB-06	28	30	29	1.48	0.08	1.63	0.07	1.42	0.08	1.51	0.08
WB-1110-MC-PCB-06	36	38	37	1.81	0.10	1.94	0.08	1.87	0.09	1.87	0.09
WB-1110-MC-PCB-06	40	42	41	1.94	0.10	2.20	0.08	2.05	0.09	2.06	0.09
WB-1110-MC-PCB-06	50	52	51	2.56	0.11	2.71	0.09	2.53	0.10	2.60	0.10
WB-1110-MC-PCB-06	60	62	61	1.90	0.08	1.90	0.06	1.68	0.07	1.82	0.07
WB-1110-MC-PCB-06	70	72	71	1.48	0.08	1.77	0.07	1.39	0.07	1.55	0.07
WB-1110-MC-PCB-06	80	82	81	1.57	0.08	1.71	0.07	1.62	0.08	1.63	0.08
WB-1110-MC-PCB-06	90	92	91	1.62	0.08	1.71	0.07	1.50	0.08	1.61	0.07
WB-1110-MC-PCB-06	100	105	102.5	1.97	0.07	2.23	0.06	2.03	0.08	2.08	0.07
WB-1110-MC-PCB-06	110	115	112.5	1.98	0.07	2.05	0.06	1.77	0.07	1.93	0.07
WB-1110-MC-PCB-06	130	135	132.5	2.13	0.07	2.05	0.06	1.97	0.07	2.05	0.07
WB-1110-MC-PCB-06	150	155	152.5	1.79	0.07	1.81	0.06	1.70	0.07	1.77	0.06
WB-1110-MC-PCB-06	170	175	172.5	1.67	0.07	1.80	0.06	1.85	0.07	1.77	0.07

Table H.4 (Continued).

Core ID	Top Depth of Interval (mm)	Bottom Depth of interval (mm)	Average Depth of Interval (mm)	^{214}Pb (295 keV) Activity (dpm/g)	^{214}Pb (295 keV) Activity error (dpm/g)	^{214}Pb (351 keV) Activity (dpm/g)	^{214}Pb (351 keV) Activity error (dpm/g)	^{214}Bi Activity (dpm/g)	^{214}Bi Activity error (dpm/g)	^{210}Pb$_{Sup}$ Activity (dpm/g)	^{210}Pb$_{Sup}$ Activity error (dpm/g)
WB-1110-MC-PCB-06	190	195	192.5	1.89	0.07	1.81	0.06	1.80	0.07	1.83	0.07
WB-1110-MC-PCB-06	200	205	202.5	1.93	0.07	2.13	0.06	1.84	0.07	1.97	0.07
WB-1110-MC-PCB-06	220	225	222.5	1.82	0.07	1.89	0.06	1.93	0.07	1.88	0.07

Table H.5. SLRad data, $^{210}Pbs_{up}$ data for core site WB-1114-MC-DSH-08. Sediment cores with sub-sample intervals (mm), and SLRad's activities of ^{214}Pb (295keV), ^{214}Pb (351keV), and ^{214}Bi (351keV) used to calculate $^{210}Pb_{Sup}$. Note: Blank cell denotes no analysis performed.

Core ID	Top Depth of Interval (mm)	Bottom Depth of interval (mm)	Average Depth of Interval (mm)	^{214}Pb (295 keV) Activity (dpm/g)	^{214}Pb (295 keV) Activity error (dpm/g)	^{214}Pb (351 keV) Activity (dpm/g)	^{214}Pb (351 keV) Activity error (dpm/g)	^{214}Bi Activity (dpm/g)	^{214}Bi Activity error (dpm/g)	$^{210}Pb_{Sup}$ Activity (dpm/g)	$^{210}Pb_{Sup}$ Activity error (dpm/g)
WB-1114-MC-DSH-08	0	2	1	1.62	0.13	1.99	0.11	2.09	0.14	1.90	0.13
WB-1114-MC-DSH-08	2	4	3	2.13	0.12	2.12	0.09	2.04	0.12	2.10	0.11
WB-1114-MC-DSH-08	4	6	5	2.00	0.12	2.00	0.09	2.23	0.13	2.08	0.11
WB-1114-MC-DSH-08	6	8	7	1.86	0.11	1.94	0.08	2.21	0.12	2.00	0.11
WB-1114-MC-DSH-08	8	10	9	1.94	0.10	1.79	0.07	0.78	0.06	1.50	0.08
WB-1114-MC-DSH-08	10	12	11	1.24	0.10	1.47	0.08	0.78	0.07	1.16	0.08
WB-1114-MC-DSH-08	12	14	13	1.86	0.11	2.14	0.08	2.14	0.11	2.05	0.10
WB-1114-MC-DSH-08	14	16	15	1.57	0.08	1.02	0.05			1.30	0.06
WB-1114-MC-DSH-08	16	18	17	2.04	0.12	1.95	0.08	1.88	0.11	1.96	0.10
WB-1114-MC-DSH-08	18	20	19	1.01	0.06	1.31	0.06	0.49	0.04	0.94	0.05
WB-1114-MC-DSH-08	24	26	25	1.86	0.10	1.99	0.08	2.14	0.11	2.00	0.09
WB-1114-MC-DSH-08	28	30	29	1.91	0.10	1.82	0.07	2.11	0.11	1.95	0.09
WB-1114-MC-DSH-08	32	34	33	1.94	0.10	1.82	0.07	2.06	0.10	1.94	0.09
WB-1114-MC-DSH-08	36	38	37	2.02	0.10	1.96	0.08	2.27	0.11	2.08	0.09
WB-1114-MC-DSH-08	40	42	41	1.60	0.09	1.89	0.07	2.05	0.10	1.85	0.09
WB-1114-MC-DSH-08	48	50	49	1.63	0.08	1.79	0.07	2.00	0.09	1.81	0.08
WB-1114-MC-DSH-08	70	75	72.5	1.64	0.07	1.95	0.06	1.94	0.07	1.84	0.06
WB-1114-MC-DSH-08	90	95	92.5	1.48	0.06	1.91	0.06	2.03	0.07	1.81	0.06
WB-1114-MC-DSH-08	110	115	112.5	1.84	0.07	2.06	0.06	2.04	0.07	1.98	0.07
WB-1114-MC-DSH-08	130	135	132.5	1.56	0.06	1.83	0.05	2.10	0.07	1.83	0.06
WB-1114-MC-DSH-08	150	155	152.5	1.91	0.07	2.11	0.06	2.34	0.08	2.12	0.07
WB-1114-MC-DSH-08	170	175	172.5	1.67	0.07	2.20	0.06	2.40	0.08	2.09	0.07
WB-1114-MC-DSH-08	180	185	182.5	2.01	0.07	2.18	0.06	2.23	0.07	2.14	0.07

Table H.5 (Continued).

Core ID	Top Depth of Interval (mm)	Bottom Depth of interval (mm)	Average Depth of Interval (mm)	^{214}Pb (295 keV) Activity (dpm/g)	^{214}Pb (295 keV) Activity error (dpm/g)	^{214}Pb (351 keV) Activity (dpm/g)	^{214}Pb (351 keV) Activity error (dpm/g)	^{214}Bi Activity (dpm/g)	^{214}Bi Activity error (dpm/g)	^{210}Pb$_{Sup}$ Activity (dpm/g)	^{210}Pb$_{Sup}$ Activity error (dpm/g)
WB-1114-MC-DSH-08	190	195	192.5	2.03	0.07	2.35	0.06	2.25	0.07	2.21	0.07
WB-1114-MC-DSH-08	200	205	202.5	1.94	0.07	2.19	0.06	2.25	0.07	2.13	0.07
WB-1114-MC-DSH-08	210	215	212.5	1.82	0.07	2.02	0.06	1.57	0.07	1.80	0.07
WB-1114-MC-DSH-08	230	235	232.5	2.15	0.11	1.74	0.08	1.17	0.09	1.68	0.09

Table H.6. SLRad data, $^{210}Pbs_{up}$ data for core site WB-1114-MC-DSH-10. Sediment cores with sub-sample intervals (mm), and SLRad's activities of ^{214}Pb (295keV), ^{214}Pb (351keV), and ^{214}Bi (351keV) used to calculate $^{210}Pb_{Sup}$. Note: Blank cell denotes no analysis performed.

Core ID	Top Depth of Interval (mm)	Bottom Depth of interval (mm)	Average Depth of Interval (mm)	^{214}Pb (295 keV) Activity (dpm/g)	^{214}Pb (295 keV) Activity error (dpm/g)	^{214}Pb (351 keV) Activity (dpm/g)	^{214}Pb (351 keV) Activity error (dpm/g)	^{214}Bi Activity (dpm/g)	^{214}Bi Activity error (dpm/g)	$^{210}Pb_{Sup}$ Activity (dpm/g)	$^{210}Pb_{Sup}$ Activity error (dpm/g)
WB-1114-MC-DSH-10	0	2	1	1.32	0.09	1.58	0.09	1.13	0.10	1.34	0.09
WB-1114-MC-DSH-10	2	4	3	1.40	0.10	1.79	0.10	1.42	0.11	1.54	0.10
WB-1114-MC-DSH-10	4	6	5	1.48	0.10	1.81	0.10	1.83	0.12	1.71	0.11
WB-1114-MC-DSH-10	6	8	7	1.41	0.09	1.76	0.08	1.76	0.11	1.64	0.09
WB-1114-MC-DSH-10	8	10	9	1.72	0.10	1.71	0.08	1.74	0.11	1.72	0.09
WB-1114-MC-DSH-10	10	12	11	1.82	0.10	1.80	0.09	1.55	0.10	1.73	0.10
WB-1114-MC-DSH-10	12	14	13	1.79	0.10	1.94	0.09	1.49	0.10	1.74	0.09
WB-1114-MC-DSH-10	14	16	15	1.50	0.09	1.63	0.08	1.50	0.10	1.54	0.09
WB-1114-MC-DSH-10	16	18	17	1.26	0.08	1.55	0.08	1.26	0.09	1.36	0.08
WB-1114-MC-DSH-10	18	20	19	1.66	0.09	1.70	0.08	1.88	0.10	1.75	0.09
WB-1114-MC-DSH-10	20	22	21	1.36	0.08	1.66	0.08	1.44	0.09	1.49	0.08
WB-1114-MC-DSH-10	24	26	25	1.38	0.08	1.72	0.07	1.48	0.09	1.52	0.08
WB-1114-MC-DSH-10	32	34	33	1.81	0.08	1.78	0.07	1.64	0.09	1.74	0.08
WB-1114-MC-DSH-10	40	42	41	1.70	0.09	1.56	0.07	1.53	0.09	1.60	0.09
WB-1114-MC-DSH-10	48	50	49	1.65	0.08	1.96	0.08	1.77	0.09	1.79	0.08
WB-1114-MC-DSH-10	56	58	57	2.56	0.10	2.43	0.09	2.29	0.11	2.43	0.10
WB-1114-MC-DSH-10	64	66	65	1.88	0.09	1.93	0.08	1.92	0.10	1.91	0.09
WB-1114-MC-DSH-10	72	74	73	2.13	0.09	2.54	0.08	1.98	0.10	2.22	0.09
WB-1114-MC-DSH-10	80	82	81	2.15	0.09	2.14	0.07	2.33	0.10	2.21	0.09
WB-1114-MC-DSH-10	90	95	92.5	2.57	0.08	2.72	0.06	2.71	0.09	2.67	0.08
WB-1114-MC-DSH-10	100	105	102.5	2.24	0.07	2.41	0.06	2.68	0.09	2.44	0.07
WB-1114-MC-DSH-10	110	115	112.5	2.34	0.08	2.44	0.06	2.41	0.08	2.39	0.07
WB-1114-MC-DSH-10	120	125	122.5	2.16	0.07	2.42	0.06	2.45	0.08	2.34	0.07

Table H.6 (Continued).

Core ID	Top Depth of Interval (mm)	Bottom Depth of interval (mm)	Average Depth of Interval (mm)	^{214}Pb (295 keV) Activity (dpm/g)	^{214}Pb (295 keV) Activity error (dpm/g)	^{214}Pb (351 keV) Activity (dpm/g)	^{214}Pb (351 keV) Activity error (dpm/g)	^{214}Bi Activity (dpm/g)	^{214}Bi Activity error (dpm/g)	^{210}Pb$_{Sup}$ Activity (dpm/g)	^{210}Pb$_{Sup}$ Activity error (dpm/g)
WB-1114-MC-DSH-10	130	135	132.5	2.01	0.07	2.10	0.06	1.98	0.07	2.03	0.07
WB-1114-MC-DSH-10	150	155	152.5	2.14	0.07	2.08	0.06	2.02	0.08	2.08	0.07
WB-1114-MC-DSH-10	170	175	172.5	1.91	0.07	2.07	0.06	1.81	0.07	1.93	0.07
WB-1114-MC-DSH-10	190	195	192.5	2.24	0.07	2.26	0.06	2.06	0.08	2.19	0.07
WB-1114-MC-DSH-10	210	215	212.5	2.17	0.07	2.22	0.06	2.00	0.08	2.13	0.07
WB-1114-MC-DSH-10	230	235	232.5	2.17	0.07	1.93	0.06	1.98	0.08	2.03	0.07
WB-1114-MC-DSH-10	250	255	252.5	2.21	0.07	2.04	0.06	2.03	0.07	2.09	0.07
WB-1114-MC-DSH-10	270	275	272.5	1.76	0.06	2.01	0.06	2.01	0.08	1.93	0.07
WB-1114-MC-DSH-10	290	295	292.5	1.60	0.08	1.85	0.07	1.76	0.09	1.74	0.08
WB-1114-MC-DSH-10	310	315	312.5	1.68	0.08	1.81	0.07	1.74	0.09	1.74	0.08

Table H.7. SLRad data, $^{210}Pbs_{up}$ data for core site WB-1114-MC-PCB-06. Sediment cores with sub-sample intervals (mm), and SLRad's activities of ^{214}Pb (295keV), ^{214}Pb (351keV), and ^{214}Bi (351keV) used to calculate $^{210}Pb_{Sup}$. Note: Blank cell denotes no analysis performed.

Core ID	Top Depth of Interval (mm)	Bottom Depth of interval (mm)	Average Depth of Interval (mm)	^{214}Pb (295 keV) Activity (dpm/g)	^{214}Pb (295 keV) Activity error (dpm/g)	^{214}Pb (351 keV) Activity (dpm/g)	^{214}Pb (351 keV) Activity error (dpm/g)	^{214}Bi Activity (dpm/g)	^{214}Bi Activity error (dpm/g)	$^{210}Pb_{Sup}$ Activity (dpm/g)	$^{210}Pb_{Sup}$ Activity error (dpm/g)
WB-1114-MC-PCB-06	0	2	1	0.97	0.08	1.54	0.08	1.18	0.09	1.23	0.08
WB-1114-MC-PCB-06	2	4	3	1.48	0.10	1.56	0.09	1.74	0.12	1.59	0.11
WB-1114-MC-PCB-06	4	6	5	1.44	0.08	1.74	0.08	1.32	0.09	1.50	0.08
WB-1114-MC-PCB-06	6	8	7	1.40	0.09	1.82	0.09	1.97	0.12	1.73	0.10
WB-1114-MC-PCB-06	8	10	9	1.56	0.09	1.84	0.09	1.63	0.10	1.68	0.09
WB-1114-MC-PCB-06	10	12	11	1.23	0.08	1.36	0.07	1.51	0.09	1.37	0.08
WB-1114-MC-PCB-06	12	14	13	1.58	0.08	1.74	0.08	1.64	0.09	1.65	0.08
WB-1114-MC-PCB-06	14	16	15	1.49	0.09	1.62	0.08	1.65	0.10	1.59	0.09
WB-1114-MC-PCB-06	16	18	17	1.40	0.08	1.69	0.08	1.49	0.09	1.53	0.09
WB-1114-MC-PCB-06	18	20	19	1.27	0.08	1.84	0.08	1.63	0.10	1.58	0.09
WB-1114-MC-PCB-06	20	22	21	1.73	0.10	1.64	0.08	1.78	0.11	1.72	0.10
WB-1114-MC-PCB-06	24	26	25	1.30	0.08	1.55	0.08	1.57	0.10	1.47	0.08
WB-1114-MC-PCB-06	32	34	33	2.18	0.10	2.76	0.10	2.69	0.13	2.54	0.11
WB-1114-MC-PCB-06	36	38	37	2.01	0.10	2.69	0.10	2.50	0.12	2.40	0.10
WB-1114-MC-PCB-06	40	42	41	2.65	0.11	3.11	0.11	2.92	0.13	2.89	0.12
WB-1114-MC-PCB-06	48	50	49	1.20	0.07	1.87	0.08	1.66	0.10	1.58	0.08
WB-1114-MC-PCB-06	56	58	57	1.60	0.09	1.43	0.07	1.74	0.10	1.59	0.09
WB-1114-MC-PCB-06	64	66	65	1.47	0.08	1.80	0.08	1.46	0.09	1.58	0.08
WB-1114-MC-PCB-06	70	75	72.5	1.73	0.07	1.76	0.06	1.71	0.07	1.73	0.07
WB-1114-MC-PCB-06	80	85	82.5	1.59	0.06	1.67	0.05	1.79	0.07	1.68	0.06
WB-1114-MC-PCB-06	90	95	92.5	1.68	0.07	1.69	0.05	1.75	0.07	1.71	0.06
WB-1114-MC-PCB-06	100	105	102.5	1.55	0.07	1.64	0.06	1.54	0.07	1.58	0.07
WB-1114-MC-PCB-06	110	115	112.5	1.70	0.06	1.75	0.05	1.81	0.07	1.75	0.06

Table H.7 (Continued).

Core ID	Top Depth of Interval (mm)	Bottom Depth of interval (mm)	Average Depth of Interval (mm)	^{214}Pb (295 keV) Activity (dpm/g)	^{214}Pb (295 keV) Activity error (dpm/g)	^{214}Pb (351 keV) Activity (dpm/g)	^{214}Pb (351 keV) Activity error (dpm/g)	^{214}Bi Activity (dpm/g)	^{214}Bi Activity error (dpm/g)	^{210}Pb$_{Sup}$ Activity (dpm/g)	^{210}Pb$_{Sup}$ Activity error (dpm/g)
WB-1114-MC-PCB-06	120	125	122.5	1.58	0.06	1.66	0.05	1.60	0.07	1.61	0.06
WB-1114-MC-PCB-06	130	135	132.5	1.57	0.06	1.82	0.06	1.82	0.07	1.74	0.06
WB-1114-MC-PCB-06	140	145	142.5	1.94	0.07	1.86	0.06	1.84	0.07	1.88	0.07
WB-1114-MC-PCB-06	150	155	152.5	1.62	0.06	1.62	0.05	1.86	0.07	1.70	0.06
WB-1114-MC-PCB-06	170	175	172.5	1.59	0.06	1.64	0.05	1.62	0.07	1.62	0.06
WB-1114-MC-PCB-06	190	195	192.5	1.74	0.06	1.58	0.05	1.68	0.07	1.67	0.06
WB-1114-MC-PCB-06	210	215	212.5	1.85	0.07	1.64	0.05	1.62	0.07	1.70	0.06
WB-1114-MC-PCB-06	230	235	232.5	1.57	0.06	1.73	0.05	1.66	0.07	1.65	0.06
WB-1114-MC-PCB-06	270	275	272.5	1.36	0.08	1.75	0.08	1.68	0.10	1.60	0.08

Table H.8. SLRad data, $^{210}Pbs_{up}$ data for core site WB-0911-BC-DSH-08. Sediment cores with sub-sample intervals (mm), and SLRad's activities of ^{214}Pb (295keV), ^{214}Pb (351keV), and ^{214}Bi (351keV) used to calculate $^{210}Pb_{Sup}$. Note: Blank cell denotes no analysis performed.

Core ID	Top Depth of Interval (mm)	Bottom Depth of interval (mm)	Average Depth of Interval (mm)	^{214}Pb (295 keV) Activity (dpm/g)	^{214}Pb (295 keV) Activity error (dpm/g)	^{214}Pb (351 keV) Activity (dpm/g)	^{214}Pb (351 keV) Activity error (dpm/g)	^{214}Bi Activity (dpm/g)	^{214}Bi Activity error (dpm/g)	$^{210}Pb_{Sup}$ Activity (dpm/g)	$^{210}Pb_{Sup}$ Activity error (dpm/g)
WB-0911-BC-DSH-08	0	2	1	1.47	0.10	1.22	0.07	0.94	0.07	1.21	0.08
WB-0911-BC-DSH-08	2	4	3	1.39	0.08	1.42	0.07	1.46	0.08	1.42	0.08
WB-0911-BC-DSH-08	4	6	5	1.57	0.08	1.48	0.06	1.32	0.07	1.46	0.07
WB-0911-BC-DSH-08	6	8	7	1.41	0.09	1.36	0.07	1.19	0.07	1.32	0.08
WB-0911-BC-DSH-08	8	10	9	1.68	0.09	1.41	0.07	1.14	0.07	1.41	0.08
WB-0911-BC-DSH-08	10	12	11	1.60	0.09	1.50	0.07	1.14	0.07	1.41	0.08
WB-0911-BC-DSH-08	12	14	13	1.56	0.09	1.39	0.07	1.38	0.08	1.45	0.08
WB-0911-BC-DSH-08	14	16	15	1.76	0.09	1.63	0.07	1.47	0.08	1.62	0.08
WB-0911-BC-DSH-08	16	18	17	1.59	0.09	1.62	0.07	1.53	0.08	1.58	0.08
WB-0911-BC-DSH-08	18	20	19	1.53	0.08	1.85	0.07	1.45	0.08	1.61	0.08
WB-0911-BC-DSH-08	24	26	25	2.41	0.10	2.23	0.08	1.93	0.09	2.19	0.09
WB-0911-BC-DSH-08	26	28	27	2.75	0.11	2.17	0.08	2.18	0.09	2.37	0.09
WB-0911-BC-DSH-08	28	30	29	2.11	0.10	2.06	0.08	2.03	0.09	2.07	0.09
WB-0911-BC-DSH-08	30	35	32.5	1.72	0.07	1.75	0.06	1.63	0.07	1.70	0.07
WB-0911-BC-DSH-08	40	45	42.5	1.65	0.07	2.05	0.06	1.83	0.07	1.84	0.07
WB-0911-BC-DSH-08	50	55	52.5	1.48	0.06	1.49	0.05	1.55	0.07	1.51	0.06
WB-0911-BC-DSH-08	60	65	62.5	1.84	0.07	1.95	0.06	1.85	0.07	1.88	0.07
WB-0911-BC-DSH-08	70	75	72.5	1.78	0.07	1.75	0.06	1.62	0.07	1.71	0.06
WB-0911-BC-DSH-08	80	85	82.5	1.97	0.07	2.10	0.06	1.98	0.07	2.02	0.07
WB-0911-BC-DSH-08	90	95	92.5	2.10	0.07	2.13	0.06	2.11	0.08	2.11	0.07
WB-0911-BC-DSH-08	100	105	102.5	1.97	0.07	1.93	0.06	1.73	0.07	1.88	0.06
WB-0911-BC-DSH-08	110	115	112.5	1.76	0.07	1.61	0.05	1.53	0.06	1.64	0.06
WB-0911-BC-DSH-08	120	125	122.5	2.05	0.07	1.92	0.06	1.79	0.07	1.92	0.07

Table H.8 (Continued).

Core ID	Top Depth of Interval (mm)	Bottom Depth of interval (mm)	Average Depth of Interval (mm)	^{214}Pb (295 keV) Activity (dpm/g)	^{214}Pb (295 keV) Activity error (dpm/g)	^{214}Pb (351 keV) Activity (dpm/g)	^{214}Pb (351 keV) Activity error (dpm/g)	^{214}Bi Activity (dpm/g)	^{214}Bi Activity error (dpm/g)	^{210}Pb$_{Sup}$ Activity (dpm/g)	^{210}Pb$_{Sup}$ Activity error (dpm/g)
WB-0911-BC-DSH-08	130	135	132.5	1.86	0.07	1.76	0.05	1.75	0.07	1.79	0.06
WB-0911-BC-DSH-08	140	145	142.5	2.12	0.07	2.11	0.06	1.90	0.07	2.04	0.07
WB-0911-BC-DSH-08	150	155	152.5	1.62	0.07	1.77	0.06	1.68	0.07	1.69	0.06
WB-0911-BC-DSH-08	170	175	172.5	1.75	0.07	1.93	0.06	1.88	0.07	1.85	0.07
WB-0911-BC-DSH-08	190	195	192.5	1.80	0.07	1.92	0.06	1.94	0.07	1.89	0.07
WB-0911-BC-DSH-08	210	215	212.5	2.32	0.08	2.22	0.06	2.20	0.08	2.25	0.07
WB-0911-BC-DSH-08	230	235	232.5	1.92	0.07	1.88	0.06	1.87	0.07	1.89	0.07
WB-0911-BC-DSH-08	250	255	252.5	2.15	0.07	2.10	0.06	2.16	0.08	2.14	0.07
WB-0911-BC-DSH-08	270	275	272.5	2.00	0.07	2.04	0.06	1.99	0.07	2.01	0.07
WB-0911-BC-DSH-08	290	295	292.5	1.83	0.07	2.04	0.06	1.95	0.07	1.94	0.07

Table H.9. SLRad data, $^{210}Pbs_{up}$ data for core site WB-0911-BC-DSH-10. Sediment cores with sub-sample intervals (mm), and SLRad's activities of ^{214}Pb (295keV), ^{214}Pb (351keV), and ^{214}Bi (351keV) used to calculate $^{210}Pb_{Sup}$. Note: Blank cell denotes no analysis performed.

Core ID	Top Depth of Interval (mm)	Bottom Depth of interval (mm)	Average Depth of Interval (mm)	^{214}Pb (295 keV) Activity (dpm/g)	^{214}Pb (295 keV) Activity error (dpm/g)	^{214}Pb (351 keV) Activity (dpm/g)	^{214}Pb (351 keV) Activity error (dpm/g)	^{214}Bi Activity (dpm/g)	^{214}Bi Activity error (dpm/g)	$^{210}Pb_{Sup}$ Activity (dpm/g)	$^{210}Pb_{Sup}$ Activity error (dpm/g)
WB-0911-BC-DSH-10	0	2	1	1.70	0.11	2.16	0.11	1.83	0.13	1.90	0.12
WB-0911-BC-DSH-10	2	4	3	1.44	0.09	2.17	0.09	1.84	0.11	1.82	0.09
WB-0911-BC-DSH-10	4	6	5	2.07	0.10	2.07	0.08	1.86	0.10	2.00	0.09
WB-0911-BC-DSH-10	6	8	7	2.28	0.10	2.20	0.09	1.93	0.10	2.14	0.10
WB-0911-BC-DSH-10	8	10	9	2.04	0.10	2.11	0.08	2.09	0.11	2.08	0.10
WB-0911-BC-DSH-10	10	12	11	2.01	0.10	2.09	0.08	2.07	0.11	2.06	0.10
WB-0911-BC-DSH-10	12	14	13	1.87	0.09	2.23	0.08	2.15	0.10	2.08	0.09
WB-0911-BC-DSH-10	14	16	15	1.88	0.09	2.05	0.08	2.15	0.11	2.03	0.09
WB-0911-BC-DSH-10	16	18	17	1.78	0.09	2.07	0.08	1.77	0.10	1.87	0.09
WB-0911-BC-DSH-10	18	20	19	2.00	0.09	2.38	0.09	1.91	0.10	2.10	0.09
WB-0911-BC-DSH-10	24	26	25	2.26	0.09	2.62	0.09	2.26	0.10	2.38	0.10
WB-0911-BC-DSH-10	32	34	33	1.99	0.10	2.16	0.09	1.71	0.10	1.96	0.09
WB-0911-BC-DSH-10	40	45	42.5	2.11	0.07	1.84	0.06	1.90	0.07	1.95	0.07
WB-0911-BC-DSH-10	50	55	52.5	2.29	0.08	2.44	0.06	2.42	0.08	2.38	0.07
WB-0911-BC-DSH-10	60	65	62.5	2.20	0.08	2.12	0.06	2.02	0.08	2.11	0.07
WB-0911-BC-DSH-10	70	75	72.5	2.29	0.07	2.52	0.06	2.52	0.08	2.44	0.07
WB-0911-BC-DSH-10	80	85	82.5	2.29	0.08	2.28	0.06	2.35	0.08	2.31	0.07
WB-0911-BC-DSH-10	90	95	92.5	2.43	0.08	2.15	0.06	2.02	0.08	2.20	0.07
WB-0911-BC-DSH-10	110	115	112.5	2.36	0.07	2.32	0.06	2.23	0.08	2.30	0.07
WB-0911-BC-DSH-10	130	135	132.5	2.19	0.07	2.19	0.06	2.02	0.07	2.13	0.07
WB-0911-BC-DSH-10	150	155	152.5	1.88	0.07	2.05	0.06	1.93	0.07	1.95	0.07
WB-0911-BC-DSH-10	170	175	172.5	1.98	0.07	1.92	0.06	1.95	0.08	1.95	0.07
WB-0911-BC-DSH-10	190	195	192.5	1.94	0.07	2.08	0.06	1.97	0.08	1.99	0.07

Table H.9 (Continued).

Core ID	Top Depth of Interval (mm)	Bottom Depth of interval (mm)	Average Depth of Interval (mm)	^{214}Pb (295 keV) Activity (dpm/g)	^{214}Pb (295 keV) Activity error (dpm/g)	^{214}Pb (351 keV) Activity (dpm/g)	^{214}Pb (351 keV) Activity error (dpm/g)	^{214}Bi Activity (dpm/g)	^{214}Bi Activity error (dpm/g)	^{210}Pb$_{Sup}$ Activity (dpm/g)	^{210}Pb$_{Sup}$ Activity error (dpm/g)
WB-0911-BC-DSH-10	210	215	212.5	2.05	0.07	2.06	0.06	2.13	0.08	2.08	0.07
WB-0911-BC-DSH-10	230	235	232.5	1.81	0.07	2.08	0.06	2.06	0.08	1.98	0.07
WB-0911-BC-DSH-10	250	255	252.5	1.97	0.07	1.98	0.06	1.93	0.07	1.96	0.06
WB-0911-BC-DSH-10	270	275	272.5	1.84	0.07	1.96	0.06	1.97	0.07	1.92	0.07
WB-0911-BC-DSH-10	310	315	312.5	1.34	0.07	1.08	0.05	1.84	0.09	1.42	0.07

Table H.10. SLRad data, $^{210}Pbs_{up}$ data for core site WB-0911-MC-PCB-06. Sediment cores with sub-sample intervals (mm), and SLRad's activities of ^{214}Pb (295keV), ^{214}Pb (351keV), and ^{214}Bi (351keV) used to calculate $^{210}Pb_{Sup}$. Note: Blank cell denotes no analysis performed.

Core ID	Top Depth of Interval (mm)	Bottom Depth of interval (mm)	Average Depth of Interval (mm)	^{214}Pb (295 keV) Activity (dpm/g)	^{214}Pb (295 keV) Activity error (dpm/g)	^{214}Pb (351 keV) Activity (dpm/g)	^{214}Pb (351 keV) Activity error (dpm/g)	^{214}Bi Activity (dpm/g)	^{214}Bi Activity error (dpm/g)	$^{210}Pb_{Sup}$ Activity (dpm/g)	$^{210}Pb_{Sup}$ Activity error (dpm/g)
WB-0911-MC-PCB-06	0	2	1	1.39	0.11	2.14	0.13	1.58	0.13	1.70	0.13
WB-0911-MC-PCB-06	2	4	3	1.12	0.11	1.94	0.13	1.83	0.16	1.63	0.13
WB-0911-MC-PCB-06	4	6	5	1.64	0.10	1.77	0.10	1.77	0.12	1.72	0.11
WB-0911-MC-PCB-06	6	8	7	1.17	0.09	1.96	0.10	1.91	0.13	1.68	0.11
WB-0911-MC-PCB-06	8	10	9	1.61	0.10	1.95	0.09	2.10	0.12	1.89	0.10
WB-0911-MC-PCB-06	10	12	11	2.02	0.11	2.23	0.10	2.14	0.12	2.13	0.11
WB-0911-MC-PCB-06	12	14	13	1.79	0.09	1.97	0.08	2.09	0.11	1.95	0.10
WB-0911-MC-PCB-06	14	16	15	1.66	0.10	2.12	0.10	1.95	0.12	1.91	0.10
WB-0911-MC-PCB-06	16	18	17	1.92	0.10	2.21	0.09	1.86	0.11	1.99	0.10
WB-0911-MC-PCB-06	18	20	19	1.95	0.10	1.90	0.08	2.18	0.11	2.01	0.10
WB-0911-MC-PCB-06	24	26	25	1.43	0.09	1.96	0.09	1.94	0.11	1.78	0.09
WB-0911-MC-PCB-06	32	34	33	1.31	0.08	1.63	0.07	1.68	0.10	1.54	0.08
WB-0911-MC-PCB-06	48	50	49	1.29	0.08	1.53	0.07	1.62	0.09	1.48	0.08
WB-0911-MC-PCB-06	70	75	72.5	1.75	0.07	1.91	0.06	1.74	0.07	1.80	0.06
WB-0911-MC-PCB-06	90	95	92.5	1.94	0.07	1.92	0.06	1.74	0.07	1.87	0.07
WB-0911-MC-PCB-06	110	115	112.5	1.61	0.06	1.78	0.05	1.66	0.07	1.68	0.06
WB-0911-MC-PCB-06	130	135	132.5	1.70	0.06	1.71	0.05	2.01	0.08	1.81	0.06
WB-0911-MC-PCB-06	150	155	152.5	1.63	0.06	1.77	0.05	1.81	0.07	1.74	0.06
WB-0911-MC-PCB-06	170	175	172.5	1.66	0.06	1.75	0.05	1.88	0.07	1.76	0.06
WB-0911-MC-PCB-06	190	195	192.5	1.60	0.06	1.67	0.05	1.66	0.07	1.64	0.06
WB-0911-MC-PCB-06	200	205	202.5	1.66	0.06	1.82	0.05	1.82	0.07	1.77	0.06
WB-0911-MC-PCB-06	210	215	212.5	1.71	0.06	1.72	0.05	1.78	0.07	1.74	0.06
WB-0911-MC-PCB-06	220	225	222.5	1.64	0.06	1.62	0.05	1.64	0.07	1.63	0.06

Table H.10 (Continued).

Core ID	Top Depth of Interval (mm)	Bottom Depth of interval (mm)	Average Depth of Interval (mm)	^{214}Pb (295 keV) Activity (dpm/g)	^{214}Pb (295 keV) Activity error (dpm/g)	^{214}Pb (351 keV) Activity (dpm/g)	^{214}Pb (351 keV) Activity error (dpm/g)	^{214}Bi Activity (dpm/g)	^{214}Bi Activity error (dpm/g)	^{210}Pb$_{Sup}$ Activity (dpm/g)	^{210}Pb$_{Sup}$ Activity error (dpm/g)
WB-0911-MC-PCB-06	230	235	232.5	1.29	0.07	1.57	0.07	1.40	0.08	1.42	0.07

Table H.11. SLRad data, $^{210}Pbs_{up}$ data for core site WB-0812-MC-DSH-08. Sediment cores with sub-sample intervals (mm), and SLRad's activities of ^{214}Pb (295keV), ^{214}Pb (351keV), and ^{214}Bi (351keV) used to calculate $^{210}Pb_{Sup}$. Note: Blank cell denotes no analysis performed.

Core ID	Top Depth of Interval (mm)	Bottom Depth of interval (mm)	Average Depth of Interval (mm)	^{214}Pb (295 keV) Activity (dpm/g)	^{214}Pb (295 keV) Activity error (dpm/g)	^{214}Pb (351 keV) Activity (dpm/g)	^{214}Pb (351 keV) Activity error (dpm/g)	^{214}Bi Activity (dpm/g)	^{214}Bi Activity error (dpm/g)	$^{210}Pb_{Sup}$ Activity (dpm/g)	$^{210}Pb_{Sup}$ Activity error (dpm/g)
WB-0812-MC-DSH-08	0	2	1	2.41	0.14	2.06	0.08	1.84	0.10	2.10	0.11
WB-0812-MC-DSH-08	2	4	3	3.12	0.16	2.04	0.08	1.89	0.10	2.35	0.11
WB-0812-MC-DSH-08	4	6	5	2.44	0.13	2.05	0.08	1.63	0.08	2.04	0.10
WB-0812-MC-DSH-08	6	8	7	2.79	0.16	1.87	0.08	1.90	0.10	2.19	0.12
WB-0812-MC-DSH-08	8	10	9	2.54	0.13	1.45	0.07	1.50	0.08	1.83	0.10
WB-0812-MC-DSH-08	10	12	11	1.89	0.11	1.58	0.07	1.54	0.08	1.67	0.09
WB-0812-MC-DSH-08	12	14	13	2.92	0.15	1.61	0.07	1.74	0.09	2.09	0.11
WB-0812-MC-DSH-08	14	16	15	2.38	0.13	1.85	0.08	1.80	0.09	2.01	0.10
WB-0812-MC-DSH-08	16	18	17	3.17	0.15	2.03	0.08	1.76	0.09	2.32	0.11
WB-0812-MC-DSH-08	18	20	19	2.85	0.14	1.85	0.08	1.76	0.09	2.16	0.10
WB-0812-MC-DSH-08	30	32	31	2.39	0.13	1.83	0.08	1.82	0.09	2.01	0.10
WB-0812-MC-DSH-08	50	55	52.5	1.82	0.07	0.98	0.04	0.43	0.03	1.08	0.05
WB-0812-MC-DSH-08	70	75	72.5	2.48	0.09	2.69	0.07	1.76	0.06	2.31	0.08
WB-0812-MC-DSH-08	90	95	92.5	2.43	0.09	2.78	0.08	1.78	0.06	2.33	0.08
WB-0812-MC-DSH-08	110	115	112.5	1.70	0.07	1.43	0.05	1.02	0.05	1.38	0.06
WB-0812-MC-DSH-08	130	135	132.5	1.80	0.10	1.87	0.08	0.87	0.06	1.51	0.08
WB-0812-MC-DSH-08	150	155	152.5	0.44	0.04	0.62	0.04	0.45	0.03	0.50	0.04
WB-0812-MC-DSH-08	170	175	172.5	2.51	0.09	2.96	0.08	1.90	0.07	2.46	0.08
WB-0812-MC-DSH-08	190	195	192.5	2.47	0.12	1.80	0.08	0.81	0.00	1.69	0.07
WB-0812-MC-DSH-08	210	215	212.5	1.15	0.08	1.00	0.06	0.45	0.00	0.87	0.05
WB-0812-MC-DSH-08	230	235	232.5	2.35	0.12	2.66	0.10	1.26	0.00	2.09	0.07
WB-0812-MC-DSH-08	265	270	267.5	2.54	0.12	2.29	0.09	1.31	0.00	2.05	0.07
WB-0812-MC-DSH-08	285	290	287.5	2.41	0.12	3.00	0.11	1.03	0.00	2.15	0.08

Table H.12. SLRad data, $^{210}Pbs_{up}$ data for core site WB-0812-MC-DSH-10. Sediment cores with sub-sample intervals (mm), and SLRad's activities of ^{214}Pb (295keV), ^{214}Pb (351keV), and ^{214}Bi (351keV) used to calculate $^{210}Pb_{Sup}$. Note: Blank cell denotes no analysis performed.

Core ID	Top Depth of Interval (mm)	Bottom Depth of interval (mm)	Average Depth of Interval (mm)	^{214}Pb (295 keV) Activity (dpm/g)	^{214}Pb (295 keV) Activity error (dpm/g)	^{214}Pb (351 keV) Activity (dpm/g)	^{214}Pb (351 keV) Activity error (dpm/g)	^{214}Bi Activity (dpm/g)	^{214}Bi Activity error (dpm/g)	$^{210}Pb_{Sup}$ Activity (dpm/g)	$^{210}Pb_{Sup}$ Activity error (dpm/g)
WB-0812-MC-DSH-10	0	2	1	1.87	0.10	2.07	0.09	1.79	0.10	1.91	0.10
WB-0812-MC-DSH-10	2	4	3	1.55	0.09	2.10	0.09	2.18	0.11	1.94	0.10
WB-0812-MC-DSH-10	4	6	5	2.02	0.10	2.27	0.09	2.12	0.11	2.14	0.10
WB-0812-MC-DSH-10	6	8	7	2.25	0.11	2.20	0.09	2.22	0.12	2.23	0.11
WB-0812-MC-DSH-10	8	10	9	2.32	0.10	2.76	0.09	2.16	0.11	2.41	0.10
WB-0812-MC-DSH-10	10	12	11	2.46	0.13	2.86	0.12	2.45	0.14	2.59	0.13
WB-0812-MC-DSH-10	12	14	13	2.44	0.10	3.00	0.09	2.73	0.11	2.72	0.10
WB-0812-MC-DSH-10	14	16	15	2.75	0.11	2.97	0.10	2.64	0.12	2.79	0.11
WB-0812-MC-DSH-10	16	18	17	2.42	0.10	2.87	0.09	2.54	0.11	2.61	0.10
WB-0812-MC-DSH-10	18	20	19	2.70	0.11	3.12	0.10	2.95	0.12	2.92	0.11
WB-0812-MC-DSH-10	20	22	21	2.94	0.11	3.72	0.11	3.18	0.13	3.28	0.12
WB-0812-MC-DSH-10	22	24	23	3.15	0.12	3.68	0.11	3.13	0.13	3.32	0.12
WB-0812-MC-DSH-10	24	26	25	2.23	0.10	2.99	0.10	2.51	0.12	2.58	0.10
WB-0812-MC-DSH-10	26	28	27	2.35	0.09	2.43	0.08	2.26	0.10	2.35	0.09
WB-0812-MC-DSH-10	28	30	29	1.75	0.09	2.09	0.08	2.07	0.11	1.97	0.09
WB-0812-MC-DSH-10	30	35	32.5	2.37	0.08	2.53	0.07	2.44	0.09	2.45	0.08
WB-0812-MC-DSH-10	35	40	37.5	1.49	0.06	1.98	0.06	1.81	0.08	1.76	0.07
WB-0812-MC-DSH-10	40	45	42.5	1.86	0.07	1.99	0.06	1.85	0.07	1.90	0.07
WB-0812-MC-DSH-10	45	50	47.5	1.84	0.07	1.86	0.06	1.84	0.07	1.84	0.07
WB-0812-MC-DSH-10	50	55	52.5	1.81	0.07	2.28	0.07	2.23	0.08	2.11	0.07
WB-0812-MC-DSH-10	55	60	57.5	1.92	0.07	2.05	0.06	1.95	0.08	1.97	0.07
WB-0812-MC-DSH-10	70	75	72.5	2.48	0.08	2.25	0.06	2.14	0.08	2.29	0.07
WB-0812-MC-DSH-10	80	85	82.5	2.24	0.07	2.29	0.06	2.13	0.08	2.22	0.07

Table H.12 (Continued).

Core ID	Top Depth of Interval (mm)	Bottom Depth of interval (mm)	Average Depth of Interval (mm)	^{214}Pb (295 keV) Activity (dpm/g)	^{214}Pb (295 keV) Activity error (dpm/g)	^{214}Pb (351 keV) Activity (dpm/g)	^{214}Pb (351 keV) Activity error (dpm/g)	^{214}Bi Activity (dpm/g)	^{214}Bi Activity error (dpm/g)	^{210}Pb$_{Sup}$ Activity (dpm/g)	^{210}Pb$_{Sup}$ Activity error (dpm/g)
WB-0812-MC-DSH-10	90	95	92.5	2.20	0.07	2.41	0.06	2.26	0.08	2.29	0.07
WB-0812-MC-DSH-10	100	105	102.5	1.85	0.07	2.04	0.06	1.96	0.07	1.95	0.07
WB-0812-MC-DSH-10	110	115	112.5	2.10	0.07	2.15	0.06	2.19	0.08	2.15	0.07
WB-0812-MC-DSH-10	130	135	132.5	1.43	0.07	1.81	0.06	1.55	0.08	1.60	0.07
WB-0812-MC-DSH-10	150	155	152.5	2.01	0.07	1.96	0.05	1.81	0.07	1.92	0.06
WB-0812-MC-DSH-10	170	175	172.5	1.45	0.07	1.59	0.06	1.46	0.08	1.50	0.07
WB-0812-MC-DSH-10	190	195	192.5	2.14	0.07	2.00	0.06	2.12	0.08	2.09	0.07
WB-0812-MC-DSH-10	210	215	212.5	1.93	0.12	1.94	0.11	1.88	0.13	1.91	0.12
WB-0812-MC-DSH-10	230	235	232.5	2.06	0.07	2.08	0.06	2.24	0.08	2.13	0.07
WB-0812-MC-DSH-10	250	255	252.5	1.74	0.11	1.97	0.10	1.56	0.12	1.76	0.11
WB-0812-MC-DSH-10	270	275	272.5	1.93	0.07	2.08	0.06	2.00	0.08	2.01	0.07
WB-0812-MC-DSH-10	310	315	312.5	1.54	0.07	1.75	0.07	1.79	0.09	1.69	0.08

Table H.13. SLRad data, $^{210}Pbs_{up}$ data for core site WB-0812-MC-PCB-06. Sediment cores with sub-sample intervals (mm), and SLRad's activities of ^{214}Pb (295keV), ^{214}Pb (351keV), and ^{214}Bi (351keV) used to calculate $^{210}Pb_{Sup}$. Note: Blank cell denotes no analysis performed.

Core ID	Top Depth of Interval (mm)	Bottom Depth of interval (mm)	Average Depth of Interval (mm)	^{214}Pb (295 keV) Activity (dpm/g)	^{214}Pb (295 keV) Activity error (dpm/g)	^{214}Pb (351 keV) Activity (dpm/g)	^{214}Pb (351 keV) Activity error (dpm/g)	^{214}Bi Activity (dpm/g)	^{214}Bi Activity error (dpm/g)	$^{210}Pb_{Sup}$ Activity (dpm/g)	$^{210}Pb_{Sup}$ Activity error (dpm/g)
WB-0812-MC-PCB-06	0	2	1	1.28	0.08	1.59	0.08	1.39	0.09	1.42	0.08
WB-0812-MC-PCB-06	2	4	3	1.54	0.09	1.42	0.07	1.77	0.10	1.58	0.09
WB-0812-MC-PCB-06	4	6	5	1.31	0.08	1.67	0.08	1.64	0.10	1.54	0.09
WB-0812-MC-PCB-06	6	8	7	1.46	0.08	1.62	0.07	1.55	0.09	1.54	0.08
WB-0812-MC-PCB-06	8	10	9	1.59	0.09	1.54	0.08	1.50	0.10	1.54	0.09
WB-0812-MC-PCB-06	10	12	11	1.58	0.08	1.70	0.07	1.34	0.08	1.54	0.08
WB-0812-MC-PCB-06	12	14	13	1.67	0.10	1.75	0.09	1.39	0.10	1.60	0.09
WB-0812-MC-PCB-06	14	16	15	1.53	0.08	1.76	0.07	1.56	0.09	1.61	0.08
WB-0812-MC-PCB-06	16	18	17	1.72	0.09	2.05	0.08	1.42	0.09	1.73	0.09
WB-0812-MC-PCB-06	18	20	19	1.50	0.08	2.01	0.08	1.67	0.09	1.73	0.08
WB-0812-MC-PCB-06	24	26	25	1.96	0.10	2.16	0.09	1.93	0.10	2.02	0.10
WB-0812-MC-PCB-06	30	32	31	2.24	0.10	2.40	0.09	2.14	0.11	2.26	0.10
WB-0812-MC-PCB-06	50	55	52.5	2.02	0.07	1.70	0.05	1.72	0.07	1.81	0.06
WB-0812-MC-PCB-06	70	75	72.5	1.36	0.06	1.72	0.05	1.54	0.07	1.54	0.06
WB-0812-MC-PCB-06	90	95	92.5	1.54	0.06	1.74	0.05	1.64	0.07	1.64	0.06
WB-0812-MC-PCB-06	110	115	112.5	1.70	0.06	1.72	0.05	1.81	0.07	1.74	0.06
WB-0812-MC-PCB-06	130	135	132.5	1.81	0.06	3.31	0.07	1.84	0.07	2.32	0.07
WB-0812-MC-PCB-06	150	155	152.5	1.84	0.07	1.64	0.05	1.71	0.07	1.73	0.06
WB-0812-MC-PCB-06	170	175	172.5	1.63	0.06	1.74	0.05	1.57	0.07	1.65	0.06
WB-0812-MC-PCB-06	190	195	192.5	1.38	0.06	1.60	0.05	1.55	0.07	1.51	0.06
WB-0812-MC-PCB-06	210	215	212.5	1.44	0.06	1.70	0.05	1.65	0.07	1.60	0.06
WB-0812-MC-PCB-06	230	235	232.5	1.45	0.06	1.61	0.05	1.58	0.07	1.55	0.06

Table H.14. SLRad data, $^{210}Pbs_{up}$ data for core site WB-1012-MC-04. Sediment cores with sub-sample intervals (mm), and SLRad's activities of ^{214}Pb (295keV), ^{214}Pb (351keV), and ^{214}Bi (351keV) used to calculate $^{210}Pb_{Sup}$. Note: Blank cell denotes no analysis performed.

Core ID	Top Depth of Interval (mm)	Bottom Depth of interval (mm)	Average Depth of Interval (mm)	^{214}Pb (295 keV) Activity (dpm/g)	^{214}Pb (295 keV) Activity error (dpm/g)	^{214}Pb (351 keV) Activity (dpm/g)	^{214}Pb (351 keV) Activity error (dpm/g)	^{214}Bi Activity (dpm/g)	^{214}Bi Activity error (dpm/g)	$^{210}Pb_{Sup}$ Activity (dpm/g)	$^{210}Pb_{Sup}$ Activity error (dpm/g)
WB-1012-MC-04	0	2	1	0.82	0.07	1.13	0.07	1.46	0.10	1.13	0.08
WB-1012-MC-04	2	4	3	1.27	0.08	1.08	0.06	1.19	0.09	1.18	0.08
WB-1012-MC-04	4	6	5	1.24	0.08	1.20	0.07	1.18	0.08	1.21	0.08
WB-1012-MC-04	6	8	7	1.24	0.08	1.28	0.07	1.39	0.09	1.30	0.08
WB-1012-MC-04	8	10	9	1.25	0.08	1.05	0.06	1.01	0.08	1.10	0.07
WB-1012-MC-04	10	12	11	1.14	0.07	1.23	0.07	1.19	0.08	1.19	0.07
WB-1012-MC-04	12	14	13	1.13	0.07	1.01	0.06	0.74	0.06	0.96	0.06
WB-1012-MC-04	14	16	15	0.91	0.06	1.18	0.06	1.04	0.07	1.05	0.07
WB-1012-MC-04	16	18	17	1.07	0.07	1.24	0.06	1.15	0.08	1.15	0.07
WB-1012-MC-04	18	20	19	1.07	0.07	1.33	0.07	1.16	0.08	1.19	0.07
WB-1012-MC-04	30	35	32.5	0.80	0.05	0.91	0.05	1.04	0.06	0.92	0.05
WB-1012-MC-04	50	55	52.5	0.94	0.05	0.89	0.04	1.04	0.06	0.96	0.05
WB-1012-MC-04	70	75	72.5	0.78	0.05	1.07	0.05	0.86	0.06	0.90	0.05
WB-1012-MC-04	90	95	92.5	0.86	0.05	0.92	0.04	1.00	0.06	0.93	0.05
WB-1012-MC-04	130	135	132.5	0.99	0.05	1.06	0.05	1.06	0.06	1.04	0.05
WB-1012-MC-04	170	175	172.5	1.09	0.06	1.05	0.05	0.89	0.06	1.01	0.05
WB-1012-MC-04	210	215	212.5	0.95	0.05	0.99	0.04	1.15	0.06	1.03	0.05
WB-1012-MC-04	250	255	252.5	0.94	0.05	1.06	0.04	1.06	0.06	1.02	0.05
WB-1012-MC-04	290	295	292.5	1.10	0.05	1.12	0.04	1.17	0.05	1.13	0.05

Table H.15. SLRad data, $^{210}Pbs_{up}$ data for core site WB-0813-MC-04. Sediment cores with sub-sample intervals (mm), and SLRad's activities of ^{214}Pb (295keV), ^{214}Pb (351keV), and ^{214}Bi (351keV) used to calculate $^{210}Pb_{Sup}$. Note: Blank cell denotes no analysis performed.

Core ID	Top Depth of Interval (mm)	Bottom Depth of interval (mm)	Average Depth of Interval (mm)	^{214}Pb (295 keV) Activity (dpm/g)	^{214}Pb (295 keV) Activity error (dpm/g)	^{214}Pb (351 keV) Activity (dpm/g)	^{214}Pb (351 keV) Activity error (dpm/g)	^{214}Bi Activity (dpm/g)	^{214}Bi Activity error (dpm/g)	$^{210}Pb_{Sup}$ Activity (dpm/g)	$^{210}Pb_{Sup}$ Activity error (dpm/g)
WB-0813-MC-04	0	2	1	1.35	0.10	1.35	0.09	1.14	0.10	1.28	0.10
WB-0813-MC-04	2	4	3	0.87	0.07	1.34	0.08	1.20	0.10	1.13	0.08
WB-0813-MC-04	4	6	5	0.84	0.07	0.94	0.06	0.93	0.08	0.90	0.07
WB-0813-MC-04	6	8	7	0.96	0.07	1.06	0.06	0.84	0.07	0.95	0.07
WB-0813-MC-04	8	10	9	0.83	0.06	1.02	0.06	0.86	0.06	0.90	0.06
WB-0813-MC-04	10	14	12	0.96	0.05	1.00	0.05	1.05	0.06	1.01	0.05
WB-0813-MC-04	14	16	15	0.98	0.07	0.99	0.06	0.92	0.07	0.96	0.07
WB-0813-MC-04	16	18	17	1.00	0.07	1.19	0.06	1.15	0.08	1.11	0.07

Table H.16. SLRad data, $^{210}Pbs_{up}$ data for core site WB-0813-MC-DSH-08. Sediment cores with sub-sample intervals (mm), and SLRad's activities of ^{214}Pb (295keV), ^{214}Pb (351keV), and ^{214}Bi (351keV) used to calculate $^{210}Pb_{Sup}$. Note: Blank cell denotes no analysis performed.

Core ID	Top Depth of Interval (mm)	Bottom Depth of interval (mm)	Average Depth of Interval (mm)	^{214}Pb (295 keV) Activity (dpm/g)	^{214}Pb (295 keV) Activity error (dpm/g)	^{214}Pb (351 keV) Activity (dpm/g)	^{214}Pb (351 keV) Activity error (dpm/g)	^{214}Bi Activity (dpm/g)	^{214}Bi Activity error (dpm/g)	$^{210}Pb_{Sup}$ Activity (dpm/g)	$^{210}Pb_{Sup}$ Activity error (dpm/g)
WB-0813-MC-DSH-08	0	2	1	1.54	0.10	1.19	0.07	1.10	0.08	1.27	0.08
WB-0813-MC-DSH-08	2	4	3	1.63	0.09	1.46	0.07	1.39	0.08	1.49	0.08
WB-0813-MC-DSH-08	4	6	5	1.45	0.09	1.36	0.07	1.32	0.08	1.38	0.08
WB-0813-MC-DSH-08	6	8	7	1.66	0.10	1.42	0.07	1.51	0.08	1.53	0.08
WB-0813-MC-DSH-08	8	10	9	1.55	0.09	1.37	0.06	1.16	0.07	1.36	0.07
WB-0813-MC-DSH-08	10	12	11	1.18	0.08	1.28	0.06	1.34	0.08	1.27	0.07
WB-0813-MC-DSH-08	12	14	13	1.49	0.08	1.40	0.06	1.48	0.08	1.46	0.08
WB-0813-MC-DSH-08	14	16	15	1.43	0.09	1.59	0.07	1.49	0.08	1.50	0.08
WB-0813-MC-DSH-08	16	18	17	1.57	0.09	1.50	0.07	1.27	0.07	1.45	0.08
WB-0813-MC-DSH-08	18	20	19	1.41	0.08	1.44	0.07	1.43	0.08	1.42	0.08

Table H.17. SLRad data, $^{210}Pbs_{up}$ data for core site WB-0813-MC-DSH-10. Sediment cores with sub-sample intervals (mm), and SLRad's activities of ^{214}Pb (295keV), ^{214}Pb (351keV), and ^{214}Bi (351keV) used to calculate $^{210}Pb_{Sup}$. Note: Blank cell denotes no analysis performed.

Core ID	Top Depth of Interval (mm)	Bottom Depth of interval (mm)	Average Depth of Interval (mm)	^{214}Pb (295 keV) Activity (dpm/g)	^{214}Pb (295 keV) Activity error (dpm/g)	^{214}Pb (351 keV) Activity (dpm/g)	^{214}Pb (351 keV) Activity error (dpm/g)	^{214}Bi Activity (dpm/g)	^{214}Bi Activity error (dpm/g)	$^{210}Pb_{Sup}$ Activity (dpm/g)	$^{210}Pb_{Sup}$ Activity error (dpm/g)
WB-0813-MC-DSH-10	0	2	1	1.84	0.09	1.74	0.08	1.88	0.10	1.82	0.09
WB-0813-MC-DSH-10	2	4	3	1.67	0.09	2.06	0.09	1.62	0.10	1.78	0.09
WB-0813-MC-DSH-10	4	6	5	1.67	0.09	2.18	0.09	1.63	0.09	1.83	0.09
WB-0813-MC-DSH-10	6	8	7	1.93	0.09	2.00	0.08	1.92	0.10	1.95	0.09
WB-0813-MC-DSH-10	8	10	9	1.66	0.09	2.17	0.08	1.81	0.10	1.88	0.09
WB-0813-MC-DSH-10	10	12	11	1.98	0.09	2.01	0.08	1.72	0.09	1.90	0.09
WB-0813-MC-DSH-10	12	14	13	1.80	0.09	2.09	0.08	1.36	0.09	1.75	0.09
WB-0813-MC-DSH-10	14	16	15	1.89	0.08	2.08	0.07	1.87	0.09	1.95	0.08
WB-0813-MC-DSH-10	16	18	17	1.72	0.09	1.97	0.08	1.85	0.10	1.85	0.09
WB-0813-MC-DSH-10	18	20	19	2.21	0.09	2.57	0.09	2.53	0.11	2.44	0.10

Table H.18. SLRad data, $^{210}Pbs_{up}$ data for core site WB-0813-MC-PCB-06. Sediment cores with sub-sample intervals (mm), and SLRad's activities of ^{214}Pb (295keV), ^{214}Pb (351keV), and ^{214}Bi (351keV) used to calculate $^{210}Pb_{Sup}$. Note: Blank cell denotes no analysis performed.

Core ID	Top Depth of Interval (mm)	Bottom Depth of interval (mm)	Average Depth of Interval (mm)	^{214}Pb (295 keV) Activity (dpm/g)	^{214}Pb (295 keV) Activity error (dpm/g)	^{214}Pb (351 keV) Activity (dpm/g)	^{214}Pb (351 keV) Activity error (dpm/g)	^{214}Bi Activity (dpm/g)	^{214}Bi Activity error (dpm/g)	$^{210}Pb_{Sup}$ Activity (dpm/g)	$^{210}Pb_{Sup}$ Activity error (dpm/g)
WB-0813-MC-PCB-06	0	4	2	1.68	0.08	1.61	0.06	1.55	0.08	1.61	0.07
WB-0813-MC-PCB-06	4	6	5	1.59	0.10	1.51	0.07	1.57	0.09	1.56	0.09
WB-0813-MC-PCB-06	6	8	7	1.60	0.09	1.57	0.07	1.42	0.08	1.53	0.08
WB-0813-MC-PCB-06	8	10	9	1.66	0.09	1.60	0.07	1.41	0.08	1.56	0.08
WB-0813-MC-PCB-06	10	12	11	1.44	0.09	1.53	0.07	1.52	0.08	1.49	0.08
WB-0813-MC-PCB-06	12	14	13	1.34	0.08	1.68	0.07	1.36	0.08	1.46	0.08
WB-0813-MC-PCB-06	14	16	15	1.58	0.09	1.45	0.07	1.51	0.08	1.51	0.08
WB-0813-MC-PCB-06	16	18	17	1.54	0.09	1.71	0.08	1.36	0.08	1.54	0.08
WB-0813-MC-PCB-06	20	22	21	1.75	0.09	1.64	0.07	1.53	0.08	1.64	0.08

Table H.19. SLRad data, $^{210}Pbs_{up}$ data for core site WB-0814-MC-04. Sediment cores with sub-sample intervals (mm), and SLRad's activities of ^{214}Pb (295keV), ^{214}Pb (351keV), and ^{214}Bi (351keV) used to calculate $^{210}Pb_{Sup}$. Note: Blank cell denotes no analysis performed.

Core ID	Top Depth of Interval (mm)	Bottom Depth of interval (mm)	Average Depth of Interval (mm)	^{214}Pb (295 keV) Activity (dpm/g)	^{214}Pb (295 keV) Activity error (dpm/g)	^{214}Pb (351 keV) Activity (dpm/g)	^{214}Pb (351 keV) Activity error (dpm/g)	^{214}Bi Activity (dpm/g)	^{214}Bi Activity error (dpm/g)	$^{210}Pb_{Sup}$ Activity (dpm/g)	$^{210}Pb_{Sup}$ Activity error (dpm/g)
WB-0814-MC-04	0	2	1	1.05	0.08	1.14	0.07	1.24	0.10	1.14	0.08
WB-0814-MC-04	2	4	3	1.19	0.09	0.97	0.07	1.27	0.10	1.15	0.09
WB-0814-MC-04	4	6	5	0.94	0.07	1.35	0.08	1.18	0.09	1.16	0.08
WB-0814-MC-04	6	8	7	1.25	0.08	1.05	0.07	1.24	0.09	1.18	0.08
WB-0814-MC-04	8	10	9	0.92	0.07	1.30	0.07	1.38	0.09	1.20	0.08
WB-0814-MC-04	10	12	11	1.08	0.07	1.33	0.07	1.03	0.08	1.15	0.07
WB-0814-MC-04	12	14	13	1.28	0.08	1.40	0.07	1.20	0.08	1.29	0.07
WB-0814-MC-04	14	16	15	1.21	0.07	1.08	0.06	1.33	0.08	1.21	0.07
WB-0814-MC-04	16	18	17	1.06	0.07	1.46	0.07	0.94	0.07	1.15	0.07
WB-0814-MC-04	18	20	19	1.06	0.06	1.10	0.06	0.92	0.07	1.02	0.06
WB-0814-MC-04	20	22	21	0.93	0.06	1.03	0.06	1.05	0.07	1.00	0.06
WB-0814-MC-04	24	26	25	0.97	0.06	1.18	0.06	0.93	0.07	1.03	0.06
WB-0814-MC-04	30	32	31	1.07	0.07	1.13	0.06	0.97	0.07	1.05	0.07
WB-0814-MC-04	36	38	37	0.87	0.06	1.03	0.06	0.77	0.06	0.89	0.06
WB-0814-MC-04	40	45	42.5	0.79	0.04	0.92	0.04	0.97	0.05	0.89	0.05
WB-0814-MC-04	50	55	52.5	0.85	0.05	1.03	0.04	1.07	0.06	0.98	0.05
WB-0814-MC-04	70	75	72.5	0.92	0.05	1.05	0.04	0.89	0.05	0.95	0.05
WB-0814-MC-04	90	95	92.5	1.06	0.05	1.01	0.04	0.99	0.05	1.02	0.05
WB-0814-MC-04	110	115	112.5	1.10	0.05	0.95	0.04	0.94	0.05	1.00	0.05
WB-0814-MC-04	130	135	132.5	1.01	0.05	1.01	0.04	0.99	0.05	1.01	0.05
WB-0814-MC-04	150	155	152.5	1.09	0.05	1.10	0.04	1.05	0.05	1.08	0.05
WB-0814-MC-04	170	175	172.5	1.12	0.05	1.10	0.04	1.14	0.06	1.12	0.05
WB-0814-MC-04	190	195	192.5	1.09	0.05	1.09	0.04	1.07	0.05	1.08	0.05

Table H.19 (Continued).

Core ID	Top Depth of Interval (mm)	Bottom Depth of interval (mm)	Average Depth of Interval (mm)	^{214}Pb (295 keV) Activity (dpm/g)	^{214}Pb (295 keV) Activity error (dpm/g)	^{214}Pb (351 keV) Activity (dpm/g)	^{214}Pb (351 keV) Activity error (dpm/g)	^{214}Bi Activity (dpm/g)	^{214}Bi Activity error (dpm/g)	^{210}Pb$_{Sup}$ Activity (dpm/g)	^{210}Pb$_{Sup}$ Activity error (dpm/g)
WB-0814-MC-04	210	215	212.5	0.93	0.04	1.15	0.04	0.96	0.05	1.01	0.04
WB-0814-MC-04	230	235	232.5	1.03	0.05	1.03	0.04	1.03	0.05	1.03	0.04
WB-0814-MC-04	250	255	252.5	1.17	0.05	1.23	0.04	0.97	0.05	1.12	0.05

Table H.20. SLRad data, $^{210}Pbs_{up}$ data for core site WB-0814-MC-DSH-08 DEP 1. Sediment cores with sub-sample intervals (mm), and SLRad's activities of ^{214}Pb (295keV), ^{214}Pb (351keV), and ^{214}Bi (351keV) used to calculate $^{210}Pb_{Sup}$. Note: Blank cell denotes no analysis performed.

Core ID	Top Depth of Interval (mm)	Bottom Depth of interval (mm)	Average Depth of Interval (mm)	^{214}Pb (295 keV) Activity (dpm/g)	^{214}Pb (295 keV) Activity error (dpm/g)	^{214}Pb (351 keV) Activity (dpm/g)	^{214}Pb (351 keV) Activity error (dpm/g)	^{214}Bi Activity (dpm/g)	^{214}Bi Activity error (dpm/g)	$^{210}Pb_{Sup}$ Activity (dpm/g)	$^{210}Pb_{Sup}$ Activity error (dpm/g)
WB-0814-MC-DSH-08 DEP 1	0	2	1	1.30	0.08	1.43	0.07	1.36	0.08	1.36	0.08
WB-0814-MC-DSH-08 DEP 1	2	4	3	1.63	0.10	1.67	0.08	1.23	0.08	1.51	0.08
WB-0814-MC-DSH-08 DEP 1	4	6	5	1.59	0.09	1.46	0.07	1.29	0.08	1.45	0.08
WB-0814-MC-DSH-08 DEP 1	6	8	7	1.34	0.08	1.47	0.07	1.17	0.07	1.33	0.07
WB-0814-MC-DSH-08 DEP 1	8	10	9	1.22	0.08	1.64	0.07	1.15	0.07	1.34	0.07
WB-0814-MC-DSH-08 DEP 1	10	12	11	1.65	0.09	1.55	0.07	1.31	0.08	1.50	0.08
WB-0814-MC-DSH-08 DEP 1	12	14	13	1.73	0.09	1.49	0.07	1.43	0.08	1.55	0.08
WB-0814-MC-DSH-08 DEP 1	14	16	15	1.31	0.08	1.60	0.07	1.19	0.07	1.37	0.07
WB-0814-MC-DSH-08 DEP 1	16	18	17	1.60	0.09	1.45	0.07	1.40	0.08	1.48	0.08
WB-0814-MC-DSH-08 DEP 1	18	20	19	1.50	0.08	1.63	0.07	1.22	0.07	1.45	0.07
WB-0814-MC-DSH-08 DEP 1	20	22	21	1.41	0.08	1.26	0.06	1.44	0.08	1.37	0.07
WB-0814-MC-DSH-08 DEP 1	24	26	25	1.72	0.09	1.48	0.06	1.50	0.08	1.56	0.08
WB-0814-MC-DSH-08 DEP 1	30	32	31	1.44	0.08	1.78	0.07	1.34	0.07	1.52	0.07
WB-0814-MC-DSH-08 DEP 1	40	45	42.5	2.02	0.07	1.97	0.06	2.01	0.07	2.00	0.07
WB-0814-MC-DSH-08 DEP 1	50	55	52.5	1.72	0.07	2.00	0.06	1.97	0.07	1.90	0.07
WB-0814-MC-DSH-08 DEP 1	70	75	72.5	2.15	0.07	2.21	0.06	2.30	0.08	2.22	0.07
WB-0814-MC-DSH-08 DEP 1	90	95	92.5	2.15	0.07	2.30	0.06	2.29	0.08	2.25	0.07
WB-0814-MC-DSH-08 DEP 1	110	115	112.5	2.23	0.08	2.18	0.06	2.14	0.08	2.18	0.07
WB-0814-MC-DSH-08 DEP 1	130	135	132.5	2.21	0.08	2.26	0.06	2.21	0.08	2.22	0.07
WB-0814-MC-DSH-08 DEP 1	150	155	152.5	2.02	0.07	2.02	0.06	2.12	0.08	2.05	0.07
WB-0814-MC-DSH-08 DEP 1	170	175	172.5	2.01	0.07	2.22	0.06	2.15	0.08	2.13	0.07
WB-0814-MC-DSH-08 DEP 1	190	195	192.5	2.07	0.07	2.11	0.06	2.03	0.08	2.07	0.07
WB-0814-MC-DSH-08 DEP 1	210	215	212.5	1.99	0.07	2.05	0.06	1.80	0.07	1.95	0.07

Table H.20 (Continued).

Core ID	Top Depth of Interval (mm)	Bottom Depth of interval (mm)	Average Depth of Interval (mm)	^{214}Pb (295 keV) Activity (dpm/g)	^{214}Pb (295 keV) Activity error (dpm/g)	^{214}Pb (351 keV) Activity (dpm/g)	^{214}Pb (351 keV) Activity error (dpm/g)	^{214}Bi Activity (dpm/g)	^{214}Bi Activity error (dpm/g)	^{210}Pb$_{Sup}$ Activity (dpm/g)	^{210}Pb$_{Sup}$ Activity error (dpm/g)
WB-0814-MC-DSH-08 DEP 1	230	235	232.5	1.79	0.07	2.03	0.06	1.62	0.07	1.81	0.07
WB-0814-MC-DSH-08 DEP 1	250	255	252.5	2.00	0.07	2.22	0.06	1.97	0.08	2.06	0.07
WB-0814-MC-DSH-08 DEP 1	270	275	272.5	1.93	0.07	2.14	0.06	2.12	0.08	2.06	0.07
WB-0814-MC-DSH-08 DEP 1	290	295	292.5	2.18	0.08	2.22	0.06	1.98	0.07	2.13	0.07

Table H.21. SLRad data, $^{210}Pbs_{up}$ data for core site WB-0814-MC-DSH-10 DEP 1. Sediment cores with sub-sample intervals (mm), and SLRad's activities of ^{214}Pb (295keV), ^{214}Pb (351keV), and ^{214}Bi (351keV) used to calculate $^{210}Pb_{Sup}$. Note: Blank cell denotes no analysis performed.

Core ID	Top Depth of Interval (mm)	Bottom Depth of interval (mm)	Average Depth of Interval (mm)	^{214}Pb (295 keV) Activity (dpm/g)	^{214}Pb (295 keV) Activity error (dpm/g)	^{214}Pb (351 keV) Activity (dpm/g)	^{214}Pb (351 keV) Activity error (dpm/g)	^{214}Bi Activity (dpm/g)	^{214}Bi Activity error (dpm/g)	$^{210}Pb_{Sup}$ Activity (dpm/g)	$^{210}Pb_{Sup}$ Activity error (dpm/g)
WB-0814-MC-DSH-10 DEP 1	0	2	1	2.54	0.14	3.35	0.14	2.96	0.17	2.95	0.15
WB-0814-MC-DSH-10 DEP 1	2	4	3	1.20	0.09	2.25	0.11	1.93	0.13	1.80	0.11
WB-0814-MC-DSH-10 DEP 1	4	6	5	1.98	0.11	2.07	0.10	2.16	0.13	2.07	0.11
WB-0814-MC-DSH-10 DEP 1	6	8	7	1.89	0.10	1.96	0.09	1.91	0.11	1.92	0.10
WB-0814-MC-DSH-10 DEP 1	8	10	9	1.77	0.10	1.78	0.08	1.88	0.11	1.81	0.10
WB-0814-MC-DSH-10 DEP 1	10	12	11	1.70	0.09	2.00	0.09	1.65	0.10	1.78	0.09
WB-0814-MC-DSH-10 DEP 1	12	14	13	1.45	0.09	1.92	0.09	1.74	0.11	1.70	0.10
WB-0814-MC-DSH-10 DEP 1	14	16	15	1.94	0.09	2.05	0.08	1.75	0.10	1.91	0.09
WB-0814-MC-DSH-10 DEP 1	16	18	17	1.59	0.09	1.95	0.08	1.68	0.10	1.74	0.09
WB-0814-MC-DSH-10 DEP 1	18	20	19	1.98	0.10	2.01	0.09	1.87	0.10	1.95	0.10
WB-0814-MC-DSH-10 DEP 1	20	22	21	2.17	0.10	2.44	0.09	1.90	0.10	2.17	0.10
WB-0814-MC-DSH-10 DEP 1	24	26	25	1.90	0.09	2.56	0.09	2.28	0.11	2.24	0.10
WB-0814-MC-DSH-10 DEP 1	30	32	31	1.73	0.08	2.35	0.08	1.98	0.10	2.02	0.09
WB-0814-MC-DSH-10 DEP 1	38	43	40.5	1.82	0.06	1.93	0.05	2.00	0.06	1.92	0.06
WB-0814-MC-DSH-10 DEP 1	53	58	55.5	1.70	0.07	1.64	0.05	1.80	0.07	1.71	0.06
WB-0814-MC-DSH-10 DEP 1	73	78	75.5	2.07	0.07	1.98	0.06	2.04	0.08	2.03	0.07
WB-0814-MC-DSH-10 DEP 1	93	98	95.5	2.21	0.07	2.28	0.06	2.05	0.08	2.18	0.07
WB-0814-MC-DSH-10 DEP 1	113	118	115.5	2.24	0.07	2.16	0.06	2.01	0.08	2.13	0.07
WB-0814-MC-DSH-10 DEP 1	133	138	135.5	2.22	0.07	2.41	0.06	2.18	0.07	2.27	0.07
WB-0814-MC-DSH-10 DEP 1	154	159	156.5	2.12	0.07	2.16	0.06	2.23	0.08	2.17	0.07
WB-0814-MC-DSH-10 DEP 1	174	179	176.5	2.01	0.07	2.19	0.06	2.17	0.08	2.13	0.07
WB-0814-MC-DSH-10 DEP 1	194	199	196.5	1.86	0.07	2.04	0.06	2.05	0.08	1.98	0.07
WB-0814-MC-DSH-10 DEP 1	214	219	216.5	1.88	0.07	1.99	0.06	1.81	0.07	1.89	0.07

Table H.21 (Continued).

Core ID	Top Depth of Interval (mm)	Bottom Depth of interval (mm)	Average Depth of Interval (mm)	^{214}Pb (295 keV) Activity (dpm/g)	^{214}Pb (295 keV) Activity error (dpm/g)	^{214}Pb (351 keV) Activity (dpm/g)	^{214}Pb (351 keV) Activity error (dpm/g)	^{214}Bi Activity (dpm/g)	^{214}Bi Activity error (dpm/g)	^{210}Pb$_{Sup}$ Activity (dpm/g)	^{210}Pb$_{Sup}$ Activity error (dpm/g)
WB-0814-MC-DSH-10 DEP 1	234	239	236.5	2.04	0.07	1.83	0.05	1.85	0.07	1.91	0.07
WB-0814-MC-DSH-10 DEP 1	254	259	256.5	1.99	0.07	2.02	0.06	1.99	0.07	2.00	0.07
WB-0814-MC-DSH-10 DEP 1	274	279	276.5	1.91	0.07	2.05	0.06	1.95	0.07	1.97	0.07
WB-0814-MC-DSH-10 DEP 1	294	299	296.5	1.90	0.07	1.95	0.05	1.82	0.07	1.89	0.06
WB-0814-MC-DSH-10 DEP 1	314	319	316.5	1.95	0.07	1.98	0.06	2.11	0.08	2.01	0.07
WB-0814-MC-DSH-10 DEP 1	53	58	55.5	2.54	0.14	3.35	0.14	2.96	0.17	2.95	0.15
WB-0814-MC-DSH-10 DEP 1	73	78	75.5	1.20	0.09	2.25	0.11	1.93	0.13	1.80	0.11
WB-0814-MC-DSH-10 DEP 1	93	98	95.5	1.98	0.11	2.07	0.10	2.16	0.13	2.07	0.11
WB-0814-MC-DSH-10 DEP 1	113	118	115.5	1.89	0.10	1.96	0.09	1.91	0.11	1.92	0.10
WB-0814-MC-DSH-10 DEP 1	133	138	135.5	1.77	0.10	1.78	0.08	1.88	0.11	1.81	0.10
WB-0814-MC-DSH-10 DEP 1	154	159	156.5	1.70	0.09	2.00	0.09	1.65	0.10	1.78	0.09
WB-0814-MC-DSH-10 DEP 1	174	179	176.5	1.45	0.09	1.92	0.09	1.74	0.11	1.70	0.10
WB-0814-MC-DSH-10 DEP 1	194	199	196.5	1.94	0.09	2.05	0.08	1.75	0.10	1.91	0.09
WB-0814-MC-DSH-10 DEP 1	214	219	216.5	1.59	0.09	1.95	0.08	1.68	0.10	1.74	0.09
WB-0814-MC-DSH-10 DEP 1	234	239	236.5	1.98	0.10	2.01	0.09	1.87	0.10	1.95	0.10
WB-0814-MC-DSH-10 DEP 1	254	259	256.5	2.17	0.10	2.44	0.09	1.90	0.10	2.17	0.10
WB-0814-MC-DSH-10 DEP 1	274	279	276.5	1.90	0.09	2.56	0.09	2.28	0.11	2.24	0.10
WB-0814-MC-DSH-10 DEP 1	294	299	296.5	1.73	0.08	2.35	0.08	1.98	0.10	2.02	0.09
WB-0814-MC-DSH-10 DEP 1	314	319	316.5	1.82	0.06	1.93	0.05	2.00	0.06	1.92	0.06

Table H.22. SLRad data, $^{210}Pbs_{up}$ data for core site WB-0814-MC-PCB-06 DEP 2. Sediment cores with sub-sample intervals (mm), and SLRad's activities of ^{214}Pb (295keV), ^{214}Pb (351keV), and ^{214}Bi (351keV) used to calculate $^{210}Pb_{Sup}$. Note: Blank cell denotes no analysis performed.

Core ID	Top Depth of Interval (mm)	Bottom Depth of interval (mm)	Average Depth of Interval (mm)	^{214}Pb (295 keV) Activity (dpm/g)	^{214}Pb (295 keV) Activity error (dpm/g)	^{214}Pb (351 keV) Activity (dpm/g)	^{214}Pb (351 keV) Activity error (dpm/g)	^{214}Bi Activity (dpm/g)	^{214}Bi Activity error (dpm/g)	$^{210}Pb_{Sup}$ Activity (dpm/g)	$^{210}Pb_{Sup}$ Activity error (dpm/g)
WB-0814-MC-PCB-06 DEP 2	0	2	1	1.54	0.10	1.58	0.08	1.31	0.08	1.48	0.09
WB-0814-MC-PCB-06 DEP 2	2	4	3	1.79	0.12	1.41	0.08	1.36	0.09	1.52	0.09
WB-0814-MC-PCB-06 DEP 2	4	6	5	1.38	0.10	1.41	0.08	1.34	0.09	1.37	0.09
WB-0814-MC-PCB-06 DEP 2	6	8	7	1.64	0.10	1.48	0.07	1.10	0.07	1.41	0.08
WB-0814-MC-PCB-06 DEP 2	8	10	9	1.47	0.10	1.33	0.07	1.27	0.08	1.36	0.08
WB-0814-MC-PCB-06 DEP 2	10	12	11	1.52	0.09	1.45	0.07	1.42	0.08	1.46	0.08
WB-0814-MC-PCB-06 DEP 2	12	14	13	1.51	0.09	1.55	0.07	1.58	0.09	1.54	0.09
WB-0814-MC-PCB-06 DEP 2	14	16	15	1.58	0.09	1.42	0.07	1.48	0.08	1.49	0.08
WB-0814-MC-PCB-06 DEP 2	16	18	17	1.48	0.09	1.50	0.07	1.48	0.08	1.49	0.08
WB-0814-MC-PCB-06 DEP 2	18	20	19	1.85	0.09	1.57	0.07	1.45	0.08	1.62	0.08
WB-0814-MC-PCB-06 DEP 2	20	22	21	1.69	0.09	1.59	0.07	1.52	0.08	1.60	0.08
WB-0814-MC-PCB-06 DEP 2	24	26	25	1.87	0.09	1.80	0.07	1.64	0.08	1.77	0.08
WB-0814-MC-PCB-06 DEP 2	30	32	31	1.99	0.09	2.10	0.08	2.00	0.09	2.03	0.09
WB-0814-MC-PCB-06 DEP 2	40	42	41	3.33	0.12	3.21	0.10	2.70	0.11	3.08	0.11
WB-0814-MC-PCB-06 DEP 2	50	55	52.5	1.75	0.07	1.83	0.06	1.72	0.07	1.77	0.06
WB-0814-MC-PCB-06 DEP 2	70	75	72.5	2.03	0.07	1.83	0.06	1.91	0.07	1.92	0.07
WB-0814-MC-PCB-06 DEP 2	90	95	92.5	2.02	0.07	2.02	0.06	1.90	0.07	1.98	0.07
WB-0814-MC-PCB-06 DEP 2	110	117	113.5	2.07	0.07	1.97	0.05	1.94	0.07	1.99	0.06
WB-0814-MC-PCB-06 DEP 2	132	137	134.5	1.93	0.07	1.87	0.06	1.90	0.07	1.90	0.07
WB-0814-MC-PCB-06 DEP 2	152	157	154.5	2.13	0.07	2.23	0.06	1.94	0.07	2.10	0.07
WB-0814-MC-PCB-06 DEP 2	172	177	174.5	2.09	0.07	2.14	0.06	1.93	0.07	2.05	0.07
WB-0814-MC-PCB-06 DEP 2	192	197	194.5	2.20	0.07	2.20	0.06	2.07	0.07	2.15	0.07
WB-0814-MC-PCB-06 DEP 2	212	217	214.5	2.06	0.07	1.91	0.06	1.97	0.07	1.98	0.07

Table H.22 (Continued).

Core ID	Top Depth of Interval (mm)	Bottom Depth of interval (mm)	Average Depth of Interval (mm)	^{214}Pb (295 keV) Activity (dpm/g)	^{214}Pb (295 keV) Activity error (dpm/g)	^{214}Pb (351 keV) Activity (dpm/g)	^{214}Pb (351 keV) Activity error (dpm/g)	^{214}Bi Activity (dpm/g)	^{214}Bi Activity error (dpm/g)	^{210}Pb$_{Sup}$ Activity (dpm/g)	^{210}Pb$_{Sup}$ Activity error (dpm/g)
WB-0814-MC-PCB-06 DEP 2	232	237	234.5	1.87	0.07	2.02	0.06	1.94	0.07	1.94	0.07
WB-0814-MC-PCB-06 DEP 2	252	257	254.5	2.04	0.07	2.01	0.06	1.99	0.07	2.01	0.07
WB-0814-MC-PCB-06 DEP 2	272	277	274.5	1.67	0.08	1.58	0.06	1.60	0.08	1.62	0.07
WB-0814-MC-PCB-06 DEP 2	292	297	294.5	1.44	0.07	1.50	0.06	1.49	0.07	1.48	0.07

Table H.23. SLRad data, $^{210}Pbs_{up}$ data for core site WB-0815-MC-04. Sediment cores with sub-sample intervals (mm), and SLRad's activities of ^{214}Pb (295keV), ^{214}Pb (351keV), and ^{214}Bi (351keV) used to calculate $^{210}Pb_{Sup}$. Note: Blank cell denotes no analysis performed.

Core ID	Top Depth of Interval (mm)	Bottom Depth of interval (mm)	Average Depth of Interval (mm)	^{214}Pb (295 keV) Activity (dpm/g)	^{214}Pb (295 keV) Activity error (dpm/g)	^{214}Pb (351 keV) Activity (dpm/g)	^{214}Pb (351 keV) Activity error (dpm/g)	^{214}Bi Activity (dpm/g)	^{214}Bi Activity error (dpm/g)	$^{210}Pb_{Sup}$ Activity (dpm/g)	$^{210}Pb_{Sup}$ Activity error (dpm/g)
WB-0815-MC-04	0	2	1	1.08	0.09	1.19	0.09	1.29	0.11	1.18	0.10
WB-0815-MC-04	2	4	3	1.04	0.08	1.31	0.08	0.95	0.08	1.10	0.08
WB-0815-MC-04	4	6	5	0.73	0.06	1.07	0.06	1.05	0.08	0.95	0.07
WB-0815-MC-04	6	8	7	1.06	0.07	1.18	0.07	1.24	0.09	1.16	0.07
WB-0815-MC-04	8	10	9	0.89	0.06	1.11	0.06	1.13	0.08	1.05	0.07
WB-0815-MC-04	10	12	11	1.15	0.07	1.23	0.07	1.02	0.08	1.13	0.07
WB-0815-MC-04	12	14	13	1.08	0.07	1.11	0.06	0.98	0.07	1.05	0.07
WB-0815-MC-04	14	16	15	0.95	0.07	1.11	0.06	0.85	0.07	0.97	0.07
WB-0815-MC-04	16	18	17	1.09	0.07	1.05	0.06	0.88	0.07	1.00	0.07

Table H.24. SLRad data, $^{210}Pbs_{up}$ data for core site WB-0815-MC-DSH-08-A. Sediment cores with sub-sample intervals (mm), and SLRad's activities of ^{214}Pb (295keV), ^{214}Pb (351keV), and ^{214}Bi (351keV) used to calculate $^{210}Pb_{Sup}$. Note: Blank cell denotes no analysis performed.

Core ID	Top Depth of Interval (mm)	Bottom Depth of interval (mm)	Average Depth of Interval (mm)	^{214}Pb (295 keV) Activity (dpm/g)	^{214}Pb (295 keV) Activity error (dpm/g)	^{214}Pb (351 keV) Activity (dpm/g)	^{214}Pb (351 keV) Activity error (dpm/g)	^{214}Bi Activity (dpm/g)	^{214}Bi Activity error (dpm/g)	$^{210}Pb_{Sup}$ Activity (dpm/g)	$^{210}Pb_{Sup}$ Activity error (dpm/g)
WB-0815-MC-DSH-08-A	0	2	1	1.89	0.12	1.85	0.09	1.39	0.09	1.71	0.10
WB-0815-MC-DSH-08-A	2	4	3	1.85	0.13	1.67	0.09	1.44	0.10	1.65	0.11
WB-0815-MC-DSH-08-A	4	6	5	1.57	0.11	1.46	0.08	1.40	0.09	1.48	0.10
WB-0815-MC-DSH-08-A	6	8	7	1.75	0.11	1.68	0.08	1.45	0.09	1.63	0.09
WB-0815-MC-DSH-08-A	8	10	9	1.89	0.11	1.36	0.07	1.63	0.09	1.63	0.09
WB-0815-MC-DSH-08-A	10	12	11	1.85	0.11	1.51	0.08	1.50	0.09	1.62	0.09
WB-0815-MC-DSH-08-A	12	14	13	1.86	0.11	1.49	0.08	1.13	0.08	1.49	0.09
WB-0815-MC-DSH-08-A	14	16	15	1.62	0.10	1.47	0.07	1.52	0.08	1.54	0.08
WB-0815-MC-DSH-08-A	16	18	17	1.58	0.10	1.67	0.08	1.61	0.09	1.62	0.09
WB-0815-MC-DSH-08-A	18	20	19	1.79	0.10	1.58	0.08	1.39	0.08	1.59	0.09

Table H.25. SLRad data, $^{210}Pbs_{up}$ data for core site WB-0815-MC-DSH-10-A. Sediment cores with sub-sample intervals (mm), and SLRad's activities of ^{214}Pb (295keV), ^{214}Pb (351keV), and ^{214}Bi (351keV) used to calculate $^{210}Pb_{Sup}$. Note: Blank cell denotes no analysis performed.

Core ID	Top Depth of Interval (mm)	Bottom Depth of interval (mm)	Average Depth of Interval (mm)	^{214}Pb (295 keV) Activity (dpm/g)	^{214}Pb (295 keV) Activity error (dpm/g)	^{214}Pb (351 keV) Activity (dpm/g)	^{214}Pb (351 keV) Activity error (dpm/g)	^{214}Bi Activity (dpm/g)	^{214}Bi Activity error (dpm/g)	$^{210}Pb_{Sup}$ Activity (dpm/g)	$^{210}Pb_{Sup}$ Activity error (dpm/g)
WB-0815-MC-DSH-10-A	0	2	1	1.60	0.11	1.95	0.11	1.97	0.13	1.84	0.12
WB-0815-MC-DSH-10-A	2	4	3	2.09	0.10	2.37	0.10	1.60	0.10	2.02	0.10
WB-0815-MC-DSH-10-A	4	6	5	2.26	0.11	2.36	0.09	1.97	0.11	2.20	0.10
WB-0815-MC-DSH-10-A	6	8	7	2.17	0.15	2.39	0.13	2.26	0.16	2.27	0.15
WB-0815-MC-DSH-10-A	8	10	9	2.18	0.10	2.23	0.09	2.00	0.11	2.14	0.10
WB-0815-MC-DSH-10-A	12	14	13	1.95	0.09	2.43	0.09	2.02	0.10	2.13	0.10
WB-0815-MC-DSH-10-A	14	16	15	1.88	0.09	2.11	0.08	1.74	0.10	1.91	0.09
WB-0815-MC-DSH-10-A	16	18	17	1.69	0.09	1.86	0.08	1.73	0.10	1.76	0.09
WB-0815-MC-DSH-10-A	18	20	19	1.69	0.09	2.29	0.09	1.87	0.10	1.95	0.09

Table H.26. SLRad data, $^{210}Pbs_{up}$ data for core site WB-0815-MC-PCB-06-A. Sediment cores with sub-sample intervals (mm), and SLRad's activities of ^{214}Pb (295keV), ^{214}Pb (351keV), and ^{214}Bi (351keV) used to calculate $^{210}Pb_{Sup}$. Note: Blank cell denotes no analysis performed.

Core ID	Top Depth of Interval (mm)	Bottom Depth of interval (mm)	Average Depth of Interval (mm)	^{214}Pb (295 keV) Activity (dpm/g)	^{214}Pb (295 keV) Activity error (dpm/g)	^{214}Pb (351 keV) Activity (dpm/g)	^{214}Pb (351 keV) Activity error (dpm/g)	^{214}Bi Activity (dpm/g)	^{214}Bi Activity error (dpm/g)	$^{210}Pb_{Sup}$ Activity (dpm/g)	$^{210}Pb_{Sup}$ Activity error (dpm/g)
WB-0815-MC-PCB-06-A	0	2	1	2.80	0.22	2.25	0.15	2.42	0.16	2.49	0.18
WB-0815-MC-PCB-06-A	2	4	3	2.02	0.13	1.66	0.09	1.31	0.09	1.66	0.10
WB-0815-MC-PCB-06-A	4	6	5	1.85	0.11	1.67	0.08	1.43	0.09	1.65	0.09
WB-0815-MC-PCB-06-A	6	8	7	1.72	0.10	1.66	0.08	1.68	0.09	1.69	0.09
WB-0815-MC-PCB-06-A	8	10	9	2.15	0.12	1.81	0.08	1.36	0.08	1.78	0.09
WB-0815-MC-PCB-06-A	10	12	11	2.33	0.11	2.19	0.08	1.98	0.09	2.17	0.09
WB-0815-MC-PCB-06-A	12	14	13	1.87	0.10	1.70	0.08	1.46	0.08	1.68	0.09
WB-0815-MC-PCB-06-A	14	16	15	1.86	0.10	1.46	0.07	1.67	0.09	1.66	0.09
WB-0815-MC-PCB-06-A	16	18	17	1.90	0.10	1.61	0.07	1.50	0.08	1.67	0.09
WB-0815-MC-PCB-06-A	18	20	19	1.59	0.09	1.76	0.08	1.44	0.08	1.60	0.08

Table H.27. SLRad data, $^{210}Pbs_{up}$ data for core site WB-0816-MC-04. Sediment cores with sub-sample intervals (mm), and SLRad's activities of ^{214}Pb (295keV), ^{214}Pb (351keV), and ^{214}Bi (351keV) used to calculate $^{210}Pb_{Sup}$. Note: Blank cell denotes no analysis performed.

Core ID	Top Depth of Interval (mm)	Bottom Depth of Interval (mm)	Average Depth of Interval (mm)	^{214}Pb (295 keV) Activity (dpm/g)	^{214}Pb (295 keV) Activity error (dpm/g)	^{214}Pb (351 keV) Activity (dpm/g)	^{214}Pb (351 keV) Activity error (dpm/g)	^{214}Bi Activity (dpm/g)	^{214}Bi Activity error (dpm/g)	$^{210}Pb_{Sup}$ Activity (dpm/g)	$^{210}Pb_{Sup}$ Activity error (dpm/g)
WB-0816-MC-04	0	2	1	1.53	0.10	1.51	0.08	1.82	0.10	1.62	0.09
WB-0816-MC-04	2	4	3	1.32	0.09	1.57	0.08	1.43	0.08	1.44	0.08
WB-0816-MC-04	4	6	5	1.04	0.07	1.32	0.06	1.37	0.08	1.24	0.07
WB-0816-MC-04	6	8	7	1.30	0.07	1.24	0.06	1.25	0.07	1.26	0.07
WB-0816-MC-04	8	10	9	1.20	0.07	1.34	0.06	1.32	0.07	1.29	0.07
WB-0816-MC-04	10	12	11	1.18	0.07	1.16	0.05	1.31	0.07	1.22	0.06
WB-0816-MC-04	12	14	13	1.31	0.07	1.23	0.05	1.27	0.06	1.27	0.06
WB-0816-MC-04	14	16	15	1.35	0.07	1.40	0.06	1.33	0.07	1.36	0.07
WB-0816-MC-04	16	18	17	1.09	0.07	1.18	0.06	1.19	0.07	1.16	0.06
WB-0816-MC-04	18	20	19	1.32	0.07	1.17	0.05	1.35	0.07	1.28	0.06
WB-0816-MC-04	20	22	21	0.98	0.06	1.11	0.05	1.09	0.06	1.06	0.06
WB-0816-MC-04	24	26	25	1.03	0.06	1.07	0.05	1.01	0.06	1.04	0.06
WB-0816-MC-04	30	32	31	1.07	0.06	1.26	0.06	1.10	0.06	1.14	0.06
WB-0816-MC-04	50	52	51	0.83	0.05	1.29	0.06	1.04	0.06	1.05	0.06
WB-0816-MC-04	70	72	71	0.98	0.06	1.30	0.06	1.13	0.06	1.14	0.06
WB-0816-MC-04	90	95	92.5	1.01	0.05	1.33	0.05	1.22	0.05	1.18	0.05
WB-0816-MC-04	110	115	112.5	1.10	0.05	1.40	0.05	1.26	0.05	1.25	0.05
WB-0816-MC-04	130	135	132.5	1.10	0.05	1.25	0.05	1.15	0.05	1.16	0.05
WB-0816-MC-04	150	155	152.5	1.17	0.05	1.39	0.05	1.19	0.05	1.25	0.05
WB-0816-MC-04	170	175	172.5	1.16	0.05	1.38	0.05	1.31	0.05	1.28	0.05
WB-0816-MC-04	190	195	192.5	1.13	0.05	1.36	0.05	1.15	0.05	1.21	0.05
WB-0816-MC-04	210	215	212.5	1.05	0.05	1.44	0.05	1.18	0.05	1.22	0.05
WB-0816-MC-04	230	235	232.5	1.14	0.07	1.36	0.07	1.16	0.07	1.22	0.07

Table H.27 (Continued).

Core ID	Top Depth of Interval (mm)	Bottom Depth of Interval (mm)	Average Depth of Interval (mm)	^{214}Pb (295 keV) Activity (dpm/g)	^{214}Pb (295 keV) Activity error (dpm/g)	^{214}Pb (351 keV) Activity (dpm/g)	^{214}Pb (351 keV) Activity error (dpm/g)	^{214}Bi Activity (dpm/g)	^{214}Bi Activity error (dpm/g)	^{210}Pb$_{Sup}$ Activity (dpm/g)	^{210}Pb$_{Sup}$ Activity error (dpm/g)
WB-0816-MC-04	250	255	252.5	1.03	0.05	1.37	0.05	1.21	0.05	1.20	0.05
WB-0816-MC-04	270	275	272.5	1.09	0.05	1.42	0.05	1.08	0.05	1.20	0.05
WB-0816-MC-04	290	295	292.5	1.11	0.05	1.31	0.05	1.12	0.05	1.18	0.05
WB-0816-MC-04	310	315	312.5	1.04	0.05	1.38	0.05	1.11	0.05	1.18	0.05
WB-0816-MC-04	330	335	332.5	1.34	0.05	1.44	0.05	1.21	0.05	1.33	0.05

Table H.28. SLRad data, $^{210}Pbs_{up}$ data for core site WB-0816-MC-DSH-08-A. Sediment cores with sub-sample intervals (mm), and SLRad's activities of ^{214}Pb (295keV), ^{214}Pb (351keV), and ^{214}Bi (351keV) used to calculate $^{210}Pb_{Sup}$. Note: Blank cell denotes no analysis performed.

Core ID	Top Depth of Interval (mm)	Bottom Depth of Interval (mm)	Average Depth of Interval (mm)	^{214}Pb (295 keV) Activity (dpm/g)	^{214}Pb (295 keV) Activity error (dpm/g)	^{214}Pb (351 keV) Activity (dpm/g)	^{214}Pb (351 keV) Activity error (dpm/g)	^{214}Bi Activity (dpm/g)	^{214}Bi Activity error (dpm/g)	$^{210}Pb_{Sup}$ Activity (dpm/g)	$^{210}Pb_{Sup}$ Activity error (dpm/g)
WB-0816-MC-DSH-08-A	0	2	1	1.41	0.10	1.17	0.07	1.35	0.09	1.31	0.09
WB-0816-MC-DSH-08-A	2	4	3	1.91	0.12	1.32	0.08	1.60	0.10	1.61	0.10
WB-0816-MC-DSH-08-A	4	6	5	1.54	0.10	1.59	0.08	1.52	0.09	1.55	0.09
WB-0816-MC-DSH-08-A	6	8	7	1.60	0.09	1.63	0.08	1.45	0.08	1.56	0.08
WB-0816-MC-DSH-08-A	8	10	9	1.58	0.09	1.68	0.07	1.51	0.08	1.59	0.08
WB-0816-MC-DSH-08-A	10	12	11	1.59	0.09	1.98	0.08	1.66	0.09	1.74	0.09
WB-0816-MC-DSH-08-A	12	14	13	1.91	0.10	1.71	0.07	1.58	0.08	1.73	0.08
WB-0816-MC-DSH-08-A	14	16	15	1.74	0.09	1.71	0.07	1.40	0.08	1.62	0.08
WB-0816-MC-DSH-08-A	16	18	17	1.89	0.10	1.81	0.07	1.48	0.08	1.73	0.08
WB-0816-MC-DSH-08-A	18	20	19	1.92	0.10	1.69	0.07	1.43	0.08	1.68	0.08
WB-0816-MC-DSH-08-A	20	22	21	2.00	0.10	1.78	0.08	1.65	0.09	1.81	0.09
WB-0816-MC-DSH-08-A	22	24	23	2.10	0.10	2.00	0.08	1.66	0.09	1.92	0.09
WB-0816-MC-DSH-08-A	24	26	25	1.62	0.09	1.73	0.07	1.42	0.08	1.59	0.08
WB-0816-MC-DSH-08-A	26	28	27	1.73	0.09	1.52	0.07	1.39	0.08	1.55	0.08
WB-0816-MC-DSH-08-A	28	30	29	1.73	0.09	1.57	0.07	1.35	0.08	1.55	0.08
WB-0816-MC-DSH-08-A	30	32	31	1.24	0.08	1.47	0.07	1.38	0.08	1.36	0.07
WB-0816-MC-DSH-08-A	50	55	52.5	1.75	0.07	1.83	0.06	1.64	0.07	1.74	0.07
WB-0816-MC-DSH-08-A	70	75	72.5	1.89	0.07	1.79	0.06	1.91	0.07	1.86	0.07
WB-0816-MC-DSH-08-A	90	95	92.5	1.70	0.07	2.01	0.06	1.65	0.07	1.79	0.07
WB-0816-MC-DSH-08-A	110	115	112.5	2.02	0.07	1.92	0.06	2.01	0.07	1.98	0.07
WB-0816-MC-DSH-08-A	130	135	132.5	1.89	0.07	2.02	0.06	1.96	0.07	1.95	0.07
WB-0816-MC-DSH-08-A	150	155	152.5	2.07	0.07	2.01	0.06	2.05	0.07	2.04	0.07
WB-0816-MC-DSH-08-A	170	175	172.5	2.09	0.07	2.04	0.06	2.05	0.08	2.06	0.07

Table H.28 (Continued).

Core ID	Top Depth of Interval (mm)	Bottom Depth of Interval (mm)	Average Depth of Interval (mm)	^{214}Pb (295 keV) Activity (dpm/g)	^{214}Pb (295 keV) Activity error (dpm/g)	^{214}Pb (351 keV) Activity (dpm/g)	^{214}Pb (351 keV) Activity error (dpm/g)	^{214}Bi Activity (dpm/g)	^{214}Bi Activity error (dpm/g)	^{210}Pb$_{Sup}$ Activity (dpm/g)	^{210}Pb$_{Sup}$ Activity error (dpm/g)
WB-0816-MC-DSH-08-A	190	195	192.5	1.89	0.07	1.88	0.06	2.04	0.07	1.93	0.07
WB-0816-MC-DSH-08-A	210	215	212.5	1.95	0.07	2.07	0.06	2.13	0.08	2.05	0.07
WB-0816-MC-DSH-08-A	250	255	252.5	1.81	0.07	1.92	0.06	1.80	0.07	1.84	0.06
WB-0816-MC-DSH-08-A	290	295	292.5	1.95	0.07	2.10	0.06	2.20	0.08	2.08	0.07

Table H.29. SLRad data, $^{210}Pbs_{up}$ data for core site WB-0816-MC-DSH-10-A. Sediment cores with sub-sample intervals (mm), and SLRad's activities of ^{214}Pb (295keV), ^{214}Pb (351keV), and ^{214}Bi (351keV) used to calculate $^{210}Pb_{Sup}$. Note: Blank cell denotes no analysis performed.

Core ID	Top Depth of Interval (mm)	Bottom Depth of Interval (mm)	Average Depth of Interval (mm)	^{214}Pb (295 keV) Activity (dpm/g)	^{214}Pb (295 keV) Activity error (dpm/g)	^{214}Pb (351 keV) Activity (dpm/g)	^{214}Pb (351 keV) Activity error (dpm/g)	^{214}Bi Activity (dpm/g)	^{214}Bi Activity error (dpm/g)	$^{210}Pb_{Sup}$ Activity (dpm/g)	$^{210}Pb_{Sup}$ Activity error (dpm/g)
WB-0816-MC-DSH-10-A	0	2	1	1.99	0.12	2.15	0.11	1.85	0.12	2.00	0.12
WB-0816-MC-DSH-10-A	2	4	3	1.78	0.10	2.09	0.09	1.99	0.12	1.95	0.10
WB-0816-MC-DSH-10-A	4	6	5	1.82	0.10	2.08	0.09	2.22	0.12	2.04	0.11
WB-0816-MC-DSH-10-A	6	8	7	1.84	0.10	2.10	0.09	2.01	0.11	1.98	0.10
WB-0816-MC-DSH-10-A	8	10	9	1.41	0.09	2.06	0.09	1.51	0.10	1.66	0.09
WB-0816-MC-DSH-10-A	10	12	11	1.59	0.09	2.30	0.09	1.70	0.10	1.86	0.09
WB-0816-MC-DSH-10-A	12	14	13	1.56	0.08	1.95	0.08	1.80	0.10	1.77	0.09
WB-0816-MC-DSH-10-A	14	16	15	1.72	0.09	1.98	0.08	1.52	0.09	1.74	0.09
WB-0816-MC-DSH-10-A	16	18	17	1.52	0.08	1.72	0.08	1.70	0.10	1.65	0.09
WB-0816-MC-DSH-10-A	18	20	19	2.04	0.10	2.08	0.08	1.92	0.10	2.01	0.09
WB-0816-MC-DSH-10-A	20	22	21	1.74	0.09	2.12	0.08	1.85	0.10	1.90	0.09
WB-0816-MC-DSH-10-A	22	24	23	2.14	0.10	2.64	0.09	2.48	0.12	2.42	0.10
WB-0816-MC-DSH-10-A	24	26	25	1.74	0.08	1.98	0.08	2.03	0.10	1.92	0.09
WB-0816-MC-DSH-10-A	26	28	27	1.86	0.09	2.29	0.08	2.17	0.10	2.11	0.09
WB-0816-MC-DSH-10-A	28	30	29	2.01	0.09	2.19	0.08	2.14	0.10	2.11	0.09
WB-0816-MC-DSH-10-A	30	32	31	1.99	0.09	2.12	0.08	1.79	0.10	1.96	0.09
WB-0816-MC-DSH-10-A	50	52	51	1.65	0.08	1.81	0.07	1.70	0.09	1.72	0.08
WB-0816-MC-DSH-10-A	70	72	71	2.03	0.09	2.07	0.08	1.95	0.10	2.02	0.09
WB-0816-MC-DSH-10-A	90	95	92.5	1.89	0.07	1.85	0.06	2.06	0.08	1.93	0.07
WB-0816-MC-DSH-10-A	110	115	112.5	2.01	0.07	2.11	0.06	1.99	0.08	2.03	0.07
WB-0816-MC-DSH-10-A	130	135	132.5	1.87	0.07	2.03	0.06	1.88	0.07	1.93	0.07
WB-0816-MC-DSH-10-A	170	175	172.5	1.86	0.07	1.75	0.05	1.64	0.07	1.75	0.06
WB-0816-MC-DSH-10-A	210	215	212.5	1.82	0.07	1.90	0.06	1.88	0.07	1.87	0.07

Table H.29 (Continued).

Core ID	Top Depth of Interval (mm)	Bottom Depth of Interval (mm)	Average Depth of Interval (mm)	^{214}Pb (295 keV) Activity (dpm/g)	^{214}Pb (295 keV) Activity error (dpm/g)	^{214}Pb (351 keV) Activity (dpm/g)	^{214}Pb (351 keV) Activity error (dpm/g)	^{214}Bi Activity (dpm/g)	^{214}Bi Activity error (dpm/g)	^{210}Pb$_{Sup}$ Activity (dpm/g)	^{210}Pb$_{Sup}$ Activity error (dpm/g)
WB-0816-MC-DSH-10-A	250	255	252.5	1.79	0.07	1.91	0.06	1.83	0.07	1.84	0.07
WB-0816-MC-DSH-10-A	290	295	292.5	1.88	0.07	2.12	0.06	1.79	0.07	1.93	0.07
WB-0816-MC-DSH-10-A	310	315	312.5	1.87	0.07	2.03	0.06	2.01	0.08	1.97	0.07

Table H.30. SLRad data, $^{210}Pbs_{up}$ data for core site WB-0816-MC-PCB-06-A. Sediment cores with sub-sample intervals (mm), and SLRad's activities of ^{214}Pb (295keV), ^{214}Pb (351keV), and ^{214}Bi (351keV) used to calculate $^{210}Pb_{Sup}$. Note: Blank cell denotes no analysis performed.

Core ID	Top Depth of Interval (mm)	Bottom Depth of Interval (mm)	Average Depth of Interval (mm)	^{214}Pb (295 keV) Activity (dpm/g)	^{214}Pb (295 keV) Activity error (dpm/g)	^{214}Pb (351 keV) Activity (dpm/g)	^{214}Pb (351 keV) Activity error (dpm/g)	^{214}Bi Activity (dpm/g)	^{214}Bi Activity error (dpm/g)	$^{210}Pb_{Sup}$ Activity (dpm/g)	$^{210}Pb_{Sup}$ Activity error (dpm/g)
WB-0816-MC-PCB-06-A	0	2	1	1.75	0.12	1.61	0.09	1.54	0.10	1.63	0.10
WB-0816-MC-PCB-06-A	2	4	3	1.79	0.15	1.69	0.11	1.55	0.11	1.68	0.12
WB-0816-MC-PCB-06-A	4	6	5	2.09	0.14	1.64	0.09	1.41	0.10	1.71	0.11
WB-0816-MC-PCB-06-A	6	8	7	1.91	0.13	1.66	0.09	1.48	0.10	1.68	0.10
WB-0816-MC-PCB-06-A	8	10	9	1.88	0.11	1.72	0.08	1.64	0.09	1.74	0.10
WB-0816-MC-PCB-06-A	10	12	11	1.73	0.10	1.76	0.08	1.35	0.08	1.61	0.08
WB-0816-MC-PCB-06-A	12	14	13	1.99	0.10	1.82	0.08	1.46	0.08	1.76	0.09
WB-0816-MC-PCB-06-A	14	16	15	1.96	0.10	1.89	0.07	1.79	0.09	1.88	0.09
WB-0816-MC-PCB-06-A	16	18	17	2.14	0.10	1.86	0.08	1.62	0.08	1.87	0.09
WB-0816-MC-PCB-06-A	18	20	19	2.28	0.10	1.93	0.08	1.92	0.09	2.04	0.09
WB-0816-MC-PCB-06-A	20	22	21	1.97	0.10	2.17	0.08	1.79	0.09	1.98	0.09
WB-0816-MC-PCB-06-A	22	24	23	1.99	0.09	2.20	0.08	1.84	0.09	2.01	0.09
WB-0816-MC-PCB-06-A	24	26	25	2.13	0.10	2.18	0.08	1.80	0.09	2.04	0.09
WB-0816-MC-PCB-06-A	26	28	27	2.50	0.11	2.50	0.09	2.02	0.09	2.34	0.09
WB-0816-MC-PCB-06-A	28	30	29	2.60	0.11	2.78	0.09	2.36	0.10	2.58	0.10
WB-0816-MC-PCB-06-A	30	32	31	2.47	0.08	2.56	0.07	2.34	0.08	2.45	0.08
WB-0816-MC-PCB-06-A	50	52	51	1.64	0.08	1.47	0.06	1.50	0.08	1.54	0.07
WB-0816-MC-PCB-06-A	70	72	71	1.65	0.08	1.70	0.07	1.49	0.07	1.61	0.07
WB-0816-MC-PCB-06-A	90	95	92.5	1.87	0.07	1.93	0.06	1.70	0.07	1.83	0.07
WB-0816-MC-PCB-06-A	110	115	112.5	1.98	0.07	2.05	0.06	1.94	0.07	1.99	0.07
WB-0816-MC-PCB-06-A	130	135	132.5	2.08	0.07	2.20	0.06	2.05	0.08	2.11	0.07
WB-0816-MC-PCB-06-A	150	155	152.5	1.95	0.07	2.08	0.06	1.94	0.07	1.99	0.07
WB-0816-MC-PCB-06-A	170	175	172.5	1.96	0.07	2.00	0.06	1.97	0.07	1.98	0.07

Table H.30 (Continued).

Core ID	Top Depth of Interval (mm)	Bottom Depth of Interval (mm)	Average Depth of Interval (mm)	^{214}Pb (295 keV) Activity (dpm/g)	^{214}Pb (295 keV) Activity error (dpm/g)	^{214}Pb (351 keV) Activity (dpm/g)	^{214}Pb (351 keV) Activity error (dpm/g)	^{214}Bi Activity (dpm/g)	^{214}Bi Activity error (dpm/g)	^{210}Pb$_{Sup}$ Activity (dpm/g)	^{210}Pb$_{Sup}$ Activity error (dpm/g)
WB-0816-MC-PCB-06-A	190	195	192.5	1.93	0.07	1.94	0.06	1.78	0.07	1.88	0.07
WB-0816-MC-PCB-06-A	210	215	212.5	1.69	0.07	1.91	0.06	1.91	0.07	1.84	0.07
WB-0816-MC-PCB-06-A	250	255	252.5	1.70	0.07	1.93	0.06	1.90	0.07	1.84	0.07
WB-0816-MC-PCB-06-A	290	295	292.5	1.94	0.07	2.03	0.06	2.03	0.07	2.00	0.07

APPENDIX I:

SHORT-LIVED RADIOISOTOPE (SLRad) DATA: $^{210}Pb_{Tot}$, $^{210}Pb_{xs}$, and Decay Corrected (D.C.) $^{210}Pb_{xs}$

Appendix I. Supplemental tables of short-lived radioisotope activities for $^{210}Pb_{Tot}$, $^{210}Pb_{xs}$, and D.C. $^{210}Pb_{xs}$.

Data are publicly available through the Gulf of Mexico Research Initiative Information & Data Cooperative (GRIIDC) at https://data.gulfresearchinitiative.org (doi: 10.7266/N7610XTJ, 10.7266/n7-81nq-dq02, 10.7266/n7-p0xt-6209, 10.7266/n7-qzw5-kc72, 10.7266/n7-xsrd-fq25, 10.7266/n7-1vvs-ef02, 10.7266/n7-4j4h-7w93, 10.7266/n7-cdrm-g239)

Table I.1. SLRad data of $^{210}Pb_{Tot}$, $^{210}Pb_{xs}$, and D.C. $^{210}Pb_{xs}$ for core site WB-1109-MC-04. Sediment cores with sub-sample intervals (mm), and SLRad activities for $^{210}Pb_{Tot}$, $^{210}Pb_{xs}$, and D.C. $^{210}Pb_{xs}$ (Decay Corrected). Note: Blank cell denotes no analysis performed.

Core ID	Top Depth of Interval (mm)	Bottom Depth of Interval (mm)	Average Depth of Interval (mm)	$^{210}Pb_{Tot}$ Activity (dpm/g)	$^{210}Pb_{Tot}$ Activity error (dpm/g)	$^{210}Pb_{xs}$ Activity (dpm/g)	$^{210}Pb_{xs}$ Activity error (dpm/g)	D.C. $^{210}Pb_{xs}$ Activity (dpm/g)	D.C. $^{210}Pb_{xs}$ Activity error (dpm/g)
WB-1109-MC-04	0	2	1	38.55	1.36	36.81	1.37	36.87	1.37
WB-1109-MC-04	2	4	3	41.23	1.17	39.62	1.18	39.69	1.18
WB-1109-MC-04	4	6	5	44.56	1.05	42.99	1.06	43.09	1.06
WB-1109-MC-04	6	8	7	44.76	1.11	43.13	1.12	43.23	1.12
WB-1109-MC-04	8	10	9	43.56	0.92	42.45	0.92	42.55	0.93
WB-1109-MC-04	10	12	11	42.74	1.10	41.13	1.10	41.23	1.11
WB-1109-MC-04	12	14	13	39.99	0.95	38.86	0.96	39.00	0.96
WB-1109-MC-04	14	16	15	37.24	0.90	35.89	0.91	36.05	0.91
WB-1109-MC-04	16	18	17	32.43	0.75	30.83	0.75	30.94	0.76
WB-1109-MC-04	18	20	19	29.78	0.78	28.60	0.79	28.73	0.79
WB-1109-MC-04	20	25	22.5	25.99	0.52	24.82	0.52	24.90	0.53
WB-1109-MC-04	30	35	32.5	20.56	0.40	19.57	0.40	19.62	0.40
WB-1109-MC-04	40	45	42.5	15.64	0.38	14.53	0.38	14.58	0.38
WB-1109-MC-04	50	55	52.5	10.51	0.29	9.49	0.30	9.52	0.30
WB-1109-MC-04	60	65	62.5	7.27	0.24	6.28	0.25	6.30	0.25
WB-1109-MC-04	70	75	72.5	7.34	0.23	6.35	0.24	6.37	0.24
WB-1109-MC-04	80	85	82.5	5.69	0.19	4.71	0.20	4.72	0.20
WB-1109-MC-04	90	95	92.5	5.13	0.20	4.08	0.21	4.09	0.21
WB-1109-MC-04	100	105	102.5	3.23	0.15	2.08	0.17	2.09	0.17
WB-1109-MC-04	110	115	112.5	3.52	0.16	2.42	0.17	2.42	0.17
WB-1109-MC-04	120	125	122.5	2.68	0.14	1.52	0.16	1.52	0.16
WB-1109-MC-04	130	135	132.5	2.57	0.13	1.61	0.15	1.61	0.15
WB-1109-MC-04	140	145	142.5	3.97	0.17	2.96	0.18	2.97	0.18
WB-1109-MC-04	150	155	152.5	2.02	0.12	1.04	0.14	1.05	0.14

Table I.1 (Continued).

Core ID	Top Depth of Interval (mm)	Bottom Depth of Interval (mm)	Average Depth of Interval (mm)	$^{210}Pb_{Tot}$ Activity (dpm/g)	$^{210}Pb_{Tot}$ Activity error (dpm/g)	$^{210}Pb_{xs}$ Activity (dpm/g)	$^{210}Pb_{xs}$ Activity error (dpm/g)	D.C. $^{210}Pb_{xs}$ Activity (dpm/g)	D.C. $^{210}Pb_{xs}$ Activity error (dpm/g)
WB-1109-MC-04	160	165	162.5	2.34	0.13	1.41	0.14	1.41	0.14
WB-1109-MC-04	170	175	172.5	2.58	0.14	1.65	0.15	1.65	0.15
WB-1109-MC-04	180	185	182.5	2.23	0.09	1.46	0.10	1.62	0.11
WB-1109-MC-04	210	215	212.5	2.02	0.11	1.01	0.13	1.25	0.16

Table I.2. SLRad data of $^{210}Pb_{Tot}$, $^{210}Pb_{xs}$, and D.C. $^{210}Pb_{xs}$ for core site WB-1110-MC-DSH-08. Sediment cores with sub-sample intervals (mm), and SLRad activities for $^{210}Pb_{Tot}$, $^{210}Pb_{xs}$, and D.C. $^{210}Pb_{xs}$ (Decay Corrected). Note: Blank cell denotes no analysis performed.

Core ID	Top Depth of Interval (mm)	Bottom Depth of Interval (mm)	Average Depth of Interval (mm)	$^{210}Pb_{Tot}$ Activity (dpm/g)	$^{210}Pb_{Tot}$ Activity error (dpm/g)	$^{210}Pb_{xs}$ Activity (dpm/g)	$^{210}Pb_{xs}$ Activity error (dpm/g)	D.C. $^{210}Pb_{xs}$ Activity (dpm/g)	D.C. $^{210}Pb_{xs}$ Activity error (dpm/g)
WB-1110-MC-DSH-08	0	2	1	65.64	1.40	63.56	1.40	63.79	1.41
WB-1110-MC-DSH-08	2	4	3	67.87	1.21	66.21	1.21	66.48	1.21
WB-1110-MC-DSH-08	4	6	5	63.29	1.12	61.74	1.13	62.09	1.13
WB-1110-MC-DSH-08	6	8	7	65.24	1.03	63.55	1.04	63.94	1.04
WB-1110-MC-DSH-08	8	10	9	64.87	0.96	63.15	0.96	63.56	0.97
WB-1110-MC-DSH-08	10	12	11	56.05	1.29	54.63	1.30	55.09	1.31
WB-1110-MC-DSH-08	12	14	13	51.82	0.83	50.39	0.83	50.77	0.84
WB-1110-MC-DSH-08	14	16	15	59.63	0.91	57.90	0.92	60.30	0.95
WB-1110-MC-DSH-08	16	18	17	47.58	0.82	46.18	0.82	47.85	0.85
WB-1110-MC-DSH-08	18	20	19	48.26	0.82	46.48	0.82	46.88	0.83
WB-1110-MC-DSH-08	22	24	23	51.56	0.82	49.00	0.83	52.21	0.88
WB-1110-MC-DSH-08	26	28	27	42.92	0.70	40.85	0.70	41.24	0.71
WB-1110-MC-DSH-08	32	34	33	36.75	0.64	35.05	0.65	36.31	0.67
WB-1110-MC-DSH-08	34	36	35	39.77	0.67	38.14	0.67	38.51	0.68
WB-1110-MC-DSH-08	38	40	39	37.22	0.65	35.99	0.65	36.50	0.66
WB-1110-MC-DSH-08	42	44	43	33.33	0.60	31.97	0.60	32.37	0.61
WB-1110-MC-DSH-08	46	48	47	31.62	0.57	30.29	0.57	30.71	0.58
WB-1110-MC-DSH-08	48	50	49	27.26	0.52	26.05	0.53	26.98	0.54
WB-1110-MC-DSH-08	50	55	52.5	26.81	0.35	24.97	0.36	25.27	0.36
WB-1110-MC-DSH-08	60	65	62.5	21.00	0.30	19.11	0.31	20.35	0.33
WB-1110-MC-DSH-08	70	75	72.5	17.83	0.28	16.20	0.29	16.40	0.29
WB-1110-MC-DSH-08	80	85	82.5	14.60	0.25	12.61	0.26	13.43	0.28
WB-1110-MC-DSH-08	90	95	92.5	11.85	0.22	10.12	0.23	10.48	0.24
WB-1110-MC-DSH-08	100	105	102.5	10.74	0.20	8.70	0.21	9.27	0.23

Table I.2 (Continued).

Core ID	Top Depth of Interval (mm)	Bottom Depth of Interval (mm)	Average Depth of Interval (mm)	$^{210}Pb_{Tot}$ Activity (dpm/g)	$^{210}Pb_{Tot}$ Activity error (dpm/g)	$^{210}Pb_{xs}$ Activity (dpm/g)	$^{210}Pb_{xs}$ Activity error (dpm/g)	D.C. $^{210}Pb_{xs}$ Activity (dpm/g)	D.C. $^{210}Pb_{xs}$ Activity error (dpm/g)
WB-1110-MC-DSH-08	110	115	112.5	7.46	0.17	5.64	0.19	5.71	0.19
WB-1110-MC-DSH-08	120	125	122.5	6.55	0.17	4.63	0.18	4.94	0.19
WB-1110-MC-DSH-08	130	135	132.5	4.60	0.14	2.57	0.15	2.70	0.16
WB-1110-MC-DSH-08	140	145	142.5	3.83	0.12	2.05	0.14	2.16	0.15
WB-1110-MC-DSH-08	150	155	152.5	3.20	0.16	1.34	0.18	1.35	0.18
WB-1110-MC-DSH-08	160	165	162.5	3.16	0.11	1.21	0.13	1.27	0.14
WB-1110-MC-DSH-08	180	185	182.5	2.93	0.11	1.09	0.13	1.15	0.14
WB-1110-MC-DSH-08	190	195	192.5	2.42	0.10	0.63	0.12	0.77	0.14
WB-1110-MC-DSH-08	210	215	212.5	2.85	0.14	1.15	0.15	1.40	0.19
WB-1110-MC-DSH-08	230	235	232.5	2.82	0.14	1.13	0.16	1.37	0.19
WB-1110-MC-DSH-08	250	255	252.5	3.09	0.15	1.52	0.16	1.86	0.20
WB-1110-MC-DSH-08	270	275	272.5	2.22	0.09	0.23	0.11	0.28	0.14

Table I.3. SLRad data of $^{210}Pb_{Tot}$, $^{210}Pb_{xs}$, and D.C. $^{210}Pb_{xs}$ for core site WB-1110-MC-DSH-10. Sediment cores with sub-sample intervals (mm), and SLRad activities for $^{210}Pb_{Tot}$, $^{210}Pb_{xs}$, and D.C. $^{210}Pb_{xs}$ (Decay Corrected). Note: Blank cell denotes no analysis performed.

Core ID	Top Depth of Interval (mm)	Bottom Depth of Interval (mm)	Average Depth of Interval (mm)	$^{210}Pb_{Tot}$ Activity (dpm/g)	$^{210}Pb_{Tot}$ Activity error (dpm/g)	$^{210}Pb_{xs}$ Activity (dpm/g)	$^{210}Pb_{xs}$ Activity error (dpm/g)	D.C. $^{210}Pb_{xs}$ Activity (dpm/g)	D.C. $^{210}Pb_{xs}$ Activity error (dpm/g)
WB-1110-MC-DSH-10	0	2	1	59.90	1.12	57.63	1.13	58.27	1.14
WB-1110-MC-DSH-10	2	4	3	52.34	0.90	50.38	0.91	50.98	0.92
WB-1110-MC-DSH-10	4	6	5	43.15	0.72	41.32	0.72	43.06	0.76
WB-1110-MC-DSH-10	6	8	7	33.21	0.67	31.21	0.67	32.50	0.70
WB-1110-MC-DSH-10	8	10	9	32.03	0.58	30.06	0.58	31.96	0.62
WB-1110-MC-DSH-10	10	12	11	30.51	0.56	28.82	0.57	29.16	0.58
WB-1110-MC-DSH-10	12	14	13	23.77	0.49	21.93	0.49	23.63	0.53
WB-1110-MC-DSH-10	14	16	15	21.28	0.45	19.27	0.46	23.44	0.56
WB-1110-MC-DSH-10	16	18	17	26.37	0.54	24.57	0.55	25.61	0.57
WB-1110-MC-DSH-10	18	20	19	20.96	0.48	18.88	0.49	22.98	0.59
WB-1110-MC-DSH-10	20	22	21	24.07	0.49	21.88	0.50	22.14	0.51
WB-1110-MC-DSH-10	24	26	25	20.58	0.44	18.74	0.45	20.19	0.48
WB-1110-MC-DSH-10	30	32	31	22.25	0.45	20.06	0.46	20.29	0.47
WB-1110-MC-DSH-10	40	42	41	22.20	0.45	20.32	0.46	20.58	0.46
WB-1110-MC-DSH-10	50	52	51	19.58	0.39	18.11	0.39	18.32	0.40
WB-1110-MC-DSH-10	60	62	61	27.23	0.46	25.25	0.47	25.57	0.47
WB-1110-MC-DSH-10	70	72	71	33.78	0.52	31.40	0.53	31.78	0.54
WB-1110-MC-DSH-10	80	85	82.5	30.21	0.34	27.71	0.35	29.24	0.37
WB-1110-MC-DSH-10	90	95	92.5	27.55	0.32	24.55	0.33	24.89	0.34
WB-1110-MC-DSH-10	100	105	102.5	13.85	0.22	11.69	0.23	12.35	0.25
WB-1110-MC-DSH-10	110	115	112.5	9.80	0.19	7.46	0.20	7.76	0.21
WB-1110-MC-DSH-10	120	125	122.5	7.89	0.17	5.30	0.19	5.71	0.20
WB-1110-MC-DSH-10	130	135	132.5	7.51	0.16	5.59	0.18	5.66	0.18
WB-1110-MC-DSH-10	140	145	142.5	6.15	0.15	4.12	0.16	4.44	0.18

Table I.3 (Continued).

Core ID	Top Depth of Interval (mm)	Bottom Depth of Interval (mm)	Average Depth of Interval (mm)	$^{210}Pb_{Tot}$ Activity (dpm/g)	$^{210}Pb_{Tot}$ Activity error (dpm/g)	$^{210}Pb_{xs}$ Activity (dpm/g)	$^{210}Pb_{xs}$ Activity error (dpm/g)	D.C. $^{210}Pb_{xs}$ Activity (dpm/g)	D.C. $^{210}Pb_{xs}$ Activity error (dpm/g)
WB-1110-MC-DSH-10	150	155	152.5	5.08	0.14	3.13	0.16	3.25	0.17
WB-1110-MC-DSH-10	160	165	162.5	4.60	0.13	2.64	0.15	2.85	0.16
WB-1110-MC-DSH-10	170	175	172.5	4.48	0.13	2.58	0.15	2.69	0.15
WB-1110-MC-DSH-10	180	185	182.5	4.21	0.13	2.21	0.14	2.33	0.15
WB-1110-MC-DSH-10	190	195	192.5	4.41	0.13	2.31	0.15	2.40	0.15
WB-1110-MC-DSH-10	200	205	202.5	2.94	0.11	1.02	0.13	1.08	0.13
WB-1110-MC-DSH-10	210	215	212.5	3.09	0.11	1.11	0.13	1.17	0.14
WB-1110-MC-DSH-10	220	225	222.5	3.09	0.11	1.10	0.13	1.16	0.13
WB-1110-MC-DSH-10	240	245	242.5	2.95	0.11	1.02	0.13	1.08	0.13
WB-1110-MC-DSH-10	250	255	252.5	1.83	0.11	0.15	0.13	0.19	0.16
WB-1110-MC-DSH-10	270	275	272.5	1.58	0.10	-0.11	0.12	-0.14	0.15
WB-1110-MC-DSH-10	290	295	292.5	1.77	0.10	0.00	0.12	0.00	0.15
WB-1110-MC-DSH-10	310	315	312.5	1.63	0.10	-0.15	0.13	-0.18	0.15

Table I.4. SLRad data of $^{210}Pb_{Tot}$, $^{210}Pb_{xs}$, and D.C. $^{210}Pb_{xs}$ for core site WB-1110-MC-PCB-06. Sediment cores with sub-sample intervals (mm), and SLRad activities for $^{210}Pb_{Tot}$, $^{210}Pb_{xs}$, and D.C. $^{210}Pb_{xs}$ (Decay Corrected). Note: Blank cell denotes no analysis performed.

Core ID	Top Depth of Interval (mm)	Bottom Depth of Interval (mm)	Average Depth of Interval (mm)	$^{210}Pb_{Tot}$ Activity (dpm/g)	$^{210}Pb_{Tot}$ Activity error (dpm/g)	$^{210}Pb_{xs}$ Activity (dpm/g)	$^{210}Pb_{xs}$ Activity error (dpm/g)	D.C. $^{210}Pb_{xs}$ Activity (dpm/g)	D.C. $^{210}Pb_{xs}$ Activity error (dpm/g)
WB-1110-MC-PCB-06	0	2	1	63.54	1.49	61.77	1.49	62.18	1.50
WB-1110-MC-PCB-06	2	4	3	60.74	1.06	59.51	1.07	60.41	1.08
WB-1110-MC-PCB-06	4	6	5	60.44	0.98	59.24	0.99	59.65	0.99
WB-1110-MC-PCB-06	6	10	8	54.51	0.62	52.98	0.62	53.69	0.63
WB-1110-MC-PCB-06	10	12	11	56.00	0.81	54.75	0.81	55.14	0.82
WB-1110-MC-PCB-06	12	14	13	51.44	0.81	49.99	0.82	53.09	0.87
WB-1110-MC-PCB-06	14	16	15	51.25	0.81	49.88	0.82	50.32	0.82
WB-1110-MC-PCB-06	16	18	17	45.32	0.74	44.07	0.75	44.73	0.76
WB-1110-MC-PCB-06	18	20	19	42.94	0.69	41.62	0.69	42.01	0.70
WB-1110-MC-PCB-06	24	26	25	36.87	0.68	35.23	0.69	37.54	0.73
WB-1110-MC-PCB-06	28	30	29	33.38	0.58	31.87	0.59	32.25	0.59
WB-1110-MC-PCB-06	36	38	37	29.70	0.59	27.83	0.60	28.12	0.60
WB-1110-MC-PCB-06	40	42	41	28.70	0.55	26.63	0.56	26.95	0.57
WB-1110-MC-PCB-06	50	52	51	19.85	0.44	17.25	0.45	17.44	0.45
WB-1110-MC-PCB-06	60	62	61	15.16	0.31	13.33	0.32	14.05	0.33
WB-1110-MC-PCB-06	70	72	71	12.50	0.32	10.96	0.33	11.09	0.33
WB-1110-MC-PCB-06	80	82	81	9.59	0.31	7.95	0.32	8.38	0.34
WB-1110-MC-PCB-06	90	92	91	8.02	0.26	6.42	0.27	6.69	0.28
WB-1110-MC-PCB-06	100	105	102.5	4.60	0.14	2.52	0.15	2.66	0.16
WB-1110-MC-PCB-06	110	115	112.5	4.48	0.14	2.55	0.16	2.58	0.16
WB-1110-MC-PCB-06	130	135	132.5	4.29	0.13	2.24	0.14	2.32	0.15
WB-1110-MC-PCB-06	150	155	152.5	3.59	0.12	1.82	0.14	1.89	0.14
WB-1110-MC-PCB-06	170	175	172.5	3.66	0.13	1.89	0.14	1.96	0.15
WB-1110-MC-PCB-06	190	195	192.5	2.64	0.11	0.80	0.13	0.84	0.13

Table I.4 (Continued).

Core ID	Top Depth of Interval (mm)	Bottom Depth of Interval (mm)	Average Depth of Interval (mm)	$^{210}Pb_{Tot}$ Activity (dpm/g)	$^{210}Pb_{Tot}$ Activity error (dpm/g)	$^{210}Pb_{xs}$ Activity (dpm/g)	$^{210}Pb_{xs}$ Activity error (dpm/g)	D.C. $^{210}Pb_{xs}$ Activity (dpm/g)	D.C. $^{210}Pb_{xs}$ Activity error (dpm/g)
WB-1110-MC-PCB-06	200	205	202.5	2.44	0.10	0.47	0.12	0.50	0.12
WB-1110-MC-PCB-06	220	225	222.5	2.36	0.10	0.47	0.12	0.54	0.13

Table I.5. SLRad data of $^{210}Pb_{Tot}$, $^{210}Pb_{xs}$, and D.C. $^{210}Pb_{xs}$ for core site WB-1114-MC-DSH-08. Sediment cores with sub-sample intervals (mm), and SLRad activities for $^{210}Pb_{Tot}$, $^{210}Pb_{xs}$, and D.C. $^{210}Pb_{xs}$ (Decay Corrected). Note: Blank cell denotes no analysis performed.

Core ID	Top Depth of Interval (mm)	Bottom Depth of Interval (mm)	Average Depth of Interval (mm)	$^{210}Pb_{Tot}$ Activity (dpm/g)	$^{210}Pb_{Tot}$ Activity error (dpm/g)	$^{210}Pb_{xs}$ Activity (dpm/g)	$^{210}Pb_{xs}$ Activity error (dpm/g)	D.C. $^{210}Pb_{xs}$ Activity (dpm/g)	D.C. $^{210}Pb_{xs}$ Activity error (dpm/g)
WB-1114-MC-DSH-08	0	2	1	57.95	1.19	56.05	1.19	56.44	1.20
WB-1114-MC-DSH-08	2	4	3	53.80	0.93	51.70	0.94	52.22	0.94
WB-1114-MC-DSH-08	4	6	5	56.11	0.97	54.04	0.97	54.59	0.98
WB-1114-MC-DSH-08	6	8	7	50.86	0.87	48.86	0.88	49.37	0.88
WB-1114-MC-DSH-08	8	10	9	35.01	0.64	33.51	0.64	40.62	0.78
WB-1114-MC-DSH-08	10	12	11	29.70	0.72	28.53	0.72	34.62	0.88
WB-1114-MC-DSH-08	12	14	13	49.05	0.80	47.01	0.81	47.53	0.81
WB-1114-MC-DSH-08	14	16	15	26.22	0.50	24.93	0.08	30.24	0.97
WB-1114-MC-DSH-08	16	18	17	50.96	0.85	49.01	0.86	49.36	0.87
WB-1114-MC-DSH-08	18	20	19	30.42	0.52	29.48	0.52	35.75	0.63
WB-1114-MC-DSH-08	24	26	25	50.34	0.76	48.34	0.76	48.99	0.77
WB-1114-MC-DSH-08	28	30	29	44.18	0.71	42.24	0.72	42.81	0.73
WB-1114-MC-DSH-08	32	34	33	43.60	0.70	41.66	0.71	41.97	0.72
WB-1114-MC-DSH-08	36	38	37	45.60	0.70	43.51	0.70	44.12	0.71
WB-1114-MC-DSH-08	40	42	41	38.73	0.64	36.88	0.65	37.40	0.66
WB-1114-MC-DSH-08	48	50	49	38.04	0.58	36.23	0.59	36.51	0.59
WB-1114-MC-DSH-08	70	75	72.5	21.90	0.33	20.05	0.33	20.21	0.34
WB-1114-MC-DSH-08	90	95	92.5	19.58	0.31	17.77	0.32	17.92	0.32
WB-1114-MC-DSH-08	110	115	112.5	13.71	0.25	11.73	0.26	11.83	0.27
WB-1114-MC-DSH-08	130	135	132.5	10.78	0.23	8.95	0.23	9.02	0.24
WB-1114-MC-DSH-08	150	155	152.5	7.17	0.19	5.05	0.20	5.16	0.20
WB-1114-MC-DSH-08	170	175	172.5	5.68	0.17	3.59	0.18	3.66	0.18
WB-1114-MC-DSH-08	180	185	182.5	3.54	0.12	1.41	0.14	1.49	0.15
WB-1114-MC-DSH-08	190	195	192.5	2.99	0.11	0.78	0.13	0.83	0.14

Table I.5 (Continued).

Core ID	Top Depth of Interval (mm)	Bottom Depth of Interval (mm)	Average Depth of Interval (mm)	$^{210}Pb_{Tot}$ Activity (dpm/g)	$^{210}Pb_{Tot}$ Activity error (dpm/g)	$^{210}Pb_{xs}$ Activity (dpm/g)	$^{210}Pb_{xs}$ Activity error (dpm/g)	D.C. $^{210}Pb_{xs}$ Activity (dpm/g)	D.C. $^{210}Pb_{xs}$ Activity error (dpm/g)
WB-1114-MC-DSH-08	200	205	202.5	3.18	0.12	1.05	0.13	1.12	0.14
WB-1114-MC-DSH-08	210	215	212.5	2.80	0.13	1.00	0.15	1.22	0.18
WB-1114-MC-DSH-08	230	235	232.5	2.67	0.18	0.99	0.20	1.21	0.25

Table I.6. SLRad data of $^{210}Pb_{Tot}$, $^{210}Pb_{xs}$, and D.C. $^{210}Pb_{xs}$ for core site WB-1114-MC-DSH-10. Sediment cores with sub-sample intervals (mm), and SLRad activities for $^{210}Pb_{Tot}$, $^{210}Pb_{xs}$, and D.C. $^{210}Pb_{xs}$ (Decay Corrected). Note: Blank cell denotes no analysis performed.

Core ID	Top Depth of Interval (mm)	Bottom Depth of Interval (mm)	Average Depth of Interval (mm)	$^{210}Pb_{Tot}$ Activity (dpm/g)	$^{210}Pb_{Tot}$ Activity error (dpm/g)	$^{210}Pb_{xs}$ Activity (dpm/g)	$^{210}Pb_{xs}$ Activity error (dpm/g)	D.C. $^{210}Pb_{xs}$ Activity (dpm/g)	D.C. $^{210}Pb_{xs}$ Activity error (dpm/g)
WB-1114-MC-DSH-10	0	2	1	72.17	1.10	70.83	1.10	71.30	1.11
WB-1114-MC-DSH-10	2	4	3	72.11	1.08	70.57	1.08	71.24	1.09
WB-1114-MC-DSH-10	4	6	5	53.16	0.93	51.45	0.94	53.66	0.98
WB-1114-MC-DSH-10	6	8	7	41.05	0.71	39.40	0.72	41.10	0.75
WB-1114-MC-DSH-10	8	10	9	37.23	0.67	35.52	0.68	37.05	0.71
WB-1114-MC-DSH-10	10	12	11	30.26	0.61	28.53	0.62	30.20	0.66
WB-1114-MC-DSH-10	12	14	13	27.09	0.56	25.35	0.57	26.45	0.60
WB-1114-MC-DSH-10	14	16	15	18.02	0.48	16.48	0.49	19.94	0.59
WB-1114-MC-DSH-10	16	18	17	27.82	0.56	26.47	0.56	26.68	0.57
WB-1114-MC-DSH-10	18	20	19	23.51	0.49	21.76	0.50	22.71	0.52
WB-1114-MC-DSH-10	20	22	21	23.48	0.50	22.00	0.51	22.96	0.53
WB-1114-MC-DSH-10	24	26	25	18.38	0.41	16.85	0.41	17.84	0.44
WB-1114-MC-DSH-10	32	34	33	23.54	0.44	21.79	0.45	21.97	0.45
WB-1114-MC-DSH-10	40	42	41	24.92	0.51	23.32	0.52	24.70	0.55
WB-1114-MC-DSH-10	48	50	49	26.32	0.47	24.53	0.48	24.69	0.48
WB-1114-MC-DSH-10	56	58	57	28.64	0.51	26.22	0.52	27.77	0.55
WB-1114-MC-DSH-10	64	66	65	34.46	0.56	32.55	0.57	32.81	0.58
WB-1114-MC-DSH-10	72	74	73	31.84	0.50	29.62	0.51	29.98	0.51
WB-1114-MC-DSH-10	80	82	81	30.01	0.45	27.80	0.46	28.02	0.46
WB-1114-MC-DSH-10	90	95	92.5	15.82	0.24	13.15	0.25	13.78	0.26
WB-1114-MC-DSH-10	100	105	102.5	9.52	0.19	7.08	0.20	7.51	0.21
WB-1114-MC-DSH-10	110	115	112.5	8.55	0.18	6.15	0.20	6.45	0.21
WB-1114-MC-DSH-10	120	125	122.5	7.79	0.18	5.44	0.19	5.48	0.19
WB-1114-MC-DSH-10	130	135	132.5	6.84	0.16	4.81	0.17	5.04	0.18

Table I.6 (Continued).

Core ID	Top Depth of Interval (mm)	Bottom Depth of Interval (mm)	Average Depth of Interval (mm)	$^{210}Pb_{Tot}$ Activity (dpm/g)	$^{210}Pb_{Tot}$ Activity error (dpm/g)	$^{210}Pb_{xs}$ Activity (dpm/g)	$^{210}Pb_{xs}$ Activity error (dpm/g)	D.C. $^{210}Pb_{xs}$ Activity (dpm/g)	D.C. $^{210}Pb_{xs}$ Activity error (dpm/g)
WB-1114-MC-DSH-10	150	155	152.5	5.32	0.14	3.25	0.16	3.40	0.17
WB-1114-MC-DSH-10	170	175	172.5	4.11	0.13	2.18	0.15	2.28	0.16
WB-1114-MC-DSH-10	190	195	192.5	3.68	0.12	1.50	0.14	1.57	0.15
WB-1114-MC-DSH-10	210	215	212.5	3.66	0.12	1.53	0.14	1.61	0.14
WB-1114-MC-DSH-10	230	235	232.5	3.69	0.12	1.66	0.14	1.74	0.14
WB-1114-MC-DSH-10	250	255	252.5	2.98	0.11	0.88	0.13	0.97	0.14
WB-1114-MC-DSH-10	270	275	272.5	3.51	0.12	1.58	0.13	1.82	0.15
WB-1114-MC-DSH-10	290	295	292.5	2.66	0.14	0.93	0.16	1.13	0.20
WB-1114-MC-DSH-10	310	315	312.5	2.71	0.14	0.97	0.17	1.20	0.20

Table I.7. SLRad data of $^{210}Pb_{Tot}$, $^{210}Pb_{xs}$, and D.C. $^{210}Pb_{xs}$ for core site WB-1114-MC-PCB-06. Sediment cores with sub-sample intervals (mm), and SLRad activities for $^{210}Pb_{Tot}$, $^{210}Pb_{xs}$, and D.C. $^{210}Pb_{xs}$ (Decay Corrected). Note: Blank cell denotes no analysis performed.

Core ID	Top Depth of Interval (mm)	Bottom Depth of Interval (mm)	Average Depth of Interval (mm)	$^{210}Pb_{Tot}$ Activity (dpm/g)	$^{210}Pb_{Tot}$ Activity error (dpm/g)	$^{210}Pb_{xs}$ Activity (dpm/g)	$^{210}Pb_{xs}$ Activity error (dpm/g)	D.C. $^{210}Pb_{xs}$ Activity (dpm/g)	D.C. $^{210}Pb_{xs}$ Activity error (dpm/g)
WB-1114-MC-PCB-06	0	2	1	46.14	0.81	44.91	0.81	45.29	0.82
WB-1114-MC-PCB-06	2	4	3	48.12	0.91	46.53	0.91	49.28	0.97
WB-1114-MC-PCB-06	4	6	5	43.68	0.69	42.18	0.69	44.49	0.73
WB-1114-MC-PCB-06	6	8	7	48.18	0.84	46.44	0.85	49.21	0.90
WB-1114-MC-PCB-06	8	10	9	36.35	0.66	34.67	0.67	36.43	0.70
WB-1114-MC-PCB-06	10	12	11	42.56	0.67	41.19	0.68	44.14	0.72
WB-1114-MC-PCB-06	12	14	13	41.89	0.64	40.23	0.64	42.45	0.68
WB-1114-MC-PCB-06	14	16	15	50.68	0.75	49.10	0.76	52.05	0.80
WB-1114-MC-PCB-06	16	18	17	58.56	0.80	57.03	0.80	57.55	0.81
WB-1114-MC-PCB-06	18	20	19	51.48	0.73	49.89	0.74	53.45	0.79
WB-1114-MC-PCB-06	20	22	21	47.29	0.78	45.57	0.79	48.32	0.84
WB-1114-MC-PCB-06	24	26	25	48.71	0.73	47.23	0.74	49.81	0.78
WB-1114-MC-PCB-06	32	34	33	47.34	0.73	44.79	0.74	45.17	0.74
WB-1114-MC-PCB-06	36	38	37	37.84	0.62	35.44	0.63	37.93	0.67
WB-1114-MC-PCB-06	40	42	41	37.73	0.64	34.84	0.65	36.94	0.69
WB-1114-MC-PCB-06	48	50	49	37.29	0.61	35.71	0.62	37.55	0.65
WB-1114-MC-PCB-06	56	58	57	28.18	0.54	26.59	0.55	28.21	0.58
WB-1114-MC-PCB-06	64	66	65	24.47	0.48	22.89	0.49	23.09	0.49
WB-1114-MC-PCB-06	70	75	72.5	16.06	0.27	14.33	0.28	15.03	0.29
WB-1114-MC-PCB-06	80	85	82.5	10.89	0.22	9.21	0.23	9.77	0.24
WB-1114-MC-PCB-06	90	95	92.5	7.48	0.18	5.77	0.19	6.06	0.20
WB-1114-MC-PCB-06	100	105	102.5	6.05	0.17	4.48	0.19	4.75	0.20
WB-1114-MC-PCB-06	110	115	112.5	5.58	0.14	3.83	0.16	4.06	0.17
WB-1114-MC-PCB-06	120	125	122.5	3.89	0.13	2.28	0.14	2.30	0.14

Table I.7 (Continued).

Core ID	Top Depth of Interval (mm)	Bottom Depth of Interval (mm)	Average Depth of Interval (mm)	$^{210}Pb_{Tot}$ Activity (dpm/g)	$^{210}Pb_{Tot}$ Activity error (dpm/g)	$^{210}Pb_{xs}$ Activity (dpm/g)	$^{210}Pb_{xs}$ Activity error (dpm/g)	D.C. $^{210}Pb_{xs}$ Activity (dpm/g)	D.C. $^{210}Pb_{xs}$ Activity error (dpm/g)
WB-1114-MC-PCB-06	130	135	132.5	2.79	0.11	1.06	0.12	1.12	0.13
WB-1114-MC-PCB-06	140	145	142.5	3.48	0.12	1.60	0.14	1.70	0.14
WB-1114-MC-PCB-06	150	155	152.5	3.19	0.11	1.49	0.13	1.56	0.13
WB-1114-MC-PCB-06	170	175	172.5	2.68	0.10	1.06	0.12	1.11	0.13
WB-1114-MC-PCB-06	190	195	192.5	2.29	0.09	0.63	0.11	0.66	0.12
WB-1114-MC-PCB-06	210	215	212.5	2.29	0.09	0.59	0.11	0.63	0.12
WB-1114-MC-PCB-06	230	235	232.5	2.43	0.10	0.78	0.11	0.85	0.13
WB-1114-MC-PCB-06	270	275	272.5	2.50	0.16	0.90	0.18	1.11	0.22

Table I.8. SLRad data of $^{210}Pb_{Tot}$, $^{210}Pb_{xs}$, and D.C. $^{210}Pb_{xs}$ for core site WB-0911-BC-DSH-08. Sediment cores with sub-sample intervals (mm), and SLRad activities for $^{210}Pb_{Tot}$, $^{210}Pb_{xs}$, and D.C. $^{210}Pb_{xs}$ (Decay Corrected). Note: Blank cell denotes no analysis performed.

Core ID	Top Depth of Interval (mm)	Bottom Depth of Interval (mm)	Average Depth of Interval (mm)	$^{210}Pb_{Tot}$ Activity (dpm/g)	$^{210}Pb_{Tot}$ Activity error (dpm/g)	$^{210}Pb_{xs}$ Activity (dpm/g)	$^{210}Pb_{xs}$ Activity error (dpm/g)	D.C. $^{210}Pb_{xs}$ Activity (dpm/g)	D.C. $^{210}Pb_{xs}$ Activity error (dpm/g)
WB-0911-BC-DSH-08	0	2	1	63.93	1.03	62.72	1.03	62.88	1.04
WB-0911-BC-DSH-08	2	4	3	66.61	0.89	65.19	0.89	65.38	0.90
WB-0911-BC-DSH-08	4	6	5	57.93	0.75	56.47	0.75	56.72	0.76
WB-0911-BC-DSH-08	6	8	7	56.97	0.83	55.65	0.84	55.93	0.84
WB-0911-BC-DSH-08	8	10	9	54.63	0.82	53.22	0.83	53.41	0.83
WB-0911-BC-DSH-08	10	12	11	53.47	0.81	52.05	0.81	52.31	0.82
WB-0911-BC-DSH-08	12	14	13	53.64	0.81	52.20	0.82	52.37	0.82
WB-0911-BC-DSH-08	14	16	15	50.32	0.72	48.70	0.72	48.98	0.73
WB-0911-BC-DSH-08	16	18	17	50.38	0.72	48.81	0.73	48.94	0.73
WB-0911-BC-DSH-08	18	20	19	48.67	0.73	47.06	0.73	47.26	0.73
WB-0911-BC-DSH-08	24	26	25	48.70	0.70	46.52	0.70	48.38	0.73
WB-0911-BC-DSH-08	26	28	27	47.28	0.69	44.91	0.70	47.19	0.73
WB-0911-BC-DSH-08	28	30	29	46.60	0.70	44.53	0.71	46.81	0.75
WB-0911-BC-DSH-08	30	35	32.5	36.77	0.44	35.07	0.45	35.41	0.45
WB-0911-BC-DSH-08	40	45	42.5	35.52	0.40	33.68	0.41	35.03	0.43
WB-0911-BC-DSH-08	50	55	52.5	24.39	0.34	22.88	0.34	23.10	0.35
WB-0911-BC-DSH-08	60	65	62.5	20.25	0.30	18.37	0.31	19.11	0.32
WB-0911-BC-DSH-08	70	75	72.5	16.06	0.26	14.35	0.27	14.48	0.27
WB-0911-BC-DSH-08	80	85	82.5	15.12	0.25	13.11	0.26	13.64	0.27
WB-0911-BC-DSH-08	90	95	92.5	13.26	0.23	11.14	0.24	11.36	0.25
WB-0911-BC-DSH-08	100	105	102.5	10.94	0.20	9.07	0.21	9.44	0.22
WB-0911-BC-DSH-08	110	115	112.5	7.67	0.17	6.04	0.18	6.11	0.19
WB-0911-BC-DSH-08	120	125	122.5	6.91	0.17	4.99	0.18	5.20	0.19
WB-0911-BC-DSH-08	130	135	132.5	5.73	0.15	3.93	0.16	3.97	0.16

Table I.8 (Continued).

Core ID	Top Depth of Interval (mm)	Bottom Depth of Interval (mm)	Average Depth of Interval (mm)	$^{210}Pb_{Tot}$ Activity (dpm/g)	$^{210}Pb_{Tot}$ Activity error (dpm/g)	$^{210}Pb_{xs}$ Activity (dpm/g)	$^{210}Pb_{xs}$ Activity error (dpm/g)	D.C. $^{210}Pb_{xs}$ Activity (dpm/g)	D.C. $^{210}Pb_{xs}$ Activity error (dpm/g)
WB-0911-BC-DSH-08	140	145	142.5	4.86	0.13	2.82	0.15	2.94	0.15
WB-0911-BC-DSH-08	150	155	152.5	3.37	0.12	1.68	0.13	1.69	0.13
WB-0911-BC-DSH-08	170	175	172.5	2.95	0.11	1.10	0.13	1.11	0.13
WB-0911-BC-DSH-08	190	195	192.5	3.12	0.11	1.23	0.13	1.24	0.13
WB-0911-BC-DSH-08	210	215	212.5	3.51	0.12	1.26	0.14	1.31	0.14
WB-0911-BC-DSH-08	230	235	232.5	3.00	0.11	1.12	0.13	1.21	0.14
WB-0911-BC-DSH-08	250	255	252.5	2.32	0.09	0.19	0.12	0.22	0.14
WB-0911-BC-DSH-08	270	275	272.5	2.42	0.10	0.41	0.12	0.49	0.14
WB-0911-BC-DSH-08	290	295	292.5	2.54	0.10	0.60	0.12	0.72	0.14

Table I.9. SLRad data of $^{210}Pb_{Tot}$, $^{210}Pb_{xs}$, and D.C. $^{210}Pb_{xs}$ for core site WB-0911-BC-DSH-10. Sediment cores with sub-sample intervals (mm), and SLRad activities for $^{210}Pb_{Tot}$, $^{210}Pb_{xs}$, and D.C. $^{210}Pb_{xs}$ (Decay Corrected). Note: Blank cell denotes no analysis performed.

Core ID	Top Depth of Interval (mm)	Bottom Depth of Interval (mm)	Average Depth of Interval (mm)	$^{210}Pb_{Tot}$ Activity (dpm/g)	$^{210}Pb_{Tot}$ Activity error (dpm/g)	$^{210}Pb_{xs}$ Activity (dpm/g)	$^{210}Pb_{xs}$ Activity error (dpm/g)	D.C. $^{210}Pb_{xs}$ Activity (dpm/g)	D.C. $^{210}Pb_{xs}$ Activity error (dpm/g)
WB-0911-BC-DSH-10	0	2	1	62.45	1.09	60.55	1.10	60.70	1.10
WB-0911-BC-DSH-10	2	4	3	58.97	0.82	57.15	0.82	57.48	0.83
WB-0911-BC-DSH-10	4	6	5	43.55	0.65	41.55	0.66	41.76	0.66
WB-0911-BC-DSH-10	6	8	7	36.75	0.61	34.61	0.62	34.80	0.62
WB-0911-BC-DSH-10	8	10	9	32.88	0.57	30.81	0.57	30.95	0.58
WB-0911-BC-DSH-10	10	12	11	33.15	0.58	31.09	0.58	31.29	0.59
WB-0911-BC-DSH-10	12	14	13	29.07	0.50	26.98	0.51	27.08	0.51
WB-0911-BC-DSH-10	14	16	15	25.84	0.50	23.81	0.51	23.97	0.52
WB-0911-BC-DSH-10	16	18	17	24.36	0.48	22.48	0.49	22.56	0.49
WB-0911-BC-DSH-10	18	20	19	20.19	0.44	18.10	0.45	21.50	0.53
WB-0911-BC-DSH-10	24	26	25	26.24	0.47	23.86	0.48	25.05	0.50
WB-0911-BC-DSH-10	32	34	33	26.11	0.52	24.15	0.53	24.43	0.53
WB-0911-BC-DSH-10	40	45	42.5	20.94	0.29	18.99	0.29	19.94	0.31
WB-0911-BC-DSH-10	50	55	52.5	22.21	0.30	19.82	0.31	20.04	0.31
WB-0911-BC-DSH-10	60	65	62.5	22.67	0.31	20.55	0.32	21.58	0.34
WB-0911-BC-DSH-10	70	75	72.5	25.04	0.31	22.60	0.32	22.83	0.32
WB-0911-BC-DSH-10	80	85	82.5	26.32	0.33	24.01	0.34	25.29	0.36
WB-0911-BC-DSH-10	90	95	92.5	20.44	0.28	18.24	0.29	18.49	0.29
WB-0911-BC-DSH-10	110	115	112.5	13.02	0.22	10.71	0.23	10.86	0.23
WB-0911-BC-DSH-10	130	135	132.5	9.12	0.18	6.98	0.20	7.04	0.20
WB-0911-BC-DSH-10	150	155	152.5	5.49	0.15	3.54	0.16	3.66	0.17
WB-0911-BC-DSH-10	170	175	172.5	4.05	0.13	2.10	0.14	2.13	0.15
WB-0911-BC-DSH-10	190	195	192.5	4.22	0.14	2.22	0.15	2.25	0.16
WB-0911-BC-DSH-10	210	215	212.5	3.82	0.12	1.74	0.14	1.79	0.14

Table I.9 (Continued).

Core ID	Top Depth of Interval (mm)	Bottom Depth of Interval (mm)	Average Depth of Interval (mm)	$^{210}Pb_{Tot}$ Activity (dpm/g)	$^{210}Pb_{Tot}$ Activity error (dpm/g)	$^{210}Pb_{xs}$ Activity (dpm/g)	$^{210}Pb_{xs}$ Activity error (dpm/g)	D.C. $^{210}Pb_{xs}$ Activity (dpm/g)	D.C. $^{210}Pb_{xs}$ Activity error (dpm/g)
WB-0911-BC-DSH-10	230	235	232.5	2.89	0.11	0.90	0.13	0.93	0.13
WB-0911-BC-DSH-10	250	255	252.5	2.76	0.10	0.80	0.12	0.87	0.13
WB-0911-BC-DSH-10	270	275	272.5	2.72	0.10	0.79	0.12	0.90	0.14
WB-0911-BC-DSH-10	310	315	312.5	3.12	0.15	1.70	0.17	2.05	0.21

Table I.10. SLRad data of $^{210}Pb_{Tot}$, $^{210}Pb_{xs}$, and D.C. $^{210}Pb_{xs}$ for core site WB-0911-MC-PCB-06. Sediment cores with sub-sample intervals (mm), and SLRad activities for $^{210}Pb_{Tot}$, $^{210}Pb_{xs}$, and D.C. $^{210}Pb_{xs}$ (Decay Corrected). Note: Blank cell denotes no analysis performed.

Core ID	Top Depth of Interval (mm)	Bottom Depth of Interval (mm)	Average Depth of Interval (mm)	$^{210}Pb_{Tot}$ Activity (dpm/g)	$^{210}Pb_{Tot}$ Activity error (dpm/g)	$^{210}Pb_{xs}$ Activity (dpm/g)	$^{210}Pb_{xs}$ Activity error (dpm/g)	D.C. $^{210}Pb_{xs}$ Activity (dpm/g)	D.C. $^{210}Pb_{xs}$ Activity error (dpm/g)
WB-0911-MC-PCB-06	0	2	1	61.07	1.23	59.36	1.23	59.58	1.24
WB-0911-MC-PCB-06	2	4	3	58.83	1.31	57.20	1.32	57.54	1.32
WB-0911-MC-PCB-06	4	6	5	55.15	0.95	53.42	0.96	53.68	0.96
WB-0911-MC-PCB-06	6	8	7	50.87	0.94	49.19	0.95	49.45	0.95
WB-0911-MC-PCB-06	8	10	9	49.67	0.81	47.79	0.82	48.03	0.82
WB-0911-MC-PCB-06	10	12	11	45.68	0.76	43.56	0.77	43.82	0.77
WB-0911-MC-PCB-06	12	14	13	39.45	0.65	37.51	0.66	37.66	0.66
WB-0911-MC-PCB-06	14	16	15	37.32	0.70	35.41	0.71	35.65	0.71
WB-0911-MC-PCB-06	16	18	17	31.63	0.62	29.64	0.63	29.78	0.63
WB-0911-MC-PCB-06	18	20	19	27.47	0.55	25.46	0.56	25.64	0.57
WB-0911-MC-PCB-06	24	26	25	20.22	0.48	18.44	0.49	19.37	0.52
WB-0911-MC-PCB-06	32	34	33	15.82	0.39	14.28	0.40	14.38	0.41
WB-0911-MC-PCB-06	48	50	49	12.66	0.35	11.18	0.36	11.37	0.36
WB-0911-MC-PCB-06	70	75	72.5	23.94	0.31	22.14	0.32	22.51	0.33
WB-0911-MC-PCB-06	90	95	92.5	24.59	0.31	22.72	0.32	23.15	0.33
WB-0911-MC-PCB-06	110	115	112.5	16.98	0.25	15.29	0.26	15.55	0.26
WB-0911-MC-PCB-06	130	135	132.5	5.77	0.15	3.97	0.16	4.04	0.17
WB-0911-MC-PCB-06	150	155	152.5	3.81	0.12	2.07	0.14	2.11	0.14
WB-0911-MC-PCB-06	170	175	172.5	2.62	0.10	0.86	0.12	0.87	0.12
WB-0911-MC-PCB-06	190	195	192.5	2.68	0.10	1.03	0.11	1.07	0.12
WB-0911-MC-PCB-06	200	205	202.5	2.62	0.10	0.86	0.12	0.88	0.12
WB-0911-MC-PCB-06	210	215	212.5	2.42	0.10	0.68	0.12	0.71	0.12
WB-0911-MC-PCB-06	220	225	222.5	2.62	0.10	0.99	0.12	1.07	0.13
WB-0911-MC-PCB-06	230	235	232.5	2.54	0.14	1.12	0.16	1.34	0.19

Table I.11. SLRad data of $^{210}Pb_{Tot}$, $^{210}Pb_{xs}$, and D.C. $^{210}Pb_{xs}$ for core site WB-0812-MC-DSH-08. Sediment cores with sub-sample intervals (mm), and SLRad activities for $^{210}Pb_{Tot}$, $^{210}Pb_{xs}$, and D.C. $^{210}Pb_{xs}$ (Decay Corrected). Note: Blank cell denotes no analysis performed.

Core ID	Top Depth of Interval (mm)	Bottom Depth of Interval (mm)	Average Depth of Interval (mm)	$^{210}Pb_{Tot}$ Activity (dpm/g)	$^{210}Pb_{Tot}$ Activity error (dpm/g)	$^{210}Pb_{xs}$ Activity (dpm/g)	$^{210}Pb_{xs}$ Activity error (dpm/g)	D.C. $^{210}Pb_{xs}$ Activity (dpm/g)	D.C. $^{210}Pb_{xs}$ Activity error (dpm/g)
WB-0812-MC-DSH-08	0	2	1	67.67	0.95	65.57	0.96	65.76	0.96
WB-0812-MC-DSH-08	2	4	3	68.09	0.97	65.74	0.98	65.96	0.98
WB-0812-MC-DSH-08	4	6	5	61.06	0.84	59.02	0.84	59.24	0.85
WB-0812-MC-DSH-08	6	8	7	62.24	1.00	60.06	1.00	60.28	1.01
WB-0812-MC-DSH-08	8	10	9	60.36	0.86	58.53	0.86	58.76	0.86
WB-0812-MC-DSH-08	10	12	11	57.93	0.82	56.26	0.82	56.50	0.83
WB-0812-MC-DSH-08	12	14	13	56.26	0.88	54.17	0.88	54.71	0.89
WB-0812-MC-DSH-08	14	16	15	53.65	0.83	51.64	0.83	52.18	0.84
WB-0812-MC-DSH-08	16	18	17	46.91	0.75	44.59	0.76	45.33	0.77
WB-0812-MC-DSH-08	18	20	19	46.24	0.75	44.09	0.76	44.84	0.77
WB-0812-MC-DSH-08	30	32	31	42.89	0.70	40.88	0.70	41.58	0.71
WB-0812-MC-DSH-08	50	55	52.5	14.52	0.25	13.45	0.25	15.58	0.29
WB-0812-MC-DSH-08	70	75	72.5	13.91	0.26	11.60	0.27	11.81	0.27
WB-0812-MC-DSH-08	90	95	92.5	8.53	0.20	6.20	0.21	6.31	0.22
WB-0812-MC-DSH-08	110	115	112.5	5.42	0.16	4.03	0.17	4.11	0.17
WB-0812-MC-DSH-08	130	135	132.5	4.47	0.20	2.96	0.21	3.43	0.25
WB-0812-MC-DSH-08	150	155	152.5	2.70	0.11	2.20	0.12	2.24	0.12
WB-0812-MC-DSH-08	170	175	172.5	4.20	0.14	1.74	0.16	1.77	0.17
WB-0812-MC-DSH-08	190	195	192.5	1.20	0.10	-0.49	0.12	-0.57	0.14
WB-0812-MC-DSH-08	210	215	212.5	2.00	0.13	1.13	0.14	1.31	0.16
WB-0812-MC-DSH-08	230	235	232.5	1.81	0.13	-0.28	0.15	-0.32	0.17
WB-0812-MC-DSH-08	265	270	267.5	2.11	0.13	0.06	0.15	0.00	0.00
WB-0812-MC-DSH-08	285	290	287.5	1.86	0.13	-0.29	0.15	-0.01	0.00

Table I.12. SLRad data of $^{210}Pb_{Tot}$, $^{210}Pb_{xs}$, and D.C. $^{210}Pb_{xs}$ for core site WB-0812-MC-DSH-10. Sediment cores with sub-sample intervals (mm), and SLRad activities for $^{210}Pb_{Tot}$, $^{210}Pb_{xs}$, and D.C. $^{210}Pb_{xs}$ (Decay Corrected). Note: Blank cell denotes no analysis performed.

Core ID	Top Depth of Interval (mm)	Bottom Depth of Interval (mm)	Average Depth of Interval (mm)	$^{210}Pb_{Tot}$ Activity (dpm/g)	$^{210}Pb_{Tot}$ Activity error (dpm/g)	$^{210}Pb_{xs}$ Activity (dpm/g)	$^{210}Pb_{xs}$ Activity error (dpm/g)	D.C. $^{210}Pb_{xs}$ Activity (dpm/g)	D.C. $^{210}Pb_{xs}$ Activity error (dpm/g)
WB-0812-MC-DSH-10	0	2	1	49.78	0.73	47.87	0.74	47.97	0.74
WB-0812-MC-DSH-10	2	4	3	39.73	0.65	37.78	0.66	37.88	0.66
WB-0812-MC-DSH-10	4	6	5	40.27	0.65	38.13	0.65	38.24	0.66
WB-0812-MC-DSH-10	6	8	7	31.04	0.61	28.81	0.62	28.91	0.62
WB-0812-MC-DSH-10	8	10	9	27.44	0.50	25.02	0.51	25.26	0.51
WB-0812-MC-DSH-10	10	12	11	23.01	0.61	20.42	0.62	22.44	0.68
WB-0812-MC-DSH-10	12	14	13	24.23	0.45	21.51	0.46	23.17	0.50
WB-0812-MC-DSH-10	14	16	15	23.11	0.47	20.33	0.49	22.00	0.53
WB-0812-MC-DSH-10	16	18	17	27.66	0.50	25.05	0.51	26.99	0.55
WB-0812-MC-DSH-10	18	20	19	23.12	0.45	20.20	0.46	23.12	0.53
WB-0812-MC-DSH-10	20	22	21	21.92	0.45	18.64	0.47	20.39	0.51
WB-0812-MC-DSH-10	22	24	23	19.63	0.43	16.30	0.45	19.15	0.53
WB-0812-MC-DSH-10	24	26	25	20.31	0.44	17.73	0.45	19.88	0.50
WB-0812-MC-DSH-10	26	28	27	21.13	0.39	18.78	0.40	21.08	0.45
WB-0812-MC-DSH-10	28	30	29	19.47	0.43	17.50	0.44	19.65	0.50
WB-0812-MC-DSH-10	30	35	32.5	20.54	0.30	18.09	0.31	19.75	0.33
WB-0812-MC-DSH-10	35	40	37.5	15.62	0.26	13.86	0.27	15.56	0.30
WB-0812-MC-DSH-10	40	45	42.5	16.09	0.26	14.19	0.27	15.91	0.30
WB-0812-MC-DSH-10	45	50	47.5	16.35	0.26	14.50	0.27	16.28	0.30
WB-0812-MC-DSH-10	50	55	52.5	20.22	0.31	18.11	0.31	19.90	0.35
WB-0812-MC-DSH-10	55	60	57.5	17.59	0.26	15.61	0.27	17.53	0.31
WB-0812-MC-DSH-10	70	75	72.5	21.36	0.29	19.07	0.30	20.82	0.33
WB-0812-MC-DSH-10	80	85	82.5	20.15	0.28	17.93	0.29	20.12	0.32
WB-0812-MC-DSH-10	90	95	92.5	22.71	0.28	20.42	0.29	22.35	0.32

Table I.12 (Continued).

Core ID	Top Depth of Interval (mm)	Bottom Depth of Interval (mm)	Average Depth of Interval (mm)	$^{210}Pb_{Tot}$ Activity (dpm/g)	$^{210}Pb_{Tot}$ Activity error (dpm/g)	$^{210}Pb_{xs}$ Activity (dpm/g)	$^{210}Pb_{xs}$ Activity error (dpm/g)	D.C. $^{210}Pb_{xs}$ Activity (dpm/g)	D.C. $^{210}Pb_{xs}$ Activity error (dpm/g)
WB-0812-MC-DSH-10	100	105	102.5	18.25	0.26	16.30	0.27	18.28	0.30
WB-0812-MC-DSH-10	110	115	112.5	13.81	0.22	11.66	0.23	12.77	0.25
WB-0812-MC-DSH-10	130	135	132.5	14.53	0.29	12.93	0.30	15.01	0.34
WB-0812-MC-DSH-10	150	155	152.5	5.71	0.14	3.79	0.16	4.14	0.17
WB-0812-MC-DSH-10	170	175	172.5	5.58	0.19	4.08	0.21	4.73	0.24
WB-0812-MC-DSH-10	190	195	192.5	3.67	0.12	1.58	0.14	1.73	0.15
WB-0812-MC-DSH-10	210	215	212.5	4.20	0.26	2.28	0.29	2.72	0.35
WB-0812-MC-DSH-10	230	235	232.5	2.93	0.11	0.80	0.13	0.88	0.14
WB-0812-MC-DSH-10	250	255	252.5	2.91	0.21	1.16	0.24	1.38	0.28
WB-0812-MC-DSH-10	270	275	272.5	2.42	0.10	0.41	0.12	0.45	0.13
WB-0812-MC-DSH-10	310	315	312.5	3.25	0.15	1.56	0.17	1.83	0.20

Table I.13. SLRad data of $^{210}Pb_{Tot}$, $^{210}Pb_{xs}$, and D.C. $^{210}Pb_{xs}$ for core site WB-0812-MC-PCB-06. Sediment cores with sub-sample intervals (mm), and SLRad activities for $^{210}Pb_{Tot}$, $^{210}Pb_{xs}$, and D.C. $^{210}Pb_{xs}$ (Decay Corrected). Note: Blank cell denotes no analysis performed.

Core ID	Top Depth of Interval (mm)	Bottom Depth of Interval (mm)	Average Depth of Interval (mm)	$^{210}Pb_{Tot}$ Activity (dpm/g)	$^{210}Pb_{Tot}$ Activity error (dpm/g)	$^{210}Pb_{xs}$ Activity (dpm/g)	$^{210}Pb_{xs}$ Activity error (dpm/g)	D.C. $^{210}Pb_{xs}$ Activity (dpm/g)	D.C. $^{210}Pb_{xs}$ Activity error (dpm/g)
WB-0812-MC-PCB-06	0	2	1	61.32	0.83	59.90	0.83	60.11	0.84
WB-0812-MC-PCB-06	2	4	3	59.09	0.79	57.51	0.79	57.72	0.80
WB-0812-MC-PCB-06	4	6	5	54.58	0.82	53.05	0.82	53.25	0.83
WB-0812-MC-PCB-06	6	8	7	52.17	0.67	50.63	0.67	50.84	0.68
WB-0812-MC-PCB-06	8	10	9	53.23	0.81	51.69	0.81	52.04	0.82
WB-0812-MC-PCB-06	10	12	11	49.45	0.69	47.91	0.69	51.72	0.75
WB-0812-MC-PCB-06	12	14	13	47.13	0.77	45.53	0.78	49.06	0.84
WB-0812-MC-PCB-06	14	16	15	42.31	0.58	40.69	0.59	43.89	0.64
WB-0812-MC-PCB-06	16	18	17	39.46	0.62	37.73	0.63	40.65	0.68
WB-0812-MC-PCB-06	18	20	19	35.68	0.56	33.96	0.57	36.67	0.61
WB-0812-MC-PCB-06	24	26	25	29.69	0.55	27.67	0.56	29.83	0.60
WB-0812-MC-PCB-06	30	32	31	25.03	0.48	22.77	0.49	24.54	0.53
WB-0812-MC-PCB-06	50	55	52.5	12.40	0.22	10.58	0.23	11.41	0.25
WB-0812-MC-PCB-06	70	75	72.5	8.41	0.18	6.87	0.19	7.42	0.21
WB-0812-MC-PCB-06	90	95	92.5	5.20	0.14	3.56	0.16	3.84	0.17
WB-0812-MC-PCB-06	110	115	112.5	5.71	0.15	3.97	0.16	4.29	0.18
WB-0812-MC-PCB-06	130	135	132.5	5.30	0.14	2.98	0.15	3.22	0.17
WB-0812-MC-PCB-06	150	155	152.5	3.90	0.12	2.17	0.14	2.35	0.15
WB-0812-MC-PCB-06	170	175	172.5	2.60	0.10	0.96	0.12	1.03	0.13
WB-0812-MC-PCB-06	190	195	192.5	2.97	0.11	1.46	0.12	1.57	0.13
WB-0812-MC-PCB-06	210	215	212.5	2.77	0.11	1.17	0.12	1.26	0.13
WB-0812-MC-PCB-06	230	235	232.5	2.32	0.10	0.77	0.11	0.83	0.12

Table I.14. SLRad data of $^{210}Pb_{Tot}$, $^{210}Pb_{xs}$, and D.C. $^{210}Pb_{xs}$ for core site WB-1012-MC-04. Sediment cores with sub-sample intervals (mm), and SLRad activities for $^{210}Pb_{Tot}$, $^{210}Pb_{xs}$, and D.C. $^{210}Pb_{xs}$ (Decay Corrected). Note: Blank cell denotes no analysis performed.

Core ID	Top Depth of Interval (mm)	Bottom Depth of Interval (mm)	Average Depth of Interval (mm)	$^{210}Pb_{Tot}$ Activity (dpm/g)	$^{210}Pb_{Tot}$ Activity error (dpm/g)	$^{210}Pb_{xs}$ Activity (dpm/g)	$^{210}Pb_{xs}$ Activity error (dpm/g)	D.C. $^{210}Pb_{xs}$ Activity (dpm/g)	D.C. $^{210}Pb_{xs}$ Activity error (dpm/g)
WB-1012-MC-04	0	2	1	47.63	0.76	46.50	0.77	46.62	0.77
WB-1012-MC-04	2	4	3	50.15	0.75	48.98	0.76	49.18	0.76
WB-1012-MC-04	4	6	5	45.81	0.72	44.60	0.73	44.76	0.73
WB-1012-MC-04	6	8	7	41.31	0.66	40.01	0.67	40.16	0.67
WB-1012-MC-04	8	10	9	40.64	0.64	39.54	0.65	39.68	0.65
WB-1012-MC-04	10	12	11	39.17	0.64	37.98	0.65	38.16	0.65
WB-1012-MC-04	12	14	13	29.02	0.54	28.06	0.54	32.45	0.63
WB-1012-MC-04	14	16	15	26.99	0.51	25.95	0.52	30.01	0.60
WB-1012-MC-04	16	18	17	24.03	0.47	22.88	0.48	26.46	0.55
WB-1012-MC-04	18	20	19	21.05	0.45	19.86	0.46	22.98	0.53
WB-1012-MC-04	30	35	32.5	10.53	0.25	9.61	0.25	11.13	0.29
WB-1012-MC-04	50	55	52.5	7.23	0.19	6.28	0.19	7.27	0.23
WB-1012-MC-04	70	75	72.5	7.26	0.21	6.36	0.22	7.37	0.25
WB-1012-MC-04	90	95	92.5	4.23	0.14	3.30	0.15	3.82	0.17
WB-1012-MC-04	130	135	132.5	2.33	0.11	1.29	0.12	1.50	0.14
WB-1012-MC-04	170	175	172.5	1.87	0.10	0.86	0.12	1.00	0.13
WB-1012-MC-04	210	215	212.5	1.63	0.08	0.60	0.10	0.70	0.11
WB-1012-MC-04	250	255	252.5	1.63	0.09	0.61	0.10	0.70	0.12
WB-1012-MC-04	290	295	292.5	1.25	0.06	0.12	0.08	0.14	0.09

Table I.15. SLRad data of $^{210}Pb_{Tot}$, $^{210}Pb_{xs}$, and D.C. $^{210}Pb_{xs}$ for core site WB-0813-MC-04. Sediment cores with sub-sample intervals (mm), and SLRad activities for $^{210}Pb_{Tot}$, $^{210}Pb_{xs}$, and D.C. $^{210}Pb_{xs}$ (Decay Corrected). Note: Blank cell denotes no analysis performed.

Core ID	Top Depth of Interval (mm)	Bottom Depth of Interval (mm)	Average Depth of Interval (mm)	$^{210}Pb_{Tot}$ Activity (dpm/g)	$^{210}Pb_{Tot}$ Activity error (dpm/g)	$^{210}Pb_{xs}$ Activity (dpm/g)	$^{210}Pb_{xs}$ Activity error (dpm/g)	D.C. $^{210}Pb_{xs}$ Activity (dpm/g)	D.C. $^{210}Pb_{xs}$ Activity error (dpm/g)
WB-0813-MC-04	0	2	1	40.78	0.87	39.50	0.88	39.60	0.88
WB-0813-MC-04	2	4	3	37.54	0.76	36.41	0.77	36.55	0.77
WB-0813-MC-04	4	6	5	32.38	0.61	31.48	0.62	31.57	0.62
WB-0813-MC-04	6	8	7	28.87	0.55	27.91	0.56	28.03	0.56
WB-0813-MC-04	8	10	9	26.60	0.47	25.69	0.47	25.77	0.47
WB-0813-MC-04	10	14	12	23.49	0.37	22.49	0.37	22.63	0.37
WB-0813-MC-04	14	16	15	24.36	0.49	23.39	0.49	23.62	0.50
WB-0813-MC-04	16	18	17	21.19	0.44	20.08	0.44	20.21	0.44

Table I.16. SLRad data of $^{210}Pb_{Tot}$, $^{210}Pb_{xs}$, and D.C. $^{210}Pb_{xs}$ for core site WB-0813-MC-DSH-08. Sediment cores with sub-sample intervals (mm), and SLRad activities for $^{210}Pb_{Tot}$, $^{210}Pb_{xs}$, and D.C. $^{210}Pb_{xs}$ (Decay Corrected). Note: Blank cell denotes no analysis performed.

Core ID	Top Depth of Interval (mm)	Bottom Depth of Interval (mm)	Average Depth of Interval (mm)	$^{210}Pb_{Tot}$ Activity (dpm/g)	$^{210}Pb_{Tot}$ Activity error (dpm/g)	$^{210}Pb_{xs}$ Activity (dpm/g)	$^{210}Pb_{xs}$ Activity error (dpm/g)	D.C. $^{210}Pb_{xs}$ Activity (dpm/g)	D.C. $^{210}Pb_{xs}$ Activity error (dpm/g)
WB-0813-MC-DSH-08	0	2	1	54.73	1.00	53.45	1.01	53.60	1.01
WB-0813-MC-DSH-08	2	4	3	59.30	0.86	57.80	0.86	58.00	0.87
WB-0813-MC-DSH-08	4	6	5	57.05	0.91	55.67	0.92	55.84	0.92
WB-0813-MC-DSH-08	6	8	7	57.39	0.87	55.85	0.87	56.05	0.88
WB-0813-MC-DSH-08	8	10	9	53.02	0.77	51.65	0.77	51.82	0.77
WB-0813-MC-DSH-08	10	12	11	53.99	0.79	52.72	0.80	53.19	0.80
WB-0813-MC-DSH-08	12	14	13	54.82	0.77	53.36	0.78	53.61	0.78
WB-0813-MC-DSH-08	14	16	15	54.30	0.81	52.79	0.81	53.28	0.82
WB-0813-MC-DSH-08	16	18	17	51.51	0.76	50.06	0.76	50.31	0.76
WB-0813-MC-DSH-08	18	20	19	49.23	0.74	47.81	0.74	48.29	0.75

Table I.17. SLRad data of $^{210}Pb_{Tot}$, $^{210}Pb_{xs}$, and D.C. $^{210}Pb_{xs}$ for core site WB-0813-MC-DSH-10. Sediment cores with sub-sample intervals (mm), and SLRad activities for $^{210}Pb_{Tot}$, $^{210}Pb_{xs}$, and D.C. $^{210}Pb_{xs}$ (Decay Corrected). Note: Blank cell denotes no analysis performed.

Core ID	Top Depth of Interval (mm)	Bottom Depth of Interval (mm)	Average Depth of Interval (mm)	$^{210}Pb_{Tot}$ Activity (dpm/g)	$^{210}Pb_{Tot}$ Activity error (dpm/g)	$^{210}Pb_{xs}$ Activity (dpm/g)	$^{210}Pb_{xs}$ Activity error (dpm/g)	D.C. $^{210}Pb_{xs}$ Activity (dpm/g)	D.C. $^{210}Pb_{xs}$ Activity error (dpm/g)
WB-0813-MC-DSH-10	0	2	1	43.97	0.65	42.15	0.66	42.26	0.66
WB-0813-MC-DSH-10	2	4	3	43.51	0.67	41.73	0.68	41.86	0.68
WB-0813-MC-DSH-10	4	6	5	39.47	0.61	37.64	0.62	37.68	0.62
WB-0813-MC-DSH-10	6	8	7	32.23	0.56	30.28	0.56	30.40	0.57
WB-0813-MC-DSH-10	8	10	9	32.00	0.55	30.12	0.56	30.21	0.56
WB-0813-MC-DSH-10	10	12	11	29.71	0.49	27.81	0.50	28.06	0.50
WB-0813-MC-DSH-10	12	14	13	31.68	0.55	29.93	0.56	30.04	0.56
WB-0813-MC-DSH-10	14	16	15	32.86	0.49	30.92	0.50	31.20	0.50
WB-0813-MC-DSH-10	16	18	17	32.01	0.58	30.16	0.58	30.28	0.59
WB-0813-MC-DSH-10	18	20	19	29.75	0.50	27.31	0.51	29.07	0.54

Table I.18. SLRad data of $^{210}Pb_{Tot}$, $^{210}Pb_{xs}$, and D.C. $^{210}Pb_{xs}$ for core site WB-0813-MC-PCB-06. Sediment cores with sub-sample intervals (mm), and SLRad activities for $^{210}Pb_{Tot}$, $^{210}Pb_{xs}$, and D.C. $^{210}Pb_{xs}$ (Decay Corrected). Note: Blank cell denotes no analysis performed.

Core ID	Top Depth of Interval (mm)	Bottom Depth of Interval (mm)	Average Depth of Interval (mm)	$^{210}Pb_{Tot}$ Activity (dpm/g)	$^{210}Pb_{Tot}$ Activity error (dpm/g)	$^{210}Pb_{xs}$ Activity (dpm/g)	$^{210}Pb_{xs}$ Activity error (dpm/g)	D.C. $^{210}Pb_{xs}$ Activity (dpm/g)	D.C. $^{210}Pb_{xs}$ Activity error (dpm/g)
WB-0813-MC-PCB-06	0	4	2	58.02	0.68	56.41	0.68	56.62	0.68
WB-0813-MC-PCB-06	4	6	5	60.88	0.94	59.32	0.94	59.56	0.95
WB-0813-MC-PCB-06	6	8	7	57.44	0.85	55.91	0.85	56.15	0.86
WB-0813-MC-PCB-06	8	10	9	56.07	0.84	54.51	0.85	54.74	0.85
WB-0813-MC-PCB-06	10	12	11	55.09	0.81	53.60	0.81	54.10	0.82
WB-0813-MC-PCB-06	12	14	13	50.60	0.77	49.14	0.78	49.36	0.78
WB-0813-MC-PCB-06	14	16	15	52.80	0.75	51.29	0.75	51.78	0.76
WB-0813-MC-PCB-06	16	18	17	54.94	0.87	53.40	0.87	53.65	0.88
WB-0813-MC-PCB-06	20	22	21	50.69	0.71	49.05	0.71	49.56	0.72

Table I.19. SLRad data of $^{210}Pb_{Tot}$, $^{210}Pb_{xs}$, and D.C. $^{210}Pb_{xs}$ for core site WB-0814-MC-04. Sediment cores with sub-sample intervals (mm), and SLRad activities for $^{210}Pb_{Tot}$, $^{210}Pb_{xs}$, and D.C. $^{210}Pb_{xs}$ (Decay Corrected). Note: Blank cell denotes no analysis performed.

Core ID	Top Depth of Interval (mm)	Bottom Depth of Interval (mm)	Average Depth of Interval (mm)	$^{210}Pb_{Tot}$ Activity (dpm/g)	$^{210}Pb_{Tot}$ Activity error (dpm/g)	$^{210}Pb_{xs}$ Activity (dpm/g)	$^{210}Pb_{xs}$ Activity error (dpm/g)	D.C. $^{210}Pb_{xs}$ Activity (dpm/g)	D.C. $^{210}Pb_{xs}$ Activity error (dpm/g)
WB-0814-MC-04	0	2	1	52.66	0.89	51.52	0.89	51.71	0.90
WB-0814-MC-04	2	4	3	51.23	0.91	50.09	0.92	50.30	0.92
WB-0814-MC-04	4	6	5	51.96	0.84	50.80	0.84	51.00	0.84
WB-0814-MC-04	6	8	7	47.34	0.76	46.15	0.76	46.39	0.77
WB-0814-MC-04	8	10	9	49.21	0.78	48.01	0.78	48.33	0.79
WB-0814-MC-04	10	12	11	44.01	0.68	42.86	0.68	43.28	0.69
WB-0814-MC-04	12	14	13	42.12	0.63	40.82	0.64	41.19	0.64
WB-0814-MC-04	14	16	15	37.48	0.59	36.27	0.60	36.64	0.60
WB-0814-MC-04	16	18	17	39.09	0.64	37.94	0.64	38.29	0.65
WB-0814-MC-04	18	20	19	32.48	0.51	31.45	0.52	31.77	0.52
WB-0814-MC-04	20	22	21	29.76	0.50	28.76	0.50	29.09	0.51
WB-0814-MC-04	24	26	25	24.42	0.45	23.39	0.46	23.97	0.47
WB-0814-MC-04	30	32	31	23.27	0.47	22.22	0.47	22.47	0.48
WB-0814-MC-04	36	38	37	22.51	0.44	21.62	0.45	22.20	0.46
WB-0814-MC-04	40	45	42.5	17.14	0.27	16.24	0.27	17.53	0.29
WB-0814-MC-04	50	55	52.5	12.84	0.23	11.85	0.24	12.12	0.24
WB-0814-MC-04	70	75	72.5	9.11	0.19	8.16	0.19	8.33	0.20
WB-0814-MC-04	90	95	92.5	6.64	0.16	5.62	0.16	5.75	0.17
WB-0814-MC-04	110	115	112.5	3.14	0.11	2.14	0.12	2.18	0.12
WB-0814-MC-04	130	135	132.5	3.00	0.10	1.99	0.11	2.04	0.12
WB-0814-MC-04	150	155	152.5	2.07	0.08	0.99	0.10	1.01	0.10
WB-0814-MC-04	170	175	172.5	1.73	0.08	0.61	0.09	0.62	0.09
WB-0814-MC-04	190	195	192.5	1.52	0.07	0.43	0.09	0.44	0.09
WB-0814-MC-04	210	215	212.5	1.68	0.07	0.67	0.09	0.68	0.09

Table I.19 (Continued).

Core ID	Top Depth of Interval (mm)	Bottom Depth of Interval (mm)	Average Depth of Interval (mm)	$^{210}Pb_{Tot}$ Activity (dpm/g)	$^{210}Pb_{Tot}$ Activity error (dpm/g)	$^{210}Pb_{xs}$ Activity (dpm/g)	$^{210}Pb_{xs}$ Activity error (dpm/g)	D.C. $^{210}Pb_{xs}$ Activity (dpm/g)	D.C. $^{210}Pb_{xs}$ Activity error (dpm/g)
WB-0814-MC-04	230	235	232.5	1.19	0.06	0.16	0.08	0.16	0.08
WB-0814-MC-04	250	255	252.5	1.20	0.06	0.07	0.08	0.07	0.08

Table I.20. SLRad data of $^{210}Pb_{Tot}$, $^{210}Pb_{xs}$, and D.C. $^{210}Pb_{xs}$ for core site WB-0814-MC-DSH-08 DEP 1. Sediment cores with sub-sample intervals (mm), and SLRad activities for $^{210}Pb_{Tot}$, $^{210}Pb_{xs}$, and D.C. $^{210}Pb_{xs}$ (Decay Corrected). Note: Blank cell denotes no analysis performed.

Core ID	Top Depth of Interval (mm)	Bottom Depth of Interval (mm)	Average Depth of Interval (mm)	$^{210}Pb_{Tot}$ Activity (dpm/g)	$^{210}Pb_{Tot}$ Activity error (dpm/g)	$^{210}Pb_{xs}$ Activity (dpm/g)	$^{210}Pb_{xs}$ Activity error (dpm/g)	D.C. $^{210}Pb_{xs}$ Activity (dpm/g)	D.C. $^{210}Pb_{xs}$ Activity error (dpm/g)
WB-0814-MC-DSH-08 DEP 1	0	2	1	49.63	0.77	48.27	0.77	48.37	0.77
WB-0814-MC-DSH-08 DEP 1	2	4	3	50.13	0.84	48.62	0.85	48.76	0.85
WB-0814-MC-DSH-08 DEP 1	4	6	5	47.26	0.80	45.82	0.81	45.92	0.81
WB-0814-MC-DSH-08 DEP 1	6	8	7	46.24	0.76	44.92	0.76	45.05	0.77
WB-0814-MC-DSH-08 DEP 1	8	10	9	44.24	0.73	42.90	0.73	43.04	0.74
WB-0814-MC-DSH-08 DEP 1	10	12	11	41.91	0.72	40.41	0.72	40.57	0.72
WB-0814-MC-DSH-08 DEP 1	12	14	13	39.85	0.69	38.29	0.69	38.42	0.69
WB-0814-MC-DSH-08 DEP 1	14	16	15	37.62	0.63	36.25	0.64	36.59	0.64
WB-0814-MC-DSH-08 DEP 1	16	18	17	37.18	0.68	35.70	0.69	35.82	0.69
WB-0814-MC-DSH-08 DEP 1	18	20	19	33.76	0.58	32.31	0.58	32.59	0.59
WB-0814-MC-DSH-08 DEP 1	20	22	21	32.56	0.59	31.19	0.59	31.78	0.60
WB-0814-MC-DSH-08 DEP 1	24	26	25	30.54	0.55	28.97	0.55	29.65	0.57
WB-0814-MC-DSH-08 DEP 1	30	32	31	28.46	0.52	26.94	0.52	27.51	0.54
WB-0814-MC-DSH-08 DEP 1	40	45	42.5	22.36	0.30	20.37	0.31	21.97	0.33
WB-0814-MC-DSH-08 DEP 1	50	55	52.5	20.85	0.30	18.95	0.30	19.54	0.31
WB-0814-MC-DSH-08 DEP 1	70	75	72.5	11.22	0.21	9.00	0.22	9.19	0.22
WB-0814-MC-DSH-08 DEP 1	90	95	92.5	5.95	0.15	3.70	0.17	3.79	0.17
WB-0814-MC-DSH-08 DEP 1	110	115	112.5	8.00	0.18	5.82	0.19	5.94	0.20
WB-0814-MC-DSH-08 DEP 1	130	135	132.5	7.76	0.18	5.53	0.20	5.68	0.20
WB-0814-MC-DSH-08 DEP 1	150	155	152.5	5.38	0.14	3.32	0.16	3.39	0.16
WB-0814-MC-DSH-08 DEP 1	170	175	172.5	4.85	0.15	2.72	0.16	2.79	0.17
WB-0814-MC-DSH-08 DEP 1	190	195	192.5	3.38	0.12	1.31	0.14	1.33	0.14
WB-0814-MC-DSH-08 DEP 1	210	215	212.5	2.89	0.11	0.94	0.13	0.97	0.14
WB-0814-MC-DSH-08 DEP 1	230	235	232.5	2.93	0.11	1.12	0.13	1.15	0.14

Table I.20 (Continued).

Core ID	Top Depth of Interval (mm)	Bottom Depth of Interval (mm)	Average Depth of Interval (mm)	$^{210}Pb_{Tot}$ Activity (dpm/g)	$^{210}Pb_{Tot}$ Activity error (dpm/g)	$^{210}Pb_{xs}$ Activity (dpm/g)	$^{210}Pb_{xs}$ Activity error (dpm/g)	D.C. $^{210}Pb_{xs}$ Activity (dpm/g)	D.C. $^{210}Pb_{xs}$ Activity error (dpm/g)
WB-0814-MC-DSH-08 DEP 1	250	255	252.5	2.84	0.11	0.78	0.13	0.79	0.14
WB-0814-MC-DSH-08 DEP 1	270	275	272.5	2.44	0.10	0.38	0.12	0.39	0.13
WB-0814-MC-DSH-08 DEP 1	290	295	292.5	2.41	0.10	0.28	0.12	0.31	0.13

Table I.21. SLRad data of $^{210}Pb_{Tot}$, $^{210}Pb_{xs}$, and D.C. $^{210}Pb_{xs}$ for core site WB-0814-MC-DSH-10 DEP 1. Sediment cores with sub-sample intervals (mm), and SLRad activities for $^{210}Pb_{Tot}$, $^{210}Pb_{xs}$, and D.C. $^{210}Pb_{xs}$ (Decay Corrected). Note: Blank cell denotes no analysis performed.

Core ID	Top Depth of Interval (mm)	Bottom Depth of Interval (mm)	Average Depth of Interval (mm)	$^{210}Pb_{Tot}$ Activity (dpm/g)	$^{210}Pb_{Tot}$ Activity error (dpm/g)	$^{210}Pb_{xs}$ Activity (dpm/g)	$^{210}Pb_{xs}$ Activity error (dpm/g)	D.C. $^{210}Pb_{xs}$ Activity (dpm/g)	D.C. $^{210}Pb_{xs}$ Activity error (dpm/g)
WB-0814-MC-DSH-10 DEP 1	0	2	1	45.69	0.96	42.74	0.97	42.82	0.97
WB-0814-MC-DSH-10 DEP 1	2	4	3	39.14	0.85	37.34	0.85	37.43	0.86
WB-0814-MC-DSH-10 DEP 1	4	6	5	33.00	0.70	30.92	0.71	30.99	0.71
WB-0814-MC-DSH-10 DEP 1	6	8	7	32.68	0.65	30.76	0.66	30.83	0.66
WB-0814-MC-DSH-10 DEP 1	8	10	9	23.07	0.53	21.26	0.53	21.32	0.54
WB-0814-MC-DSH-10 DEP 1	10	12	11	27.95	0.58	26.17	0.59	26.40	0.59
WB-0814-MC-DSH-10 DEP 1	12	14	13	28.48	0.62	26.78	0.63	26.86	0.63
WB-0814-MC-DSH-10 DEP 1	14	16	15	24.75	0.50	22.84	0.51	23.05	0.51
WB-0814-MC-DSH-10 DEP 1	16	18	17	25.60	0.50	23.86	0.51	23.94	0.51
WB-0814-MC-DSH-10 DEP 1	18	20	19	23.52	0.51	21.56	0.51	22.06	0.53
WB-0814-MC-DSH-10 DEP 1	20	22	21	25.57	0.52	23.40	0.53	23.64	0.54
WB-0814-MC-DSH-10 DEP 1	24	26	25	23.00	0.46	20.75	0.47	21.39	0.48
WB-0814-MC-DSH-10 DEP 1	30	32	31	23.83	0.45	21.80	0.46	22.30	0.47
WB-0814-MC-DSH-10 DEP 1	38	43	40.5	18.81	0.23	16.89	0.23	18.21	0.25
WB-0814-MC-DSH-10 DEP 1	53	58	55.5	18.31	0.27	16.59	0.28	16.89	0.29
WB-0814-MC-DSH-10 DEP 1	73	78	75.5	20.21	0.28	18.18	0.29	18.50	0.29
WB-0814-MC-DSH-10 DEP 1	93	98	95.5	16.64	0.26	14.46	0.27	14.71	0.27
WB-0814-MC-DSH-10 DEP 1	113	118	115.5	11.75	0.21	9.61	0.22	9.80	0.23
WB-0814-MC-DSH-10 DEP 1	133	138	135.5	10.15	0.18	7.88	0.20	8.04	0.20
WB-0814-MC-DSH-10 DEP 1	154	159	156.5	10.21	0.19	8.04	0.21	8.18	0.21
WB-0814-MC-DSH-10 DEP 1	174	179	176.5	5.23	0.14	3.10	0.16	3.16	0.16
WB-0814-MC-DSH-10 DEP 1	194	199	196.5	4.81	0.14	2.83	0.15	2.88	0.16
WB-0814-MC-DSH-10 DEP 1	214	219	216.5	3.76	0.12	1.87	0.14	1.91	0.14
WB-0814-MC-DSH-10 DEP 1	234	239	236.5	3.07	0.11	1.17	0.13	1.19	0.13

Table I.21 (Continued).

Core ID	Top Depth of Interval (mm)	Bottom Depth of Interval (mm)	Average Depth of Interval (mm)	$^{210}Pb_{Tot}$ Activity (dpm/g)	$^{210}Pb_{Tot}$ Activity error (dpm/g)	$^{210}Pb_{xs}$ Activity (dpm/g)	$^{210}Pb_{xs}$ Activity error (dpm/g)	D.C. $^{210}Pb_{xs}$ Activity (dpm/g)	D.C. $^{210}Pb_{xs}$ Activity error (dpm/g)
WB-0814-MC-DSH-10 DEP 1	254	259	256.5	2.99	0.11	0.99	0.13	1.01	0.13
WB-0814-MC-DSH-10 DEP 1	274	279	276.5	2.44	0.10	0.47	0.12	0.48	0.12
WB-0814-MC-DSH-10 DEP 1	294	299	296.5	3.28	0.11	1.39	0.12	1.42	0.13
WB-0814-MC-DSH-10 DEP 1	314	319	316.5	2.90	0.11	0.88	0.13	0.91	0.13

Table I.22. SLRad data of $^{210}Pb_{Tot}$, $^{210}Pb_{xs}$, and D.C. $^{210}Pb_{xs}$ for core site WB-0814-MC-PCB-06 DEP 2. Sediment cores with sub-sample intervals (mm), and SLRad activities for $^{210}Pb_{Tot}$, $^{210}Pb_{xs}$, and D.C. $^{210}Pb_{xs}$ (Decay Corrected). Note: Blank cell denotes no analysis performed.

Core ID	Top Depth of Interval (mm)	Bottom Depth of Interval (mm)	Average Depth of Interval (mm)	$^{210}Pb_{Tot}$ Activity (dpm/g)	$^{210}Pb_{Tot}$ Activity error (dpm/g)	$^{210}Pb_{xs}$ Activity (dpm/g)	$^{210}Pb_{xs}$ Activity error (dpm/g)	D.C. $^{210}Pb_{xs}$ Activity (dpm/g)	D.C. $^{210}Pb_{xs}$ Activity error (dpm/g)
WB-0814-MC-PCB-06 DEP 2	0	2	1	71.52	1.15	70.04	1.15	70.33	1.15
WB-0814-MC-PCB-06 DEP 2	2	4	3	71.89	1.19	70.37	1.19	70.68	1.20
WB-0814-MC-PCB-06 DEP 2	4	6	5	71.03	1.15	69.66	1.15	69.95	1.16
WB-0814-MC-PCB-06 DEP 2	6	8	7	70.93	1.03	69.52	1.03	69.92	1.04
WB-0814-MC-PCB-06 DEP 2	8	10	9	67.26	1.05	65.90	1.06	66.29	1.06
WB-0814-MC-PCB-06 DEP 2	10	12	11	64.95	0.96	63.49	0.96	64.09	0.97
WB-0814-MC-PCB-06 DEP 2	12	14	13	61.09	0.93	59.54	0.94	60.01	0.95
WB-0814-MC-PCB-06 DEP 2	14	16	15	62.64	0.89	61.15	0.89	61.74	0.90
WB-0814-MC-PCB-06 DEP 2	16	18	17	56.55	0.81	55.06	0.81	55.50	0.82
WB-0814-MC-PCB-06 DEP 2	18	20	19	50.84	0.76	49.22	0.76	49.70	0.77
WB-0814-MC-PCB-06 DEP 2	20	22	21	49.06	0.77	47.46	0.77	48.53	0.79
WB-0814-MC-PCB-06 DEP 2	24	26	25	43.24	0.67	41.47	0.68	42.40	0.69
WB-0814-MC-PCB-06 DEP 2	30	32	31	38.47	0.62	36.44	0.63	37.15	0.64
WB-0814-MC-PCB-06 DEP 2	40	42	41	26.03	0.52	22.95	0.53	24.81	0.57
WB-0814-MC-PCB-06 DEP 2	50	55	52.5	15.49	0.26	13.73	0.27	14.03	0.27
WB-0814-MC-PCB-06 DEP 2	70	75	72.5	9.41	0.20	7.49	0.21	7.63	0.22
WB-0814-MC-PCB-06 DEP 2	90	95	92.5	7.29	0.17	5.31	0.18	5.41	0.19
WB-0814-MC-PCB-06 DEP 2	110	117	113.5	3.88	0.11	1.88	0.13	1.92	0.13
WB-0814-MC-PCB-06 DEP 2	132	137	134.5	3.84	0.13	1.94	0.14	1.98	0.15
WB-0814-MC-PCB-06 DEP 2	152	157	154.5	2.55	0.10	0.45	0.12	0.45	0.12
WB-0814-MC-PCB-06 DEP 2	172	177	174.5	2.42	0.10	0.37	0.12	0.38	0.12
WB-0814-MC-PCB-06 DEP 2	192	197	194.5	2.60	0.10	0.44	0.12	0.45	0.12
WB-0814-MC-PCB-06 DEP 2	212	217	214.5	3.07	0.11	1.09	0.13	1.12	0.13
WB-0814-MC-PCB-06 DEP 2	232	237	234.5	3.36	0.12	1.41	0.13	1.44	0.14

Table I.22 (Continued).

Core ID	Top Depth of Interval (mm)	Bottom Depth of Interval (mm)	Average Depth of Interval (mm)	$^{210}Pb_{Tot}$ Activity (dpm/g)	$^{210}Pb_{Tot}$ Activity error (dpm/g)	$^{210}Pb_{xs}$ Activity (dpm/g)	$^{210}Pb_{xs}$ Activity error (dpm/g)	D.C. $^{210}Pb_{xs}$ Activity (dpm/g)	D.C. $^{210}Pb_{xs}$ Activity error (dpm/g)
WB-0814-MC-PCB-06 DEP 2	252	257	254.5	2.58	0.10	0.56	0.12	0.58	0.12
WB-0814-MC-PCB-06 DEP 2	272	277	274.5	3.21	0.15	1.59	0.17	1.73	0.18
WB-0814-MC-PCB-06 DEP 2	292	297	294.5	2.63	0.14	1.15	0.16	1.25	0.17

Table I.23. SLRad data of $^{210}Pb_{Tot}$, $^{210}Pb_{xs}$, and D.C. $^{210}Pb_{xs}$ for core site WB-0815-MC-04. Sediment cores with sub-sample intervals (mm), and SLRad activities for $^{210}Pb_{Tot}$, $^{210}Pb_{xs}$, and D.C. $^{210}Pb_{xs}$ (Decay Corrected). Note: Blank cell denotes no analysis performed.

Core ID	Top Depth of Interval (mm)	Bottom Depth of Interval (mm)	Average Depth of Interval (mm)	$^{210}Pb_{Tot}$ Activity (dpm/g)	$^{210}Pb_{Tot}$ Activity error (dpm/g)	$^{210}Pb_{xs}$ Activity (dpm/g)	$^{210}Pb_{xs}$ Activity error (dpm/g)	D.C. $^{210}Pb_{xs}$ Activity (dpm/g)	D.C. $^{210}Pb_{xs}$ Activity error (dpm/g)
WB-0815-MC-04	0	2	1	40.53	0.90	39.35	0.91	39.45	0.91
WB-0815-MC-04	2	4	3	40.12	0.74	39.02	0.74	39.14	0.75
WB-0815-MC-04	4	6	5	38.73	0.67	37.78	0.67	37.90	0.68
WB-0815-MC-04	6	8	7	37.29	0.64	36.13	0.65	36.30	0.65
WB-0815-MC-04	8	10	9	35.62	0.60	34.58	0.61	34.69	0.61
WB-0815-MC-04	10	12	11	33.27	0.58	32.14	0.59	32.31	0.59
WB-0815-MC-04	12	14	13	35.48	0.59	34.42	0.59	34.55	0.59
WB-0815-MC-04	14	16	15	30.95	0.56	29.98	0.56	31.26	0.59
WB-0815-MC-04	16	18	17	29.87	0.54	28.87	0.54	28.96	0.54

Table I.24. SLRad data of $^{210}Pb_{Tot}$, $^{210}Pb_{xs}$, and D.C. $^{210}Pb_{xs}$ for core site WB-0815-MC-DSH-08-A. Sediment cores with sub-sample intervals (mm), and SLRad activities for $^{210}Pb_{Tot}$, $^{210}Pb_{xs}$, and D.C. $^{210}Pb_{xs}$ (Decay Corrected). Note: Blank cell denotes no analysis performed.

Core ID	Top Depth of Interval (mm)	Bottom Depth of Interval (mm)	Average Depth of Interval (mm)	$^{210}Pb_{Tot}$ Activity (dpm/g)	$^{210}Pb_{Tot}$ Activity error (dpm/g)	$^{210}Pb_{xs}$ Activity (dpm/g)	$^{210}Pb_{xs}$ Activity error (dpm/g)	D.C. $^{210}Pb_{xs}$ Activity (dpm/g)	D.C. $^{210}Pb_{xs}$ Activity error (dpm/g)
WB-0815-MC-DSH-08-A	0	2	1	51.36	1.05	49.65	1.06	49.76	1.06
WB-0815-MC-DSH-08-A	2	4	3	53.48	1.18	51.83	1.19	51.96	1.19
WB-0815-MC-DSH-08-A	4	6	5	53.82	1.07	52.34	1.08	52.48	1.08
WB-0815-MC-DSH-08-A	6	8	7	54.87	0.99	53.24	0.99	53.42	0.99
WB-0815-MC-DSH-08-A	8	10	9	54.10	0.96	52.47	0.96	52.62	0.97
WB-0815-MC-DSH-08-A	10	12	11	56.27	0.95	54.65	0.96	54.86	0.96
WB-0815-MC-DSH-08-A	12	14	13	58.22	0.96	56.73	0.97	56.86	0.97
WB-0815-MC-DSH-08-A	14	16	15	55.70	0.87	54.17	0.88	54.39	0.88
WB-0815-MC-DSH-08-A	16	18	17	56.74	0.90	55.12	0.91	55.29	0.91
WB-0815-MC-DSH-08-A	18	20	19	54.31	0.89	52.72	0.89	53.34	0.90

Table I.25. SLRad data of $^{210}Pb_{Tot}$, $^{210}Pb_{xs}$, and D.C. $^{210}Pb_{xs}$ for core site WB-0815-MC-DSH-10-A. Sediment cores with sub-sample intervals (mm), and SLRad activities for $^{210}Pb_{Tot}$, $^{210}Pb_{xs}$, and D.C. $^{210}Pb_{xs}$ (Decay Corrected). Note: Blank cell denotes no analysis performed.

Core ID	Top Depth of Interval (mm)	Bottom Depth of Interval (mm)	Average Depth of Interval (mm)	$^{210}Pb_{Tot}$ Activity (dpm/g)	$^{210}Pb_{Tot}$ Activity error (dpm/g)	$^{210}Pb_{xs}$ Activity (dpm/g)	$^{210}Pb_{xs}$ Activity error (dpm/g)	D.C. $^{210}Pb_{xs}$ Activity (dpm/g)	D.C. $^{210}Pb_{xs}$ Activity error (dpm/g)
WB-0815-MC-DSH-10-A	0	2	1	59.79	1.04	57.95	1.05	58.16	1.05
WB-0815-MC-DSH-10-A	2	4	3	41.51	0.70	39.49	0.70	39.63	0.71
WB-0815-MC-DSH-10-A	4	6	5	33.39	0.61	31.19	0.62	31.32	0.62
WB-0815-MC-DSH-10-A	6	8	7	26.05	0.76	23.78	0.77	23.89	0.77
WB-0815-MC-DSH-10-A	8	10	9	24.83	0.50	22.70	0.51	25.03	0.57
WB-0815-MC-DSH-10-A	12	14	13	22.97	0.48	20.84	0.49	20.93	0.49
WB-0815-MC-DSH-10-A	14	16	15	22.64	0.47	20.73	0.48	21.62	0.50
WB-0815-MC-DSH-10-A	16	18	17	24.14	0.50	22.39	0.50	22.48	0.51
WB-0815-MC-DSH-10-A	18	20	19	22.04	0.48	20.09	0.49	20.95	0.51

Table I.26. SLRad data of $^{210}Pb_{Tot}$, $^{210}Pb_{xs}$, and D.C. $^{210}Pb_{xs}$ for core site WB-0815-MC-PCB-06-A. Sediment cores with sub-sample intervals (mm), and SLRad activities for $^{210}Pb_{Tot}$, $^{210}Pb_{xs}$, and D.C. $^{210}Pb_{xs}$ (Decay Corrected). Note: Blank cell denotes no analysis performed.

Core ID	Top Depth of Interval (mm)	Bottom Depth of Interval (mm)	Average Depth of Interval (mm)	$^{210}Pb_{Tot}$ Activity (dpm/g)	$^{210}Pb_{Tot}$ Activity error (dpm/g)	$^{210}Pb_{xs}$ Activity (dpm/g)	$^{210}Pb_{xs}$ Activity error (dpm/g)	D.C. $^{210}Pb_{xs}$ Activity (dpm/g)	D.C. $^{210}Pb_{xs}$ Activity error (dpm/g)
WB-0815-MC-PCB-06-A	0	2	1	62.35	1.81	59.86	1.82	59.96	1.82
WB-0815-MC-PCB-06-A	2	4	3	59.66	1.12	58.00	1.13	58.10	1.13
WB-0815-MC-PCB-06-A	4	6	5	50.93	0.93	49.28	0.93	49.38	0.93
WB-0815-MC-PCB-06-A	6	8	7	40.77	0.75	39.09	0.75	39.23	0.76
WB-0815-MC-PCB-06-A	8	10	9	43.75	0.83	41.98	0.84	42.07	0.84
WB-0815-MC-PCB-06-A	10	12	11	23.39	0.50	21.23	0.51	21.33	0.51
WB-0815-MC-PCB-06-A	12	14	13	56.56	0.88	54.88	0.89	55.08	0.89
WB-0815-MC-PCB-06-A	14	16	15	60.31	0.87	58.64	0.87	58.95	0.88
WB-0815-MC-PCB-06-A	16	18	17	66.57	0.95	64.90	0.96	65.05	0.96
WB-0815-MC-PCB-06-A	18	20	19	64.12	0.90	62.53	0.91	64.23	0.93

Table I.27. SLRad data of $^{210}Pb_{Tot}$, $^{210}Pb_{xs}$, and D.C. $^{210}Pb_{xs}$ for core site WB-0816-MC-04. Sediment cores with sub-sample intervals (mm), and SLRad activities for $^{210}Pb_{Tot}$, $^{210}Pb_{xs}$, and D.C. $^{210}Pb_{xs}$ (Decay Corrected). Note: Blank cell denotes no analysis performed.

Core ID	Top Depth of Interval (mm)	Bottom Depth of Interval (mm)	Average Depth of Interval (mm)	$^{210}Pb_{Tot}$ Activity (dpm/g)	$^{210}Pb_{Tot}$ Activity error (dpm/g)	$^{210}Pb_{xs}$ Activity (dpm/g)	$^{210}Pb_{xs}$ Activity error (dpm/g)	D.C. $^{210}Pb_{xs}$ Activity (dpm/g)	D.C. $^{210}Pb_{xs}$ Activity error (dpm/g)
WB-0816-MC-04	0	2	1	38.55	0.84	36.93	0.84	37.04	0.84
WB-0816-MC-04	2	4	3	37.95	0.74	36.51	0.75	36.63	0.75
WB-0816-MC-04	4	6	5	37.28	0.67	36.04	0.67	36.17	0.67
WB-0816-MC-04	6	8	7	33.52	0.58	32.25	0.58	32.37	0.58
WB-0816-MC-04	8	10	9	31.05	0.56	29.77	0.56	29.88	0.56
WB-0816-MC-04	10	12	11	30.92	0.52	29.70	0.53	29.88	0.53
WB-0816-MC-04	12	14	13	24.17	0.45	22.90	0.46	23.00	0.46
WB-0816-MC-04	14	16	15	19.92	0.41	18.56	0.42	18.67	0.42
WB-0816-MC-04	16	18	17	18.64	0.42	17.48	0.42	23.98	0.58
WB-0816-MC-04	18	20	19	16.87	0.38	15.59	0.38	15.66	0.39
WB-0816-MC-04	20	22	21	14.34	0.35	13.28	0.36	13.74	0.37
WB-0816-MC-04	24	26	25	13.44	0.33	12.40	0.34	12.84	0.35
WB-0816-MC-04	30	32	31	13.54	0.34	12.40	0.35	12.60	0.35
WB-0816-MC-04	50	52	51	8.94	0.27	7.89	0.28	8.02	0.28
WB-0816-MC-04	70	72	71	7.98	0.26	6.84	0.26	6.97	0.27
WB-0816-MC-04	90	95	92.5	4.67	0.14	3.49	0.15	3.55	0.15
WB-0816-MC-04	110	115	112.5	5.54	0.15	4.29	0.16	4.37	0.16
WB-0816-MC-04	130	135	132.5	4.96	0.15	3.80	0.16	3.86	0.16
WB-0816-MC-04	150	155	152.5	4.53	0.13	3.28	0.14	3.34	0.14
WB-0816-MC-04	170	175	172.5	2.49	0.10	1.21	0.11	1.23	0.11
WB-0816-MC-04	190	195	192.5	3.18	0.11	1.96	0.12	2.00	0.12
WB-0816-MC-04	210	215	212.5	2.14	0.09	0.92	0.11	0.93	0.11
WB-0816-MC-04	230	235	232.5	2.76	0.15	1.54	0.17	1.57	0.17
WB-0816-MC-04	250	255	252.5	2.80	0.11	1.60	0.12	1.63	0.12

Table I.27 (Continued).

Core ID	Top Depth of Interval (mm)	Bottom Depth of Interval (mm)	Average Depth of Interval (mm)	$^{210}Pb_{Tot}$ Activity (dpm/g)	$^{210}Pb_{Tot}$ Activity error (dpm/g)	$^{210}Pb_{xs}$ Activity (dpm/g)	$^{210}Pb_{xs}$ Activity error (dpm/g)	D.C. $^{210}Pb_{xs}$ Activity (dpm/g)	D.C. $^{210}Pb_{xs}$ Activity error (dpm/g)
WB-0816-MC-04	270	275	272.5	2.00	0.09	0.80	0.10	0.82	0.10
WB-0816-MC-04	290	295	292.5	2.80	0.11	1.61	0.12	1.64	0.12
WB-0816-MC-04	310	315	312.5	1.83	0.09	0.65	0.10	0.67	0.10
WB-0816-MC-04	330	335	332.5	2.11	0.09	0.78	0.11	0.80	0.11

Table I.28. SLRad data of $^{210}Pb_{Tot}$, $^{210}Pb_{xs}$, and D.C. $^{210}Pb_{xs}$ for core site WB-0816-MC-DSH-08-A. Sediment cores with sub-sample intervals (mm), and SLRad activities for $^{210}Pb_{Tot}$, $^{210}Pb_{xs}$, and D.C. $^{210}Pb_{xs}$ (Decay Corrected). Note: Blank cell denotes no analysis performed.

Core ID	Top Depth of Interval (mm)	Bottom Depth of Interval (mm)	Average Depth of Interval (mm)	$^{210}Pb_{Tot}$ Activity (dpm/g)	$^{210}Pb_{Tot}$ Activity error (dpm/g)	$^{210}Pb_{xs}$ Activity (dpm/g)	$^{210}Pb_{xs}$ Activity error (dpm/g)	D.C. $^{210}Pb_{xs}$ Activity (dpm/g)	D.C. $^{210}Pb_{xs}$ Activity error (dpm/g)
WB-0816-MC-DSH-08-A	0	2	1	49.74	0.97	48.43	0.97	48.50	0.98
WB-0816-MC-DSH-08-A	2	4	3	59.49	1.10	57.88	1.11	57.97	1.11
WB-0816-MC-DSH-08-A	4	6	5	60.14	0.98	58.59	0.98	58.70	0.98
WB-0816-MC-DSH-08-A	6	8	7	59.22	0.90	57.66	0.90	57.77	0.90
WB-0816-MC-DSH-08-A	8	10	9	56.18	0.81	54.59	0.82	54.76	0.82
WB-0816-MC-DSH-08-A	10	12	11	56.82	0.86	55.08	0.87	55.25	0.87
WB-0816-MC-DSH-08-A	12	14	13	56.97	0.82	55.24	0.82	55.42	0.83
WB-0816-MC-DSH-08-A	14	16	15	56.26	0.81	54.64	0.82	54.87	0.82
WB-0816-MC-DSH-08-A	16	18	17	55.18	0.78	53.45	0.79	53.64	0.79
WB-0816-MC-DSH-08-A	18	20	19	55.39	0.82	53.70	0.82	53.94	0.82
WB-0816-MC-DSH-08-A	20	22	21	52.12	0.81	50.31	0.82	51.49	0.84
WB-0816-MC-DSH-08-A	22	24	23	49.80	0.76	47.88	0.77	48.97	0.78
WB-0816-MC-DSH-08-A	24	26	25	48.51	0.75	46.92	0.76	48.00	0.77
WB-0816-MC-DSH-08-A	26	28	27	47.71	0.75	46.16	0.75	47.23	0.77
WB-0816-MC-DSH-08-A	28	30	29	46.49	0.71	44.94	0.71	46.05	0.73
WB-0816-MC-DSH-08-A	30	32	31	44.33	0.71	42.97	0.71	43.71	0.73
WB-0816-MC-DSH-08-A	50	55	52.5	28.78	0.38	27.04	0.39	27.52	0.39
WB-0816-MC-DSH-08-A	70	75	72.5	19.53	0.29	17.67	0.29	18.06	0.30
WB-0816-MC-DSH-08-A	90	95	92.5	14.76	0.25	12.97	0.26	13.20	0.27
WB-0816-MC-DSH-08-A	110	115	112.5	10.47	0.21	8.49	0.22	8.68	0.22
WB-0816-MC-DSH-08-A	130	135	132.5	7.06	0.17	5.10	0.18	5.19	0.19
WB-0816-MC-DSH-08-A	150	155	152.5	4.69	0.14	2.64	0.15	2.70	0.16
WB-0816-MC-DSH-08-A	170	175	172.5	4.06	0.13	2.00	0.15	2.04	0.15

Table I.28 (Continued).

Core ID	Top Depth of Interval (mm)	Bottom Depth of Interval (mm)	Average Depth of Interval (mm)	$^{210}Pb_{Tot}$ Activity (dpm/g)	$^{210}Pb_{Tot}$ Activity error (dpm/g)	$^{210}Pb_{xs}$ Activity (dpm/g)	$^{210}Pb_{xs}$ Activity error (dpm/g)	D.C. $^{210}Pb_{xs}$ Activity (dpm/g)	D.C. $^{210}Pb_{xs}$ Activity error (dpm/g)
WB-0816-MC-DSH-08-A	190	195	192.5	3.41	0.12	1.48	0.13	1.51	0.14
WB-0816-MC-DSH-08-A	210	215	212.5	3.67	0.12	1.62	0.14	1.65	0.14
WB-0816-MC-DSH-08-A	250	255	252.5	2.25	0.09	0.41	0.11	0.42	0.12
WB-0816-MC-DSH-08-A	290	295	292.5	2.47	0.10	0.39	0.12	0.40	0.13

Table I.29. SLRad data of $^{210}Pb_{Tot}$, $^{210}Pb_{xs}$, and D.C. $^{210}Pb_{xs}$ for core site WB-0816-MC-DSH-10-A. Sediment cores with sub-sample intervals (mm), and SLRad activities for $^{210}Pb_{Tot}$, $^{210}Pb_{xs}$, and D.C. $^{210}Pb_{xs}$ (Decay Corrected). Note: Blank cell denotes no analysis performed.

Core ID	Top Depth of Interval (mm)	Bottom Depth of Interval (mm)	Average Depth of Interval (mm)	$^{210}Pb_{Tot}$ Activity (dpm/g)	$^{210}Pb_{Tot}$ Activity error (dpm/g)	$^{210}Pb_{xs}$ Activity (dpm/g)	$^{210}Pb_{xs}$ Activity error (dpm/g)	D.C. $^{210}Pb_{xs}$ Activity (dpm/g)	D.C. $^{210}Pb_{xs}$ Activity error (dpm/g)
WB-0816-MC-DSH-10-A	0	2	1	48.71	0.91	46.71	0.92	46.79	0.92
WB-0816-MC-DSH-10-A	2	4	3	44.70	0.76	42.75	0.77	42.83	0.77
WB-0816-MC-DSH-10-A	4	6	5	38.62	0.71	36.57	0.72	36.66	0.72
WB-0816-MC-DSH-10-A	6	8	7	32.58	0.62	30.60	0.63	30.68	0.63
WB-0816-MC-DSH-10-A	8	10	9	33.33	0.62	31.67	0.63	31.94	0.64
WB-0816-MC-DSH-10-A	10	12	11	30.80	0.57	28.94	0.57	29.10	0.58
WB-0816-MC-DSH-10-A	12	14	13	32.26	0.57	30.49	0.58	30.77	0.58
WB-0816-MC-DSH-10-A	14	16	15	32.12	0.57	30.38	0.57	30.95	0.58
WB-0816-MC-DSH-10-A	16	18	17	32.16	0.57	30.51	0.57	31.09	0.58
WB-0816-MC-DSH-10-A	18	20	19	32.29	0.55	30.28	0.56	30.85	0.57
WB-0816-MC-DSH-10-A	20	22	21	31.33	0.55	29.42	0.55	30.18	0.57
WB-0816-MC-DSH-10-A	22	24	23	30.09	0.54	27.67	0.55	28.41	0.57
WB-0816-MC-DSH-10-A	24	26	25	26.93	0.49	25.02	0.49	25.65	0.51
WB-0816-MC-DSH-10-A	26	28	27	25.36	0.46	23.26	0.47	23.88	0.48
WB-0816-MC-DSH-10-A	28	30	29	23.33	0.44	21.22	0.45	21.95	0.47
WB-0816-MC-DSH-10-A	30	32	31	23.00	0.46	21.03	0.47	21.46	0.48
WB-0816-MC-DSH-10-A	50	52	51	21.41	0.41	19.69	0.42	20.07	0.43
WB-0816-MC-DSH-10-A	70	72	71	23.62	0.44	21.60	0.45	22.14	0.46
WB-0816-MC-DSH-10-A	90	95	92.5	11.52	0.21	9.59	0.22	9.77	0.23
WB-0816-MC-DSH-10-A	110	115	112.5	8.19	0.18	6.16	0.19	6.31	0.20
WB-0816-MC-DSH-10-A	130	135	132.5	4.91	0.14	2.98	0.15	3.04	0.16
WB-0816-MC-DSH-10-A	170	175	172.5	2.96	0.11	1.21	0.13	1.23	0.13
WB-0816-MC-DSH-10-A	210	215	212.5	3.71	0.12	1.85	0.14	1.88	0.14
WB-0816-MC-DSH-10-A	250	255	252.5	3.31	0.12	1.46	0.13	1.49	0.14

Table I.29 (Continued).

Core ID	Top Depth of Interval (mm)	Bottom Depth of Interval (mm)	Average Depth of Interval (mm)	$^{210}Pb_{Tot}$ Activity (dpm/g)	$^{210}Pb_{Tot}$ Activity error (dpm/g)	$^{210}Pb_{xs}$ Activity (dpm/g)	$^{210}Pb_{xs}$ Activity error (dpm/g)	D.C. $^{210}Pb_{xs}$ Activity (dpm/g)	D.C. $^{210}Pb_{xs}$ Activity error (dpm/g)
WB-0816-MC-DSH-10-A	290	295	292.5	2.04	0.09	0.11	0.11	0.11	0.11
WB-0816-MC-DSH-10-A	310	315	312.5	2.57	0.10	0.60	0.12	0.62	0.13

Table I.30. SLRad data of $^{210}Pb_{Tot}$, $^{210}Pb_{xs}$, and D.C. $^{210}Pb_{xs}$ for core site WB-0816-MC-PCB-06-A. Sediment cores with sub-sample intervals (mm), and SLRad activities for $^{210}Pb_{Tot}$, $^{210}Pb_{xs}$, and D.C. $^{210}Pb_{xs}$ (Decay Corrected). Note: Blank cell denotes no analysis performed.

Core ID	Top Depth of Interval (mm)	Bottom Depth of Interval (mm)	Average Depth of Interval (mm)	$^{210}Pb_{Tot}$ Activity (dpm/g)	$^{210}Pb_{Tot}$ Activity error (dpm/g)	$^{210}Pb_{xs}$ Activity (dpm/g)	$^{210}Pb_{xs}$ Activity error (dpm/g)	D.C. $^{210}Pb_{xs}$ Activity (dpm/g)	D.C. $^{210}Pb_{xs}$ Activity error (dpm/g)
WB-0816-MC-PCB-06-A	0	2	1	70.52	1.28	68.89	1.28	69.03	1.28
WB-0816-MC-PCB-06-A	2	4	3	62.50	1.48	60.83	1.49	60.97	1.49
WB-0816-MC-PCB-06-A	4	6	5	65.94	1.25	64.23	1.26	64.39	1.26
WB-0816-MC-PCB-06-A	6	8	7	68.66	1.25	66.98	1.25	67.16	1.26
WB-0816-MC-PCB-06-A	8	10	9	64.49	1.04	62.75	1.05	62.92	1.05
WB-0816-MC-PCB-06-A	10	12	11	60.25	0.88	58.63	0.88	58.90	0.89
WB-0816-MC-PCB-06-A	12	14	13	54.04	0.81	52.29	0.82	52.48	0.82
WB-0816-MC-PCB-06-A	14	16	15	49.42	0.73	47.53	0.73	47.76	0.74
WB-0816-MC-PCB-06-A	16	18	17	45.69	0.72	43.82	0.72	43.99	0.72
WB-0816-MC-PCB-06-A	18	20	19	41.95	0.66	39.90	0.67	40.10	0.67
WB-0816-MC-PCB-06-A	20	22	21	35.03	0.64	33.06	0.65	33.91	0.67
WB-0816-MC-PCB-06-A	22	24	23	33.37	0.58	31.36	0.59	32.17	0.60
WB-0816-MC-PCB-06-A	24	26	25	31.09	0.58	29.05	0.59	29.73	0.60
WB-0816-MC-PCB-06-A	26	28	27	30.40	0.56	28.06	0.57	29.02	0.59
WB-0816-MC-PCB-06-A	28	30	29	28.20	0.52	25.62	0.53	26.50	0.55
WB-0816-MC-PCB-06-A	30	32	31	26.50	0.41	24.05	0.42	24.56	0.43
WB-0816-MC-PCB-06-A	50	52	51	17.65	0.38	16.11	0.39	16.41	0.39
WB-0816-MC-PCB-06-A	70	72	71	10.24	0.29	8.63	0.30	8.81	0.30
WB-0816-MC-PCB-06-A	90	95	92.5	4.65	0.14	2.82	0.16	2.87	0.16
WB-0816-MC-PCB-06-A	110	115	112.5	3.38	0.12	1.38	0.14	1.41	0.14
WB-0816-MC-PCB-06-A	130	135	132.5	2.86	0.11	0.75	0.13	0.77	0.13
WB-0816-MC-PCB-06-A	150	155	152.5	2.65	0.10	0.66	0.12	0.67	0.13
WB-0816-MC-PCB-06-A	170	175	172.5	2.66	0.10	0.69	0.12	0.70	0.12
WB-0816-MC-PCB-06-A	190	195	192.5	2.53	0.10	0.64	0.12	0.66	0.13

Table I.30 (Continued).

Core ID	Top Depth of Interval (mm)	Bottom Depth of Interval (mm)	Average Depth of Interval (mm)	$^{210}Pb_{Tot}$ Activity (dpm/g)	$^{210}Pb_{Tot}$ Activity error (dpm/g)	$^{210}Pb_{xs}$ Activity (dpm/g)	$^{210}Pb_{xs}$ Activity error (dpm/g)	D.C. $^{210}Pb_{xs}$ Activity (dpm/g)	D.C. $^{210}Pb_{xs}$ Activity error (dpm/g)
WB-0816-MC-PCB-06-A	210	215	212.5	2.51	0.10	0.67	0.12	0.68	0.12
WB-0816-MC-PCB-06-A	250	255	252.5	2.76	0.11	0.91	0.13	0.93	0.13
WB-0816-MC-PCB-06-A	290	295	292.5	2.40	0.10	0.40	0.12	0.40	0.12

APPENDIX J:

SEDIMENT TEXTURE AND COMPOSITION DATA

Appendix J. Supplemental tables of sediment texture and composition data for cores with texture described as %Gravel, %Sand, %Silt, and %Clay, as well as %Mud, and composition described as %Carbonate, %TOM (LOI), and %Other (non-carbonate, non-organic).

Data are publicly available through the Gulf of Mexico Research Initiative Information & Data Cooperative (GRIIDC) at https://data.gulfresearchinitiative.org (doi: 10.7266/N79S1PJZ, 10.7266/n7-kzww-0995, 10.7266/n7-c8va-fr98, 10.7266/n7-bkvk-wr98, 10.7266/n7-b0y2-f117, 10.7266/n7-380p-k210)

Table J.1. Sediment texture and composition data for core site WB-1109-MC-04. Sediment cores with sub-sample intervals (mm), texture described as %Gravel, % Sand, % Silt, and % Clay, as well as %Mud, and composition described as %Carbonate, %TOM (LOI), and % Other (non-carbonate, non-organic). Note: Blank cell denotes no analysis performed.

Core ID	Top Depth of Interval (mm)	Bottom Depth of Interval (mm)	Average Depth of Interval (mm)	% Gravel	% Sand	% Silt	% Clay	% Mud (% Silt + % Clay)	% Carbonate	% TOM (LOI)	% Other
WB-1109-MC-04	0	2	1	0.0	5.8	57.5	36.7	94.2	54.2	6.5	39.3
WB-1109-MC-04	2	4	3	0.0	7.8	67.3	24.9	92.2			
WB-1109-MC-04	4	6	5	0.0	13.9	64.2	21.9	86.1	59.1	6.6	34.3
WB-1109-MC-04	6	8	7	0.0	9.2	59.0	31.8	90.8			
WB-1109-MC-04	8	10	9	0.0	5.5	65.4	29.1	94.5	54.7	6.8	38.5
WB-1109-MC-04	10	12	11	0.0	9.2	62.7	28.1	90.8	54.9	6.4	38.7
WB-1109-MC-04	12	14	13	0.0	13.6	58.7	27.7	86.4			
WB-1109-MC-04	14	16	15	0.0	14.1	58.6	27.3	85.9	59.6	6.5	33.9
WB-1109-MC-04	16	18	17	0.0	11.8	56.8	31.4	88.2	54.7	7.6	37.7
WB-1109-MC-04	18	20	19	0.0	19.6	51.8	28.6	80.4			
WB-1109-MC-04	20	25	22.5	0.0	14.3	55.7	29.9	85.7	55.7	5.7	38.5
WB-1109-MC-04	30	35	32.5	0.0	13.4	53.5	33.0	86.6	55.7	6.1	38.2
WB-1109-MC-04	40	45	42.5	0.0	21.8	46.2	32.0	78.2	54.9	7.5	37.6
WB-1109-MC-04	50	55	52.5	0.0	20.4	50.4	29.2	79.6	59.0	6.7	34.3
WB-1109-MC-04	60	65	62.5	0.0	21.3	47.3	31.4	78.7	54.3	7.6	38.1
WB-1109-MC-04	70	75	72.5	0.0	14.4	49.4	36.2	85.6	55.4	6.1	38.4
WB-1109-MC-04	80	85	82.5	0.0	22.1	47.4	30.5	77.9	58.4	6.6	35.0
WB-1109-MC-04	90	95	92.5	0.0	17.2	49.9	32.9	82.8	56.6	6.1	37.3
WB-1109-MC-04	100	105	102.5	0.0	21.6	46.6	31.8	78.4	56.5	7.0	36.5
WB-1109-MC-04	110	115	112.5	0.0	26.2	47.5	26.3	73.8	57.7	5.1	37.2
WB-1109-MC-04	120	125	122.5	0.0	23.5	48.0	28.6	76.5	57.7	6.8	35.5
WB-1109-MC-04	130	135	132.5	0.0	27.9	47.5	24.6	72.1	58.8	5.7	35.5
WB-1109-MC-04	140	145	142.5	0.0	27.7	46.9	25.3	72.3	61.9	6.0	32.0
WB-1109-MC-04	150	155	152.5	0.0	28.1	42.7	29.1	71.9	60.2	5.3	34.5

Table J.1 (Continued).

Core ID	Top Depth of Interval (mm)	Bottom Depth of Interval (mm)	Average Depth of Interval (mm)	% Gravel	% Sand	% Silt	% Clay	% Mud (% Silt + % Clay)	% Carbonate	% TOM (LOI)	% Other
WB-1109-MC-04	160	165	162.5	0.0	28.1	44.2	27.8	71.9	59.1	6.9	34.0
WB-1109-MC-04	170	175	172.5	0.0	29.8	44.7	25.5	70.2	58.7	4.9	36.3
WB-1109-MC-04	190	195	192.5	0.0	25.0	47.9	27.1	75.0	60.6	5.3	34.1
WB-1109-MC-04	200	205	202.5	0.0	23.7	45.7	30.6	76.3	58.2	6.9	34.9
WB-1109-MC-04	210	215	212.5	0.0	15.6	50.9	33.6	84.4	59.9	4.2	35.9
WB-1109-MC-04	220	225	222.5	0.0	23.8	44.9	31.3	76.2	59.8	6.4	33.8
WB-1109-MC-04	230	235	232.5	0.0	21.7	49.4	29.0	78.3	60.7	5.3	34.0

Table J.2. Sediment texture and composition data for core site WB-1110-MC-DSH-08. Sediment cores with sub-sample intervals (mm), texture described as %Gravel, % Sand, % Silt, and % Clay, as well as %Mud, and composition described as %Carbonate, %TOM (LOI), and % Other (non-carbonate, non-organic). Note: Blank cell denotes no analysis performed.

Core ID	Top Depth of Interval (mm)	Bottom Depth of Interval (mm)	Average Depth of Interval (mm)	% Gravel	% Sand	% Silt	% Clay	% Mud (% Silt + % Clay)	% Carbonate	% TOM (LOI)	% Other
WB-1110-MC-DSH-08	0	2	1	0.0	0.9	67.4	31.7	99.1	44.4	6.3	49.3
WB-1110-MC-DSH-08	2	4	3	0.0	0.8	42.1	57.1	99.2			
WB-1110-MC-DSH-08	4	6	5	0.0	0.5	48.4	51.2	99.5	38.3	7.8	53.9
WB-1110-MC-DSH-08	6	8	7	0.0	0.4	50.3	49.3	99.6	36.6	8.0	55.5
WB-1110-MC-DSH-08	8	10	9	0.0	0.7	46.3	53.0	99.3	35.4	8.8	55.8
WB-1110-MC-DSH-08	10	12	11	0.0	0.5	44.8	54.7	99.5			
WB-1110-MC-DSH-08	12	14	13	0.0	0.5	55.5	44.0	99.5			
WB-1110-MC-DSH-08	14	16	15	0.0	0.9	47.6	51.5	99.1			
WB-1110-MC-DSH-08	16	18	17	0.0	0.6	46.4	53.0	99.4	36.4	7.4	56.2
WB-1110-MC-DSH-08	18	20	19	0.0	0.9	49.9	49.2	99.1			
WB-1110-MC-DSH-08	22	24	23	0.0	0.5	41.9	57.6	99.5	34.0	8.2	57.7
WB-1110-MC-DSH-08	26	28	27	0.0	0.8	35.4	63.8	99.2	33.6	6.6	59.7
WB-1110-MC-DSH-08	32	34	33	0.0	0.7	31.7	67.6	99.3	32.3	8.5	59.2
WB-1110-MC-DSH-08	34	36	35	0.0	0.3	39.0	60.7	99.7			
WB-1110-MC-DSH-08	38	40	39	0.0	0.9	30.1	69.0	99.1			
WB-1110-MC-DSH-08	42	44	43	0.0	0.5	30.6	68.9	99.5	33.5	5.4	61.1
WB-1110-MC-DSH-08	46	48	47	0.0	0.5	33.4	66.1	99.5	31.2	6.3	62.6
WB-1110-MC-DSH-08	48	50	49	0.0	0.5	26.4	73.1	99.5			
WB-1110-MC-DSH-08	50	55	52.5	0.0	0.3	32.8	66.9	99.7	28.7	8.7	62.6
WB-1110-MC-DSH-08	70	75	72.5	0.0	0.4	26.5	73.1	99.6	30.9	5.4	63.8
WB-1110-MC-DSH-08	80	85	82.5	0.0	0.3	26.8	72.9	99.7	30.1	4.8	65.1
WB-1110-MC-DSH-08	90	95	92.5	0.0	0.4	31.0	68.7	99.6	24.0	10.2	65.8
WB-1110-MC-DSH-08	100	105	102.5	0.0	0.5	25.5	74.0	99.5	30.1	5.1	64.7
WB-1110-MC-DSH-08	110	115	112.5	0.0	0.6	28.2	71.3	99.4	26.1	8.5	65.4
WB-1110-MC-DSH-08	120	125	122.5	0.0	0.7	25.3	74.0	99.3	29.7	5.4	64.9

Table J.2 (Continued).

Core ID	Top Depth of Interval (mm)	Bottom Depth of Interval (mm)	Average Depth of Interval (mm)	% Gravel	% Sand	% Silt	% Clay	% Mud (% Silt + % Clay)	% Carbonate	% TOM (LOI)	% Other
WB-1110-MC-DSH-08	130	135	132.5	0.0	0.3	31.6	68.1	99.7	27.0	8.3	64.7
WB-1110-MC-DSH-08	140	145	142.5	0.0	1.3	27.9	70.8	98.7	30.5	5.5	64.0
WB-1110-MC-DSH-08	150	155	152.5	0.0	1.2	30.2	68.7	98.8	27.3	8.2	64.5
WB-1110-MC-DSH-08	160	165	162.5	0.0	0.8	25.8	73.4	99.2	31.6	4.1	64.3
WB-1110-MC-DSH-08	180	185	182.5	0.0	0.8	24.4	74.8	99.2	32.3	3.8	63.9
WB-1110-MC-DSH-08	210	215	212.5	0.0	0.6	36.1	63.3	99.4	30.2	8.0	61.9
WB-1110-MC-DSH-08	220	225	222.5	0.0	0.6	29.4	70.0	99.4	34.9	4.3	60.8
WB-1110-MC-DSH-08	230	235	232.5	0.0	0.6	30.3	69.1	99.4	36.2	4.4	59.4
WB-1110-MC-DSH-08	240	245	242.5	0.0	0.5	29.8	69.7	99.5	36.8	5.3	57.9
WB-1110-MC-DSH-08	250	255	252.5	0.0	1.8	40.1	58.1	98.2	31.9	10.0	58.1
WB-1110-MC-DSH-08	260	265	262.5	0.0	1.0	31.7	67.3	99.0	39.3	4.4	56.4

Table J.3. Sediment texture and composition data for core site WB-1110-MC-DSH-10. Sediment cores with sub-sample intervals (mm), texture described as %Gravel, % Sand, % Silt, and % Clay, as well as %Mud, and composition described as %Carbonate, %TOM (LOI), and % Other (non-carbonate, non-organic). Note: Blank cell denotes no analysis performed.

Core ID	Top Depth of Interval (mm)	Bottom Depth of Interval (mm)	Average Depth of Interval (mm)	% Gravel	% Sand	% Silt	% Clay	% Mud (% Silt + % Clay)	% Carbonate	% TOM (LOI)	% Other
WB-1110-MC-DSH-10	0	2	1	0.0	0.5	16.3	83.2	99.5	32.4	8.8	58.9
WB-1110-MC-DSH-10	2	4	3	0.0	1.3	33.2	65.5	98.7			
WB-1110-MC-DSH-10	4	6	5	0.0	0.7	29.7	69.6	99.3	30.1	7.9	62.0
WB-1110-MC-DSH-10	6	8	7	0.0	0.7	49.3	50.0	99.3	31.2	7.0	61.7
WB-1110-MC-DSH-10	8	10	9	0.0	0.8	31.6	67.6	99.2	28.7	9.3	61.9
WB-1110-MC-DSH-10	10	12	11	0.0	0.8	32.7	66.5	99.2	27.1	8.4	64.6
WB-1110-MC-DSH-10	12	14	13	0.0	0.0	35.9	64.0	100.0	32.9	7.0	60.1
WB-1110-MC-DSH-10	14	16	15	0.0	0.7	33.9	65.5	99.3	31.2	8.1	60.6
WB-1110-MC-DSH-10	16	18	17	0.0	0.6	38.6	60.8	99.4	27.0	8.5	64.6
WB-1110-MC-DSH-10	18	20	19	0.0	0.0	73.5	26.5	100.0	28.5	11.3	60.2
WB-1110-MC-DSH-10	20	22	21	0.0	0.4	33.6	66.1	99.6	27.4	9.3	63.4
WB-1110-MC-DSH-10	24	26	25	0.0	0.2	35.8	64.0	99.8	31.4	7.3	61.3
WB-1110-MC-DSH-10	30	32	31	0.0	0.5	32.3	67.3	99.5	23.6	10.0	66.4
WB-1110-MC-DSH-10	40	42	41	0.0	0.6	37.6	61.8	99.4	30.4	7.6	62.0
WB-1110-MC-DSH-10	50	52	51	0.0	0.7	33.7	65.6	99.3	25.3	9.1	65.6
WB-1110-MC-DSH-10	60	62	61	0.0	0.6	26.3	73.1	99.4	29.1	8.0	62.8
WB-1110-MC-DSH-10	70	72	71	0.0	0.8	29.0	70.2	99.2	20.3	12.1	67.6
WB-1110-MC-DSH-10	80	85	82.5	0.0	0.7	31.8	67.5	99.3	29.2	6.9	63.9
WB-1110-MC-DSH-10	90	95	92.5	0.0	0.6	30.1	69.4	99.4	22.8	10.1	67.1
WB-1110-MC-DSH-10	100	105	102.5	0.0	0.6	32.0	67.3	99.4	28.3	7.5	64.2
WB-1110-MC-DSH-10	110	115	112.5	0.0	1.0	21.4	77.6	99.0	25.7	9.3	65.0
WB-1110-MC-DSH-10	120	125	122.5	0.0	0.4	33.3	66.3	99.6	28.3	7.6	64.2
WB-1110-MC-DSH-10	130	135	132.5	0.0	0.7	32.8	66.5	99.3	26.0	8.9	65.1
WB-1110-MC-DSH-10	140	145	142.5	0.0	0.4	30.5	69.1	99.6	29.4	8.3	62.4
WB-1110-MC-DSH-10	150	155	152.5	0.0	0.7	23.7	75.6	99.3	29.5	8.7	61.8

Table J.3 (Continued).

Core ID	Top Depth of Interval (mm)	Bottom Depth of Interval (mm)	Average Depth of Interval (mm)	% Gravel	% Sand	% Silt	% Clay	% Mud (% Silt + % Clay)	% Carbonate	% TOM (LOI)	% Other
WB-1110-MC-DSH-10	160	165	162.5	0.0	0.5	35.8	63.7	99.5	32.1	7.3	60.6
WB-1110-MC-DSH-10	170	175	172.5	0.0	1.1	34.5	64.4	98.9	31.8	8.3	59.9
WB-1110-MC-DSH-10	180	185	182.5	0.0	1.5	30.5	68.0	98.5	35.1	6.5	58.4
WB-1110-MC-DSH-10	190	195	192.5	0.0	1.8	30.6	67.6	98.2	33.4	8.1	58.4
WB-1110-MC-DSH-10	200	205	202.5	0.0	1.4	35.2	63.5	98.6	36.0	6.5	57.5
WB-1110-MC-DSH-10	210	215	212.5	0.0	1.3	24.1	74.7	98.7	34.2	8.1	57.6
WB-1110-MC-DSH-10	220	225	222.5	0.0	1.2	33.5	65.3	98.8	37.1	6.6	56.3
WB-1110-MC-DSH-10	230	235	232.5	0.0	1.1	38.1	60.8	98.9	39.1	3.0	58.0
WB-1110-MC-DSH-10	240	245	242.5	0.0	1.2	31.5	67.3	98.8	37.6	6.5	55.9
WB-1110-MC-DSH-10	250	255	252.5	0.0	1.8	4.6	93.7	98.2	34.4	8.2	57.5
WB-1110-MC-DSH-10	260	265	262.5	0.0	0.8	32.4	66.8	99.2	37.7	5.3	57.0
WB-1110-MC-DSH-10	270	275	272.5	0.0	1.3	26.3	72.4	98.7	34.2	8.2	57.6
WB-1110-MC-DSH-10	280	285	282.5	0.0	1.4	38.7	59.8	98.6	37.4	6.3	56.3
WB-1110-MC-DSH-10	290	295	292.5	0.0	1.5	34.6	63.9	98.5	38.3	5.3	56.4
WB-1110-MC-DSH-10	300	305	302.5	0.0	1.5	36.4	62.1	98.5	31.0	8.8	60.2
WB-1110-MC-DSH-10	310	315	312.5	0.0	1.3	37.2	61.5	98.7	36.1	6.5	57.4

Table J.4. Sediment texture and composition data for core site WB-1110-MC-PCB-06. Sediment cores with sub-sample intervals (mm), texture described as %Gravel, % Sand, % Silt, and % Clay, as well as %Mud, and composition described as %Carbonate, %TOM (LOI), and % Other (non-carbonate, non-organic). Note: Blank cell denotes no analysis performed.

Core ID	Top Depth of Interval (mm)	Bottom Depth of Interval (mm)	Average Depth of Interval (mm)	% Gravel	% Sand	% Silt	% Clay	% Mud (% Silt + % Clay)	% Carbonate	% TOM (LOI)	% Other
WB-1110-MC-PCB-06	0	2	1	0.0	0.4	3.8	95.8	99.6	30.4	7.8	61.8
WB-1110-MC-PCB-06	2	4	3	0.0	2.1	49.5	48.4	97.9			
WB-1110-MC-PCB-06	4	6	5	0.0	1.3	39.5	59.2	98.7	35.0	7.3	57.7
WB-1110-MC-PCB-06	6	10	8	0.0	1.3	36.0	62.8	98.7	38.2	7.3	54.5
WB-1110-MC-PCB-06	10	12	11	0.0	2.5	53.9	43.6	97.5	34.7	7.5	57.8
WB-1110-MC-PCB-06	12	14	13	0.0	1.7	35.2	63.1	98.3			
WB-1110-MC-PCB-06	14	16	15	0.0	0.9	33.0	66.1	99.1			
WB-1110-MC-PCB-06	16	18	17	0.0	0.7	35.6	63.7	99.3	38.9	7.0	54.1
WB-1110-MC-PCB-06	18	20	19	0.6	0.8	27.8	70.8	98.6			
WB-1110-MC-PCB-06	24	26	25	0.0	0.5	26.3	73.2	99.5			
WB-1110-MC-PCB-06	28	30	29	0.0	0.4	22.3	77.3	99.6	36.2	7.2	56.6
WB-1110-MC-PCB-06	36	38	37	0.0	3.0	77.5	19.4	97.0			
WB-1110-MC-PCB-06	40	42	41	0.0	0.7	41.4	57.8	99.2	37.1	7.5	55.4
WB-1110-MC-PCB-06	50	52	51	0.0	1.3	28.5	70.2	98.7	37.3	7.0	55.8
WB-1110-MC-PCB-06	60	62	61	0.0	0.8	30.3	68.9	99.2	34.6	7.1	58.3
WB-1110-MC-PCB-06	70	72	71	0.0	1.4	33.2	65.4	98.6	33.2	7.5	59.4
WB-1110-MC-PCB-06	80	82	81	0.0	1.3	23.5	75.1	98.7	35.0	4.8	60.2
WB-1110-MC-PCB-06	90	92	91	0.0	1.4	31.7	66.9	98.6	33.3	7.5	59.2
WB-1110-MC-PCB-06	100	105	102.5	0.0	1.5	27.9	70.6	98.5	37.0	5.5	57.5
WB-1110-MC-PCB-06	110	115	112.5	0.0	2.1	36.0	61.9	97.9	38.1	5.9	55.9
WB-1110-MC-PCB-06	130	135	132.5	0.0	1.9	42.2	55.9	98.1	37.6	7.4	55.0
WB-1110-MC-PCB-06	150	155	152.5	0.0	4.2	38.4	57.4	95.8	42.2	6.2	51.6
WB-1110-MC-PCB-06	170	175	172.5	0.0	4.7	44.2	51.2	95.4	39.4	7.4	53.2
WB-1110-MC-PCB-06	190	195	192.5	0.0	2.5	30.4	67.0	97.4	39.8	7.1	53.1
WB-1110-MC-PCB-06	210	215	212.5	0.0	3.2	43.7	53.2	96.9	38.8	5.7	55.5

Table J.4 (Continued).

Core ID	Top Depth of Interval (mm)	Bottom Depth of Interval (mm)	Average Depth of Interval (mm)	% Gravel	% Sand	% Silt	% Clay	% Mud (% Silt + % Clay)	% Carbonate	% TOM (LOI)	% Other
WB-1110-MC-PCB-06	230	235	232.5	0.0	1.8	37.9	60.3	98.2	41.6	3.3	55.1
WB-1110-MC-PCB-06	240	245	242.5	0.0	1.9	32.6	65.5	98.1	37.0	6.2	56.8
WB-1110-MC-PCB-06	250	255	252.5	0.0	1.0	31.0	68.1	99.0	39.5	5.3	55.2
WB-1110-MC-PCB-06	260	265	262.5	0.0	1.6	33.7	64.7	98.4	38.3	5.3	56.4
WB-1110-MC-PCB-06	270	275	272.5	0.0	2.9	47.5	49.6	97.1	36.5	7.5	56.1
WB-1110-MC-PCB-06	280	285	282.5	0.0	1.3	34.9	63.8	98.7	37.7	5.4	56.9
WB-1110-MC-PCB-06	290	295	292.5	0.0	1.5	35.0	63.4	98.5	37.7	5.1	57.2
WB-1110-MC-PCB-06	300	305	302.5	0.0	1.8	33.3	64.9	98.2	38.5	6.8	54.8
WB-1110-MC-PCB-06	310	315	312.5	0.0	1.6	29.2	69.2	98.4	39.5	5.2	55.2

Table J.5. Sediment texture and composition data for core site WB-1114-MC-DSH-08. Sediment cores with sub-sample intervals (mm), texture described as %Gravel, % Sand, % Silt, and % Clay, as well as %Mud, and composition described as %Carbonate, %TOM (LOI), and % Other (non-carbonate, non-organic). Note: Blank cell denotes no analysis performed.

Core ID	Top Depth of Interval (mm)	Bottom Depth of Interval (mm)	Average Depth of Interval (mm)	% Gravel	% Sand	% Silt	% Clay	% Mud (% Silt + % Clay)	% Carbonate	% TOM (LOI)	% Other
WB-1114-MC-DSH-08	0	2	1	0.0	0.8	35.2	64.0	99.2	35.0	7.4	57.6
WB-1114-MC-DSH-08	2	4	3	0.0	0.6	1.6	97.8	99.4			
WB-1114-MC-DSH-08	4	6	5	0.0	1.0	40.0	59.0	99.0	38.7	6.9	54.4
WB-1114-MC-DSH-08	6	8	7	0.0	0.6	4.1	95.3	99.4			
WB-1114-MC-DSH-08	8	10	9	0.0	0.3	43.1	56.6	99.7			
WB-1114-MC-DSH-08	10	12	11	0.0	0.8	22.8	76.4	99.2			
WB-1114-MC-DSH-08	12	14	13	0.0	0.4	40.7	58.9	99.6			
WB-1114-MC-DSH-08	14	16	15	0.0	0.5	45.7	53.8	99.5			
WB-1114-MC-DSH-08	16	18	17	0.0	0.6	32.0	67.4	99.4	31.8	7.8	60.4
WB-1114-MC-DSH-08	18	20	19	0.0	0.3	46.5	53.2	99.7	31.4	9.1	59.5
WB-1114-MC-DSH-08	24	26	25	0.0	0.6	24.1	75.4	99.4			
WB-1114-MC-DSH-08	28	30	29	0.0	6.6	0.2	93.1	93.4	33.7	7.6	58.7
WB-1114-MC-DSH-08	32	34	33	0.0	0.7	28.3	71.0	99.3	32.9	7.5	59.6
WB-1114-MC-DSH-08	36	38	37	0.0	0.7	6.1	93.2	99.3	33.9	6.9	59.2
WB-1114-MC-DSH-08	40	42	41	0.0	1.1	12.9	86.0	98.9	33.9	6.9	59.2
WB-1114-MC-DSH-08	48	50	49	0.0	0.8	13.8	85.4	99.2	31.7	8.3	60.0
WB-1114-MC-DSH-08	70	75	72.5	0.0	0.6	30.5	68.9	99.4	27.8	8.0	64.2
WB-1114-MC-DSH-08	90	95	92.5	0.0	0.4	25.2	74.4	99.6	28.5	8.0	63.5
WB-1114-MC-DSH-08	110	115	112.5	0.0	3.1	0.9	96.0	96.9	33.1	4.8	62.1
WB-1114-MC-DSH-08	130	135	132.5	0.0	0.6	26.8	72.6	99.4	28.7	7.9	63.4
WB-1114-MC-DSH-08	150	155	152.5	0.0	0.4	25.7	73.9	99.6	31.5	5.8	62.7
WB-1114-MC-DSH-08	170	175	172.5	0.0	0.4	16.4	83.2	99.6	32.0	5.8	62.2
WB-1114-MC-DSH-08	180	185	182.5	0.0	0.6	0.8	98.5	99.4	26.4	8.5	65.1
WB-1114-MC-DSH-08	190	195	192.5	0.0	0.6	1.6	97.8	99.4	28.1	7.6	64.3
WB-1114-MC-DSH-08	200	205	202.5	0.0	0.4	36.1	63.4	99.6	30.2	10.1	59.7

Table J.5 (Continued).

Core ID	Top Depth of Interval (mm)	Bottom Depth of Interval (mm)	Average Depth of Interval (mm)	% Gravel	% Sand	% Silt	% Clay	% Mud (% Silt + % Clay)	% Carbonate	% TOM (LOI)	% Other
WB-1114-MC-DSH-08	210	215	212.5	0.0	0.6	1.2	98.2	99.4	28.7	8.6	62.7
WB-1114-MC-DSH-08	230	235	232.5	0.0	1.2	37.0	61.9	98.8	30.4	7.7	61.9

Table J.6. Sediment texture and composition data for core site WB-1114-MC-DSH-10. Sediment cores with sub-sample intervals (mm), texture described as %Gravel, % Sand, % Silt, and % Clay, as well as %Mud, and composition described as %Carbonate, %TOM (LOI), and % Other (non-carbonate, non-organic). Note: Blank cell denotes no analysis performed.

Core ID	Top Depth of Interval (mm)	Bottom Depth of Interval (mm)	Average Depth of Interval (mm)	% Gravel	% Sand	% Silt	% Clay	% Mud (% Silt + % Clay)	% Carbonate	% TOM (LOI)	% Other
WB-1114-MC-DSH-10	0	2	1	0.0	0.2	54.3	45.6	99.8			
WB-1114-MC-DSH-10	2	4	3	0.0	1.2	56.0	42.9	98.8			
WB-1114-MC-DSH-10	4	6	5	0.0	0.1	52.9	47.0	99.9			
WB-1114-MC-DSH-10	6	8	7	0.0	0.7	40.2	59.0	99.3			
WB-1114-MC-DSH-10	8	10	9	0.0	0.3	44.5	55.2	99.7			
WB-1114-MC-DSH-10	10	12	11	0.0	0.7	46.1	53.2	99.3			
WB-1114-MC-DSH-10	12	14	13	0.0	0.3	43.2	56.5	99.7			
WB-1114-MC-DSH-10	14	16	15	0.0	0.5	46.3	53.2	99.5			
WB-1114-MC-DSH-10	16	18	17	0.0	0.2	41.6	58.3	99.8			
WB-1114-MC-DSH-10	18	20	19	0.0	0.4	35.3	64.3	99.6			
WB-1114-MC-DSH-10	20	22	21	0.0	0.1	47.3	52.6	99.9			
WB-1114-MC-DSH-10	24	26	25	0.0	0.5	25.5	74.0	99.5			
WB-1114-MC-DSH-10	32	34	33	0.0	0.2	37.2	62.7	99.8	31.3	6.3	62.5
WB-1114-MC-DSH-10	40	42	41	0.0	0.6	40.8	58.5	99.4	28.0	6.7	65.3
WB-1114-MC-DSH-10	48	50	49	0.0	0.2	40.6	59.3	99.8	29.3	7.5	63.2
WB-1114-MC-DSH-10	56	58	57	0.0	0.4	37.9	61.8	99.6	27.5	7.2	65.4
WB-1114-MC-DSH-10	64	66	65	0.0	1.3	39.1	59.6	98.7	27.3	7.2	65.5
WB-1114-MC-DSH-10	72	74	73	0.0	0.1	30.4	69.5	99.9	30.6	6.4	63.0
WB-1114-MC-DSH-10	80	82	81	0.0	0.2	30.8	68.9	99.8	26.3	7.0	66.7
WB-1114-MC-DSH-10	90	95	92.5	0.0	0.2	31.3	68.5	99.8	27.1	6.2	66.7
WB-1114-MC-DSH-10	100	105	102.5	0.0	0.9	36.0	63.2	99.1	28.0	4.6	67.4
WB-1114-MC-DSH-10	110	115	112.5	0.0	0.6	34.3	65.1	99.4	27.1	7.4	65.5
WB-1114-MC-DSH-10	120	125	122.5	0.0	0.1	35.2	64.7	99.9	26.7	6.2	67.0
WB-1114-MC-DSH-10	130	135	132.5	0.0	0.1	35.9	64.0	99.9	30.0	5.2	64.7
WB-1114-MC-DSH-10	150	155	152.5	0.0	0.5	33.8	65.7	99.5	30.5	6.1	63.5

Table J.6 (Continued).

Core ID	Top Depth of Interval (mm)	Bottom Depth of Interval (mm)	Average Depth of Interval (mm)	% Gravel	% Sand	% Silt	% Clay	% Mud (% Silt + % Clay)	% Carbonate	% TOM (LOI)	% Other
WB-1114-MC-DSH-10	170	175	172.5	0.0	1.6	46.1	52.3	98.4	30.7	5.5	63.7
WB-1114-MC-DSH-10	190	195	192.5	0.0	1.2	36.2	62.6	98.8	33.4	5.7	60.9
WB-1114-MC-DSH-10	210	215	212.5	0.0	0.6	42.0	57.4	99.4	32.3	6.3	61.4
WB-1114-MC-DSH-10	230	235	232.5	0.0	0.7	34.0	65.3	99.3	35.0	5.7	59.3
WB-1114-MC-DSH-10	250	255	252.5	0.0	3.6	44.6	51.8	96.4	35.8	6.0	58.3
WB-1114-MC-DSH-10	270	275	272.5	0.0	2.8	47.5	49.7	97.2	38.2	4.8	57.0
WB-1114-MC-DSH-10	290	295	292.5	0.0	1.4	44.0	54.6	98.6	38.1	4.9	57.0
WB-1114-MC-DSH-10	310	315	312.5	0.0	1.7	43.5	54.7	98.3	38.5	5.2	56.4

Table J.7. Sediment texture and composition data for core site WB-1114-MC-PCB-06. Sediment cores with sub-sample intervals (mm), texture described as %Gravel, % Sand, % Silt, and % Clay, as well as %Mud, and composition described as %Carbonate, %TOM (LOI), and % Other (non-carbonate, non-organic). Note: Blank cell denotes no analysis performed.

Core ID	Top Depth of Interval (mm)	Bottom Depth of Interval (mm)	Average Depth of Interval (mm)	% Gravel	% Sand	% Silt	% Clay	% Mud (% Silt + % Clay)	% Carbonate	% TOM (LOI)	% Other
WB-1114-MC-PCB-06	0	2	1	0.0	0.1	62.8	37.1	99.9			
WB-1114-MC-PCB-06	2	4	3	0.0	0.4	40.7	58.9	99.6			
WB-1114-MC-PCB-06	4	6	5	0.0	1.5	54.4	44.1	98.5			
WB-1114-MC-PCB-06	6	8	7	0.0	0.9	51.0	48.1	99.1			
WB-1114-MC-PCB-06	8	10	9	0.0	1.1	45.8	53.1	98.9			
WB-1114-MC-PCB-06	10	12	11	0.0	0.7	44.7	54.5	99.3			
WB-1114-MC-PCB-06	12	14	13	0.0	0.8	42.3	56.9	99.2	39.7	7.2	53.0
WB-1114-MC-PCB-06	14	16	15	0.0	0.9	47.6	51.5	99.1			
WB-1114-MC-PCB-06	16	18	17	0.0	0.8	40.5	58.8	99.2			
WB-1114-MC-PCB-06	18	20	19	0.0	0.7	46.5	52.8	99.3	39.0	7.9	53.2
WB-1114-MC-PCB-06	20	22	21	0.0	0.3	35.3	64.4	99.7			
WB-1114-MC-PCB-06	24	26	25	0.0	0.6	30.8	68.6	99.4			
WB-1114-MC-PCB-06	32	34	33	0.0	5.5	34.2	60.3	94.5			
WB-1114-MC-PCB-06	36	38	37						39.7	8.4	52.0
WB-1114-MC-PCB-06	40	42	41						37.7	9.7	52.6
WB-1114-MC-PCB-06	48	50	49	0.0	0.5	46.3	53.3	99.5	37.6	7.6	54.8
WB-1114-MC-PCB-06	56	58	57						36.6	9.8	53.6
WB-1114-MC-PCB-06	64	66	65						34.3	10.9	54.8
WB-1114-MC-PCB-06	70	75	72.5	0.0	0.8	40.9	58.3	99.2	35.3	8.3	56.4
WB-1114-MC-PCB-06	80	85	82.5						33.5	10.7	55.8
WB-1114-MC-PCB-06	90	95	92.5	0.0	1.5	38.0	60.5	98.5	36.0	7.7	56.3
WB-1114-MC-PCB-06	100	105	102.5						34.1	10.0	55.9
WB-1114-MC-PCB-06	110	115	112.5	0.0	0.6	33.9	65.5	99.4	36.4	8.3	55.3
WB-1114-MC-PCB-06	120	125	122.5						35.8	7.1	57.2
WB-1114-MC-PCB-06	130	135	132.5	0.0	1.3	56.1	42.6	98.7	37.1	9.5	53.4

Table J.7 (Continued).

Core ID	Top Depth of Interval (mm)	Bottom Depth of Interval (mm)	Average Depth of Interval (mm)	% Gravel	% Sand	% Silt	% Clay	% Mud (% Silt + % Clay)	% Carbonate	% TOM (LOI)	% Other
WB-1114-MC-PCB-06	140	145	142.5						37.1	9.3	53.6
WB-1114-MC-PCB-06	150	155	152.5	0.0	0.8	37.6	61.7	99.2	39.4	7.0	53.5
WB-1114-MC-PCB-06	170	175	172.5						37.2	10.0	52.8
WB-1114-MC-PCB-06	190	195	192.5	0.0	1.1	34.4	64.5	98.9	39.2	9.1	51.7
WB-1114-MC-PCB-06	210	215	212.5						39.1	8.4	52.5
WB-1114-MC-PCB-06	230	235	232.5						40.0	7.9	52.1
WB-1114-MC-PCB-06	250	255	252.5						34.5	12.6	52.9
WB-1114-MC-PCB-06	270	275	272.5						37.1	9.2	53.7
WB-1114-MC-PCB-06	290	295	292.5						35.4	9.5	55.1
WB-1114-MC-PCB-06	310	315	312.5						39.4	8.2	52.4
WB-1114-MC-PCB-06	330	335	332.5						34.7	10.8	54.6

Table J.8. Sediment texture and composition data for core site WB-0911-BC-DSH-08. Sediment cores with sub-sample intervals (mm), texture described as %Gravel, % Sand, % Silt, and % Clay, as well as %Mud, and composition described as %Carbonate, %TOM (LOI), and % Other (non-carbonate, non-organic). Note: Blank cell denotes no analysis performed.

Core ID	Top Depth of Interval (mm)	Bottom Depth of Interval (mm)	Average Depth of Interval (mm)	% Gravel	% Sand	% Silt	% Clay	% Mud (% Silt + % Clay)	% Carbonate	% TOM (LOI)	% Other
WB-0911-BC-DSH-08	0	2	1	0.0	0.9	24.8	74.3	99.1	34.4	9.6	56.0
WB-0911-BC-DSH-08	2	4	3	0.4	0.4	32.6	66.6	99.2			
WB-0911-BC-DSH-08	4	6	5	0.0	0.8	16.9	82.3	99.2	33.1	8.0	58.9
WB-0911-BC-DSH-08	6	8	7	0.0	0.8	42.6	56.6	99.2			
WB-0911-BC-DSH-08	8	10	9	0.0	0.7	15.6	83.7	99.3	31.7	8.0	60.3
WB-0911-BC-DSH-08	10	12	11	0.0	0.6	38.1	61.3	99.4			
WB-0911-BC-DSH-08	12	14	13	0.0	0.2	45.9	53.8	99.8			
WB-0911-BC-DSH-08	14	16	15	0.0	0.7	34.7	64.5	99.3	32.5	10.1	57.4
WB-0911-BC-DSH-08	16	18	17	0.0	0.3	22.9	76.8	99.7	32.7	8.3	59.0
WB-0911-BC-DSH-08	18	20	19	0.0	0.7	38.4	60.9	99.3	35.9	7.0	57.1
WB-0911-BC-DSH-08	24	26	25	0.0	0.6	35.6	63.8	99.4	29.5	11.7	58.7
WB-0911-BC-DSH-08	26	28	27	0.0	0.6	37.1	62.3	99.4	30.1	11.7	58.2
WB-0911-BC-DSH-08	28	30	29	0.0	1.0	39.1	59.9	99.0	31.5	9.7	58.9
WB-0911-BC-DSH-08	30	35	32.5	0.0	0.7	35.7	63.5	99.3	30.4	8.0	61.6
WB-0911-BC-DSH-08	40	45	42.5	0.2	0.3	34.6	65.0	99.6	31.4	6.6	62.0
WB-0911-BC-DSH-08	50	55	52.5	0.0	0.6	38.3	61.0	99.4	25.3	8.6	66.1
WB-0911-BC-DSH-08	60	65	62.5	0.0	0.2	33.2	66.6	99.8	28.6	9.9	61.6
WB-0911-BC-DSH-08	70	75	72.5	0.0	0.3	26.8	72.9	99.7	24.2	8.9	66.9
WB-0911-BC-DSH-08	80	85	82.5	0.0	0.3	27.6	72.2	99.7	27.7	9.1	63.2
WB-0911-BC-DSH-08	90	95	92.5	0.0	0.2	26.9	72.9	99.8	24.6	12.0	63.5
WB-0911-BC-DSH-08	100	105	102.5	0.0	0.2	27.8	72.0	99.8	25.6	11.2	63.3
WB-0911-BC-DSH-08	110	115	112.5	0.0	0.1	27.8	72.1	99.9	31.6	6.1	62.3
WB-0911-BC-DSH-08	120	125	122.5	0.0	0.3	25.3	74.3	99.7	27.0	9.8	63.2
WB-0911-BC-DSH-08	130	135	132.5	0.0	0.5	34.7	64.7	99.5	21.8	9.9	68.3
WB-0911-BC-DSH-08	140	145	142.5	0.0	0.2	23.9	75.9	99.8	30.9	6.0	63.2

Table J.8 (Continued).

Core ID	Top Depth of Interval (mm)	Bottom Depth of Interval (mm)	Average Depth of Interval (mm)	% Gravel	% Sand	% Silt	% Clay	% Mud (% Silt + % Clay)	% Carbonate	% TOM (LOI)	% Other
WB-0911-BC-DSH-08	150	155	152.5	0.0	0.1	33.0	66.9	99.9	30.2	6.3	63.4
WB-0911-BC-DSH-08	170	175	172.5	0.0	0.7	34.3	65.0	99.3	18.6	13.5	68.0
WB-0911-BC-DSH-08	190	195	192.5	0.0	0.1	27.4	72.4	99.9	32.6	6.7	60.7
WB-0911-BC-DSH-08	210	215	212.5	0.0	0.2	32.4	67.4	99.8	33.3	6.9	59.8
WB-0911-BC-DSH-08	230	235	232.5	0.0	0.1	30.6	69.2	99.9	31.3	9.1	59.6
WB-0911-BC-DSH-08	250	255	252.5	0.0	0.2	23.6	76.2	99.8	33.5	7.0	59.4
WB-0911-BC-DSH-08	270	275	272.5	0.0	0.3	28.5	71.2	99.7	32.6	9.3	58.1
WB-0911-BC-DSH-08	290	295	292.5	0.0	0.3	24.6	75.1	99.7	35.9	7.6	56.5
WB-0911-BC-DSH-08	300	305	302.5	0.0	1.7	40.2	58.1	98.3	32.5	8.3	59.2
WB-0911-BC-DSH-08	310	315	312.5	0.0	0.9	39.9	59.2	99.1	36.4	9.1	54.5

Table J.9. Sediment texture and composition data for core site WB-0911-BC-DSH-10. Sediment cores with sub-sample intervals (mm), texture described as %Gravel, % Sand, % Silt, and % Clay, as well as %Mud, and composition described as %Carbonate, %TOM (LOI), and % Other (non-carbonate, non-organic). Note: Blank cell denotes no analysis performed.

Core ID	Top Depth of Interval (mm)	Bottom Depth of Interval (mm)	Average Depth of Interval (mm)	% Gravel	% Sand	% Silt	% Clay	% Mud (% Silt + % Clay)	% Carbonate	% TOM (LOI)	% Other
WB-0911-BC-DSH-10	0	2	1	0.0	3.0	5.0	92.0	97.0	30.8	9.5	59.7
WB-0911-BC-DSH-10	2	4	3	0.0	0.7	33.8	65.6	99.3	32.1	10.1	57.9
WB-0911-BC-DSH-10	4	6	5	1.1	1.5	24.6	72.9	97.4	29.4	8.6	62.1
WB-0911-BC-DSH-10	6	8	7	0.0	0.7	34.4	65.0	99.3	27.6	11.6	60.8
WB-0911-BC-DSH-10	8	10	9	0.0	0.4	36.5	63.1	99.6	30.3	7.7	61.9
WB-0911-BC-DSH-10	10	12	11	0.0	0.4	31.5	68.1	99.6	25.8	12.2	62.1
WB-0911-BC-DSH-10	12	14	13	0.0	0.4	27.3	72.3	99.6	24.5	13.8	61.7
WB-0911-BC-DSH-10	14	16	15	0.0	0.3	26.5	73.2	99.7	25.3	11.3	63.4
WB-0911-BC-DSH-10	16	18	17	0.0	8.9	30.1	61.1	91.1	25.2	8.7	66.1
WB-0911-BC-DSH-10	18	20	19	0.0	0.0	33.3	66.7	100.0	26.8	10.7	62.5
WB-0911-BC-DSH-10	24	26	25	0.0	0.2	32.8	67.0	99.8	25.1	12.1	62.8
WB-0911-BC-DSH-10	32	34	33	0.0	0.8	29.2	69.9	99.2	29.3	7.7	63.0
WB-0911-BC-DSH-10	40	45	42.5	0.0	0.3	31.3	68.4	99.7	24.7	11.1	64.2
WB-0911-BC-DSH-10	50	55	52.5	0.0	4.7	31.3	64.0	95.3	24.3	9.0	66.8
WB-0911-BC-DSH-10	60	65	62.5	0.0	0.3	29.0	70.7	99.7	24.7	11.0	64.2
WB-0911-BC-DSH-10	70	75	72.5	0.0	0.6	31.0	68.4	99.4	24.2	9.0	66.8
WB-0911-BC-DSH-10	80	85	82.5	0.0	0.3	29.9	69.7	99.7	25.3	10.9	63.8
WB-0911-BC-DSH-10	90	95	92.5	0.0	0.8	30.6	68.6	99.2	22.1	9.7	68.2
WB-0911-BC-DSH-10	110	115	112.5	0.0	0.5	28.9	70.6	99.5	25.8	9.9	64.3
WB-0911-BC-DSH-10	130	135	132.5	0.0	0.6	28.7	70.7	99.4	21.3	9.9	68.7
WB-0911-BC-DSH-10	150	155	152.5	0.0	0.5	37.2	62.3	99.5	28.2	10.2	61.6
WB-0911-BC-DSH-10	170	175	172.5	0.0	1.0	39.8	59.2	99.0	25.9	9.7	64.5
WB-0911-BC-DSH-10	190	195	192.5	0.0	0.6	46.3	53.1	99.4	30.9	9.8	59.3
WB-0911-BC-DSH-10	210	215	212.5	0.0	1.1	37.9	61.1	98.9	30.2	11.5	58.3
WB-0911-BC-DSH-10	230	235	232.5	0.0	0.8	34.9	64.3	99.2	32.4	10.6	56.9

Table J.9 (Continued).

Core ID	Top Depth of Interval (mm)	Bottom Depth of Interval (mm)	Average Depth of Interval (mm)	% Gravel	% Sand	% Silt	% Clay	% Mud (% Silt + % Clay)	% Carbonate	% TOM (LOI)	% Other
WB-0911-BC-DSH-10	270	275	272.5	0.0	1.4	39.5	59.1	98.6	33.4	9.1	57.5
WB-0911-BC-DSH-10	290	295	292.5	0.0	0.9	39.7	59.3	99.1	31.1	10.1	58.7
WB-0911-BC-DSH-10	300	305	302.5	0.0	1.5	33.3	65.3	98.5	30.7	7.4	62.0
WB-0911-BC-DSH-10	310	315	312.5	0.0	0.8	45.5	53.7	99.2	29.8	11.6	58.5

Table J.10. Sediment texture and composition data for core site WB-0911-MC-PCB-06. Sediment cores with sub-sample intervals (mm), texture described as %Gravel, % Sand, % Silt, and % Clay, as well as %Mud, and composition described as %Carbonate, %TOM (LOI), and % Other (non-carbonate, non-organic). Note: Blank cell denotes no analysis performed.

Core ID	Top Depth of Interval (mm)	Bottom Depth of Interval (mm)	Average Depth of Interval (mm)	% Gravel	% Sand	% Silt	% Clay	% Mud (% Silt + % Clay)	% Carbonate	% TOM (LOI)	% Other
WB-0911-MC-PCB-06	0	2	1	0.0	2.1	70.1	27.8	97.9	45.8	6.3	47.8
WB-0911-MC-PCB-06	2	4	3	0.0	0.8	45.0	54.2	99.2			
WB-0911-MC-PCB-06	4	6	5	2.0	1.0	54.8	42.2	97.0	43.9	6.7	49.3
WB-0911-MC-PCB-06	6	8	7	0.0	0.3	44.4	55.3	99.7			
WB-0911-MC-PCB-06	8	10	9	0.0	0.9	43.6	55.5	99.1	43.4	6.7	49.9
WB-0911-MC-PCB-06	10	12	11	0.0	0.7	39.7	59.5	99.3			
WB-0911-MC-PCB-06	12	14	13	0.0	0.8	36.3	62.9	99.2			
WB-0911-MC-PCB-06	14	16	15	0.0	0.8	39.9	59.3	99.2			
WB-0911-MC-PCB-06	16	18	17	0.0	1.1	44.7	54.2	98.9	40.8	7.0	52.2
WB-0911-MC-PCB-06	18	20	19	0.0	0.8	30.2	69.0	99.2			
WB-0911-MC-PCB-06	24	26	25	0.0	0.4	27.7	71.9	99.6			
WB-0911-MC-PCB-06	32	34	33	0.0	1.4	37.9	60.7	98.6	35.6	7.5	56.9
WB-0911-MC-PCB-06	48	50	49	0.0	1.2	32.7	66.1	98.8			
WB-0911-MC-PCB-06	70	75	72.5	0.0	1.6	39.1	59.3	98.4	33.9	8.0	58.1
WB-0911-MC-PCB-06	90	95	92.5	0.0	1.2	39.2	59.5	98.8	33.7	8.1	58.3
WB-0911-MC-PCB-06	110	115	112.5	0.0	0.3	33.1	66.6	99.7			
WB-0911-MC-PCB-06	130	135	132.5	0.0	1.8	37.7	60.4	98.2	35.6	7.3	57.1
WB-0911-MC-PCB-06	150	155	152.5	0.0	1.2	33.6	65.2	98.8			
WB-0911-MC-PCB-06	170	175	172.5	0.0	2.2	37.3	60.4	97.8	39.1	6.6	54.3
WB-0911-MC-PCB-06	190	195	192.5	0.0	1.7	31.5	66.8	98.3			
WB-0911-MC-PCB-06	200	205	202.5	0.0	1.9	50.8	47.3	98.1			
WB-0911-MC-PCB-06	210	215	212.5	0.0	2.5	31.0	66.5	97.5			
WB-0911-MC-PCB-06	220	225	222.5	0.0	2.7	36.3	61.0	97.3			
WB-0911-MC-PCB-06	230	235	232.5	0.0	2.3	46.2	51.5	97.7			
WB-0911-MC-PCB-06	250	255	252.5	0.0	2.5	48.5	49.0	97.5			

Table J.10 (Continued).

Core ID	Top Depth of Interval (mm)	Bottom Depth of Interval (mm)	Average Depth of Interval (mm)	% Gravel	% Sand	% Silt	% Clay	% Mud (% Silt + % Clay)	% Carbonate	% TOM (LOI)	% Other
WB-0911-MC-PCB-06	270	275	272.5	0.0	1.7	44.7	53.6	98.3			
WB-0911-MC-PCB-06	290	295	292.5	0.0	2.4	50.3	47.3	97.6			
WB-0911-MC-PCB-06	310	315	312.5	0.0	0.8	32.5	66.7	99.2			
WB-0911-MC-PCB-06	330	335	332.5	0.0	1.1	26.6	72.2	98.9			
WB-0911-MC-PCB-06	350	355	352.5	0.0	1.4	36.5	62.2	98.6	34.8	7.0	58.2

Table J.11. Sediment texture and composition data for core site WB-0812-MC-DSH-08. Sediment cores with sub-sample intervals (mm), texture described as %Gravel, % Sand, % Silt, and % Clay, as well as %Mud, and composition described as %Carbonate, %TOM (LOI), and % Other (non-carbonate, non-organic). Note: Blank cell denotes no analysis performed.

Core ID	Top Depth of Interval (mm)	Bottom Depth of Interval (mm)	Average Depth of Interval (mm)	% Gravel	% Sand	% Silt	% Clay	% Mud (% Silt + % Clay)	% Carbonate	% TOM (LOI)	% Other
WB-0812-MC-DSH-08	0	2	1	0.0	0.8	43.4	55.8	99.2			
WB-0812-MC-DSH-08	4	6	5	0.0	0.4	34.7	64.9	99.6	25.0	13.1	61.9
WB-0812-MC-DSH-08	6	8	7	0.0	0.2	36.9	62.9	99.8			
WB-0812-MC-DSH-08	8	10	9	0.0	0.6	42.3	57.2	99.4	24.9	12.9	62.2
WB-0812-MC-DSH-08	10	12	11	0.0	0.6	42.4	56.9	99.4	27.6	9.9	62.5
WB-0812-MC-DSH-08	12	14	13	0.0	0.3	30.4	69.3	99.7			
WB-0812-MC-DSH-08	14	16	15	0.0	0.5	39.0	60.5	99.5			
WB-0812-MC-DSH-08	16	18	17	0.0	0.3	32.3	67.4	99.7	22.2	13.5	64.2
WB-0812-MC-DSH-08	18	20	19	0.0	0.7	42.5	56.8	99.3			
WB-0812-MC-DSH-08	30	32	31	0.0	0.3	30.9	68.8	99.7	24.8	10.8	64.4
WB-0812-MC-DSH-08	50	55	52.5	0.0	0.1	33.2	66.6	99.9	24.3	7.4	68.3
WB-0812-MC-DSH-08	70	75	72.5	0.0	0.7	33.9	65.4	99.3	24.6	10.4	65.0
WB-0812-MC-DSH-08	90	95	92.5	0.0	0.2	27.6	72.2	99.8	21.3	11.5	67.2
WB-0812-MC-DSH-08	110	115	112.5	0.0	0.2	28.0	71.8	99.8	23.3	10.6	66.1
WB-0812-MC-DSH-08	130	135	132.5	0.0	0.2	36.5	63.3	99.8	25.1	6.9	68.0
WB-0812-MC-DSH-08	150	155	152.5	0.0	0.7	39.2	60.1	99.3	25.5	10.8	63.8
WB-0812-MC-DSH-08	170	175	172.5	0.0	0.3	31.6	68.0	99.7	26.8	11.0	62.2
WB-0812-MC-DSH-08	190	195	192.5	0.4	0.4	39.5	59.8	99.3	29.8	6.9	63.3
WB-0812-MC-DSH-08	210	215	212.5	0.1	0.3	41.4	58.2	99.6	33.0	6.2	60.7
WB-0812-MC-DSH-08	230	235	232.5	0.0	0.3	37.0	62.7	99.7	31.1	6.7	62.2
WB-0812-MC-DSH-08	250	255	252.5	0.0	0.3	37.4	62.2	99.7	32.1	6.3	61.6
WB-0812-MC-DSH-08	270	275	272.5	0.0	0.4	39.6	60.0	99.6	31.2	6.7	62.1
WB-0812-MC-DSH-08	290	295	292.5	0.0	0.4	39.6	60.0	99.6	35.0	6.3	58.7
WB-0812-MC-DSH-08	310	315	312.5	0.0	0.3	40.4	59.2	99.6	35.8	6.6	57.5
WB-0812-MC-DSH-08	330	335	332.5	0.0	0.4	42.5	57.2	99.6	40.1	6.3	53.5

Table J.12. Sediment texture and composition data for core site WB-0812-MC-DSH-10. Sediment cores with sub-sample intervals (mm), texture described as %Gravel, % Sand, % Silt, and % Clay, as well as %Mud, and composition described as %Carbonate, %TOM (LOI), and % Other (non-carbonate, non-organic). Note: Blank cell denotes no analysis performed.

Core ID	Top Depth of Interval (mm)	Bottom Depth of Interval (mm)	Average Depth of Interval (mm)	% Gravel	% Sand	% Silt	% Clay	% Mud (% Silt + % Clay)	% Carbonate	% TOM (LOI)	% Other
WB-0812-MC-DSH-10	0	2	1	0.0	0.5	45.3	54.3	99.5	28.5	9.9	61.6
WB-0812-MC-DSH-10	2	4	3	0.0	0.2	43.7	56.1	99.8	27.5	11.2	61.4
WB-0812-MC-DSH-10	4	6	5	0.0	0.2	36.3	63.6	99.8	26.5	11.2	62.4
WB-0812-MC-DSH-10	6	8	7	0.0	0.2	41.2	58.7	99.8	26.0	11.5	62.4
WB-0812-MC-DSH-10	8	10	9	0.0	0.3	28.8	70.9	99.7	25.4	10.0	64.6
WB-0812-MC-DSH-10	10	12	11	0.0	0.2	31.0	68.8	99.8			
WB-0812-MC-DSH-10	12	14	13	0.0	0.2	29.6	70.2	99.8	24.0	11.9	64.1
WB-0812-MC-DSH-10	14	16	15	0.0	0.1	26.7	73.2	99.9	23.7	12.0	64.3
WB-0812-MC-DSH-10	16	18	17	0.0	0.2	33.4	66.4	99.8	27.3	8.6	64.1
WB-0812-MC-DSH-10	18	20	19	0.0	0.1	33.5	66.4	99.9	27.7	9.5	62.8
WB-0812-MC-DSH-10	20	22	21	0.0	0.1	36.5	63.4	99.9	24.5	11.1	64.4
WB-0812-MC-DSH-10	24	26	25	0.0	0.1	36.4	63.5	99.9	29.8	7.7	62.6
WB-0812-MC-DSH-10	26	28	27	0.0	0.2	32.2	67.6	99.8	27.8	9.0	63.2
WB-0812-MC-DSH-10	28	30	29	0.0	0.1	30.9	69.0	99.9	29.5	8.0	62.5
WB-0812-MC-DSH-10	30	35	32.5	0.0	0.2	38.7	61.1	99.8	24.5	11.4	64.1
WB-0812-MC-DSH-10	35	40	37.5	0.0	0.2	35.7	64.1	99.8	28.0	7.9	64.0
WB-0812-MC-DSH-10	40	45	42.5	0.0	0.2	34.2	65.5	99.8	28.2	7.3	64.5
WB-0812-MC-DSH-10	45	50	47.5	0.0	0.2	32.3	67.5	99.8	28.1	6.7	65.1
WB-0812-MC-DSH-10	50	55	52.5	0.0	0.3	32.8	66.8	99.7	24.5	11.1	64.4
WB-0812-MC-DSH-10	55	60	57.5	0.0	0.3	29.7	70.0	99.7	27.4	7.3	65.2
WB-0812-MC-DSH-10	70	75	72.5	0.0	0.3	30.7	69.0	99.7	23.7	11.3	65.1
WB-0812-MC-DSH-10	80	85	82.5	0.0	0.3	27.0	72.7	99.7	25.5	8.5	66.0
WB-0812-MC-DSH-10	90	95	92.5	0.0	0.1	30.3	69.6	99.9	24.1	11.2	64.7
WB-0812-MC-DSH-10	100	105	102.5	0.0	0.3	28.5	71.2	99.7	26.3	8.1	65.6
WB-0812-MC-DSH-10	110	115	112.5	0.0	0.1	32.6	67.3	99.9	24.6	11.1	64.3

Table J.12 (Continued).

Core ID	Top Depth of Interval (mm)	Bottom Depth of Interval (mm)	Average Depth of Interval (mm)	% Gravel	% Sand	% Silt	% Clay	% Mud (% Silt + % Clay)	% Carbonate	% TOM (LOI)	% Other
WB-0812-MC-DSH-10	150	155	152.5	0.0	0.4	34.4	65.2	99.6	27.4	10.5	62.1
WB-0812-MC-DSH-10	190	195	192.5	0.0	1.1	36.6	62.3	98.9	31.4	10.1	58.5
WB-0812-MC-DSH-10	230	235	232.5	0.0	0.4	33.0	66.6	99.6	33.3	9.8	56.9
WB-0812-MC-DSH-10	270	275	272.5	0.0	0.9	34.3	64.8	99.1	31.6	9.9	58.5

Table J.13. Sediment texture and composition data for core site WB-0812-MC-PCB-06. Sediment cores with sub-sample intervals (mm), texture described as %Gravel, % Sand, % Silt, and % Clay, as well as %Mud, and composition described as %Carbonate, %TOM (LOI), and % Other (non-carbonate, non-organic). Note: Blank cell denotes no analysis performed.

Core ID	Top Depth of Interval (mm)	Bottom Depth of Interval (mm)	Average Depth of Interval (mm)	% Gravel	% Sand	% Silt	% Clay	% Mud (% Silt + % Clay)	% Carbonate	% TOM (LOI)	% Other
WB-0812-MC-PCB-06	0	2	1	0.0	0.9	49.2	49.9	99.1	34.7	11.9	53.4
WB-0812-MC-PCB-06	2	4	3	0.0	0.8	38.9	60.4	99.2	33.2	13.1	53.7
WB-0812-MC-PCB-06	4	6	5	0.0	0.4	36.4	63.2	99.6			
WB-0812-MC-PCB-06	6	8	7	0.0	0.4	42.1	57.5	99.6	36.6	10.0	53.4
WB-0812-MC-PCB-06	8	10	9	0.0	0.2	36.1	63.7	99.8			
WB-0812-MC-PCB-06	10	12	11	0.0	0.1	40.9	59.1	99.9	35.2	10.6	54.2
WB-0812-MC-PCB-06	12	14	13	0.0	0.7	49.0	50.3	99.3			
WB-0812-MC-PCB-06	14	16	15	0.0	0.5	42.7	56.8	99.5	35.1	10.1	
WB-0812-MC-PCB-06	16	18	17	0.0	0.8	39.6	59.7	99.2	35.8	10.2	54.0
WB-0812-MC-PCB-06	18	20	19	0.0	4.0	35.5	60.4	96.0	32.7	12.2	55.1
WB-0812-MC-PCB-06	24	26	25	0.0	0.8	40.1	59.1	99.2	34.9	10.5	54.6
WB-0812-MC-PCB-06	30	32	31	0.0	0.9	38.5	60.6	99.1	33.5	10.3	56.2
WB-0812-MC-PCB-06	50	55	52.5	0.0	0.7	39.1	60.3	99.3	31.1	9.9	59.0
WB-0812-MC-PCB-06	70	75	72.5	0.0	1.2	68.0	30.8	98.8	30.8	11.7	57.5
WB-0812-MC-PCB-06	90	95	92.5	0.0	1.2	72.8	26.1	98.8	33.7	8.9	57.4
WB-0812-MC-PCB-06	130	135	132.5	0.0	2.3	64.4	33.3	97.7	37.1	6.7	56.2
WB-0812-MC-PCB-06	150	155	152.5	0.0	2.4	68.7	28.9	97.6	36.6	10.4	53.1
WB-0812-MC-PCB-06	170	175	172.5	0.0	2.4	56.8	40.8	97.6	36.6	11.3	52.1
WB-0812-MC-PCB-06	190	195	192.5	0.0	2.6	65.9	31.6	97.4	39.1	9.2	51.7
WB-0812-MC-PCB-06	210	215	212.5	0.0	2.9	62.4	34.7	97.1	40.8	5.8	53.3
WB-0812-MC-PCB-06	230	235	232.5	0.0	3.8	47.1	49.0	96.2	42.1	7.5	50.4
WB-0812-MC-PCB-06	250	255	252.5	0.0	3.9	82.1	14.0	96.1			
WB-0812-MC-PCB-06	270	275	272.5	0.0	3.4	65.9	30.7	96.6			
WB-0812-MC-PCB-06	290	295	292.5	0.0	2.6	76.9	20.5	97.4			
WB-0812-MC-PCB-06	310	315	312.5	0.0	2.1	84.1	13.8	97.9			

Table J.13 (Continued).

Core ID	Top Depth of Interval (mm)	Bottom Depth of Interval (mm)	Average Depth of Interval (mm)	% Gravel	% Sand	% Silt	% Clay	% Mud (% Silt + % Clay)	% Carbonate	% TOM (LOI)	% Other
WB-0812-MC-PCB-06	330	335	332.5	0.0	2.6	89.4	8.0	97.4			
WB-0812-MC-PCB-06	350	355	352.5	0.0	1.5	55.5	43.0	98.5			
WB-0812-MC-PCB-06	370	375	372.5	0.0	2.5	76.4	21.1	97.5			
WB-0812-MC-PCB-06	390	395	392.5	0.0	3.1	83.6	13.3	96.9			
WB-0812-MC-PCB-06	410	415	412.5	0.0	3.2	55.2	41.6	96.8			

Table J.14. Sediment texture and composition data for core site WB-1012-MC-04. Sediment cores with sub-sample intervals (mm), texture described as %Gravel, % Sand, % Silt, and % Clay, as well as %Mud, and composition described as %Carbonate, %TOM (LOI), and % Other (non-carbonate, non-organic). Note: Blank cell denotes no analysis performed.

Core ID	Top Depth of Interval (mm)	Bottom Depth of Interval (mm)	Average Depth of Interval (mm)	% Gravel	% Sand	% Silt	% Clay	% Mud (% Silt + % Clay)	% Carbonate	% TOM (LOI)	% Other
WB-1012-MC-04	0	2	1	0.0	3.0	67.1	29.9	97.0	55.2		
WB-1012-MC-04	2	4	3	0.0	4.2	62.5	33.4	95.8	45.2		
WB-1012-MC-04	4	6	5	0.0	2.4	54.0	43.6	97.6	53.1		
WB-1012-MC-04	6	8	7	0.0	1.9	65.3	32.8	98.1	55.0		
WB-1012-MC-04	8	10	9	0.0	5.4	67.5	27.1	94.6	52.1		
WB-1012-MC-04	10	12	11	0.0	6.0	62.7	31.3	94.0	51.9		
WB-1012-MC-04	12	14	13	0.0	3.4	65.0	31.6	96.6	52.1		
WB-1012-MC-04	14	16	15	0.0	4.4	56.0	39.6	95.6	48.9		
WB-1012-MC-04	16	18	17	0.0	9.3	59.0	31.7	90.7	41.0		
WB-1012-MC-04	18	20	19	0.0	6.8	62.6	30.5	93.2	47.7		
WB-1012-MC-04	30	35	32.5	0.0	14.0	60.1	25.9	86.0	51.6		
WB-1012-MC-04	50	55	52.5	0.0	13.9	61.0	25.1	86.1	42.5		
WB-1012-MC-04	70	75	72.5	0.0	6.7	67.8	25.4	93.3	55.1		
WB-1012-MC-04	90	95	92.5	0.0	10.8	48.3	40.9	89.2	52.5		
WB-1012-MC-04	110	115	112.5	0.0	10.0	54.5	35.5	90.0	47.9		
WB-1012-MC-04	130	135	132.5	0.0	14.7	54.4	30.9	85.3	47.4		
WB-1012-MC-04	150	155	152.5	0.0	16.9	49.8	33.3	83.1	46.8		
WB-1012-MC-04	170	175	172.5	0.0	14.0	57.8	28.8	86.6	49.3		
WB-1012-MC-04	190	195	192.5	0.0	14.1	52.0	33.9	85.9	52.5		
WB-1012-MC-04	210	215	212.5	0.0	10.3	50.3	39.4	89.7	44.3		
WB-1012-MC-04	230	235	232.5	0.0	14.7	56.3	29.0	85.3	46.7		
WB-1012-MC-04	250	255	252.5	0.0	10.8	55.4	33.9	89.2	50.4		

Table J.15. Sediment texture and composition data for core site WB-0814-MC-04. Sediment cores with sub-sample intervals (mm), texture described as %Gravel, % Sand, % Silt, and % Clay, as well as %Mud, and composition described as %Carbonate, %TOM (LOI), and % Other (non-carbonate, non-organic). Note: Blank cell denotes no analysis performed.

Core ID	Top Depth of Interval (mm)	Bottom Depth of Interval (mm)	Average Depth of Interval (mm)	% Gravel	% Sand	% Silt	% Clay	% Mud (% Silt + % Clay)	% Carbonate	% TOM (LOI)	% Other
WB-0814-MC-04	0	2	1	0.0	3.0	59.6	37.4	97.0			
WB-0814-MC-04	2	4	3	0.0	1.8	65.7	32.5	98.2			
WB-0814-MC-04	4	6	5	0.0	2.1	60.7	37.2	97.9			
WB-0814-MC-04	6	8	7	0.0	2.3	49.3	48.4	97.7			
WB-0814-MC-04	8	10	9	0.0	1.8	57.0	41.1	98.2			
WB-0814-MC-04	10	12	11	0.0	2.4	60.0	37.5	97.6			
WB-0814-MC-04	12	14	13	0.0	1.5	54.5	44.0	98.5	53.7	6.8	39.5
WB-0814-MC-04	14	16	15	0.0	6.0	53.1	40.9	94.0	55.0	6.3	38.7
WB-0814-MC-04	16	18	17	0.0	5.9	60.7	33.4	94.1			
WB-0814-MC-04	18	20	19	0.0	1.7	63.1	35.2	98.3	56.2	5.7	38.1
WB-0814-MC-04	20	22	21	0.0	8.1	57.1	34.8	91.9	55.7	6.1	38.2
WB-0814-MC-04	24	26	25	0.0	8.5	50.4	41.0	91.5	57.1	5.2	37.7
WB-0814-MC-04	30	32	31	0.0	6.0	54.3	39.7	94.0	56.2	6.0	37.7
WB-0814-MC-04	36	38	37	0.0	11.4	44.1	44.5	88.6	55.6	7.2	37.2
WB-0814-MC-04	40	45	42.5	0.0	13.1	54.2	32.8	86.9	55.9	6.2	37.9
WB-0814-MC-04	50	55	52.5	0.0	10.4	49.4	40.2	89.6	56.1	5.3	38.6
WB-0814-MC-04	70	75	72.5	0.0	10.4	46.5	43.1	89.6	50.7	7.7	41.6
WB-0814-MC-04	90	95	92.5	0.0	9.7	46.4	43.9	90.3	55.7	5.5	38.8
WB-0814-MC-04	110	115	112.5	0.0	9.1	47.4	43.5	90.9	56.1	6.1	37.9
WB-0814-MC-04	130	135	132.5	0.0	15.9	45.8	38.3	84.1	57.3	5.9	36.9
WB-0814-MC-04	150	155	152.5	0.0	10.6	47.9	41.5	89.4	58.2	5.7	36.1
WB-0814-MC-04	170	175	172.5	0.0	14.4	45.6	40.0	85.6	56.4	6.0	37.6
WB-0814-MC-04	190	195	192.5	0.0	4.1	47.9	48.0	95.9	54.6	5.8	39.5
WB-0814-MC-04	210	215	212.5	0.0	12.8	45.7	41.5	87.2	56.1	6.4	37.5
WB-0814-MC-04	230	235	232.5	0.0	4.5	48.9	46.6	95.5	55.1	6.7	38.2

Table J.15 (Continued).

Core ID	Top Depth of Interval (mm)	Bottom Depth of Interval (mm)	Average Depth of Interval (mm)	% Gravel	% Sand	% Silt	% Clay	% Mud (% Silt + % Clay)	% Carbonate	% TOM (LOI)	% Other
WB-0814-MC-04	250	255	252.5	0.0	12.8	47.1	40.1	87.2	58.5	6.1	35.3

Table J.16. Sediment texture and composition data for core site WB-0814-MC-DSH-08 DEP 1. Sediment cores with sub-sample intervals (mm), texture described as %Gravel, % Sand, % Silt, and % Clay, as well as %Mud, and composition described as %Carbonate, %TOM (LOI), and % Other (non-carbonate, non-organic). Note: Blank cell denotes no analysis performed.

Core ID	Top Depth of Interval (mm)	Bottom Depth of Interval (mm)	Average Depth of Interval (mm)	% Gravel	% Sand	% Silt	% Clay	% Mud (% Silt + % Clay)	% Carbonate	% TOM (LOI)	% Other
WB-0814-MC-DSH-08 DEP 1	0	2	1	0.0	0.7	51.8	47.5	99.3	37.2	7.5	55.2
WB-0814-MC-DSH-08 DEP 1	2	4	3	0.0	0.3	47.2	52.6	99.7			
WB-0814-MC-DSH-08 DEP 1	4	6	5	0.0	0.2	47.6	52.1	99.8			
WB-0814-MC-DSH-08 DEP 1	6	8	7	0.0	0.2	46.9	52.9	99.8			
WB-0814-MC-DSH-08 DEP 1	8	10	9	0.0	0.2	49.7	50.1	99.8	32.9	6.8	60.3
WB-0814-MC-DSH-08 DEP 1	10	12	11	0.0	0.2	50.1	49.7	99.8			
WB-0814-MC-DSH-08 DEP 1	12	14	13	0.0	0.2	48.5	51.3	99.8			
WB-0814-MC-DSH-08 DEP 1	14	16	15	0.0	0.2	49.5	50.3	99.8	31.2	7.2	61.6
WB-0814-MC-DSH-08 DEP 1	16	18	17	0.0	0.2	44.3	55.5	99.8			
WB-0814-MC-DSH-08 DEP 1	18	20	19	0.0	0.4	42.1	57.6	99.6	29.4	8.1	62.5
WB-0814-MC-DSH-08 DEP 1	20	22	21	0.0	0.4	38.9	60.7	99.6			
WB-0814-MC-DSH-08 DEP 1	24	26	25	0.0	0.3	42.2	57.5	99.7	29.1	7.9	62.9
WB-0814-MC-DSH-08 DEP 1	30	32	31	0.0	0.4	40.6	59.0	99.6	28.5	8.0	63.5
WB-0814-MC-DSH-08 DEP 1	40	45	42.5	0.0	0.3	39.9	59.8	99.7			
WB-0814-MC-DSH-08 DEP 1	50	55	52.5	0.0	0.1	35.9	64.1	99.9	24.8	8.7	66.5
WB-0814-MC-DSH-08 DEP 1	70	75	72.5	0.0	0.3	37.4	62.3	99.7			
WB-0814-MC-DSH-08 DEP 1	90	95	92.5	0.0	0.2	40.3	59.5	99.8	24.0	8.1	67.9
WB-0814-MC-DSH-08 DEP 1	110	115	112.5	0.0	0.4	41.7	58.0	99.6			
WB-0814-MC-DSH-08 DEP 1	130	135	132.5	0.0	0.1	33.7	66.2	99.9	25.0	7.8	67.3
WB-0814-MC-DSH-08 DEP 1	150	155	152.5	0.0	0.5	43.8	55.7	99.5			
WB-0814-MC-DSH-08 DEP 1	170	175	172.5	0.0	0.4	39.6	60.0	99.6	28.3	6.9	64.8
WB-0814-MC-DSH-08 DEP 1	190	195	192.5	0.0	0.6	44.5	54.9	99.4			
WB-0814-MC-DSH-08 DEP 1	210	215	212.5	0.0	0.3	41.6	58.2	99.7	32.2	7.5	60.3
WB-0814-MC-DSH-08 DEP 1	230	235	232.5	0.0	1.1	49.6	49.3	98.9			
WB-0814-MC-DSH-08 DEP 1	250	255	252.5	0.0	1.1	34.6	64.3	98.9	32.5	7.3	60.2

Table J.16 (Continued).

Core ID	Top Depth of Interval (mm)	Bottom Depth of Interval (mm)	Average Depth of Interval (mm)	% Gravel	% Sand	% Silt	% Clay	% Mud (% Silt + % Clay)	% Carbonate	% TOM (LOI)	% Other
WB-0814-MC-DSH-08 DEP 1	270	275	272.5	0.0	0.6	41.5	57.9	99.4			
WB-0814-MC-DSH-08 DEP 1	290	295	292.5	0.0	0.8	47.4	51.8	99.2			
WB-0814-MC-DSH-08 DEP 1	310	315	312.5	0.0	1.8	51.5	46.8	98.2			
WB-0814-MC-DSH-08 DEP 1	330	335	332.5	0.0	2.0	46.2	51.8	98.0			
WB-0814-MC-DSH-08 DEP 1	350	355	352.5	0.0	1.3	52.0	46.7	98.7			
WB-0814-MC-DSH-08 DEP 1	370	375	372.5	0.0	0.3	37.4	62.3	99.7	37.5	6.9	55.6

Table J.17. Sediment texture and composition data for core site WB-0814-MC-DSH-10 DEP 1. Sediment cores with sub-sample intervals (mm), texture described as %Gravel, % Sand, % Silt, and % Clay, as well as %Mud, and composition described as %Carbonate, %TOM (LOI), and % Other (non-carbonate, non-organic). Note: Blank cell denotes no analysis performed.

Core ID	Top Depth of Interval (mm)	Bottom Depth of Interval (mm)	Average Depth of Interval (mm)	% Gravel	% Sand	% Silt	% Clay	% Mud (% Silt + % Clay)	% Carbonate	% TOM (LOI)	% Other
WB-0814-MC-DSH-10 DEP 1	0	2	1	0.0	1.4	46.8	51.8	98.6			
WB-0814-MC-DSH-10 DEP 1	2	4	3	0.0	0.8	46.7	52.5	99.2			
WB-0814-MC-DSH-10 DEP 1	4	6	5	0.0	0.4	43.9	55.7	99.6			
WB-0814-MC-DSH-10 DEP 1	6	8	7	0.0	0.3	41.9	57.8	99.7			
WB-0814-MC-DSH-10 DEP 1	8	10	9	0.0	0.2	42.8	57.0	99.8			
WB-0814-MC-DSH-10 DEP 1	10	12	11	0.0	0.5	40.6	59.0	99.5			
WB-0814-MC-DSH-10 DEP 1	12	14	13	0.0	0.3	37.7	62.0	99.7			
WB-0814-MC-DSH-10 DEP 1	14	16	15	0.0	0.3	38.8	60.9	99.7			
WB-0814-MC-DSH-10 DEP 1	16	18	17	0.0	0.2	34.9	64.9	99.8	34.3	9.2	56.5
WB-0814-MC-DSH-10 DEP 1	18	20	19	0.0	0.2	40.1	59.7	99.8			
WB-0814-MC-DSH-10 DEP 1	20	22	21	0.0	0.2	37.8	62.0	99.8			
WB-0814-MC-DSH-10 DEP 1	24	26	25	0.0	0.5	30.9	68.6	99.5	36.9	6.9	56.2
WB-0814-MC-DSH-10 DEP 1	30	32	31	0.0	0.2	41.5	58.4	99.8	27.6	12.0	60.4
WB-0814-MC-DSH-10 DEP 1	38	43	40.5	0.0	0.9	48.4	50.7	99.1	26.4	9.0	64.6
WB-0814-MC-DSH-10 DEP 1	53	58	55.5	0.0	0.3	38.3	61.5	99.7	12.0	13.2	74.8
WB-0814-MC-DSH-10 DEP 1	73	78	75.5	0.0	0.3	36.6	63.2	99.7	21.8	13.1	65.1
WB-0814-MC-DSH-10 DEP 1	93	98	95.5	0.0	0.4	38.0	61.6	99.6	25.5	8.4	66.1
WB-0814-MC-DSH-10 DEP 1	113	118	115.5	0.0	0.3	34.7	65.0	99.7	25.5	11.0	63.5
WB-0814-MC-DSH-10 DEP 1	133	138	135.5	0.0	0.4	36.0	63.6	99.6	27.2	7.2	65.6
WB-0814-MC-DSH-10 DEP 1	154	159	156.5	0.0	0.3	38.0	61.7	99.7	25.1	12.1	62.8
WB-0814-MC-DSH-10 DEP 1	174	179	176.5	0.0	0.7	49.1	50.2	99.3	28.3	9.4	62.3
WB-0814-MC-DSH-10 DEP 1	194	199	196.5	0.0	0.6	34.3	65.0	99.4	31.5	10.0	58.5
WB-0814-MC-DSH-10 DEP 1	214	219	216.5	0.0	1.6	51.8	46.6	98.4	31.1	8.6	60.3
WB-0814-MC-DSH-10 DEP 1	234	239	236.5	0.0	0.4	39.1	60.5	99.6	32.4	10.9	56.8
WB-0814-MC-DSH-10 DEP 1	274	279	276.5	0.0	0.4	36.2	63.4	99.6	36.7	9.1	54.2

Table J.17 (Continued).

Core ID	Top Depth of Interval (mm)	Bottom Depth of Interval (mm)	Average Depth of Interval (mm)	% Gravel	% Sand	% Silt	% Clay	% Mud (% Silt + % Clay)	% Carbonate	% TOM (LOI)	% Other
WB-0814-MC-DSH-10 DEP 1	294	299	296.5	0.0	0.6	43.0	56.4	99.4	27.5	8.4	64.1
WB-0814-MC-DSH-10 DEP 1	314	319	316.5	0.0	0.3	37.2	62.5	99.7	35.8	9.2	55.0
WB-0814-MC-DSH-10 DEP 1	334	339	336.5	0.0	1.2	44.6	54.2	98.8	36.1	8.1	55.8
WB-0814-MC-DSH-10 DEP 1	354	359	356.5	0.0	1.2	50.9	47.9	98.8	26.6	8.5	64.9
WB-0814-MC-DSH-10 DEP 1	374	379	376.5	0.0	0.9	44.7	54.4	99.1	38.7	8.2	53.1
WB-0814-MC-DSH-10 DEP 1	394	399	396.5	0.0	0.8	50.0	49.1	99.2	30.3	8.5	61.2
WB-0814-MC-DSH-10 DEP 1	414	419	416.5	0.0	0.8	41.7	57.5	99.2	30.0	8.2	61.8

Table J.18. Sediment texture and composition data for core site WB-0814-MC-PCB-06 DEP 2. Sediment cores with sub-sample intervals (mm), texture described as %Gravel, % Sand, % Silt, and % Clay, as well as %Mud, and composition described as %Carbonate, %TOM (LOI), and % Other (non-carbonate, non-organic). Note: Blank cell denotes no analysis performed.

Core ID	Top Depth of Interval (mm)	Bottom Depth of Interval (mm)	Average Depth of Interval (mm)	% Gravel	% Sand	% Silt	% Clay	% Mud (% Silt + % Clay)	% Carbonate	% TOM (LOI)	% Other
WB-0814-MC-PCB-06 DEP 2	0	2	1	0.0	1.1	53.6	45.3	98.9			
WB-0814-MC-PCB-06 DEP 2	2	4	3	0.0	0.8	48.9	50.2	99.2			
WB-0814-MC-PCB-06 DEP 2	4	6	5	0.0	1.3	49.2	49.6	98.8			
WB-0814-MC-PCB-06 DEP 2	6	8	7	0.0	1.1	45.5	53.4	98.9			
WB-0814-MC-PCB-06 DEP 2	8	10	9	0.0	0.8	47.0	52.2	99.2			
WB-0814-MC-PCB-06 DEP 2	10	12	11	0.0	0.7	40.2	59.1	99.3			
WB-0814-MC-PCB-06 DEP 2	12	14	13	0.0	0.4	38.6	61.0	99.6			
WB-0814-MC-PCB-06 DEP 2	14	16	15	0.0	0.7	48.3	51.0	99.3			
WB-0814-MC-PCB-06 DEP 2	16	18	17	0.0	0.8	43.0	56.2	99.2			
WB-0814-MC-PCB-06 DEP 2	18	20	19	0.0	0.4	39.0	60.6	99.6	39.7	6.2	54.1
WB-0814-MC-PCB-06 DEP 2	20	22	21	0.0	0.7	38.7	60.6	99.3			
WB-0814-MC-PCB-06 DEP 2	24	26	25	0.0	0.4	38.3	61.4	99.6	37.4	6.7	55.9
WB-0814-MC-PCB-06 DEP 2	30	32	31	0.0	0.5	36.0	63.6	99.5	36.8	6.8	56.4
WB-0814-MC-PCB-06 DEP 2	40	42	41						33.6	8.0	58.4
WB-0814-MC-PCB-06 DEP 2	50	55	52.5	0.0	0.6	36.3	63.1	99.4	35.2	6.5	58.3
WB-0814-MC-PCB-06 DEP 2	70	75	72.5						33.7	6.7	
WB-0814-MC-PCB-06 DEP 2	90	95	92.5	0.0	0.6	34.2	65.2	99.4	36.3	6.4	57.3
WB-0814-MC-PCB-06 DEP 2	110	117	113.5						35.3	6.4	58.3
WB-0814-MC-PCB-06 DEP 2	132	137	134.5	0.0	1.0	36.4	62.6	99.0	39.6	6.1	54.3
WB-0814-MC-PCB-06 DEP 2	152	157	154.5						38.1	6.4	55.5
WB-0814-MC-PCB-06 DEP 2	172	177	174.5	0.0	1.6	35.7	62.8	98.4	39.3	6.3	54.5
WB-0814-MC-PCB-06 DEP 2	192	197	194.5						36.3	7.2	56.5
WB-0814-MC-PCB-06 DEP 2	212	217	214.5	0.0	0.9	37.4	61.8	99.1	38.1	6.4	55.5
WB-0814-MC-PCB-06 DEP 2	232	237	234.5						36.2	6.6	57.2
WB-0814-MC-PCB-06 DEP 2	252	257	254.5	0.0	0.5	36.8	62.7	99.5	37.4	6.2	56.4

Table J.18 (Continued).

Core ID	Top Depth of Interval (mm)	Bottom Depth of Interval (mm)	Average Depth of Interval (mm)	% Gravel	% Sand	% Silt	% Clay	% Mud (% Silt + % Clay)	% Carbonate	% TOM (LOI)	% Other
WB-0814-MC-PCB-06 DEP 2	272	277	274.5						36.2	6.0	57.8
WB-0814-MC-PCB-06 DEP 2	292	297	294.5						37.8	5.6	56.5
WB-0814-MC-PCB-06 DEP 2	312	317	314.5						37.6	5.7	56.8
WB-0814-MC-PCB-06 DEP 2	332	337	334.5						35.6	7.3	57.1
WB-0814-MC-PCB-06 DEP 2	352	357	354.5						38.7	6.1	55.3
WB-0814-MC-PCB-06 DEP 2	372	377	374.5						39.8	6.6	53.7
WB-0814-MC-PCB-06 DEP 2	392	397	394.5	0.0	1.2	41.0	57.9	98.8	42.8	5.7	51.5

Table J.19. Sediment texture and composition data for core site WB-0816-MC-04. Sediment cores with sub-sample intervals (mm), texture described as %Gravel, % Sand, % Silt, and % Clay, as well as %Mud, and composition described as %Carbonate, %TOM (LOI), and % Other (non-carbonate, non-organic). Note: Blank cell denotes no analysis performed.

Core ID	Top Depth of Interval (mm)	Bottom Depth of Interval (mm)	Average Depth of Interval (mm)	% Gravel	% Sand	% Silt	% Clay	% Mud (% Silt + % Clay)	% Carbonate	% TOM (LOI)	% Other
WB-0816-MC-04	0	2	1	0.0	4.4	62.0	33.6	95.6			
WB-0816-MC-04	2	4	3	0.0	5.3	60.3	34.4	94.7			
WB-0816-MC-04	4	6	5	0.0	6.7	56.3	37.0	93.3	51.8	8.3	40.0
WB-0816-MC-04	6	8	7	0.0	9.8	54.3	35.9	90.2	55.9	6.9	37.2
WB-0816-MC-04	8	10	9	0.0	7.8	49.2	43.0	92.2	55.5	6.9	37.5
WB-0816-MC-04	10	12	11	0.0	6.7	55.1	38.2	93.3	53.2	8.0	38.8
WB-0816-MC-04	12	14	13	0.0	10.0	55.4	34.6	90.0	55.9	7.5	36.6
WB-0816-MC-04	14	16	15	0.0	8.2	50.0	41.8	91.8	57.3	6.8	35.9
WB-0816-MC-04	16	18	17	0.0	12.2	54.5	33.3	87.8	57.8	6.1	36.1
WB-0816-MC-04	18	20	19	0.0	13.0	50.5	36.5	87.0	56.7	6.9	36.3
WB-0816-MC-04	20	22	21	0.0	17.3	49.5	33.2	82.7	52.6	9.2	38.3
WB-0816-MC-04	24	26	25	0.0	7.2	61.9	30.9	92.8	55.0	6.8	38.2
WB-0816-MC-04	30	32	31	0.0	13.4	44.6	42.1	86.6	54.5	8.3	37.2
WB-0816-MC-04	50	52	51	0.0	11.7	51.3	37.0	88.3	53.8	8.8	37.4
WB-0816-MC-04	70	72	71	0.0	10.8	56.8	32.4	89.2	55.1	7.0	37.9
WB-0816-MC-04	90	95	92.5	0.0	10.1	54.1	35.8	89.9	55.5	6.9	37.6
WB-0816-MC-04	110	115	112.5	0.0	12.6	52.3	35.1	87.4	56.3	7.3	36.3
WB-0816-MC-04	130	135	132.5	0.0	14.0	51.0	35.0	86.0	57.1	6.8	36.1
WB-0816-MC-04	150	155	152.5	0.0	12.1	53.1	34.7	87.9	49.5	10.0	40.5
WB-0816-MC-04	170	175	172.5	0.0	10.5	49.9	39.6	89.5	55.3	7.6	37.1
WB-0816-MC-04	190	195	192.5	0.0	16.3	40.4	43.3	83.7	51.2	8.9	39.9
WB-0816-MC-04	210	215	212.5	0.0	9.7	52.0	38.4	90.3	57.8	6.9	35.3
WB-0816-MC-04	230	235	232.5	0.0	14.4	54.4	31.2	85.6	64.3	4.5	31.2
WB-0816-MC-04	250	255	252.5	0.0	10.0	55.6	34.4	90.0	60.5	6.5	33.1
WB-0816-MC-04	270	275	272.5	0.0	17.9	43.0	39.1	82.1	61.5	4.8	33.7

Table J.19 (Continued).

Core ID	Top Depth of Interval (mm)	Bottom Depth of Interval (mm)	Average Depth of Interval (mm)	% Gravel	% Sand	% Silt	% Clay	% Mud (% Silt + % Clay)	% Carbonate	% TOM (LOI)	% Other
WB-0816-MC-04	290	295	292.5	0.0	8.6	57.0	34.3	91.4	60.6	6.6	32.7
WB-0816-MC-04	310	315	312.5	0.1	15.0	46.4	38.5	84.9	55.2	8.4	36.4
WB-0816-MC-04	330	335	332.5	0.0	16.4	44.1	39.4	83.6	62.2	4.7	33.1
WB-0816-MC-04	350	355	352.5	0.1	10.6	55.4	33.8	89.3	61.1	5.3	33.6

Table J.20. Sediment texture and composition data for core site WB-0816-MC-DSH-08-A. Sediment cores with sub-sample intervals (mm), texture described as %Gravel, % Sand, % Silt, and % Clay, as well as %Mud, and composition described as %Carbonate, %TOM (LOI), and % Other (non-carbonate, non-organic). Note: Blank cell denotes no analysis performed.

Core ID	Top Depth of Interval (mm)	Bottom Depth of Interval (mm)	Average Depth of Interval (mm)	% Gravel	% Sand	% Silt	% Clay	% Mud (% Silt + % Clay)	% Carbonate	% TOM (LOI)	% Other
WB-0816-MC-DSH-08-A	2	4	3	0.0	0.3	47.3	52.4	99.7			
WB-0816-MC-DSH-08-A	4	6	5	0.0	0.1	47.6	52.3	99.9			
WB-0816-MC-DSH-08-A	6	8	7	0.0	0.1	52.3	47.6	99.9			
WB-0816-MC-DSH-08-A	8	10	9	0.0	0.1	51.1	48.8	99.9			
WB-0816-MC-DSH-08-A	10	12	11	0.0	0.2	52.9	46.9	99.8			
WB-0816-MC-DSH-08-A	12	14	13	0.0	0.5	42.5	57.0	99.5			
WB-0816-MC-DSH-08-A	14	16	15	0.0	0.2	45.1	54.6	99.8			
WB-0816-MC-DSH-08-A	16	18	17	0.0	0.3	50.9	48.8	99.7	28.3	10.9	60.8
WB-0816-MC-DSH-08-A	18	20	19	0.0	0.3	53.4	46.3	99.7			
WB-0816-MC-DSH-08-A	20	22	21	0.0	0.4	47.8	51.8	99.6			
WB-0816-MC-DSH-08-A	22	24	23	0.0	0.4	42.6	57.1	99.6			
WB-0816-MC-DSH-08-A	24	26	25	0.0	0.3	47.2	52.5	99.7			
WB-0816-MC-DSH-08-A	26	28	27	0.0	0.4	52.7	46.9	99.6			
WB-0816-MC-DSH-08-A	28	30	29	0.0	0.3	53.2	46.5	99.7	33.0	7.2	59.8
WB-0816-MC-DSH-08-A	30	32	31	0.0	0.8	52.7	46.5	99.2			
WB-0816-MC-DSH-08-A	50	55	52.5	0.0	0.5	44.8	54.7	99.5	23.0	10.7	66.3
WB-0816-MC-DSH-08-A	70	75	72.5	0.0	0.6	41.7	57.7	99.4	21.8	10.8	67.5
WB-0816-MC-DSH-08-A	90	95	92.5	0.0	0.5	41.0	58.4	99.5	23.1	9.9	67.0
WB-0816-MC-DSH-08-A	110	115	112.5	0.0	0.4	40.8	58.8	99.6	21.8	10.1	68.2
WB-0816-MC-DSH-08-A	130	135	132.5	0.0	0.6	43.0	56.4	99.4	21.1	10.7	68.2
WB-0816-MC-DSH-08-A	150	155	152.5	0.0	0.4	43.7	55.9	99.6	22.8	8.8	68.5
WB-0816-MC-DSH-08-A	170	175	172.5	0.0	0.7	44.4	54.9	99.3	24.2	9.6	66.3
WB-0816-MC-DSH-08-A	190	195	192.5	0.0	0.3	40.4	59.3	99.7	28.7	7.1	64.3
WB-0816-MC-DSH-08-A	210	215	212.5	0.0	0.9	43.8	55.3	99.1	26.4	9.9	63.7
WB-0816-MC-DSH-08-A	230	235	232.5	0.0	0.4	39.4	60.3	99.6	31.6	7.3	61.2

Table J.20 (Continued).

Core ID	Top Depth of Interval (mm)	Bottom Depth of Interval (mm)	Average Depth of Interval (mm)	% Gravel	% Sand	% Silt	% Clay	% Mud (% Silt + % Clay)	% Carbonate	% TOM (LOI)	% Other
WB-0816-MC-DSH-08-A	250	255	252.5	0.0	1.4	47.0	51.6	98.6	29.6	9.6	60.8
WB-0816-MC-DSH-08-A	270	275	272.5	0.0	0.7	35.6	63.7	99.3	31.8	7.6	60.7
WB-0816-MC-DSH-08-A	290	295	292.5	0.0	0.9	48.0	51.0	99.1	29.6	9.8	60.6
WB-0816-MC-DSH-08-A	310	315	312.5	0.0	0.4	36.5	63.1	99.6	37.7	6.2	56.1
WB-0816-MC-DSH-08-A	330	335	332.5	0.0	0.5	34.6	64.9	99.5	33.1	8.3	58.5
WB-0816-MC-DSH-08-A	350	355	352.5	0.0	1.1	42.4	56.5	98.9	37.4	6.9	55.7
WB-0816-MC-DSH-08-A	370	375	372.5	0.0	1.8	40.5	57.7	98.2	38.2	7.3	54.5
WB-0816-MC-DSH-08-A	390	395	392.5	0.0	0.5	47.2	52.3	99.5	37.3	7.5	55.2
WB-0816-MC-DSH-08-A	410	415	412.5	0.0	0.9	39.8	59.2	99.1	38.4	7.3	54.4

Table J.21. Sediment texture and composition data for core site WB-0816-MC-DSH-10-A. Sediment cores with sub-sample intervals (mm), texture described as %Gravel, % Sand, % Silt, and % Clay, as well as %Mud, and composition described as %Carbonate, %TOM (LOI), and % Other (non-carbonate, non-organic). Note: Blank cell denotes no analysis performed.

Core ID	Top Depth of Interval (mm)	Bottom Depth of Interval (mm)	Average Depth of Interval (mm)	% Gravel	% Sand	% Silt	% Clay	% Mud (% Silt + % Clay)	% Carbonate	% TOM (LOI)	% Other
WB-0816-MC-DSH-10-A	0	2	1	0.0	0.7	44.2	55.1	99.3			
WB-0816-MC-DSH-10-A	2	4	3	0.0	1.0	50.9	48.0	99.0			
WB-0816-MC-DSH-10-A	4	6	5	0.0	0.5	40.5	59.1	99.5			
WB-0816-MC-DSH-10-A	6	8	7	0.0	1.1	47.8	51.1	98.9			
WB-0816-MC-DSH-10-A	8	10	9	0.0	1.2	46.2	52.6	98.8			
WB-0816-MC-DSH-10-A	10	12	11	0.0	0.3	40.3	59.4	99.7	26.9	8.8	64.3
WB-0816-MC-DSH-10-A	12	14	13	0.0	0.6	45.2	54.3	99.4	27.0	8.5	64.5
WB-0816-MC-DSH-10-A	14	16	15	0.0	0.5	37.1	62.3	99.5	26.7	8.3	64.9
WB-0816-MC-DSH-10-A	16	18	17	0.0	0.3	44.7	55.0	99.7	27.0	8.3	64.7
WB-0816-MC-DSH-10-A	18	20	19	0.0	0.2	36.0	63.8	99.8	26.2	8.7	65.1
WB-0816-MC-DSH-10-A	20	22	21	0.0	0.1	40.1	59.7	99.9	31.4	8.7	59.9
WB-0816-MC-DSH-10-A	22	24	23	0.0	0.7	36.7	62.6	99.3	29.9	9.6	60.5
WB-0816-MC-DSH-10-A	24	26	25	0.0	0.4	42.0	57.6	99.6	29.2	10.1	60.8
WB-0816-MC-DSH-10-A	26	28	27	0.0	2.0	44.6	53.5	98.0	29.3	10.0	60.7
WB-0816-MC-DSH-10-A	28	30	29	0.0	0.1	34.0	65.9	99.9	35.4	5.8	58.8
WB-0816-MC-DSH-10-A	30	32	31	0.0	0.3	38.2	61.4	99.7	23.8	10.1	66.1
WB-0816-MC-DSH-10-A	50	52	51	0.0	0.6	44.7	54.7	99.4	25.0	7.8	67.1
WB-0816-MC-DSH-10-A	70	72	71	0.0	0.1	79.6	20.2	99.9	29.4	9.6	61.1
WB-0816-MC-DSH-10-A	90	95	92.5	0.0	0.6	40.0	59.3	99.4	21.7	9.4	68.9
WB-0816-MC-DSH-10-A	110	115	112.5	0.0	0.1	50.1	49.7	99.9	27.9	10.0	62.1
WB-0816-MC-DSH-10-A	130	135	132.5	0.0	0.5	44.2	55.3	99.5	24.5	9.2	66.3
WB-0816-MC-DSH-10-A	150	155	152.5	0.0	0.4	42.2	57.4	99.6	28.1	11.0	61.0
WB-0816-MC-DSH-10-A	170	175	172.5	0.0	0.7	43.4	55.9	99.3	28.2	9.2	62.5
WB-0816-MC-DSH-10-A	190	195	192.5	0.0	0.8	37.3	61.9	99.2	35.3	9.5	55.2
WB-0816-MC-DSH-10-A	210	215	212.5	0.0	1.1	46.5	52.5	98.9	31.9	8.8	59.3

Table J.21 (Continued).

Core ID	Top Depth of Interval (mm)	Bottom Depth of Interval (mm)	Average Depth of Interval (mm)	% Gravel	% Sand	% Silt	% Clay	% Mud (% Silt + % Clay)	% Carbonate	% TOM (LOI)	% Other
WB-0816-MC-DSH-10-A	230	235	232.5	0.0	1.0	37.9	61.1	99.0	38.3	9.1	52.6
WB-0816-MC-DSH-10-A	250	255	252.5	0.0	1.4	43.6	54.9	98.6	34.1	7.6	58.2
WB-0816-MC-DSH-10-A	270	275	272.5	0.0	0.8	43.0	56.2	99.2	38.4	8.5	53.0
WB-0816-MC-DSH-10-A	290	295	292.5	0.0	1.0	51.5	47.5	99.0	30.6	9.3	60.1
WB-0816-MC-DSH-10-A	310	315	312.5	0.0	0.8	45.8	53.4	99.2	36.0	9.4	54.6
WB-0816-MC-DSH-10-A	330	335	332.5	0.0	1.0	39.4	59.6	99.0	33.2	9.9	56.9
WB-0816-MC-DSH-10-A	350	355	352.5	0.0	0.9	35.7	63.5	99.1	33.8	10.1	56.2
WB-0816-MC-DSH-10-A	370	375	372.5	0.0	0.4	39.0	60.6	99.6	29.9	10.2	59.9
WB-0816-MC-DSH-10-A	390	395	392.5	0.0	0.7	39.3	60.0	99.3	31.0	10.4	58.6
WB-0816-MC-DSH-10-A	410	415	412.5	0.0	0.3	31.6	68.0	99.7	28.1	10.5	61.4
WB-0816-MC-DSH-10-A	430	435	432.5	0.0	0.2	34.8	65.0	99.8	29.9	8.7	61.4

Table J.22. Sediment texture and composition data for core site WB-0816-MC-PCB-06-A. Sediment cores with sub-sample intervals (mm), texture described as %Gravel, % Sand, % Silt, and % Clay, as well as %Mud, and composition described as %Carbonate, %TOM (LOI), and % Other (non-carbonate, non-organic). Note: Blank cell denotes no analysis performed.

Core ID	Top Depth of Interval (mm)	Bottom Depth of Interval (mm)	Average Depth of Interval (mm)	% Gravel	% Sand	% Silt	% Clay	% Mud (% Silt + % Clay)	% Carbonate	% TOM (LOI)	% Other
WB-0816-MC-PCB-06-A	0	2	1	0.0	0.4	43.0	56.7	99.6			
WB-0816-MC-PCB-06-A	2	6	4	0.0	0.6	44.3	55.1	99.4			
WB-0816-MC-PCB-06-A	6	8	7	0.0	0.6	46.9	52.5	99.4			
WB-0816-MC-PCB-06-A	8	10	9	0.0	0.4	37.8	61.8	99.6			
WB-0816-MC-PCB-06-A	10	12	11	0.0	0.2	45.5	54.3	99.8			
WB-0816-MC-PCB-06-A	12	14	13	0.0	0.3	42.4	57.3	99.7			
WB-0816-MC-PCB-06-A	14	16	15	0.0	0.5	42.5	57.1	99.5	39.8	6.5	53.7
WB-0816-MC-PCB-06-A	16	18	17	0.0	0.2	37.2	62.6	99.8			
WB-0816-MC-PCB-06-A	18	20	19	0.0	0.2	46.7	53.1	99.8	38.0	6.8	55.2
WB-0816-MC-PCB-06-A	20	22	21	0.0	0.2	47.8	52.0	99.8			
WB-0816-MC-PCB-06-A	22	24	23	0.0	0.3	40.5	59.2	99.7			
WB-0816-MC-PCB-06-A	24	26	25	0.0	0.4	43.9	55.6	99.6			
WB-0816-MC-PCB-06-A	26	28	27	0.0	0.4	46.4	53.2	99.6			
WB-0816-MC-PCB-06-A	28	30	29	0.0	0.4	42.5	57.2	99.6			
WB-0816-MC-PCB-06-A	30	32	31	0.0	0.3	47.1	52.6	99.7	35.8	8.1	56.1
WB-0816-MC-PCB-06-A	50	52	51	0.0	0.3	35.2	64.5	99.7	36.3	6.9	56.8
WB-0816-MC-PCB-06-A	70	72	71	0.0	0.7	35.8	63.4	99.3	35.5	7.3	57.2
WB-0816-MC-PCB-06-A	90	95	92.5	0.0	0.8	47.0	52.2	99.2	35.5	7.3	57.2
WB-0816-MC-PCB-06-A	110	115	112.5	0.0	0.4	51.8	47.8	99.6	36.0	7.3	56.7
WB-0816-MC-PCB-06-A	130	135	132.5	0.0	1.0	52.2	46.9	99.0	36.3	7.7	56.0
WB-0816-MC-PCB-06-A	150	155	152.5	0.0	0.4	48.0	51.5	99.6			
WB-0816-MC-PCB-06-A	170	175	172.5	0.0	0.3	55.4	44.3	99.7	39.7	5.6	54.7
WB-0816-MC-PCB-06-A	190	195	192.5	0.0	0.6	52.9	46.5	99.4			
WB-0816-MC-PCB-06-A	210	215	212.5	0.0	0.7	55.9	43.4	99.3	34.7	11.1	54.2
WB-0816-MC-PCB-06-A	230	235	232.5	0.0	2.0	48.4	49.6	98.0			

Table J.22 (Continued).

Core ID	Top Depth of Interval (mm)	Bottom Depth of Interval (mm)	Average Depth of Interval (mm)	% Gravel	% Sand	% Silt	% Clay	% Mud (% Silt + % Clay)	% Carbonate	% TOM (LOI)	% Other
WB-0816-MC-PCB-06-A	250	255	252.5	0.0	0.3	61.4	38.4	99.7	37.6	7.0	55.4
WB-0816-MC-PCB-06-A	270	275	272.5	0.0	2.3	42.4	55.3	97.7			
WB-0816-MC-PCB-06-A	290	295	292.5	0.0	0.7	50.7	48.6	99.3	36.0	7.5	56.5
WB-0816-MC-PCB-06-A	310	315	312.5	0.0	0.9	42.7	56.4	99.1			
WB-0816-MC-PCB-06-A	330	335	332.5	0.0	1.2	42.2	56.5	98.8			
WB-0816-MC-PCB-06-A	350	355	352.5	0.0	1.4	42.8	55.8	98.6			
WB-0816-MC-PCB-06-A	370	375	372.5	0.0	1.4	43.6	55.0	98.6			
WB-0816-MC-PCB-06-A	390	395	392.5	0.0	2.6	43.5	53.9	97.4			
WB-0816-MC-PCB-06-A	410	415	412.5	0.0	3.7	43.2	53.1	96.3			
WB-0816-MC-PCB-06-A	430	435	432.5	0.0	3.0	44.8	52.2	97.0			

APPENDIX K:

BULK DENSITY DATA FROM SEDIMENT CORES

Appendix K. Supplemental tables of sediment core sub-sample wet weight (g), dry weight (g), sub-sample volume (cm^3), and bulk density (g/cm^3).

Data are publicly available through the Gulf of Mexico Research Initiative Information & Data Cooperative (GRIIDC) at https://data.gulfresearchinitiative.org (doi: 10.7266/N7FJ2F94, 10.7266/N7FJ2F94, 10.7266/N74B2Z7K, 10.7266/n7-k9s6-4b11, 10.7266/n7-pb9j-t538, 10.7266/n7-c88d-pn57, 10.7266/n7-qzyx-sz24, 10.7266/N7BR8QHJ)

Table K.1. Bulk density data for core site WB-1109-MC-04. Sediment core sub-sample intervals (mm), sub-sample wet weight (g), dry weight (g), sub-sample volume (cm^3), and bulk density (g/cm^3). Note: Blank cell denotes no analysis performed.

Core ID	Top Depth of Interval (mm)	Bottom Depth of Interval (mm)	Average Depth of Interval (mm)	Wet Weight (g)	Dry Weight (g)	Sample Volume (cm^3)	Bulk Density (g/cm^3)
WB-1109-MC-04	0	2	1	9.71	1.84	14.257	0.13
WB-1109-MC-04	2	4	3	13.82	2.84	14.257	0.20
WB-1109-MC-04	4	6	5	16.34	3.95	14.257	0.28
WB-1109-MC-04	6	8	7	14.12	3.53	14.257	0.25
WB-1109-MC-04	8	10	9	20.13	5.16	14.257	0.36
WB-1109-MC-04	10	12	11	13.02	3.39	14.257	0.24
WB-1109-MC-04	12	14	13	16.34	4.36	14.257	0.31
WB-1109-MC-04	14	16	15	16.19	4.46	14.257	0.31
WB-1109-MC-04	16	18	17	19.41	5.51	14.257	0.39
WB-1109-MC-04	18	20	19	17.09	4.99	14.257	0.35
WB-1109-MC-04	20	25	22.5	45.27	13.77	35.642	0.39
WB-1109-MC-04	25	30	27.5	42.09	13.25	35.642	0.37
WB-1109-MC-04	30	35	32.5	45.11	14.59	35.642	0.41
WB-1109-MC-04	35	40	37.5	46.34	15.53	35.642	0.44
WB-1109-MC-04	40	45	42.5	42.47	14.64	35.642	0.41
WB-1109-MC-04	45	50	47.5	45.27	16.09	35.642	0.45
WB-1109-MC-04	50	55	52.5	45.94	16.46	35.642	0.46
WB-1109-MC-04	55	60	57.5	46.19	16.80	35.642	0.47
WB-1109-MC-04	60	65	62.5	47.17	17.41	35.642	0.49
WB-1109-MC-04	65	70	67.5	42.79	16.00	35.642	0.45
WB-1109-MC-04	70	75	72.5	49.58	18.97	35.642	0.53
WB-1109-MC-04	75	80	77.5	46.40	18.25	35.642	0.51
WB-1109-MC-04	80	85	82.5	53.22	20.81	35.642	0.58
WB-1109-MC-04	85	90	87.5	37.33	14.28	35.642	0.40
WB-1109-MC-04	90	95	92.5	46.28	18.15	35.642	0.51
WB-1109-MC-04	95	100	97.5	48.43	19.21	35.642	0.54
WB-1109-MC-04	100	105	102.5	52.83	21.05	35.642	0.59
WB-1109-MC-04	105	110	107.5	51.28	20.48	35.642	0.57
WB-1109-MC-04	110	115	112.5	46.06	18.57	35.642	0.52
WB-1109-MC-04	115	120	117.5	52.34	21.23	35.642	0.60
WB-1109-MC-04	120	125	122.5	42.74	17.25	35.642	0.48
WB-1109-MC-04	125	130	127.5	51.01	20.72	35.642	0.58
WB-1109-MC-04	130	135	132.5	43.46	17.67	35.642	0.50
WB-1109-MC-04	135	140	137.5	52.13	21.59	35.642	0.61
WB-1109-MC-04	140	145	142.5	47.56	19.55	35.642	0.55

Table K.1 (Continued).

Core ID	Top Depth of Interval (mm)	Bottom Depth of Interval (mm)	Average Depth of Interval (mm)	Wet Weight (g)	Dry Weight (g)	Sample Volume (cm^3)	Bulk Density (g/cm^3)
WB-1109-MC-04	145	150	147.5	49.63	20.49	35.642	0.57
WB-1109-MC-04	150	155	152.5	45.46	18.92	35.642	0.53
WB-1109-MC-04	155	160	157.5	52.74	22.21	35.642	0.62
WB-1109-MC-04	160	165	162.5	46.28	19.28	35.642	0.54
WB-1109-MC-04	165	170	167.5	48.40	20.03	35.642	0.56
WB-1109-MC-04	170	175	172.5	47.66	19.69	35.642	0.55
WB-1109-MC-04	175	180	177.5	48.57	19.92	35.642	0.56
WB-1109-MC-04	180	185	182.5	44.14	18.11	35.642	0.51
WB-1109-MC-04	185	190	187.5	60.76	25.36	35.642	0.71
WB-1109-MC-04	190	195	192.5	49.46	21.06	35.642	0.59
WB-1109-MC-04	195	200	197.5	43.50	18.58	35.642	0.52
WB-1109-MC-04	200	205	202.5	48.99	21.01	35.642	0.59
WB-1109-MC-04	205	210	207.5	61.57	27.15	35.642	0.76
WB-1109-MC-04	210	215	212.5	42.66	19.18	35.642	0.54
WB-1109-MC-04	215	220	217.5	54.47	25.00	35.642	0.70
WB-1109-MC-04	220	225	222.5	49.83	23.09	35.642	0.65
WB-1109-MC-04	225	230	227.5	58.24	27.25	35.642	0.76
WB-1109-MC-04	230	235	232.5	45.42	21.56	35.642	0.60
WB-1109-MC-04	235	240	237.5	53.62	25.81	35.642	0.72
WB-1109-MC-04	240	Base		12.83	6.13		

Table K.2. Bulk density data for core site WB-1110-MC-DSH-08. Sediment core sub-sample intervals (mm), sub-sample wet weight (g), dry weight (g), sub-sample volume (cm^3), and bulk density (g/cm^3). Note: Blank cell denotes no analysis performed.

Core ID	Top Depth of Interval (mm)	Bottom Depth of Interval (mm)	Average Depth of Interval (mm)	Wet Weight (g)	Dry Weight (g)	Sample Volume (cm^3)	Bulk Density (g/cm^3)
WB-1110-MC-DSH-08	0	2	1	7.97	1.59	14.257	0.11
WB-1110-MC-DSH-08	2	4	3	11.06	2.21	14.257	0.16
WB-1110-MC-DSH-08	4	6	5	12.12	2.44	14.257	0.17
WB-1110-MC-DSH-08	6	8	7	14.40	2.93	14.257	0.21
WB-1110-MC-DSH-08	8	10	9	16.56	3.42	14.257	0.24
WB-1110-MC-DSH-08	10	12	11	14.48	3.25	14.257	0.23
WB-1110-MC-DSH-08	12	14	13	16.80	3.73	14.257	0.26
WB-1110-MC-DSH-08	14	16	15	15.83	3.57	14.257	0.25
WB-1110-MC-DSH-08	16	18	17	15.64	3.52	14.257	0.25
WB-1110-MC-DSH-08	18	20	19	15.57	3.54	14.257	0.25
WB-1110-MC-DSH-08	20	22	21	17.31	4.18	14.257	0.29
WB-1110-MC-DSH-08	22	24	23	16.29	3.91	14.257	0.27
WB-1110-MC-DSH-08	24	26	25	17.48	4.29	14.257	0.30
WB-1110-MC-DSH-08	26	28	27	17.77	4.50	14.257	0.32
WB-1110-MC-DSH-08	28	30	29	16.30	4.15	14.257	0.29
WB-1110-MC-DSH-08	30	32	31	16.62	4.34	14.257	0.30
WB-1110-MC-DSH-08	32	34	33	17.22	4.49	14.257	0.31
WB-1110-MC-DSH-08	34	36	35	17.28	4.57	14.257	0.32
WB-1110-MC-DSH-08	36	38	37	17.16	4.68	14.257	0.33
WB-1110-MC-DSH-08	38	40	39	16.37	4.53	14.257	0.32
WB-1110-MC-DSH-08	40	42	41	17.22	4.91	14.257	0.34
WB-1110-MC-DSH-08	42	44	43	16.08	4.66	14.257	0.33
WB-1110-MC-DSH-08	44	46	45	18.09	5.40	14.257	0.38
WB-1110-MC-DSH-08	46	48	47	16.72	4.99	14.257	0.35
WB-1110-MC-DSH-08	48	50	49	17.46	5.21	14.257	0.37
WB-1110-MC-DSH-08	50	55	52.5	45.80	14.30	35.642	0.40
WB-1110-MC-DSH-08	55	60	57.5	43.58	13.73	35.642	0.39
WB-1110-MC-DSH-08	60	65	62.5	45.36	15.32	35.642	0.43
WB-1110-MC-DSH-08	65	70	67.5	49.00	16.42	35.642	0.46
WB-1110-MC-DSH-08	70	75	72.5	42.42	14.57	35.642	0.41
WB-1110-MC-DSH-08	75	80	77.5	44.54	15.32	35.642	0.43
WB-1110-MC-DSH-08	80	85	82.5	44.44	15.42	35.642	0.43
WB-1110-MC-DSH-08	85	90	87.5	44.86	15.83	35.642	0.44
WB-1110-MC-DSH-08	90	95	92.5	54.56	16.67	35.642	0.47
WB-1110-MC-DSH-08	95	100	97.5	47.97	17.73	35.642	0.50
WB-1110-MC-DSH-08	100	105	102.5	46.41	19.98	35.642	0.56

Table K.2 (Continued).

Core ID	Top Depth of Interval (mm)	Bottom Depth of Interval (mm)	Average Depth of Interval (mm)	Wet Weight (g)	Dry Weight (g)	Sample Volume (cm^3)	Bulk Density (g/cm^3)
WB-1110-MC-DSH-08	105	110	107.5	49.69	18.67	35.642	0.52
WB-1110-MC-DSH-08	110	115	112.5	50.86	19.59	35.642	0.55
WB-1110-MC-DSH-08	115	120	117.5	40.44	15.52	35.642	0.44
WB-1110-MC-DSH-08	120	125	122.5	46.80	17.88	35.642	0.50
WB-1110-MC-DSH-08	125	130	127.5	47.30	18.10	35.642	0.51
WB-1110-MC-DSH-08	130	135	132.5	46.85	17.97	35.642	0.50
WB-1110-MC-DSH-08	135	140	137.5	45.38	17.25	35.642	0.48
WB-1110-MC-DSH-08	140	145	142.5	46.45	17.75	35.642	0.50
WB-1110-MC-DSH-08	145	150	147.5	46.18	17.62	35.642	0.49
WB-1110-MC-DSH-08	150	155	152.5	48.85	19.05	35.642	0.53
WB-1110-MC-DSH-08	155	160	157.5	46.80	17.95	35.642	0.50
WB-1110-MC-DSH-08	160	165	162.5	48.19	18.54	35.642	0.52
WB-1110-MC-DSH-08	165	170	167.5	45.35	17.44	35.642	0.49
WB-1110-MC-DSH-08	170	175	172.5	45.66	17.77	35.642	0.50
WB-1110-MC-DSH-08	175	180	177.5	48.89	18.78	35.642	0.53
WB-1110-MC-DSH-08	180	185	182.5	44.86	16.92	35.642	0.47
WB-1110-MC-DSH-08	185	190	187.5	47.82	18.03	35.642	0.51
WB-1110-MC-DSH-08	190	195	192.5	47.46	18.07	35.642	0.51
WB-1110-MC-DSH-08	195	200	197.5	47.15	17.63	35.642	0.49
WB-1110-MC-DSH-08	200	205	202.5	48.25	18.30	35.642	0.51
WB-1110-MC-DSH-08	205	210	207.5	46.50	17.68	35.642	0.50
WB-1110-MC-DSH-08	210	215	212.5	44.79	17.22	35.642	0.48
WB-1110-MC-DSH-08	215	220	217.5	47.97	18.17	35.642	0.51
WB-1110-MC-DSH-08	220	225	222.5	50.36	19.07	35.642	0.54
WB-1110-MC-DSH-08	225	230	227.5	45.27	17.10	35.642	0.48
WB-1110-MC-DSH-08	230	235	232.5	48.72	18.46	35.642	0.52
WB-1110-MC-DSH-08	235	240	237.5	45.45	16.94	35.642	0.48
WB-1110-MC-DSH-08	240	245	242.5	48.15	17.83	35.642	0.50
WB-1110-MC-DSH-08	245	250	247.5	41.94	15.49	35.642	0.43
WB-1110-MC-DSH-08	250	255	252.5	48.83	18.24	35.642	0.51
WB-1110-MC-DSH-08	255	260	257.5	45.91	17.41	35.642	0.49
WB-1110-MC-DSH-08	260	265	262.5	50.75	19.35	35.642	0.54
WB-1110-MC-DSH-08	265	270	267.5	44.79	17.16	35.642	0.48
WB-1110-MC-DSH-08	270	275	272.5	52.31	20.54	35.642	0.58
WB-1110-MC-DSH-08	275	280	277.5	46.06	17.50	35.642	0.49
WB-1110-MC-DSH-08	280	Base		44.13	16.92		

Table K.3. Bulk density data for core site WB-1110-MC-DSH-10. Sediment core sub-sample intervals (mm), sub-sample wet weight (g), dry weight (g), sub-sample volume (cm^3), and bulk density (g/cm^3). Note: Blank cell denotes no analysis performed.

Core ID	Top Depth of Interval (mm)	Bottom Depth of Interval (mm)	Average Depth of Interval (mm)	Wet Weight (g)	Dry Weight (g)	Sample Volume (cm^3)	Bulk Density (g/cm^3)
WB-1110-MC-DSH-10	0	2	1	13.09	2.17	14.257	0.15
WB-1110-MC-DSH-10	2	4	3	14.05	3.00	14.257	0.21
WB-1110-MC-DSH-10	4	6	5	17.26	4.09	14.257	0.29
WB-1110-MC-DSH-10	6	8	7	14.69	3.71	14.257	0.26
WB-1110-MC-DSH-10	8	10	9	17.51	4.72	14.257	0.33
WB-1110-MC-DSH-10	10	12	11	17.26	4.76	14.257	0.33
WB-1110-MC-DSH-10	12	14	13	17.93	5.09	14.257	0.36
WB-1110-MC-DSH-10	14	16	15	18.72	5.28	14.257	0.37
WB-1110-MC-DSH-10	16	18	17	15.58	4.45	14.257	0.31
WB-1110-MC-DSH-10	18	20	19	15.57	4.57	14.257	0.32
WB-1110-MC-DSH-10	20	22	21	16.45	4.88	14.257	0.34
WB-1110-MC-DSH-10	22	24	23	15.12	4.55	14.257	0.32
WB-1110-MC-DSH-10	24	26	25	17.59	5.39	14.257	0.38
WB-1110-MC-DSH-10	26	28	27	18.50	5.78	14.257	0.41
WB-1110-MC-DSH-10	28	30	29	15.77	4.99	14.257	0.35
WB-1110-MC-DSH-10	30	32	31	16.95	5.45	14.257	0.38
WB-1110-MC-DSH-10	32	34	33	19.58	6.49	14.257	0.46
WB-1110-MC-DSH-10	34	36	35	26.72	8.91	14.257	0.62
WB-1110-MC-DSH-10	36	38	37	18.16	5.95	14.257	0.42
WB-1110-MC-DSH-10	38	40	39	14.55	4.89	14.257	0.34
WB-1110-MC-DSH-10	40	42	41	16.40	5.58	14.257	0.39
WB-1110-MC-DSH-10	42	44	43	19.39	6.66	14.257	0.47
WB-1110-MC-DSH-10	44	46	45	15.86	5.38	14.257	0.38
WB-1110-MC-DSH-10	46	48	47	21.85	7.50	14.257	0.53
WB-1110-MC-DSH-10	48	50	49	18.77	6.52	14.257	0.46
WB-1110-MC-DSH-10	50	52	51	18.43	7.09	14.257	0.50
WB-1110-MC-DSH-10	52	54	53	16.58	5.70	14.257	0.40
WB-1110-MC-DSH-10	54	56	55	17.52	6.06	14.257	0.43
WB-1110-MC-DSH-10	56	58	57	21.64	7.60	14.257	0.53
WB-1110-MC-DSH-10	58	60	59	17.45	6.07	14.257	0.43
WB-1110-MC-DSH-10	60	62	61	19.00	6.67	14.257	0.47
WB-1110-MC-DSH-10	62	64	63	19.23	6.82	14.257	0.48
WB-1110-MC-DSH-10	64	66	65	18.75	6.56	14.257	0.46
WB-1110-MC-DSH-10	66	68	67	18.18	6.42	14.257	0.45
WB-1110-MC-DSH-10	68	70	69	19.20	6.80	14.257	0.48
WB-1110-MC-DSH-10	70	72	71	18.06	6.51	14.257	0.46

Table K.3 (Continued).

Core ID	Top Depth of Interval (mm)	Bottom Depth of Interval (mm)	Average Depth of Interval (mm)	Wet Weight (g)	Dry Weight (g)	Sample Volume (cm^3)	Bulk Density (g/cm^3)
WB-1110-MC-DSH-10	72	74	73	19.77	7.14	14.257	0.50
WB-1110-MC-DSH-10	74	76	75	18.06	6.62	14.257	0.46
WB-1110-MC-DSH-10	76	78	77	18.85	6.86	14.257	0.48
WB-1110-MC-DSH-10	78	80	79	17.78	6.54	14.257	0.46
WB-1110-MC-DSH-10	80	85	82.5	44.42	16.57	35.642	0.46
WB-1110-MC-DSH-10	85	90	87.5	47.87	18.39	35.642	0.52
WB-1110-MC-DSH-10	90	95	92.5	50.13	19.43	35.642	0.55
WB-1110-MC-DSH-10	95	100	97.5	50.34	19.76	35.642	0.55
WB-1110-MC-DSH-10	100	105	102.5	46.04	18.11	35.642	0.51
WB-1110-MC-DSH-10	105	110	107.5	45.93	18.35	35.642	0.51
WB-1110-MC-DSH-10	110	115	112.5	50.16	20.05	35.642	0.56
WB-1110-MC-DSH-10	115	120	117.5	53.97	21.58	35.642	0.61
WB-1110-MC-DSH-10	120	125	122.5	50.12	20.07	35.642	0.56
WB-1110-MC-DSH-10	125	130	127.5	39.59	15.89	35.642	0.45
WB-1110-MC-DSH-10	130	135	132.5	49.02	19.29	35.642	0.54
WB-1110-MC-DSH-10	135	140	137.5	50.69	19.34	35.642	0.54
WB-1110-MC-DSH-10	140	145	142.5	49.81	18.97	35.642	0.53
WB-1110-MC-DSH-10	145	150	147.5	46.65	17.71	35.642	0.50
WB-1110-MC-DSH-10	150	155	152.5	45.31	16.90	35.642	0.47
WB-1110-MC-DSH-10	155	160	157.5	46.56	17.14	35.642	0.48
WB-1110-MC-DSH-10	160	165	162.5	48.53	17.95	35.642	0.50
WB-1110-MC-DSH-10	165	170	167.5	50.14	18.32	35.642	0.51
WB-1110-MC-DSH-10	170	175	172.5	46.83	17.01	35.642	0.48
WB-1110-MC-DSH-10	175	180	177.5	48.77	17.84	35.642	0.50
WB-1110-MC-DSH-10	180	185	182.5	44.69	16.24	35.642	0.46
WB-1110-MC-DSH-10	185	190	187.5	48.81	17.69	35.642	0.50
WB-1110-MC-DSH-10	190	195	192.5	48.94	17.54	35.642	0.49
WB-1110-MC-DSH-10	195	200	197.5	44.80	15.92	35.642	0.45
WB-1110-MC-DSH-10	200	205	202.5	42.35	15.07	35.642	0.42
WB-1110-MC-DSH-10	205	210	207.5	47.33	16.98	35.642	0.48
WB-1110-MC-DSH-10	210	215	212.5	43.95	15.78	35.642	0.44
WB-1110-MC-DSH-10	215	220	217.5	51.00	18.71	35.642	0.52
WB-1110-MC-DSH-10	220	225	222.5	48.51	17.76	35.642	0.50
WB-1110-MC-DSH-10	225	230	227.5	45.11	16.47	35.642	0.46
WB-1110-MC-DSH-10	230	235	232.5	46.52	17.12	35.642	0.48
WB-1110-MC-DSH-10	235	240	237.5	47.30	17.35	35.642	0.49
WB-1110-MC-DSH-10	240	245	242.5	46.31	17.06	35.642	0.48
WB-1110-MC-DSH-10	245	250	247.5	49.37	18.32	35.642	0.51

Table K.3 (Continued).

Core ID	Top Depth of Interval (mm)	Bottom Depth of Interval (mm)	Average Depth of Interval (mm)	Wet Weight (g)	Dry Weight (g)	Sample Volume (cm^3)	Bulk Density (g/cm^3)
WB-1110-MC-DSH-10	250	255	252.5	47.02	17.48	35.642	0.49
WB-1110-MC-DSH-10	255	260	257.5	45.71	16.92	35.642	0.47
WB-1110-MC-DSH-10	260	265	262.5	50.47	18.54	35.642	0.52
WB-1110-MC-DSH-10	265	270	267.5	44.20	16.24	35.642	0.46
WB-1110-MC-DSH-10	270	275	272.5	49.29	17.82	35.642	0.50
WB-1110-MC-DSH-10	275	280	277.5	43.54	15.90	35.642	0.45
WB-1110-MC-DSH-10	280	285	282.5	51.16	18.75	35.642	0.53
WB-1110-MC-DSH-10	285	290	287.5	43.34	15.96	35.642	0.45
WB-1110-MC-DSH-10	290	295	292.5	52.94	19.72	35.642	0.55
WB-1110-MC-DSH-10	295	300	297.5	45.13	16.92	35.642	0.47
WB-1110-MC-DSH-10	300	305	302.5	50.68	19.08	35.642	0.54
WB-1110-MC-DSH-10	305	310	307.5	54.01	16.00	35.642	0.45
WB-1110-MC-DSH-10	310	315	312.5	46.34	17.57	35.642	0.49
WB-1110-MC-DSH-10	315	320	317.5	46.36	17.69	35.642	0.50
WB-1110-MC-DSH-10	320	325	322.5	48.12	18.60	35.642	0.52
WB-1110-MC-DSH-10	325	Base		44.42	17.20		

Table K.4. Bulk density data for core site WB-1110-MC-PCB-06. Sediment core sub-sample intervals (mm), sub-sample wet weight (g), dry weight (g), sub-sample volume (cm^3), and bulk density (g/cm^3). Note: Blank cell denotes no analysis performed.

Core ID	Top Depth of Interval (mm)	Bottom Depth of Interval (mm)	Average Depth of Interval (mm)	Wet Weight (g)	Dry Weight (g)	Sample Volume (cm^3)	Bulk Density (g/cm^3)
WB-1110-MC-PCB-06	0	2	1	7.88	1.35	14.257	0.09
WB-1110-MC-PCB-06	2	4	3	12.70	2.61	14.257	0.18
WB-1110-MC-PCB-06	4	6	5	13.40	3.01	14.257	0.21
WB-1110-MC-PCB-06	6	10	8	33.19	7.90	14.257	0.55
WB-1110-MC-PCB-06	10	12	11	18.04	4.32	14.257	0.30
WB-1110-MC-PCB-06	12	14	13	16.19	3.86	14.257	0.27
WB-1110-MC-PCB-06	14	16	15	15.88	3.90	14.257	0.27
WB-1110-MC-PCB-06	16	18	17	16.19	4.16	14.257	0.29
WB-1110-MC-PCB-06	18	20	19	17.20	4.52	14.257	0.32
WB-1110-MC-PCB-06	20	22	21	16.15	4.39	14.257	0.31
WB-1110-MC-PCB-06	22	24	23	13.99	3.94	14.257	0.28
WB-1110-MC-PCB-06	24	26	25	14.63	4.07	14.257	0.29
WB-1110-MC-PCB-06	26	28	27	11.08	3.26	14.257	0.23
WB-1110-MC-PCB-06	28	30	29	17.35	5.14	14.257	0.36
WB-1110-MC-PCB-06	30	32	31	22.63	6.76	14.257	0.47
WB-1110-MC-PCB-06	32	34	33	18.26	5.45	14.257	0.38
WB-1110-MC-PCB-06	34	36	35	15.27	4.62	14.257	0.32
WB-1110-MC-PCB-06	36	38	37	15.01	4.47	14.257	0.31
WB-1110-MC-PCB-06	38	40	39	15.90	4.93	14.257	0.35
WB-1110-MC-PCB-06	40	42	41	16.42	4.74	14.257	0.33
WB-1110-MC-PCB-06	42	44	43	19.16	5.97	14.257	0.42
WB-1110-MC-PCB-06	44	46	45	18.58	5.76	14.257	0.40
WB-1110-MC-PCB-06	46	48	47	15.96	4.93	14.257	0.35
WB-1110-MC-PCB-06	48	50	49	17.21	5.30	14.257	0.37
WB-1110-MC-PCB-06	50	52	51	17.94	5.54	14.257	0.39
WB-1110-MC-PCB-06	52	54	53	19.07	5.95	14.257	0.42
WB-1110-MC-PCB-06	54	56	55	13.94	4.40	14.257	0.31
WB-1110-MC-PCB-06	56	58	57	14.71	4.68	14.257	0.33
WB-1110-MC-PCB-06	58	60	59	12.54	3.95	14.257	0.28
WB-1110-MC-PCB-06	60	62	61	28.39	9.16	14.257	0.64
WB-1110-MC-PCB-06	62	64	63	18.80	6.06	14.257	0.43
WB-1110-MC-PCB-06	64	66	65	14.73	4.76	14.257	0.33
WB-1110-MC-PCB-06	66	68	67	16.41	5.29	14.257	0.37
WB-1110-MC-PCB-06	68	70	69	15.59	5.01	14.257	0.35
WB-1110-MC-PCB-06	70	72	71	20.74	6.68	14.257	0.47
WB-1110-MC-PCB-06	72	74	73	19.15	6.14	14.257	0.43

Table K.4 (Continued).

Core ID	Top Depth of Interval (mm)	Bottom Depth of Interval (mm)	Average Depth of Interval (mm)	Wet Weight (g)	Dry Weight (g)	Sample Volume (cm^3)	Bulk Density (g/cm^3)
WB-1110-MC-PCB-06	74	76	75	16.97	5.46	14.257	0.38
WB-1110-MC-PCB-06	76	78	77	16.77	5.49	14.257	0.39
WB-1110-MC-PCB-06	78	80	79	17.89	5.86	14.257	0.41
WB-1110-MC-PCB-06	80	82	81	16.06	5.23	14.257	0.37
WB-1110-MC-PCB-06	82	84	83	15.19	4.94	14.257	0.35
WB-1110-MC-PCB-06	84	86	85	23.21	7.66	14.257	0.54
WB-1110-MC-PCB-06	86	88	87	16.87	5.60	14.257	0.39
WB-1110-MC-PCB-06	88	90	89	20.86	7.04	14.257	0.49
WB-1110-MC-PCB-06	90	92	91	19.25	6.41	14.257	0.45
WB-1110-MC-PCB-06	92	94	93	13.30	4.45	14.257	0.31
WB-1110-MC-PCB-06	94	96	95	15.91	5.30	14.257	0.37
WB-1110-MC-PCB-06	96	98	97	20.97	7.15	14.257	0.50
WB-1110-MC-PCB-06	98	100	99	16.67	5.65	14.257	0.40
WB-1110-MC-PCB-06	100	105	102.5	45.77	15.68	35.642	0.44
WB-1110-MC-PCB-06	105	110	107.5	41.15	14.20	35.642	0.40
WB-1110-MC-PCB-06	110	115	112.5	45.02	14.92	35.642	0.42
WB-1110-MC-PCB-06	115	120	117.5	44.22	16.30	35.642	0.46
WB-1110-MC-PCB-06	120	125	122.5	49.22	18.92	35.642	0.53
WB-1110-MC-PCB-06	125	130	127.5	45.08	17.01	35.642	0.48
WB-1110-MC-PCB-06	130	135	132.5	50.72	19.26	35.642	0.54
WB-1110-MC-PCB-06	135	140	137.5	45.30	17.01	35.642	0.48
WB-1110-MC-PCB-06	140	145	142.5	44.41	17.29	35.642	0.49
WB-1110-MC-PCB-06	145	150	147.5	49.92	19.52	35.642	0.55
WB-1110-MC-PCB-06	150	155	152.5	45.92	17.83	35.642	0.50
WB-1110-MC-PCB-06	155	160	157.5	46.33	17.92	35.642	0.50
WB-1110-MC-PCB-06	160	165	162.5	43.01	16.66	35.642	0.47
WB-1110-MC-PCB-06	165	170	167.5	61.39	23.82	35.642	0.67
WB-1110-MC-PCB-06	170	175	172.5	40.40	15.53	35.642	0.44
WB-1110-MC-PCB-06	175	180	177.5	49.20	18.96	35.642	0.53
WB-1110-MC-PCB-06	180	185	182.5	45.01	16.99	35.642	0.48
WB-1110-MC-PCB-06	185	190	187.5	44.96	16.94	35.642	0.48
WB-1110-MC-PCB-06	190	195	192.5	44.12	16.69	35.642	0.47
WB-1110-MC-PCB-06	195	200	197.5	45.66	17.15	35.642	0.48
WB-1110-MC-PCB-06	200	205	202.5	50.65	20.14	35.642	0.57
WB-1110-MC-PCB-06	205	210	207.5	43.58	16.29	35.642	0.46
WB-1110-MC-PCB-06	210	215	212.5	47.60	20.39	35.642	0.57
WB-1110-MC-PCB-06	215	220	217.5	46.35	17.50	35.642	0.49
WB-1110-MC-PCB-06	220	225	222.5	45.23	17.66	35.642	0.50

Table K.4 (Continued).

Core ID	Top Depth of Interval (mm)	Bottom Depth of Interval (mm)	Average Depth of Interval (mm)	Wet Weight (g)	Dry Weight (g)	Sample Volume (cm^3)	Bulk Density (g/cm^3)
WB-1110-MC-PCB-06	225	230	227.5	48.35	18.25	35.642	0.51
WB-1110-MC-PCB-06	230	235	232.5	48.34	18.23	35.642	0.51
WB-1110-MC-PCB-06	235	240	237.5	44.64	16.65	35.642	0.47
WB-1110-MC-PCB-06	240	245	242.5	47.14	17.78	35.642	0.50
WB-1110-MC-PCB-06	245	250	247.5	46.01	17.36	35.642	0.49
WB-1110-MC-PCB-06	250	255	252.5	46.31	21.06	35.642	0.59
WB-1110-MC-PCB-06	255	260	257.5	48.41	18.30	35.642	0.51
WB-1110-MC-PCB-06	260	265	262.5	47.12	17.83	35.642	0.50
WB-1110-MC-PCB-06	265	270	267.5	48.32	18.32	35.642	0.51
WB-1110-MC-PCB-06	270	275	272.5	43.22	16.82	35.642	0.47
WB-1110-MC-PCB-06	275	280	277.5	50.59	19.16	35.642	0.54
WB-1110-MC-PCB-06	280	285	282.5	45.25	17.12	35.642	0.48
WB-1110-MC-PCB-06	285	290	287.5	46.33	17.58	35.642	0.49
WB-1110-MC-PCB-06	290	295	292.5	51.12	19.41	35.642	0.54
WB-1110-MC-PCB-06	295	300	297.5	44.05	16.86	35.642	0.47
WB-1110-MC-PCB-06	300	305	302.5	45.55	19.75	35.642	0.55
WB-1110-MC-PCB-06	305	310	307.5	55.94	21.12	35.642	0.59
WB-1110-MC-PCB-06	310	315	312.5	51.00	22.83	35.642	0.64
WB-1110-MC-PCB-06	315	320	317.5	45.09	18.00	35.642	0.51
WB-1110-MC-PCB-06	320	325	322.5	38.91	15.70	35.642	0.44
WB-1110-MC-PCB-06	325	330	327.5	53.39	21.82	35.642	0.61
WB-1110-MC-PCB-06	330	Base		58.43	26.54		

Table K.5. Bulk density data for core site WB-1114-MC-DSH-08. Sediment core sub-sample intervals (mm), sub-sample wet weight (g), dry weight (g), sub-sample volume (cm^3), and bulk density (g/cm^3). Note: Blank cell denotes no analysis performed.

Core ID	Top Depth of Interval (mm)	Bottom Depth of Interval (mm)	Average Depth of Interval (mm)	Wet Weight (g)	Dry Weight (g)	Sample Volume (cm^3)	Bulk Density (g/cm^3)
WB-1114-MC-DSH-08	0	2	1	10.28	2.16	14.257	0.15
WB-1114-MC-DSH-08	2	4	3	15.83	3.44	14.257	0.24
WB-1114-MC-DSH-08	4	6	5	15.46	3.30	14.257	0.23
WB-1114-MC-DSH-08	6	8	7	17.18	3.67	14.257	0.26
WB-1114-MC-DSH-08	8	10	9	17.00	3.75	14.257	0.26
WB-1114-MC-DSH-08	10	12	11	18.16	4.29	14.257	0.30
WB-1114-MC-DSH-08	12	14	13	18.02	4.37	14.257	0.31
WB-1114-MC-DSH-08	14	16	15	16.57	3.43	14.257	0.24
WB-1114-MC-DSH-08	16	18	17	15.47	3.92	14.257	0.27
WB-1114-MC-DSH-08	18	20	19	19.40	5.15	14.257	0.36
WB-1114-MC-DSH-08	20	22	21	16.53	4.44	14.257	0.31
WB-1114-MC-DSH-08	22	24	23	18.45	5.12	14.257	0.36
WB-1114-MC-DSH-08	24	26	25	18.29	5.13	14.257	0.36
WB-1114-MC-DSH-08	26	28	27	16.17	4.55	14.257	0.32
WB-1114-MC-DSH-08	28	30	29	17.73	5.07	14.257	0.36
WB-1114-MC-DSH-08	30	32	31	18.03	5.34	14.257	0.37
WB-1114-MC-DSH-08	32	34	33	17.21	5.12	14.257	0.36
WB-1114-MC-DSH-08	34	36	35	17.13	5.08	14.257	0.36
WB-1114-MC-DSH-08	36	38	37	18.27	5.52	14.257	0.39
WB-1114-MC-DSH-08	38	40	39	17.48	5.36	14.257	0.38
WB-1114-MC-DSH-08	40	42	41	18.15	5.59	14.257	0.39
WB-1114-MC-DSH-08	42	44	43	18.24	5.71	14.257	0.40
WB-1114-MC-DSH-08	44	46	45	16.87	5.35	14.257	0.38
WB-1114-MC-DSH-08	46	48	47	16.18	5.15	14.257	0.36
WB-1114-MC-DSH-08	48	50	49	20.96	6.87	14.257	0.48
WB-1114-MC-DSH-08	50	55	52.5	45.53	16.06	35.642	0.45
WB-1114-MC-DSH-08	55	60	57.5	47.49	16.08	35.642	0.45
WB-1114-MC-DSH-08	60	65	62.5	45.33	15.49	35.642	0.43
WB-1114-MC-DSH-08	65	70	67.5	44.18	15.09	35.642	0.42
WB-1114-MC-DSH-08	70	75	72.5	46.59	16.01	35.642	0.45
WB-1114-MC-DSH-08	75	80	77.5	44.07	15.38	35.642	0.43
WB-1114-MC-DSH-08	80	85	82.5	46.09	16.05	35.642	0.45
WB-1114-MC-DSH-08	85	90	87.5	44.85	15.75	35.642	0.44
WB-1114-MC-DSH-08	90	95	92.5	46.09	16.18	35.642	0.45
WB-1114-MC-DSH-08	95	100	97.5	44.26	15.80	35.642	0.44
WB-1114-MC-DSH-08	100	105	102.5	45.45	16.24	35.642	0.46

Table K.5 (Continued).

Core ID	Top Depth of Interval (mm)	Bottom Depth of Interval (mm)	Average Depth of Interval (mm)	Wet Weight (g)	Dry Weight (g)	Sample Volume (cm^3)	Bulk Density (g/cm^3)
WB-1114-MC-DSH-08	105	110	107.5	45.94	16.55	35.642	0.46
WB-1114-MC-DSH-08	110	115	112.5	47.23	16.97	35.642	0.48
WB-1114-MC-DSH-08	115	120	117.5	45.80	16.65	35.642	0.47
WB-1114-MC-DSH-08	120	125	122.5	46.47	17.02	35.642	0.48
WB-1114-MC-DSH-08	125	130	127.5	46.44	16.98	35.642	0.48
WB-1114-MC-DSH-08	130	135	132.5	46.82	17.10	35.642	0.48
WB-1114-MC-DSH-08	135	140	137.5	45.96	16.87	35.642	0.47
WB-1114-MC-DSH-08	140	145	142.5	46.66	17.26	35.642	0.48
WB-1114-MC-DSH-08	145	150	147.5	46.02	17.45	35.642	0.49
WB-1114-MC-DSH-08	150	155	152.5	46.41	17.62	35.642	0.49
WB-1114-MC-DSH-08	155	160	157.5	48.88	18.57	35.642	0.52
WB-1114-MC-DSH-08	160	165	162.5	46.81	17.94	35.642	0.50
WB-1114-MC-DSH-08	165	170	167.5	47.44	18.33	35.642	0.51
WB-1114-MC-DSH-08	170	175	172.5	46.49	17.99	35.642	0.50
WB-1114-MC-DSH-08	175	180	177.5	47.42	18.40	35.642	0.52
WB-1114-MC-DSH-08	180	185	182.5	46.83	18.48	35.642	0.52
WB-1114-MC-DSH-08	185	190	187.5	48.05	19.10	35.642	0.54
WB-1114-MC-DSH-08	190	195	192.5	45.80	18.17	35.642	0.51
WB-1114-MC-DSH-08	195	200	197.5	47.29	18.87	35.642	0.53
WB-1114-MC-DSH-08	200	205	202.5	51.07	20.38	35.642	0.57
WB-1114-MC-DSH-08	205	210	207.5	49.13	19.57	35.642	0.55
WB-1114-MC-DSH-08	210	215	212.5	48.42	19.27	35.642	0.54
WB-1114-MC-DSH-08	215	220	217.5	48.65	19.57	35.642	0.55
WB-1114-MC-DSH-08	220	225	222.5	47.55	19.06	35.642	0.53
WB-1114-MC-DSH-08	225	230	227.5	53.64	21.64	35.642	0.61
WB-1114-MC-DSH-08	230	235	232.5	47.29	18.98	35.642	0.53
WB-1114-MC-DSH-08	235	240	237.5	49.05	19.91	35.642	0.56
WB-1114-MC-DSH-08	240	245	242.5	51.23	20.53	35.642	0.58
WB-1114-MC-DSH-08	245	Base		34.64	13.74		

Table K.6. Bulk density data for core site WB-1114-MC-DSH-10. Sediment core sub-sample intervals (mm), sub-sample wet weight (g), dry weight (g), sub-sample volume (cm^3), and bulk density (g/cm^3). Note: Blank cell denotes no analysis performed.

Core ID	Top Depth of Interval (mm)	Bottom Depth of Interval (mm)	Average Depth of Interval (mm)	Wet Weight (g)	Dry Weight (g)	Sample Volume (cm^3)	Bulk Density (g/cm^3)
WB-1114-MC-DSH-10	0	2	1	17.98	2.78	14.257	0.19
WB-1114-MC-DSH-10	2	4	3	16.56	2.89	14.257	0.20
WB-1114-MC-DSH-10	4	6	5	15.50	2.97	14.257	0.21
WB-1114-MC-DSH-10	6	8	7	18.54	3.98	14.257	0.28
WB-1114-MC-DSH-10	8	10	9	17.48	3.95	14.257	0.28
WB-1114-MC-DSH-10	10	12	11	16.18	3.83	14.257	0.27
WB-1114-MC-DSH-10	12	14	13	17.43	4.31	14.257	0.30
WB-1114-MC-DSH-10	14	16	15	15.68	4.00	14.257	0.28
WB-1114-MC-DSH-10	16	18	17	16.53	4.39	14.257	0.31
WB-1114-MC-DSH-10	18	20	19	17.65	4.82	14.257	0.34
WB-1114-MC-DSH-10	20	22	21	17.24	4.69	14.257	0.33
WB-1114-MC-DSH-10	22	24	23	18.91	5.29	14.257	0.37
WB-1114-MC-DSH-10	24	26	25	15.76	4.56	14.257	0.32
WB-1114-MC-DSH-10	26	28	27	17.50	5.18	14.257	0.36
WB-1114-MC-DSH-10	28	30	29	19.27	5.78	14.257	0.41
WB-1114-MC-DSH-10	30	32	31	17.77	5.37	14.257	0.38
WB-1114-MC-DSH-10	32	34	33	20.69	6.28	14.257	0.44
WB-1114-MC-DSH-10	34	36	35	17.54	5.45	14.257	0.38
WB-1114-MC-DSH-10	36	38	37	17.53	5.37	14.257	0.38
WB-1114-MC-DSH-10	38	40	39	18.83	5.75	14.257	0.40
WB-1114-MC-DSH-10	40	42	41	16.11	4.85	14.257	0.34
WB-1114-MC-DSH-10	42	44	43	18.03	5.39	14.257	0.38
WB-1114-MC-DSH-10	44	46	45	15.21	4.52	14.257	0.32
WB-1114-MC-DSH-10	46	48	47	19.11	5.81	14.257	0.41
WB-1114-MC-DSH-10	48	50	49	20.22	6.21	14.257	0.44
WB-1114-MC-DSH-10	50	52	51	19.46	6.04	14.257	0.42
WB-1114-MC-DSH-10	52	54	53	16.64	5.10	14.257	0.36
WB-1114-MC-DSH-10	54	56	55	19.22	5.90	14.257	0.41
WB-1114-MC-DSH-10	56	58	57	18.39	5.69	14.257	0.40
WB-1114-MC-DSH-10	58	60	59	19.85	6.24	14.257	0.44
WB-1114-MC-DSH-10	60	62	61	15.34	4.80	14.257	0.34
WB-1114-MC-DSH-10	62	64	63	17.42	5.43	14.257	0.38
WB-1114-MC-DSH-10	64	66	65	17.17	5.50	14.257	0.39
WB-1114-MC-DSH-10	66	68	67	18.95	6.21	14.257	0.44
WB-1114-MC-DSH-10	68	70	69	20.54	6.72	14.257	0.47
WB-1114-MC-DSH-10	70	72	71	18.01	5.98	14.257	0.42

Table K.6 (Continued).

Core ID	Top Depth of Interval (mm)	Bottom Depth of Interval (mm)	Average Depth of Interval (mm)	Wet Weight (g)	Dry Weight (g)	Sample Volume (cm^3)	Bulk Density (g/cm^3)
WB-1114-MC-DSH-10	72	74	73	19.28	6.62	14.257	0.46
WB-1114-MC-DSH-10	74	76	75	19.07	6.56	14.257	0.46
WB-1114-MC-DSH-10	76	78	77	16.61	5.70	14.257	0.40
WB-1114-MC-DSH-10	78	80	79	20.51	7.14	14.257	0.50
WB-1114-MC-DSH-10	80	82	81	22.04	8.01	14.257	0.56
WB-1114-MC-DSH-10	82	84	83	15.80	5.67	14.257	0.40
WB-1114-MC-DSH-10	84	86	85	19.89	7.26	14.257	0.51
WB-1114-MC-DSH-10	86	88	87	16.68	6.22	14.257	0.44
WB-1114-MC-DSH-10	88	90	89	19.18	7.24	14.257	0.51
WB-1114-MC-DSH-10	90	95	92.5	47.15	17.98	35.642	0.50
WB-1114-MC-DSH-10	95	100	97.5	50.86	19.52	35.642	0.55
WB-1114-MC-DSH-10	100	105	102.5	47.30	17.95	35.642	0.50
WB-1114-MC-DSH-10	105	110	107.5	46.96	17.70	35.642	0.50
WB-1114-MC-DSH-10	110	115	112.5	45.36	16.75	35.642	0.47
WB-1114-MC-DSH-10	115	120	117.5	47.61	17.70	35.642	0.50
WB-1114-MC-DSH-10	120	125	122.5	44.83	16.38	35.642	0.46
WB-1114-MC-DSH-10	125	130	127.5	47.47	17.12	35.642	0.48
WB-1114-MC-DSH-10	130	135	132.5	45.62	16.85	35.642	0.47
WB-1114-MC-DSH-10	135	140	137.5	46.47	16.92	35.642	0.47
WB-1114-MC-DSH-10	140	145	142.5	47.94	17.55	35.642	0.49
WB-1114-MC-DSH-10	145	150	147.5	45.98	16.81	35.642	0.47
WB-1114-MC-DSH-10	150	155	152.5	44.79	15.60	35.642	0.44
WB-1114-MC-DSH-10	155	160	157.5	53.47	19.39	35.642	0.54
WB-1114-MC-DSH-10	160	165	162.5	46.25	16.80	35.642	0.47
WB-1114-MC-DSH-10	165	170	167.5	46.75	16.92	35.642	0.47
WB-1114-MC-DSH-10	170	175	172.5	40.79	14.60	35.642	0.41
WB-1114-MC-DSH-10	175	180	177.5	43.32	15.52	35.642	0.44
WB-1114-MC-DSH-10	180	185	182.5	49.66	17.82	35.642	0.50
WB-1114-MC-DSH-10	185	190	187.5	50.19	17.89	35.642	0.50
WB-1114-MC-DSH-10	190	195	192.5	41.60	15.00	35.642	0.42
WB-1114-MC-DSH-10	195	200	197.5	45.51	16.44	35.642	0.46
WB-1114-MC-DSH-10	200	205	202.5	45.38	16.38	35.642	0.46
WB-1114-MC-DSH-10	205	210	207.5	46.19	16.67	35.642	0.47
WB-1114-MC-DSH-10	210	215	212.5	45.45	16.38	35.642	0.46
WB-1114-MC-DSH-10	215	220	217.5	49.41	17.77	35.642	0.50
WB-1114-MC-DSH-10	220	225	222.5	46.45	16.90	35.642	0.47
WB-1114-MC-DSH-10	225	230	227.5	47.46	17.26	35.642	0.48
WB-1114-MC-DSH-10	230	235	232.5	46.30	16.87	35.642	0.47

Table K.6 (Continued).

Core ID	Top Depth of Interval (mm)	Bottom Depth of Interval (mm)	Average Depth of Interval (mm)	Wet Weight (g)	Dry Weight (g)	Sample Volume (cm^3)	Bulk Density (g/cm^3)
WB-1114-MC-DSH-10	235	240	237.5	40.05	14.57	35.642	0.41
WB-1114-MC-DSH-10	240	245	242.5	43.63	15.91	35.642	0.45
WB-1114-MC-DSH-10	245	250	247.5	47.62	17.46	35.642	0.49
WB-1114-MC-DSH-10	250	255	252.5	47.38	17.40	35.642	0.49
WB-1114-MC-DSH-10	255	260	257.5	47.55	17.34	35.642	0.49
WB-1114-MC-DSH-10	260	265	262.5	46.40	16.88	35.642	0.47
WB-1114-MC-DSH-10	265	270	267.5	46.97	17.01	35.642	0.48
WB-1114-MC-DSH-10	270	275	272.5	46.25	16.74	35.642	0.47
WB-1114-MC-DSH-10	275	280	277.5	44.87	16.51	35.642	0.46
WB-1114-MC-DSH-10	280	285	282.5	48.00	17.77	35.642	0.50
WB-1114-MC-DSH-10	285	290	287.5	45.86	17.09	35.642	0.48
WB-1114-MC-DSH-10	290	295	292.5	48.75	18.35	35.642	0.51
WB-1114-MC-DSH-10	295	300	297.5	47.50	18.01	35.642	0.51
WB-1114-MC-DSH-10	300	305	302.5	49.51	18.78	35.642	0.53
WB-1114-MC-DSH-10	305	310	307.5	48.08	18.19	35.642	0.51
WB-1114-MC-DSH-10	310	315	312.5	50.38	18.97	35.642	0.53
WB-1114-MC-DSH-10	315	320	317.5	50.74	19.31	35.642	0.54
WB-1114-MC-DSH-10	320	325	322.5	61.73	24.02	35.642	0.67
WB-1114-MC-DSH-10	325	Base		53.70	21.34		

Table K.7. Bulk density data for core site WB-1114-MC-PCB-06. Sediment core sub-sample intervals (mm), sub-sample wet weight (g), dry weight (g), sub-sample volume (cm^3), and bulk density (g/cm^3). Note: Blank cell denotes no analysis performed.

Core ID	Top Depth of Interval (mm)	Bottom Depth of Interval (mm)	Average Depth of Interval (mm)	Wet Weight (g)	Dry Weight (g)	Sample Volume (cm^3)	Bulk Density (g/cm^3)
WB-1114-MC-PCB-06	0	2	1	27.74	3.31	14.257	0.23
WB-1114-MC-PCB-06	2	4	3	13.94	2.79	14.257	0.20
WB-1114-MC-PCB-06	4	6	5	18.22	4.25	14.257	0.30
WB-1114-MC-PCB-06	6	8	7	15.90	3.72	14.257	0.26
WB-1114-MC-PCB-06	8	10	9	15.80	3.98	14.257	0.28
WB-1114-MC-PCB-06	10	12	11	17.77	4.53	14.257	0.32
WB-1114-MC-PCB-06	12	14	13	18.97	4.84	14.257	0.34
WB-1114-MC-PCB-06	14	16	15	16.25	4.12	14.257	0.29
WB-1114-MC-PCB-06	16	18	17	17.9	4.52	14.257	0.32
WB-1114-MC-PCB-06	18	20	19	19.03	4.82	14.257	0.34
WB-1114-MC-PCB-06	20	22	21	14.41	3.55	14.257	0.25
WB-1114-MC-PCB-06	22	24	23	19.17	4.71	14.257	0.33
WB-1114-MC-PCB-06	24	26	25	17.69	4.41	14.257	0.31
WB-1114-MC-PCB-06	26	28	27	17.81	4.53	14.257	0.32
WB-1114-MC-PCB-06	28	30	29	16.22	4.11	14.257	0.29
WB-1114-MC-PCB-06	30	32	31	17.54	4.46	14.257	0.31
WB-1114-MC-PCB-06	32	34	33	17.51	4.42	14.257	0.31
WB-1114-MC-PCB-06	34	36	35	18.62	4.78	14.257	0.34
WB-1114-MC-PCB-06	36	38	37	17.45	4.51	14.257	0.32
WB-1114-MC-PCB-06	38	40	39	17.43	4.62	14.257	0.32
WB-1114-MC-PCB-06	40	42	41	17.03	4.54	14.257	0.32
WB-1114-MC-PCB-06	42	44	43	17.83	4.72	14.257	0.33
WB-1114-MC-PCB-06	44	46	45	18.04	4.82	14.257	0.34
WB-1114-MC-PCB-06	46	48	47	17.71	4.82	14.257	0.34
WB-1114-MC-PCB-06	48	50	49	17.76	4.86	14.257	0.34
WB-1114-MC-PCB-06	50	52	51	18.8	5.26	14.257	0.37
WB-1114-MC-PCB-06	52	54	53	16.07	4.52	14.257	0.32
WB-1114-MC-PCB-06	54	56	55	16.93	4.86	14.257	0.34
WB-1114-MC-PCB-06	56	58	57	17.83	4.95	14.257	0.35
WB-1114-MC-PCB-06	58	60	59	18.14	5.1	14.257	0.36
WB-1114-MC-PCB-06	60	62	61	17.96	5.07	14.257	0.36
WB-1114-MC-PCB-06	62	64	63	16.88	4.81	14.257	0.34
WB-1114-MC-PCB-06	64	66	65	18.52	5.36	14.257	0.38
WB-1114-MC-PCB-06	66	68	67	15.89	4.66	14.257	0.33
WB-1114-MC-PCB-06	68	70	69	18.89	5.64	14.257	0.40
WB-1114-MC-PCB-06	70	75	72.5	43.02	13.64	35.642	0.38

Table K.7 (Continued).

Core ID	Top Depth of Interval (mm)	Bottom Depth of Interval (mm)	Average Depth of Interval (mm)	Wet Weight (g)	Dry Weight (g)	Sample Volume (cm^3)	Bulk Density (g/cm^3)
WB-1114-MC-PCB-06	75	80	77.5	45.17	14.45	35.642	0.41
WB-1114-MC-PCB-06	80	85	82.5	48.25	15.07	35.642	0.42
WB-1114-MC-PCB-06	85	90	87.5	42.64	14.02	35.642	0.39
WB-1114-MC-PCB-06	90	95	92.5	45.18	14.86	35.642	0.42
WB-1114-MC-PCB-06	95	100	97.5	44.26	23.62	35.642	0.66
WB-1114-MC-PCB-06	100	105	102.5	34.75	11.68	35.642	0.33
WB-1114-MC-PCB-06	105	110	107.5	44.31	15.66	35.642	0.44
WB-1114-MC-PCB-06	110	115	112.5	50.71	17.66	35.642	0.50
WB-1114-MC-PCB-06	115	120	117.5	44.01	15.18	35.642	0.43
WB-1114-MC-PCB-06	120	125	122.5	45.33	15.76	35.642	0.44
WB-1114-MC-PCB-06	125	130	127.5	44.06	15.57	35.642	0.44
WB-1114-MC-PCB-06	130	135	132.5	45.43	16.67	35.642	0.47
WB-1114-MC-PCB-06	135	140	137.5	48.02	17.59	35.642	0.49
WB-1114-MC-PCB-06	140	145	142.5	47.73	17.57	35.642	0.49
WB-1114-MC-PCB-06	145	150	147.5	46.5	17.15	35.642	0.48
WB-1114-MC-PCB-06	150	155	152.5	46.55	16.78	35.642	0.47
WB-1114-MC-PCB-06	155	160	157.5	48.67	18.02	35.642	0.51
WB-1114-MC-PCB-06	160	165	162.5	43.47	16.14	35.642	0.45
WB-1114-MC-PCB-06	165	170	167.5	53.85	18.14	35.642	0.51
WB-1114-MC-PCB-06	170	175	172.5	45.94	16.79	35.642	0.47
WB-1114-MC-PCB-06	175	180	177.5	48.18	17.82	35.642	0.50
WB-1114-MC-PCB-06	180	185	182.5	44.35	16.19	35.642	0.45
WB-1114-MC-PCB-06	185	190	187.5	47.52	17.53	35.642	0.49
WB-1114-MC-PCB-06	190	195	192.5	46.32	17.19	35.642	0.48
WB-1114-MC-PCB-06	195	200	197.5	44.69	16.58	35.642	0.47
WB-1114-MC-PCB-06	200	205	202.5	49.17	17.83	35.642	0.50
WB-1114-MC-PCB-06	205	210	207.5	45.22	16.75	35.642	0.47
WB-1114-MC-PCB-06	210	215	212.5	46.69	17.14	35.642	0.48
WB-1114-MC-PCB-06	215	220	217.5	45	16.8	35.642	0.47
WB-1114-MC-PCB-06	220	225	222.5	49.48	18.45	35.642	0.52
WB-1114-MC-PCB-06	225	230	227.5	43.11	16.22	35.642	0.46
WB-1114-MC-PCB-06	230	235	232.5	46.58	17.37	35.642	0.49
WB-1114-MC-PCB-06	235	240	237.5	46.41	17.44	35.642	0.49
WB-1114-MC-PCB-06	240	245	242.5	47.13	17.69	35.642	0.50
WB-1114-MC-PCB-06	245	250	247.5	43.34	15.87	35.642	0.45
WB-1114-MC-PCB-06	250	255	252.5	49.65	18.36	35.642	0.52
WB-1114-MC-PCB-06	255	260	257.5	43.88	16.18	35.642	0.45
WB-1114-MC-PCB-06	260	265	262.5	47.77	17.63	35.642	0.49

Table K.7 (Continued).

Core ID	Top Depth of Interval (mm)	Bottom Depth of Interval (mm)	Average Depth of Interval (mm)	Wet Weight (g)	Dry Weight (g)	Sample Volume (cm^3)	Bulk Density (g/cm^3)
WB-1114-MC-PCB-06	265	270	267.5	48.42	18.44	35.642	0.52
WB-1114-MC-PCB-06	270	275	272.5	44.31	16.87	35.642	0.47
WB-1114-MC-PCB-06	275	280	277.5	49.89	19.06	35.642	0.53
WB-1114-MC-PCB-06	280	285	282.5	46.34	17.65	35.642	0.50
WB-1114-MC-PCB-06	285	290	287.5	48.65	18.63	35.642	0.52
WB-1114-MC-PCB-06	290	295	292.5	43.67	16.59	35.642	0.47
WB-1114-MC-PCB-06	295	300	297.5	47.88	18.69	35.642	0.52
WB-1114-MC-PCB-06	300	305	302.5	47.34	18.71	35.642	0.52
WB-1114-MC-PCB-06	305	310	307.5	47.42	18.78	35.642	0.53
WB-1114-MC-PCB-06	310	315	312.5	58.12	23.53	35.642	0.66
WB-1114-MC-PCB-06	315	320	317.5	47.09	19.17	35.642	0.54
WB-1114-MC-PCB-06	320	325	322.5	56.62	23.04	35.642	0.65
WB-1114-MC-PCB-06	325	330	327.5	53.84	21.63	35.642	0.61
WB-1114-MC-PCB-06	330	335	332.5	52.97	21.41	35.642	0.60
WB-1114-MC-PCB-06	335	340	337.5	47.54	19.31	35.642	0.54
WB-1114-MC-PCB-06	340	345	342.5	39.51	16.26	35.642	0.46
WB-1114-MC-PCB-06	345	Base		16.55	6.94		

Table K.8. Bulk density data for core site WB-0911-BC-DSH-08. Sediment core sub-sample intervals (mm), sub-sample wet weight (g), dry weight (g), sub-sample volume (cm^3), and bulk density (g/cm^3). Note: Blank cell denotes no analysis performed.

Core ID	Top Depth of Interval (mm)	Bottom Depth of Interval (mm)	Average Depth of Interval (mm)	Wet Weight (g)	Dry Weight (g)	Sample Volume (cm^3)	Bulk Density (g/cm^3)
WB-0911-BC-DSH-08	0	2	1	11.18	3.04	14.257	0.21
WB-0911-BC-DSH-08	2	4	3	15.67	4.17	14.257	0.29
WB-0911-BC-DSH-08	4	6	5	20.48	5.43	14.257	0.38
WB-0911-BC-DSH-08	6	8	7	15.56	4.14	14.257	0.29
WB-0911-BC-DSH-08	8	10	9	15.01	4.09	14.257	0.29
WB-0911-BC-DSH-08	10	12	11	14.92	4.14	14.257	0.29
WB-0911-BC-DSH-08	12	14	13	14.35	3.99	14.257	0.28
WB-0911-BC-DSH-08	14	16	15	18.84	5.26	14.257	0.37
WB-0911-BC-DSH-08	16	18	17	17.14	4.88	14.257	0.34
WB-0911-BC-DSH-08	18	20	19	16.45	4.65	14.257	0.33
WB-0911-BC-DSH-08	20	22	21	17.16	4.85	14.257	0.34
WB-0911-BC-DSH-08	22	24	23	18.06	5.12	14.257	0.36
WB-0911-BC-DSH-08	24	26	25	18.34	5.28	14.257	0.37
WB-0911-BC-DSH-08	26	28	27	16.91	4.85	14.257	0.34
WB-0911-BC-DSH-08	28	30	29	16.18	4.70	14.257	0.33
WB-0911-BC-DSH-08	30	35	32.5	40.23	11.73	35.642	0.33
WB-0911-BC-DSH-08	35	40	37.5	43.89	12.90	35.642	0.36
WB-0911-BC-DSH-08	40	45	42.5	44.77	13.64	35.642	0.38
WB-0911-BC-DSH-08	45	50	47.5	47.21	14.57	35.642	0.41
WB-0911-BC-DSH-08	50	55	52.5	42.38	13.72	35.642	0.38
WB-0911-BC-DSH-08	55	60	57.5	43.06	14.27	35.642	0.40
WB-0911-BC-DSH-08	60	65	62.5	43.09	14.86	35.642	0.42
WB-0911-BC-DSH-08	65	70	67.5	47.17	16.67	35.642	0.47
WB-0911-BC-DSH-08	70	75	72.5	43.99	15.93	35.642	0.45
WB-0911-BC-DSH-08	75	80	77.5	43.53	16.16	35.642	0.45
WB-0911-BC-DSH-08	80	85	82.5	45.97	17.67	35.642	0.50
WB-0911-BC-DSH-08	85	90	87.5	48.34	18.89	35.642	0.53
WB-0911-BC-DSH-08	90	95	92.5	47.63	18.56	35.642	0.52
WB-0911-BC-DSH-08	95	100	97.5	43.77	17.25	35.642	0.48
WB-0911-BC-DSH-08	100	105	102.5	46.98	18.79	35.642	0.53
WB-0911-BC-DSH-08	105	110	107.5	48.63	19.65	35.642	0.55
WB-0911-BC-DSH-08	110	115	112.5	49.59	19.55	35.642	0.55
WB-0911-BC-DSH-08	115	120	117.5	42.52	16.73	35.642	0.47
WB-0911-BC-DSH-08	120	125	122.5	39.40	16.03	35.642	0.45
WB-0911-BC-DSH-08	125	130	127.5	55.27	22.60	35.642	0.63
WB-0911-BC-DSH-08	130	135	132.5	46.56	18.86	35.642	0.53

Table K.8 (Continued).

Core ID	Top Depth of Interval (mm)	Bottom Depth of Interval (mm)	Average Depth of Interval (mm)	Wet Weight (g)	Dry Weight (g)	Sample Volume (cm^3)	Bulk Density (g/cm^3)
WB-0911-BC-DSH-08	135	140	137.5	46.06	18.67	35.642	0.52
WB-0911-BC-DSH-08	140	145	142.5	51.07	20.68	35.642	0.58
WB-0911-BC-DSH-08	145	150	147.5	44.64	17.93	35.642	0.50
WB-0911-BC-DSH-08	150	155	152.5	46.49	18.45	35.642	0.52
WB-0911-BC-DSH-08	155	160	157.5	47.61	18.81	35.642	0.53
WB-0911-BC-DSH-08	160	165	162.5	46.80	18.68	35.642	0.52
WB-0911-BC-DSH-08	165	170	167.5	47.72	19.39	35.642	0.54
WB-0911-BC-DSH-08	170	175	172.5	46.22	18.16	35.642	0.51
WB-0911-BC-DSH-08	175	180	177.5	45.70	18.18	35.642	0.51
WB-0911-BC-DSH-08	180	185	182.5	53.96	21.63	35.642	0.61
WB-0911-BC-DSH-08	185	190	187.5	47.07	18.92	35.642	0.53
WB-0911-BC-DSH-08	190	195	192.5	43.45	16.90	35.642	0.47
WB-0911-BC-DSH-08	195	200	197.5	47.29	18.41	35.642	0.52
WB-0911-BC-DSH-08	200	205	202.5	44.77	17.39	35.642	0.49
WB-0911-BC-DSH-08	205	210	207.5	47.79	18.76	35.642	0.53
WB-0911-BC-DSH-08	210	215	212.5	48.27	18.92	35.642	0.53
WB-0911-BC-DSH-08	215	220	217.5	48.16	18.80	35.642	0.53
WB-0911-BC-DSH-08	220	225	222.5	51.20	19.95	35.642	0.56
WB-0911-BC-DSH-08	225	230	227.5	41.75	16.39	35.642	0.46
WB-0911-BC-DSH-08	230	235	232.5	47.52	18.85	35.642	0.53
WB-0911-BC-DSH-08	235	240	237.5	38.34	15.08	35.642	0.42
WB-0911-BC-DSH-08	240	245	242.5	53.59	21.13	35.642	0.59
WB-0911-BC-DSH-08	245	250	247.5	44.27	17.67	35.642	0.50
WB-0911-BC-DSH-08	250	255	252.5	48.22	18.53	35.642	0.52
WB-0911-BC-DSH-08	255	260	257.5	45.16	17.84	35.642	0.50
WB-0911-BC-DSH-08	260	265	262.5	46.16	17.93	35.642	0.50
WB-0911-BC-DSH-08	265	270	267.5	47.56	18.20	35.642	0.51
WB-0911-BC-DSH-08	270	275	272.5	45.53	17.51	35.642	0.49
WB-0911-BC-DSH-08	275	280	277.5	47.90	18.10	35.642	0.51
WB-0911-BC-DSH-08	280	285	282.5	48.27	18.34	35.642	0.51
WB-0911-BC-DSH-08	285	290	287.5	46.36	17.68	35.642	0.50
WB-0911-BC-DSH-08	290	295	292.5	47.22	18.10	35.642	0.51
WB-0911-BC-DSH-08	295	300	297.5	42.84	16.95	35.642	0.48
WB-0911-BC-DSH-08	300	305	302.5	51.82	20.07	35.642	0.56
WB-0911-BC-DSH-08	305	310	307.5	46.68	18.48	35.642	0.52
WB-0911-BC-DSH-08	310	315	312.5	53.47	21.14	35.642	0.59
WB-0911-BC-DSH-08	315	320	317.5	33.06	12.92	35.642	0.36
WB-0911-BC-DSH-08	320	Base		43.91	17.30		

Table K.9. Bulk density data for core site WB-0911-BC-DSH-10. Sediment core sub-sample intervals (mm), sub-sample wet weight (g), dry weight (g), sub-sample volume (cm^3), and bulk density (g/cm^3). Note: Blank cell denotes no analysis performed.

Core ID	Top Depth of Interval (mm)	Bottom Depth of Interval (mm)	Average Depth of Interval (mm)	Wet Weight (g)	Dry Weight (g)	Sample Volume (cm^3)	Bulk Density (g/cm^3)
WB-0911-BC-DSH-10	0	2	1	9.40	2.54	14.257	0.18
WB-0911-BC-DSH-10	2	4	3	16.69	4.63	14.257	0.32
WB-0911-BC-DSH-10	4	6	5	18.13	5.33	14.257	0.37
WB-0911-BC-DSH-10	6	8	7	16.31	4.78	14.257	0.34
WB-0911-BC-DSH-10	8	10	9	17.17	5.19	14.257	0.36
WB-0911-BC-DSH-10	10	12	11	16.81	5.15	14.257	0.36
WB-0911-BC-DSH-10	12	14	13	18.74	5.87	14.257	0.41
WB-0911-BC-DSH-10	14	16	15	15.97	5.02	14.257	0.35
WB-0911-BC-DSH-10	16	18	17	16.84	5.23	14.257	0.37
WB-0911-BC-DSH-10	18	20	19	16.46	5.20	14.257	0.36
WB-0911-BC-DSH-10	20	22	21	18.07	5.79	14.257	0.41
WB-0911-BC-DSH-10	22	24	23	18.12	5.82	14.257	0.41
WB-0911-BC-DSH-10	24	26	25	18.64	5.98	14.257	0.42
WB-0911-BC-DSH-10	26	28	27	19.52	6.32	14.257	0.44
WB-0911-BC-DSH-10	28	30	29	17.64	5.80	14.257	0.41
WB-0911-BC-DSH-10	30	32	31	20.10	6.73	14.257	0.47
WB-0911-BC-DSH-10	32	34	33	15.50	5.07	14.257	0.36
WB-0911-BC-DSH-10	34	36	35	16.96	5.92	14.257	0.42
WB-0911-BC-DSH-10	36	38	37	19.92	6.86	14.257	0.48
WB-0911-BC-DSH-10	38	40	39	16.90	5.82	14.257	0.41
WB-0911-BC-DSH-10	40	45	42.5	48.19	16.60	35.642	0.47
WB-0911-BC-DSH-10	45	50	47.5	45.12	15.52	35.642	0.44
WB-0911-BC-DSH-10	50	55	52.5	45.77	15.94	35.642	0.45
WB-0911-BC-DSH-10	55	60	57.5	46.15	16.19	35.642	0.45
WB-0911-BC-DSH-10	60	65	62.5	40.54	14.12	35.642	0.40
WB-0911-BC-DSH-10	65	70	67.5	48.36	17.19	35.642	0.48
WB-0911-BC-DSH-10	70	75	72.5	49.13	17.76	35.642	0.50
WB-0911-BC-DSH-10	75	80	77.5	50.93	18.68	35.642	0.52
WB-0911-BC-DSH-10	80	85	82.5	40.36	14.44	35.642	0.41
WB-0911-BC-DSH-10	85	90	87.5	42.33	15.77	35.642	0.44
WB-0911-BC-DSH-10	90	95	92.5	47.36	18.08	35.642	0.51
WB-0911-BC-DSH-10	95	100	97.5	46.53	18.25	35.642	0.51
WB-0911-BC-DSH-10	100	105	102.5	49.62	19.98	35.642	0.56
WB-0911-BC-DSH-10	105	110	107.5	44.51	18.56	35.642	0.52
WB-0911-BC-DSH-10	110	115	112.5	47.52	19.17	35.642	0.54
WB-0911-BC-DSH-10	115	120	117.5	49.64	20.20	35.642	0.57

Table K.9 (Continued).

Core ID	Top Depth of Interval (mm)	Bottom Depth of Interval (mm)	Average Depth of Interval (mm)	Wet Weight (g)	Dry Weight (g)	Sample Volume (cm^3)	Bulk Density (g/cm^3)
WB-0911-BC-DSH-10	120	125	122.5	40.43	16.29	35.642	0.46
WB-0911-BC-DSH-10	125	130	127.5	51.40	19.87	35.642	0.56
WB-0911-BC-DSH-10	130	135	132.5	46.41	18.08	35.642	0.51
WB-0911-BC-DSH-10	135	140	137.5	46.00	17.49	35.642	0.49
WB-0911-BC-DSH-10	140	145	142.5	44.98	16.76	35.642	0.47
WB-0911-BC-DSH-10	145	150	147.5	44.94	16.37	35.642	0.46
WB-0911-BC-DSH-10	150	155	152.5	47.25	17.72	35.642	0.50
WB-0911-BC-DSH-10	155	160	157.5	47.48	17.73	35.642	0.50
WB-0911-BC-DSH-10	160	165	162.5	46.32	17.36	35.642	0.49
WB-0911-BC-DSH-10	165	170	167.5	48.63	17.73	35.642	0.50
WB-0911-BC-DSH-10	170	175	172.5	43.87	16.34	35.642	0.46
WB-0911-BC-DSH-10	175	180	177.5	45.56	17.38	35.642	0.49
WB-0911-BC-DSH-10	180	185	182.5	45.35	17.17	35.642	0.48
WB-0911-BC-DSH-10	185	190	187.5	57.97	21.98	35.642	0.62
WB-0911-BC-DSH-10	190	195	192.5	38.92	14.38	35.642	0.40
WB-0911-BC-DSH-10	195	200	197.5	43.87	16.62	35.642	0.47
WB-0911-BC-DSH-10	200	205	202.5	44.60	16.55	35.642	0.46
WB-0911-BC-DSH-10	205	210	207.5	43.93	16.26	35.642	0.46
WB-0911-BC-DSH-10	210	215	212.5	48.16	18.03	35.642	0.51
WB-0911-BC-DSH-10	215	220	217.5	45.02	16.72	35.642	0.47
WB-0911-BC-DSH-10	220	225	222.5	48.02	17.85	35.642	0.50
WB-0911-BC-DSH-10	225	230	227.5	46.12	16.79	35.642	0.47
WB-0911-BC-DSH-10	230	235	232.5	46.76	17.04	35.642	0.48
WB-0911-BC-DSH-10	235	240	237.5	45.32	16.72	35.642	0.47
WB-0911-BC-DSH-10	240	245	242.5	46.88	17.56	35.642	0.49
WB-0911-BC-DSH-10	245	250	247.5	45.68	16.89	35.642	0.47
WB-0911-BC-DSH-10	250	255	252.5	48.11	18.88	35.642	0.53
WB-0911-BC-DSH-10	255	260	257.5	45.57	16.90	35.642	0.47
WB-0911-BC-DSH-10	260	265	262.5	48.87	18.25	35.642	0.51
WB-0911-BC-DSH-10	265	270	267.5	44.05	16.52	35.642	0.46
WB-0911-BC-DSH-10	270	275	272.5	46.88	17.20	35.642	0.48
WB-0911-BC-DSH-10	275	280	277.5	45.88	17.07	35.642	0.48
WB-0911-BC-DSH-10	280	285	282.5	45.59	16.90	35.642	0.47
WB-0911-BC-DSH-10	285	290	287.5	49.90	19.01	35.642	0.53
WB-0911-BC-DSH-10	290	295	292.5	47.82	17.88	35.642	0.50
WB-0911-BC-DSH-10	295	300	297.5	49.56	18.89	35.642	0.53
WB-0911-BC-DSH-10	300	305	302.5	43.17	16.17	35.642	0.45
WB-0911-BC-DSH-10	305	310	307.5	46.16	17.53	35.642	0.49

Table K.9 (Continued).

Core ID	Top Depth of Interval (mm)	Bottom Depth of Interval (mm)	Average Depth of Interval (mm)	Wet Weight (g)	Dry Weight (g)	Sample Volume (cm^3)	Bulk Density (g/cm^3)
WB-0911-BC-DSH-10	310	315	312.5	45.21	17.24	35.642	0.48
WB-0911-BC-DSH-10	315	320	317.5	48.73	18.66	35.642	0.52
WB-0911-BC-DSH-10	320	325	322.5	48.39	18.63	35.642	0.52
WB-0911-BC-DSH-10	325	330	327.5	36.10	13.93	35.642	0.39
WB-0911-BC-DSH-10	330	Base		39.89	14.90		

Table K.10. Bulk density data for core site WB-0911-MC-PCB-06. Sediment core sub-sample intervals (mm), sub-sample wet weight (g), dry weight (g), sub-sample volume (cm^3), and bulk density (g/cm^3). Note: Blank cell denotes no analysis performed.

Core ID	Top Depth of Interval (mm)	Bottom Depth of Interval (mm)	Average Depth of Interval (mm)	Wet Weight (g)	Dry Weight (g)	Sample Volume (cm^3)	Bulk Density (g/cm^3)
WB-0911-MC-PCB-06	0	2	1	8.75	1.90	14.257	0.13
WB-0911-MC-PCB-06	2	4	3	7.79	1.59	14.257	0.11
WB-0911-MC-PCB-06	4	6	5	14.35	2.90	14.257	0.20
WB-0911-MC-PCB-06	6	8	7	12.61	2.63	14.257	0.18
WB-0911-MC-PCB-06	8	10	9	16.56	3.57	14.257	0.25
WB-0911-MC-PCB-06	10	12	11	16.59	3.75	14.257	0.26
WB-0911-MC-PCB-06	12	14	13	18.83	4.49	14.257	0.31
WB-0911-MC-PCB-06	14	16	15	14.06	3.62	14.257	0.25
WB-0911-MC-PCB-06	16	18	17	15.59	3.98	14.257	0.28
WB-0911-MC-PCB-06	18	20	19	16.56	4.35	14.257	0.31
WB-0911-MC-PCB-06	20	22	21	16.41	4.35	14.257	0.31
WB-0911-MC-PCB-06	22	24	23	16.67	4.49	14.257	0.31
WB-0911-MC-PCB-06	24	26	25	15.61	4.30	14.257	0.30
WB-0911-MC-PCB-06	26	28	27	15.49	4.31	14.257	0.30
WB-0911-MC-PCB-06	28	30	29	17.89	5.06	14.257	0.35
WB-0911-MC-PCB-06	30	32	31	16.03	4.63	14.257	0.32
WB-0911-MC-PCB-06	32	34	33	17.66	5.12	14.257	0.36
WB-0911-MC-PCB-06	34	36	35	16.90	4.96	14.257	0.35
WB-0911-MC-PCB-06	36	38	37	18.43	5.51	14.257	0.39
WB-0911-MC-PCB-06	38	40	39	16.94	5.05	14.257	0.35
WB-0911-MC-PCB-06	40	42	41	15.62	4.77	14.257	0.33
WB-0911-MC-PCB-06	42	44	43	18.14	5.54	14.257	0.39
WB-0911-MC-PCB-06	44	46	45	19.64	6.09	14.257	0.43
WB-0911-MC-PCB-06	46	48	47	15.63	4.89	14.257	0.34
WB-0911-MC-PCB-06	48	50	49	16.72	5.33	14.257	0.37
WB-0911-MC-PCB-06	50	55	52.5	46.35	15.06	35.642	0.42
WB-0911-MC-PCB-06	55	60	57.5	51.79	17.72	35.642	0.50
WB-0911-MC-PCB-06	60	65	62.5	41.53	14.06	35.642	0.39
WB-0911-MC-PCB-06	65	70	67.5	43.59	15.00	35.642	0.42
WB-0911-MC-PCB-06	70	75	72.5	45.16	15.63	35.642	0.44
WB-0911-MC-PCB-06	75	80	77.5	48.08	16.87	35.642	0.47
WB-0911-MC-PCB-06	80	85	82.5	43.57	15.21	35.642	0.43
WB-0911-MC-PCB-06	85	90	87.5	47.24	16.69	35.642	0.47
WB-0911-MC-PCB-06	90	95	92.5	44.49	16.03	35.642	0.45
WB-0911-MC-PCB-06	95	100	97.5	44.64	16.44	35.642	0.46
WB-0911-MC-PCB-06	100	105	102.5	49.31	18.69	35.642	0.52

Table K.10 (Continued).

Core ID	Top Depth of Interval (mm)	Bottom Depth of Interval (mm)	Average Depth of Interval (mm)	Wet Weight (g)	Dry Weight (g)	Sample Volume (cm^3)	Bulk Density (g/cm^3)
WB-0911-MC-PCB-06	105	110	107.5	47.08	18.02	35.642	0.51
WB-0911-MC-PCB-06	110	115	112.5	48.62	18.09	35.642	0.51
WB-0911-MC-PCB-06	115	120	117.5	44.89	16.88	35.642	0.47
WB-0911-MC-PCB-06	120	125	122.5	43.70	16.04	35.642	0.45
WB-0911-MC-PCB-06	125	130	127.5	47.99	18.31	35.642	0.51
WB-0911-MC-PCB-06	130	135	132.5	47.85	17.93	35.642	0.50
WB-0911-MC-PCB-06	135	140	137.5	46.05	17.38	35.642	0.49
WB-0911-MC-PCB-06	140	145	142.5	46.45	17.52	35.642	0.49
WB-0911-MC-PCB-06	145	150	147.5	50.21	19.13	35.642	0.54
WB-0911-MC-PCB-06	150	155	152.5	43.12	16.18	35.642	0.45
WB-0911-MC-PCB-06	155	160	157.5	44.52	16.62	35.642	0.47
WB-0911-MC-PCB-06	160	165	162.5	50.15	18.77	35.642	0.53
WB-0911-MC-PCB-06	165	170	167.5	50.07	18.76	35.642	0.53
WB-0911-MC-PCB-06	170	175	172.5	45.08	16.98	35.642	0.48
WB-0911-MC-PCB-06	175	180	177.5	42.44	16.33	35.642	0.46
WB-0911-MC-PCB-06	180	185	182.5	45.98	17.01	35.642	0.48
WB-0911-MC-PCB-06	185	190	187.5	43.59	16.41	35.642	0.46
WB-0911-MC-PCB-06	190	195	192.5	51.19	19.23	35.642	0.54
WB-0911-MC-PCB-06	195	200	197.5	53.08	20.06	35.642	0.56
WB-0911-MC-PCB-06	200	205	202.5	49.14	18.37	35.642	0.52
WB-0911-MC-PCB-06	205	210	207.5	41.32	15.54	35.642	0.44
WB-0911-MC-PCB-06	210	215	212.5	41.57	15.24	35.642	0.43
WB-0911-MC-PCB-06	215	220	217.5	46.28	17.79	35.642	0.50
WB-0911-MC-PCB-06	220	225	222.5	44.37	16.54	35.642	0.46
WB-0911-MC-PCB-06	225	230	227.5	46.42	17.74	35.642	0.50
WB-0911-MC-PCB-06	230	235	232.5	43.70	15.80	35.642	0.44
WB-0911-MC-PCB-06	235	240	237.5	49.87	19.03	35.642	0.53
WB-0911-MC-PCB-06	240	245	242.5	43.46	16.08	35.642	0.45
WB-0911-MC-PCB-06	245	250	247.5	49.65	18.84	35.642	0.53
WB-0911-MC-PCB-06	250	255	252.5	44.33	17.01	35.642	0.48
WB-0911-MC-PCB-06	255	260	257.5	40.39	15.48	35.642	0.43
WB-0911-MC-PCB-06	260	265	262.5	46.25	17.69	35.642	0.50
WB-0911-MC-PCB-06	265	270	267.5	52.24	19.94	35.642	0.56
WB-0911-MC-PCB-06	270	275	272.5	46.61	17.84	35.642	0.50
WB-0911-MC-PCB-06	275	280	277.5	57.37	22.26	35.642	0.62
WB-0911-MC-PCB-06	280	285	282.5	42.11	16.14	35.642	0.45
WB-0911-MC-PCB-06	285	290	287.5	47.82	18.54	35.642	0.52
WB-0911-MC-PCB-06	290	295	292.5	41.09	15.97	35.642	0.45

Table K.10 (Continued).

Core ID	Top Depth of Interval (mm)	Bottom Depth of Interval (mm)	Average Depth of Interval (mm)	Wet Weight (g)	Dry Weight (g)	Sample Volume (cm^3)	Bulk Density (g/cm^3)
WB-0911-MC-PCB-06	295	300	297.5	46.52	18.12	35.642	0.51
WB-0911-MC-PCB-06	300	305	302.5	46.79	17.96	35.642	0.50
WB-0911-MC-PCB-06	305	310	307.5	47.68	18.76	35.642	0.53
WB-0911-MC-PCB-06	310	315	312.5	46.40	18.08	35.642	0.51
WB-0911-MC-PCB-06	315	320	317.5	46.74	18.36	35.642	0.52
WB-0911-MC-PCB-06	320	325	322.5	45.10	17.52	35.642	0.49
WB-0911-MC-PCB-06	325	330	327.5	48.44	18.73	35.642	0.53
WB-0911-MC-PCB-06	330	335	332.5	45.56	17.91	35.642	0.50
WB-0911-MC-PCB-06	335	340	337.5	49.21	19.39	35.642	0.54
WB-0911-MC-PCB-06	340	345	342.5	45.29	17.77	35.642	0.50
WB-0911-MC-PCB-06	345	350	347.5	49.12	19.47	35.642	0.55
WB-0911-MC-PCB-06	350	355	352.5	45.69	18.23	35.642	0.51
WB-0911-MC-PCB-06	355	360	357.5	47.88	19.27	35.642	0.54
WB-0911-MC-PCB-06	360	365	362.5	50.04	20.29	35.642	0.57
WB-0911-MC-PCB-06	365	370	367.5	49.85	20.68	35.642	0.58
WB-0911-MC-PCB-06	370	375	372.5	37.61	15.96	35.642	0.45
WB-0911-MC-PCB-06	375	Base		51.45	22.25		

Table K.11. Bulk density data for core site WB-0812-MC-DSH-08. Sediment core sub-sample intervals (mm), sub-sample wet weight (g), dry weight (g), sub-sample volume (cm^3), and bulk density (g/cm^3). Note: Blank cell denotes no analysis performed.

Core ID	Top Depth of Interval (mm)	Bottom Depth of Interval (mm)	Average Depth of Interval (mm)	Wet Weight (g)	Dry Weight (g)	Sample Volume (cm^3)	Bulk Density (g/cm^3)
WB-0812-MC-DSH-08	0	2	1	14.92	4.25	14.257	0.30
WB-0812-MC-DSH-08	2	4	3	14.70	4.09	14.257	0.29
WB-0812-MC-DSH-08	4	6	5	18.15	5.05	14.257	0.35
WB-0812-MC-DSH-08	6	8	7	12.55	3.46	14.257	0.24
WB-0812-MC-DSH-08	8	10	9	16.91	4.74	14.257	0.33
WB-0812-MC-DSH-08	10	12	11	17.39	5.00	14.257	0.35
WB-0812-MC-DSH-08	12	14	13	14.05	4.13	14.257	0.29
WB-0812-MC-DSH-08	14	16	15	15.27	4.48	14.257	0.31
WB-0812-MC-DSH-08	16	18	17	16.04	4.80	14.257	0.34
WB-0812-MC-DSH-08	18	20	19	15.53	4.72	14.257	0.33
WB-0812-MC-DSH-08	20	22	21	17.04	5.25	14.257	0.37
WB-0812-MC-DSH-08	22	24	23	18.19	5.74	14.257	0.40
WB-0812-MC-DSH-08	24	26	25	18.18	5.79	14.257	0.41
WB-0812-MC-DSH-08	26	28	27	15.77	5.10	14.257	0.36
WB-0812-MC-DSH-08	28	30	29	19.01	6.23	14.257	0.44
WB-0812-MC-DSH-08	30	32	31	15.62	5.17	14.257	0.36
WB-0812-MC-DSH-08	32	34	33	16.60	5.54	14.257	0.39
WB-0812-MC-DSH-08	34	36	35	17.66	5.96	14.257	0.42
WB-0812-MC-DSH-08	36	38	37	10.46	3.52	14.257	0.25
WB-0812-MC-DSH-08	38	40	39	17.75	6.10	14.257	0.43
WB-0812-MC-DSH-08	40	42	41	14.79	5.14	14.257	0.36
WB-0812-MC-DSH-08	42	44	43	15.66	5.59	14.257	0.39
WB-0812-MC-DSH-08	44	46	45	12.65	4.49	14.257	0.31
WB-0812-MC-DSH-08	46	48	47	17.90	6.48	14.257	0.45
WB-0812-MC-DSH-08	48	50	49	16.31	5.93	14.257	0.42
WB-0812-MC-DSH-08	50	55	52.5	45.12	16.79	35.642	0.47
WB-0812-MC-DSH-08	55	60	57.5	47.15	17.77	35.642	0.50
WB-0812-MC-DSH-08	60	65	62.5	46.09	17.32	35.642	0.49
WB-0812-MC-DSH-08	65	70	67.5	44.82	12.92	35.642	0.36
WB-0812-MC-DSH-08	70	75	72.5	43.10	16.73	35.642	0.47
WB-0812-MC-DSH-08	75	80	77.5	46.33	17.95	35.642	0.50
WB-0812-MC-DSH-08	80	85	82.5	43.57	17.27	35.642	0.48
WB-0812-MC-DSH-08	85	90	87.5	47.85	18.92	35.642	0.53
WB-0812-MC-DSH-08	90	95	92.5	43.83	17.21	35.642	0.48
WB-0812-MC-DSH-08	95	100	97.5	45.17	17.41	35.642	0.49
WB-0812-MC-DSH-08	100	105	102.5	41.99	16.69	35.642	0.47

Table K.11 (Continued).

Core ID	Top Depth of Interval (mm)	Bottom Depth of Interval (mm)	Average Depth of Interval (mm)	Wet Weight (g)	Dry Weight (g)	Sample Volume (cm^3)	Bulk Density (g/cm^3)
WB-0812-MC-DSH-08	105	110	107.5	51.52	20.17	35.642	0.57
WB-0812-MC-DSH-08	110	115	112.5	45.46	17.43	35.642	0.49
WB-0812-MC-DSH-08	115	120	117.5	45.30	17.50	35.642	0.49
WB-0812-MC-DSH-08	120	125	122.5	44.89	17.24	35.642	0.48
WB-0812-MC-DSH-08	125	130	127.5	43.21	16.62	35.642	0.47
WB-0812-MC-DSH-08	130	135	132.5	43.08	16.69	35.642	0.47
WB-0812-MC-DSH-08	135	140	137.5	48.88	18.58	35.642	0.52
WB-0812-MC-DSH-08	140	145	142.5	43.17	16.23	35.642	0.46
WB-0812-MC-DSH-08	145	150	147.5	43.97	16.42	35.642	0.46
WB-0812-MC-DSH-08	150	155	152.5	44.53	16.44	35.642	0.46
WB-0812-MC-DSH-08	155	160	157.5	45.71	16.78	35.642	0.47
WB-0812-MC-DSH-08	160	165	162.5	43.28	15.79	35.642	0.44
WB-0812-MC-DSH-08	165	170	167.5	47.49	17.77	35.642	0.50
WB-0812-MC-DSH-08	170	175	172.5	43.96	16.46	35.642	0.46
WB-0812-MC-DSH-08	175	180	177.5	48.14	18.40	35.642	0.52
WB-0812-MC-DSH-08	180	185	182.5	53.11	20.09	35.642	0.56
WB-0812-MC-DSH-08	185	190	187.5	42.01	15.98	35.642	0.45
WB-0812-MC-DSH-08	190	195	192.5	45.99	17.59	35.642	0.49
WB-0812-MC-DSH-08	195	200	197.5	42.68	16.41	35.642	0.46
WB-0812-MC-DSH-08	200	205	202.5	47.85	18.53	35.642	0.52
WB-0812-MC-DSH-08	205	210	207.5	45.92	17.80	35.642	0.50
WB-0812-MC-DSH-08	210	215	212.5	44.46	17.13	35.642	0.48
WB-0812-MC-DSH-08	215	220	217.5	50.68	19.59	35.642	0.55
WB-0812-MC-DSH-08	220	225	222.5	44.58	17.17	35.642	0.48
WB-0812-MC-DSH-08	225	230	227.5	51.38	19.50	35.642	0.55
WB-0812-MC-DSH-08	230	235	232.5	43.41	16.71	35.642	0.47
WB-0812-MC-DSH-08	235	240	237.5	43.84	16.61	35.642	0.47
WB-0812-MC-DSH-08	240	245	242.5	48.55	18.69	35.642	0.52
WB-0812-MC-DSH-08	245	250	247.5	47.03	17.77	35.642	0.50
WB-0812-MC-DSH-08	250	255	252.5	44.45	16.83	35.642	0.47
WB-0812-MC-DSH-08	255	260	257.5	45.99	17.43	35.642	0.49
WB-0812-MC-DSH-08	260	265	262.5	46.43	17.61	35.642	0.49
WB-0812-MC-DSH-08	265	270	267.5	50.13	19.51	35.642	0.55
WB-0812-MC-DSH-08	270	275	272.5	44.87	17.40	35.642	0.49
WB-0812-MC-DSH-08	275	280	277.5	47.06	18.25	35.642	0.51
WB-0812-MC-DSH-08	280	285	282.5	48.19	18.77	35.642	0.53
WB-0812-MC-DSH-08	285	290	287.5	46.60	17.98	35.642	0.50
WB-0812-MC-DSH-08	290	295	292.5	47.99	18.57	35.642	0.52

Table K.11 (Continued).

Core ID	Top Depth of Interval (mm)	Bottom Depth of Interval (mm)	Average Depth of Interval (mm)	Wet Weight (g)	Dry Weight (g)	Sample Volume (cm^3)	Bulk Density (g/cm^3)
WB-0812-MC-DSH-08	295	300	297.5	48.20	18.79	35.642	0.53
WB-0812-MC-DSH-08	300	305	302.5	46.36	18.22	35.642	0.51
WB-0812-MC-DSH-08	305	310	307.5	51.01	19.94	35.642	0.56
WB-0812-MC-DSH-08	310	315	312.5	46.00	18.17	35.642	0.51
WB-0812-MC-DSH-08	315	320	317.5	42.46	16.91	35.642	0.47
WB-0812-MC-DSH-08	320	325	322.5	51.10	19.91	35.642	0.56
WB-0812-MC-DSH-08	325	330	327.5	44.54	17.51	35.642	0.49
WB-0812-MC-DSH-08	330	335	332.5	50.47	19.76	35.642	0.55
WB-0812-MC-DSH-08	335	340	337.5	49.74	19.81	35.642	0.56
WB-0812-MC-DSH-08	340	345	342.5	45.08	18.06	35.642	0.51
WB-0812-MC-DSH-08	345	350	347.5	38.98	15.69	35.642	0.44
WB-0812-MC-DSH-08	350	Base		61.29	25.28		

Table K.12. Bulk density data for core site WB-0812-MC-DSH-10. Sediment core sub-sample intervals (mm), sub-sample wet weight (g), dry weight (g), sub-sample volume (cm^3), and bulk density (g/cm^3). Note: Blank cell denotes no analysis performed.

Core ID	Top Depth of Interval (mm)	Bottom Depth of Interval (mm)	Average Depth of Interval (mm)	Wet Weight (g)	Dry Weight (g)	Sample Volume (cm^3)	Bulk Density (g/cm^3)
WB-0812-MC-DSH-10	0	2	1	16.10	4.57	14.257	0.32
WB-0812-MC-DSH-10	2	4	3	15.91	4.69	14.257	0.33
WB-0812-MC-DSH-10	4	6	5	15.79	4.71	14.257	0.33
WB-0812-MC-DSH-10	6	8	7	13.53	4.07	14.257	0.29
WB-0812-MC-DSH-10	8	10	9	18.04	5.50	14.257	0.39
WB-0812-MC-DSH-10	10	12	11	9.44	2.93	14.257	0.21
WB-0812-MC-DSH-10	12	14	13	19.06	6.03	14.257	0.42
WB-0812-MC-DSH-10	14	16	15	16.29	5.21	14.257	0.37
WB-0812-MC-DSH-10	16	18	17	17.22	5.60	14.257	0.39
WB-0812-MC-DSH-10	18	20	19	18.13	5.89	14.257	0.41
WB-0812-MC-DSH-10	20	22	21	16.41	5.32	14.257	0.37
WB-0812-MC-DSH-10	22	24	23	16.52	5.32	14.257	0.37
WB-0812-MC-DSH-10	24	26	25	16.52	5.33	14.257	0.37
WB-0812-MC-DSH-10	26	28	27	22.76	7.48	14.257	0.52
WB-0812-MC-DSH-10	28	30	29	15.19	5.00	14.257	0.35
WB-0812-MC-DSH-10	30	35	32.5	44.95	14.75	35.642	0.41
WB-0812-MC-DSH-10	35	40	37.5	43.51	14.60	35.642	0.41
WB-0812-MC-DSH-10	40	45	42.5	44.25	15.04	35.642	0.42
WB-0812-MC-DSH-10	45	50	47.5	45.44	15.34	35.642	0.43
WB-0812-MC-DSH-10	50	55	52.5	43.13	15.09	35.642	0.42
WB-0812-MC-DSH-10	55	60	57.5	47.60	16.96	35.642	0.48
WB-0812-MC-DSH-10	60	65	62.5	43.17	15.50	35.642	0.43
WB-0812-MC-DSH-10	65	70	67.5	41.03	15.16	35.642	0.43
WB-0812-MC-DSH-10	70	75	72.5	43.56	16.32	35.642	0.46
WB-0812-MC-DSH-10	75	80	77.5	50.59	19.56	35.642	0.55
WB-0812-MC-DSH-10	80	85	82.5	44.36	17.18	35.642	0.48
WB-0812-MC-DSH-10	85	90	87.5	46.89	18.45	35.642	0.52
WB-0812-MC-DSH-10	90	95	92.5	47.14	18.76	35.642	0.53
WB-0812-MC-DSH-10	95	100	97.5	43.83	17.59	35.642	0.49
WB-0812-MC-DSH-10	100	105	102.5	47.25	19.01	35.642	0.53
WB-0812-MC-DSH-10	105	110	107.5	50.27	20.28	35.642	0.57
WB-0812-MC-DSH-10	110	115	112.5	48.89	19.77	35.642	0.55
WB-0812-MC-DSH-10	115	120	117.5	57.68	23.16	35.642	0.65
WB-0812-MC-DSH-10	120	125	122.5	42.70	17.24	35.642	0.48
WB-0812-MC-DSH-10	125	130	127.5	38.04	15.16	35.642	0.43
WB-0812-MC-DSH-10	130	135	132.5	51.10	20.45	35.642	0.57

Table K.12 (Continued).

Core ID	Top Depth of Interval (mm)	Bottom Depth of Interval (mm)	Average Depth of Interval (mm)	Wet Weight (g)	Dry Weight (g)	Sample Volume (cm^3)	Bulk Density (g/cm^3)
WB-0812-MC-DSH-10	135	140	137.5	41.82	16.52	35.642	0.46
WB-0812-MC-DSH-10	140	145	142.5	47.86	19.01	35.642	0.53
WB-0812-MC-DSH-10	145	150	147.5	42.69	17.02	35.642	0.48
WB-0812-MC-DSH-10	150	155	152.5	50.50	20.05	35.642	0.56
WB-0812-MC-DSH-10	155	160	157.5	43.51	16.96	35.642	0.48
WB-0812-MC-DSH-10	160	165	162.5	52.95	20.55	35.642	0.58
WB-0812-MC-DSH-10	165	170	167.5	42.67	16.22	35.642	0.46
WB-0812-MC-DSH-10	170	175	172.5	49.50	18.66	35.642	0.52
WB-0812-MC-DSH-10	175	180	177.5	47.10	17.69	35.642	0.50
WB-0812-MC-DSH-10	180	185	182.5	45.93	17.13	35.642	0.48
WB-0812-MC-DSH-10	185	190	187.5	47.04	17.51	35.642	0.49
WB-0812-MC-DSH-10	190	195	192.5	44.86	16.62	35.642	0.47
WB-0812-MC-DSH-10	195	200	197.5	44.99	16.65	35.642	0.47
WB-0812-MC-DSH-10	200	205	202.5	46.55	17.15	35.642	0.48
WB-0812-MC-DSH-10	205	210	207.5	46.18	16.80	35.642	0.47
WB-0812-MC-DSH-10	210	215	212.5	45.10	16.56	35.642	0.46
WB-0812-MC-DSH-10	215	220	217.5	46.23	17.07	35.642	0.48
WB-0812-MC-DSH-10	220	225	222.5	43.94	16.15	35.642	0.45
WB-0812-MC-DSH-10	225	230	227.5	48.75	17.90	35.642	0.50
WB-0812-MC-DSH-10	230	235	232.5	45.48	16.83	35.642	0.47
WB-0812-MC-DSH-10	235	240	237.5	46.77	17.57	35.642	0.49
WB-0812-MC-DSH-10	240	245	242.5	46.58	17.33	35.642	0.49
WB-0812-MC-DSH-10	245	250	247.5	44.86	16.93	35.642	0.48
WB-0812-MC-DSH-10	250	255	252.5	46.63	17.37	35.642	0.49
WB-0812-MC-DSH-10	255	260	257.5	47.35	17.57	35.642	0.49
WB-0812-MC-DSH-10	260	265	262.5	46.74	17.45	35.642	0.49
WB-0812-MC-DSH-10	265	270	267.5	45.56	16.98	35.642	0.48
WB-0812-MC-DSH-10	270	275	272.5	46.79	17.46	35.642	0.49
WB-0812-MC-DSH-10	275	280	277.5	44.67	16.67	35.642	0.47
WB-0812-MC-DSH-10	280	285	282.5	48.15	18.11	35.642	0.51
WB-0812-MC-DSH-10	285	290	287.5	46.46	17.35	35.642	0.49
WB-0812-MC-DSH-10	290	295	292.5	45.58	17.16	35.642	0.48
WB-0812-MC-DSH-10	295	300	297.5	48.20	18.88	35.642	0.53
WB-0812-MC-DSH-10	300	305	302.5	46.92	18.01	35.642	0.51
WB-0812-MC-DSH-10	305	310	307.5	46.43	17.81	35.642	0.50
WB-0812-MC-DSH-10	310	315	312.5	48.92	18.82	35.642	0.53
WB-0812-MC-DSH-10	315	320	317.5	45.84	17.76	35.642	0.50
WB-0812-MC-DSH-10	320	325	322.5	46.53	18.12	35.642	0.51

Table K.12 (Continued).

Core ID	Top Depth of Interval (mm)	Bottom Depth of Interval (mm)	Average Depth of Interval (mm)	Wet Weight (g)	Dry Weight (g)	Sample Volume (cm^3)	Bulk Density (g/cm^3)
WB-0812-MC-DSH-10	325	330	327.5	46.47	18.19	35.642	0.51
WB-0812-MC-DSH-10	330	335	332.5	47.57	18.54	35.642	0.52
WB-0812-MC-DSH-10	335	340	337.5	49.39	19.16	35.642	0.54
WB-0812-MC-DSH-10	340	345	342.5	44.98	17.36	35.642	0.49
WB-0812-MC-DSH-10	345	350	347.5	47.26	18.10	35.642	0.51
WB-0812-MC-DSH-10	350	355	352.5	46.94	18.36	35.642	0.52
WB-0812-MC-DSH-10	355	360	357.5	47.33	18.58	35.642	0.52
WB-0812-MC-DSH-10	360	365	362.5	49.15	19.36	35.642	0.54
WB-0812-MC-DSH-10	365	Base		32.09	12.81		

Table K.13. Bulk density data for core site WB-0812-MC-PCB-06. Sediment core sub-sample intervals (mm), sub-sample wet weight (g), dry weight (g), sub-sample volume (cm^3), and bulk density (g/cm^3). Note: Blank cell denotes no analysis performed.

Core ID	Top Depth of Interval (mm)	Bottom Depth of Interval (mm)	Average Depth of Interval (mm)	Wet Weight (g)	Dry Weight (g)	Sample Volume (cm^3)	Bulk Density (g/cm^3)
WB-0812-MC-PCB-06	0	2	1	16.50	4.54	14.257	0.32
WB-0812-MC-PCB-06	2	4	3	17.09	4.72	14.257	0.33
WB-0812-MC-PCB-06	4	6	5	14.70	4.03	14.257	0.28
WB-0812-MC-PCB-06	6	8	7	21.53	5.89	14.257	0.41
WB-0812-MC-PCB-06	8	10	9	14.28	3.92	14.257	0.27
WB-0812-MC-PCB-06	10	12	11	18.70	5.16	14.257	0.36
WB-0812-MC-PCB-06	12	14	13	13.78	3.83	14.257	0.27
WB-0812-MC-PCB-06	14	16	15	22.21	6.36	14.257	0.45
WB-0812-MC-PCB-06	16	18	17	18.46	5.10	14.257	0.36
WB-0812-MC-PCB-06	18	20	19	19.98	5.56	14.257	0.39
WB-0812-MC-PCB-06	20	22	21	21.02	6.31	14.257	0.44
WB-0812-MC-PCB-06	22	24	23	11.40	3.22	14.257	0.23
WB-0812-MC-PCB-06	24	26	25	17.04	4.92	14.257	0.35
WB-0812-MC-PCB-06	26	28	27	17.02	5.07	14.257	0.36
WB-0812-MC-PCB-06	28	30	29	16.92	5.09	14.257	0.36
WB-0812-MC-PCB-06	30	32	31	17.35	5.28	14.257	0.37
WB-0812-MC-PCB-06	32	34	33	14.33	4.42	14.257	0.31
WB-0812-MC-PCB-06	34	36	35	18.66	5.96	14.257	0.42
WB-0812-MC-PCB-06	36	38	37	17.45	5.63	14.257	0.39
WB-0812-MC-PCB-06	38	40	39	16.94	5.39	14.257	0.38
WB-0812-MC-PCB-06	40	45	42.5	45.23	25.17	35.642	0.71
WB-0812-MC-PCB-06	45	50	47.5	40.14	12.84	35.642	0.36
WB-0812-MC-PCB-06	50	55	52.5	48.28	15.63	35.642	0.44
WB-0812-MC-PCB-06	55	60	57.5	39.77	17.92	35.642	0.50
WB-0812-MC-PCB-06	60	65	62.5	43.47	14.35	35.642	0.40
WB-0812-MC-PCB-06	65	70	67.5	43.90	24.09	35.642	0.68
WB-0812-MC-PCB-06	70	75	72.5	48.42	31.73	35.642	0.89
WB-0812-MC-PCB-06	75	80	77.5	45.27	22.69	35.642	0.64
WB-0812-MC-PCB-06	80	85	82.5	40.75	21.86	35.642	0.61
WB-0812-MC-PCB-06	85	90	87.5	50.62	32.32	35.642	0.91
WB-0812-MC-PCB-06	90	95	92.5	45.20	21.89	35.642	0.61
WB-0812-MC-PCB-06	95	100	97.5	43.77	17.72	35.642	0.50
WB-0812-MC-PCB-06	100	105	102.5	33.71	13.76	35.642	0.39
WB-0812-MC-PCB-06	105	110	107.5	50.11	18.34	35.642	0.51
WB-0812-MC-PCB-06	110	115	112.5	45.25	20.93	35.642	0.59
WB-0812-MC-PCB-06	115	120	117.5	52.10	32.10	35.642	0.90

Table K.13 (Continued).

Core ID	Top Depth of Interval (mm)	Bottom Depth of Interval (mm)	Average Depth of Interval (mm)	Wet Weight (g)	Dry Weight (g)	Sample Volume (cm^3)	Bulk Density (g/cm^3)
WB-0812-MC-PCB-06	120	125	122.5	50.93	30.30	35.642	0.85
WB-0812-MC-PCB-06	125	130	127.5	38.81	23.17	35.642	0.65
WB-0812-MC-PCB-06	130	135	132.5	52.33	27.24	35.642	0.76
WB-0812-MC-PCB-06	135	140	137.5	39.54	19.42	35.642	0.54
WB-0812-MC-PCB-06	140	145	142.5	42.96	16.15	35.642	0.45
WB-0812-MC-PCB-06	145	150	147.5	40.48	18.30	35.642	0.51
WB-0812-MC-PCB-06	150	155	152.5	47.27	27.41	35.642	0.77
WB-0812-MC-PCB-06	155	160	157.5	42.67	19.42	35.642	0.54
WB-0812-MC-PCB-06	160	165	162.5	47.84	20.11	35.642	0.56
WB-0812-MC-PCB-06	165	170	167.5	43.38	15.56	35.642	0.44
WB-0812-MC-PCB-06	170	175	172.5	45.83	16.75	35.642	0.47
WB-0812-MC-PCB-06	175	180	177.5	48.39	19.99	35.642	0.56
WB-0812-MC-PCB-06	180	185	182.5	43.80	15.98	35.642	0.45
WB-0812-MC-PCB-06	185	190	187.5	46.38	17.88	35.642	0.50
WB-0812-MC-PCB-06	190	195	192.5	48.95	19.65	35.642	0.55
WB-0812-MC-PCB-06	195	200	197.5	47.76	21.84	35.642	0.61
WB-0812-MC-PCB-06	200	205	202.5	44.86	19.55	35.642	0.55
WB-0812-MC-PCB-06	205	210	207.5	48.51	22.13	35.642	0.62
WB-0812-MC-PCB-06	210	215	212.5	40.57	18.61	35.642	0.52
WB-0812-MC-PCB-06	215	220	217.5	43.04	18.56	35.642	0.52
WB-0812-MC-PCB-06	220	225	222.5	46.16	22.27	35.642	0.62
WB-0812-MC-PCB-06	225	230	227.5	44.42	18.52	35.642	0.52
WB-0812-MC-PCB-06	230	235	232.5	44.88	16.43	35.642	0.46
WB-0812-MC-PCB-06	235	240	237.5	41.01	20.94	35.642	0.59
WB-0812-MC-PCB-06	240	245	242.5	46.83	17.24	35.642	0.48
WB-0812-MC-PCB-06	245	250	247.5	44.74	20.26	35.642	0.57
WB-0812-MC-PCB-06	250	255	252.5	45.29	27.01	35.642	0.76
WB-0812-MC-PCB-06	255	260	257.5	42.56	15.71	35.642	0.44
WB-0812-MC-PCB-06	260	265	262.5	43.47	16.08	35.642	0.45
WB-0812-MC-PCB-06	265	270	267.5	42.14	15.62	35.642	0.44
WB-0812-MC-PCB-06	270	275	272.5	43.71	16.15	35.642	0.45
WB-0812-MC-PCB-06	275	280	277.5	41.84	15.22	35.642	0.43
WB-0812-MC-PCB-06	280	285	282.5	48.90	17.60	35.642	0.49
WB-0812-MC-PCB-06	285	290	287.5	43.47	15.69	35.642	0.44
WB-0812-MC-PCB-06	290	295	292.5	45.36	16.84	35.642	0.47
WB-0812-MC-PCB-06	295	300	297.5	44.51	16.15	35.642	0.45
WB-0812-MC-PCB-06	300	305	302.5	48.59	17.62	35.642	0.49
WB-0812-MC-PCB-06	305	310	307.5	43.31	15.63	35.642	0.44

Table K.13 (Continued).

Core ID	Top Depth of Interval (mm)	Bottom Depth of Interval (mm)	Average Depth of Interval (mm)	Wet Weight (g)	Dry Weight (g)	Sample Volume (cm^3)	Bulk Density (g/cm^3)
WB-0812-MC-PCB-06	310	315	312.5	46.51	16.83	35.642	0.47
WB-0812-MC-PCB-06	315	320	317.5	43.38	15.80	35.642	0.44
WB-0812-MC-PCB-06	320	325	322.5	49.15	18.03	35.642	0.51
WB-0812-MC-PCB-06	325	330	327.5	47.64	17.54	35.642	0.49
WB-0812-MC-PCB-06	330	335	332.5	48.23	17.82	35.642	0.50
WB-0812-MC-PCB-06	335	340	337.5	50.69	18.99	35.642	0.53
WB-0812-MC-PCB-06	340	345	342.5	49.09	19.10	35.642	0.54
WB-0812-MC-PCB-06	345	350	347.5	46.45	21.35	35.642	0.60
WB-0812-MC-PCB-06	350	355	352.5	44.68	17.30	35.642	0.49
WB-0812-MC-PCB-06	355	360	357.5	49.85	20.79	35.642	0.58
WB-0812-MC-PCB-06	360	365	362.5	47.57	22.86	35.642	0.64
WB-0812-MC-PCB-06	365	370	367.5	45.98	19.82	35.642	0.56
WB-0812-MC-PCB-06	370	375	372.5	49.52	19.44	35.642	0.55
WB-0812-MC-PCB-06	375	380	377.5	47.58	18.47	35.642	0.52
WB-0812-MC-PCB-06	380	385	382.5	42.89	17.03	35.642	0.48
WB-0812-MC-PCB-06	385	390	387.5	45.83	17.92	35.642	0.50
WB-0812-MC-PCB-06	390	395	392.5	48.27	18.97	35.642	0.53
WB-0812-MC-PCB-06	395	400	397.5	47.82	18.77	35.642	0.53
WB-0812-MC-PCB-06	400	405	402.5	37.87	15.08	35.642	0.42
WB-0812-MC-PCB-06	405	410	407.5	49.07	19.16	35.642	0.54
WB-0812-MC-PCB-06	410	415	412.5	47.95	18.86	35.642	0.53
WB-0812-MC-PCB-06	415	420	417.5	55.44	21.57	35.642	0.61
WB-0812-MC-PCB-06	420	425	422.5	38.74	15.24	35.642	0.43
WB-0812-MC-PCB-06	425	430	427.5	44.84	17.83	35.642	0.50
WB-0812-MC-PCB-06	430	Base		37.42	14.99		

Table K.14. Bulk density data for core site WB-1012-MC-04. Sediment core sub-sample intervals (mm), sub-sample wet weight (g), dry weight (g), sub-sample volume (cm^3), and bulk density (g/cm^3). Note: Blank cell denotes no analysis performed.

Core ID	Top Depth of Interval (mm)	Bottom Depth of Interval (mm)	Average Depth of Interval (mm)	Wet Weight (g)	Dry Weight (g)	Sample Volume (cm^3)	Bulk Density (g/cm^3)
WB-1012-MC-04	0	2	1	16.31	3.93	14.257	0.28
WB-1012-MC-04	2	4	3	17.32	4.43	14.257	0.31
WB-1012-MC-04	4	6	5	16.24	4.24	14.257	0.30
WB-1012-MC-04	6	8	7	17.12	4.59	14.257	0.32
WB-1012-MC-04	8	10	9	17.83	4.88	14.257	0.34
WB-1012-MC-04	10	12	11	16.98	4.73	14.257	0.33
WB-1012-MC-04	12	14	13	17.38	4.98	14.257	0.35
WB-1012-MC-04	14	16	15	17.57	5.18	14.257	0.36
WB-1012-MC-04	16	18	17	17.86	5.42	14.257	0.38
WB-1012-MC-04	18	20	19	16.37	5.10	14.257	0.36
WB-1012-MC-04	20	22	21	17.04	5.45	14.257	0.38
WB-1012-MC-04	22	24	23	17.98	5.76	14.257	0.40
WB-1012-MC-04	24	26	25	17.71	5.88	14.257	0.41
WB-1012-MC-04	26	28	27	19.85	6.60	14.257	0.46
WB-1012-MC-04	28	30	29	17.82	5.95	14.257	0.42
WB-1012-MC-04	30	35	32.5	43.64	14.78	35.642	0.41
WB-1012-MC-04	35	40	37.5	45.57	15.92	35.642	0.45
WB-1012-MC-04	40	45	42.5	46.87	16.46	35.642	0.46
WB-1012-MC-04	45	50	47.5	47.27	16.97	35.642	0.48
WB-1012-MC-04	50	55	52.5	45.98	16.24	35.642	0.46
WB-1012-MC-04	55	60	57.5	45.89	16.67	35.642	0.47
WB-1012-MC-04	60	65	62.5	46.34	17.08	35.642	0.48
WB-1012-MC-04	65	70	67.5	43.39	15.98	35.642	0.45
WB-1012-MC-04	70	75	72.5	48.28	17.80	35.642	0.50
WB-1012-MC-04	75	80	77.5	45.76	17.26	35.642	0.48
WB-1012-MC-04	80	85	82.5	46.56	17.72	35.642	0.50
WB-1012-MC-04	85	90	87.5	47.35	18.07	35.642	0.51
WB-1012-MC-04	90	95	92.5	45.66	17.47	35.642	0.49
WB-1012-MC-04	95	100	97.5	48.45	19.03	35.642	0.53
WB-1012-MC-04	100	105	102.5	44.79	17.80	35.642	0.50
WB-1012-MC-04	105	110	107.5	48.50	19.21	35.642	0.54
WB-1012-MC-04	110	115	112.5	48.06	18.70	35.642	0.52
WB-1012-MC-04	115	120	117.5	47.96	19.49	35.642	0.55
WB-1012-MC-04	120	125	122.5	45.57	18.81	35.642	0.53
WB-1012-MC-04	125	130	127.5	47.34	19.63	35.642	0.55
WB-1012-MC-04	130	135	132.5	52.06	21.40	35.642	0.60

Table K.14 (Continued).

Core ID	Top Depth of Interval (mm)	Bottom Depth of Interval (mm)	Average Depth of Interval (mm)	Wet Weight (g)	Dry Weight (g)	Sample Volume (cm^3)	Bulk Density (g/cm^3)
WB-1012-MC-04	135	140	137.5	48.36	20.25	35.642	0.57
WB-1012-MC-04	140	145	142.5	52.39	21.81	35.642	0.61
WB-1012-MC-04	145	150	147.5	43.06	17.77	35.642	0.50
WB-1012-MC-04	150	155	152.5	46.63	18.74	35.642	0.53
WB-1012-MC-04	155	160	157.5	46.03	19.21	35.642	0.54
WB-1012-MC-04	160	165	162.5	47.96	19.43	35.642	0.55
WB-1012-MC-04	165	170	167.5	49.00	20.02	35.642	0.56
WB-1012-MC-04	170	175	172.5	47.38	19.48	35.642	0.55
WB-1012-MC-04	175	180	177.5	46.47	19.43	35.642	0.55
WB-1012-MC-04	180	185	182.5	52.04	22.16	35.642	0.62
WB-1012-MC-04	185	190	187.5	48.29	20.50	35.642	0.58
WB-1012-MC-04	190	195	192.5	48.55	21.09	35.642	0.59
WB-1012-MC-04	195	200	197.5	48.62	21.17	35.642	0.59
WB-1012-MC-04	200	205	202.5	49.02	21.86	35.642	0.61
WB-1012-MC-04	205	210	207.5	45.69	20.73	35.642	0.58
WB-1012-MC-04	210	215	212.5	52.29	23.68	35.642	0.66
WB-1012-MC-04	215	220	217.5	52.24	23.98	35.642	0.67
WB-1012-MC-04	220	225	222.5	53.28	24.70	35.642	0.69
WB-1012-MC-04	225	230	227.5	52.18	24.21	35.642	0.68
WB-1012-MC-04	230	235	232.5	46.86	20.98	35.642	0.59
WB-1012-MC-04	235	240	237.5	54.02	24.47	35.642	0.69
WB-1012-MC-04	240	245	242.5	49.88	22.26	35.642	0.62
WB-1012-MC-04	245	250	247.5	45.61	20.46	35.642	0.57
WB-1012-MC-04	250	255	252.5	52.70	23.35	35.642	0.66
WB-1012-MC-04	255	260	257.5	48.16	21.64	35.642	0.61
WB-1012-MC-04	260	265	262.5	50.29	22.53	35.642	0.63
WB-1012-MC-04	265	270	267.5	46.03	20.99	35.642	0.59
WB-1012-MC-04	270	275	272.5	49.48	22.40	35.642	0.63
WB-1012-MC-04	275	280	277.5	49.95	23.13	35.642	0.65
WB-1012-MC-04	280	285	282.5	52.45	24.37	35.642	0.68
WB-1012-MC-04	285	290	287.5	51.75	24.09	35.642	0.68
WB-1012-MC-04	290	295	292.5	51.10	24.58	35.642	0.69
WB-1012-MC-04	295	300	297.5	48.98	22.86	35.642	0.64
WB-1012-MC-04	300	305	302.5	54.10	25.32	35.642	0.71
WB-1012-MC-04	305	310	307.5	50.21	23.70	35.642	0.66
WB-1012-MC-04	310	315	312.5	53.87	25.22	35.642	0.71
WB-1012-MC-04	315	320	317.5	52.74	24.92	35.642	0.70
WB-1012-MC-04	320	325	322.5	53.47	25.25	35.642	0.71

Table K.14 (Continued).

Core ID	Top Depth of Interval (mm)	Bottom Depth of Interval (mm)	Average Depth of Interval (mm)	Wet Weight (g)	Dry Weight (g)	Sample Volume (cm^3)	Bulk Density (g/cm^3)
WB-1012-MC-04	325	330	327.5	45.81	21.42	35.642	0.60
WB-1012-MC-04	330	Base		40.42	18.65		

Table K.15. Bulk density data for core site WB-0813-MC-04. Sediment core sub-sample intervals (mm), sub-sample wet weight (g), dry weight (g), sub-sample volume (cm^3), and bulk density (g/cm^3). Note: Blank cell denotes no analysis performed.

Core ID	Top Depth of Interval (mm)	Bottom Depth of Interval (mm)	Average Depth of Interval (mm)	Wet Weight (g)	Dry Weight (g)	Sample Volume (cm^3)	Bulk Density (g/cm^3)
WB-0813-MC-04	0	2	1	15.93	2.53	14.257	0.18
WB-0813-MC-04	2	4	3	11.44	2.85	14.257	0.20
WB-0813-MC-04	4	6	5	14.29	4.34	14.257	0.30
WB-0813-MC-04	6	8	7	14.74	4.65	14.257	0.33
WB-0813-MC-04	8	10	9	20.68	6.62	14.257	0.46
WB-0813-MC-04	10	14	12	30.74	10.09	28.514	0.35
WB-0813-MC-04	14	16	15	16.22	5.35	14.257	0.38
WB-0813-MC-04	16	18	17	16.69	5.63	14.257	0.39
WB-0813-MC-04	18	20	19	16.97	5.79	14.257	0.41
WB-0813-MC-04	20	22	21	17.46	6.07	14.257	0.43
WB-0813-MC-04	22	24	23	18.89	6.58	14.257	0.46
WB-0813-MC-04	24	26	25	19.60	6.88	14.257	0.48
WB-0813-MC-04	26	28	27	17.59	6.18	14.257	0.43
WB-0813-MC-04	28	30	29	17.84	6.30	14.257	0.44
WB-0813-MC-04	30	32	31	18.58	6.60	14.257	0.46
WB-0813-MC-04	32	34	33	17.51	6.22	14.257	0.44
WB-0813-MC-04	34	36	35	19.49	6.89	14.257	0.48
WB-0813-MC-04	36	38	37	17.46	6.16	14.257	0.43
WB-0813-MC-04	38	40	39	19.07	6.75	14.257	0.47
WB-0813-MC-04	40	42	41	18.18	6.47	14.257	0.45
WB-0813-MC-04	42	47	44.5	46.35	13.72	35.642	0.38
WB-0813-MC-04	47	52	49.5	44.71	16.24	35.642	0.46
WB-0813-MC-04	52	57	54.5	45.40	16.86	35.642	0.47
WB-0813-MC-04	57	62	59.5	42.62	16.08	35.642	0.45
WB-0813-MC-04	62	67	64.5	43.06	16.52	35.642	0.46
WB-0813-MC-04	67	72	69.5	43.22	16.92	35.642	0.47
WB-0813-MC-04	72	77	74.5	49.70	19.64	35.642	0.55
WB-0813-MC-04	77	82	79.5	49.73	19.19	35.642	0.54
WB-0813-MC-04	82	87	84.5	49.91	19.23	35.642	0.54
WB-0813-MC-04	87	92	89.5	48.79	18.97	35.642	0.53
WB-0813-MC-04	92	97	94.5	45.59	17.81	35.642	0.50
WB-0813-MC-04	97	102	99.5	41.95	16.72	35.642	0.47
WB-0813-MC-04	102	107	104.5	45.95	18.12	35.642	0.51
WB-0813-MC-04	107	112	109.5	49.28	19.97	35.642	0.56
WB-0813-MC-04	112	117	114.5	45.06	18.46	35.642	0.52
WB-0813-MC-04	117	122	119.5	45.43	18.55	35.642	0.52

Table K.15 (Continued).

Core ID	Top Depth of Interval (mm)	Bottom Depth of Interval (mm)	Average Depth of Interval (mm)	Wet Weight (g)	Dry Weight (g)	Sample Volume (cm^3)	Bulk Density (g/cm^3)
WB-0813-MC-04	122	127	124.5	47.49	19.61	35.642	0.55
WB-0813-MC-04	127	132	129.5	46.70	19.18	35.642	0.54
WB-0813-MC-04	132	137	134.5	49.28	20.45	35.642	0.57
WB-0813-MC-04	137	142	139.5	50.25	20.91	35.642	0.59
WB-0813-MC-04	142	147	144.5	48.07	19.64	35.642	0.55
WB-0813-MC-04	147	152	149.5	50.92	20.66	35.642	0.58
WB-0813-MC-04	152	157	154.5	41.52	16.70	35.642	0.47
WB-0813-MC-04	157	162	159.5	48.32	19.48	35.642	0.55
WB-0813-MC-04	162	167	164.5	47.57	19.71	35.642	0.55
WB-0813-MC-04	167	172	169.5	48.82	20.69	35.642	0.58
WB-0813-MC-04	172	177	174.5	47.37	19.95	35.642	0.56
WB-0813-MC-04	177	182	179.5	43.41	18.10	35.642	0.51
WB-0813-MC-04	182	187	184.5	47.89	20.43	35.642	0.57
WB-0813-MC-04	187	192	189.5	37.52	16.55	35.642	0.46
WB-0813-MC-04	192	197	194.5	42.32	18.89	35.642	0.53
WB-0813-MC-04	197	202	199.5	68.74	30.44	35.642	0.85
WB-0813-MC-04	202	207	204.5	45.69	20.25	35.642	0.57
WB-0813-MC-04	207	212	209.5	49.39	21.59	35.642	0.61
WB-0813-MC-04	212	217	214.5	50.08	21.85	35.642	0.61
WB-0813-MC-04	217	222	219.5	48.67	21.36	35.642	0.60
WB-0813-MC-04	222	227	224.5	48.57	21.16	35.642	0.59
WB-0813-MC-04	227	232	229.5	48.71	21.32	35.642	0.60
WB-0813-MC-04	232	237	234.5	48.66	21.17	35.642	0.59
WB-0813-MC-04	237	242	239.5	47.81	20.91	35.642	0.59
WB-0813-MC-04	242	247	244.5	52.43	23.00	35.642	0.65
WB-0813-MC-04	247	252	249.5	46.83	20.66	35.642	0.58
WB-0813-MC-04	252	257	254.5	46.23	20.56	35.642	0.58
WB-0813-MC-04	257	262	259.5	47.97	21.45	35.642	0.60
WB-0813-MC-04	262	267	264.5	53.72	24.29	35.642	0.68
WB-0813-MC-04	267	272	269.5	50.54	22.76	35.642	0.64
WB-0813-MC-04	272	277	274.5	45.03	20.32	35.642	0.57
WB-0813-MC-04	277	282	279.5	48.88	21.98	35.642	0.62
WB-0813-MC-04	282	287	284.5	52.62	23.46	35.642	0.66
WB-0813-MC-04	287	292	289.5	54.27	24.41	35.642	0.68
WB-0813-MC-04	292	297	294.5	46.29	20.70	35.642	0.58
WB-0813-MC-04	297	302	299.5	45.17	20.16	35.642	0.57
WB-0813-MC-04	302	307	304.5	47.60	21.64	35.642	0.61
WB-0813-MC-04	307	312	309.5	48.88	22.47	35.642	0.63

Table K.15 (Continued).

Core ID	Top Depth of Interval (mm)	Bottom Depth of Interval (mm)	Average Depth of Interval (mm)	Wet Weight (g)	Dry Weight (g)	Sample Volume (cm^3)	Bulk Density (g/cm^3)
WB-0813-MC-04	312	317	314.5	51.34	23.88	35.642	0.67
WB-0813-MC-04	317	322	319.5	50.78	23.67	35.642	0.66
WB-0813-MC-04	322	327	324.5	50.24	23.30	35.642	0.65
WB-0813-MC-04	327	332	329.5	50.36	23.55	35.642	0.66
WB-0813-MC-04	332	337	334.5	54.85	26.22	35.642	0.74
WB-0813-MC-04	337	342	339.5	50.90	24.57	35.642	0.69
WB-0813-MC-04	342	347	344.5	49.92	23.97	35.642	0.67
WB-0813-MC-04	347	352	349.5	47.93	23.03	35.642	0.65
WB-0813-MC-04	352	Base		57.03	27.68		

Table K.16. Bulk density data for core site WB-0813-MC-DSH-08. Sediment core sub-sample intervals (mm), sub-sample wet weight (g), dry weight (g), sub-sample volume (cm^3), and bulk density (g/cm^3). Note: Blank cell denotes no analysis performed.

Core ID	Top Depth of Interval (mm)	Bottom Depth of Interval (mm)	Average Depth of Interval (mm)	Wet Weight (g)	Dry Weight (g)	Sample Volume (cm^3)	Bulk Density (g/cm^3)
WB-0813-MC-DSH-08	0	2	1	16.65	2.73	14.257	0.19
WB-0813-MC-DSH-08	2	4	3	17.69	3.97	14.257	0.28
WB-0813-MC-DSH-08	4	6	5	14.23	3.41	14.257	0.24
WB-0813-MC-DSH-08	6	8	7	14.72	3.73	14.257	0.26
WB-0813-MC-DSH-08	8	10	9	17.52	4.59	14.257	0.32
WB-0813-MC-DSH-08	10	12	11	15.70	4.10	14.257	0.29
WB-0813-MC-DSH-08	12	14	13	18.16	4.67	14.257	0.33
WB-0813-MC-DSH-08	14	16	15	16.56	4.34	14.257	0.30
WB-0813-MC-DSH-08	16	18	17	17.38	4.51	14.257	0.32
WB-0813-MC-DSH-08	18	20	19	16.46	4.46	14.257	0.31
WB-0813-MC-DSH-08	20	22	21	16.30	4.35	14.257	0.31
WB-0813-MC-DSH-08	22	24	23	18.10	4.84	14.257	0.34
WB-0813-MC-DSH-08	24	26	25	16.31	4.36	14.257	0.31
WB-0813-MC-DSH-08	26	28	27	20.30	5.53	14.257	0.39
WB-0813-MC-DSH-08	28	30	29	16.17	4.52	14.257	0.32
WB-0813-MC-DSH-08	30	35	32.5	43.72	12.22	35.642	0.34
WB-0813-MC-DSH-08	35	40	37.5	41.80	12.50	35.642	0.35
WB-0813-MC-DSH-08	40	45	42.5	44.82	13.92	35.642	0.39
WB-0813-MC-DSH-08	45	50	47.5	41.42	13.20	35.642	0.37
WB-0813-MC-DSH-08	50	55	52.5	46.20	14.69	35.642	0.41
WB-0813-MC-DSH-08	55	60	57.5	47.18	17.77	35.642	0.50
WB-0813-MC-DSH-08	60	65	62.5	41.27	14.49	35.642	0.41
WB-0813-MC-DSH-08	65	70	67.5	45.29	15.27	35.642	0.43
WB-0813-MC-DSH-08	70	75	72.5	45.46	16.03	35.642	0.45
WB-0813-MC-DSH-08	75	80	77.5	44.29	15.98	35.642	0.45
WB-0813-MC-DSH-08	80	85	82.5	46.43	17.69	35.642	0.50
WB-0813-MC-DSH-08	85	90	87.5	45.89	19.32	35.642	0.54
WB-0813-MC-DSH-08	90	95	92.5	44.28	16.85	35.642	0.47
WB-0813-MC-DSH-08	95	100	97.5	53.98	21.06	35.642	0.59
WB-0813-MC-DSH-08	100	105	102.5	41.08	15.86	35.642	0.44
WB-0813-MC-DSH-08	105	110	107.5	51.79	20.71	35.642	0.58
WB-0813-MC-DSH-08	110	115	112.5	47.93	8.00	35.642	0.22
WB-0813-MC-DSH-08	115	120	117.5	40.41	14.95	35.642	0.42
WB-0813-MC-DSH-08	120	125	122.5	48.22	18.54	35.642	0.52
WB-0813-MC-DSH-08	125	130	127.5	47.99	18.04	35.642	0.51
WB-0813-MC-DSH-08	130	135	132.5	46.67	17.43	35.642	0.49

Table K.16 (Continued).

Core ID	Top Depth of Interval (mm)	Bottom Depth of Interval (mm)	Average Depth of Interval (mm)	Wet Weight (g)	Dry Weight (g)	Sample Volume (cm^3)	Bulk Density (g/cm^3)
WB-0813-MC-DSH-08	135	140	137.5	47.19	17.58	35.642	0.49
WB-0813-MC-DSH-08	140	145	142.5	49.10	18.57	35.642	0.52
WB-0813-MC-DSH-08	145	155	150	92.77	39.37	71.284	0.55
WB-0813-MC-DSH-08	155	160	157.5	40.78	15.45	35.642	0.43
WB-0813-MC-DSH-08	160	165	162.5	48.40	18.42	35.642	0.52
WB-0813-MC-DSH-08	165	170	167.5	40.48	15.60	35.642	0.44
WB-0813-MC-DSH-08	170	175	172.5	51.69	19.57	35.642	0.55
WB-0813-MC-DSH-08	175	180	177.5	43.02	16.31	35.642	0.46
WB-0813-MC-DSH-08	180	185	182.5	50.16	19.18	35.642	0.54
WB-0813-MC-DSH-08	185	190	187.5	42.92	16.49	35.642	0.46
WB-0813-MC-DSH-08	190	195	192.5	52.91	19.79	35.642	0.56
WB-0813-MC-DSH-08	195	200	197.5	43.84	16.72	35.642	0.47
WB-0813-MC-DSH-08	200	205	202.5	52.95	19.89	35.642	0.56
WB-0813-MC-DSH-08	205	210	207.5	48.68	17.76	35.642	0.50
WB-0813-MC-DSH-08	210	215	212.5	44.63	16.26	35.642	0.46
WB-0813-MC-DSH-08	215	220	217.5	41.46	15.10	35.642	0.42
WB-0813-MC-DSH-08	220	225	222.5	49.95	18.53	35.642	0.52
WB-0813-MC-DSH-08	225	230	227.5	46.08	16.95	35.642	0.48
WB-0813-MC-DSH-08	230	235	232.5	44.62	16.41	35.642	0.46
WB-0813-MC-DSH-08	235	240	237.5	48.90	17.45	35.642	0.49
WB-0813-MC-DSH-08	240	245	242.5	53.20	19.52	35.642	0.55
WB-0813-MC-DSH-08	245	250	247.5	41.16	14.53	35.642	0.41
WB-0813-MC-DSH-08	250	255	252.5	47.32	16.72	35.642	0.47
WB-0813-MC-DSH-08	255	260	257.5	43.71	15.27	35.642	0.43
WB-0813-MC-DSH-08	260	265	262.5	49.18	19.97	35.642	0.56
WB-0813-MC-DSH-08	265	270	267.5	43.74	15.87	35.642	0.45
WB-0813-MC-DSH-08	270	275	272.5	39.47	14.26	35.642	0.40
WB-0813-MC-DSH-08	275	280	277.5	53.95	19.79	35.642	0.56
WB-0813-MC-DSH-08	280	285	282.5	42.41	15.75	35.642	0.44
WB-0813-MC-DSH-08	285	290	287.5	49.53	19.50	35.642	0.55
WB-0813-MC-DSH-08	290	295	292.5	50.50	18.58	35.642	0.52
WB-0813-MC-DSH-08	295	300	297.5	46.36	17.49	35.642	0.49
WB-0813-MC-DSH-08	300	305	302.5	43.02	16.40	35.642	0.46
WB-0813-MC-DSH-08	305	310	307.5	51.26	20.01	35.642	0.56
WB-0813-MC-DSH-08	310	315	312.5	41.90	15.85	35.642	0.44
WB-0813-MC-DSH-08	315	320	317.5	53.95	21.12	35.642	0.59
WB-0813-MC-DSH-08	320	325	322.5	39.68	14.92	35.642	0.42
WB-0813-MC-DSH-08	325	330	327.5	49.87	19.68	35.642	0.55

Table K.16 (Continued).

Core ID	Top Depth of Interval (mm)	Bottom Depth of Interval (mm)	Average Depth of Interval (mm)	Wet Weight (g)	Dry Weight (g)	Sample Volume (cm^3)	Bulk Density (g/cm^3)
WB-0813-MC-DSH-08	330	335	332.5	42.85	16.41	35.642	0.46
WB-0813-MC-DSH-08	335	340	337.5	56.96	22.30	35.642	0.63
WB-0813-MC-DSH-08	340	345	342.5	42.83	16.60	35.642	0.47
WB-0813-MC-DSH-08	345	350	347.5	44.99	17.62	35.642	0.49
WB-0813-MC-DSH-08	350	355	352.5	52.70	20.06	35.642	0.56
WB-0813-MC-DSH-08	355	360	357.5	45.25	17.36	35.642	0.49
WB-0813-MC-DSH-08	360	365	362.5	57.83	22.40	35.642	0.63
WB-0813-MC-DSH-08	365	370	367.5	39.43	15.15	35.642	0.43
WB-0813-MC-DSH-08	370	375	372.5	70.09	26.62	35.642	0.75
WB-0813-MC-DSH-08	375	Base		82.58	32.28		

Table K.17. Bulk density data for core site WB-0813-MC-DSH-10. Sediment core sub-sample intervals (mm), sub-sample wet weight (g), dry weight (g), sub-sample volume (cm^3), and bulk density (g/cm^3). Note: Blank cell denotes no analysis performed.

Core ID	Top Depth of Interval (mm)	Bottom Depth of Interval (mm)	Average Depth of Interval (mm)	Wet Weight (g)	Dry Weight (g)	Sample Volume (cm^3)	Bulk Density (g/cm^3)
WB-0813-MC-DSH-10	0	2	1	17.73	5.07	14.257	0.36
WB-0813-MC-DSH-10	2	4	3	16.57	4.72	14.257	0.33
WB-0813-MC-DSH-10	4	6	5	18.32	5.34	14.257	0.37
WB-0813-MC-DSH-10	6	8	7	17.37	5.17	14.257	0.36
WB-0813-MC-DSH-10	8	10	9	17.52	5.26	14.257	0.37
WB-0813-MC-DSH-10	10	12	11	21.55	6.58	14.257	0.46
WB-0813-MC-DSH-10	12	14	13	17.45	5.38	14.257	0.38
WB-0813-MC-DSH-10	14	16	15	22.37	7.07	14.257	0.50
WB-0813-MC-DSH-10	16	18	17	15.37	4.83	14.257	0.34
WB-0813-MC-DSH-10	18	20	19	19.13	6.15	14.257	0.43
WB-0813-MC-DSH-10	20	22	21	20.18	6.57	14.257	0.46
WB-0813-MC-DSH-10	22	24	23	20.28	6.63	14.257	0.47
WB-0813-MC-DSH-10	24	26	25	17.95	5.82	14.257	0.41
WB-0813-MC-DSH-10	26	28	27	21.40	7.19	14.257	0.50
WB-0813-MC-DSH-10	28	30	29	17.48	5.69	14.257	0.40
WB-0813-MC-DSH-10	30	32	31	19.80	6.51	14.257	0.46
WB-0813-MC-DSH-10	32	34	33	16.68	5.42	14.257	0.38
WB-0813-MC-DSH-10	34	36	35	20.44	6.74	14.257	0.47
WB-0813-MC-DSH-10	36	38	37	19.38	6.53	14.257	0.46
WB-0813-MC-DSH-10	38	40	39	20.28	6.82	14.257	0.48
WB-0813-MC-DSH-10	40	42	41	15.32	5.15	14.257	0.36
WB-0813-MC-DSH-10	42	44	43	17.05	5.76	14.257	0.40
WB-0813-MC-DSH-10	44	46	45	18.69	6.50	14.257	0.46
WB-0813-MC-DSH-10	46	48	47	17.41	6.11	14.257	0.43
WB-0813-MC-DSH-10	48	50	49	19.18	6.73	14.257	0.47
WB-0813-MC-DSH-10	50	52	51	16.01	5.53	14.257	0.39
WB-0813-MC-DSH-10	52	54	53	14.94	5.14	14.257	0.36
WB-0813-MC-DSH-10	54	56	55	18.67	6.60	14.257	0.46
WB-0813-MC-DSH-10	56	58	57	17.26	6.11	14.257	0.43
WB-0813-MC-DSH-10	58	60	59	17.86		14.257	
WB-0813-MC-DSH-10	60	62	61	19.78	7.18	14.257	0.50
WB-0813-MC-DSH-10	62	64	63	17.97	6.48	14.257	0.45
WB-0813-MC-DSH-10	64	66	65	18.41	6.72	14.257	0.47
WB-0813-MC-DSH-10	66	68	67	16.70		14.257	
WB-0813-MC-DSH-10	68	70	69	20.97		14.257	
WB-0813-MC-DSH-10	70	72	71	18.55	7.15	14.257	0.50

Table K.17 (Continued).

Core ID	Top Depth of Interval (mm)	Bottom Depth of Interval (mm)	Average Depth of Interval (mm)	Wet Weight (g)	Dry Weight (g)	Sample Volume (cm^3)	Bulk Density (g/cm^3)
WB-0813-MC-DSH-10	72	74	73	17.03	6.63	14.257	0.47
WB-0813-MC-DSH-10	74	76	75	16.23	6.37	14.257	0.45
WB-0813-MC-DSH-10	76	78	77	17.60	6.91	14.257	0.48
WB-0813-MC-DSH-10	78	80	79	18.93	7.26	14.257	0.51
WB-0813-MC-DSH-10	80	82	81	18.55	7.34	14.257	0.51
WB-0813-MC-DSH-10	82	84	83	18.21	7.14	14.257	0.50
WB-0813-MC-DSH-10	84	86	85	17.32	6.89	14.257	0.48
WB-0813-MC-DSH-10	86	88	87	19.92	7.90	14.257	0.55
WB-0813-MC-DSH-10	88	90	89	16.14	6.48	14.257	0.45
WB-0813-MC-DSH-10	90	92	91	19.98	8.05	14.257	0.56
WB-0813-MC-DSH-10	92	94	93	17.83	7.11	14.257	0.50
WB-0813-MC-DSH-10	94	96	95	18.57	7.42	14.257	0.52
WB-0813-MC-DSH-10	96	98	97	19.48	7.68	14.257	0.54
WB-0813-MC-DSH-10	98	100	99	17.73	7.19	14.257	0.50
WB-0813-MC-DSH-10	100	105	102.5	53.11	21.32	35.642	0.60
WB-0813-MC-DSH-10	105	110	107.5	46.80	18.37	35.642	0.52
WB-0813-MC-DSH-10	110	115	112.5	46.26	17.81	35.642	0.50
WB-0813-MC-DSH-10	115	120	117.5	45.86	17.49	35.642	0.49
WB-0813-MC-DSH-10	120	125	122.5	47.54	18.16	35.642	0.51
WB-0813-MC-DSH-10	125	130	127.5	43.58	16.33	35.642	0.46
WB-0813-MC-DSH-10	130	135	132.5	47.89	18.30	35.642	0.51
WB-0813-MC-DSH-10	135	140	137.5	45.19	17.02	35.642	0.48
WB-0813-MC-DSH-10	140	145	142.5	48.13	18.20	35.642	0.51
WB-0813-MC-DSH-10	145	150	147.5	42.65	16.14	35.642	0.45
WB-0813-MC-DSH-10	150	155	152.5	47.83	17.88	35.642	0.50
WB-0813-MC-DSH-10	155	160	157.5	42.73	16.10	35.642	0.45
WB-0813-MC-DSH-10	160	165	162.5	48.07	17.69	35.642	0.50
WB-0813-MC-DSH-10	165	170	167.5	44.63	16.69	35.642	0.47
WB-0813-MC-DSH-10	170	175	172.5	45.61	16.86	35.642	0.47
WB-0813-MC-DSH-10	175	180	177.5	46.11	17.23	35.642	0.48
WB-0813-MC-DSH-10	180	185	182.5	55.70	20.37	35.642	0.57
WB-0813-MC-DSH-10	185	190	187.5	46.83	17.21	35.642	0.48
WB-0813-MC-DSH-10	190	195	192.5	42.86	15.79	35.642	0.44
WB-0813-MC-DSH-10	195	200	197.5	47.91	18.04	35.642	0.51
WB-0813-MC-DSH-10	200	205	202.5	44.15	16.46	35.642	0.46
WB-0813-MC-DSH-10	205	210	207.5	45.62	16.90	35.642	0.47
WB-0813-MC-DSH-10	210	215	212.5	44.77	16.52	35.642	0.46
WB-0813-MC-DSH-10	215	220	217.5	48.58	18.01	35.642	0.51

Table K.17 (Continued).

Core ID	Top Depth of Interval (mm)	Bottom Depth of Interval (mm)	Average Depth of Interval (mm)	Wet Weight (g)	Dry Weight (g)	Sample Volume (cm^3)	Bulk Density (g/cm^3)
WB-0813-MC-DSH-10	220	225	222.5	43.29	16.58	35.642	0.47
WB-0813-MC-DSH-10	225	230	227.5	45.57	17.15	35.642	0.48
WB-0813-MC-DSH-10	230	235	232.5	45.12	17.26	35.642	0.48
WB-0813-MC-DSH-10	235	240	237.5	46.77	18.17	35.642	0.51
WB-0813-MC-DSH-10	240	245	242.5	47.26	17.98	35.642	0.50
WB-0813-MC-DSH-10	245	250	247.5	45.15	16.60	35.642	0.47
WB-0813-MC-DSH-10	250	255	252.5	44.26	16.19	35.642	0.45
WB-0813-MC-DSH-10	255	260	257.5	47.24	17.78	35.642	0.50
WB-0813-MC-DSH-10	260	265	262.5	45.45	17.22	35.642	0.48
WB-0813-MC-DSH-10	265	270	267.5	47.26	17.47	35.642	0.49
WB-0813-MC-DSH-10	270	275	272.5	45.53	17.30	35.642	0.49
WB-0813-MC-DSH-10	275	280	277.5	47.14	17.92	35.642	0.50
WB-0813-MC-DSH-10	280	285	282.5	45.36	17.62	35.642	0.49
WB-0813-MC-DSH-10	285	290	287.5	47.77	18.58	35.642	0.52
WB-0813-MC-DSH-10	290	295	292.5	45.62	17.60	35.642	0.49
WB-0813-MC-DSH-10	295	300	297.5	45.96	17.59	35.642	0.49
WB-0813-MC-DSH-10	300	305	302.5	45.41	17.44	35.642	0.49
WB-0813-MC-DSH-10	305	310	307.5	48.64	18.47	35.642	0.52
WB-0813-MC-DSH-10	310	315	312.5	42.87	16.50	35.642	0.46
WB-0813-MC-DSH-10	315	320	317.5	47.02	18.09	35.642	0.51
WB-0813-MC-DSH-10	320	325	322.5	46.41	17.53	35.642	0.49
WB-0813-MC-DSH-10	325	330	327.5	45.68	17.28	35.642	0.48
WB-0813-MC-DSH-10	330	335	332.5	43.78	16.64	35.642	0.47
WB-0813-MC-DSH-10	335	340	337.5	48.99	18.68	35.642	0.52
WB-0813-MC-DSH-10	340	345	342.5	46.03	17.60	35.642	0.49
WB-0813-MC-DSH-10	345	350	347.5	47.00	17.96	35.642	0.50
WB-0813-MC-DSH-10	350	355	352.5	47.24	18.32	35.642	0.51
WB-0813-MC-DSH-10	355	360	357.5	46.55	17.47	35.642	0.49
WB-0813-MC-DSH-10	360	365	362.5	42.40	16.25	35.642	0.46
WB-0813-MC-DSH-10	365	370	367.5	49.49	19.31	35.642	0.54
WB-0813-MC-DSH-10	370	375	372.5	44.99	17.31	35.642	0.49
WB-0813-MC-DSH-10	375	380	377.5	45.94	17.90	35.642	0.50
WB-0813-MC-DSH-10	380	385	382.5	46.52	18.30	35.642	0.51
WB-0813-MC-DSH-10	385	390	387.5	47.40	18.45	35.642	0.52
WB-0813-MC-DSH-10	390	395	392.5	46.31	18.26	35.642	0.51
WB-0813-MC-DSH-10	395	400	397.5	47.54	18.75	35.642	0.53
WB-0813-MC-DSH-10	400	405	402.5	46.61	18.52	35.642	0.52
WB-0813-MC-DSH-10	405	410	407.5	48.69	19.38	35.642	0.54

Table K.17 (Continued).

Core ID	Top Depth of Interval (mm)	Bottom Depth of Interval (mm)	Average Depth of Interval (mm)	Wet Weight (g)	Dry Weight (g)	Sample Volume (cm^3)	Bulk Density (g/cm^3)
WB-0813-MC-DSH-10	410	415	412.5	46.17	18.58	35.642	0.52
WB-0813-MC-DSH-10	415	420	417.5	39.48	16.02	35.642	0.45
WB-0813-MC-DSH-10	420	Base		60.28	24.31		

Table K.18. Bulk density data for core site WB-0813-MC-PCB-06. Sediment core sub-sample intervals (mm), sub-sample wet weight (g), dry weight (g), sub-sample volume (cm^3), and bulk density (g/cm^3). Note: Blank cell denotes no analysis performed.

Core ID	Top Depth of Interval (mm)	Bottom Depth of Interval (mm)	Average Depth of Interval (mm)	Wet Weight (g)	Dry Weight (g)	Sample Volume (cm^3)	Bulk Density (g/cm^3)
WB-0813-MC-PCB-06	0	4	2	25.50	6.71	28.514	0.24
WB-0813-MC-PCB-06	4	6	5	13.76	3.45	14.257	0.24
WB-0813-MC-PCB-06	6	8	7	15.60	3.94	14.257	0.28
WB-0813-MC-PCB-06	8	10	9	15.41	3.88	14.257	0.27
WB-0813-MC-PCB-06	10	12	11	16.60	4.29	14.257	0.30
WB-0813-MC-PCB-06	12	14	13	16.43	4.23	14.257	0.30
WB-0813-MC-PCB-06	14	16	15	18.00	4.74	14.257	0.33
WB-0813-MC-PCB-06	16	18	17	14.31	3.65	14.257	0.26
WB-0813-MC-PCB-06	18	20	19	16.43	4.33	14.257	0.30
WB-0813-MC-PCB-06	20	22	21	18.42	4.89	14.257	0.34
WB-0813-MC-PCB-06	22	24	23	16.77	4.50	14.257	0.32
WB-0813-MC-PCB-06	24	26	25	15.68	4.27	14.257	0.30
WB-0813-MC-PCB-06	26	28	27	14.51	3.95	14.257	0.28
WB-0813-MC-PCB-06	28	30	29	17.06	4.74	14.257	0.33
WB-0813-MC-PCB-06	30	32	31	16.80	4.68	14.257	0.33
WB-0813-MC-PCB-06	32	37	34.5	44.35	12.88	35.642	0.36
WB-0813-MC-PCB-06	37	42	39.5	44.38	13.06	35.642	0.37
WB-0813-MC-PCB-06	42	47	44.5	41.98	12.74	35.642	0.36
WB-0813-MC-PCB-06	47	52	49.5	46.52	14.85	35.642	0.42
WB-0813-MC-PCB-06	52	57	54.5	42.41	13.57	35.642	0.38
WB-0813-MC-PCB-06	57	62	59.5	44.47	14.77	35.642	0.41
WB-0813-MC-PCB-06	62	67	64.5	45.93	15.91	35.642	0.45
WB-0813-MC-PCB-06	67	72	69.5	51.46	18.37	35.642	0.52
WB-0813-MC-PCB-06	72	77	74.5	46.50	16.75	35.642	0.47
WB-0813-MC-PCB-06	77	82	79.5	43.05	15.47	35.642	0.43
WB-0813-MC-PCB-06	82	87	84.5	36.49	13.18	35.642	0.37
WB-0813-MC-PCB-06	87	92	89.5	47.16	17.69	35.642	0.50
WB-0813-MC-PCB-06	92	97	94.5	44.54	16.72	35.642	0.47
WB-0813-MC-PCB-06	97	102	99.5	47.15	16.48	35.642	0.46
WB-0813-MC-PCB-06	102	107	104.5	49.71	18.43	35.642	0.52
WB-0813-MC-PCB-06	107	112	109.5	41.65	15.00	35.642	0.42
WB-0813-MC-PCB-06	112	117	114.5	48.78	17.84	35.642	0.50
WB-0813-MC-PCB-06	117	122	119.5	54.21	19.82	35.642	0.56
WB-0813-MC-PCB-06	122	127	124.5	51.64	18.94	35.642	0.53
WB-0813-MC-PCB-06	127	132	129.5	49.35	18.48	35.642	0.52
WB-0813-MC-PCB-06	132	137	134.5	41.00	14.92	35.642	0.42

Table K.18 (Continued).

Core ID	Top Depth of Interval (mm)	Bottom Depth of Interval (mm)	Average Depth of Interval (mm)	Wet Weight (g)	Dry Weight (g)	Sample Volume (cm^3)	Bulk Density (g/cm^3)
WB-0813-MC-PCB-06	137	142	139.5	32.65	11.58	35.642	0.32
WB-0813-MC-PCB-06	142	147	144.5	40.45	14.26	35.642	0.40
WB-0813-MC-PCB-06	147	152	149.5	45.33	15.87	35.642	0.45
WB-0813-MC-PCB-06	152	157	154.5	45.67	16.13	35.642	0.45
WB-0813-MC-PCB-06	157	162	159.5	49.35	17.63	35.642	0.49
WB-0813-MC-PCB-06	162	167	164.5	42.87	15.26	35.642	0.43
WB-0813-MC-PCB-06	167	172	169.5	44.33	15.99	35.642	0.45
WB-0813-MC-PCB-06	172	177	174.5	42.89	15.15	35.642	0.43
WB-0813-MC-PCB-06	177	182	179.5	45.19	16.09	35.642	0.45
WB-0813-MC-PCB-06	182	187	184.5	47.09	17.02	35.642	0.48
WB-0813-MC-PCB-06	187	192	189.5	42.74	15.36	35.642	0.43
WB-0813-MC-PCB-06	192	197	194.5	45.78	16.30	35.642	0.46
WB-0813-MC-PCB-06	197	202	199.5	47.09	16.79	35.642	0.47
WB-0813-MC-PCB-06	202	207	204.5	43.92	15.69	35.642	0.44
WB-0813-MC-PCB-06	207	212	209.5	45.69	16.48	35.642	0.46
WB-0813-MC-PCB-06	212	217	214.5	45.27	16.73	35.642	0.47
WB-0813-MC-PCB-06	217	222	219.5	46.33	17.34	35.642	0.49
WB-0813-MC-PCB-06	222	227	224.5	46.42	17.50	35.642	0.49
WB-0813-MC-PCB-06	227	232	229.5	46.17	17.68	35.642	0.50
WB-0813-MC-PCB-06	232	237	234.5	47.04	17.93	35.642	0.50
WB-0813-MC-PCB-06	237	242	239.5	45.47	17.07	35.642	0.48
WB-0813-MC-PCB-06	242	247	244.5	48.81	18.32	35.642	0.51
WB-0813-MC-PCB-06	247	252	249.5	45.45	16.93	35.642	0.48
WB-0813-MC-PCB-06	252	257	254.5	45.50	17.10	35.642	0.48
WB-0813-MC-PCB-06	257	262	259.5	47.65	18.88	35.642	0.53
WB-0813-MC-PCB-06	262	267	264.5	47.44	18.36	35.642	0.52
WB-0813-MC-PCB-06	267	272	269.5	46.30	18.04	35.642	0.51
WB-0813-MC-PCB-06	272	277	274.5	46.41	18.51	35.642	0.52
WB-0813-MC-PCB-06	277	282	279.5	45.91	18.25	35.642	0.51
WB-0813-MC-PCB-06	282	287	284.5	49.03	19.37	35.642	0.54
WB-0813-MC-PCB-06	287	292	289.5	46.71	18.97	35.642	0.53
WB-0813-MC-PCB-06	292	297	294.5	46.18	18.71	35.642	0.52
WB-0813-MC-PCB-06	297	302	299.5	46.23	18.89	35.642	0.53
WB-0813-MC-PCB-06	302	307	304.5	47.85	19.71	35.642	0.55
WB-0813-MC-PCB-06	307	312	309.5	47.22	19.50	35.642	0.55
WB-0813-MC-PCB-06	312	317	314.5	48.90	19.90	35.642	0.56
WB-0813-MC-PCB-06	317	322	319.5	46.36	19.11	35.642	0.54
WB-0813-MC-PCB-06	322	327	324.5	46.60	19.23	35.642	0.54

Table K.18 (Continued).

Core ID	Top Depth of Interval (mm)	Bottom Depth of Interval (mm)	Average Depth of Interval (mm)	Wet Weight (g)	Dry Weight (g)	Sample Volume (cm^3)	Bulk Density (g/cm^3)
WB-0813-MC-PCB-06	327	332	329.5	47.52	19.64	35.642	0.55
WB-0813-MC-PCB-06	332	337	334.5	50.64	20.55	35.642	0.58
WB-0813-MC-PCB-06	337	342	339.5	47.29	18.90	35.642	0.53
WB-0813-MC-PCB-06	342	347	344.5	47.85	19.17	35.642	0.54
WB-0813-MC-PCB-06	347	352	349.5	48.27	19.23	35.642	0.54
WB-0813-MC-PCB-06	352	357	354.5	48.04	19.00	35.642	0.53
WB-0813-MC-PCB-06	357	362	359.5	47.31	18.77	35.642	0.53
WB-0813-MC-PCB-06	362	367	364.5	47.95	19.00	35.642	0.53
WB-0813-MC-PCB-06	367	372	369.5	47.49	18.71	35.642	0.52
WB-0813-MC-PCB-06	372	377	374.5	45.98	17.85	35.642	0.50
WB-0813-MC-PCB-06	377	382	379.5	49.01	19.24	35.642	0.54
WB-0813-MC-PCB-06	382	387	384.5	47.31	18.62	35.642	0.52
WB-0813-MC-PCB-06	387	392	389.5	47.95	19.15	35.642	0.54
WB-0813-MC-PCB-06	392	397	394.5	49.17	19.94	35.642	0.56
WB-0813-MC-PCB-06	397	402	399.5	49.52	20.24	35.642	0.57
WB-0813-MC-PCB-06	402	407	404.5	49.10	20.04	35.642	0.56
WB-0813-MC-PCB-06	407	412	409.5	49.67	20.24	35.642	0.57
WB-0813-MC-PCB-06	412	417	414.5	48.53	19.78	35.642	0.55
WB-0813-MC-PCB-06	417	422	419.5	48.32	19.70	35.642	0.55
WB-0813-MC-PCB-06	422	427	424.5	45.82	19.09	35.642	0.54
WB-0813-MC-PCB-06	427	Base		49.44	20.68		

Table K.19. Bulk density data for core site WB-0814-MC-04. Sediment core sub-sample intervals (mm), sub-sample wet weight (g), dry weight (g), sub-sample volume (cm^3), and bulk density (g/cm^3). Note: Blank cell denotes no analysis performed.

Core ID	Top Depth of Interval (mm)	Bottom Depth of Interval (mm)	Average Depth of Interval (mm)	Wet Weight (g)	Dry Weight (g)	Sample Volume (cm^3)	Bulk Density (g/cm^3)
WB-0814-MC-04	0	2	1	10.78	3.10	14.257	0.22
WB-0814-MC-04	2	4	3	10.09	2.91	14.257	0.20
WB-0814-MC-04	4	6	5	12.19	3.54	14.257	0.25
WB-0814-MC-04	6	8	7	13.82	3.99	14.257	0.28
WB-0814-MC-04	8	10	9	13.69	3.93	14.257	0.28
WB-0814-MC-04	10	12	11	16.05	4.06	14.257	0.28
WB-0814-MC-04	12	14	13	18.09	5.42	14.257	0.38
WB-0814-MC-04	14	16	15	17.16	5.33	14.257	0.37
WB-0814-MC-04	16	18	17	15.13	4.80	14.257	0.34
WB-0814-MC-04	18	20	19	19.16	6.21	14.257	0.44
WB-0814-MC-04	20	22	21	18.19	5.97	14.257	0.42
WB-0814-MC-04	22	24	23	18.20	6.01	14.257	0.42
WB-0814-MC-04	24	26	25	18.22	6.05	14.257	0.42
WB-0814-MC-04	26	28	27	17.82	5.92	14.257	0.42
WB-0814-MC-04	28	30	29	20.37	6.79	14.257	0.48
WB-0814-MC-04	30	32	31	16.90	5.58	14.257	0.39
WB-0814-MC-04	32	34	33	16.95	5.60	14.257	0.39
WB-0814-MC-04	34	36	35	18.15	5.96	14.257	0.42
WB-0814-MC-04	36	38	37	17.57	5.82	14.257	0.41
WB-0814-MC-04	38	40	39	18.30	6.07	14.257	0.43
WB-0814-MC-04	40	45	42.5	45.04	15.40	35.642	0.43
WB-0814-MC-04	45	50	47.5	45.29	15.60	35.642	0.44
WB-0814-MC-04	50	55	52.5	43.70	15.14	35.642	0.42
WB-0814-MC-04	55	60	57.5	46.26	16.34	35.642	0.46
WB-0814-MC-04	60	65	62.5	44.49	15.94	35.642	0.45
WB-0814-MC-04	65	70	67.5	47.33	17.34	35.642	0.49
WB-0814-MC-04	70	75	72.5	43.70	16.74	35.642	0.47
WB-0814-MC-04	75	80	77.5	46.04	18.10	35.642	0.51
WB-0814-MC-04	80	85	82.5	47.75	18.90	35.642	0.53
WB-0814-MC-04	85	90	87.5	49.05	19.51	35.642	0.55
WB-0814-MC-04	90	95	92.5	46.32	18.61	35.642	0.52
WB-0814-MC-04	95	100	97.5	48.44	19.41	35.642	0.54
WB-0814-MC-04	100	105	102.5	48.48	19.47	35.642	0.55
WB-0814-MC-04	105	110	107.5	45.23	18.11	35.642	0.51
WB-0814-MC-04	110	115	112.5	43.96	17.52	35.642	0.49
WB-0814-MC-04	115	120	117.5	47.30	33.00	35.642	0.93

Table K.19 (Continued).

Core ID	Top Depth of Interval (mm)	Bottom Depth of Interval (mm)	Average Depth of Interval (mm)	Wet Weight (g)	Dry Weight (g)	Sample Volume (cm^3)	Bulk Density (g/cm^3)
WB-0814-MC-04	120	125	122.5	47.10	19.04	35.642	0.53
WB-0814-MC-04	125	130	127.5	49.37	20.15	35.642	0.57
WB-0814-MC-04	130	135	132.5	47.57	19.53	35.642	0.55
WB-0814-MC-04	135	140	137.5	49.73	20.56	35.642	0.58
WB-0814-MC-04	140	145	142.5	46.84	19.32	35.642	0.54
WB-0814-MC-04	145	150	147.5	51.81	21.48	35.642	0.60
WB-0814-MC-04	150	155	152.5	48.45	20.55	35.642	0.58
WB-0814-MC-04	155	160	157.5	42.74	18.17	35.642	0.51
WB-0814-MC-04	160	165	162.5	48.50	20.94	35.642	0.59
WB-0814-MC-04	165	170	167.5	52.33	23.19	35.642	0.65
WB-0814-MC-04	170	175	172.5	44.74	20.04	35.642	0.56
WB-0814-MC-04	175	180	177.5	52.07	23.36	35.642	0.66
WB-0814-MC-04	180	185	182.5	47.41	21.20	35.642	0.59
WB-0814-MC-04	185	190	187.5	48.93	21.83	35.642	0.61
WB-0814-MC-04	190	195	192.5	45.11	20.24	35.642	0.57
WB-0814-MC-04	195	200	197.5	52.43	23.52	35.642	0.66
WB-0814-MC-04	200	205	202.5	49.58	22.34	35.642	0.63
WB-0814-MC-04	205	210	207.5	45.37	20.55	35.642	0.58
WB-0814-MC-04	210	215	212.5	51.69	23.76	35.642	0.67
WB-0814-MC-04	215	220	217.5	49.49	22.84	35.642	0.64
WB-0814-MC-04	220	225	222.5	54.64	25.27	35.642	0.71
WB-0814-MC-04	225	230	227.5	59.72	27.48	35.642	0.77
WB-0814-MC-04	230	235	232.5	52.14	24.17	35.642	0.68
WB-0814-MC-04	235	240	237.5	57.93	26.90	35.642	0.75
WB-0814-MC-04	240	245	242.5	46.20	21.49	35.642	0.60
WB-0814-MC-04	245	250	247.5	60.97	28.65	35.642	0.80
WB-0814-MC-04	250	255	252.5	51.03	23.88	35.642	0.67
WB-0814-MC-04	255	Base		48.68	22.88		

Table K.20. Bulk density data for core site WB-0814-MC-DSH-08 DEP 1. Sediment core sub-sample intervals (mm), sub-sample wet weight (g), dry weight (g), sub-sample volume (cm^3), and bulk density (g/cm^3). Note: Blank cell denotes no analysis performed.

Core ID	Top Depth of Interval (mm)	Bottom Depth of Interval (mm)	Average Depth of Interval (mm)	Wet Weight (g)	Dry Weight (g)	Sample Volume (cm^3)	Bulk Density (g/cm^3)
WB-0814-MC-DSH-08 DEP 1	0	2	1	22.65	4.16	14.257	0.29
WB-0814-MC-DSH-08 DEP 1	2	4	3	15.38	3.44	14.257	0.24
WB-0814-MC-DSH-08 DEP 1	4	6	5	15.25	3.62	14.257	0.25
WB-0814-MC-DSH-08 DEP 1	6	8	7	16.11	3.85	14.257	0.27
WB-0814-MC-DSH-08 DEP 1	8	10	9	16.75	4.21	14.257	0.30
WB-0814-MC-DSH-08 DEP 1	10	12	11	16.38	4.10	14.257	0.29
WB-0814-MC-DSH-08 DEP 1	12	14	13	16.03	4.18	14.257	0.29
WB-0814-MC-DSH-08 DEP 1	14	16	15	18.03	4.83	14.257	0.34
WB-0814-MC-DSH-08 DEP 1	16	18	17	13.85	3.88	14.257	0.27
WB-0814-MC-DSH-08 DEP 1	18	20	19	18.06	5.10	14.257	0.36
WB-0814-MC-DSH-08 DEP 1	20	22	21	16.84	4.90	14.257	0.34
WB-0814-MC-DSH-08 DEP 1	22	24	23	17.93	5.27	14.257	0.37
WB-0814-MC-DSH-08 DEP 1	24	26	25	16.97	5.07	14.257	0.36
WB-0814-MC-DSH-08 DEP 1	26	28	27	18.69	5.62	14.257	0.39
WB-0814-MC-DSH-08 DEP 1	28	30	29	17.63	5.52	14.257	0.39
WB-0814-MC-DSH-08 DEP 1	30	32	31	17.10	5.44	14.257	0.38
WB-0814-MC-DSH-08 DEP 1	32	34	33	18.57	5.98	14.257	0.42
WB-0814-MC-DSH-08 DEP 1	34	36	35	15.87	5.20	14.257	0.36
WB-0814-MC-DSH-08 DEP 1	36	38	37	17.24	5.75	14.257	0.40
WB-0814-MC-DSH-08 DEP 1	38	40	39	19.68	6.72	14.257	0.47
WB-0814-MC-DSH-08 DEP 1	40	45	42.5	51.84	18.05	35.642	0.51
WB-0814-MC-DSH-08 DEP 1	45	50	47.5	39.48	14.18	35.642	0.40
WB-0814-MC-DSH-08 DEP 1	50	55	52.5	44.31	16.19	35.642	0.45
WB-0814-MC-DSH-08 DEP 1	55	60	57.5	42.69	16.71	35.642	0.47
WB-0814-MC-DSH-08 DEP 1	60	65	62.5	45.94	18.09	35.642	0.51
WB-0814-MC-DSH-08 DEP 1	65	70	67.5	45.94	18.44	35.642	0.52
WB-0814-MC-DSH-08 DEP 1	70	75	72.5	46.70	18.96	35.642	0.53
WB-0814-MC-DSH-08 DEP 1	75	80	77.5	48.03	18.30	35.642	0.51
WB-0814-MC-DSH-08 DEP 1	80	85	82.5	46.29	18.43	35.642	0.52
WB-0814-MC-DSH-08 DEP 1	85	90	87.5	47.83	19.43	35.642	0.55
WB-0814-MC-DSH-08 DEP 1	90	95	92.5	45.57	18.15	35.642	0.51
WB-0814-MC-DSH-08 DEP 1	95	100	97.5	43.83	17.35	35.642	0.49
WB-0814-MC-DSH-08 DEP 1	100	105	102.5	50.21	19.96	35.642	0.56
WB-0814-MC-DSH-08 DEP 1	105	110	107.5	46.03	18.07	35.642	0.51
WB-0814-MC-DSH-08 DEP 1	110	115	112.5	45.82	17.93	35.642	0.50
WB-0814-MC-DSH-08 DEP 1	115	120	117.5	44.36	17.09	35.642	0.48

Table K.20 (Continued).

Core ID	Top Depth of Interval (mm)	Bottom Depth of Interval (mm)	Average Depth of Interval (mm)	Wet Weight (g)	Dry Weight (g)	Sample Volume (cm^3)	Bulk Density (g/cm^3)
WB-0814-MC-DSH-08 DEP 1	120	125	122.5	46.61	17.96	35.642	0.50
WB-0814-MC-DSH-08 DEP 1	125	130	127.5	46.03	17.76	35.642	0.50
WB-0814-MC-DSH-08 DEP 1	130	135	132.5	43.50	16.52	35.642	0.46
WB-0814-MC-DSH-08 DEP 1	135	140	137.5	46.94	17.72	35.642	0.50
WB-0814-MC-DSH-08 DEP 1	140	145	142.5	50.71	19.23	35.642	0.54
WB-0814-MC-DSH-08 DEP 1	145	150	147.5	44.96	17.16	35.642	0.48
WB-0814-MC-DSH-08 DEP 1	150	155	152.5	50.18	18.95	35.642	0.53
WB-0814-MC-DSH-08 DEP 1	155	160	157.5	44.61	16.67	35.642	0.47
WB-0814-MC-DSH-08 DEP 1	160	165	162.5	45.85	17.05	35.642	0.48
WB-0814-MC-DSH-08 DEP 1	165	170	167.5	43.28	15.59	35.642	0.44
WB-0814-MC-DSH-08 DEP 1	170	175	172.5	42.05	15.14	35.642	0.42
WB-0814-MC-DSH-08 DEP 1	175	180	177.5	48.76	17.55	35.642	0.49
WB-0814-MC-DSH-08 DEP 1	180	185	182.5	43.06	15.18	35.642	0.43
WB-0814-MC-DSH-08 DEP 1	185	190	187.5	47.58	16.76	35.642	0.47
WB-0814-MC-DSH-08 DEP 1	190	195	192.5	43.24	15.32	35.642	0.43
WB-0814-MC-DSH-08 DEP 1	195	200	197.5	46.41	16.41	35.642	0.46
WB-0814-MC-DSH-08 DEP 1	200	205	202.5	44.32	15.63	35.642	0.44
WB-0814-MC-DSH-08 DEP 1	205	210	207.5	45.23	15.86	35.642	0.44
WB-0814-MC-DSH-08 DEP 1	210	215	212.5	45.25	15.72	35.642	0.44
WB-0814-MC-DSH-08 DEP 1	215	220	217.5	44.45	15.32	35.642	0.43
WB-0814-MC-DSH-08 DEP 1	220	225	222.5	43.63	14.86	35.642	0.42
WB-0814-MC-DSH-08 DEP 1	225	230	227.5	44.14	14.91	35.642	0.42
WB-0814-MC-DSH-08 DEP 1	230	235	232.5	44.47	14.91	35.642	0.42
WB-0814-MC-DSH-08 DEP 1	235	240	237.5	44.78	15.28	35.642	0.43
WB-0814-MC-DSH-08 DEP 1	240	245	242.5	44.31	15.13	35.642	0.42
WB-0814-MC-DSH-08 DEP 1	245	250	247.5	43.83	14.89	35.642	0.42
WB-0814-MC-DSH-08 DEP 1	250	255	252.5	42.65	14.53	35.642	0.41
WB-0814-MC-DSH-08 DEP 1	255	260	257.5	44.24	15.60	35.642	0.44
WB-0814-MC-DSH-08 DEP 1	260	265	262.5	45.61	16.13	35.642	0.45
WB-0814-MC-DSH-08 DEP 1	265	270	267.5	43.48	15.66	35.642	0.44
WB-0814-MC-DSH-08 DEP 1	270	275	272.5	47.41	17.33	35.642	0.49
WB-0814-MC-DSH-08 DEP 1	275	280	277.5	44.42	16.11	35.642	0.45
WB-0814-MC-DSH-08 DEP 1	280	285	282.5	44.82	16.39	35.642	0.46
WB-0814-MC-DSH-08 DEP 1	285	290	287.5	44.16	16.32	35.642	0.46
WB-0814-MC-DSH-08 DEP 1	290	295	292.5	48.08	17.92	35.642	0.50
WB-0814-MC-DSH-08 DEP 1	295	300	297.5	44.28	16.30	35.642	0.46
WB-0814-MC-DSH-08 DEP 1	300	305	302.5	45.79	17.14	35.642	0.48
WB-0814-MC-DSH-08 DEP 1	305	310	307.5	47.84	17.85	35.642	0.50

Table K.20 (Continued).

Core ID	Top Depth of Interval (mm)	Bottom Depth of Interval (mm)	Average Depth of Interval (mm)	Wet Weight (g)	Dry Weight (g)	Sample Volume (cm^3)	Bulk Density (g/cm^3)
WB-0814-MC-DSH-08 DEP 1	310	315	312.5	44.80	16.77	35.642	0.47
WB-0814-MC-DSH-08 DEP 1	315	320	317.5	46.88	17.20	35.642	0.48
WB-0814-MC-DSH-08 DEP 1	320	325	322.5	43.97	15.96	35.642	0.45
WB-0814-MC-DSH-08 DEP 1	325	330	327.5	46.27	16.84	35.642	0.47
WB-0814-MC-DSH-08 DEP 1	330	335	332.5	44.57	16.21	35.642	0.45
WB-0814-MC-DSH-08 DEP 1	335	340	337.5	45.28	16.47	35.642	0.46
WB-0814-MC-DSH-08 DEP 1	340	345	342.5	45.96	16.83	35.642	0.47
WB-0814-MC-DSH-08 DEP 1	345	350	347.5	46.31	17.23	35.642	0.48
WB-0814-MC-DSH-08 DEP 1	350	355	352.5	46.67	17.35	35.642	0.49
WB-0814-MC-DSH-08 DEP 1	355	360	357.5	46.75	17.74	35.642	0.50
WB-0814-MC-DSH-08 DEP 1	360	365	362.5	46.08	17.37	35.642	0.49
WB-0814-MC-DSH-08 DEP 1	365	370	367.5	46.39	17.42	35.642	0.49
WB-0814-MC-DSH-08 DEP 1	370	375	372.5	44.80	16.68	35.642	0.47
WB-0814-MC-DSH-08 DEP 1	375	380	377.5	46.89	17.67	35.642	0.50
WB-0814-MC-DSH-08 DEP 1	380	385	382.5	46.32	17.83	35.642	0.50
WB-0814-MC-DSH-08 DEP 1	385	Base		48.49	18.81		

Table K.21. Bulk density data for core site WB-0814-MC-DSH-10 DEP 1. Sediment core sub-sample intervals (mm), sub-sample wet weight (g), dry weight (g), sub-sample volume (cm^3), and bulk density (g/cm^3). Note: Blank cell denotes no analysis performed.

Core ID	Top Depth of Interval (mm)	Bottom Depth of Interval (mm)	Average Depth of Interval (mm)	Wet Weight (g)	Dry Weight (g)	Sample Volume (cm^3)	Bulk Density (g/cm^3)
WB-0814-MC-DSH-10 DEP 1	0	2	1	9.23	2.33	14.257	0.16
WB-0814-MC-DSH-10 DEP 1	2	4	3	9.93	2.54	14.257	0.18
WB-0814-MC-DSH-10 DEP 1	4	6	5	12.38	3.22	14.257	0.23
WB-0814-MC-DSH-10 DEP 1	6	8	7	13.73	3.67	14.257	0.26
WB-0814-MC-DSH-10 DEP 1	8	10	9	14.83	4.06	14.257	0.28
WB-0814-MC-DSH-10 DEP 1	10	12	11	13.74	3.92	14.257	0.27
WB-0814-MC-DSH-10 DEP 1	12	14	13	12.14	3.55	14.257	0.25
WB-0814-MC-DSH-10 DEP 1	14	16	15	16.30	4.91	14.257	0.34
WB-0814-MC-DSH-10 DEP 1	16	18	17	16.45	5.01	14.257	0.35
WB-0814-MC-DSH-10 DEP 1	18	20	19	13.79	4.26	14.257	0.30
WB-0814-MC-DSH-10 DEP 1	20	22	21	14.62	4.53	14.257	0.32
WB-0814-MC-DSH-10 DEP 1	22	24	23	15.71	4.97	14.257	0.35
WB-0814-MC-DSH-10 DEP 1	24	26	25	16.79	5.35	14.257	0.38
WB-0814-MC-DSH-10 DEP 1	26	28	27	17.59	5.67	14.257	0.40
WB-0814-MC-DSH-10 DEP 1	28	30	29	10.25	3.46	14.257	0.24
WB-0814-MC-DSH-10 DEP 1	30	32	31	18.08	6.00	14.257	0.42
WB-0814-MC-DSH-10 DEP 1	32	34	33	15.37	5.15	14.257	0.36
WB-0814-MC-DSH-10 DEP 1	34	36	35	16.98	5.72	14.257	0.40
WB-0814-MC-DSH-10 DEP 1	36	38	37	15.93	5.44	14.257	0.38
WB-0814-MC-DSH-10 DEP 1	38	43	40.5	45.28	16.08	35.642	0.45
WB-0814-MC-DSH-10 DEP 1	43	48	45.5	42.42	15.08	35.642	0.42
WB-0814-MC-DSH-10 DEP 1	48	53	50.5	44.00	15.96	35.642	0.45
WB-0814-MC-DSH-10 DEP 1	53	58	55.5	42.96	15.64	35.642	0.44
WB-0814-MC-DSH-10 DEP 1	58	63	60.5	47.83	17.70	35.642	0.50
WB-0814-MC-DSH-10 DEP 1	63	68	65.5	42.96	16.61	35.642	0.47
WB-0814-MC-DSH-10 DEP 1	68	73	70.5	46.99	18.25	35.642	0.51
WB-0814-MC-DSH-10 DEP 1	73	78	75.5	44.60	17.44	35.642	0.49
WB-0814-MC-DSH-10 DEP 1	78	83	80.5	42.51	16.33	35.642	0.46
WB-0814-MC-DSH-10 DEP 1	83	88	85.5	47.91	18.69	35.642	0.52
WB-0814-MC-DSH-10 DEP 1	88	93	90.5	45.92	18.24	35.642	0.51
WB-0814-MC-DSH-10 DEP 1	93	98	95.5	42.70	17.18	35.642	0.48
WB-0814-MC-DSH-10 DEP 1	98	103	100.5	44.27	18.13	35.642	0.51
WB-0814-MC-DSH-10 DEP 1	103	108	105.5	44.15	18.16	35.642	0.51
WB-0814-MC-DSH-10 DEP 1	108	113	110.5	49.64	20.56	35.642	0.58
WB-0814-MC-DSH-10 DEP 1	113	118	115.5	42.04	17.50	35.642	0.49
WB-0814-MC-DSH-10 DEP 1	118	123	120.5	50.93	21.22	35.642	0.60

Table K.21 (Continued).

Core ID	Top Depth of Interval (mm)	Bottom Depth of Interval (mm)	Average Depth of Interval (mm)	Wet Weight (g)	Dry Weight (g)	Sample Volume (cm^3)	Bulk Density (g/cm^3)
WB-0814-MC-DSH-10 DEP 1	123	128	125.5	42.91	17.78	35.642	0.50
WB-0814-MC-DSH-10 DEP 1	128	133	130.5	45.81	19.07	35.642	0.54
WB-0814-MC-DSH-10 DEP 1	133	138	135.5	51.60	21.36	35.642	0.60
WB-0814-MC-DSH-10 DEP 1	138	143	140.5	43.09	17.89	35.642	0.50
WB-0814-MC-DSH-10 DEP 1	143	148	145.5	52.11	21.74	35.642	0.61
WB-0814-MC-DSH-10 DEP 1	148	154	151	63.05	26.31	42.7705	0.62
WB-0814-MC-DSH-10 DEP 1	154	159	156.5	46.12	18.62	35.642	0.52
WB-0814-MC-DSH-10 DEP 1	159	164	161.5	42.94	17.15	35.642	0.48
WB-0814-MC-DSH-10 DEP 1	164	169	166.5	34.94	13.62	35.642	0.38
WB-0814-MC-DSH-10 DEP 1	169	174	171.5	46.56	18.12	35.642	0.51
WB-0814-MC-DSH-10 DEP 1	174	179	176.5	46.00	17.61	35.642	0.49
WB-0814-MC-DSH-10 DEP 1	179	184	181.5	46.73	17.86	35.642	0.50
WB-0814-MC-DSH-10 DEP 1	184	189	186.5	42.22	16.15	35.642	0.45
WB-0814-MC-DSH-10 DEP 1	189	194	191.5	50.78	19.26	35.642	0.54
WB-0814-MC-DSH-10 DEP 1	194	199	196.5	44.30	16.57	35.642	0.46
WB-0814-MC-DSH-10 DEP 1	199	204	201.5	48.64	18.30	35.642	0.51
WB-0814-MC-DSH-10 DEP 1	204	209	206.5	45.34	17.09	35.642	0.48
WB-0814-MC-DSH-10 DEP 1	209	214	211.5	46.55	17.48	35.642	0.49
WB-0814-MC-DSH-10 DEP 1	214	219	216.5	44.38	16.55	35.642	0.46
WB-0814-MC-DSH-10 DEP 1	219	224	221.5	47.14	17.62	35.642	0.49
WB-0814-MC-DSH-10 DEP 1	224	229	226.5	46.50	17.34	35.642	0.49
WB-0814-MC-DSH-10 DEP 1	229	234	231.5	46.28	17.14	35.642	0.48
WB-0814-MC-DSH-10 DEP 1	234	239	236.5	45.99	17.33	35.642	0.49
WB-0814-MC-DSH-10 DEP 1	239	244	241.5	45.29	17.06	35.642	0.48
WB-0814-MC-DSH-10 DEP 1	244	249	246.5	46.74	17.74	35.642	0.50
WB-0814-MC-DSH-10 DEP 1	249	254	251.5	45.04	17.07	35.642	0.48
WB-0814-MC-DSH-10 DEP 1	254	259	256.5	48.55	18.46	35.642	0.52
WB-0814-MC-DSH-10 DEP 1	259	264	261.5	40.58	15.53	35.642	0.44
WB-0814-MC-DSH-10 DEP 1	264	269	266.5	46.19	17.46	35.642	0.49
WB-0814-MC-DSH-10 DEP 1	269	274	271.5	45.00	17.12	35.642	0.48
WB-0814-MC-DSH-10 DEP 1	274	279	276.5	46.34	17.83	35.642	0.50
WB-0814-MC-DSH-10 DEP 1	279	284	281.5	46.64	17.90	35.642	0.50
WB-0814-MC-DSH-10 DEP 1	284	289	286.5	46.29	18.10	35.642	0.51
WB-0814-MC-DSH-10 DEP 1	289	294	291.5	46.20	18.24	35.642	0.51
WB-0814-MC-DSH-10 DEP 1	294	299	296.5	47.82	18.91	35.642	0.53
WB-0814-MC-DSH-10 DEP 1	299	304	301.5	44.80	17.61	35.642	0.49
WB-0814-MC-DSH-10 DEP 1	304	309	306.5	47.17	18.40	35.642	0.52
WB-0814-MC-DSH-10 DEP 1	309	314	311.5	47.31	18.31	35.642	0.51

Table K.21 (Continued).

Core ID	Top Depth of Interval (mm)	Bottom Depth of Interval (mm)	Average Depth of Interval (mm)	Wet Weight (g)	Dry Weight (g)	Sample Volume (cm^3)	Bulk Density (g/cm^3)
WB-0814-MC-DSH-10 DEP 1	314	319	316.5	43.70	17.01	35.642	0.48
WB-0814-MC-DSH-10 DEP 1	319	324	321.5	48.97	19.14	35.642	0.54
WB-0814-MC-DSH-10 DEP 1	324	329	326.5	44.11	17.16	35.642	0.48
WB-0814-MC-DSH-10 DEP 1	329	334	331.5	44.97	17.61	35.642	0.49
WB-0814-MC-DSH-10 DEP 1	334	339	336.5	47.24	18.52	35.642	0.52
WB-0814-MC-DSH-10 DEP 1	339	344	341.5	46.70	17.79	35.642	0.50
WB-0814-MC-DSH-10 DEP 1	344	349	346.5	45.78	17.24	35.642	0.48
WB-0814-MC-DSH-10 DEP 1	349	354	351.5	46.34	17.48	35.642	0.49
WB-0814-MC-DSH-10 DEP 1	354	359	356.5	45.52	17.04	35.642	0.48
WB-0814-MC-DSH-10 DEP 1	359	364	361.5	45.78	17.34	35.642	0.49
WB-0814-MC-DSH-10 DEP 1	364	369	366.5	45.81	17.15	35.642	0.48
WB-0814-MC-DSH-10 DEP 1	369	374	371.5	46.99	17.53	35.642	0.49
WB-0814-MC-DSH-10 DEP 1	374	379	376.5	44.96	16.93	35.642	0.48
WB-0814-MC-DSH-10 DEP 1	379	384	381.5	47.65	18.10	35.642	0.51
WB-0814-MC-DSH-10 DEP 1	384	389	386.5	45.58	17.28	35.642	0.48
WB-0814-MC-DSH-10 DEP 1	389	394	391.5	44.76	17.08	35.642	0.48
WB-0814-MC-DSH-10 DEP 1	394	399	396.5	48.09	18.18	35.642	0.51
WB-0814-MC-DSH-10 DEP 1	399	404	401.5	45.48	17.15	35.642	0.48
WB-0814-MC-DSH-10 DEP 1	404	409	406.5	47.35	18.21	35.642	0.51
WB-0814-MC-DSH-10 DEP 1	409	414	411.5	47.14	18.24	35.642	0.51
WB-0814-MC-DSH-10 DEP 1	414	419	416.5	48.21	18.59	35.642	0.52
WB-0814-MC-DSH-10 DEP 1	419	424	421.5	44.83	17.34	35.642	0.49
WB-0814-MC-DSH-10 DEP 1	424	429	426.5	52.43	20.34	35.642	0.57
WB-0814-MC-DSH-10 DEP 1	429	Base		61.30	24.28		

Table K.22. Bulk density data for core site WB-0814-MC-PCB-06 DEP 2. Sediment core sub-sample intervals (mm), sub-sample wet weight (g), dry weight (g), sub-sample volume (cm^3), and bulk density (g/cm^3). Note: Blank cell denotes no analysis performed.

Core ID	Top Depth of Interval (mm)	Bottom Depth of Interval (mm)	Average Depth of Interval (mm)	Wet Weight (g)	Dry Weight (g)	Sample Volume (cm^3)	Bulk Density (g/cm^3)
WB-0814-MC-PCB-06 DEP 2	0	2	1	12.99	2.56	14.257	0.18
WB-0814-MC-PCB-06 DEP 2	2	4	3	11.57	2.39	14.257	0.17
WB-0814-MC-PCB-06 DEP 2	4	6	5	12.14	2.58	14.257	0.18
WB-0814-MC-PCB-06 DEP 2	6	8	7	14.67	3.23	14.257	0.23
WB-0814-MC-PCB-06 DEP 2	8	10	9	11.04	2.87	14.257	0.20
WB-0814-MC-PCB-06 DEP 2	10	12	11	13.34	3.42	14.257	0.24
WB-0814-MC-PCB-06 DEP 2	12	14	13	13.40	3.41	14.257	0.24
WB-0814-MC-PCB-06 DEP 2	14	16	15	15.12	3.94	14.257	0.28
WB-0814-MC-PCB-06 DEP 2	16	18	17	15.95	4.24	14.257	0.30
WB-0814-MC-PCB-06 DEP 2	18	20	19	16.15	4.40	14.257	0.31
WB-0814-MC-PCB-06 DEP 2	20	22	21	14.92	4.11	14.257	0.29
WB-0814-MC-PCB-06 DEP 2	22	24	23	16.47	4.53	14.257	0.32
WB-0814-MC-PCB-06 DEP 2	24	26	25	17.53	4.92	14.257	0.35
WB-0814-MC-PCB-06 DEP 2	26	28	27	19.32	5.56	14.257	0.39
WB-0814-MC-PCB-06 DEP 2	28	30	29	17.39	5.01	14.257	0.35
WB-0814-MC-PCB-06 DEP 2	30	32	31	17.90	5.19	14.257	0.36
WB-0814-MC-PCB-06 DEP 2	32	34	33	15.53	4.66	14.257	0.33
WB-0814-MC-PCB-06 DEP 2	34	36	35	15.54	4.71	14.257	0.33
WB-0814-MC-PCB-06 DEP 2	36	38	37	16.08	4.91	14.257	0.34
WB-0814-MC-PCB-06 DEP 2	38	40	39	18.09	5.59	14.257	0.39
WB-0814-MC-PCB-06 DEP 2	40	42	41	15.17	4.97	14.257	0.35
WB-0814-MC-PCB-06 DEP 2	42	44	43	18.67	5.92	14.257	0.42
WB-0814-MC-PCB-06 DEP 2	44	46	45	15.43	5.01	14.257	0.35
WB-0814-MC-PCB-06 DEP 2	46	48	47	15.97	5.19	14.257	0.36
WB-0814-MC-PCB-06 DEP 2	48	50	49	17.20	5.63	14.257	0.39
WB-0814-MC-PCB-06 DEP 2	50	55	52.5	43.79	14.42	35.642	0.40
WB-0814-MC-PCB-06 DEP 2	55	60	57.5	43.59	14.21	35.642	0.40
WB-0814-MC-PCB-06 DEP 2	60	65	62.5	44.86	14.75	35.642	0.41
WB-0814-MC-PCB-06 DEP 2	65	70	67.5	41.76	14.06	35.642	0.39
WB-0814-MC-PCB-06 DEP 2	70	75	72.5	44.38	15.16	35.642	0.43
WB-0814-MC-PCB-06 DEP 2	75	80	77.5	42.25	14.71	35.642	0.41
WB-0814-MC-PCB-06 DEP 2	80	85	82.5	47.92	17.18	35.642	0.48
WB-0814-MC-PCB-06 DEP 2	85	90	87.5	41.08	15.14	35.642	0.42
WB-0814-MC-PCB-06 DEP 2	90	95	92.5	50.08	18.49	35.642	0.52
WB-0814-MC-PCB-06 DEP 2	95	100	97.5	42.72	16.00	35.642	0.45
WB-0814-MC-PCB-06 DEP 2	100	105	102.5	45.85	17.50	35.642	0.49

Table K.22 (Continued).

Core ID	Top Depth of Interval (mm)	Bottom Depth of Interval (mm)	Average Depth of Interval (mm)	Wet Weight (g)	Dry Weight (g)	Sample Volume (cm^3)	Bulk Density (g/cm^3)
WB-0814-MC-PCB-06 DEP 2	105	110	107.5	47.41	18.14	35.642	0.51
WB-0814-MC-PCB-06 DEP 2	110	117	113.5	67.98	26.17	49.899	0.52
WB-0814-MC-PCB-06 DEP 2	117	122	119.5	43.24	16.78	35.642	0.47
WB-0814-MC-PCB-06 DEP 2	122	127	124.5	42.94	16.68	35.642	0.47
WB-0814-MC-PCB-06 DEP 2	127	132	129.5	48.89	18.65	35.642	0.52
WB-0814-MC-PCB-06 DEP 2	132	137	134.5	46.19	17.50	35.642	0.49
WB-0814-MC-PCB-06 DEP 2	137	142	139.5	44.69	16.82	35.642	0.47
WB-0814-MC-PCB-06 DEP 2	142	147	144.5	46.77	17.73	35.642	0.50
WB-0814-MC-PCB-06 DEP 2	147	152	149.5	47.85	18.19	35.642	0.51
WB-0814-MC-PCB-06 DEP 2	152	157	154.5	50.12	19.35	35.642	0.54
WB-0814-MC-PCB-06 DEP 2	157	162	159.5	44.65	17.31	35.642	0.49
WB-0814-MC-PCB-06 DEP 2	162	167	164.5	45.88	17.95	35.642	0.50
WB-0814-MC-PCB-06 DEP 2	167	172	169.5	44.46	17.62	35.642	0.49
WB-0814-MC-PCB-06 DEP 2	172	177	174.5	44.87	17.92	35.642	0.50
WB-0814-MC-PCB-06 DEP 2	177	182	179.5	49.65	20.16	35.642	0.57
WB-0814-MC-PCB-06 DEP 2	182	187	184.5	45.21	18.64	35.642	0.52
WB-0814-MC-PCB-06 DEP 2	187	192	189.5	48.09	19.98	35.642	0.56
WB-0814-MC-PCB-06 DEP 2	192	197	194.5	49.29	20.63	35.642	0.58
WB-0814-MC-PCB-06 DEP 2	197	202	199.5	43.78	18.03	35.642	0.51
WB-0814-MC-PCB-06 DEP 2	202	207	204.5	50.87	20.97	35.642	0.59
WB-0814-MC-PCB-06 DEP 2	207	212	209.5	49.86	20.61	35.642	0.58
WB-0814-MC-PCB-06 DEP 2	212	217	214.5	49.06	19.96	35.642	0.56
WB-0814-MC-PCB-06 DEP 2	217	222	219.5	45.59	18.02	35.642	0.51
WB-0814-MC-PCB-06 DEP 2	222	227	224.5	42.44	16.94	35.642	0.48
WB-0814-MC-PCB-06 DEP 2	227	232	229.5	50.16	20.54	35.642	0.58
WB-0814-MC-PCB-06 DEP 2	232	237	234.5	42.74	17.75	35.642	0.50
WB-0814-MC-PCB-06 DEP 2	237	242	239.5	51.17	21.47	35.642	0.60
WB-0814-MC-PCB-06 DEP 2	242	247	244.5	43.80	18.35	35.642	0.51
WB-0814-MC-PCB-06 DEP 2	247	252	249.5	47.97	20.04	35.642	0.56
WB-0814-MC-PCB-06 DEP 2	252	257	254.5	44.40	18.43	35.642	0.52
WB-0814-MC-PCB-06 DEP 2	257	262	259.5	54.17	22.45	35.642	0.63
WB-0814-MC-PCB-06 DEP 2	262	267	264.5	49.68	20.38	35.642	0.57
WB-0814-MC-PCB-06 DEP 2	267	272	269.5	47.51	19.32	35.642	0.54
WB-0814-MC-PCB-06 DEP 2	272	277	274.5	45.01	18.28	35.642	0.51
WB-0814-MC-PCB-06 DEP 2	277	282	279.5	48.20	19.09	35.642	0.54
WB-0814-MC-PCB-06 DEP 2	282	287	284.5	45.51	17.86	35.642	0.50
WB-0814-MC-PCB-06 DEP 2	287	292	289.5	44.61	17.28	35.642	0.48
WB-0814-MC-PCB-06 DEP 2	292	297	294.5	44.48	17.13	35.642	0.48

Table K.22 (Continued).

Core ID	Top Depth of Interval (mm)	Bottom Depth of Interval (mm)	Average Depth of Interval (mm)	Wet Weight (g)	Dry Weight (g)	Sample Volume (cm^3)	Bulk Density (g/cm^3)
WB-0814-MC-PCB-06 DEP 2	297	302	299.5	48.28	18.46	35.642	0.52
WB-0814-MC-PCB-06 DEP 2	302	307	304.5	44.48	17.01	35.642	0.48
WB-0814-MC-PCB-06 DEP 2	307	312	309.5	47.77	18.36	35.642	0.52
WB-0814-MC-PCB-06 DEP 2	312	317	314.5	48.54	18.59	35.642	0.52
WB-0814-MC-PCB-06 DEP 2	317	322	319.5	43.99	17.00	35.642	0.48
WB-0814-MC-PCB-06 DEP 2	322	327	324.5	48.92	19.33	35.642	0.54
WB-0814-MC-PCB-06 DEP 2	327	332	329.5	45.27	18.26	35.642	0.51
WB-0814-MC-PCB-06 DEP 2	332	337	334.5	47.76	20.00	35.642	0.56
WB-0814-MC-PCB-06 DEP 2	337	342	339.5	45.85	19.44	35.642	0.55
WB-0814-MC-PCB-06 DEP 2	342	347	344.5	50.51	21.57	35.642	0.61
WB-0814-MC-PCB-06 DEP 2	347	352	349.5	47.72	20.58	35.642	0.58
WB-0814-MC-PCB-06 DEP 2	352	357	354.5	49.17	21.16	35.642	0.59
WB-0814-MC-PCB-06 DEP 2	357	362	359.5	48.84	20.95	35.642	0.59
WB-0814-MC-PCB-06 DEP 2	362	367	364.5	48.37	20.76	35.642	0.58
WB-0814-MC-PCB-06 DEP 2	367	372	369.5	47.11	20.17	35.642	0.57
WB-0814-MC-PCB-06 DEP 2	372	377	374.5	46.25	19.95	35.642	0.56
WB-0814-MC-PCB-06 DEP 2	377	382	379.5	49.66	21.65	35.642	0.61
WB-0814-MC-PCB-06 DEP 2	382	387	384.5	50.97	22.15	35.642	0.62
WB-0814-MC-PCB-06 DEP 2	387	392	389.5	48.76	21.42	35.642	0.60
WB-0814-MC-PCB-06 DEP 2	392	397	394.5	49.37	21.41	35.642	0.60
WB-0814-MC-PCB-06 DEP 2	397	402	399.5	49.91	21.62	35.642	0.61
WB-0814-MC-PCB-06 DEP 2	402	407	404.5	48.29	20.82	35.642	0.58
WB-0814-MC-PCB-06 DEP 2	407	412	409.5	47.84	20.45	35.642	0.57
WB-0814-MC-PCB-06 DEP 2	412	417	414.5	52.39	22.44	35.642	0.63
WB-0814-MC-PCB-06 DEP 2	417	Base		7.32	3.09		

Table K.23. Bulk density data for core site WB-0815-MC-04. Sediment core sub-sample intervals (mm), sub-sample wet weight (g), dry weight (g), sub-sample volume (cm^3), and bulk density (g/cm^3). Note: Blank cell denotes no analysis performed.

Core ID	Top Depth of Interval (mm)	Bottom Depth of Interval (mm)	Average Depth of Interval (mm)	Wet Weight (g)	Dry Weight (g)	Sample Volume (cm^3)	Bulk Density (g/cm^3)
WB-0815-MC-04	0	2	1	8.83	2.30	14.257	0.16
WB-0815-MC-04	2	4	3	12.42	3.48	14.257	0.24
WB-0815-MC-04	4	6	5	14.69	4.13	14.257	0.29
WB-0815-MC-04	6	8	7	15.88	4.47	14.257	0.31
WB-0815-MC-04	8	10	9	16.89	4.85	14.257	0.34
WB-0815-MC-04	10	12	11	16.92	4.93	14.257	0.35
WB-0815-MC-04	12	14	13	17.07	5.07	14.257	0.36
WB-0815-MC-04	14	16	15	16.44	4.98	14.257	0.35
WB-0815-MC-04	16	18	17	16.69	5.08	14.257	0.36
WB-0815-MC-04	18	20	19	15.86	4.88	14.257	0.34
WB-0815-MC-04	20	22	21	16.05	5.01	14.257	0.35
WB-0815-MC-04	22	24	23	17.68	5.60	14.257	0.39
WB-0815-MC-04	24	26	25	17.31	5.53	14.257	0.39
WB-0815-MC-04	26	28	27	18.50	5.96	14.257	0.42
WB-0815-MC-04	28	30	29	15.91	5.18	14.257	0.36
WB-0815-MC-04	30	35	32.5	40.42	13.68	35.642	0.38
WB-0815-MC-04	35	40	37.5	42.94	14.42	35.642	0.40
WB-0815-MC-04	40	45	42.5	44.49	14.86	35.642	0.42
WB-0815-MC-04	45	50	47.5	44.93	15.01	35.642	0.42
WB-0815-MC-04	50	55	52.5	44.18	14.96	35.642	0.42
WB-0815-MC-04	55	60	57.5	43.67	15.25	35.642	0.43
WB-0815-MC-04	60	65	62.5	46.72	17.00	35.642	0.48
WB-0815-MC-04	65	70	67.5	46.64	17.34	35.642	0.49
WB-0815-MC-04	70	75	72.5	42.80	16.23	35.642	0.46
WB-0815-MC-04	75	80	77.5	47.41	18.23	35.642	0.51
WB-0815-MC-04	80	85	82.5	44.98	17.38	35.642	0.49
WB-0815-MC-04	85	90	87.5	47.30	18.49	35.642	0.52
WB-0815-MC-04	90	95	92.5	47.66	18.91	35.642	0.53
WB-0815-MC-04	95	100	97.5	45.73	18.08	35.642	0.51
WB-0815-MC-04	100	105	102.5	46.47	18.49	35.642	0.52
WB-0815-MC-04	105	110	107.5	48.04	19.11	35.642	0.54
WB-0815-MC-04	110	115	112.5	46.59	18.73	35.642	0.53
WB-0815-MC-04	115	120	117.5	45.32	18.53	35.642	0.52
WB-0815-MC-04	120	125	122.5	49.86	20.55	35.642	0.58
WB-0815-MC-04	125	130	127.5	45.80	18.85	35.642	0.53
WB-0815-MC-04	130	135	132.5	47.27	19.54	35.642	0.55

Table K.23 (Continued).

Core ID	Top Depth of Interval (mm)	Bottom Depth of Interval (mm)	Average Depth of Interval (mm)	Wet Weight (g)	Dry Weight (g)	Sample Volume (cm^3)	Bulk Density (g/cm^3)
WB-0815-MC-04	135	140	137.5	47.14	19.40	35.642	0.54
WB-0815-MC-04	140	145	142.5	45.75	18.95	35.642	0.53
WB-0815-MC-04	145	150	147.5	49.42	20.70	35.642	0.58
WB-0815-MC-04	150	155	152.5	46.43	19.62	35.642	0.55
WB-0815-MC-04	155	160	157.5	50.02	21.17	35.642	0.59
WB-0815-MC-04	160	165	162.5	47.20	19.98	35.642	0.56
WB-0815-MC-04	165	170	167.5	47.99	20.45	35.642	0.57
WB-0815-MC-04	170	175	172.5	50.10	21.47	35.642	0.60
WB-0815-MC-04	175	180	177.5	46.35	19.88	35.642	0.56
WB-0815-MC-04	180	185	182.5	49.28	21.23	35.642	0.60
WB-0815-MC-04	185	190	187.5	47.42	20.62	35.642	0.58
WB-0815-MC-04	190	195	192.5	51.20	22.37	35.642	0.63
WB-0815-MC-04	195	200	197.5	42.85	18.75	35.642	0.53
WB-0815-MC-04	200	205	202.5	48.61	21.61	35.642	0.61
WB-0815-MC-04	205	210	207.5	50.59	22.66	35.642	0.64
WB-0815-MC-04	210	215	212.5	48.40	21.64	35.642	0.61
WB-0815-MC-04	215	220	217.5	47.70	21.25	35.642	0.60
WB-0815-MC-04	220	225	222.5	48.66	21.78	35.642	0.61
WB-0815-MC-04	225	230	227.5	48.68	22.03	35.642	0.62
WB-0815-MC-04	230	235	232.5	49.80	22.62	35.642	0.63
WB-0815-MC-04	235	240	237.5	49.60	22.58	35.642	0.63
WB-0815-MC-04	240	245	242.5	47.91	21.97	35.642	0.62
WB-0815-MC-04	245	250	247.5	50.61	23.41	35.642	0.66
WB-0815-MC-04	250	255	252.5	49.54	23.03	35.642	0.65
WB-0815-MC-04	255	260	257.5	55.54	25.85	35.642	0.73
WB-0815-MC-04	260	265	262.5	46.67	21.72	35.642	0.61
WB-0815-MC-04	265	270	267.5	51.29	23.79	35.642	0.67
WB-0815-MC-04	270	275	272.5		22.54	35.642	0.63
WB-0815-MC-04	275	280	277.5		24.32	35.642	0.68
WB-0815-MC-04	280	Base		10.50	4.91		

Table K.24. Bulk density data for core site WB-0815-MC-DSH-08-A. Sediment core sub-sample intervals (mm), sub-sample wet weight (g), dry weight (g), sub-sample volume (cm^3), and bulk density (g/cm^3). Note: Blank cell denotes no analysis performed.

Core ID	Top Depth of Interval (mm)	Bottom Depth of Interval (mm)	Average Depth of Interval (mm)	Wet Weight (g)	Dry Weight (g)	Sample Volume (cm^3)	Bulk Density (g/cm^3)
WB-0815-MC-DSH-08-A	0	2	1	9.78	2.18	14.257	0.15
WB-0815-MC-DSH-08-A	2	4	3	7.84	1.79	14.257	0.13
WB-0815-MC-DSH-08-A	4	6	5	9.78	2.19	14.257	0.15
WB-0815-MC-DSH-08-A	6	8	7	12.18	2.70	14.257	0.19
WB-0815-MC-DSH-08-A	8	10	9	13.13	2.86	14.257	0.20
WB-0815-MC-DSH-08-A	10	12	11	13.43	3.00	14.257	0.21
WB-0815-MC-DSH-08-A	12	14	13	13.44	3.05	14.257	0.21
WB-0815-MC-DSH-08-A	14	16	15	15.43	3.56	14.257	0.25
WB-0815-MC-DSH-08-A	16	18	17	14.27	3.35	14.257	0.23
WB-0815-MC-DSH-08-A	18	20	19	14.57	3.46	14.257	0.24
WB-0815-MC-DSH-08-A	20	22	21	15.18	3.61	14.257	0.25
WB-0815-MC-DSH-08-A	22	24	23	15.03	3.64	14.257	0.26
WB-0815-MC-DSH-08-A	24	26	25	14.49	3.54	14.257	0.25
WB-0815-MC-DSH-08-A	26	28	27	15.19	3.83	14.257	0.27
WB-0815-MC-DSH-08-A	28	30	29	16.02	4.05	14.257	0.28
WB-0815-MC-DSH-08-A	30	32	31	14.89	3.75	14.257	0.26
WB-0815-MC-DSH-08-A	32	34	33	15.65	3.95	14.257	0.28
WB-0815-MC-DSH-08-A	34	36	35	16.15	4.12	14.257	0.29
WB-0815-MC-DSH-08-A	36	38	37	15.89	4.10	14.257	0.29
WB-0815-MC-DSH-08-A	38	40	39	17.15	4.50	14.257	0.32
WB-0815-MC-DSH-08-A	40	42	41	15.48	4.11	14.257	0.29
WB-0815-MC-DSH-08-A	42	44	43	14.48	3.89	14.257	0.27
WB-0815-MC-DSH-08-A	44	46	45	15.07	4.18	14.257	0.29
WB-0815-MC-DSH-08-A	46	48	47	16.82	4.70	14.257	0.33
WB-0815-MC-DSH-08-A	48	50	49	16.94	4.78	14.257	0.34
WB-0815-MC-DSH-08-A	50	52	51	15.03	4.39	14.257	0.31
WB-0815-MC-DSH-08-A	52	54	53	17.48	5.15	14.257	0.36
WB-0815-MC-DSH-08-A	54	56	55	16.04	4.74	14.257	0.33
WB-0815-MC-DSH-08-A	56	58	57	18.22	5.51	14.257	0.39
WB-0815-MC-DSH-08-A	58	60	59	15.80	4.84	14.257	0.34
WB-0815-MC-DSH-08-A	60	65	62.5	44.83	14.05	35.642	0.39
WB-0815-MC-DSH-08-A	65	70	67.5	42.85	13.80	35.642	0.39
WB-0815-MC-DSH-08-A	70	75	72.5	48.91	22.08	35.642	0.62
WB-0815-MC-DSH-08-A	75	80	77.5	50.58	22.51	35.642	0.63
WB-0815-MC-DSH-08-A	80	85	82.5	49.12	22.11	35.642	0.62
WB-0815-MC-DSH-08-A	85	90	87.5	46.69	20.52	35.642	0.58

Table K.24 (Continued).

Core ID	Top Depth of Interval (mm)	Bottom Depth of Interval (mm)	Average Depth of Interval (mm)	Wet Weight (g)	Dry Weight (g)	Sample Volume (cm^3)	Bulk Density (g/cm^3)
WB-0815-MC-DSH-08-A	90	95	92.5	49.34	21.22	35.642	0.60
WB-0815-MC-DSH-08-A	95	100	97.5	42.20	18.37	35.642	0.52
WB-0815-MC-DSH-08-A	100	105	102.5	50.14	21.99	35.642	0.62
WB-0815-MC-DSH-08-A	105	110	107.5	50.69	21.88	35.642	0.61
WB-0815-MC-DSH-08-A	110	115	112.5	52.01	22.22	35.642	0.62
WB-0815-MC-DSH-08-A	115	120	117.5	50.49	21.21	35.642	0.60
WB-0815-MC-DSH-08-A	120	125	122.5	51.82	21.27	35.642	0.60
WB-0815-MC-DSH-08-A	125	130	127.5	46.87	19.34	35.642	0.54
WB-0815-MC-DSH-08-A	130	135	132.5	50.79	21.30	35.642	0.60
WB-0815-MC-DSH-08-A	135	140	137.5	46.10	19.42	35.642	0.54
WB-0815-MC-DSH-08-A	140	145	142.5	47.54	20.36	35.642	0.57
WB-0815-MC-DSH-08-A	145	150	147.5	48.55	21.49	35.642	0.60
WB-0815-MC-DSH-08-A	150	155	152.5	50.87	22.22	35.642	0.62
WB-0815-MC-DSH-08-A	155	160	157.5	51.39	23.06	35.642	0.65
WB-0815-MC-DSH-08-A	160	165	162.5	46.89	18.00	35.642	0.51
WB-0815-MC-DSH-08-A	165	170	167.5	46.55	17.81	35.642	0.50
WB-0815-MC-DSH-08-A	170	175	172.5	46.05	17.26	35.642	0.48
WB-0815-MC-DSH-08-A	175	180	177.5	45.77	16.95	35.642	0.48
WB-0815-MC-DSH-08-A	180	185	182.5	43.77	16.00	35.642	0.45
WB-0815-MC-DSH-08-A	185	190	187.5	45.65	16.64	35.642	0.47
WB-0815-MC-DSH-08-A	190	195	192.5	45.21	16.63	35.642	0.47
WB-0815-MC-DSH-08-A	195	200	197.5	44.65	16.51	35.642	0.46
WB-0815-MC-DSH-08-A	200	205	202.5	46.02	17.13	35.642	0.48
WB-0815-MC-DSH-08-A	205	210	207.5	44.59	16.74	35.642	0.47
WB-0815-MC-DSH-08-A	210	215	212.5	47.99	18.13	35.642	0.51
WB-0815-MC-DSH-08-A	215	220	217.5	46.27	17.67	35.642	0.50
WB-0815-MC-DSH-08-A	220	225	222.5	45.47	17.46	35.642	0.49
WB-0815-MC-DSH-08-A	225	230	227.5	49.17	18.91	35.642	0.53
WB-0815-MC-DSH-08-A	230	235	232.5	44.71	17.23	35.642	0.48
WB-0815-MC-DSH-08-A	235	240	237.5	46.85	18.23	35.642	0.51
WB-0815-MC-DSH-08-A	240	245	242.5	47.25	18.53	35.642	0.52
WB-0815-MC-DSH-08-A	245	250	247.5	44.96	17.75	35.642	0.50
WB-0815-MC-DSH-08-A	250	255	252.5	49.35	19.41	35.642	0.54
WB-0815-MC-DSH-08-A	255	260	257.5	44.75	17.54	35.642	0.49
WB-0815-MC-DSH-08-A	260	265	262.5	49.52	19.36	35.642	0.54
WB-0815-MC-DSH-08-A	265	270	267.5	48.35	18.82	35.642	0.53
WB-0815-MC-DSH-08-A	270	275	272.5	44.32	17.17	35.642	0.48
WB-0815-MC-DSH-08-A	275	280	277.5	48.21	18.78	35.642	0.53

Table K.24 (Continued).

Core ID	Top Depth of Interval (mm)	Bottom Depth of Interval (mm)	Average Depth of Interval (mm)	Wet Weight (g)	Dry Weight (g)	Sample Volume (cm^3)	Bulk Density (g/cm^3)
WB-0815-MC-DSH-08-A	280	285	282.5	45.53	17.84	35.642	0.50
WB-0815-MC-DSH-08-A	285	290	287.5	46.71	18.41	35.642	0.52
WB-0815-MC-DSH-08-A	290	295	292.5	46.47	18.29	35.642	0.51
WB-0815-MC-DSH-08-A	295	300	297.5	46.34	18.24	35.642	0.51
WB-0815-MC-DSH-08-A	300	305	302.5	48.24	18.78	35.642	0.53
WB-0815-MC-DSH-08-A	305	310	307.5	46.23	17.71	35.642	0.50
WB-0815-MC-DSH-08-A	310	315	312.5	44.89	17.22	35.642	0.48
WB-0815-MC-DSH-08-A	315	320	317.5	47.71	18.34	35.642	0.51
WB-0815-MC-DSH-08-A	320	325	322.5	46.80	18.10	35.642	0.51
WB-0815-MC-DSH-08-A	325	330	327.5	45.97	18.05	35.642	0.51
WB-0815-MC-DSH-08-A	330	335	332.5	47.63	18.91	35.642	0.53
WB-0815-MC-DSH-08-A	335	340	337.5	46.79	18.81	35.642	0.53
WB-0815-MC-DSH-08-A	340	345	342.5	45.93	18.80	35.642	0.53
WB-0815-MC-DSH-08-A	345	350	347.5	51.83	21.54	35.642	0.60
WB-0815-MC-DSH-08-A	350	355	352.5	46.66	19.51	35.642	0.55
WB-0815-MC-DSH-08-A	355	360	357.5	45.29	18.92	35.642	0.53
WB-0815-MC-DSH-08-A	360	365	362.5	50.90	21.38	35.642	0.60
WB-0815-MC-DSH-08-A	365	370	367.5	46.84	19.53	35.642	0.55
WB-0815-MC-DSH-08-A	370	375	372.5	46.79	19.51	35.642	0.55
WB-0815-MC-DSH-08-A	375	380	377.5	48.62	20.38	35.642	0.57
WB-0815-MC-DSH-08-A	380	385	382.5	47.20	19.86	35.642	0.56
WB-0815-MC-DSH-08-A	385	390	387.5	50.17	21.03	35.642	0.59
WB-0815-MC-DSH-08-A	390	395	392.5	46.32	19.22	35.642	0.54
WB-0815-MC-DSH-08-A	395	400	397.5	48.01	19.85	35.642	0.56
WB-0815-MC-DSH-08-A	400	405	402.5	47.70	19.51	35.642	0.55
WB-0815-MC-DSH-08-A	405	410	407.5	51.12	21.35	35.642	0.60
WB-0815-MC-DSH-08-A	410	415	412.5	47.60	18.79	35.642	0.53
WB-0815-MC-DSH-08-A	415	420	417.5	47.88	18.52	35.642	0.52
WB-0815-MC-DSH-08-A	420	Base		40.67	15.95		

Table K.25. Bulk density data for core site WB-0815-MC-DSH-10-A. Sediment core sub-sample intervals (mm), sub-sample wet weight (g), dry weight (g), sub-sample volume (cm^3), and bulk density (g/cm^3). Note: Blank cell denotes no analysis performed.

Core ID	Top Depth of Interval (mm)	Bottom Depth of Interval (mm)	Average Depth of Interval (mm)	Wet Weight (g)	Dry Weight (g)	Sample Volume (cm^3)	Bulk Density (g/cm^3)
WB-0815-MC-DSH-10-A	0	2	1	9.86	2.55	14.257	0.18
WB-0815-MC-DSH-10-A	2	4	3	14.94	4.14	14.257	0.29
WB-0815-MC-DSH-10-A	4	6	5	15.14	4.32	14.257	0.30
WB-0815-MC-DSH-10-A	6	8	7	14.99	4.35	14.257	0.31
WB-0815-MC-DSH-10-A	8	10	9	16.06	4.78	14.257	0.34
WB-0815-MC-DSH-10-A	10	12	11	15.81	4.72	14.257	0.33
WB-0815-MC-DSH-10-A	12	14	13	16.32	4.99	14.257	0.35
WB-0815-MC-DSH-10-A	14	16	15	16.48	5.08	14.257	0.36
WB-0815-MC-DSH-10-A	16	18	17	15.51	4.81	14.257	0.34
WB-0815-MC-DSH-10-A	18	20	19	15.05	4.71	14.257	0.33
WB-0815-MC-DSH-10-A	20	22	21	16.05	5.13	14.257	0.36
WB-0815-MC-DSH-10-A	22	24	23	17.47	5.59	14.257	0.39
WB-0815-MC-DSH-10-A	24	26	25	16.09	5.21	14.257	0.37
WB-0815-MC-DSH-10-A	26	28	27	15.68	5.14	14.257	0.36
WB-0815-MC-DSH-10-A	28	30	29	16.76	5.50	14.257	0.39
WB-0815-MC-DSH-10-A	30	35	32.5	43.23	14.35	35.642	0.40
WB-0815-MC-DSH-10-A	35	40	37.5	46.13	15.25	35.642	0.43
WB-0815-MC-DSH-10-A	40	45	42.5	47.54	15.91	35.642	0.45
WB-0815-MC-DSH-10-A	45	50	47.5	40.24	13.42	35.642	0.38
WB-0815-MC-DSH-10-A	50	55	52.5	46.08	15.80	35.642	0.44
WB-0815-MC-DSH-10-A	55	60	57.5	45.37	15.40	35.642	0.43
WB-0815-MC-DSH-10-A	60	65	62.5	44.58	15.56	35.642	0.44
WB-0815-MC-DSH-10-A	65	70	67.5	52.44	19.01	35.642	0.53
WB-0815-MC-DSH-10-A	70	75	72.5	33.45	12.33	35.642	0.35
WB-0815-MC-DSH-10-A	75	80	77.5	45.65	17.44	35.642	0.49
WB-0815-MC-DSH-10-A	80	85	82.5	44.23	16.81	35.642	0.47
WB-0815-MC-DSH-10-A	85	90	87.5	44.15	17.24	35.642	0.48
WB-0815-MC-DSH-10-A	90	95	92.5	45.89	17.64	35.642	0.49
WB-0815-MC-DSH-10-A	95	100	97.5	44.51	18.24	35.642	0.51
WB-0815-MC-DSH-10-A	100	105	102.5	48.07	17.87	35.642	0.50
WB-0815-MC-DSH-10-A	105	110	107.5	46.05	17.81	35.642	0.50
WB-0815-MC-DSH-10-A	110	115	112.5	46.92	16.78	35.642	0.47
WB-0815-MC-DSH-10-A	115	120	117.5	45.13	18.49	35.642	0.52
WB-0815-MC-DSH-10-A	120	125	122.5	47.65	15.43	35.642	0.43
WB-0815-MC-DSH-10-A	125	130	127.5	43.35	17.05	35.642	0.48
WB-0815-MC-DSH-10-A	130	135	132.5	45.35	16.72	35.642	0.47

Table K.25 (Continued).

Core ID	Top Depth of Interval (mm)	Bottom Depth of Interval (mm)	Average Depth of Interval (mm)	Wet Weight (g)	Dry Weight (g)	Sample Volume (cm^3)	Bulk Density (g/cm^3)
WB-0815-MC-DSH-10-A	135	140	137.5	46.30	16.44	35.642	0.46
WB-0815-MC-DSH-10-A	140	145	142.5	45.78	16.70	35.642	0.47
WB-0815-MC-DSH-10-A	145	150	147.5	45.86	16.06	35.642	0.45
WB-0815-MC-DSH-10-A	150	155	152.5	44.82	17.36	35.642	0.49
WB-0815-MC-DSH-10-A	155	160	157.5	46.22	14.59	35.642	0.41
WB-0815-MC-DSH-10-A	160	165	162.5	44.07	16.25	35.642	0.46
WB-0815-MC-DSH-10-A	165	170	167.5	45.82	16.63	35.642	0.47
WB-0815-MC-DSH-10-A	170	175	172.5	46.43	16.14	35.642	0.45
WB-0815-MC-DSH-10-A	175	180	177.5	43.81	16.86	35.642	0.47
WB-0815-MC-DSH-10-A	180	185	182.5	45.47	16.77	35.642	0.47
WB-0815-MC-DSH-10-A	185	190	187.5	45.11	17.53	35.642	0.49
WB-0815-MC-DSH-10-A	190	195	192.5	47.26	17.06	35.642	0.48
WB-0815-MC-DSH-10-A	195	200	197.5	46.10	18.05	35.642	0.51
WB-0815-MC-DSH-10-A	200	205	202.5	47.25	17.64	35.642	0.49
WB-0815-MC-DSH-10-A	205	210	207.5	44.65	16.51	35.642	0.46
WB-0815-MC-DSH-10-A	210	215	212.5	46.50	17.16	35.642	0.48
WB-0815-MC-DSH-10-A	215	220	217.5	47.76	17.75	35.642	0.50
WB-0815-MC-DSH-10-A	220	225	222.5	43.62	16.35	35.642	0.46
WB-0815-MC-DSH-10-A	225	230	227.5	44.45	16.46	35.642	0.46
WB-0815-MC-DSH-10-A	230	235	232.5	44.64	16.49	35.642	0.46
WB-0815-MC-DSH-10-A	235	240	237.5	46.03	17.12	35.642	0.48
WB-0815-MC-DSH-10-A	240	245	242.5	44.64	16.72	35.642	0.47
WB-0815-MC-DSH-10-A	245	250	247.5	46.38	17.40	35.642	0.49
WB-0815-MC-DSH-10-A	250	255	252.5	45.91	17.12	35.642	0.48
WB-0815-MC-DSH-10-A	255	260	257.5	45.13	16.86	35.642	0.47
WB-0815-MC-DSH-10-A	260	265	262.5	47.91	17.83	35.642	0.50
WB-0815-MC-DSH-10-A	265	270	267.5	44.62	16.60	35.642	0.47
WB-0815-MC-DSH-10-A	270	275	272.5	45.66	16.97	35.642	0.48
WB-0815-MC-DSH-10-A	275	280	277.5	44.46	16.57	35.642	0.46
WB-0815-MC-DSH-10-A	280	285	282.5	46.75	17.39	35.642	0.49
WB-0815-MC-DSH-10-A	285	290	287.5	45.86	16.89	35.642	0.47
WB-0815-MC-DSH-10-A	290	295	292.5	46.56	17.08	35.642	0.48
WB-0815-MC-DSH-10-A	295	300	297.5	43.76	15.82	35.642	0.44
WB-0815-MC-DSH-10-A	300	305	302.5	45.06	16.27	35.642	0.46
WB-0815-MC-DSH-10-A	305	310	307.5	45.28	16.48	35.642	0.46
WB-0815-MC-DSH-10-A	310	315	312.5	46.40	17.02	35.642	0.48
WB-0815-MC-DSH-10-A	315	320	317.5	48.73	18.16	35.642	0.51
WB-0815-MC-DSH-10-A	320	325	322.5	44.74	16.63	35.642	0.47

Table K.25 (Continued).

Core ID	Top Depth of Interval (mm)	Bottom Depth of Interval (mm)	Average Depth of Interval (mm)	Wet Weight (g)	Dry Weight (g)	Sample Volume (cm^3)	Bulk Density (g/cm^3)
WB-0815-MC-DSH-10-A	325	330	327.5	44.43	16.65	35.642	0.47
WB-0815-MC-DSH-10-A	330	335	332.5	45.01	17.06	35.642	0.48
WB-0815-MC-DSH-10-A	335	340	337.5	45.90	17.49	35.642	0.49
WB-0815-MC-DSH-10-A	340	345	342.5	45.23	16.94	35.642	0.48
WB-0815-MC-DSH-10-A	345	350	347.5	46.53	17.26	35.642	0.48
WB-0815-MC-DSH-10-A	350	355	352.5	45.34	16.83	35.642	0.47
WB-0815-MC-DSH-10-A	355	360	357.5	46.30	17.16	35.642	0.48
WB-0815-MC-DSH-10-A	360	365	362.5	45.85	17.01	35.642	0.48
WB-0815-MC-DSH-10-A	365	370	367.5	45.45	16.73	35.642	0.47
WB-0815-MC-DSH-10-A	370	375	372.5	46.06	16.94	35.642	0.48
WB-0815-MC-DSH-10-A	375	380	377.5	45.02	16.47	35.642	0.46
WB-0815-MC-DSH-10-A	380	385	382.5	46.30	16.84	35.642	0.47
WB-0815-MC-DSH-10-A	385	390	387.5	43.93	15.92	35.642	0.45
WB-0815-MC-DSH-10-A	390	395	392.5	45.47	16.57	35.642	0.46
WB-0815-MC-DSH-10-A	395	400	397.5	46.36	16.93	35.642	0.48
WB-0815-MC-DSH-10-A	400	405	402.5	45.24	16.51	35.642	0.46
WB-0815-MC-DSH-10-A	405	410	407.5	44.29	16.99	35.642	0.48
WB-0815-MC-DSH-10-A	410	415	412.5	48.25	17.74	35.642	0.50
WB-0815-MC-DSH-10-A	415	420	417.5	45.92	16.98	35.642	0.48
WB-0815-MC-DSH-10-A	420	425	422.5	46.19	17.19	35.642	0.48
WB-0815-MC-DSH-10-A	425	430	427.5	44.57	16.73	35.642	0.47
WB-0815-MC-DSH-10-A	430	435	432.5	48.12	18.14	35.642	0.51
WB-0815-MC-DSH-10-A	435	440	437.5	47.37	17.83	35.642	0.50
WB-0815-MC-DSH-10-A	440	445	442.5	46.39	17.43	35.642	0.49
WB-0815-MC-DSH-10-A	445	450	447.5	45.83	17.26	35.642	0.48
WB-0815-MC-DSH-10-A	450	455	452.5	47.94	18.37	35.642	0.52
WB-0815-MC-DSH-10-A	455	Base		22.57	8.74		

Table K.26. Bulk density data for core site WB-0815-MC-PCB-06-A. Sediment core sub-sample intervals (mm), sub-sample wet weight (g), dry weight (g), sub-sample volume (cm^3), and bulk density (g/cm^3). Note: Blank cell denotes no analysis performed.

Core ID	Top Depth of Interval (mm)	Bottom Depth of Interval (mm)	Average Depth of Interval (mm)	Wet Weight (g)	Dry Weight (g)	Sample Volume (cm^3)	Bulk Density (g/cm^3)
WB-0815-MC-PCB-06-A	0	2	1	3.61	0.86	14.257	0.06
WB-0815-MC-PCB-06-A	2	4	3	9.79	2.24	14.257	0.16
WB-0815-MC-PCB-06-A	4	6	5	11.80	2.85	14.257	0.20
WB-0815-MC-PCB-06-A	6	8	7	13.93	3.57	14.257	0.25
WB-0815-MC-PCB-06-A	8	10	9	11.98	3.10	14.257	0.22
WB-0815-MC-PCB-06-A	10	12	11	15.52	4.04	14.257	0.28
WB-0815-MC-PCB-06-A	12	14	13	13.73	3.55	14.257	0.25
WB-0815-MC-PCB-06-A	14	16	15	15.24	3.94	14.257	0.28
WB-0815-MC-PCB-06-A	16	18	17	13.79	3.62	14.257	0.25
WB-0815-MC-PCB-06-A	18	20	19	14.51	3.88	14.257	0.27
WB-0815-MC-PCB-06-A	20	22	21	16.94	4.56	14.257	0.32
WB-0815-MC-PCB-06-A	22	24	23	16.42	4.44	14.257	0.31
WB-0815-MC-PCB-06-A	24	26	25	15.58	4.25	14.257	0.30
WB-0815-MC-PCB-06-A	26	28	27	15.65	4.30	14.257	0.30
WB-0815-MC-PCB-06-A	28	30	29	15.84	4.42	14.257	0.31
WB-0815-MC-PCB-06-A	30	32	31	15.60	4.41	14.257	0.31
WB-0815-MC-PCB-06-A	32	34	33	16.40	4.69	14.257	0.33
WB-0815-MC-PCB-06-A	34	36	35	15.11	4.34	14.257	0.30
WB-0815-MC-PCB-06-A	36	38	37	16.79	4.90	14.257	0.34
WB-0815-MC-PCB-06-A	38	40	39	17.26	5.03	14.257	0.35
WB-0815-MC-PCB-06-A	40	42	41	14.75	4.37	14.257	0.31
WB-0815-MC-PCB-06-A	42	44	43	15.29	4.60	14.257	0.32
WB-0815-MC-PCB-06-A	44	46	45	17.35	5.28	14.257	0.37
WB-0815-MC-PCB-06-A	46	48	47	15.55	4.82	14.257	0.34
WB-0815-MC-PCB-06-A	48	50	49	15.70	4.92	14.257	0.35
WB-0815-MC-PCB-06-A	50	52	51	16.07	5.06	14.257	0.35
WB-0815-MC-PCB-06-A	52	54	53	16.15	5.10	14.257	0.36
WB-0815-MC-PCB-06-A	54	56	55	16.04	5.09	14.257	0.36
WB-0815-MC-PCB-06-A	56	58	57	19.82	6.37	14.257	0.45
WB-0815-MC-PCB-06-A	58	60	59	15.38	5.00	14.257	0.35
WB-0815-MC-PCB-06-A	60	65	62.5	41.27	13.64	35.642	0.38
WB-0815-MC-PCB-06-A	65	70	67.5	44.73	15.10	35.642	0.42
WB-0815-MC-PCB-06-A	70	75	72.5	45.06	15.61	35.642	0.44
WB-0815-MC-PCB-06-A	75	80	77.5	44.80	15.78	35.642	0.44
WB-0815-MC-PCB-06-A	80	85	82.5	43.45	15.21	35.642	0.43
WB-0815-MC-PCB-06-A	85	90	87.5	39.11	13.74	35.642	0.39

Table K.26 (Continued).

Core ID	Top Depth of Interval (mm)	Bottom Depth of Interval (mm)	Average Depth of Interval (mm)	Wet Weight (g)	Dry Weight (g)	Sample Volume (cm^3)	Bulk Density (g/cm^3)
WB-0815-MC-PCB-06-A	90	95	92.5	48.51	17.10	35.642	0.48
WB-0815-MC-PCB-06-A	95	100	97.5	44.42	15.43	35.642	0.43
WB-0815-MC-PCB-06-A	100	105	102.5	43.70	15.24	35.642	0.43
WB-0815-MC-PCB-06-A	105	110	107.5	40.83	14.33	35.642	0.40
WB-0815-MC-PCB-06-A	110	115	112.5	46.16	16.17	35.642	0.45
WB-0815-MC-PCB-06-A	115	120	117.5	46.60	16.37	35.642	0.46
WB-0815-MC-PCB-06-A	120	125	122.5	42.30	14.74	35.642	0.41
WB-0815-MC-PCB-06-A	125	130	127.5	43.65	15.21	35.642	0.43
WB-0815-MC-PCB-06-A	130	135	132.5	44.98	15.75	35.642	0.44
WB-0815-MC-PCB-06-A	135	140	137.5	45.55	16.03	35.642	0.45
WB-0815-MC-PCB-06-A	140	145	142.5	45.17	16.07	35.642	0.45
WB-0815-MC-PCB-06-A	145	150	147.5	44.25	15.87	35.642	0.45
WB-0815-MC-PCB-06-A	150	155	152.5	44.41	15.83	35.642	0.44
WB-0815-MC-PCB-06-A	155	160	157.5	44.39	15.82	35.642	0.44
WB-0815-MC-PCB-06-A	160	165	162.5	44.39	15.90	35.642	0.45
WB-0815-MC-PCB-06-A	165	170	167.5	46.32	16.65	35.642	0.47
WB-0815-MC-PCB-06-A	170	175	172.5	41.51	14.84	35.642	0.42
WB-0815-MC-PCB-06-A	175	180	177.5	48.50	17.57	35.642	0.49
WB-0815-MC-PCB-06-A	180	185	182.5	44.10	15.78	35.642	0.44
WB-0815-MC-PCB-06-A	185	190	187.5	42.76	15.27	35.642	0.43
WB-0815-MC-PCB-06-A	190	195	192.5	44.41	15.98	35.642	0.45
WB-0815-MC-PCB-06-A	195	200	197.5	43.97	15.94	35.642	0.45
WB-0815-MC-PCB-06-A	200	205	202.5	46.64	17.26	35.642	0.48
WB-0815-MC-PCB-06-A	205	210	207.5	46.63	17.36	35.642	0.49
WB-0815-MC-PCB-06-A	210	215	212.5	41.05	15.22	35.642	0.43
WB-0815-MC-PCB-06-A	215	220	217.5	49.15	17.90	35.642	0.50
WB-0815-MC-PCB-06-A	220	225	222.5	42.03	15.15	35.642	0.43
WB-0815-MC-PCB-06-A	225	230	227.5	45.67	16.44	35.642	0.46
WB-0815-MC-PCB-06-A	230	235	232.5	46.49	16.70	35.642	0.47
WB-0815-MC-PCB-06-A	235	240	237.5	43.95	15.90	35.642	0.45
WB-0815-MC-PCB-06-A	240	245	242.5	46.40	16.96	35.642	0.48
WB-0815-MC-PCB-06-A	245	250	247.5	44.95	16.68	35.642	0.47
WB-0815-MC-PCB-06-A	250	255	252.5	48.21	18.06	35.642	0.51
WB-0815-MC-PCB-06-A	255	260	257.5	47.87	18.15	35.642	0.51
WB-0815-MC-PCB-06-A	260	265	262.5	51.30	19.66	35.642	0.55
WB-0815-MC-PCB-06-A	265	270	267.5	49.87	19.26	35.642	0.54
WB-0815-MC-PCB-06-A	270	275	272.5	41.85	16.10	35.642	0.45
WB-0815-MC-PCB-06-A	275	280	277.5	39.39	15.13	35.642	0.42

Table K.26 (Continued).

Core ID	Top Depth of Interval (mm)	Bottom Depth of Interval (mm)	Average Depth of Interval (mm)	Wet Weight (g)	Dry Weight (g)	Sample Volume (cm^3)	Bulk Density (g/cm^3)
WB-0815-MC-PCB-06-A	280	285	282.5	43.44	16.71	35.642	0.47
WB-0815-MC-PCB-06-A	285	290	287.5	45.57	17.46	35.642	0.49
WB-0815-MC-PCB-06-A	290	295	292.5	42.14	15.88	35.642	0.45
WB-0815-MC-PCB-06-A	295	300	297.5	46.89	17.75	35.642	0.50
WB-0815-MC-PCB-06-A	300	305	302.5	45.82	17.51	35.642	0.49
WB-0815-MC-PCB-06-A	305	310	307.5	46.92	17.96	35.642	0.50
WB-0815-MC-PCB-06-A	310	315	312.5	46.05	17.49	35.642	0.49
WB-0815-MC-PCB-06-A	315	320	317.5	45.56	17.21	35.642	0.48
WB-0815-MC-PCB-06-A	320	325	322.5	45.65	17.22	35.642	0.48
WB-0815-MC-PCB-06-A	325	330	327.5	47.08	17.94	35.642	0.50
WB-0815-MC-PCB-06-A	330	335	332.5	45.57	17.30	35.642	0.49
WB-0815-MC-PCB-06-A	335	340	337.5	46.85	17.76	35.642	0.50
WB-0815-MC-PCB-06-A	340	345	342.5	45.91	17.38	35.642	0.49
WB-0815-MC-PCB-06-A	345	350	347.5	46.10	17.43	35.642	0.49
WB-0815-MC-PCB-06-A	350	355	352.5	45.81	17.50	35.642	0.49
WB-0815-MC-PCB-06-A	355	360	357.5	45.79	17.46	35.642	0.49
WB-0815-MC-PCB-06-A	360	365	362.5	44.74	16.97	35.642	0.48
WB-0815-MC-PCB-06-A	365	370	367.5	45.94	17.40	35.642	0.49
WB-0815-MC-PCB-06-A	370	375	372.5	47.27	18.29	35.642	0.51
WB-0815-MC-PCB-06-A	375	380	377.5	45.35	17.32	35.642	0.49
WB-0815-MC-PCB-06-A	380	385	382.5	45.74	17.78	35.642	0.50
WB-0815-MC-PCB-06-A	385	390	387.5	47.73	18.68	35.642	0.52
WB-0815-MC-PCB-06-A	390	395	392.5	45.14	17.77	35.642	0.50
WB-0815-MC-PCB-06-A	395	400	397.5	46.63	18.40	35.642	0.52
WB-0815-MC-PCB-06-A	400	405	402.5	46.95	18.63	35.642	0.52
WB-0815-MC-PCB-06-A	405	410	407.5		18.30	35.642	0.51
WB-0815-MC-PCB-06-A	410	415	412.5		18.25	35.642	0.51
WB-0815-MC-PCB-06-A	415	420	417.5		19.45	35.642	0.55
WB-0815-MC-PCB-06-A	420	425	422.5		18.67	35.642	0.52
WB-0815-MC-PCB-06-A	425	430	427.5		20.18	35.642	0.57
WB-0815-MC-PCB-06-A	430	435	432.5		18.11	35.642	0.51
WB-0815-MC-PCB-06-A	435	440	437.5		19.44	35.642	0.55
WB-0815-MC-PCB-06-A	440	445	442.5		18.51	35.642	0.52
WB-0815-MC-PCB-06-A	445	450	447.5		19.49	35.642	0.55
WB-0815-MC-PCB-06-A	450	455	452.5		20.04	35.642	0.56
WB-0815-MC-PCB-06-A	455	460	457.5		19.63	35.642	0.55
WB-0815-MC-PCB-06-A	460	465	462.5		20.17	35.642	0.57
WB-0815-MC-PCB-06-A	465	470	467.5		20.87	35.642	0.59

Table K.26 (Continued).

Core ID	Top Depth of Interval (mm)	Bottom Depth of Interval (mm)	Average Depth of Interval (mm)	Wet Weight (g)	Dry Weight (g)	Sample Volume (cm^3)	Bulk Density (g/cm^3)
WB-0815-MC-PCB-06-A	470	Base			14.81		

Table K.27. Bulk density data for core site WB-0816-MC-04. Sediment core sub-sample intervals (mm), sub-sample wet weight (g), dry weight (g), sub-sample volume (cm^3), and bulk density (g/cm^3). Note: Blank cell denotes no analysis performed.

Core ID	Top Depth of Interval (mm)	Bottom Depth of Interval (mm)	Average Depth of Interval (mm)	Wet Weight (g)	Dry Weight (g)	Sample Volume (cm^3)	Bulk Density (g/cm^3)
WB-0816-MC-04	0	2	1	8.92	2.58	14.257	0.18
WB-0816-MC-04	2	4	3	10.87	3.26	14.257	0.23
WB-0816-MC-04	4	6	5	13.77	4.21	14.257	0.30
WB-0816-MC-04	6	8	7	16.90	5.12	14.257	0.36
WB-0816-MC-04	8	10	9	16.53	5.17	14.257	0.36
WB-0816-MC-04	10	12	11	17.88	5.78	14.257	0.41
WB-0816-MC-04	12	14	13	18.90	6.30	14.257	0.44
WB-0816-MC-04	14	16	15	18.31	6.24	14.257	0.44
WB-0816-MC-04	16	18	17	16.33	5.59	14.257	0.39
WB-0816-MC-04	18	20	19	19.04	6.53	14.257	0.46
WB-0816-MC-04	20	22	21	18.45	6.35	14.257	0.45
WB-0816-MC-04	22	24	23	17.08	5.98	14.257	0.42
WB-0816-MC-04	24	26	25	18.58	6.47	14.257	0.45
WB-0816-MC-04	26	28	27	18.17	6.32	14.257	0.44
WB-0816-MC-04	28	30	29	18.20	6.33	14.257	0.44
WB-0816-MC-04	30	32	31	18.11	6.30	14.257	0.44
WB-0816-MC-04	32	34	33	17.67	6.16	14.257	0.43
WB-0816-MC-04	34	36	35	18.70	6.53	14.257	0.46
WB-0816-MC-04	36	38	37	18.91	6.65	14.257	0.47
WB-0816-MC-04	38	40	39	16.81	5.93	14.257	0.42
WB-0816-MC-04	40	42	41	17.68	6.24	14.257	0.44
WB-0816-MC-04	42	44	43	18.55	6.60	14.257	0.46
WB-0816-MC-04	44	46	45	17.76	6.32	14.257	0.44
WB-0816-MC-04	46	48	47	19.49	6.92	14.257	0.49
WB-0816-MC-04	48	50	49	16.81	5.99	14.257	0.42
WB-0816-MC-04	50	52	51	17.74	6.41	14.257	0.45
WB-0816-MC-04	52	54	53	18.21	6.63	14.257	0.47
WB-0816-MC-04	54	56	55	18.25	6.64	14.257	0.47
WB-0816-MC-04	56	58	57	17.98	6.59	14.257	0.46
WB-0816-MC-04	58	60	59	19.35	7.08	14.257	0.50
WB-0816-MC-04	60	62	61	18.04	6.63	14.257	0.47
WB-0816-MC-04	62	64	63	17.82	6.59	14.257	0.46
WB-0816-MC-04	64	66	65	18.26	6.73	14.257	0.47
WB-0816-MC-04	66	68	67	18.29	6.81	14.257	0.48
WB-0816-MC-04	68	70	69	18.30	6.89	14.257	0.48
WB-0816-MC-04	70	72	71	17.63	6.62	14.257	0.46

Table K.27 (Continued).

Core ID	Top Depth of Interval (mm)	Bottom Depth of Interval (mm)	Average Depth of Interval (mm)	Wet Weight (g)	Dry Weight (g)	Sample Volume (cm^3)	Bulk Density (g/cm^3)
WB-0816-MC-04	72	74	73	18.87	7.16	14.257	0.50
WB-0816-MC-04	74	76	75	18.79	7.16	14.257	0.50
WB-0816-MC-04	76	78	77	18.97	7.24	14.257	0.51
WB-0816-MC-04	78	80	79	18.07	6.93	14.257	0.49
WB-0816-MC-04	80	82	81	18.36	7.04	14.257	0.49
WB-0816-MC-04	82	84	83	18.68	7.13	14.257	0.50
WB-0816-MC-04	84	86	85	19.83	7.69	14.257	0.54
WB-0816-MC-04	86	88	87	15.14	5.92	14.257	0.42
WB-0816-MC-04	88	90	89	21.05	8.28	14.257	0.58
WB-0816-MC-04	90	95	92.5	48.48	19.54	35.642	0.55
WB-0816-MC-04	95	100	97.5	45.60	18.29	35.642	0.51
WB-0816-MC-04	100	105	102.5	48.18	19.47	35.642	0.55
WB-0816-MC-04	105	110	107.5	48.41	19.79	35.642	0.56
WB-0816-MC-04	110	115	112.5	47.94	19.73	35.642	0.55
WB-0816-MC-04	115	120	117.5	47.66	19.87	35.642	0.56
WB-0816-MC-04	120	125	122.5	56.26	23.62	35.642	0.66
WB-0816-MC-04	125	130	127.5	50.73	20.88	35.642	0.59
WB-0816-MC-04	130	135	132.5	38.03	15.57	35.642	0.44
WB-0816-MC-04	135	140	137.5	44.38	18.66	35.642	0.52
WB-0816-MC-04	140	145	142.5	46.12	20.05	35.642	0.56
WB-0816-MC-04	145	150	147.5	50.10	22.34	35.642	0.63
WB-0816-MC-04	150	155	152.5	48.53	21.79	35.642	0.61
WB-0816-MC-04	155	160	157.5	49.21	22.16	35.642	0.62
WB-0816-MC-04	160	165	162.5	49.04	22.21	35.642	0.62
WB-0816-MC-04	165	170	167.5	48.16	22.17	35.642	0.62
WB-0816-MC-04	170	175	172.5	52.02	23.92	35.642	0.67
WB-0816-MC-04	175	180	177.5	52.71	24.09	35.642	0.68
WB-0816-MC-04	180	185	182.5	48.94	22.29	35.642	0.63
WB-0816-MC-04	185	190	187.5	49.10	22.39	35.642	0.63
WB-0816-MC-04	190	195	192.5	53.56	24.45	35.642	0.69
WB-0816-MC-04	195	200	197.5	51.45	23.38	35.642	0.66
WB-0816-MC-04	200	205	202.5	63.80	28.71	35.642	0.81
WB-0816-MC-04	205	210	207.5	47.02	21.26	35.642	0.60
WB-0816-MC-04	210	215	212.5	44.18	19.83	35.642	0.56
WB-0816-MC-04	215	220	217.5	47.93	21.60	35.642	0.61
WB-0816-MC-04	220	225	222.5	45.27	20.34	35.642	0.57
WB-0816-MC-04	225	230	227.5	46.78	20.94	35.642	0.59
WB-0816-MC-04	230	235	232.5	41.62	18.41	35.642	0.52

Table K.27 (Continued).

Core ID	Top Depth of Interval (mm)	Bottom Depth of Interval (mm)	Average Depth of Interval (mm)	Wet Weight (g)	Dry Weight (g)	Sample Volume (cm^3)	Bulk Density (g/cm^3)
WB-0816-MC-04	235	240	237.5	50.58	22.47	35.642	0.63
WB-0816-MC-04	240	245	242.5	49.37	21.97	35.642	0.62
WB-0816-MC-04	245	250	247.5	48.50	21.46	35.642	0.60
WB-0816-MC-04	250	255	252.5	45.85	20.42	35.642	0.57
WB-0816-MC-04	255	260	257.5	50.39	22.44	35.642	0.63
WB-0816-MC-04	260	265	262.5	49.66	22.29	35.642	0.63
WB-0816-MC-04	265	270	267.5	49.49	22.44	35.642	0.63
WB-0816-MC-04	270	275	272.5	54.26	24.88	35.642	0.70
WB-0816-MC-04	275	280	277.5	55.33	25.37	35.642	0.71
WB-0816-MC-04	280	285	282.5	59.78	27.29	35.642	0.77
WB-0816-MC-04	285	290	287.5	49.04	22.10	35.642	0.62
WB-0816-MC-04	290	295	292.5	40.99	18.08	35.642	0.51
WB-0816-MC-04	295	300	297.5	45.75	19.63	35.642	0.55
WB-0816-MC-04	300	305	302.5	42.96	17.71	35.642	0.50
WB-0816-MC-04	305	310	307.5	44.10	17.92	35.642	0.50
WB-0816-MC-04	310	315	312.5	48.74	19.86	35.642	0.56
WB-0816-MC-04	315	320	317.5		19.17	35.642	0.54
WB-0816-MC-04	320	325	322.5	47.84	19.95	35.642	0.56
WB-0816-MC-04	325	330	327.5	48.84	20.71	35.642	0.58
WB-0816-MC-04	330	335	332.5	47.06	19.98	35.642	0.56
WB-0816-MC-04	335	340	337.5	49.79	21.27	35.642	0.60
WB-0816-MC-04	340	345	342.5	50.84	21.89	35.642	0.61
WB-0816-MC-04	345	350	347.5	47.17	20.50	35.642	0.58
WB-0816-MC-04	350	355	352.5	52.26	22.56	35.642	0.63
WB-0816-MC-04	355	360	357.5	48.19	21.15	35.642	0.59
WB-0816-MC-04	360	365	362.5	49.88	22.06	35.642	0.62
WB-0816-MC-04	365	370	367.5	49.40	22.02	35.642	0.62
WB-0816-MC-04	370	Base		19.38	8.81		

Table K.28. Bulk density data for core site WB-0816-MC-DSH-08-A. Sediment core sub-sample intervals (mm), sub-sample wet weight (g), dry weight (g), sub-sample volume (cm^3), and bulk density (g/cm^3). Note: Blank cell denotes no analysis performed.

Core ID	Top Depth of Interval (mm)	Bottom Depth of Interval (mm)	Average Depth of Interval (mm)	Wet Weight (g)	Dry Weight (g)	Sample Volume (cm^3)	Bulk Density (g/cm^3)
WB-0816-MC-DSH-08-A	0	2	1	21.31	2.49	14.257	0.17
WB-0816-MC-DSH-08-A	2	4	3	12.03	2.32	14.257	0.16
WB-0816-MC-DSH-08-A	4	6	5	13.51	2.99	14.257	0.21
WB-0816-MC-DSH-08-A	6	8	7	15.65	3.69	14.257	0.26
WB-0816-MC-DSH-08-A	8	10	9	17.16	4.19	14.257	0.29
WB-0816-MC-DSH-08-A	10	12	11	15.30	3.83	14.257	0.27
WB-0816-MC-DSH-08-A	12	14	13	16.43	4.23	14.257	0.30
WB-0816-MC-DSH-08-A	14	16	15	16.15	4.20	14.257	0.29
WB-0816-MC-DSH-08-A	16	18	17	17.72	4.65	14.257	0.33
WB-0816-MC-DSH-08-A	18	20	19	15.74	4.14	14.257	0.29
WB-0816-MC-DSH-08-A	20	22	21	14.47	3.84	14.257	0.27
WB-0816-MC-DSH-08-A	22	24	23	16.36	4.39	14.257	0.31
WB-0816-MC-DSH-08-A	24	26	25	15.75	4.27	14.257	0.30
WB-0816-MC-DSH-08-A	26	28	27	15.71	4.30	14.257	0.30
WB-0816-MC-DSH-08-A	28	30	29	16.66	4.64	14.257	0.33
WB-0816-MC-DSH-08-A	30	32	31	15.84	4.44	14.257	0.31
WB-0816-MC-DSH-08-A	32	34	33	16.71	4.77	14.257	0.33
WB-0816-MC-DSH-08-A	34	36	35	16.26	4.70	14.257	0.33
WB-0816-MC-DSH-08-A	36	38	37	16.26	4.81	14.257	0.34
WB-0816-MC-DSH-08-A	38	40	39	15.47	4.67	14.257	0.33
WB-0816-MC-DSH-08-A	40	42	41	14.91	4.60	14.257	0.32
WB-0816-MC-DSH-08-A	42	44	43	18.17	5.66	14.257	0.40
WB-0816-MC-DSH-08-A	44	46	45	17.15	5.40	14.257	0.38
WB-0816-MC-DSH-08-A	46	48	47	16.44	5.30	14.257	0.37
WB-0816-MC-DSH-08-A	48	50	49	20.46	6.63	14.257	0.47
WB-0816-MC-DSH-08-A	50	55	52.5	35.69	12.27	35.642	0.34
WB-0816-MC-DSH-08-A	55	60	57.5	46.25	15.95	35.642	0.45
WB-0816-MC-DSH-08-A	60	65	62.5	45.62	15.83	35.642	0.44
WB-0816-MC-DSH-08-A	65	70	67.5	42.84	15.37	35.642	0.43
WB-0816-MC-DSH-08-A	70	75	72.5	46.21	16.53	35.642	0.46
WB-0816-MC-DSH-08-A	75	80	77.5	44.61	16.29	35.642	0.46
WB-0816-MC-DSH-08-A	80	85	82.5	43.93	16.30	35.642	0.46
WB-0816-MC-DSH-08-A	85	90	87.5	46.81	17.67	35.642	0.50
WB-0816-MC-DSH-08-A	90	95	92.5	41.47	15.78	35.642	0.44
WB-0816-MC-DSH-08-A	95	100	97.5	40.63	15.46	35.642	0.43
WB-0816-MC-DSH-08-A	100	105	102.5	44.64	17.17	35.642	0.48

Table K.28 (Continued).

Core ID	Top Depth of Interval (mm)	Bottom Depth of Interval (mm)	Average Depth of Interval (mm)	Wet Weight (g)	Dry Weight (g)	Sample Volume (cm^3)	Bulk Density (g/cm^3)
WB-0816-MC-DSH-08-A	105	110	107.5	46.91	18.13	35.642	0.51
WB-0816-MC-DSH-08-A	110	115	112.5	43.22	16.87	35.642	0.47
WB-0816-MC-DSH-08-A	115	120	117.5	48.81	19.11	35.642	0.54
WB-0816-MC-DSH-08-A	120	125	122.5	41.87	16.29	35.642	0.46
WB-0816-MC-DSH-08-A	125	130	127.5	51.08	20.03	35.642	0.56
WB-0816-MC-DSH-08-A	130	135	132.5	44.81	17.38	35.642	0.49
WB-0816-MC-DSH-08-A	135	140	137.5	45.87	18.03	35.642	0.51
WB-0816-MC-DSH-08-A	140	145	142.5	46.98	18.52	35.642	0.52
WB-0816-MC-DSH-08-A	145	150	147.5	46.36	18.23	35.642	0.51
WB-0816-MC-DSH-08-A	150	155	152.5	47.34	18.47	35.642	0.52
WB-0816-MC-DSH-08-A	155	160	157.5	46.57	18.02	35.642	0.51
WB-0816-MC-DSH-08-A	160	165	162.5	46.75	17.94	35.642	0.50
WB-0816-MC-DSH-08-A	165	170	167.5	45.35	17.29	35.642	0.49
WB-0816-MC-DSH-08-A	170	175	172.5	46.68	17.60	35.642	0.49
WB-0816-MC-DSH-08-A	175	180	177.5	45.33	17.11	35.642	0.48
WB-0816-MC-DSH-08-A	180	185	182.5	46.87	17.68	35.642	0.50
WB-0816-MC-DSH-08-A	185	190	187.5	45.31	17.30	35.642	0.49
WB-0816-MC-DSH-08-A	190	195	192.5	47.05	18.06	35.642	0.51
WB-0816-MC-DSH-08-A	195	200	197.5	43.93	16.94	35.642	0.48
WB-0816-MC-DSH-08-A	200	205	202.5	52.28	20.45	35.642	0.57
WB-0816-MC-DSH-08-A	205	210	207.5	46.78	18.66	35.642	0.52
WB-0816-MC-DSH-08-A	210	215	212.5	45.46	18.15	35.642	0.51
WB-0816-MC-DSH-08-A	215	220	217.5	48.25	19.15	35.642	0.54
WB-0816-MC-DSH-08-A	220	225	222.5	42.97	16.85	35.642	0.47
WB-0816-MC-DSH-08-A	225	230	227.5	47.25	18.56	35.642	0.52
WB-0816-MC-DSH-08-A	230	235	232.5	46.57	18.18	35.642	0.51
WB-0816-MC-DSH-08-A	235	240	237.5	49.12	19.01	35.642	0.53
WB-0816-MC-DSH-08-A	240	245	242.5	40.52	15.48	35.642	0.43
WB-0816-MC-DSH-08-A	245	250	247.5	47.92	18.31	35.642	0.51
WB-0816-MC-DSH-08-A	250	255	252.5	49.84	18.75	35.642	0.53
WB-0816-MC-DSH-08-A	255	260	257.5	45.28	16.77	35.642	0.47
WB-0816-MC-DSH-08-A	260	265	262.5	48.20	17.56	35.642	0.49
WB-0816-MC-DSH-08-A	265	270	267.5	44.72	15.91	35.642	0.45
WB-0816-MC-DSH-08-A	270	275	272.5	47.46	16.47	35.642	0.46
WB-0816-MC-DSH-08-A	275	280	277.5	40.57	13.88	35.642	0.39
WB-0816-MC-DSH-08-A	280	285	282.5	42.41	14.60	35.642	0.41
WB-0816-MC-DSH-08-A	285	290	287.5	44.97	15.55	35.642	0.44
WB-0816-MC-DSH-08-A	290	295	292.5	46.77	16.37	35.642	0.46

Table K.28 (Continued).

Core ID	Top Depth of Interval (mm)	Bottom Depth of Interval (mm)	Average Depth of Interval (mm)	Wet Weight (g)	Dry Weight (g)	Sample Volume (cm^3)	Bulk Density (g/cm^3)
WB-0816-MC-DSH-08-A	295	300	297.5	45.18	15.72	35.642	0.44
WB-0816-MC-DSH-08-A	300	305	302.5	44.52	15.43	35.642	0.43
WB-0816-MC-DSH-08-A	305	310	307.5	45.14	15.68	35.642	0.44
WB-0816-MC-DSH-08-A	310	315	312.5	46.85	16.46	35.642	0.46
WB-0816-MC-DSH-08-A	315	320	317.5	44.85	15.94	35.642	0.45
WB-0816-MC-DSH-08-A	320	325	322.5	46.89	16.80	35.642	0.47
WB-0816-MC-DSH-08-A	325	330	327.5	46.99	16.96	35.642	0.48
WB-0816-MC-DSH-08-A	330	335	332.5	45.96	16.75	35.642	0.47
WB-0816-MC-DSH-08-A	335	340	337.5	44.38	16.13	35.642	0.45
WB-0816-MC-DSH-08-A	340	345	342.5	44.32	16.04	35.642	0.45
WB-0816-MC-DSH-08-A	345	350	347.5	44.45	16.17	35.642	0.45
WB-0816-MC-DSH-08-A	350	355	352.5	47.75	17.55	35.642	0.49
WB-0816-MC-DSH-08-A	355	360	357.5	46.25	17.09	35.642	0.48
WB-0816-MC-DSH-08-A	360	365	362.5	50.00	18.61	35.642	0.52
WB-0816-MC-DSH-08-A	365	370	367.5	43.25	16.09	35.642	0.45
WB-0816-MC-DSH-08-A	370	375	372.5	44.98	16.67	35.642	0.47
WB-0816-MC-DSH-08-A	375	380	377.5	46.52	17.16	35.642	0.48
WB-0816-MC-DSH-08-A	380	385	382.5	45.17	16.58	35.642	0.47
WB-0816-MC-DSH-08-A	385	390	387.5	46.20	17.03	35.642	0.48
WB-0816-MC-DSH-08-A	390	395	392.5	45.56	16.75	35.642	0.47
WB-0816-MC-DSH-08-A	395	400	397.5	46.86	17.40	35.642	0.49
WB-0816-MC-DSH-08-A	400	405	402.5	48.37	18.02	35.642	0.51
WB-0816-MC-DSH-08-A	405	410	407.5	46.24	17.27	35.642	0.48
WB-0816-MC-DSH-08-A	410	415	412.5	48.32	18.37	35.642	0.52
WB-0816-MC-DSH-08-A	415	420	417.5	41.58	15.94	35.642	0.45
WB-0816-MC-DSH-08-A	420	425	422.5	54.03	20.77	35.642	0.58
WB-0816-MC-DSH-08-A	425	430	427.5	32.29	12.81	35.642	0.36
WB-0816-MC-DSH-08-A	430	Base		41.60	17.01		

Table K.29. Bulk density data for core site WB-0816-MC-DSH-10-A. Sediment core sub-sample intervals (mm), sub-sample wet weight (g), dry weight (g), sub-sample volume (cm^3), and bulk density (g/cm^3). Note: Blank cell denotes no analysis performed.

Core ID	Top Depth of Interval (mm)	Bottom Depth of Interval (mm)	Average Depth of Interval (mm)	Wet Weight (g)	Dry Weight (g)	Sample Volume (cm^3)	Bulk Density (g/cm^3)
WB-0816-MC-DSH-10-A	0	2	1	10.02	2.74	14.257	0.19
WB-0816-MC-DSH-10-A	2	4	3	13.64	3.61	14.257	0.25
WB-0816-MC-DSH-10-A	4	6	5	14.01	3.69	14.257	0.26
WB-0816-MC-DSH-10-A	6	8	7	15.41	4.13	14.257	0.29
WB-0816-MC-DSH-10-A	8	10	9	15.23	4.21	14.257	0.30
WB-0816-MC-DSH-10-A	10	12	11	16.70	4.72	14.257	0.33
WB-0816-MC-DSH-10-A	12	14	13	17.12	4.90	14.257	0.34
WB-0816-MC-DSH-10-A	14	16	15	17.04	5.03	14.257	0.35
WB-0816-MC-DSH-10-A	16	18	17	16.60	4.92	14.257	0.35
WB-0816-MC-DSH-10-A	18	20	19	17.30	5.30	14.257	0.37
WB-0816-MC-DSH-10-A	20	22	21	16.16	5.02	14.257	0.35
WB-0816-MC-DSH-10-A	22	24	23	16.94	5.30	14.257	0.37
WB-0816-MC-DSH-10-A	24	26	25	17.65	5.70	14.257	0.40
WB-0816-MC-DSH-10-A	26	28	27	18.67	6.07	14.257	0.43
WB-0816-MC-DSH-10-A	28	30	29	17.91	5.85	14.257	0.41
WB-0816-MC-DSH-10-A	30	32	31	16.81	5.49	14.257	0.39
WB-0816-MC-DSH-10-A	32	34	33	17.48	5.76	14.257	0.40
WB-0816-MC-DSH-10-A	34	36	35	17.66	5.88	14.257	0.41
WB-0816-MC-DSH-10-A	36	38	37	19.18	6.39	14.257	0.45
WB-0816-MC-DSH-10-A	38	40	39	22.26	7.61	14.257	0.53
WB-0816-MC-DSH-10-A	40	42	41	16.48	5.59	14.257	0.39
WB-0816-MC-DSH-10-A	42	44	43	17.65	6.10	14.257	0.43
WB-0816-MC-DSH-10-A	44	46	45	16.25	5.43	14.257	0.38
WB-0816-MC-DSH-10-A	46	48	47	17.62	5.96	14.257	0.42
WB-0816-MC-DSH-10-A	48	50	49	17.50	6.06	14.257	0.43
WB-0816-MC-DSH-10-A	50	52	51	17.93	6.43	14.257	0.45
WB-0816-MC-DSH-10-A	52	54	53	16.95	5.93	14.257	0.42
WB-0816-MC-DSH-10-A	54	56	55	17.06	5.95	14.257	0.42
WB-0816-MC-DSH-10-A	56	58	57	16.76	5.82	14.257	0.41
WB-0816-MC-DSH-10-A	58	60	59	17.77	6.20	14.257	0.43
WB-0816-MC-DSH-10-A	60	62	61	18.90	6.63	14.257	0.47
WB-0816-MC-DSH-10-A	62	64	63	19.04	6.73	14.257	0.47
WB-0816-MC-DSH-10-A	64	66	65	18.86	6.75	14.257	0.47
WB-0816-MC-DSH-10-A	66	68	67	17.97	6.34	14.257	0.44
WB-0816-MC-DSH-10-A	68	70	69	18.33	6.44	14.257	0.45
WB-0816-MC-DSH-10-A	70	72	71	17.97	6.39	14.257	0.45

Table K.29 (Continued).

Core ID	Top Depth of Interval (mm)	Bottom Depth of Interval (mm)	Average Depth of Interval (mm)	Wet Weight (g)	Dry Weight (g)	Sample Volume (cm^3)	Bulk Density (g/cm^3)
WB-0816-MC-DSH-10-A	72	74	73	18.95	6.85	14.257	0.48
WB-0816-MC-DSH-10-A	74	76	75	18.61	6.69	14.257	0.47
WB-0816-MC-DSH-10-A	76	78	77	19.13	7.08	14.257	0.50
WB-0816-MC-DSH-10-A	78	80	79	17.56	6.47	14.257	0.45
WB-0816-MC-DSH-10-A	80	85	82.5	39.75	14.34	35.642	0.40
WB-0816-MC-DSH-10-A	85	90	87.5	48.75	17.85	35.642	0.50
WB-0816-MC-DSH-10-A	90	95	92.5	45.26	16.80	35.642	0.47
WB-0816-MC-DSH-10-A	95	100	97.5	46.25	17.39	35.642	0.49
WB-0816-MC-DSH-10-A	100	105	102.5	44.50	16.85	35.642	0.47
WB-0816-MC-DSH-10-A	105	110	107.5	45.77	17.40	35.642	0.49
WB-0816-MC-DSH-10-A	110	115	112.5	42.37	15.92	35.642	0.45
WB-0816-MC-DSH-10-A	115	120	117.5	45.81	17.45	35.642	0.49
WB-0816-MC-DSH-10-A	120	125	122.5	45.69	17.36	35.642	0.49
WB-0816-MC-DSH-10-A	125	130	127.5	46.41	17.65	35.642	0.50
WB-0816-MC-DSH-10-A	130	135	132.5	46.37	17.37	35.642	0.49
WB-0816-MC-DSH-10-A	135	140	137.5	44.59	16.55	35.642	0.46
WB-0816-MC-DSH-10-A	140	145	142.5	48.55	17.89	35.642	0.50
WB-0816-MC-DSH-10-A	145	150	147.5	43.74	15.71	35.642	0.44
WB-0816-MC-DSH-10-A	150	155	152.5	46.84	16.65	35.642	0.47
WB-0816-MC-DSH-10-A	155	160	157.5	44.25	15.53	35.642	0.44
WB-0816-MC-DSH-10-A	160	165	162.5	45.36	15.96	35.642	0.45
WB-0816-MC-DSH-10-A	165	170	167.5	45.27	15.79	35.642	0.44
WB-0816-MC-DSH-10-A	170	175	172.5	44.27	15.44	35.642	0.43
WB-0816-MC-DSH-10-A	175	180	177.5	45.82	16.00	35.642	0.45
WB-0816-MC-DSH-10-A	180	185	182.5	44.57	15.64	35.642	0.44
WB-0816-MC-DSH-10-A	185	190	187.5	47.29	16.71	35.642	0.47
WB-0816-MC-DSH-10-A	190	195	192.5	43.42	15.35	35.642	0.43
WB-0816-MC-DSH-10-A	195	200	197.5	45.21	15.99	35.642	0.45
WB-0816-MC-DSH-10-A	200	205	202.5	44.64	15.90	35.642	0.45
WB-0816-MC-DSH-10-A	205	210	207.5	45.97	16.43	35.642	0.46
WB-0816-MC-DSH-10-A	210	215	212.5	44.73	16.06	35.642	0.45
WB-0816-MC-DSH-10-A	215	220	217.5	47.90	17.26	35.642	0.48
WB-0816-MC-DSH-10-A	220	225	222.5	44.96	15.97	35.642	0.45
WB-0816-MC-DSH-10-A	225	230	227.5	45.22	15.93	35.642	0.45
WB-0816-MC-DSH-10-A	230	235	232.5	46.25	16.22	35.642	0.46
WB-0816-MC-DSH-10-A	235	240	237.5	44.19	15.52	35.642	0.44
WB-0816-MC-DSH-10-A	240	245	242.5	45.07	15.93	35.642	0.45
WB-0816-MC-DSH-10-A	245	250	247.5	44.89	15.90	35.642	0.45

Table K.29 (Continued).

Core ID	Top Depth of Interval (mm)	Bottom Depth of Interval (mm)	Average Depth of Interval (mm)	Wet Weight (g)	Dry Weight (g)	Sample Volume (cm^3)	Bulk Density (g/cm^3)
WB-0816-MC-DSH-10-A	250	255	252.5	45.40	16.10	35.642	0.45
WB-0816-MC-DSH-10-A	255	260	257.5	45.83	16.24	35.642	0.46
WB-0816-MC-DSH-10-A	260	265	262.5	44.28	15.59	35.642	0.44
WB-0816-MC-DSH-10-A	265	270	267.5	45.35	16.01	35.642	0.45
WB-0816-MC-DSH-10-A	270	275	272.5	44.26	15.58	35.642	0.44
WB-0816-MC-DSH-10-A	275	280	277.5	45.36	16.06	35.642	0.45
WB-0816-MC-DSH-10-A	280	285	282.5	44.97	16.21	35.642	0.45
WB-0816-MC-DSH-10-A	285	290	287.5	44.62	16.30	35.642	0.46
WB-0816-MC-DSH-10-A	290	295	292.5	46.86	17.38	35.642	0.49
WB-0816-MC-DSH-10-A	295	300	297.5	49.07	18.12	35.642	0.51
WB-0816-MC-DSH-10-A	300	305	302.5	45.32	16.75	35.642	0.47
WB-0816-MC-DSH-10-A	305	310	307.5	45.63	16.78	35.642	0.47
WB-0816-MC-DSH-10-A	310	315	312.5	45.32	16.43	35.642	0.46
WB-0816-MC-DSH-10-A	315	320	317.5	43.65	15.65	35.642	0.44
WB-0816-MC-DSH-10-A	320	325	322.5	47.83	17.12	35.642	0.48
WB-0816-MC-DSH-10-A	325	330	327.5	45.10	16.08	35.642	0.45
WB-0816-MC-DSH-10-A	330	335	332.5	43.58	15.65	35.642	0.44
WB-0816-MC-DSH-10-A	335	340	337.5	45.58	16.28	35.642	0.46
WB-0816-MC-DSH-10-A	340	345	342.5	45.76	16.36	35.642	0.46
WB-0816-MC-DSH-10-A	345	350	347.5	47.63	17.33	35.642	0.49
WB-0816-MC-DSH-10-A	350	355	352.5	44.19	15.97	35.642	0.45
WB-0816-MC-DSH-10-A	355	360	357.5	44.59	15.95	35.642	0.45
WB-0816-MC-DSH-10-A	360	365	362.5	44.65	15.92	35.642	0.45
WB-0816-MC-DSH-10-A	365	370	367.5	46.35	16.52	35.642	0.46
WB-0816-MC-DSH-10-A	370	375	372.5	44.41	16.03	35.642	0.45
WB-0816-MC-DSH-10-A	375	380	377.5	46.11	16.76	35.642	0.47
WB-0816-MC-DSH-10-A	380	385	382.5	44.93	16.49	35.642	0.46
WB-0816-MC-DSH-10-A	385	390	387.5	46.71	17.30	35.642	0.49
WB-0816-MC-DSH-10-A	390	395	392.5	45.52	16.90	35.642	0.47
WB-0816-MC-DSH-10-A	395	400	397.5	47.04	17.59	35.642	0.49
WB-0816-MC-DSH-10-A	400	405	402.5	45.73	17.14	35.642	0.48
WB-0816-MC-DSH-10-A	405	410	407.5	47.18	17.71	35.642	0.50
WB-0816-MC-DSH-10-A	410	415	412.5	47.54	17.86	35.642	0.50
WB-0816-MC-DSH-10-A	415	420	417.5	45.11	16.98	35.642	0.48
WB-0816-MC-DSH-10-A	420	425	422.5	46.35	17.44	35.642	0.49
WB-0816-MC-DSH-10-A	425	430	427.5	45.95	17.38	35.642	0.49
WB-0816-MC-DSH-10-A	430	435	432.5	47.10	17.89	35.642	0.50
WB-0816-MC-DSH-10-A	435	440	437.5	46.21	17.91	35.642	0.50

Table K.29 (Continued).

Core ID	Top Depth of Interval (mm)	Bottom Depth of Interval (mm)	Average Depth of Interval (mm)	Wet Weight (g)	Dry Weight (g)	Sample Volume (cm^3)	Bulk Density (g/cm^3)
WB-0816-MC-DSH-10-A	440	Base		22.52	9.10		

Table K.30. Bulk density data for core site WB-0816-MC-PCB-06-A. Sediment core sub-sample intervals (mm), sub-sample wet weight (g), dry weight (g), sub-sample volume (cm^3), and bulk density (g/cm^3). Note: Blank cell denotes no analysis performed.

Core ID	Top Depth of Interval (mm)	Bottom Depth of Interval (mm)	Average Depth of Interval (mm)	Wet Weight (g)	Dry Weight (g)	Sample Volume (cm^3)	Bulk Density (g/cm^3)
WB-0816-MC-PCB-06-A	0	2	1	8.06	2.04	14.257	0.14
WB-0816-MC-PCB-06-A	2	4	3	5.59	1.32	14.257	0.09
WB-0816-MC-PCB-06-A	4	6	5	8.97	1.95	14.257	0.14
WB-0816-MC-PCB-06-A	6	8	7	9.99	2.07	14.257	0.15
WB-0816-MC-PCB-06-A	8	10	9	12.34	2.86	14.257	0.20
WB-0816-MC-PCB-06-A	10	12	11	15.82	3.95	14.257	0.28
WB-0816-MC-PCB-06-A	12	14	13	15.44	3.99	14.257	0.28
WB-0816-MC-PCB-06-A	14	16	15	17.15	4.57	14.257	0.32
WB-0816-MC-PCB-06-A	16	18	17	16.54	4.48	14.257	0.31
WB-0816-MC-PCB-06-A	18	20	19	17.49	4.80	14.257	0.34
WB-0816-MC-PCB-06-A	20	22	21	16.10	4.48	14.257	0.31
WB-0816-MC-PCB-06-A	22	24	23	17.11	4.87	14.257	0.34
WB-0816-MC-PCB-06-A	24	26	25	16.00	4.64	14.257	0.33
WB-0816-MC-PCB-06-A	26	28	27	16.67	4.98	14.257	0.35
WB-0816-MC-PCB-06-A	28	30	29	17.38	5.32	14.257	0.37
WB-0816-MC-PCB-06-A	30	32	31	17.40	5.38	14.257	0.38
WB-0816-MC-PCB-06-A	32	34	33	15.85	4.91	14.257	0.34
WB-0816-MC-PCB-06-A	34	36	35	17.86	5.62	14.257	0.39
WB-0816-MC-PCB-06-A	36	38	37	17.55	5.48	14.257	0.38
WB-0816-MC-PCB-06-A	38	40	39	17.75	5.59	14.257	0.39
WB-0816-MC-PCB-06-A	40	42	41	16.17	5.18	14.257	0.36
WB-0816-MC-PCB-06-A	42	44	43	18.24	5.91	14.257	0.41
WB-0816-MC-PCB-06-A	44	46	45	16.09	5.23	14.257	0.37
WB-0816-MC-PCB-06-A	46	48	47	18.92	6.16	14.257	0.43
WB-0816-MC-PCB-06-A	48	50	49	15.51	5.12	14.257	0.36
WB-0816-MC-PCB-06-A	50	52	51	19.24	6.40	14.257	0.45
WB-0816-MC-PCB-06-A	52	54	53	18.62	6.89	14.257	0.48
WB-0816-MC-PCB-06-A	54	56	55	16.56	5.55	14.257	0.39
WB-0816-MC-PCB-06-A	56	58	57	16.17	5.43	14.257	0.38
WB-0816-MC-PCB-06-A	58	60	59	18.64	6.32	14.257	0.44
WB-0816-MC-PCB-06-A	60	62	61	17.02	5.82	14.257	0.41
WB-0816-MC-PCB-06-A	62	64	63	18.21	6.25	14.257	0.44
WB-0816-MC-PCB-06-A	64	66	65	18.36	6.27	14.257	0.44
WB-0816-MC-PCB-06-A	66	68	67	17.88	6.13	14.257	0.43
WB-0816-MC-PCB-06-A	68	70	69	16.27	5.60	14.257	0.39
WB-0816-MC-PCB-06-A	70	72	71	19.11	6.64	14.257	0.47

Table K.30 (Continued).

Core ID	Top Depth of Interval (mm)	Bottom Depth of Interval (mm)	Average Depth of Interval (mm)	Wet Weight (g)	Dry Weight (g)	Sample Volume (cm^3)	Bulk Density (g/cm^3)
WB-0816-MC-PCB-06-A	72	74	73	16.89	5.87	14.257	0.41
WB-0816-MC-PCB-06-A	74	76	75	18.63	6.47	14.257	0.45
WB-0816-MC-PCB-06-A	76	78	77	16.95	5.95	14.257	0.42
WB-0816-MC-PCB-06-A	78	80	79	18.51	6.50	14.257	0.46
WB-0816-MC-PCB-06-A	80	85	82.5	45.18	15.85	35.642	0.44
WB-0816-MC-PCB-06-A	85	90	87.5	44.50	15.78	35.642	0.44
WB-0816-MC-PCB-06-A	90	95	92.5	44.77	15.79	35.642	0.44
WB-0816-MC-PCB-06-A	95	100	97.5	46.20	16.37	35.642	0.46
WB-0816-MC-PCB-06-A	100	105	102.5	45.65	16.23	35.642	0.46
WB-0816-MC-PCB-06-A	105	110	107.5	45.57	16.20	35.642	0.45
WB-0816-MC-PCB-06-A	110	115	112.5	46.52	16.74	35.642	0.47
WB-0816-MC-PCB-06-A	115	120	117.5	43.90	15.84	35.642	0.44
WB-0816-MC-PCB-06-A	120	125	122.5	46.66	16.73	35.642	0.47
WB-0816-MC-PCB-06-A	125	130	127.5	45.26	16.26	35.642	0.46
WB-0816-MC-PCB-06-A	130	135	132.5	45.65	16.43	35.642	0.46
WB-0816-MC-PCB-06-A	135	140	137.5	46.33	16.82	35.642	0.47
WB-0816-MC-PCB-06-A	140	145	142.5	42.06	15.35	35.642	0.43
WB-0816-MC-PCB-06-A	145	150	147.5	45.37	16.35	35.642	0.46
WB-0816-MC-PCB-06-A	150	155	152.5	47.27	17.38	35.642	0.49
WB-0816-MC-PCB-06-A	155	160	157.5	44.74	16.63	35.642	0.47
WB-0816-MC-PCB-06-A	160	165	162.5	45.79	16.94	35.642	0.48
WB-0816-MC-PCB-06-A	165	170	167.5	44.89	16.69	35.642	0.47
WB-0816-MC-PCB-06-A	170	175	172.5	50.20	18.63	35.642	0.52
WB-0816-MC-PCB-06-A	175	180	177.5	43.17	15.88	35.642	0.45
WB-0816-MC-PCB-06-A	180	185	182.5	46.08	17.02	35.642	0.48
WB-0816-MC-PCB-06-A	185	190	187.5	45.00	16.45	35.642	0.46
WB-0816-MC-PCB-06-A	190	195	192.5	44.94	16.42	35.642	0.46
WB-0816-MC-PCB-06-A	195	200	197.5	46.75	17.03	35.642	0.48
WB-0816-MC-PCB-06-A	200	205	202.5	45.75	16.69	35.642	0.47
WB-0816-MC-PCB-06-A	205	210	207.5	45.65	16.62	35.642	0.47
WB-0816-MC-PCB-06-A	210	215	212.5	46.43	16.88	35.642	0.47
WB-0816-MC-PCB-06-A	215	220	217.5	44.89	16.03	35.642	0.45
WB-0816-MC-PCB-06-A	220	225	222.5	47.15	16.82	35.642	0.47
WB-0816-MC-PCB-06-A	225	230	227.5	44.16	15.76	35.642	0.44
WB-0816-MC-PCB-06-A	230	235	232.5	45.20	16.21	35.642	0.45
WB-0816-MC-PCB-06-A	235	240	237.5	44.60	16.32	35.642	0.46
WB-0816-MC-PCB-06-A	240	245	242.5	47.88	17.42	35.642	0.49
WB-0816-MC-PCB-06-A	245	250	247.5	45.80	16.65	35.642	0.47

Table K.30 (Continued).

Core ID	Top Depth of Interval (mm)	Bottom Depth of Interval (mm)	Average Depth of Interval (mm)	Wet Weight (g)	Dry Weight (g)	Sample Volume (cm^3)	Bulk Density (g/cm^3)
WB-0816-MC-PCB-06-A	260	265	262.5	45.75	16.64	35.642	0.47
WB-0816-MC-PCB-06-A	265	270	267.5	45.34	16.75	35.642	0.47
WB-0816-MC-PCB-06-A	270	275	272.5	47.51	17.60	35.642	0.49
WB-0816-MC-PCB-06-A	275	280	277.5	44.57	16.48	35.642	0.46
WB-0816-MC-PCB-06-A	280	285	282.5	47.92	17.76	35.642	0.50
WB-0816-MC-PCB-06-A	285	290	287.5	45.66	17.10	35.642	0.48
WB-0816-MC-PCB-06-A	290	295	292.5	46.75	17.69	35.642	0.50
WB-0816-MC-PCB-06-A	295	300	297.5	45.29	17.11	35.642	0.48
WB-0816-MC-PCB-06-A	300	305	302.5	46.26	17.58	35.642	0.49
WB-0816-MC-PCB-06-A	305	310	307.5	46.67	17.90	35.642	0.50
WB-0816-MC-PCB-06-A	310	315	312.5	46.66	17.71	35.642	0.50
WB-0816-MC-PCB-06-A	315	320	317.5	45.31	17.07	35.642	0.48
WB-0816-MC-PCB-06-A	320	325	322.5	48.14	17.87	35.642	0.50
WB-0816-MC-PCB-06-A	325	330	327.5	45.68	16.87	35.642	0.47
WB-0816-MC-PCB-06-A	330	335	332.5	46.76	17.39	35.642	0.49
WB-0816-MC-PCB-06-A	335	340	337.5	44.51	16.83	35.642	0.47
WB-0816-MC-PCB-06-A	340	345	342.5	46.92	17.90	35.642	0.50
WB-0816-MC-PCB-06-A	345	350	347.5	45.24	17.17	35.642	0.48
WB-0816-MC-PCB-06-A	350	355	352.5	47.76	18.17	35.642	0.51
WB-0816-MC-PCB-06-A	355	360	357.5	46.66	17.71	35.642	0.50
WB-0816-MC-PCB-06-A	360	365	362.5	46.89	17.89	35.642	0.50
WB-0816-MC-PCB-06-A	365	370	367.5	45.96	17.48	35.642	0.49
WB-0816-MC-PCB-06-A	370	375	372.5	47.04	17.81	35.642	0.50
WB-0816-MC-PCB-06-A	375	380	377.5	45.77	17.38	35.642	0.49
WB-0816-MC-PCB-06-A	380	385	382.5	47.58	18.28	35.642	0.51
WB-0816-MC-PCB-06-A	385	390	387.5	46.53	18.02	35.642	0.51
WB-0816-MC-PCB-06-A	390	395	392.5	46.17	18.01	35.642	0.51
WB-0816-MC-PCB-06-A	395	400	397.5	46.53	18.35	35.642	0.51
WB-0816-MC-PCB-06-A	400	405	402.5	47.95	19.06	35.642	0.53
WB-0816-MC-PCB-06-A	405	410	407.5	47.09	18.72	35.642	0.53
WB-0816-MC-PCB-06-A	410	415	412.5	47.03	18.75	35.642	0.53
WB-0816-MC-PCB-06-A	415	420	417.5	49.78	20.14	35.642	0.57
WB-0816-MC-PCB-06-A	420	425	422.5	46.84	18.95	35.642	0.53
WB-0816-MC-PCB-06-A	425	430	427.5	47.31	19.27	35.642	0.54
WB-0816-MC-PCB-06-A	430	435	432.5	46.39	19.12	35.642	0.54
WB-0816-MC-PCB-06-A	435	Base		61.48	25.85		